An Observational Study of the Austral Spring Stratosphere: Dynamics, Ozone Transport and the 'Ozone Dilution Effect'

by

Roger John Atkinson

B.E. (Hons), University of Melbourne (1989)
Dip. Meteor., Australian Bureau of Meteorology (1978)

Submitted to the Department of
Earth, Atmospheric, and Planetary Sciences
in Partial Fulfillment of the Requirements
for the Degree of

Doctor of Science in Meteorology

at the

Massachusetts Institute of Technology

July 1993

Signature of Author _____
Center for Meteorology and Physical Oceanography
July 1993

Certified by _____
R. Alan Plumb
Professor of Meteorology
Thesis Supervisor

Accepted by _____
Thomas Jordan, Head
Dept. of Earth, Atmospheric and Planetary Sciences

An Observational Study of the Austral Spring Stratosphere: Dynamics, Ozone Transport and the 'Ozone Dilution Effect'

by

Roger John Atkinson

Submitted to the Department of Earth, Atmospheric and Planetary Sciences on 31 July 1993 in partial fulfillment of the requirements for the Degree of Doctor of Science in Meteorology

Abstract

Since the onset of springtime ozone depletion in the Antarctic lower stratosphere, a question has arisen concerning the extent to which the dynamical extrusion of 'ozone hole' material out into the surrounding regions, either before or accompanying the breakup of the polar vortex, might influence ozone levels at mid-latitudes, through a so-called 'ozone dilution effect'. One such event was previously identified which followed the vortex breakup during early December 1987, but the extent to which it comprised an actual dilution event, and not just a 'natural' process, was not assessed. The question also remains as to the overall frequency and severity of such events during the past decade or so, and whether they might together contribute significantly to observed long-term mid-latitude ozone decreases. In the present work, we have carried out an observational investigation of the ozone dilution issue, by examining the evolution of the austral spring stratosphere in each year from 1979 to 1989.

The December 1987 event is first examined in more detail. A coordinate transformation technique is used on SAGE ozone data to obtain a three-dimensional description of the hemispheric ozone distribution immediately prior to the event. Contour advection with surgery (CAS) is used to describe the stratospheric material evolution during the period of the event, and this provides a detailed description of the quasi-horizontal ozone transports which occcurred. The 'potential vorticity tendency' form of the quasi-geostrophic omega equation is solved to provide insight into the horizontal scales and vertical domain of the dynamical processes primarily responsible for the component of the total ozone changes due to vertical advection. Finally, by imposing a 'no ozone hole' ozone distribution during the period, and comparing the implied ozone changes with those obtained from the unmodified reconstruction, we isolate the component of the observed ozone changes attributable to the presence of Antarctic ozone depletion. The analysis reveals that the event contained a significant ozone dilution component, and that a smaller but more widespread effect may have followed during the latter part of the month. This subsequent period is next examined more briefly to provide a crude estimate of the overall impact of the 1987 Antarctic ozone hole on the summertime mid-latitude ozone column.

The broader issue of ozone dilution occurring in other years, and at other stages of the season, is then considered. A synoptic analysis of the springtime dynamical evolution each year is performed to identify other potential dilution events. The springtime SAGE ozone data from 1979 to 1989 are used, via the coordinate transformation technique, to provide a detailed description of the day-to-day evolution of the ozone distribution during each season. Additional CAS simulations are then performed for each potential event. These, together with the corresponding reconstructed ozone distributions, enable crude assessment of the extent of mid-latitude ozone dilution prior to and accompanying the vortex breakup in each of the years examined, which in turn provides insight into the long-term impact on mid-latitude ozone of the ozone dilution effect.

Thesis Supervisor: Dr. R. Alan Plumb
Professor of Meteorology

Acknowledgements

I have numerous people to thank for the encouragement, assistance and support so generously provided during the last several years. Foremost among these I wish to thank my advisor, Alan Plumb, for his encouragement and advice in relation to my research, and for sharing his knowledge and understanding throughout the course of my studies at MIT.

Without the benefit of support under an Australian Government Scholarship, which was funded by the Bureau of Meteorology, my studies at MIT would not have been possible. I also acknowledge partial assistance during the latter stages of my research from NASA Grant NAGW 1727.

I am particularly grateful to the numerous members of the MIT faculty from whom I have had the opportunity to learn; in particular to Kerry Emanuel, Dick Lindzen and Ron Prinn, who, as members of my thesis committee, also provided helpful advice and criticism on my research. Others I also wish to thank in this latter regard include Mark Schoeberl, Paul Newman and Darryn Waugh.

My research being observationally based, it could not have been performed without data, and I extend my thanks to all who assisted in providing the various datasets used. In particular, I wish to acknowledge the generous assistance of the following: to Albert Fleig and the TOMS data processing team at NASA GSFC, for the TOMS total ozone dataset; to the SAGE data processing team at the EOS Distributed Active Archive Center of the Global Change Data Center, for the SAGE ozone data; to Paul Newman and Eric Nash at NASA GSFC, for the gridded NMC data; to Sam Oltmans at NOAA ERL for ozone sonde data from the NOAA stations; to Andrew Matthews of NIWA (formerly DSIR), New Zealand, for the Lauder ozone sonde data; to Larry Morrison at the World Ozone Data Center, Toronto, for the ozone sonde data from the remaining southern hemisphere stations; and to my colleague Jim Easson, for the Melbourne Dobson total ozone data. Thanks are also due to Darryn Waugh for

the use of his Contour Advection with Surgery code, and to Bob Boldi for his colour graphics code.

Naturally, there are many others I should also like to thank. Among these are Michael McIntyre, whose few words of encouragement at the Polar Ozone Workshop sparked the course of events which brought me here, and Eric Jesson and Peter Shaw, who provided encouragement and support over several years prior to my stint at MIT. Then there are all those in Boston, both at MIT and off-campus, who have made my experience here such an enjoyable and fulfilling one, and all my friends back home, in particular Mark Halse, and the Downey family, the benefit of whose continual support and friendship has been immeasurable.

Last but by no means least, I am indebted to my family: to my parents who set me off in the right direction, and my brothers, who have been such ideal companions along the way. Most of all, of course, to my wife, Julie, for her constant companionship and selfless support, and to Jack and Christina, for their patience, if not their understanding: it is to these three I dedicate this thesis.

Contents

Chapter 1

Introduction

Since the detection by Farman *et al* (1985) of marked spring-time reductions in total ozone at Halley Bay, Antarctica, rapid progress has been made in understanding the chemistry, dynamics and radiative processes of the extra-tropical stratosphere. This understanding remains far from complete, however. One question that remains concerns the extent to which the Antarctic ozone hole might influence ozone levels elsewhere in the hemisphere. Atkinson *et al* (1989) examined an incident during December 1987 in which very low ozone was observed in the southern hemisphere mid-latitudes, and suggested a connection with the ozone hole. In the work described below we examine this 1987 'ozone hole dilution event' in more detail. Using NMC observational data we also examine and describe the dynamical evolution in the Austral spring stratosphere from 1979 to 1989, and build up a picture of the corresponding ozone evolution by employing a relatively novel and powerful coordinate transformation technique on the available SAGE ozone data. The dynamical analysis leads to the identification of other potential dilution events during the period, which we examine and discuss in an attempt to characterise the frequency and severity of such events, and to assess the role that Antarctic ozone loss and dynamical transport may together play in influencing the behaviour of mid-latitude ozone.

1.1 The Antarctic Ozone Hole

After the Farman *et al* (1985) Halley Bay Dobson spectrophotometer data findings were released, a re-appraisal of data from the Total Ozone Mapping Spectrometer (TOMS) on the Nimbus-7 satellite (Stolarski *et al*, 1986) revealed the full extent of the Antarctic 'ozone hole'. An intensive observational mission conducted during the following spring resulted in several theories being advanced, invoking either dynamical, chemical or radiative changes in the polar stratosphere, to explain the observed ozone reductions (see e.g. Schoeberl and Krueger, 1986, and references therein). A second mission in 1987 established that the springtime ozone decrease was essentially the result of increasing anthropogenic emissions of chlorofluorocarbons (CFCs) (Anderson *et al*, 1989). After photochemical breakdown of the CFCs filtering into the upper stratosphere, heterogeneous processing of stratospheric chlorine occurs on the surfaces of polar stratospheric clouds (PSCs) present in the Antarctic winter stratosphere, converting much of the chlorine from passive reservoir species into active radicals. Then, after the PSCs have partially precipitated, leaving behind a highly chlorinated, denitrified and dehydrated stratosphere, the return of sunlight in the spring brings about rapid and almost total ozone destruction in the polar lower stratosphere, a process which is only halted by renitrification of the region, either by reevaporation of the remaining PSCs within the warming polar vortex, or by the inward mixing of fresh sub-polar air rich in both nitrogen species and ozone. (Comprehensive reviews of the chemical and dynamical evolution of the Antarctic ozone hole are given, respectively, by Anderson *et al*, 1991, and Schoeberl and Hartmann, 1991.)

1.2 The Ozone Hole 'Dilution Effect': Analysis of the 1987 Event

On the strength of both observational and modelling studies (Hartmann, 1990; Hartmann *et al*, 1989a, 1989b; Juckes and McIntyre, 1987; McIntyre, 1989), which suggested that the polar vortex acts as a materially isolated entity, or 'chemical containment vessel', the ozone hole came for a time to be generally regarded as a uniquely Antarctic phenomenon, essentially divorced from the remainder of the stratosphere. Subsequently, numerous modelling studies (Chipperfield and Pyle, 1988; Grose *et al*, 1990; Ko *et al*, 1993; Pitari *et al*, 1992; Prather *et al*, 1990; Rodriguez *et al*, 1988; Sze *et al*, 1989) have indicated that, irrespective of whether or not the polar vortex might remain isolated while intact, the potential exists for transport of ozone-depleted air to lower latitudes as the vortex collapses during the final warming. Earlier, Atkinson and Easson (1988) had identified a sudden decrease in Dobson total ozone levels over southern Australia coincident with the vortex breakdown in 1987, and using potential vorticity diagnostics and TOMS data, Atkinson *et al* (1989) both demonstrated the large areal extent of the decrease and linked it with the quasi-horizontal transport of ozone-depleted lower stratospheric air from the vortex into mid-latitudes.

While Atkinson *et al* produced *prima facie* evidence of an observed 'ozone dilution' effect, they stopped short of quantifying the relative contributions to the observed decrease, from horizontal advection into the region of ozone-depleted vortex air (a true 'ozone dilution' effect), 'natural' horizontal advection (which would have occurred in the absence of Antarctic ozone depletion), and vertical advection from below of air 'naturally' low in ozone (isentropic uplift), a quite normal and inevitable dynamical adjustment process which must accompany the advection of high latitude stratospheric air into middle latitudes. In the absence of further evidence, it would not be inconceivable that such a decrease might be due solely to isentropic uplift, if the 'origin' of the high latitude air were the circumpolar ozone ridge rather than the ozone hole itself. Although Atkinson *et al* found support for their claims of a dilution

effect in trajectory analyses, they were cautious not to claim irrefutable proof.

To determine quantitatively the extent to which the mid-latitude ozone decrease observed during the first two weeks of December 1987 was an ozone dilution event, the first major objective of the present work, first requires the four-dimensional reconstruction of the hemispheric distribution of ozone (volumetric) mixing ratio (OMR), which is a conserved property, or material tracer, when photochemical processes can be neglected, a reasonable first order assumption for periods of up to a few weeks in the lower stratosphere. This task is by no means straightforward.

Firstly, the scarcity of available ozone data precludes direct four-dimensional reconstruction of the OMR fields for the period. While daily hemispheric gridded fields of total ozone data are available, observations of OMR are much more limited, particularly for the period covering the 1987 event. To overcome this problem we employ a coordinate transformation technique, similar to that recently developed by Schoeberl *et al* (1989a) for use with aircraft observations of long-lived chemical tracers, and the need for which was first alluded to by McIntyre (1980). On the assumption that non-conservative processes acting on OMR, Ertel potential vorticity (EPV) and potential temperature in the lower stratosphere during the month before the period of interest can be essentially neglected, we take the available ozone observations from that earlier period, and transform them into a quasi-Lagrangian reference frame (from 'latitude-longitude-potential temperature' space into 'normalised EPV-potential temperature' space), in which we are able to construct a dynamical or vortex-relative cross-section of OMR for the hemisphere. Then by using the EPV distribution from a particular day of the investigation, we perform the inverse transformation, to produce daily gridded hemispheric reconstructions of the OMR distribution.

While the use of the transformation technique overcomes to a large extent the scarcity of ozone data, it introduces another problem, because the December 1987 event occurs as the polar vortex breaks up. The transformation technique employed is tailored to cope with occasional instances of apparent non-conservation of the features in the isentropic EPV analyses, which coincide with large amplitude wave

events during the spring season each year. However, accompanying the vortex breakup a more marked EPV relaxation is observed in the analyses, which has a significant and adverse effect on the quality of the OMR reconstructions for the post-breakup period. The possible causes of this EPV relaxation are severalfold. Firstly, the large meridional excursions of both material and isentropic EPV which occur at this time result in a diabatic response which is not negligible. Secondly, there is a marked potential enstrophy cascade to horizontal scales below the adequate resolution of the satellite instrument whose retrieved data comprise the basis of the dynamical analyses, resulting in non-conservation of 'analysed' EPV, irrespective of whether or not actual EPV is conserved. Contributions attributable to other sources, such as limited vertical resolution and overall accuracy of the meteorological data, are also expected to arise. It would be desirable then to take such processes into account in our analysis.

Quantitative assessment of the diabatic response is a particularly complex problem requiring full treatment of radiative transfer for all but the simplest cases (Pawson *et al*, 1992), and is beyond the scope of the present work. Since there appears to be no worthwhile middle road in such circumstances, we make no attempt to take into *direct* account this contribution.

In an endeavour to minimise the effect of the other potential contributions, and to counter, *indirectly*, the effects of diabatic processes, we employ Contour Advection with Surgery (CAS) (Waugh and Plumb, 1993), a relatively novel innovation on trajectory analysis, wherein the analysed isentropic EPV contours from the start day of the investigation, which are taken to represent material contours on that day, are advected using the 'analysed' balanced winds for each day. The resulting contour patterns for each day of interest are then inverted and reinverted to retrieve gridded fields of the approximate material distribution, which are used subsequently as the basis of the OMR reconstructions for the latter stages of the detailed analysis period for the 1987 event.

Equipped with the resulting detailed OMR reconstructions, then, we examine in

more detail the contributions to the observed ozone decline due, respectively, to quasi-horizontal advection and isentropic uplift. The latter of these we approach directly at first, by simply calculating the effect on the total ozone distribution of the observed local isentropic pressure changes. We then employ an alternative procedure, which involves inversion of the 'potential vorticity tendency' form of the quasigeostrophic (QG) omega equation, after spherical harmonic decomposition of the input geopotential height fields, to obtain the vertical motion fields associated with the event. By adopting this alternative approach we confine ourselves to considering relatively large scales of motion (implicit in applying QG assumptions, but consistent with the limitations of the base satellite data set) but are able to retain computational manageability, and can obtain linearly superposable solutions which provide information on the horizontal scales and vertical domain of the QG potential vorticity (hereafter QPV) changes primarily responsible for the observed isentropic uplift.

Having examined the effect on the total ozone distribution of vertical motion occurring during the period, we turn to the contribution to the changes which is attributable to quasi-horizontal transport, and attempt to isolate the component of this contribution resulting solely from the presence of the Antarctic ozone hole, the true ozone dilution component of the observed total ozone changes.

Finally, since the detailed analysis covers only the early December period, we consider more briefly the expected impact of the dynamical transports occurring later in the month.

1.3 The Ozone Hole 'Dilution Effect': Additional Events, 1979 to 1989

By establishing that a component of the December 1987 mid-latitude ozone decrease was due to an ozone hole dilution effect, we may conclude that there has occurred at least once a mid-latitude impact of the Antarctic ozone hole. The question remains

as to whether this event was unique, rare, or just a marked and easily identifiable example of a relatively common but perhaps generally more subtle occurrence.

As well as the detection of the Antarctic ozone hole during the last decade, trend analysis of TOMS total ozone data by the International Ozone Trends Panel (OTP) indicated a mid-latitude total ozone decrease in each hemisphere during the preceding decade which was about a factor of two larger than that predicted by homogeneous chemistry models to have occurred as a result of anthropogenic influences (WMO, 1988). The OTP considered the observations to be 'qualitatively consistent' with the model predictions, taking into account model uncertainties, observational data accuracy, and uncertainties about the magnitude of 'natural' contributions to the observed decline, such as the solar cycle. More recently, however, Stolarski *et al* (1991), who repeated the TOMS trend analysis using data reprocessed to include allowance for internal calibration of the instrument for diffuser plate drift (Herman *et al*, 1991), found the previous trend estimates to have been substantially underestimated. Their reevaluated trends are quantitatively consistent with those made by Atkinson and Easson (1988), who used independent reevaluated Australian Dobson spectrophotometer total ozone data, and suggest that the observed mid-latitude ozone decline is several times larger than that predicted by the chemical models to have occurred. The cause of the discrepancy is yet to be identified. Given that the homogeneous chemistry of the stratosphere is reasonably well understood, and given the close quantitative agreement between the independent TOMS and Dobson trends, it is unlikely that the disparity is solely due to model and/or observational error. The remaining potential culprits are direct dynamical changes, in-situ heterogeneous chemistry, and advected chemistry, a combination of chemistry occurring elsewhere and dynamical transport of the perturbed chemistry into the mid-latitudes.

Lehmann *et al* (1992a, 1992b) recently performed a detailed examination of Macquarie Island ($55^{o}S$ $159^{o}E$) Dobson data extending back to 1963 and found a decadal mid-winter decrease in total ozone during the 1980s of about 12%, consistent with the latest TOMS findings, which they claim to be both zonally representative and

inconsistent with the hypothesis that the cause is dynamical changes in the lower stratosphere during the period. This would appear to rule out direct dynamical change. The potential role of 'advected chemistry' has been addressed elsewhere (Prather and Jaffe, 1990) and the question of in-situ heterogeneous chemistry is the subject of current research, in particular whether significant ozone destruction might result from heterogeneous reactions involving liquid sulphate aerosol at sub-polar lower stratospheric temperatures (Zhang *et al*, 1993 and references therein). Although the interhemispheric symmetry of the observed mid-latitude ozone decline and its mid-winter extremum suggest that dynamics is probably not the major player in winter, there remains the need to address the question of whether the observed decadal trend in spring and/or early summer might be due, at least in part, either to the occurrence of intermittent ozone dilution events of increasing severity during the decade, concommitant with the increasing severity of the ozone hole, or to an integrated ozone dilution effect during the 1980s, with chemical replacement too slow in the lower stratosphere to prevent an accumulating deficit.

This, then, comprises the second major objective of the present work, wherein we endeavour to identify and analyse, using essentially the same technique employed for the 1987 event, other potential ozone dilution events which might have occurred during each spring from 1979 to 1989, the seasons for which routine hemispheric monitoring of the meteorology of the stratosphere has been provided by satellite.

1.4 Dynamical Evolution of the Austral Spring Stratosphere

The provisional stage of this broader examination necessitated examination of the daily synoptic evolution of the southern hemisphere stratosphere over the eleven spring seasons considered. Copious literature is available concerning past endeavours to describe and explain the observed features in each hemisphere of the spring stratospheric evolution, a topic which has received so much attention because of

the dramatic and often sudden nature of the annual transition from winter westerly to summer easterly circulations which occurs in each hemisphere, and the opportunity these 'final warmings' provide to test our understanding of the underlying dynamical theory. While the gross observed features are now quite well characterised, doubts remain as to which particular theoretical mechanisms are important and which merely incidental. It is now generally accepted, since the pioneering work of Charney and Drazin (1961) and Matsuno (1970, 1971), and subsequent refinements (see e.g. Schoeberl, 1978 for a discussion of the development of ideas), that the essential gross features of a sudden warming probably involve the upward propagation of forced planetary scale tropospheric Rossby waves. While these ideas have provided an understanding of sorts, a number of key issues remain unresolved (McIntyre, 1982). Previous observational examinations tend to emphasize just one year, so attempting to piece together a coherent picture which distinguishes apparently essential features of the dynamical evolution from those which may be prominent one year but entirely absent another, can be a laborious and unprofitable task. We therefore hold that the construction of a consistent EPV-based description of the synoptic evolution of the austral spring stratosphere over the decade considered is a worthwhile task in itself. This is the third objective of the present work, the intention of which is primarily to describe and discuss the observed features of a typical or 'average' seasonal evolution, drawing on the work of others, and to compare and contrast departures from this typical behaviour noted in each of the seasons examined, to serve mainly as a reference for discussion of the features observed in the ozone evolution, but also perhaps as an aid to future dynamical studies.

1.5 Ozone Evolution in the Austral Spring Stratosphere

Finally, since the broader analysis also required several essentially monthly mean OMR distributions to be constructed for each year examined, we also find ourselves

in the possession of a rather detailed climatology of the southern hemisphere spring OMR distribution. While climatologies of OMR in the southern hemisphere have been assembled before, based on data from surface-based (Dutsch, 1978) and space-based (McPeters *et al*, 1984; Nagatani *et al*, 1988) measurements, our use here of the coordinate transformation technique on an independent satellite data set, to be described below, provides complementary information and an opportunity for an independent assessment to be made. Our last objective, then, is to present this climatology and discuss its major features, relating them to the observed dynamical behaviour, and comparing and contrasting the picture obtained with that gained from the earlier work.

1.6 Thesis Layout

In Chapter 2 below, we describe and discuss the basic dynamical data employed in the analysis, and provide details of the computational techniques used to obtain the derived quantities. Chapter 3 contains a similar description of the ozone data employed, and discusses the motivation for, and presents details of, the coordinate transformation technique adopted. In Chapter 4 we describe and discuss the dynamical climatology of the southern hemisphere stratosphere, while Chapter 5 contains a brief account of the synoptic evolution observed in each winter/spring season from 1979 to 1989. Chapter 6 is concerned with both the climatological evolution of the OMR distribution during the spring season and the noteworthy features of the evolution observed or implied for each year examined.

In Chapter 7 we then present the detailed examination of the 1987 ozone dilution event and the briefer analysis of the subsequent period in 1987, and follow this up in Chapter 8 with an account of the broader search for and examination of other potential events during the spring seasons from 1979 to 1989. In Chapter 9 we present our conclusions, and discuss a number of avenues for further research.

Chapter 2

Meteorological Data Employed and Computational Technique

2.1 Basic Meteorological Data

The primary data set employed for the derivation and construction of all dynamical fields in the analysis described below is that generated since 1978 by the Climate Analysis Center (CAC) at the National Meteorological Center (NMC), Washington. The original NMC southern hemisphere data set has been mapped, prior to use here, from its original 65 by 65 polar stereographic grid onto a 5^o latitude by 5^o longitude hemispheric grid by the Laboratory for Atmospheres at NASA Goddard SFC, from where the data set was obtained. The data comprise daily asynoptic (12 UTC centred) isobaric geopotential height and temperature fields for the southern hemisphere at 18 pressure levels (1000, 850, 700, 500, 400, 300, 250, 200, 150, 100, 70, 50, 30, 10, 5, 2, 1 and 0.4 hPa). Since our aim is to examine the dynamical evolution of the southern hemisphere spring stratosphere during the period for which routine satellite monitoring has been performed, we confine ourselves to the 'spring' period in each year from 1979 to 1989. We examine eleven six month periods from August to January, commencing 01 August 1979 and terminating on 31 January 1990.

Details of the retrieval scheme by which the NMC fields are generated from the original satellite radiances, and the modifications which have been incorporated into the analysis scheme over the years, are provided elsewhere (Gelman *et al*, 1983, 1984, 1986 and references therein). Perhaps the most critical of these changes was the cessation of use, after October 1980, of any surface-based observations in the analysis scheme. In effect, this means that subsequent to this change the data are exclusively a satellite-derived product, other than the extent to which the tropospheric analyses at and below the 100 hPa level (McPherson *et al*, 1979), upon which the stratospheric thickness analyses are stacked, and the radiosonde-derived regression coefficients for first guess temperature retrievals, influence the upper levels. While the need to exclude surface-baced input from the analyses might raise doubts about the quality of the product, the NMC data set is the only routine stratospheric data set available for the years prior to 1986. Although the gridded operational ECMWF stratospheric data set covers the period since May 1986 it employs first guess fields from the ECMWF high resolution global model, which can introduce an additional source of error into the final analysis fields (Shaw *et al*, 1987).

A critical appraisal of the NMC CAC data quality has been performed by Karoly and Graves (1990). They note that the two most significant sources of error in the data are that due to errors in the 100 hPa base level analysis upon which the upper levels are constructed, and that due to errors in the inversion and analysis of the satellite radiance data. They find that the analyses at levels above 2 hPa are unreliable owing to the coarse resolution of the highest SSU channel, which has maximum response near 2 hPa. At other levels they find the basic fields to be well represented, but note reservations about the quality of fields of derived quantities (e.g. E-P fluxes), and suggest that most problems stem from the failure of the satellite sampling to represent transient features adequately. They assess the reliable resolution of the data to be about 5° latitude by 30° longitude by 10 km height. The use of invariant first guess regression coefficients above 10 hPa, as opposed to the regular updating of the algorithms for lower levels (Newman and Randel, 1988; Randel, 1992) may also compromise data quality at these levels (Randel, 1988b).

As a last comment on the quality of the data employed in the present work, we note the polar stereographic to latitude-longitude mapping performed at NASA GSFC, for which bilinear interpolation was used, introduces spikes into the fields of second and higher order derivatives, which need to be filtered out for some purposes.

While the input NMC data set is isobaric, and extends from the lower troposphere to the upper stratosphere, our primary concern is the dynamical evolution of EPV and OMR in the lower stratosphere. The sensible vertical coordinate for this purpose is potential temperature (θ), so all quantities used in the analysis are transformed into isentropic coordinates prior to use. For this purpose, 24 'standard' levels were selected between $300K$ (about 500 hPa) and $1200K$ (about 5 hPa) (see Table 2.1, which also shows approximately representative values of pressure and altitude at each level during late winter at sub-polar latitudes).

For simplicity, in all calculations we perform linear interpolation of potential temperature with respect to pressure and all vertical derivatives are calculated by finite differencing in pressure. While it can be argued that this approach is overly simple (e.g. log pressure interpolation would be superior in most cases) and is not self-consistent for some calculations, we find the simple approach generally adequate for our purposes, and note potential improvements in Chapter 9.

2.2 Calculation of Isentropic Pressure

As noted above, hemispheric arrays of isentropic pressure at the 24 standard levels are calculated using the daily NMC isobaric temperature fields by simple finite differencing of θ against pressure, where θ is defined by

$$\theta = T\left(\frac{p_0}{p}\right)^{\kappa}, \tag{2.1}$$

where T is temperature (K), p_0 is reference pressure (1000 hPa), and $\kappa = R/C_p$, where R is the gas constant for dry air (287 $JKg^{-1}K^{-1}$) and C_p is the specific heat of dry air at constant pressure (1004 $JKg^{-1}K^{-1}$).

Potential Temperature (K)	Pressure (hPa)	Height (km)
300	500	5.5
310	350	8
320	250	10.5
340	200	12
360	175	13
380	140	14
400	120	15
425	100	16
450	85	17
475	70	18.5
500	60	19.5
525	50	20.5
550	40	22
575	35	23
600	30	24
650	26	25
700	23	26
750	20	27
800	16	28
850	13	29.5
900	10	31
1000	8	33
1100	6	35
1200	5	36

Table 2.1: 'Standard' isentropic analysis levels (^{o}K), and approximately corresponding pressure levels (hPa) and altitudes (km) for a sub-polar location in late winter.

2.3 Calculation of Balanced Winds

The vectorial form of the horizontal momentum equation may be written

$$\frac{d\vec{\mathbf{u}}}{dt} + 2\vec{\Omega} \times \vec{\mathbf{u}} + \nabla\Phi = \frac{\vec{\mathbf{F}}}{\rho}, \tag{2.2}$$

which represents the balance between inertial, Coriolis, body and frictional forces acting on a fluid (Pedlosky, 1987). Assuming the flow to be steady and frictionless, and employing the vector identity

$$(\nabla \times \vec{\mathbf{u}}) \times \vec{\mathbf{u}} = (\vec{\mathbf{u}}.\nabla)\vec{\mathbf{u}} - \nabla\Big(\frac{|\vec{\mathbf{u}}|^2}{2}\Big), \tag{2.3}$$

then Equation 2.2 can be written

$$\vec{\xi}_a \times \vec{\mathbf{u}} = -\nabla\Big(\Phi + \frac{|\vec{\mathbf{u}}|^2}{2}\Big), \tag{2.4}$$

where $\vec{\xi}_a$ is the absolute vorticity vector which we represent in component form as $\eta_a\vec{\mathbf{i}}+\zeta_a\vec{\mathbf{j}}+\xi_a\vec{\mathbf{k}}$, and $\vec{u} = u\vec{\mathbf{i}}+v\vec{\mathbf{j}}+w\vec{\mathbf{k}}$. Then, assuming that $\eta_a w \ll \xi_a u$ and $\zeta_a w \ll \xi_a v$, and expanding into spherical coordinates, we have

$$u \approx \frac{1}{a\xi_a}\frac{\partial}{\partial\varphi}\Big(\Phi + \frac{|\vec{\mathbf{u}}|^2}{2}\Big) \tag{2.5}$$

and

$$v \approx \frac{1}{acos\varphi\xi_a}\frac{\partial}{\partial\lambda}\Big(\Phi + \frac{|\vec{\mathbf{u}}|^2}{2}\Big), \tag{2.6}$$

where u and v are, respectively, the zonal and meridional wind components, a is earth radius, φ is latitude, λ longitude, and Φ is the geopotential.

By first assuming that $\xi_a = f$, the local magnitude of the Coriolis force, and $|\vec{\mathbf{u}}| = 0$ we may obtain a first guess of u and v, hence $|\vec{\mathbf{u}}|$ (the geostrophic wind). On substitution of $|\vec{\mathbf{u}}|$ back into the above expressions, finite differencing u and v to obtain the vertical component of relative vorticity, and substituting in a new estimate for ξ_a, we obtain iteratively balanced winds. Two iterations is generally sufficient for adequate convergence of the solutions. Finally, by implicitly employing the low Rossby Number, high Richardson Number (hereinafter 'loRohiRi') assumption (Hartmann, 1977a), we interpolate (as noted above) to obtain the isentropic wind distribution.

Winds derived from the non-linear balance equations generally provide considerably better representation of the true wind field at extra-tropical locations than lower order balance approximations (Randel, 1987b), a particularly important consideration for the CAS simulations described below.

2.4 Calculation of Ertel Potential Vorticity

Ertel potential vorticity (EPV), q, arguably the most essential and revealing quantity in atmospheric dynamics (Hoskins *et al*, 1985), is defined as

$$q = \rho^{-1}\vec{\xi}_a.\nabla\theta, \tag{2.7}$$

where ρ is atmospheric density and the other quantities are as described above.

Adopting the hydrostatic and loRohiRi assumptions appropriate for large scale stratospheric flows, we may approximate Equation 2.7 by

$$q \approx -g\xi_a\frac{\partial\theta}{\partial p}, \tag{2.8}$$

where g is the gravitational acceleration (9.81 ms^{-2}).

To ensure smooth variation of analysed EPV between consecutive isentropic levels, four level finite differencing is used in the evaluation of the $\partial\theta/\partial p$ term. Also, to avoid spikes in the analysed isentropic distribution, introduced by the mapping of the original data described above, we perform a latitude-dependent binomial filtering of the isobaric vorticity prior to its interpolation into θ space.

In all the work that follows EPV values will be referred to in PV units (PVU), where 1 PVU $= -1.0 \times 10^{-6} m^2 K s^{-1} K g^{-1}$, and in all cases 'high' EPV may be taken to mean large negative EPV, as associated with air from high altitude or latitude, and 'low' EPV to mean a small absolute value of EPV, as associated with tropical or low altitude origin.

2.5 Calculation of 'Vertical Motion'

Lagrangian vertical displacements in (x, y, z) space of a material parcel in generalised atmospheric motion can be viewed as having components due to isentropic upglide (the adiabatic motion of a parcel along an isentrope), vertical motion of a material parcel relative to the isentropes due to diabatic heating in the interior, and the vertical motion of the isentropes themselves, due to potential vorticity advection in the interior, temperature advection at the boundary, viscous dissipation in the interior, Ekman pumping in the boundary layer, or topographic forcing at the boundary.

Since our purpose in the present work primarily is to examine *localised* dynamical effects on the ozone distribution, in essence to separate approximately the contributions to an observed local change in total column ozone due to horizontal and vertical *material* motion, then if we can assume that diabatic processes are negligible in the region of our interest for the time scales we consider, then the isentropes become material surfaces, and we need merely to consider the observed pressure changes on the isentropes.

Several techniques are available to us for the calculation of the rate of 'isentropic uplift'. Defining the total rate of change of pressure by ω, we have

$$\omega = \frac{dp}{dt} = \left.\frac{\partial p}{\partial t}\right|_{\theta} + u_{\theta}.\nabla_{\theta} p + \dot{\theta}\frac{\partial p}{\partial \theta}, \tag{2.9}$$

where all symbols carry their normal meaning.

Rearranging, and defining the local pressure tendency in our isentropic coordinates as $\tilde{\omega}$, gives

$$\tilde{\omega} = \left.\frac{\partial p}{\partial t}\right|_{\theta} = \omega - u_{\theta}.\nabla_{\theta} p - \dot{\theta}\frac{\partial p}{\partial \theta}. \tag{2.10}$$

So $\tilde{\omega}$ is the rate of isentropic uplift, i.e. the total rate of pressure change following an air parcel (including e.g. viscous contributions) minus the contribution to this total change from isentropic pressure advection and diabatic mass fluxes, which, in the absence of diabatic processes, becomes the local rate of uplift of *material* surfaces.

The simplest and computationally the most direct approach to calculating $\tilde{\omega}$, and

that used for the bulk of the analysis to follow, is to use simple differencing of the observed isentropic pressure fields at the beginning and end of a particular period of interest to obtain the local pressure changes.

Alternatively, by considering the thermodynamic equation expanded in pressure coordinates,

$$\frac{d\theta}{dt} = \dot{\theta} = \left.\frac{\partial\theta}{\partial t}\right|_p + u_p.\nabla_p\theta + \omega\frac{\partial\theta}{\partial p}, \tag{2.11}$$

we have, after rearranging,

$$-\frac{\partial\theta/\partial t|_p}{\partial\theta/\partial p} = \omega + \frac{u_p.\nabla_p\theta}{\partial\theta/\partial p} - \dot{\theta}\frac{\partial p}{\partial\theta} \approx \tilde{\omega} \tag{2.12}$$

as before, where we have also made the loRohiRi assumption, since then

$$\left.\frac{\partial p}{\partial t}\right|_\theta \approx -\frac{\partial\theta/\partial t|_p}{\partial\theta/\partial p}. \tag{2.13}$$

Hence we might also calculate the local isentropic pressure changes by determining $\tilde{\omega}$ from the isobaric temperature analyses and interpolating to the 'standard' isentropic levels. Under adiabatic conditions, which we assume throughout, and QG scaling, the zonal mean of Equation 2.12 corresponds to the 'residual' vertical velocity of Andrews and McIntyre (1976).

While calculation of vertical motion by either of the above methods is quite straightforward, it allows no insight into the dynamical changes responsible for the resulting motion. Instead we can adopt another technique.

Since we are primarily interested in motions of large horizontal scales, hence low Rossby Number, then assuming the region of the atmosphere of interest to be inviscid, unforced and adiabatic, the QPV (q_p) equation reduces to

$$D_g q_p = 0 \tag{2.14}$$

or

$$\vec{\mathbf{u}}_g.\nabla_\mathbf{p} q_p = -\frac{\partial q_p}{\partial t}, \tag{2.15}$$

where

$$D_g = \frac{\partial}{\partial t} + u_g\frac{\partial}{\partial x} + v_g\frac{\partial}{\partial y} \tag{2.16}$$

and where we define

$$q_p = f_0 + \beta y + \frac{1}{f_0}\nabla_p^2\Phi + f_0\frac{\partial}{\partial p}\Big(\frac{\theta'}{d\bar{\theta}/dp}\Big), \tag{2.17}$$

where $\vec{\mathbf{u}}_g$, u_g and v_g are the geostrophic velocity and the magnitudes of its zonal and meridional components, respectively, ∇_p^2 is the horizontal Laplacian operator, Φ is the geopotential, f_0 the planetary vorticity at some reference latitude (chosen to be $60^o S$ for our purposes), β its meridional gradient, and where, to ensure exact balance in the expressions to follow, we have strictly defined the components of θ such that

$$\theta(x,y,p,t) = \tilde{\theta}(p,t) + \theta'(x,y,p,t) \tag{2.18}$$

and

$$\tilde{\theta}(p,t) = \bar{\theta}(p) + \bar{\theta}'(p,t) \tag{2.19}$$

i.e. $\bar{\theta}$ is the temporally and horizontally averaged potential temperature, and θ' is the local departure of θ from the horizontal average.

Alternatively, by employing the hydrostatic relationship

$$-\Re\theta = \frac{\partial\Phi}{\partial p}, \tag{2.20}$$

where $\Re = \frac{d\Pi}{dp}$, with $\Pi = C_p(p/p_0)^\kappa$ the Exner function, we may write

$$q_p = f_0 + \beta y + \frac{1}{f_0}\nabla_p^2\Phi' + f_0\frac{\partial}{\partial p}\Big[\frac{\Re^{-1}\partial\Phi'/\partial p}{\frac{d}{dp}(\Re^{-1}d\bar{\Phi}/dp)}\Big], \tag{2.21}$$

where we have defined the components of Φ by the same notation as used for θ, to express q_p solely in terms of the geopotential (a two-edged sword, the advantages and disadvantages of which we discuss below).

Then, by taking partial derivatives with respect to pressure and temperature, putting $\aleph^2 = -\Re d\bar{\theta}/dp$, and rearranging, we have

$$\Big(\aleph^2\nabla_p^2 + f_0^2\frac{\partial^2}{\partial p^2}\Big)\tilde{\omega} = f_0\frac{\partial}{\partial p}\Big(-\frac{\partial q_p}{\partial t}\Big) = F, \tag{2.22}$$

or, making use of Equation 2.15

$$\Big(\aleph^2\nabla_p^2 + f_0^2\frac{\partial^2}{\partial p^2}\Big)\tilde{\omega} = f_0\frac{\partial}{\partial p}\Big(\vec{\mathbf{u}}_g.\nabla_p q_p\Big) = F, \tag{2.23}$$

where

$$\tilde{\omega} = -\frac{\partial\theta'/\partial t}{d\bar{\theta}/dp} = \frac{\partial}{\partial t}\left(\frac{\Re^{-1}\frac{d\Phi'}{dp}}{\frac{d}{dp}[\Re^{-1}\frac{d\bar{\Phi}}{dp}]}\right), \tag{2.24}$$

as before.

Equation 2.23 is the 'potential vorticity advection' form of the QG omega equation. Its utility in this form lies in the way the dynamics behind local vertical motion are laid bare: the vertical motion is determined, via the inverse three-dimensional Laplacian-type operator, by vertical gradients in the horizontal advection of potential vorticity. As well as providing a clear dynamical expression for the vertical motion mechanism, which avoids the classical need to differentiate between the often competing effects of 'differential vorticity advection' and 'thickness advection' (Holton, 1992, Chapter 6; Hoskins *et al*, 1978), an additional feature makes its use particularly appealing. This arises via the numerical procedure employed to solve for $\tilde{\omega}$. Before providing details of this numerical procedure, however, two points should be noted.

First, it is found in practice that use of the 'QPV advection' form of the forcing term (i.e. use of Equation 2.23), which involves calculation by finite differencing of the dot products of second and third order horizontal derivatives of the geopotential, produces forcing fields which are overly sensitive to inaccuracies in the geopotential fields and results in unrealistic vertical motion distributions. Since the use instead of Equation 2.22 overcomes the problem, this is the approach adopted for all calculations. This introduces a subtle difference in the $\tilde{\omega}$ for which we are solving. Whereas the validity of Equation 2.23 is dependent, at the outset, on the adiabatic and inviscid assumptions being satisfied, to obtain the contribution to observed $\tilde{\omega}$ from QPV advection alone (subject to appropriate selection of boundary conditions), Equation 2.22 is valid irrespective of any large scale internal forcing which might exist: it is after the event that we apply these assumptions, in interpreting the solution obtained as being essentially due to QPV advection.

Second, all calculations are performed employing only the NMC geopotential fields (e.g. Equation 2.21 is used rather than Equation 2.17). This circumvents problems resulting from hydrostatic imbalance between the input geopotential and temperature

fields, and also enables us to ensure internal balance in the omega equation solution, despite the crude finite differencing technique employed. The price to be paid as a result, is the need to go one order higher in vertical derivatives than would be necessary using the temperature fields, which in turn either reduces the useful vertical domain of the data set, or expands the region near the boundaries where we are required to impose assumptions regarding vertical structure. The latter course is adopted. Numbering the 18 vertical levels of the input NMC fields from $i = 1$ (1000 hPa) to $i = 18$ (0.4 hPa), the hydrostatic relation (Equation 2.20) is used to calculate θ' and $\bar{\theta}$ at the 'half' levels $(i + \frac{1}{2})$ from $1\frac{1}{2}$ to $17\frac{1}{2}$, then $d\bar{\theta}/dp$ at levels 1 to 17. At this stage 'virtual' levels $\frac{1}{2}$ and $18\frac{1}{2}$ are 'envisaged', and the assumption is made that both $d\bar{\theta}/dp$ and $\partial\theta'/\partial p$ are constant within $1\frac{1}{2}$ levels of levels 1 and 18. Hence θ' and $d\bar{\theta}/dp$ can be calculated at all remaining 'half' levels from $\frac{1}{2}$ to $18\frac{1}{2}$. Using this artefact, we calculate $\partial/\partial p(\theta'/d\bar{\theta}/dp)$, hence QPV, at each i level from 1 to 18, to evaluate the forcing term F in Equation 2.22 (or more correctly, as discussed below, Λ in Equation 2.32 to follow) at each 'half' level from $1\frac{1}{2}$ to $17\frac{1}{2}$.

To solve Equation 2.22 it is first assumed that the $\tilde{\omega}$ distribution and QPV 'forcing' at each level may each be adequately expressed as the sum of a finite number of spherical harmonics,

$$\tilde{\omega} = \sum_{n=-N}^{N} \sum_{m=0}^{n} \Omega_{nm}(p) Y_n^m(\varphi, \lambda) \tag{2.25}$$

and

$$F = \sum_{n=-N}^{N} \sum_{m=0}^{n} \Lambda_{nm}(p) Y_n^m(\varphi, \lambda), \tag{2.26}$$

where

$$Y_n^m(\varphi, \lambda) = C_n^m e^{im\lambda} P_n^m(sin\varphi), \tag{2.27}$$

with P_n^m the associated Legendre function of the first kind of degree n and order m, and

$$C_n^m = \sqrt{\frac{2n+1}{4\pi} \frac{(n-m)!}{(n+m)!}} \tag{2.28}$$

its normalising coefficient, and where, as before, φ is latitude and λ longitude. Then,

by making use of the orthogonality relationship for normalised spherical harmonics

$$\int_0^{2\pi} d\lambda \int_{-1}^{1} d(sin\varphi) Y_{n'}^{m'\star}(\varphi,\lambda) Y_n^m(\varphi,\lambda) = \delta_{nn'}\delta_{mm'} \tag{2.29}$$

and the conjugate relation

$$Y_n^{-m}(\varphi,\lambda) = (-1)^m Y_n^{m\star}(\varphi,\lambda), \tag{2.30}$$

and by employing Poisson's Equation as applied to spherical harmonics

$$\nabla^2 Y_n^m = -\frac{n(n+1)}{a_2} Y_n^m, \tag{2.31}$$

we may reexpress each harmonic of Equation 2.22 as

$$f_0^2 \frac{\partial^2}{\partial p^2}\Omega_{nm} - \frac{\aleph^2 n(n+1)}{a^2}\Omega_{nm} = \Lambda_{nm}, \tag{2.32}$$

which, being a second order ordinary differential equation, can be reduced, by finite differencing in the vertical, to an algebraic expression relating values of Ω_{nm} at three adjoining levels in the vertical. i.e. For each (n,m)

$$A_{i+\frac{1}{2}}\Omega_{i+1\frac{1}{2}} + B_{i+\frac{1}{2}}\Omega_{i+\frac{1}{2}} + C_{i+\frac{1}{2}}\Omega_{i-\frac{1}{2}} = \Lambda_{i+\frac{1}{2}} + D_{i+\frac{1}{2}} \quad for \quad i = 1,...,17, \tag{2.33}$$

where

$$A_{i+\frac{1}{2}} = \begin{cases} \frac{2f_0^2}{(p_{i+1}-p_i)(p_{i+2}-p_i)} & i = 1,..,16 \\ 0 & i = 17, \end{cases} \tag{2.34}$$

$$B_{i+\frac{1}{2}} = -\left\{ \aleph_{i+\frac{1}{2}}^2 \frac{n(n+1)}{a^2} + \frac{2f_0^2}{(p_{i+1}-p_i)}\left(\frac{1}{(p_{i+2}-p_i)} + \frac{1}{(p_{i+1}-p_{i-1})}\right)\right\}, \tag{2.35}$$

$$C_{i+\frac{1}{2}} = \begin{cases} 0 & i = 1 \\ \frac{2f_0^2}{(p_{i+1}-p_i)(p_{i+1}-p_{i-1})} & i = 2,..,17, \end{cases} \tag{2.36}$$

$$D_{i+\frac{1}{2}} = \begin{cases} \frac{f_0^2}{(p_{i+1}-p_i)(p_{i+\frac{1}{2}}-p_{i-\frac{1}{2}})}\Omega_{nmi-\frac{1}{2}} & i = 1 \\ 0 & i = 2,..,16 \\ \frac{f_0^2}{(p_{i+1}-p_i)(p_{i+1\frac{1}{2}}-p_{i+\frac{1}{2}})}\Omega_{nmi+1\frac{1}{2}} & i = 17, \end{cases} \tag{2.37}$$

and where $\Omega_{nmi-\frac{1}{2}}$ and $\Omega_{nmi+1\frac{1}{2}}$ are such that

$$\sum_{n=-N}^{N}\sum_{m=0}^{n}\Omega_{nmk}Y_n^m(\varphi,\lambda)=\tilde{\omega}_k=-\left(\frac{\partial\theta'/\partial t}{d\bar{\theta}/dp}\right)_k \qquad k=\frac{1}{2},18\frac{1}{2}. \tag{2.38}$$

The set of Equations 2.33 to 2.38 for each level of the inversion domain ($i = 1\frac{1}{2},..,17\frac{1}{2}$) are then solved numerically, for each (n,m), using a tridiagonal technique, to field the spherical harmonic coefficients of the $\tilde{\omega}$ distribution at each level resulting from QPV forcing everywhere in the vertical domain, from which the $\tilde{\omega}$ distribution itself can be simply recomposed then interpolated to the desired isentropic levels.

The boundary conditions on the full domain solution have been implicitly incorporated into the problem through the terms $D_{i+\frac{1}{2}}$, required to close the problem. These are equivalent, physically, to defining boundaries at levels $i = \frac{1}{2}$ and $18\frac{1}{2}$, at which the interior forcing is zero but thermal advection is present (realised in the problem as $-(\partial\theta/\partial t/d\bar{\theta}/dp)$). These boundary contributions are treated, in the finite differencing equivalent to the Bretherton(1966) approach, as contributions to the interior forcing at the levels adjoining the boundaries ($i = 1\frac{1}{2}, 17\frac{1}{2}$).

In this manner, then, under adiabatic and inviscid QG assumptions, we solve for the vertical motion field resulting from QPV advection throughout the interior, and boundary temperature advection (i.e ω_{PVA} and ω_{BTA} of Hoskins *et al*, 1985).

Solving for the vertical motion field resulting from QPV advection occurring in a vertical sub-domain of interest is not quite so straightforward. By way of illustration, suppose we wish to obtain the $\tilde{\omega}$ distribution attributable to the QPV advection occurring in the lower stratosphere only, say between 200 hPa ($i = 8$) and 30 hPa ($i =$ 13). Simply eliminating the forcing contributions from the boundaries and the levels outside this sub-domain (i.e. setting $D_{i+\frac{1}{2}} = 0$ everywhere and $\Lambda_{nmi+\frac{1}{2}} = 0$ for $i =$ $1,..,7,13,..,17$) will generally result in the occurrence of a large and spurious response of complicated vertical structure beyond the sub-domain boundaries, reflecting the requirement of the calculated response to overcome the gross imbalance introduced by arbitrarily imposing this unrealistic 'total' forcing distribution. The appropriate way to prevent the occurrence of such imbalance is to collapse the residual forcing

(i.e. that actually present above and/or below the sub-domain) onto the respective 'internal boundary' of the sub-domain, such that the vertical integral of the 'internal boundary' forcing equals that of the residual forcing beyond that boundary. This 'delta function' internal boundary forcing is represented in our restricted domain finite difference calculations by placing half of each integrated residual at the first level beyond the internal boundary and half at the first level within (i.e. in the above example, the vertical integral of the forcing between levels $1\frac{1}{2}$ and $7\frac{1}{2}$ is equally shared between levels $7\frac{1}{2}$ and $8\frac{1}{2}$). While applying this technique allows realistic solutions to be obtained, those obtained for each sub-domain of the total vertical domain are not linearly superposable without yet further modification e.g. summation of solutions obtained for sub-domains 1 to 8, 8 to 13 and 13 to 18, will not result, in general, in the same $\tilde{\omega}$ field as is obtained from a single full domain calculation. This is a direct consequence of the vertical integral of the total forcing at a given location being non-zero. While the mass conservation requirement for the vanishing of the global volume integral of the forcing (and the response) is always met by virtue of the spherical harmonic approach (i.e. $\Omega_{00} = 0$ always), there is no such requirement locally. The problem enters the calculations as follows.

At any location the vertical integral of the total forcing can be expressed in finite difference form using e.g. Equation 2.22 as

$$\int_{1000hPa}^{0.4hPa} F.dp \approx \sum_{i=1}^{17} F_{i+\frac{1}{2}} \Delta p_{i+\frac{1}{2}} = -f_0 \left(\frac{\partial q_p}{\partial t}_{18} - \frac{\partial q_p}{\partial t}_{1} \right) = \epsilon_F \neq 0. \tag{2.39}$$

For a given sub-domain, say levels 8 to 13 as before,

$$\int_{1000hPa}^{0.4hPa} (F.dp)_{8-13} \approx \sum_{i=8}^{12} F_{i+\frac{1}{2}} \Delta p_{i+\frac{1}{2}} + Res_{1-8} + Res_{13-18} = \epsilon_F, \tag{2.40}$$

as for the full solution, since

$$Res_{1-8} = \sum_{i=1}^{7} F_{i+\frac{1}{2}} \Delta p_{i+\frac{1}{2}} \tag{2.41}$$

and

$$Res_{13-18} = \sum_{i=13}^{17} F_{i+\frac{1}{2}} \Delta p_{i+\frac{1}{2}}. \tag{2.42}$$

Hence the sum of the forcing integrals for the three sub-domain solutions is

$$\int_{1000hPa}^{0.4hPa}(F.dp)_{1-8} + \int_{1000hPa}^{0.4hPa}(F.dp)_{8-13} + \int_{1000hPa}^{0.4hPa}(F.dp)_{13-18} = 3\epsilon_F \qquad (2.43)$$

i.e.

$$Res_{1-8} + Res_{8-18} = Res_{1-13} + Res_{13-18} = \epsilon_F, \qquad (2.44)$$

so the nonvanishing of the total forcing integral results in the overall noncancellation between boundary 'delta functions', and is due, as is evident from Equation 2.39, to non-zero 'QPV advection' at levels 1 and 18. This final problem is overcome by ensuring, somewhat artificially, that the local vertical integral of the *interior* forcing vanishes everywhere. This is accomplished by redefining the domain boundaries to be at $i = 1 - \delta$ and $i = 18 + \delta$, where δ is some infinitessimal distance, and viewing all the effective *internal* forcing at levels 1 and 18 (which includes both the QPV advection and the boundary thermal advection component assigned to these levels for the full domain calculation) as *boundary* forcing at $i = 1-\delta$ and $i = 18+\delta$, so that there is no contribution to the vertical integral of interior forcing from levels 1 and 18. This is essentially an 'inverse Bretherton' approach, the baroclinic component of the $f_0(\partial q/\partial t)$ terms being treated as though a boundary temperature advection contribution, whereas the barotropic component might perhaps be viewed as something akin to an Ekman pumping tendency effect occurring in infinitessimally thin boundary layers between levels 1 and 18 and their respective neighbouring boundary.

In this manner, then, because $(\partial q/\partial t)_1 = (\partial q/\partial t)_{18} = 0$ now, the vertical integral of the 'modified' interior forcing vanishes, and by calculating the residual associated with an interior sub-domain boundary, by excluding the contribution from the 'effective' boundary forcing, we ensure that the sums of the residuals vanish, and the solutions obtained will be linearly superposable to give the total solution.

By employing the above approach, then, we are able both to analyse the QG picture of the isentropic uplift fields, and, by recomposing the $\tilde{\omega}$ fields by restricting ourselves to more limited ranges of horizontal wavenumber, or by moving upper and lower boundaries to enclose a specific vertical sub-domain of interest, or both, we are

able to investigate the horizontal scales and vertical region of the QG 'forcing' which brings about the observed vertical motion 'response'.

By using the terms 'forcing' and 'response' here, it is not our intention to imply that we are able, by this analysis technique, to identify the true forcing mechanisms responsible for the observed stratospheric dynamics. Our stratospheric 'QPV forcing' is most probably, in itself, a response to the true forcing which, according to the Charney-Drazin hypothesis, likely originates in the troposphere below. Instead, we use the term rather loosely, in the sense that QPV advection, or local rate of change, *causes* a more generalised (via the three dimensional Laplacian-type operator) vertical motion response.

Although the spherical harmonic approach is numerically time-consuming, a number of savings can be made to minimise this disadvantage. First, by employing the conjugate relation Equation 2.30 we avoid the need to calculate coefficients of the harmonics of negative order. By calculating the forcing term by using Equation 2.21 rather than Equation 2.17, we need only decompose the input geopotential fields, rather than both temperature and geopotential fields. Because of the linear superposability of solutions which results from the orthogonality of the spherical harmonics, we are able to perform the time-consuming decomposition on the raw geopotential fields, and make all subsequent calculations prior to final recomposition of the solution, using the harmonic coefficients. Because we are only concerned with the southern hemisphere, and because geopotential displays approximately even symmetry about the equator, we can eliminate from the calculation the coefficients of the odd Legendre functions ($n - m$ odd). Care in selection both of the recurrence relation used for calculating the Legendre functions, some of which can be inefficient or unstable and therefore dangerous (Press *et al*, 1986, Chapter 6), and of the technique used to calculate the normalising coefficients and the harmonic coefficients themselves (a technique is used in which, after the harmonics of a given degree and order are calculated, the component of the input field they account for is recomposed and subtracted from the input field, and the residual field used to derive the next set of coefficients),

enables us to obtain reliable solutions out to degree 26 using single precision. Finally, since we are primarily interested in the dynamics occurring at large spatial scales, and since the satellite data resolution limits us anyway to looking at these scales (a marked increase in the zonal wavenumber power spectrum occurs near $m = 14$, particularly at the upper levels of the NMC data, approximately coinciding with the satellite daily overpass frequency and leads us to suspect a data aliasing problem), we make all decomposition calculations by triangularly truncating at degree 20 (T20), essentially enabling us to represent accurately 'analysed' features at spatial scales larger than effective wavenumber 14.

If, then, all the assumptions regarding QG balance and conservative motion were exactly met, the observational data set were perfect and the spherical harmonic truncation produced no error, calculation of isentropic uplift by each of the three above techniques (i.e. Equation 2.10, 2.12 or 2.22) should produce three sets of identical results. This turns out not to be the case.

Small differences result between the fields derived using each of the first two techniques for three reasons. Firstly, the linear interpolation in pressure of both θ and $\partial\theta/\partial p$, an internal inconsistency noted above, produces small disparities in the results. The second reason is occasional violation of the loRohiRi assumption, which invalidates Equation 2.13. Thirdly, evaluation of $\tilde{\omega}$ by the second method requires use of a temporal mean value for $\partial\theta/\partial p$, a further small source of discrepancy.

Larger and quantitatively significant differences occur between results obtained from the omega equation solution and those from either of the other two methods. These occur for several reasons, amongst which are the three above. e.g. Linear interpolation in pressure of Φ and its first three pressure derivatives is implicitly performed in the calculation, and the stability term used in the QG formulation must be both the temporal and horizontal mean value for internal balance of the omega equation to be achieved. As well as these factors, use of just the geopotential height fields produces discrepancies wherever hydrostatic balance is not achieved between the temperature and height fields. While only small differences result from the har-

monic truncation, another noteworthy source of disagreement stems from an apparent internal problem within the geopotential height fields, such that the 70 hPa heights often appear inconsistent with the 100 hPa heights. While the source of this problem has not been fully identified, it is suspected to be a result of imperfect matching of the NMC 'tropospheric' base analyses with the stratospheric levels above (similar signs of such an effect are evident in the plots of Randel, 1987a and Randel *et al*, 1987).

Notwithstanding these differences, the vertical motion fields obtained from each method are semi-quantitatively consistent with one another: values calculated by each technique generally lie within about ten percent of one another, and their horizontal and vertical structures are virtually identical.

2.6 Contour Advection with Surgery (CAS)

In the present work, the major question we address in investigating the ozone dilution effect, is the redistribution of vortex material which accompanies the final warming. Although necessarily to a lesser extent, we also wish to address the question of the extent to which the vortex remains materially isolated prior to its breakup. Sole use of the NMC satellite-derived data analyses, with their coarse resolution, makes each of these tasks difficult at best. In an attempt to ameliorate this satellite resolution problem, we make use of CAS.

CAS is essentially no more than a sophisticated multiple trajectory analysis method which involves the renoding and surgery techniques originally developed for contour dynamics modelling (Dritschel, 1988, 1989). Our use here comprises advecting a set of points, or nodes, which describes a material contour of interest (represented by an EPV contour), using consecutive daily balanced wind analyses obtained from the NMC geopotential height fields. At each small time step, the advected contour is redrawn and renoded, the surgery technique being employed to amputate strings of nodes, or filaments, which fail to meet a specified minimum scale criterion. In this manner the flow can develop small scale features without suffering the chaotic evo-

lution which results from the use of more conventional trajectory analysis methods. The philosophy behind the CAS technique, its strengths and weaknesses, the precise details of the scheme employed and previous examples of its successful use are to be found elsewhere (e.g. Waugh and Plumb, 1993; Waugh *et al*, 1993; Plumb *et al*, 1993).

The first application in the present work is in the detailed reconstruction of the 1987 dilution event, at which time CAS allows the opportunity to overcome to some extent the problems of the aforementioned EPV relaxation. Waugh and Plumb (1993) find that by using CAS to advect analysed EPV contours with the analysed wind fields, the resulting EPV-conserving flow evolution appears to depict the details of the enstrophy cascade in a realistic manner, while maintaining close agreement with the larger scale features evident in the day-to-day EPV analyses. We make the assumption, then, that CAS can reproduce the details of the real stratospheric material evolution better than the EPV analyses themselves, even though we employ the southern hemisphere NMC analyses, which are considered by some (e.g. Mechoso *et al*, 1988) to be of poorer quality than their northern counterparts used by Waugh and Plumb, and we use the CAS depictions of the evolution during the 1987 vortex breakup in place of the EPV analyses themselves. In this manner we can treat the advected EPV contours as *material* contours irrespective of whether or not the EPV is conserved, while allowing the real atmospheric forcing to feed into the flow development through the analysed wind fields. Hence nonconservation during the period of analysed EPV *per se* becomes essentially immaterial. Rather, it is only unaccounted for diabatic mass fluxes and errors in the advecting wind fields which are of concern. We discuss these matters further in Chapter 7 below.

CAS, in itself, does not provide regularly gridded EPV data, which are what we require. The CAS output comprises hemispheric contour patterns, but provides no information on the EPV distribution between the contours. To overcome this problem, we use a technique borrowed from contour dynamics, to convert a given contour pattern to a field of regularly gridded data. First it is necessary to ensure sufficiently

close separation of contours over the hemisphere (advecting 20 to 25 contours suffices for our purposes). Then by temporarily defining a hypothetical 'pseudo-velocity' $\vec{\mathbf{u}}$ (which is related to EPV in the same manner as is true velocity to relative vorticity), such that

$$q = \nabla \times \vec{\mathbf{u}}, \tag{2.45}$$

then the same contour integral technique valid for deriving velocity fields from a relative vorticity contour distribution (Dritschel, 1989) can be used to invert the EPV contour distribution to obtain gridded pseudo-velocity data of whatever spatial resolution is desired (within practical constraints imposed by the physical separation of the EPV contours to be inverted). Finally, by simple finite differencing, the EPV distribution is recalculated from the pseudo-velocity distribution, subject to an appropriate boundary, or far-field, condition, to give the regularly gridded fields required for the subsequent analysis.

While it is also possible to recompose the EPV fields from the pseudo winds using a Green's function technique, which would provide esssentially 'point' EPV data (resolution limited only by the resolution of the pseudo-velocity grid), the finite differencing approach is preferred for its smoothing properties. By performing the recomposition step using finite differencing over different spatial scales, we are able to obtain pictures of the EPV distribution at progressively coarser resolution, which enables us, by comparison with the NMC analyses, to obtain information on the 'effective EPV resolution' of the NMC data, the relative contribution to the analysed EPV relaxation from the potential enstrophy cascade, and the effectiveness of the CAS simulations at describing the EPV evolution.

It was intended, at the outset, to carry out detailed CAS simulations on a number of periods during the eleven seasons examined. However, the computational expense of performing CAS on many contours at many isentropic levels, which is required for the task, and of performing the subsequent inversion/recomposition of the EPV contours/fields, precluded this. Although full (multi-level, multi-contour) CAS simulations are computationally expensive and need to be carried out on a supercomputer,

much simpler simulations, wherein advection of just one or two strategically chosen contours at a single level is performed, are possible on a workstation.

This is the second way in which we use CAS in the analysis described below. Although the NMC analyses suggest that the polar vortex generally remains materially isolated, at least at ozone hole levels, prior to the final warming, the question remains as to whether small scale irreversible mixing between the vortex and its surroundings may be occurring on a regular basis during the spring season. Were this the case, then there would be some prospect for a more gradual and subtle dilution effect to be at play prior to the vortex breakup. In order, then, to assess the extent of mixing which occurs both with the vortex breakup in each of the other years examined, and prior to the breakup each year, we perform numerous simplified CAS simulations on a few EPV contours at an isentropic level of interest, carefully selecting the contours to be advected to represent approximately the material boundary of the vortex at that level.

Chapter 3

Ozone Data Employed and Computational Technique

3.1 Total Ozone Data

Since its launch in October 1978, the Total Ozone Mapping Spectrometer (TOMS) on board the Nimbus-7 satellite has provided continuous daily measurements of the total ozone column over the southern hemisphere. Because of their accuracy (absolute error $\pm 3\%$, random error $\pm 2\%$) and high resolution hemispheric coverage over the entire period of interest to us, almost exclusive use is made herein of the Version 6 GRIDTOMS data set for definitive analysis of total ozone. For full details of the instrument design and performance, measurement and data retrieval techniques and resulting data quality, the reader is referred to Fleig *et al* (1993) and references therein.

Total ozone over the southern hemisphere has also been routinely monitored since the 1950s and earlier by a surface network of Dobson ozone spectrophotometers (WMO 1962-1992). Indeed, the original detection of the Antarctic ozone hole resulted from analysis of Dobson data from Halley Bay, Antarctica (Farman *et al*, 1985) and the possibility of a 1987 ozone hole dilution event was originally alluded to by Atkinson and Easson (1988) who used Australian Dobson data. Nevertheless, for

present purposes, the daily hemispheric coverage and consistency of the TOMS data is preferred, and Dobson data are not used in the present work.

The Version 6 GRIDTOMS data set, obtained on CD-ROM and magnetic tape from the Ozone Processing Team at the National Space Science Data Center (NSSDC), NASA GSFC, consists of daily asynoptic global data on a 1° latitude by 1.25° longitude grid. Prior to their use here, and consistent with the resolution of the NMC CAC data and the gridded 'reconstructed SAGE' data to be described in the next Sections, the original daily GRIDTOMS data have been transformed to a 5° latitude by 5° longitude hemispheric grid and interpolated in time to produce 12 UTC synoptic analyses of daily total ozone for the period of the investigation. For the spatial mapping, the mapped values were determined as the 'four neighbouring point' mean of the original high resolution gridded data. Where data were missing the adopted value was determined from the remaining points of the four, and where all four values were missing on the original grid, a missing data flag was assigned to that point on the mapped grid. In this manner, the effective 'footprint' of the mapped data is generally about 2° by 2.5°.

Because the TOMS data only provide information on the total ozone column, they can not be used alone to describe ozone's three dimensional evolution. Even the pioneering efforts of Dobson (1956), in interpreting the observed total ozone distribution to deduce the essential features of the global stratospheric circulation, served only to confirm and extend the earlier interpretation of stratospheric water vapour measurements by Brewer (1949). Analyses of total ozone have also been used more recently to infer lower stratospheric transport (e.g. Bowman, 1990, 1993; Bowman and Mangus, 1993; Salby and Callaghan, 1993; Vaughan and Price, 1991; Vaughan *et al*, 1993), although these must inevitably rely on the assumption that significant perturbations in the lower stratosphere are of deep vertical structure and little vertical tilt (equivalent barotropic), so lead to only broad generalisations being made possible, or worse, as will be shown in Chapter 8, to erroneous conclusions. The prospects are very limited, then, for using total ozone to describe the details of

stratospheric evolution, and we use the TOMS data only for the subsidiary purpose of providing 'ground truth' (and, at the outset, a limited amount of subjective 'tuning') for the three-dimensional ozone reconstructions described below.

3.2 Ozone Vertical Profile Data

3.2.1 Ozone Sondes

Although the Dobson spectrophotometer can, and has, been used at many stations in the aforementioned surface network to make coarse estimates of the ozone vertical distribution using the Umkehr technique, the relatively low accuracy (especially below the middle stratosphere) and crude vertical resolution make them unsuitable for the present purposes.

The most common and reliable surface-based technique for detailed measurement of ozone profiles involves the deployment of balloon-borne electrochemical ozone sondes. Unfortunately, despite operation of a relatively extensive northern hemisphere network of ozone sonde stations during the last few decades, prior to 1986 only three permanent stations existed in the southern hemisphere, at Aspendale (Australia), Natal (Brazil) and the Japanese base at Syowa (Antarctica). Since the detection of the ozone hole the southern hemisphere network has expanded considerably, with several new permanent stations making weekly or twice-weekly soundings, and sporadic observations being made at a number of other locations. Details of the southern hemisphere network can be found in WMO (1962-1992). The data from most stations in the network are archived at the World Ozone Data Center, Toronto (WODC), while those from the remaining stations are generally available from the respective operating agency. Those data used in the present work were obtained either from WODC or from the NOAA/ERL Climate Monitoring and Diagnostics Laboratory at Boulder, Colorado.

The electrochemical ozone sonde generally provides reliable measurements in the

lower stratosphere below the ozone maximum ($\pm 5\%$), but some types can be subject to tropospheric contamination, and measurement error increases rapidly in the middle and upper stratosphere ($> 10\%$) where mechanical pump efficiency is compromised in the low pressure environment. The reader is referred to e.g. Whitten and Prasad (1985), and references therein, for a detailed discussion of measurement technique and accuracy.

Although the southern hemisphere ozone sonde network now provides a reasonable data set for analysis, at least during the spring period (a claim discussed further in Chapter 9 below), the scarcity of data for the period prior to 1986, which makes their use for the present purposes inadequate, and our late acquisition of the available data for the more recent years, accomplished only at the closing stages of the analysis, together result in our employment of these data only for comparison and validation purposes in the main analysis. The analysis to follow is instead based almost solely on satellite ozone data.

3.2.2 Stratospheric Aerosol and Gas Experiment (SAGE)

Several satellite instruments have provided vertical ozone profiles on a regular basis using different techniques and for different periods, during the last 15 years (for a review see Miller (1989)). Only two of these instruments have provided data for most of the period of the present analysis, these being the SBUV/SBUV II and the SAGE/SAGE II instruments.

SBUV is a nadir viewing instrument which, from October 1978 to September 1987, measured solar back-scattered ultraviolet radiation to provide ozone data at levels above 100 hPa with a resolution of approximately 200 km by 200 km in the horizontal and 8 km in the vertical (Fleig *et al*, 1990). While SBUV measurement errors, other than those due to long term drift, are small at altitudes above 30 hPa, below 40 hPa multiple scattering produces increasingly large errors with decreasing height. Also, until recently, the significant long term drift in the retrieved data due

to diffuser plate degradation (the same diffuser plate used for the TOMS instrument) reduced confidence in the use of the long term data set. Recently, with the advent of the self-calibration technique proposed by Herman *et al* (1991), this problem has been overcome. Nonetheless, because of lack of confidence in the data at the outset of the present investigation, and the data quality deterioration in the lower stratosphere, the SBUV data set is not directly employed in the present analysis. Rather, in Chapter 6 below, we draw some comparisons between the SBUV climatology assembled by Nagatani *et al* (1988) and that which we derive using the SAGE data set, of which we make exclusive use in the analysis to follow.

The SAGE instruments are limb-scanners employing the solar occultation technique to measure ozone absorption in the Chappuis band (about 600 nm) of the solar spectrum. A highly precessing inclined orbit provides southern hemisphere sampling north of about $70^{o}S$ during the spring season. With about 15 orbits per day, and one 'sunrise' and one 'sunset' observation made per orbit, there are usually about 15 southern hemisphere observations per day, successive orbits shifting about 25^{o} westward and a fraction of a degree in latitude, so that full hemispheric coverage (a single 'sweep') is completed in an average of about 20 days. The major exception to continual coverage is during brief periods each year when the orbit is such that both sunrise and sunset observations are made in the northern hemisphere, or when viewing geometry prevents any observations being made for up to two weeks (an unfortunate situation for the analysis of the 1987 dilution event, which occurred during one of these periods). The spatial resolution of the retrieved data is about 200 km along scan, by 5 km across, by 0.5 km in the vertical, and the estimated data accuracy is better than $\pm 10\%$ from cloud top to 55 km altitude. The SAGE instrument operated from February 1978 to November 1981 and SAGE II has been in operation since October 1984. A spacecraft power problem on SAGE which occurred after only six months of operation prevented sunrise profiles from being obtained thereafter, greatly reducing the amount of useful data for the southern hemisphere spring season for the three years from 1979 to 1981. For more details of the SAGE instruments, measurement technique, data coverage and quality, the reader is referred to McCormick *et al*

(1989), or WMO (1988), and references therein.

The SAGE data used were obtained on magnetic tape from the EOS Distributed Active Archive Center of the Global Change Data Center (formally the Central Data Services Facility of the National Space Science Data Center) at NASA GSFC. The data set comprises all SAGE and SAGE II ozone observations from February 1979 to November 1989, and for each profile includes date, time, location, type of event, and temperature, pressure, density, geometric height and ozone volumetric mixing ratio (OMR), with associated error estimates, at 1 km intervals from 1 to 70 km.

3.3 Motivation and Foundation for Performing a Coordinate Transformation

The first objective of the present work, as discussed in Chapter 1 above, is an in-depth analysis of the 1987 ozone dilution event examined by Atkinson *et al* (1989). For the proposed analysis we require detailed information on the three-dimensional distribution of ozone mixing ratio throughout the middle and high latitudes of the southern hemisphere on each day of the period during which the polar vortex breaks up and its material begins to be redistributed about the hemisphere. Examination of the lower stratospheric EPV evolution depicted by the NMC analyses, to be described in more detail in the next two Chapters, suggested that the most critical period of concern spanned the first two weeks of December 1987. Detailed examination of other potential events which might have occurred during the eleven seasons considered, the task which comprises the broader objective of the work herein, involves similar requirements for the particular events concerned.

Unfortunately, the approximately 15 southern hemisphere SAGE ozone profiles available each day, although evenly distributed in longitude, are taken at approximately the same latitude. While there may also be one or two balloon soundings available on a given day, the total amount of ozone data is obviously insufficient for

direct analysis of the daily three dimensional hemispheric distribution. Even more restricting for the 1987 event, is that there are no SAGE observations at all from 05 December to 16 December due to the aforementioned occurrence of one of the observation blackout periods.

If, then, we are to attempt the analysis at all without resorting to complex theoretical modelling, a prospect we specifically wish to avoid in this *observational* analysis, it is necessary to make optimal use of the scant data available by carefully selecting the reference frame in which to perform the analysis.

The tracer continuity equation for OMR (χ) can be written

$$\frac{d\chi}{dt} = \frac{\partial\chi}{\partial t} + \vec{\mathbf{u}}.\nabla\chi = S, \tag{3.1}$$

where $\vec{\mathbf{u}}$ is the vector flow field and S accounts for all 'nonconservative' contributions such as those from sources, sinks and non-advective transports (Andrews, 1987a; Schoeberl and Lait, 1993). In the classical Eulerian reference frame (x, y, p), Equation 3.1 can be expanded to give

$$\frac{\partial\chi}{\partial t} = S - \left(u\frac{\partial\chi}{\partial x} + v\frac{\partial\chi}{\partial y} + \omega\frac{\partial\chi}{\partial p}\right). \tag{3.2}$$

Irrespective of the size of the contribution from the source term, which varies greatly from one region of the atmosphere to another, the contribution to local changes in χ from each of the advective terms in Equation 3.2 is generally substantial, resulting from normal meteorological variability. While sufficient observations evenly distributed in space and time enable a zonal mean, temporal mean ozone distribution to be described, significant local advection-induced departures from this state will exist at any particular instant. The classical reference frame therefore severely limits our ability to describe anything other than the most general features of the instantaneous ozone distribution.

McIntyre (1980) was the first to suggest that the use of potential vorticity - potential temperature (q, θ) coordinates, or a 'modified Lagrangian mean' (MLM) reference frame, a simpler but more practicable alternative to the generalised Lagrangian mean

of Andrews and McIntyre (1978), might be a more appropriate perspective from which to view the mean state of the stratosphere. After Dunkerton *et al* (1981) first applied the concept to model data, Butchart and Remsberg (1986) developed their 'area diagnostic' as a means by which both the dynamical and chemical tracer evolutions could be viewed from a 'vortex-relative' perspective, enabling them to obtain a clearer picture of the essential features than that which results from considering the Eulerian zonal mean state when wave amplitudes are large.

More recently Schoeberl *et al* (1989a), by transforming ER-2 aircraft observations of trace gas species concentrations into (q, θ) space were able to obtain a picture, relatively unclouded by meteorological variability, of the trace gas evolution near the vortex edge during the Airborne Antarctic Ozone Experiment (AAOE) in August/September 1987. Lait *et al* (1990) extended the analysis to include ozone data from balloon, lidar and SAGE measurement platforms, demonstrating the general applicability of the technique. Most recently, Schoeberl *et al* (1992) applied the method to data from both the AAOE and the Airborne Arctic Stratospheric Expedition (AASE) during January/February 1989 to compare and contrast the vortex evolution in each hemisphere and to assess the strength and three dimensional structure of the lower stratospheric residual circulation near the vortex edge at these times.

Schoeberl and Lait (1993) describe and discuss the motivation and theoretical basis for performing the coordinate transformation. In essence, by defining a coordinate system (s, q, θ), where s represents displacement along an isentropic EPV contour, q is EPV, and θ is potential temperature, Equation 3.1 can be expanded in these coordinates to give

$$\frac{\partial \chi}{\partial t} = S - \left(\dot{s} \frac{\partial \chi}{\partial s} + \dot{q} \frac{\partial \chi}{\partial q} + \dot{\theta} \frac{\partial \chi}{\partial \theta} \right), \tag{3.3}$$

where the dot notation is used for Lagrangian time derivatives. Leovy *et al* (1985) have shown that variations in χ along isentropic EPV contours are small (i.e. χ and q are highly correlated on a given isentropic surface in the winter lower and middle stratosphere, or χ is well-mixed along q contours), so $\partial \chi / \partial s \approx 0$ and Equation 3.3

essentially collapses to a two dimensional expression for tracer continuity

$$\frac{\partial \chi}{\partial t} \approx S - \left(\dot{q} \frac{\partial \chi}{\partial q} + \dot{\theta} \frac{\partial \chi}{\partial \theta} \right). \tag{3.4}$$

By the choice of q and θ as coordinates, which themselves are both quasi-conserved tracers in the extratropical lower stratosphere for periods of a few weeks to a month, most meteorological variability is removed and local 'conservative' variations in χ will be small.

In the hypothetical situation where photochemical production and destruction of ozone, other 'effective' sources and sinks of ozone and diabatic processes were absent, then χ would be exactly conserved. Then all available observations at a particular isentropic level, irrespective of location or time, could be mapped into the 'dynamical' coordinate system, to describe the variation of χ with q at each level. Finally, if the temporal evolution of the EPV distribution were known, the reverse transformation could be made to obtain a complete description in physical space of the ozone evolution.

Of course, in the real stratosphere, neither χ, q, or θ is exactly conserved. Nonetheless, over short periods in the region of our interest, each is quasi-conserved and the technique can be used on the limited ozone data available, but with ready availability of EPV analyses, to obtain adequate ozone reconstructions.

That the assumption of conservation of each variable leads, for our purposes, to only small errors in OMR, at least in the extratropical lower stratosphere during the spring period prior to the vortex breakup, can be seen via a simple scale analysis. To do this we assume a representative ozone photochemical time scale of around 80 days (Garcia and Solomon, 1985), typical departures of OMR from photochemical equilibrium of, say, 10%, net diabatic heating rates of the order of $10^{-1} K/day$ and vertical gradients of diabatic heating of about $10^{-1} K/day/100K$ (Shine, 1989), normalised 'horizontal' OMR gradients of unity ($q\Delta\chi/\chi\Delta q \sim 1$) and normalised vertical OMR gradients of around $3\%/K$ (see Chapter 6 below). Under these circumstances, and noting that $\dot{q}/q \sim \partial\dot{\theta}/\theta$, then by substituting into the right hand side of Equation 3.4

we can crudely estimate the magnitude of the impact on local OMR values arising from each of the three contributions. In a two week period, the typical timescale we need to consider, the associated error in reconstructed OMR resulting from the neglect of each of the three 'non-conservative' terms turns out to be 1-2% due to photochemistry, 1-2% due to 'horizontal' fluxes, and about 4% due to 'vertical' fluxes. So the use of the reconstruction technique will result in errors in OMR which are generally less than 10% in the extratropical lower stratosphere prior to the vortex breakup.

Of course, accompanying the breakup (with which we shall be concerned in Chapters 7 and 8 below) the net diabatic heating rates, their vertical gradients, and the OMR perturbations from photochemical equilibrium are expected to be considerably larger (up to an order of magnitude so), leading to respective error contributions which will also be up to an order of magnitude larger. Nonetheless, because of the use to which we put the OMR reconstructions in the work to follow, the impact of these potentially serious errors is not critical. By using CAS to represent the material evolution during the vortex breakup rather than the EPV analyses themselves, the 'horizontal' flux contribution is essentially eliminated (in the absence of observational errors). The photochemical contribution turns out merely to impose an acceptable limit on the accuracy of our 'ozone dilution' assessment, and because we will primarily consider contributions to the total ozone column rather than local OMR values *per se*, it is not the magnitude of the local error in OMR itself which is important, but the unaccounted-for diabatic displacement which produces it (up to, say, $15K$ in two weeks during the vortex breakup period). For the analysis described in the Chapters to follow to remain valid, it is only required that these diabatic displacements are significantly smaller than the vertical scale of variation of the horizontal wind (generally in excess of $100K$).

Schoeberl and Lait (1993) describe how, in principle, 'diabatic drift' can be accounted for in detail. So, too, might photochemical changes to ozone. This is beyond the scope of the present work, however. Other than the simple modification described

next, the effects of nonconservative processes are not directly included in our analysis.

Rather than introduce the necessary complexity of fully treating nonconservative processes, Schoeberl *et al* (1989a) and Lait *et al* (1990) take simple account of them by parameterising all the terms on the right hand side of Equation 3.4 as a simple constant for given (q, θ). i.e. they assume that

$$S - \left(\dot{q}\frac{\partial \chi}{\partial q} + \dot{\theta}\frac{\partial \chi}{\partial \theta}\right) = \alpha(q, \theta) \tag{3.5}$$

at each point in (q, θ) space and determine the constant α by linear least squares fit to their observational data. In this way, they essentially allow for a local linear temporal trend in OMR of unspecified cause and unspecified (empirically determined) meridional (q) and vertical (θ) structure. This approach serves as a simple and effective means of allowing for most of the local temporal variation of OMR during mid- to late winter in the vicinity of the polar vortex edge when the vortex is relatively quiescent.

Examination of the EPV analyses for the spring period leading up to the final warming, and of (q, χ) scatter plots for different isentropic levels during the spring period, suggested that for our purposes, a linear fit in time such as that above might not be the best approach. Rather than diabatic 'drift', the scatter plots tended to display occasional large 'jolts' superimposed on a more gradual diabatic drift. These 'jolts' were observed generally to accompany significant wave events. The suddenness of these occurrences and the accompanying signs of extensive lateral mixing indicated by the CAS simulations, described later for the 1987 dilution event, suggested a significant contribution may have come from 'apparent' non-conservation of EPV by the NMC analyses resulting from their limited spatial resolution. While real diabatic effects will also contribute, occurring as a response to large amplitude wave events, a different technique was adopted to that described above to account for these sudden shifts.

The main feature of these 'jolts' is sudden relaxation of isentropic EPV values occurring throughout the polar vortex and its surroundings. The magnitude of the EPV

change at a given vortex-relative location appeared to be approximately proportional to the magnitude of the EPV at that location, a symptom not inconsistent with the supposition that the feature was due to rather evenly-distributed lateral mixing of the limited vortex material with the much more massive 'surf zone' volume.

Assuming this to be the case and that the rate of change to EPV observed in the analysed fields can be described by a simple linear relation in q space such that

$$\dot{q} = -kq, \tag{3.6}$$

where $k = k(t, \theta)$ only, then by choosing, instead of the (q, θ) coordinate system the coordinates $(\hat{q}, \theta)$, where $\hat{q}$ is normalised EPV (the local EPV value normalised by a representative value of the 'vortex maximum' EPV), then Equation 3.4 becomes

$$\frac{\partial \chi}{\partial t} \approx S - \left(\dot{\hat{q}} \frac{\partial \chi}{\partial \hat{q}} + \dot{\theta} \frac{\partial \chi}{\partial \theta} \right). \tag{3.7}$$

In this reference frame, if analysed EPV is everywhere conserved, then so too will be normalised EPV, and the new coordinate system is essentially equivalent to the (q, θ) system. Now, however, if the real flow is conservative but 'apparent' changes to analysed EPV occur, of arbitrary temporal and vertical structure but with the simple 'meridional' structure described by Equation 3.6, then OMR will still be locally conserved. While somewhat contrived, and not as well founded as the former technique, the normalised EPV transformation considerably reduced the scatter in the (q, χ) correlation diagrams, attesting to its effectiveness, particularly in the mid-latitude and sub-polar regions, with which we are primarily concerned.

3.4 Use of the Coordinate Transformation Technique

Schoeberl *et al* (1989,1992) and Lait *et al* (1990) demonstrated that the coordinate transformation technique could be employed to make optimal use of a limited number of observations from different platforms in a relatively localised region and period, to

describe the trace gas distribution for that period over a broader region (extended around the hemisphere in the zonal direction) in considerably more detail than is possible than by conventional analysis techniques. Our intention is to go beyond the earlier work and use the technique on the available SAGE ozone data to describe the ozone distribution over the entire extratropical region for periods when SAGE data are available, and also to speculate on the distribution during periods for which there are none.

The first step performed in the process was to take all available SAGE profiles south of $10°S$ from August 1979 to November 1989 and interpolate the data to the 24 isentropic levels selected for the study. The EPV distribution at each level was then computed for each day of the eleven seasons examined. A representative value of the vortex maximum EPV for each day and level was next determined, and the EPV distributions linearly interpolated in space and time to provide, at each level, estimates of $\hat{q}$ corresponding to each SAGE observation.

As described in Section 3.2 above, the nature of the satellite orbit results in the SAGE instrument generally taking about 20 days (from 6 days, when both sunset and sunrise observations fall in the southern hemisphere, to 25 days) to sample the full hemisphere, or perform a hemispheric 'sweep'. The assumption was made next that χ, q, and θ are all essentially conserved for the duration of each sweep. While this assumption is expected to be reasonable in the extratropical lower stratosphere, the dynamical control region, it is rather poor in the tropics and at the highest levels of our analysis, where photochemical/radiative control comes into play because both the diabatic and ozone photochemical timescales are relatively short. Nonetheless, we are primarily interested in the cause of changes in the mid- to high latitude ozone column, and the total contribution to the column from these upper levels is very small, so we expect that the contribution to changes in the total column from assumed dynamical changes to the upper level ozone distribution will also be small. We therefore treat the upper levels in the same manner as the lower levels on the assumption that our results will be relatively insensitive to errors in the depicted upper level changes.

On the basis of the 'conservation' assumption, all the $(\hat{q}, \chi)$ data were binned by isentropic level and sweep, and scatter plots of χ vs $\hat{q}$ constructed. These, despite careful selection of the coordinate system, still showed considerable scatter at some levels, so to describe the average distribution of χ with respect to $\hat{q}$ for each level and sweep, a 'least squares error in χ' polynomial curve was fitted by Gaussian elimination, and the resulting curve taken as representative of the average 'meridional' χ variation.

An element of subjectivity was required in the curve fitting, insofar as the order of polynomial chosen to 'best represent' each distribution. At the lower levels in the vicinity of the tropopause, where the SAGE data quality deteriorates, a large degree of scatter in the data results in higher order solutions becoming unstable and in any case pointless, so the fit selected was generally a cubic. At higher levels in the lower and middle stratosphere, where data scatter is much reduced, sharp 'meridional' gradients in χ occur at the vortex edge and at the tropical/extratropical transition, requiring higher order components for reasonable representation, so at these levels an eighth order polynomial was generally selected. Finally, for some sweeps a particular order of fit can be badly behaved near the range limits of the data points. In these cases fitting a curve of one order higher or lower generally overcame this problem.

Despite the subjective input to the curve fitting procedure, the fitting technique often fails to capture the apparent true magnitude of maxima and minima in the meridional distribution, and fails to provide an accurate portrayal where meridional gradients are particularly steep. These shortcomings result from the least squares error in χ approach, in which it is implicitly assumed that all the mismatch between a data point and the fitted curve results from an 'error' in χ_i $(\delta\chi_i)$ which is independent of the magnitude of χ_i, while $\hat{q}_i$ is exact $(\delta\hat{q}_i = 0)$, so the selected fit minimises $\sum(\delta\chi_i)^2$. In reality, although difficult to assess the likely errors in $\hat{q}$ resulting from satellite resolution problems, they are probably substantially larger than those for χ (less than $\pm 10\%$), so each data point would be better described by an error ellipse with major axis horizontal, rather than the vertical error bar implicit in the adopted technique. Hence a superior curve fitting technique would choose the curve

to minimise $\sum((\delta\chi_i/\epsilon_\chi)^2 + (\delta\hat{q}_i/\epsilon_{\hat{q}})^2)$ where ϵ_χ and $\epsilon_{\hat{q}}$ provide a measure of the expected errors associated with a given $(\hat{q}, \chi)$ data point. Nonetheless, in the interests of simplicity and computational economy, the cruder technique was retained for the analysis herein.

Having derived a set of polynomial coefficients to describe the variation of χ with $\hat{q}$ for each SAGE sweep and isentropic level, it was possible to produce a 'dynamical cross-section' of the period-mean distribution of χ for each sweep. Moreover, given daily three dimensional distributions of EPV during the relevant period, it was possible to perform the reverse transformation back into real space, to produce three dimensional reconstructions of the daily distribution of χ over the hemisphere. Then from these reconstructions, almost any χ analysis desired could be produced, e.g. period means, meridional or zonal cross-sections, or three dimensional analyses of local day-to-day changes in the χ distribution, with which we are specifically interested.

3.5 Total Ozone Reconstructions

The reconstruction technique described in 3.4 above was first tested on the SAGE sweep of 10 November to 04 December 1987, preparatory to the analysis of the 1987 dilution event described in Chapter 7 below, to produce gridded hemispheric fields of OMR on each isentropic surface for selected days during that period. At this stage it was important to assess the effectiveness of the technique for reproducing the observed ozone distribution.

One means by which this might have been accomplished is by comparison of reconstructed ozone profiles with available ozone sonde profiles at the same location and time. Although some intercomparisons were performed later in the analysis, this was not the primary validation technique adopted, for several reasons. In the first place, the reconstructions, being based on the satellite derived EPV analyses, could not hope to reproduce the small scale features ubiquitous in ozone sonde profiles, whose effective horizontal resolution is of the order of $10^3 km^2$ (assuming an instru-

ment response time of around 10 s, an ascent rate of around 1500 ft/min and a representative atmospheric deformation ratio between 10^2 and 10^3). Further, for the period prior to 1987, too few ozone sonde profiles are generally available at sufficiently varied locations during a given SAGE sweep, for such comparisons to be representative of the overall effectiveness of the reconstruction technique. (While for the trial period in 1987 this might have been attempted, a technique was required which could be used equally effectively for the earlier years.) Also, while ozone sonde data might produce reasonable 'ground truth' at the lower levels, in the middle stratosphere and higher, where SAGE is at its best, any discrepancies noted between sonde and reconstructed profiles could just as likely be due to sonde inaccuracies as inadequacies in the reconstructions. Finally, and as mentioned in Section 3.2 above, most of the ozone sonde data set was obtained during the closing stages of the analysis, too late for inclusion in the basic validation process.

Instead, the TOMS total ozone data set was used to assess the effectiveness of the reconstructions. In effect, the success of the reconstructions was assessed in terms of how well they were able to reproduce the hemispheric distribution of total ozone observed by TOMS. But first it was necessary to integrate the reconstructed three dimensional ozone distributions in the vertical to obtain reconstructed total ozone amounts.

Total ozone is usually measured in Dobson Units (1 DU = 1.0×10^{-5} $atmosphere-metre$), and expresses the total amount of ozone in a vertical column of unit area, in terms of the equivalent depth the column would occupy were it to comprise a layer of pure ozone at STP. Accordingly, total ozone (Ω, in DU) can be expressed as

$$\Omega = 0.78826 \int_0^{p_0} \chi \, dp, \tag{3.8}$$

where χ is in units of parts per million volume ($ppmv$) and p, the total pressure, is in hPa. Alternatively, in terms of ozone partial pressure (p_{O_3}), where $p_{O_3} = \chi p$, Equation 3.8 may be re-expressed as

$$\Omega = 7.8826 \int p_{O_3} d(lnp), \tag{3.9}$$

with p_{O_3} and p in units of mPa and hPa respectively. While Equation 3.8 represents a generally more meaningful context in which to view the total ozone column, in that potential photochemical production/loss processes are directly related to local values of χ rather than p_{O_3}, and it is χ, not p_{O_3}, that is a long-lived dynamical tracer in the lower stratosphere, the form Equation 3.9 is that used more commonly by ozone climatologists, because by plotting the vertical distribution of p_{O_3} against a log-pressure scale, equal contributions to the ozone column are represented by equal areas under (or more accurately, beside) the curve. A third alternative appropriate to our isentropic perspective, but which is strictly valid only for an isothermal atmosphere, is

$$\Omega \approx 27.575 \int \frac{p_{O_3}}{\theta} d\theta = 27.575 \int p_{O_3} d(ln\theta), \tag{3.10}$$

which implies that the 'equal area' property approximately holds for plots of p_{O_3} vs log-potential temperature, or the area under a portion of a p_{O_3} vs θ curve must be weighted inversely with θ to assess qualitatively its contribution to the total ozone column.

The vertical integral of reconstructed ozone at any location can be expressed approximately in the finite difference form of Equation 3.8 as

$$\Omega \approx 0.78826 \sum_{i=1}^{24} \chi_{\theta_i} \Delta p_{\theta_i} + R_{strat} + R_{trop}, \tag{3.11}$$

where χ_{θ_i} is the value of χ at the ith isentropic level of the analysis, Δp_{θ_i} is half the pressure difference between isentropic levels above and below (except at highest and lowest levels, where one-sided finite differencing is used) and R_{strat} and R_{trop} represent, respectively, total ozone residuals above and below the highest ($1200K$) and lowest ($300K$) reconstruction levels. At the outset the residuals were estimated simply by assuming that χ decreases linearly in pressure to zero at the surface (at standard pressure) and at the top of the atmosphere ($p = 0$) i.e.

$$R_{strat} = 0.39413 \chi_{1200K} p_{1200K} \tag{3.12}$$

and

$$R_{trop} = 0.39413 \chi_{300K} (1013 - p_{300K}). \tag{3.13}$$

Comparison of reconstructed total ozone by this technique with TOMS total ozone revealed that in general the reconstructions grossly overestimated the total ozone column. Subsequent comparison of local reconstructed ozone profiles and original SAGE profiles with ozone sonde profiles revealed the major cause of the discrepancy to be due to gross overestimation of χ by SAGE at levels below the local tropopause. To overcome the problem, and in view of the generally small contribution to the total ozone column from tropospheric ozone, a simple algorithm was sought to represent the tropospheric component.

Examination of the ozone sonde data from Laverton (Australia) and Lauder (New Zealand) during November/December 1987 suggested that a temporally invariant tropospheric column of 1.5 mPa ozone partial pressure provided a reasonable representation for the mid-latitudes at that time. In the absence of other sonde data, ascertaining similar estimates for other latitudes was not so straightforward. The only known past attempts to describe the climatology of tropospheric ozone in the southern hemisphere are those of Logan (1985), Levy *et al* (1985), Fishman *et al* (1990) and Komhyr *et al* (1993).

Fishman *et al* essentially performed the reverse process to that here. That is, they used the difference between integrated SAGE profiles above the tropopause and coincident TOMS total ozone observations to represent the tropospheric column. Since this provides no independent information for our purposes, their results were excluded from consideration.

While Logan's work was primarily concerned with tropospheric ozone chemistry and trends, examination of her Figures 18 to 22, which are based on sonde and aircraft data available then, suggests constant p_{O_3} with height to be a reasonable approximation at all latitudes in spring. It also suggests little evidence of meridional gradients in p_{O_3} during the spring season, although her tropical values (4 mPa) are substantially higher than those in mid-latitudes (2 mPa). Logan notes, however, that the tropical data employed (primarily from Natal, Brazil) probably reflect local biomass burning, and may not be representative of the tropics as a whole.

Leovy *et al* (1985) used a GCM to model the influence on the tropospheric ozone distribution of both chemistry and dynamics. Their results suggest a monotonic increase in tropospheric OMR at all levels from equator to pole, the polar values being about twice as large as those in the tropics.

In the light of the information available from these latter investigations, and the evidence from the mid-latitude sonde flights from 1987, a simple algorithm was selected to represent the tropospheric ozone contribution as a column of constant p_{O_3} extending from the surface (at 1013 hPa everywhere) to the tropopause, the value of p_{O_3} increasing with the sine of latitude (φ) from a minimum at the equator, i.e.

$$p_{O_3}(\varphi) = A + Bsin\varphi. \tag{3.14}$$

After limited subjective tuning of the coefficients to minimise the difference between reconstructed and TOMS total ozone distributions on 02 December 1987, the values of A and B selected were 1.0 and 1.5 mPa respectively. While it might be argued that the subjective tuning is tantamount to employing circular reasoning, once selected, the same values of the coefficients A and B were rigidly adhered to for the entire 11 year analysis period.

The recent and detailed analysis of southern hemisphere tropospheric ozone climatology of Komhyr *et al* (1993), which is based solely on ozone sonde data from stations at Samoa (15^oS), Lauder (45^oS), Syowa (69^oS) and South Pole (90^oS), suggests that the use of Equation 3.14 will typically result in underestimating the true springtime tropospheric column by about 5 DU in the tropics, overestimating by about 5 DU in the polar region, but being about right in the mid-latitudes. More significant underestimation of the true tropical tropospheric column probably occurs in some locations during the biomass burning pollution episodes discussed by Fishman *et al* (1991). Since the influence of these events is primarily confined to latitudes equatorward of 25^oS, they are not expected to be of major concern in the present analysis. The reconstruction technique is in any case not expected to perform well at low latitudes, essentially a result of calculating EPV everywhere using winds derived by the nonlinear balance method, a technique known to be unsuitable at low latitudes

(Randel, 1987b).

Having adopted Equation 3.14 to describe the tropospheric residual, reconstructed total ozone was subsequently calculated by first determining the 'height' of the dynamical tropopause (the pressure and potential temperature at which EPV first exceeds 1.5 PVU). Then all reconstructed χ data corresponding to levels below the tropopause were discarded, the total column being calculated by computing the contribution from the remaining reconstruction data and adding the upper and lower residuals, the latter of which, using Equation 3.14 and Equation 3.9 is now given by

$$R_{trop} = 7.8826(1.0 + 1.5sin\varphi)ln\frac{1013}{p_{trop}}, \tag{3.15}$$

where p_{trop} is tropopause pressure, in hPa.

3.6 Total Ozone Change - Contributions from Vertical and Horizontal Transport

A critical component in assessing the extent to which an observed mid-latitude ozone decrease is the result of an ozone hole dilution effect, first involves separating the contributions to the 'observed' change which arise from (a) quasi-horizontal ozone advection, and (b) the isentropic uplift (vertical ozone advection) which will accompany such horizontal advection, as described, for example, by the QG omega equation described in Section 2.5 above. It has long been known that under natural (anthropogenically unperturbed) stratospheric conditions, normal dynamical wave activity and ozone gradients will lead to comparable contributions to total ozone fluctuations from each of the above processes (Reed, 1949; Kurjeza, 1984). In assessing the extent of an ozone dilution event we need also to separate the contributions to the observed change in the ozone column which arise from a 'natural' component of quasi-horizontal transport, and an 'unnatural' component (due to springtime Antarctic ozone depletion).

The first of the above requirements is not difficult to meet. Let us assume that

during a given period (from time 1 to time 2, say) local vertical displacements of the tropopause are realised by a change in tropopause pressure, but that tropopause potential temperature remains locally constant. (This amounts to assuming that the tropopause can be locally defined by a fixed isentropic surface during the period, which is expected to be a reasonable assumption under most circumstances, in the absence of significant stratosphere-troposphere exchange.) Then, using Equation 3.11 as modified to take into account the parameterisation of the tropopause level given by Equation 3.15, and denoting $i_{t_1}(=i_{t_2})$ as the local isentropic level of the tropopause, the local change in total ozone ($\Delta\Omega$) according to the reconstructions can be expressed as

$$\begin{aligned}\Delta\Omega &= \Omega_2 - \Omega_1 \\ &= 0.78826 \sum_{i=i_{t_1}}^{24} \left\{ (\chi_{\theta_{i_2}} \Delta p_{\theta_{i_2}}) - (\chi_{\theta_{i_1}} \Delta p_{\theta_{i_1}}) \right\} + (R_{strat2} - R_{strat1}) + (R_{trop_2} - R_{trop_1}).\end{aligned} \tag{3.16}$$

Under the above circumstances a change in the tropospheric residual ($R_{trop_2} - R_{trop_1}$) can only result from a change in tropopause pressure, because of the simple parameterisation selected to represent the tropospheric column (Equation 3.15), so can be viewed as a contribution arising solely from vertical motion. If, however, the tropopause potential temperature does in fact change locally during the period (i.e. $i_{t_1} \neq i_{t_2}$), then there will result an additional component of what might be regarded as an *effective* tropospheric contribution to $\Delta\Omega$, proportional to $\sum_{i_{t_2}}^{i_{t_1}} (\chi_{\theta_i} \Delta p_{\theta_i})$. Such a contribution, again because of the parameterisation of the tropospheric column, can not strictly be considered as representing solely a vertical motion contribution. Nonetheless, in view of its small relative magnitude under most circumstances, and within the level of approximation involved in the remainder of the procedure to follow, we treat all changes in total ozone arising from vertical motion of the tropopause as vertical transport contributions.

Turning to the first bracketed term on the right hand side of Equation 3.16, neglecting the aforementioned possible differences in i_{t1} and i_{t2}, and putting

$$\chi_{\theta_{i_2}} = \chi_{\theta_{i_1}} + \delta\chi_{\theta_i} \tag{3.17}$$

and

$$\Delta p_{\theta_{i_2}} = \Delta p_{\theta_{i_1}} + \delta \Delta p_{\theta_i}, \tag{3.18}$$

we have, temporarily dropping the θ_i subscripts for clarity,

$$\sum_{i_{t_1}}^{24} (\chi_2 \Delta p_2 - \chi_1 \Delta p_1) = \sum_{i_{t_1}}^{24} ((\chi_1 + \delta\chi)(\Delta p_1 + \delta \Delta p) - (\chi_1 \Delta p_1)). \tag{3.19}$$

Assuming $\delta\chi \ll \chi$ and $\delta\Delta p \ll \Delta p$ and linearising, we may reexpress Equation 3.19 approximately as

$$\sum_{i_{t_1}}^{24} (\chi_2 \Delta p_2 - \chi_1 \Delta p_1) \approx \sum_{i_{t_1}}^{24} \chi(\delta \Delta p) + \sum_{i_{t_1}}^{24} (\delta\chi) \Delta p. \tag{3.20}$$

The stratospheric residuals may be treated in the same manner, so that we may write

$$R_{strat2} - R_{strat1} = \Delta R_{strat} = \Delta R_{stratV} + \Delta R_{stratH}.$$

Hence, defining hypothetical ozone columns Ω_{2V} and Ω_{2H} such that

$$\Omega_{2V} = 0.78826 \sum_{i=i_{t_2}}^{24} \chi_{\theta_{i_1}} \Delta p_{\theta_{i_2}} + R_{strat2V} + R_{trop_2} \tag{3.21}$$

and

$$\Omega_{2H} = 0.78826 \sum_{i=i_{t_1}}^{24} \chi_{\theta_{i_2}} \Delta p_{\theta_{i_1}} + R_{strat2H} + R_{trop_1}, \tag{3.22}$$

where $R_{strat2V}$ ($R_{strat2H}$) is the stratospheric residual obtained using the chi_2 (chi_1) distribution with the Δp_1 (Δp_2) distribution, then, by substituting Equations 3.20, 3.21 and 3.22 into Equation 3.16, we have

$$\begin{aligned} \Delta\Omega &\approx (\Omega_{2V} - \Omega_1) + (\Omega_{2H} - \Omega_1). \\ &= \Delta\Omega_{vertical} + \Delta\Omega_{horizontal} \end{aligned} \tag{3.23}$$

So under the linearising assumptions, the reconstructed distribution of total ozone change will approximately equal the sum of the separate contributions from vertical and horizontal motion.

The vertical contribution is determined as the difference between the 'observed' total ozone distribution at t_1 and the hypothetical distribution resulting from 'observed' vertical, but no horizontal, advection between t_1 and t_2 (Ω_{2V}). This 'vertical

motion only' hypothetical distribution is determined by artificially freezing all isentropic (quasi-horizontal) advection of ozone throughout the hemisphere between t_1 and t_2, while allowing the tropopause and isentropes to move up or down as observed, i.e. by calculating the total ozone distribution at t_2 using the isentropic OMR distribution observed at t_1 and the tropopause and isentropic pressure distributions at t_2 (Equation 3.21).

Conversely, the horizontal contribution is determined as the difference between the 'observed' total ozone distribution at t_1 and the hypothetical distribution resulting from 'observed' horizontal, but no vertical, advection between t_1 and t_2 (Ω_{2H}). This hypothetical 'horizontal motion only' distribution can be calculated by artificially freezing the tropopause and isentropic pressure distributions at their t_1 state, while allowing the isentropic distribution of OMR on each surface to develop as 'observed' between t_1 and t_2, i.e. calculating the total ozone distribution at t_2 using the isentropic OMR distribution observed at t_2 and the tropopause and isentropic pressure distributions at t_1 (Equation 3.22).

It is not so straightforward to separate the respective contributions to the total ozone change from natural quasi-horizontal transport and true ozone dilution, since this requires a knowledge of the 'control' distribution of ozone i.e. the dynamical cross-section which would be present in the absence of ozone depletion. It also requires making the implicit assumption that ozone depletion produces no dynamical feedback, although this is probably a reasonal assumption in view of all the other approximations made *en route*. The precise manner in which we attempt to quantify the ozone dilution contribution to observed total ozone decreases is described in Chapters 7 and 8 below.

Chapter 4

Dynamical Climatology of the Austral Spring Stratosphere

The springtime evolution of the total ozone distribution over the hemisphere is primarily determined by the isentropic distributions of OMR and pressure in the lower stratosphere. These, in turn, are dependent on the dynamical evolution of the stratosphere. To understand the ozone evolution, then, we need to know the dynamical evolution that brings it about. The purpose of this Chapter is to describe and discuss the observed dynamical climatology, with emphasis on the spring period, the aim being primarily to provide a context in which the observed ozone evolution can then be viewed.

The description to follow is somewhat mixed. At times it is more appropriate and convenient to view the climatological evolution from the Eulerian wave/zonal mean flow perspective. This tends to be the case when the zonal mean dominates the hemispheric flow, such as is the case in summer and mid-winter, or when use is made of the analyses of others, most of which are from the Eulerian wave mean flow perspective. At other times, it seems more appropriate to consider the synoptic evolution of interacting dynamical entities. This is particularly so when we consider the evolution of the 'final warming', which occurs once the 'mean' flow has weakened

and tends to be zonally asymmetric, perturbation amplitudes are large, and nonlinear processes may be important to the dynamics. The overall aim of this Chapter, then, is to describe the observed wave/zonal mean behaviour and what we see from the synoptic perspective, and relate this to what is understood of the underlying dynamical and radiative causes.

Since our focus in the Chapters following is on the 'final warming', we commence in Section 4.1 below with a brief description of what we mean by the term 'final warming'. In Sections 4.2 and 4.3 we describe and discuss the observed climatological features of the annual stratospheric evolution, by drawing extensively on the work of others. The description of the planetary wave evolution in Section 4.2 is taken largely from the work of Randel (1988a, 1992) and Geller and Wu (1987). That of the zonal mean temperature and zonal wind evolution in Section 4.3 is based primarily on the analyses of Barnett and Corney (1985), Geller and Wu (1987) and Nagatani *et al* (1988), and the radiative equilibrium temperature distribution referred to is that of the time-marched radiative-convective-photochemical model of Fels (1985). Additional sources are as noted in the text. In Section 4.4 we then describe, from the synoptic perspective, the climatological features of the evolution for the period leading up to and including the 'final warming'. Finally, in Section 4.5 we briefly discuss the extent of interannual variability in the dynamical evolution during the winter/spring season.

4.1 Defining the 'Final Warming'

The term 'final warming', when applied to the winter to summer transition in the southern hemisphere stratosphere, is subject to some ambiguity in interpretation, which results from employing a term originally coined to describe late winter northern hemisphere 'major' warmings. Use of the expression in relation to the boreal seasonal transition is a concise way to describe the almost simultaneous reversal of both the large scale wind field and the zonal mean meridional temperature gradient in the mid-

dle/upper stratosphere, which results when a large amplitude planetary wave event, of the magnitude observed in a northern hemisphere 'major' warming, irreversibly disrupts the vortex simultaneously through substantial depth. In the southern hemisphere, a 'major' warming, by the WMO definition, has not been observed, and the seasonal transition tends to involve a more gradual, downward progressing, destruction/decay process which results in the temperature gradient reversal at middle and upper levels preceding the flow reversal there by up to several weeks.

Further ambiguity arises for the austral case in choosing a representative level for the seasonal transition. Whereas some authors choose the WMO reference level of 10 hPa (e.g. Farrara and Mechoso, 1986), others choose a different level (e.g. Newman, 1986, adopts the 30 hPa level as representative).

In the present work, we use the term to describe the overall spring transition throughout the stratosphere, from about the time of the temperature gradient reversal at upper levels to the vortex breakdown in the lower/middle stratosphere.

4.2 Annual Climatology of Stratospheric Wave Activity

4.2.1 Planetary Scale Forced Rossby Waves

4.2.1.1 Climatological Behaviour

By far the dominant contribution to extra-tropical stratospheric annual mean wave activity comes from forced planetary scale Rossby waves, which display a strong seasonal cycle.

During the summer, with a stratospheric easterly flow regime prevailing throughout the hemisphere above about 60 hPa, vertical propagation of forced Rossby waves is prohibited by the Charney and Drazin (1961) mechanism, and any such wave ac-

tivity forced from below should rapidly evanesce in the lower stratosphere.

With the establishment of a generally westerly regime throughout the extra-tropical stratosphere by the autumnal equinox, however, the region becomes more receptive to vertical propagation by the graver (planetary scale) modes.

From the start of April, early winter wave activity in the lower and middle stratosphere is observed to increase from near zero to a climatological peak around winter solstice, a similar progression occuring about a month earlier in the upper stratosphere. Virtually all of the activity is due to planetary scale Rossby waves with equivalent barotropic structure (small westward tilt with height), primarily of the gravest zonal mode (W1), but with a small contribution from transient wave number 2 (hereafter referred to as TW2, which is mainly eastward travelling with period from 1 to 3 weeks). The W1 contribution is about equally divided between stationary (with geopotential height ridge over the central Pacific Ocean near $160^{o}W$) and mainly eastward travelling (Farrara *et al*, 1992) transient components (hereafter SW1 and TW1 respectively). Maximum amplitudes occur at about $60^{o}S$ throughout the stratosphere, peaking near the stratopause (the density-weighted amplitude maximum is observed in the middle to upper troposphere for SW1 and the lower to middle stratosphere (near 40 hPa) for TW1).

After the winter solstice the total wave activity declines to a minimum in early August, as first noted by Hirota *et al* (1983). The decline is more marked for SW1 than TW1, so that TW1 dominates SW1 during the June to August period (Hartmann, 1977b; Randel, 1987a; Hartmann *et al*, 1984). The reasons for this decrease, which comprises a mid-winter lull, are not yet clear. One might suppose it to be due to the basic state westerlies in the extra-tropical stratosphere exceeding the upper cutoff for vertical propagation predicted by the Charney-Drazin mechanism (Plumb, 1989). However, Randel (1988a) notes that lower stratospheric refractive index for SW1 is most favourable for vertical propagation during the lull, and implies that this should overcome the slight decrease apparent in tropospheric planetary wave amplitude at the same time, were stratospheric wave activity merely the result of simple propagation

from below. Wirth (1990) investigated the matter using a hemispheric, linear, QG model of the stratosphere with prescribed stationary tropospheric forcing. Rather than a midwinter lull, or a midwinter peak, he found a monotonic increase in wave activity throughout the winter with the peak in September/October, which was rather insensitive to tropospheric wave amplitudes and suggested to him that stratospheric wave amplitudes were most sensitive to the propagation characteristics of the lowest levels of the stratosphere, rather than Randel's overall 'lower stratospheric' refractive index. Nonetheless, Wirth also concluded that, in view of his model's essential failure to produce the midwinter lull, the answer must lie elsewhere, such as in critical layer wave reflection or nonlinear processes.

During late July, while climatological W1 amplitudes are still decreasing, TW2 amplitudes begin to increase. Shortly thereafter the polar jet core moves suddenly downward and poleward. Shiotani and Hirota (1985), who examined the 1981 winter season, attributed this shift in 1981 to what they termed a 'wave 2 minor warming', wherein a renewed burst of TW2 activity produced an episode of Eliassen-Palm (EP) flux convergence/divergence at middle/high latitudes in the upper/middle stratosphere, decelerating the mean zonal flow in the vicinity of the jet core while accelerating it at lower levels poleward. They further noted that it was after this that W1 began to strengthen in the stratosphere, suggesting the jet core movement served to tune the stratosphere for vertical propagation of W1. On the other hand, Shiotani *et al* (1990) examined the dynamical evolution in 1983, suggesting that in that year the jet shift was caused by a SW1 event, after which stratospheric TW2 amplitudes increased markedly. Irrespective of whether the jet shift is generally brought about by SW1 or TW2, a number of authors (e.g. Mechoso *et al*, 1985; Randel *et al*, 1987) have noted that it is after the jet shift that total planetary wave activity increases, suggesting that the jet shift may serve as a tuning mechanism for subsequent planetary wave propagation.

The upper level EP flux divergence dipole pattern accompanying the jet shift is a feature which has been observed by many to occur with southern hemisphere

planetary wave amplification in general (e.g. Hartmann *et al*, 1984; Mechoso *et al*, 1985, Randel *et al*, 1987; Randel, 1988a; Manney *et al*, 1991). While many of these observational studies have used geostrophic winds to estimate EP fluxes, which are prone to exaggerate high latitude divergences due to lack of allowance for flow curvature (Randel, 1987b), there seems to be little doubt that the positive divergence feature is real. It is also seen in primitive equation modelling studies (e.g. Young and Houben, 1989). Some authors have interpreted its existence as an indication of an in-situ source of wave activity, indicating instability of the basic state. Others claim it may reflect the presence of nonlinear interactions, since in some cases the dipole pattern occurs in association with positive meridional potential vorticity gradients (e.g. Andrews, 1987b; Randel, 1988a). O'Neill and Pope (1988) describe how an EP flux divergence dipole can result from nonlinear vortex interaction in which a Rossby wave breaking signature produces a localised zonally-asymmetric jet between the vortices, with net poleward momentum transport (equatorward EP flux) focussed at the jet entrance. They suggest that this situation may correspond to that of the observed southern hemisphere EP flux divergence pattern.

By early August, W1 activity begins to increase, continuing to do so until mid-October, and again becomes about evenly partitioned between SW1 and TW1. Unlike the early winter period, TW2 also grows to account for a significant proportion of the total variance, reaching maximum amplitude during September (Manney *et al*, 1991). A small contribution to the total wave activity also comes from an eastward travelling wave 3 (TW3) component, which achieves maximum amplitude in the vertical near 7 hPa and which has a period of about 6 days, as first noted by Harwood (1975), Hartmann (1976) and Leovy and Webster (1976). According to Randel (1988a) each of the stratospheric transients displays equivalent barotropic structure similar to the early winter period, although Manney *et al* (1991) find TW2 sometimes shows significant baroclinicity. SW1, on the other hand, shows a marked difference in structure, becoming strongly baroclinic during the late winter period, its climatological tropospheric ridge progressing to be near $120^{o}W$ (central/eastern Pacific Ocean), while the 10 hPa ridge moves rapidly westwards to $135^{o}E$ (Australia) during August. This baroclinic

structure, with associated strong vertical EP flux component and mid-latitude EP flux convergence, leads SW1 to dominate the wave driving of the mean flow when the annual planetary wave amplitude maximum occurs in October, this late spring maximum being substantialy larger than that in early winter. As the season progresses into spring, the height of maximum wave amplitudes follows the gradual downward movement of the jet core so that by the time of the October maximum in total wave activity, maximum amplitudes occur between 5 and 10 hPa (Shiotani and Gille, 1987; Geller and Wu, 1987).

After the mid-October planetary wave amplitude maximum, the height of maximum amplitude descends further, and the wave activity rapidly decreases to near zero by the completion of the seasonal transition, at which stage the easterly flow regime has become re-established and the waves are again barred from the stratosphere.

4.2.1.2 The Source of Stationary Wave 1

James (1988) has shown that the Antarctic land mass, which dominates the planetary scale projection of the hemispheric topographic distribution, can account qualitatively for the magnitude and phase of SW1 in the southern hemisphere winter. He further shows that inclusion of allowance for planetary scale extra-tropical thermal forcing improves the agreement between model and observed behaviour, but suggests that tropical thermal forcing may also play a significant role. Randel (1988a) suggests that a region of observed strong subtropical tropospheric upward SW1 EP flux indicates a significant contribution to SW1 from a low latitude thermal source. Mechoso *et al* (1988) claim that the observed tendency for the stratospheric final warming process to commence and develop over a preferred geographical region year after year points to a surface topography source for the wave activity. They further attribute the occurrence of stratospheric SW1 to the preferential formation during the winter/spring season of an upper tropospheric split jet over the Australian region and the downstream formation of a climatological blocking pattern over the southwest Pacific, much as depicted by James' modelling study. Kodera and Yamazaki (1990) show that during

the 1980s the concentration of this tropospheric blocking pattern over the southwest Pacific, as opposed to a broad region of high pressure spanning the entire Pacific, is well correlated with the occurrence of positive sea surface temperature anomalies in the tropical east Pacific (ENSO), and they attribute a trend during the 1980s in stratospheric SW1 wave activity (Newman and Randel, 1988) to a trend in the occurrence of the tropical SST anomalies. Finally, Randel (1987a, 1988a) and Randel *et al* (1987), by lag-correlation analysis and examination of EP flux cross-sections, present strong evidence to connect episodes of enhanced SW1 activity in the mid-stratosphere to periods of enhanced propagation of the wave activity from the middle and upper troposphere about 4 days earlier, consistent with the theoretical ray tracing calculations of Karoly and Hoskins (1982).

Overall, then, the general consensus is that the primary source of SW1 in the southern hemisphere stratosphere is combined tropospheric topographic and thermal forcing, and subsequent vertical propagation aloft.

4.2.1.3 The Source(s) of the Transients

Randel's aforementioned lag-correlations and EP flux statistics lead him to conclude a 'clear tropospheric source' for TW1, but he notes that the mechanism of the tropospheric forcing awaits clarification, suggesting that wave-wave interaction in the troposphere may play an important role. Farrara *et al* (1992) examined TW1 during the early winter period and modelled the observed behaviour, reinforcing Randel's findings, but noting that not all observed stratospheric TW1 events could be traced to the troposphere. Their modelling study suggested, however, that the development and eastward propagation of mid-stratospheric TW1 disturbances requires the development and eastward movement of a disturbance in the lower stratosphere and that year to year variations in stratospheric TW1 amplitudes are more likely due to variations in tropospheric forcing than variations in the mean flow characteristics of the stratosphere.

Since its occurrence and peculiarity to the southern hemisphere were first noted

by Phillpot (1969) and Deland (1973), respectively, the source of TW2 has been the subject of numerous investigations, but the reasons for its existence are yet to be firmly established.

The early attempts by Harwood (1975) and Hartmann (1976) to describe the wave's characteristics led Leovy and Webster (1976), who further examined the satellite-depicted behaviour of TW2, to suggest that it might comprise the stratospheric projection of a tropospheric baroclinically unstable Green mode. Hartmann (1979) suggested the observed structures of TW2 and TW3 agreed more closely with modelled tropospheric baroclinically unstable Charney modes, but noted that the wave's definitive identification would require confirmation of its tropospheric signature, a difficult task in the poorly sampled southern hemisphere. Mechoso and Hartmann (1982) then used the FGGE data set from 1979 to find very little coherence in TW1 and TW2 amplitude signals between the troposphere and stratosphere, whereas they were able to identify TW3 and TW4 as being Charney modes. They suggested that three possible explanations for the lack of coherence for each wave would be (i) finite propagation time, and/or non-linear interaction in transit, modifying the wave's structure between troposphere and stratosphere, (ii) an in-situ source of stratospheric wave activity, and (iii) the existence of two linearly independent modes in the troposphere (Charney mode) and stratosphere (Green mode), the explanation they leaned towards.

Hartmann (1983) later investigated the second of these mechanisms by modelling the stratospheric response to in-situ barotropic instability resulting from reversal of the meridional gradient of potential vorticity (Charney and Stern, 1962) on either flank of the polar night jet. As well as finding fast eastward modes in the upper stratosphere on the poleward side of the jet, one of which resembled in many respects the '4 day wave' of Venne and Stanford (1979, 1982), and another of which was a wave numer 2 equivalent (similar to that later detected in the stratosphere by Prata, 1984), he found slower eastward moving mid-latitude modes of zonal wavenumbers 1 and 2 which he suggested might account for the observed lack of coherence in both

TW1 and TW2 between troposphere and stratosphere.

More recently, Shiotani *et al* (1990) examined the 1983 season, a year when TW2 was particularly active and persistent. They found the polar jet to have been marked in 1983 by particularly large curvature and local vorticity gradient reversal on its flanks, suggesting a connection between the strong narrow jet and the enhanced TW2 activity, and citing this as evidence in favour of the in-situ barotropic instability mechanism as the source of TW2.

The aforementioned lag-correlation and EP flux distribution analyses of Randel (1987a) and Randel *et al* (1987) led these authors to prefer Mechoso and Hartmann's first hypothesis, claiming that it was unneccessary to invoke in-situ instability to explain the source of TW2. i.e. They concluded that the observed lack of coherence between tropospheric and stratospheric signals for TW2 was probably due to the 1 to 2 day transit time indicated in their analysis for a burst of TW2 activity to reach the stratosphere, this observed transit time once again corresponding well with the theoretical calculations of Karoly and Hoskins (1982).

Young and Houben (1989), noting that finite transit time alone could not account for the poor coherence in TW1 and TW2 signals between troposphere and stratosphere, modelled the possibility of non-linear interaction in the stratosphere between baroclinically unstable modes arising in the troposphere. They found support for the hypothesis and concluded that the lack of vertical coherence was due both to finite propagation time (their transit times were similar to Randel's), and, more importantly, to non-linear coupling between the unstable modes in the upper troposphere and stratosphere. They also noted, however, that while TW1 behaviour was well explained by the mechanism, TW2 in their model still showed too much vertical coherence compared with the observations.

Robinson (1986) and Marks (1988) each modelled the effects on the stratosphere of localised stationary but unsteady 'tropospheric' forcing and found that travelling waves could be excited in the stratosphere which amplified with height under some conditions, particularly when trapped at high latitudes in the presence of a region of

reversed meridional potential vorticity gradient. Marks suggested this overall mechanism might be the cause of the observed TW2 in the stratosphere.

Manney *et al* (1988, 1989) have further examined the question of barotropic instability, and suggest that regions of tight curvature on the equatorward side of a zonally symmetric jet can both give rise to instabilities resembling the observed TW2 and TW3, and also serve to amplify preexisting modes resulting from some other cause.

In a recent detailed study of TW2 episodes in the southern hemisphere winter/spring period, Manney *et al* (1991) found two distinct types of TW2 behaviour. When TW2 amplitudes grow to be large, which tends to coincide with its eastward propagation being most regular, the waves display baroclinic structure and can clearly be traced into the troposphere. On other occasions, however, there are periods of moderate stratospheric amplification of waves with equivalent barotropic structure which are unrelated to behaviour in the troposphere. Manney *et al* conclude that a separate mechanism may be responsible for each type of event. The former, they suggest, is primarily driven from the troposphere (they do not specify the mechanism) and is perhaps reinforced by insitu stratospheric instability, while the latter probably results from barotropic instability on the equatorward flank of the jet.

4.2.2 Normal Modes and 'Fast Eastward' Modes

Although the dominant contribution to the total stratospheric wave activity in the winter/spring season is accounted for by the planetary scale forced Rossby waves discussed above, these are not the sole cause of day-to-day stratospheric dynamical variability.

Numerous observational studies have identified the presence in the southern hemisphere stratosphere at most times of the year (Hirooka and Hirota, 1989) of what are understood to be free Rossby waves, the normal modes of the global atmosphere. Most notable among these are the first and second symmetric modes of zonal wavenumber 1, the first symmetric and second antisymmetric modes of zonal wavenumber 2, and

the first antisymmetric mode of zonal wavenumber 3, known respectively as the '5 day wave' (Rodgers, 1976; Hirota and Hirooka, 1984), the '16 day wave' (e.g. Hirooka and Hirota, 1985), the '4 day wave' (Hirota and Hirooka, 1984), the '10 day wave' (Hirooka and Hirota, 1985), and the '2 day wave' (Rodgers and Prata, 1981).

All of these are westward propagating modes, with amplitude increasing with height, so that they are generally most noticeable in the upper stratosphere, and they exhibit an essentially barotropic structure, although westward tilt with height increases with increasing period, due to radiative 'leakage'. Madden (1979) and Salby (1984) provide reviews of the observed and modelled features of these more prominent modes. More recently Hirooka and Hirota (1989) and Venne (1989) have identified several additional modes.

The indirect effect of the normal modes on the overall dynamical state of the stratosphere is probably not negligible. It has been suggested that interference between forced stationary waves and normal modes may explain fluctuations in stratospheric wave transports, upward propagation of wave vacillations and the observed switching (from equatorward to poleward) of stratospheric EP flux vectors prior to sudden stratospheric warmings (see WMO, 1985, and references therein). McIntyre (1982) suggests they may thus have a significant influence on the development of sudden warmings.

As well as the normal modes, fast eastward moving disturbances have been identified in the southern hemisphere upper stratosphere, most notably the zonal wavenumber 1 '4 day wave' of Venne and Stanford (1979, 1982) and its wavenumber 2 to 4 equivalents (Prata, 1984; Venne, 1985; Lait and Stanford, 1988). These 'fast eastward' modes, observed in upper stratospheric temperature fields, have been observed to move together quasi-nondispersively (Prata, 1984; Lait and Stanford, 1988). A slower eastward moving synoptic scale wavenumber 5 feature has also been identified (Miles and Grose, 1989). These waves may be the result of barotropic instability on the poleward flank of the polar jet during winter (Hartmann, 1983; Manney *et al*, 1988, 1989; Manney, 1993; Randel and Lait, 1991) or on some occasions due to

baroclinic instability near the polar stratopause (Randel and Lait, 1991). On the other hand Prata (1984) notes that the quasi-nondispersive character of waves 1 to 4 suggests a nonlinear mechanism.

4.2.3 Medium and Synoptic Scale Rossby Waves

At the lowest levels of the polar winter stratosphere, close to the tropopause, a proportion of the total wave variance results from tropospheric synoptic and medium scale forced Rossby waves (zonal wavenumbers 4 to 7 or so). Although these waves may play a role in defining the base of the polar vortex, and in trace gas transport at the lowest stratospheric levels (Tuck, 1989), their vertical penetration into the stratosphere is severely limited, and they do not contribute significantly to wave variance aloft.

4.3 Annual Climatology of the Zonal Mean Flow Evolution

4.3.1 Mid-summer Conditions

The southern hemisphere mid-summer stratosphere is characterised by maximum solar heating over the pole, a poleward meridional temperature gradient at all levels, and, by thermal wind balance, an easterly stratospheric circulation above about 50 hPa. Below 50 hPa the dominent influence of the generally equatorward temperature gradient results in zonal mean westerlies which peak at 200 hPa in the subtropical jet near $45^{o}S$.

The stratospheric circulation at this time is dynamically quiescent, vertical propagation of forced Rossby waves being prohibited in the easterly regime by the Charney-Drazin mechanism, and the stratosphere is close to radiative equilibrium.

4.3.2 Mid-summer to Autumnal Equinox

During the three months after mid-summer the northward seasonal progression of the stratospheric solar heating maximum results in increased net radiative cooling of the dynamically undisturbed polar stratosphere, and a temperature minimum forms over the polar region. Maintaining thermal wind balance, the high latitude easterlies reverse, and a weak westerly circumpolar jet develops in the sub-polar upper stratosphere - the precursor to the polar night jet.

4.3.3 Autumnal Equinox to Winter Solstice

Between equinox and mid-winter, the stratospheric winter circulation becomes firmly established. As the solar heating maximum retreats into the northern hemisphere and the polar night sets in, enhanced net radiative cooling throughout the middle and high latitudes intensifies the westerlies and the polar vortex grows to dominate the stratospheric flow. By winter solstice the core of the polar jet lies just above the stratopause (at about 0.4 hPa) near $40^{o}S$, with maximum geostrophic winds around 130 ms^{-1}, the jet axis sloping poleward and downward into the lower stratosphere to be near $60^{o}S$ at 100 hPa where maximum zonal mean geostrophic winds are around 45 ms^{-1}. Below this level the jet axis broadens and becomes indistinct, the subtropical jet near $30^{o}S$ dominating the flow at lower levels.

In the vicinity of the polar stratopause, a local temperature maximum forms by May (Hirota *et al*, 1983) which is attributed by Kanzawa (1989) to gravity wave dissipation further aloft (the effect of which is understood to contribute significantly to the large net diabatic cooling rates), and results in minimum stratopause temperatures occurring at mid-latitudes during winter. Elsewhere in the middle and upper stratosphere the meridional temperature gradient is equatorward at all latitudes so isentropes slope upward from equator to pole. A cold tropical lower stratosphere results in maximum temperatures at mid-latitudes and isentropes in the lower stratosphere slope downward from the tropics to mid-latitudes, then upward towards the

pole, most steeply near the vortex edge.

With the establishment of the generally westerly flow regime by the autumnal equinox, forced planetary wave activity undergoes a climatological monotonic increase until mid-winter, as described in Section 4.2 above. Dissipation of the stratospheric waves during this period, either frictional, diabatic, or by some form of 'wave breaking' (McIntyre and Palmer, 1983, 1984) process (see Farrara *et al*, 1992, for an apparent southern hemisphere mid-winter example), leads generally to mean flow deceleration (Andrews *et al*, 1987) and the attendent residual circulation which, by inducing adiabatic warming at high latitudes and cooling at lower latitudes, works against the establishment of radiative equilibrium (and aids the maintenance of net diabatic cooling rates in the polar winter stratosphere). As a result of this dynamical activity, observed mid-winter temperatures in the high latitude lower stratosphere are 10 to $20K$ warmer than those corresponding to radiative equilibrium. Much larger departures (more than $100K$) are observed in the polar upper stratosphere and mesosphere, but these are thought to be largely gravity wave driven.

Identifying the vortex edge as the location of the jet axis, by winter solstice the polar vortex takes on the appearance of an inverted, truncated cone (Mechoso, 1990), extending upwards from a rather flat-bottomed but ill-defined base just below 100 hPa (at about 400K). At each isentropic level the vortex edge, thus defined, is characterised by strongest meridional gradients of EPV and trace gas mixing ratios (Schoeberl *et al*, 1992), poleward of which horizontal gradients are weak. Outside the vortex a moderate gradient extends into low latitudes, except for a narrow region of weak meridional EPV gradient near the vortex edge at upper levels. A narrow 'surf zone' signature (McIntyre and Palmer, 1983, 1984) might be implied here (see Figure 4 of McIntyre, 1989), but Farrara *et al* (1992) claim that a surf zone does not form at this time of year, so the feature may merely be the result of zonal and temporal averaging.

From the EPV perspective, the vortex growth process is most simply understood by considering the EPV 'conservation equation' in the absence of frictional forces,

which can be written

$$\frac{dq}{dt} = q\frac{d\dot{\theta}}{d\theta}. \tag{4.1}$$

In isentropic coordinates, we may reexpress Equation 4.1, following Hoskins *et al* (1985), as

$$\frac{Dq}{Dt} = q\frac{d\dot{\theta}}{d\theta} - \dot{\theta}\frac{dq}{d\theta} = q^2\frac{d}{d\theta}\left(\frac{\dot{\theta}}{q}\right), \tag{4.2}$$

where

$$\frac{D}{Dt} = \frac{\partial}{\partial t} + \vec{\mathbf{u}}.\nabla_\theta. \tag{4.3}$$

During the early winter season, net radiative cooling rates in the Antarctic stratosphere increase with height (Kiehl and Solomon 1986), so that, by Equation 4.1, EPV generally decreases following the Lagrangian motion of a material parcel. However, the magnitude of q, being directly related to $d\theta/dp$ by Equation 2.8, tends to increase more rapidly than $\dot{\theta}$ from the lower to the upper stratosphere, so $|\dot{\theta}/q|$ decreases with height. Hence by Equation 4.2, isentropic EPV values steadily increase in the polar region as winter progresses. i.e. The gradual Lagrangian EPV decreases in the polar region are more than compensated for by downward cross-isentropic (diabatic) fluxes of higher EPV from aloft, which result from significant large scale cooling and the strong vertical gradient of EPV. This, of course, also implies that, in order to meet the global conservation constraint on volume-integrated 'pv substance' discussed by Haynes and McIntyre (1987), at lower latitudes beyond the strong cooling region, a net isentropic EPV decrease must occur, and the two effects together result in the vortex becoming rather sharply defined in the EPV analyses.

This vortex intensification process can be seen more clearly with the help of a simple model. From Figure 8 of Kiehl and Solomon (1986), we might loosely approximate the net diabatic cooling rate in the austral winter stratosphere (Q, in $^\circ/day$) by a simple expression of the form

$$Q \approx -\frac{z}{H}, \tag{4.4}$$

where z is geopotential height in km, and H is the stratospheric scale height (about

7 km). From Andrews (1987a), we have

$$\dot{\theta} = Qe^{\frac{\kappa z}{H}}. \tag{4.5}$$

If we assume that the planetary vorticity dominates the absolute vorticity in the polar stratosphere, we can approximate Equation 2.8 by

$$q \approx -gf\frac{d\theta}{dp}. \tag{4.6}$$

Then, by using the definition of potential temperature given by Equation 2.1, assuming that $p \approx exp(-z/H)$, where p is in units of $10^5 Pa$, (so $p_0 = 1$ in Equation 2.1) and that the atmosphere is approximately isothermal ($T = \bar{T}$, a crude approximation but adequate for present purposes), we may substitute into Equation 4.2, after some manipulation, to yield

$$\frac{1}{q}\frac{Dq}{Dt} = q\frac{d}{d\theta}\left(\frac{\dot{\theta}}{q}\right) \approx \frac{1}{\kappa\bar{T}}\left\{\frac{z}{H} - 1\right\}. \tag{4.7}$$

So this simple representation suggests that, despite diabatic relaxation of *Lagrangian* EPV, there will be a continual fractional rate of increase in *isentropic* EPV everywhere in the polar stratosphere in a region whose base lies about a scale height above the base of the net cooling region (the surface, in this simple example).

4.3.4 July

The planetary wave-driving of the mean flow during early winter slows the transition to 'meteorological mid-winter' conditions in the lower and middle stratosphere. As a result, after the winter solstice, whereas upper stratospheric temperatures at high latitudes increase (Harwood, 1975; Hartmann, 1976; Hartmann *et al*, 1984) and the jet maximum begins to weaken slowly (Shiotani and Hirota, 1985), at lower levels polar temperatures continue to decrease slowly (Hartmann *et al*, 1984) and the jet continues to strengthen.

By late July the general vortex structure is similar to that at winter solstice, but extends downward to near 150 hPa (360-380K) with temperatures below 190K inside the vortex between the base and about 20 hPa (Hartmann *et al*, 1984). Then at

about the end of July, as mentioned in Section 4.2 above, while the jet axis maintains its mid-winter position, the jet core (the location of maximum winds) shifts suddenly downward to about 5 hPa and poleward to $60°S$ (Leovy and Webster, 1976; Hartmann, 1976; Hartmann *et al* 1984).

4.3.5 Early August to Spring Equinox

At the beginning of August, the commencement of our analysis period, planetary wave activity is at its mid-winter minimum, as discussed in Section 4.2 above.

The meridional cross-section shown in Figure 4.1(a) broadly represents the 11 year (1979-1989) climatological average state of the austral stratosphere during early August, as obtained from our present analysis. It shows the 'average' meridional distribution, from our isentropic coordinate perspective (potential temperature versus latitude), of pressure, zonal wind and EPV between the $300K$ and $1200K$ surfaces, obtained by simple averaging of temporal average distributions corresponding to the first 'SAGE sweep' for each year. (See Chapter 6 for details of the precise period from each year. For the years 1985 to 1989 these correspond to actual SAGE sweeps, whereas for the other years they may or may not, depending on SAGE data availability. While it might make more sense from a purely climatological perspective, were the same period from each year chosen, those selected are more useful for our ultimate purpose, as will become clearer in the Chapters to follow.)

Evident in the smoothed Eulerian picture of Figure 4.1(a) is the location of the vortex edge, which corresponds to the location of the polar jet axis and the steepest isentropic EPV gradients at each level. In climatological early August the edge slopes slightly with height, from about $55°S$ at $1200K$ to near $60°S$ at the vortex base and separates the region of relatively flat EPV isopleths inside the vortex, from the region of moderate meridional gradient outside. The polar jet core, with maximum (balanced) winds of about 85 ms^{-1} (geostrophic winds are closer to 95 ms^{-1} at this time), has already shifted down to be near $1100K$ (about 5 hPa). The pole

is cold at all levels inside the vortex (isentropes slope downward into the vortex) and below $600K$ the warmest temperatures are in mid-latitudes (where the isobars bulge upward). Winds are westerly throughout the extratropical stratosphere, turning easterly near 15^oS according to Figure 4.1(a), although the true climatological zero wind line is actually located closer to 20^oS. The more northward location in Figure 4.1(a) is spurious and a result of poorly behaved nonlinear balance winds at low latitudes (see Randel, 1987b). The location of the dynamical tropopause coincides with the lowest EPV contour.

The situation about a month later, leading up to the spring equinox, is shown in Figure 4.1(b). The combined effects of the wave driving and the seasonal march of the solar heating maximum southward, which work in concert rather than opposition in the spring, have brought about a weakening and shrinkage of the vortex in the middle and upper stratosphere. This effect is strongest at the highest levels, where wave amplitudes grow sufficiently during a series of wave amplification events, to begin to produce apparent moderate Rossby wave breaking episodes (irreversible buckling of isentropic EPV contours at the outer edge of the vortex). The combination of dynamical and radiative processes has resulted in the vortex gradually taking on a cylindrical shape (edge vertically aligned near 60^oS), as opposed to the inverted cone of mid-winter. Temperatures have begun to increase throughout the vortex, particularly at the higher levels (note the upward displacement of the isobars above $450K$ in the polar region between August and early September in Figure 4.1), and the jet has narrowed and weakened above about $600K$. The jet maximum, now about 75 ms^{-1} (85 ms^{-1} geostrophic), has moved downward to about 7 hPa. In the lower stratosphere the vortex is at its peak, having intensified slightly since August (this is not obvious in Figure 4.1), and the equatorial easterly wind region has begun to encroach southward, the mid-stratospheric zero wind line reaching as far as 25^oS.

Figure 4.1(c) shows the climatological situation around the end of September, shortly after spring equinox. The general progression noted between August and early September has continued, the vortex at middle and upper levels having weakened

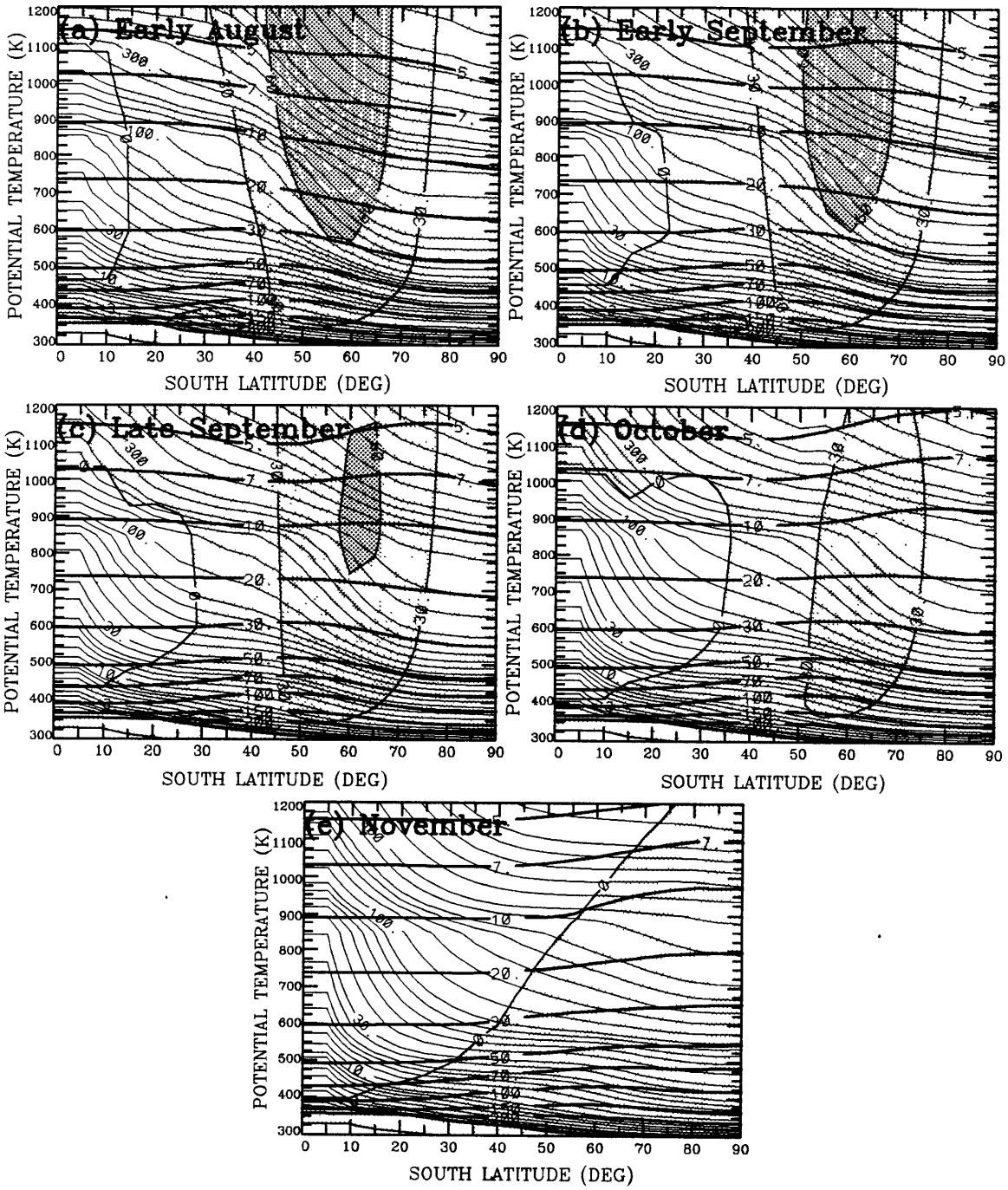

Figure 4.1: Climatological Evolution of the Austral Spring Stratosphere, showing the meridional distributions (potential temperature vs south latitude) of pressure (thick black contours at 200, 150, 100, 70, 50, 30, 20, 10, 7 and 5 hPa), EPV (thin black contours at 1.5, 1.75, 2.0, 2.5, 3, 4, 5, 6, 7, 8, 10, 12.5, 15, 17.5 etc. to 3000 PV units), and zonal wind (white contours every 5 ms^{-1}, easterlies unshaded, and light, medium and darker shading separated by black contours for westerly wind speed ranges of 0 to 30, 30 to 60, and 60 to 90 ms^{-1} respectively). See text for further details.

further to take on the the shape of an upright cone. 65 ms^{-1} maximum winds in the jet are now seen nearer 10 hPa ($900K$), and the upward bulge in the isobars near 75^oS at the upper levels in Figure 4.1(c) heralds the approach of the meridional temperature gradient reversal in the polar region at these levels. Changes at lower levels are not as obvious, but temperatures have increased everywhere inside the vortex and the jet has begun to weaken in the lower stratosphere. In the middle stratosphere the zero wind line has reached 30^oS.

4.3.6 The Final Warming

After September the most dramatic and rapid changes to the circulation culminate in the final warming.

Figure 4.1(d) shows the climatological mean situation for October. By mid-October total wave amplitude reaches its maximum. The series of wave amplification events of September continues into October, each event producing more substantial upper level vortex erosion, by stripping increasingly larger amounts of material from the vortex edge in the upper stratosphere, and on occasion from deep within the vortex. At the same time, the wave breaking process extends downward through the stratosphere. The accompanying dynamical adjustment produces adiabatic warming throughout the vortex interior, which, together with the effects of broad-scale solar radiative heating, results in the high latitude meridional temperature gradient reversal progressing downward, to affect the 10 hPa level during early October, as evident in Figure 4.1(d), and reaching 50 hPa by the end of the month. (During this period, small temperature decreases are observed at lower latitudes (Harwood, 1975; Farrara and Mechoso, 1986; Yamazaki, 1987), consistent with net vertical motion in the ascending branch of the residual circulation.) Although the October mean flow remains westerly, it has weakened markedly, and the conical shape of the vortex has become more pronounced, the jet core having descended slowly to be near 20 hPa at 65^oS with maximum winds of about 45 ms^{-1}.

Although wave amplitudes at upper levels tend to decrease markedly after a large wave event during mid- to late October, significant wave activity continues lower down while the westerly regime remains, further eroding the otherwise radiatively decaying vortex during November. By mid-November the zonal mean meridional temperature gradient reversal reaches 70 hPa (see Figure 4.1(e)), easterlies appear everywhere below 5 hPa in the tropical stratosphere, and the zero wind line moves progressively poleward and downward during the month. By the end of November the temperature maximum lies over the pole at all levels above about 200 hPa, so that the isentropes slope downward from equator to pole throughout the lower and middle stratosphere (i.e. the isobars slope upward in Figure 4.1(e)), and the high latitude wind reversal has reached down to about 20 hPa.

December brings about the completion of the seasonal transition. Continuing radiative decay sees the zero wind line descend further, and precedes a final weak wave event early in December which pushes the vortex remains above about 60 hPa off the pole, to be sheared out in the hemispheric flow. While a westerly regime persists throughout the year below 70 hPa, above this level, in the absence of further forced Rossby wave activity, radiative processes resume control, and by summer solstice the flow above 50 hPa is again characterised by a rather undisturbed zonally symmetric easterly regime throughout the hemisphere.

4.4 The Synoptic Evolution of the Final Warming

While the description of Section 4.3 provides a picture of the final warming evolution which accounts for the features observed from the Eulerian wave-mean flow perspective, examination of the synoptic evolution reveals a rather zonally asymmetric picture which occurs each year, as first pointed out by Mechoso *et al* (1988) (hereafter MOPF) for the September/October period. This alternative viewpoint also provides a perspective which is valuable for our present analysis of the ozone dilution effect, and also suggests the Eulerian wave-mean flow approach may perhaps mislead efforts

to understand the dynamical causes of the latter stages of the observed evolution by disguising some of the key dynamical processes at work.

MOPF examined the synoptic evolution of the isobaric geopotential height distribution during the final warming in each season from 1979 to 1986, focussing on 1982, and found that the vortex decay process during September and October involved a cycle of growth, movement and decay of mid-latitude anticyclones (A/Cs) in a preferred geographical location.

They found that at the beginning of September a stratospheric A/C (most clearly seen at 10 hPa) formed over the western Indian Ocean near $60^{o}E$ and intensified as it tracked eastward, eventually to decay about 10 days later over the eastern Pacific Ocean about 180^{o} east of its origin. As the first A/C decays, a second forms in the western Indian Ocean, and repeats the cycle of movement and decay. At the end of September, after three such cycles, the A/C does not decay on reaching the eastern Pacific, but becomes quasi-stationary and continues to intensify, rapidly eroding the polar vortex by advecting vortex material around its eastern flank into mid-latitudes. During this erosion process, additional, weaker A/Cs form in turn over the Indian Ocean, to track eastwards and merge with the stationary A/C. The stationary A/C eventually dissipates at the end of October, to leave a greatly weakened vortex which subsequently decays radiatively, before 'migrating' into the Atlantic Ocean at the end of November, to complete the seasonal transition.

MOPF suggest that the overall cyclic process, particularly during October, which projects onto the Eulerian wave mean flow reference frame as an anti-correlated vacillation of SW1 and TW2 (originally noted by Leovy and Webster (1976) and found by Manney et al (1991) to be statistically significant in October over a ten year period) points to the importance of nonlinear interactions in the final warming process. MOPF claim that the broad pattern of the cyclic process is much the same from one year to the next, despite a degree of interannual variability.

Similar examination of the synoptic evolution of the EPV distribution over the extended period of the present analysis suggests that while most aspects of the MOPF

mechanism are quite general from year to year, the observed interannual variability is considerably greater than they imply, and we find a slightly different description of the process, from the EPV perspective, to be not only generally more applicable to the September/October behaviour each year, but also applicable to the behaviour before and after. It must be added that the following description is intended as nothing more than than an attempt to summarise the essential features of the synoptic evolution as perceived by close examination of the EPV analyses for the eleven seasons studied, and we do not provide a rigorous explanation for the observed behaviour in terms of forcing mechanisms.

The EPV analyses show that the cyclic behaviour typical of the entire springtime evolution involves vortex-relative EPV perturbations which travel eastwards around the hemisphere. Although harmonic analysis and linear theory might generally explain the behaviour of these observed perturbations early in the season, consistent with our synoptic perspective we view each as an individual entity. There are generally between two and four, not always evenly spaced about the hemisphere, but identifiable as lasting features in the analyses. In general one, or two approximately on opposite sides of the hemisphere, dominate over the others at any given time, hence the pattern projects primarily as either wave 1 or wave 2, or a combination of these, in a harmonic decomposition. As each disturbance crosses the Atlantic Ocean and approaches Africa it tends to amplify, followed by local contour buckling as it crosses the Indian Ocean, and eventually a patch of low EPV may be cut off from its low latitude environment as the disturbance reaches peak intensity south of Australia. The disturbance then weakens as it tracks across the Pacific Ocean, generally to leave just an undulation in mid-latitude EPV contours by the time it reaches South America. This residual disturbance continues eastward and begins to reamplify as it crosses the Atlantic, repeating the process. A cyclic process typically involving three of these disturbances, each at a different stage of development, describes the essential feature of the behaviour throughout the season. However, the impact of a perturbation on the overall flow evolution is dramatically different at different stages of the season, seemingly dependent on the initial horizontal scale and amplitude of

the perturbation, and on the size and intensity of the polar vortex.

In this respect, and for the sake of describing a climatological picture, we classify four stages of the evolution, being broadly typical of late winter (LW), early spring (ES), late spring (LS) and transition time (TT).

4.4.1 LW Stage

In the LW stage (say August), temporal mean perturbation amplitudes are small and the vortex is large and intense. This is, relatively speaking, a dynamically inconsequential stage with respect to the vortex destruction process. The amplification stage of each perturbation is not marked, and any limited contour buckling associated with a perturbation appears to be localised and involves contours beyond the vortex edge. At the vortex edge the perturbations are observed to propagate eastward causing essentially elastic and reversible deformations, suggestive of rather linear behaviour, in which slow vortex decay during the period is due to radiative relaxation and gradual wave dissipation rather than noticeable Rossby wave breaking.

The LW stage tends to end shortly after the poleward/downward shift of the jet core discussed in Sections 4.2 and 4.3 above. Amidst a sea of weak perturbations, at some stage a single perturbation will be observed to amplify rapidly with height for some reason (not identified here) to produce the first significant Rossby wave breaking signature of the season at the highest analysis levels. This tends to coincide with the jet shift, as depicted in the 1 hPa zonal wind plots of Randel (1992).

4.4.2 ES Stage

The ES stage (climatological September) we view as a vortex conditioning stage, and the behaviour corresponds to the MOPF description of September. It is characterised by a still large and intense vortex, but the perturbation amplitudes are larger.

Generally within the space of a week or so after the jet shift, EPV perturbation

amplitudes in general increase markedly, signalling the commencement of the ES stage. This feature is consistent with the previously discussed notion that the jet shift serves to tune the stratosphere for planetary wave activity, although whether this is by enhancing vertical wave propagation or in-situ growth is not clear from the present analysis.

As well as increased overall perturbation amplitudes, the amplification process is observed to become more marked. Contour buckling during the amplification process occurs at larger horizontal scales and at the outer edge of the vortex itself at upper levels, a reflection of the associated A/C (via the invertibility of the EPV distribution) stripping material from the vortex edge and advecting it around the flank of the A/C into lower latitudes, a process which in itself can be expected to intensify the A/C. Successive A/Cs gouging the vortex during this period bring about a more rapid weakening of the vortex than during the LW stage, and during the amplification/gouging process the vortex centre is itself displaced off the pole away from the A/C, the more intense the A/C the more marked the overall displacement.

4.4.3 LS Stage

The LS stage is the upper level vortex destruction phase and sees the most rapid erosion of the upper level circulation and the high latitude temperature gradient reversal, in a series of major wave breaking events wherein significant amounts of upper level vortex material, eventually from deep within the vortex, are stripped away and deposited in mid-latitudes. Wave breaking is also seen at lower levels during this stage, although not as pronounced as that aloft. There appear to be two alternative mechanisms characteristic of this period, and from our synoptic perspective both seem to require peak perturbation amplitudes and the polar vortex to have weakened somewhat. Only then can the A/Cs associated with the perturbations have a major influence on the flow field, in the sense that they can strip large amounts of material from the vortex. The features of the two observed scenarios correspond to a wave 1 and wave 2 warming, respectively, although we view the former of these processes

somewhat differently from the generally adopted view of a quasi-stationary wave 1 event such as occurs in the northern hemisphere.

In our typical wave 1 scenario (which corresponds to the MOPF description of October) the EPV analyses suggest that the same perturbation amplification and decay cycle continues throughout, and that this may be important in determining the overall degree of vortex erosion which occurs. While the associated geopotential pattern comprises a quasi-stationary (or more often slowly eastward moving) A/C, the EPV analyses suggest that rather than the MOPF picture of weaker circulations moving in from the west, and continually *merging* with the quasi-stationary A/C in a *reinforcement* process, the sequence might more appropriately be described as one of cyclic *replacement* of EPV perturbations i.e. MOPF describe the 1982 final warming as being due to a single sustained wave breaking event, whereas the EPV analyses suggest it more likely comprised a series of events following one after the other in the same general region.

In such a scenario a point is reached in the ES stage that a perturbation achieves very large amplitude in the Australia/New Zealand region and its A/C begins to gouge the vortex, the vortex centre being displaced somewhat off the pole. A tongue of relatively high EPV is extruded into the mid-latitudes by the A/C, which in turn intensifies the A/C circulation. As the tongue is advected westward across the mid-latitudes to the north of the A/C, it in turn enhances the southward advection of more low EPV to its west. As the A/C gouges its way eastward, its movement slowing in the process, the zonal scale of the perturbation increases (it spreads out in longitude) due to the continued southward advection of low EPV to the west, so the next perturbation following behind closes the distance on the trailing edge of the former. Eventually the leading patch of low EPV becomes cut off, the gouging process ceases, and the rapidly weakening patch is advected away eastward as the next patch arrives to repeat the process a little further east and before the vortex moves back onto the pole, hence maintaining the presence of a slowly eastward moving A/C. In this way the upper level vortex is rapidly eroded, culminating in either a collapse

of the pattern once the upper vortex has greatly weakened, or in the upper vortex remnants being sufficiently displaced from the pole that they are subsequently sheared out in mid-latitudes.

The wave 2 process is considerably different. Rather than decaying over South America, at some point an ES stage perturbation continues on into the Atlantic Ocean after undergoing only slight weakening near South America. Arriving over the Atlantic Ocean just as another perturbation reaches maximum intensity and begins gouging the vortex in the Australia/New Zealand region, the analyses give the impression that the vortex is pinned between the two A/Cs and the gouging becomes much more extensive than when the vortex centre moves off the pole in retreat. Rapid vortex erosion then continues as the larger A/C crosses the Pacific Ocean, until the Atlantic perturbation reaches Africa and itself intensifies and begins to erode the vortex. In this manner, with neither A/C dissipating as the pattern continues to rotate, the A/Cs eventually spiral their way in towards the pole, distending the upper levels of the vortex into an hour glass or Z shape, before finally, either the pattern collapses to leave the weak upper vortex remains on the pole, or the A/Cs pinch the upper vortex in two and merge over the pole in its place.

4.4.4 TT Stage

The final stage involves rapid weakening and eventual destruction of the vortex at the low levels.

Whereas MOPF focussed on the 10 hPA evolution in 1982, in the present analysis we are more concerned with the evolution in the lower stratosphere, at ozone hole levels. Indeed, one of the major aims of the present work is to determine the extent to which material is eroded from *within* the low level vortex as the season progresses. MOPF describe November behaviour to be characterised by little dynamical activity and radiative decay of the vortex remains, a common but we believe mistaken perception of the closing stages of the seasonal transition which results from examining only

the upper level behaviour. We observe in the present analysis, where we consider the synoptic evolution at a range of isentropic levels, that while MOPF's description of primarily radiative decay during November is adequate for the upper levels in 1982, this is not the case lower down.

Unlike northern hemisphere sudden warmings, the final warming in the southern hemisphere tends to progress gradually downward, as noted above, so that although climatological October sees the upper level transition to the LS stage, substantial wave activity and ES-type behaviour continue at the lower levels throughout October, each successive event tending to have a more marked effect on progressively lower levels. At the lowest levels where the wind reversal occurs (climatologically around $475K$) ES-type behaviour continues well into November. By the end of the month the low level vortex has been greatly weakened, and the vortex is eventually displaced permanently from the pole and its remains are sheared out into the mid-latitudes, the precise nature (wave 1 or wave 2) and timing of the final push varying from year to year.

4.5 Interannual Variability

Were the southern hemisphere stratospheric evolution, particularly in the spring season, as regular and predictable as suggested by the climatological picture described above, then the task of describing in detail the evolution of the ozone distribution each year would be made relatively simple. Given sufficient ozone data over a few years to describe the evolution during those years, we might be able to use the resulting ozone climatology, with suitable allowance for photochemical trends in ozone, to examine, with or without ozone data for other years, ozone transports resulting from significant dynamical events occurring in those other years. Unfortunately, although the degree of interannual variability in the southern hemisphere stratospheric evolution is smaller than that in the northern hemisphere, the details of the resulting ozone evolution appear to be rather sensitive to the details of the dynamical evolution, as

will be shown in Chapter 6 below.

Hence, if we are to be able not only to describe the ozone evolution in a given spring season, but to understand it, and further, if we are to attempt to speculate on the ozone evolution occurring in years for which ozone data are unavailable, then it is important to consider the interannual differences in the dynamical evolution.

Most of the interannual variability in the dynamical evolution of the stratosphere results, as expected, from variability in planetary wave driving. The effective absence of such wave activity during the summer and the expected small interannual variability in the solar heating cycle, together result in relatively little year to year variability in the summer easterly circulation. However, whereas the climatological picture suggests a smoothly varying bi-modal pattern of planetary wave amplitudes in winter/spring, it has long been known that in an individual year the planetary wave activity tends to comprise a series of bursts generally lasting a week to ten days, clustered within larger envelopes of moderate activity of several weeks' duration. Even the mid-winter lull tends only to be a statistical tendency. During the early winter period, although largest wave amplitudes occur most frequently in June, they have occurred as early as April and as late as July (Farrara *et al*, 1992). About the only regularly recurring feature in the seasonal behaviour is the tendency for the largest wave amplitude events in a given year to occur during late September or October. Total wave activity from year to year also varies considerably: while some years are dynamically active, with numerous large amplitude wave events occurring throughout the season, others are quiet, with no more than one or two noteworthy events.

The result of this variability in wave activity is to produce considerable variability at a given time of year in the hemispheric temperature, wind and trace gas distributions, and the size and intensity of the polar vortex. Since these distributions at a given time are all dependent to a greater or lesser extent on the time-integrated wave activity (during a period whose representative length depends on the quantity considered and the location), the interannual variability in their distributions tends to increase as the season progresses, to a maximum in late spring. Much of this late

spring variability is reflected by the timing and nature of the final warming, which itself appears to be sensitive not only to the wave events in late spring but also to the seasonal wave history (this essentially amounts to a claim that preconditioning is important to the timing of the austral final warming). At the completion of the final warming process, which sees both a return to essentially radiative control over the temperature and wind distributions, and also the breakdown of the meridional mixing barrier provided by the polar vortex edge, interannual variability in the hemispheric distributions again becomes relatively small.

The reasons for the winter/spring variability in planetary wave activity are not well understood.

Perhaps the most prominent feature apparent in the observations is a link between the level of planetary wave activity during a particular season and the phase of the quasi-biennial oscillation (QBO) in tropical stratospheric winds. There is a well-documented tendency for dynamically active seasons to coincide with the easterly phase of the QBO. Newman (1986), in an examination of the final warming each year from 1979 to 1985, classified two types of seasonal transition: a major mid-October wave event and a mid-October warming, which tends to coincide with the QBO easterly phase, or no mid-October wave event and a mid-November warming (generally westerly QBO), either of which is followed by a minor wave event and vortex breakdown (zonal wind reversal) in late November or early December. Since Oltmans and London (1982) first pointed out a QBO in extratropical ozone, an observed correlation between ozone hole severity and the phase of the equatorial QBO has been noted (Garcia and Solomon, 1987), and related to interannual variations in stratospheric planetary wave activity (Lait *et al*, 1989; Newman *et al*, 1990). A westerly QBO phase generally coincides with a dynamically quiet spring season, which in turn results in a more zonally symmetric and intense vortex, weaker eddy transports and cooler polar temperatures, hence more extensive chemical destruction of ozone and, possibly, less ozone transport into the high latitude region during winter.

Whether the QBO/wave activity correlation results directly from the relative prox-

imity of the zero wind line and an associated critical layer during the easterly phase, serving to focus wave activity into the high latitude stratosphere throughout the season (McIntyre, 1982), or just long enough to aid an early poleward/downward shift of the jet, after which the jet takes over the role of wave guide (Shiotani and Hirota, 1985), or by some other mechanism, has not been determined.

As well as the QBO in wave activity, a downward trend has been noted in October planetary wave activity during the early eighties (Nagatani and Miller, 1987). Newman and Randel (1988) relate a decrease in polar stratospheric temperatures during October from 1979 to 1986 to a decrease in SW1 heat fluxes, but other than noting that the decrease is due to the combined effects of changes in both wave amplitude and vertical structure, do not suggest a possible cause. As noted in Section 4.2 above, Kodera and Yamazaki (1990) suggest the observed SW1 trend might be attributable to a trend in net tropospheric forcing resulting from changes in the tropical tropospheric thermal forcing component, thus hinting at an ENSO connection.

Quite apart from the general trend and QBO cycle in seasonal wave activity, there are also significant differences from year to year in the spectral composition of the forcing. Although SW1 and TW2 are ubiquitous in the austral spring stratosphere, their relative magnitudes are highly variable from year to year. Whereas MOPF suggest the typical synoptic evolution involves a transition from a primarily TW2 dominated pattern in September to a SW1 dominated pattern in October, our present analysis suggests such a simple classification to be unique to 1982, the year focussed on by MOPF, and that a broad spectrum of behaviour occurs over the eleven seasons examined here, from almost pure SW1 behaviour throughout a season, to almost pure SW2 behaviour throughout, TW3 also contributing to different extents in different years.

Chapter 5

Dynamical Evolution of the Austral Spring Stratosphere: 1979 to 1989

In Chapter 4 above we described the dynamical climatology of the austral spring stratosphere. However we noted in Section 4.5, and will show in Chapter 6 below, how the evolution of the ozone distribution in a given year appears to be particularly sensitive to the details of the dynamical evolution in that year. Also, our eventual aim is to identify and analyse potential ozone dilution events which might have occurred from 1979 to 1989, which themselves will be tied to the occurrence of specific dynamical events. So an essentially preparatory component of the present work was to examine closely the day-to day dynamical evolution of the austral spring stratosphere in each season. The purpose of this Chapter, then, is to summarise this dynamical evolution each year, to provide a framework for the Chapters to follow, in which we switch our attention to the ozone distribution. Using the climatology described in Chapter 4 as a basis, the focus here will be on the noteworthy characteristics of each year's evolution, in particular those which seem to produce the most marked impact on the ozone evolution, and on the individual dynamical events which showed apparent ozone dilution potential.

Randel (1992) provides maps of 10 hPa total geopotential height wave amplitude vs day number for each year from 1979 to 1990. Farrara *et al* (1992) provide similar plots for the zonal wavenumber 1 component from April to July for the same years, and Manney *et al* (1991) for each of wavenumbers 1 and 2, with data at $60°S$ for wavenumber 3, from July to October of the years 1979 to 1988. The information contained in these plots (not shown) is used in the following description as an aid in assessing the overall level of wave activity in each season, and to provide a guide to the timing of individual wave events and their harmonic composition, particularly for the period in each year prior to August, for which no information is available from the present analysis.

More detailed information on the synoptic evolution of the EPV distribution for the spring period in each year has been obtained from the examination of daily analyses of the isentropic EPV distribution at a range of stratospheric levels. Few of the details of this examination are described here, to avoid getting the reader too bogged down in this subsidiary component of the present work, the primary focus of which is the ozone evolution. Instead we have endeavoured to confine the account to the more essential features of the evolution each season and the general impressions gained from the synoptic analysis. While only a small selection of the daily EPV analyses will be shown for brevity, the dynamical evolution in the lower stratosphere each season is depicted graphically in the Hovmoller diagrams of Figures A.1(a) to A.11(a) (to be found in the Appendix), which show the daily evolution of EPV vs longitude at $50°S$ on the $525K$ surface for the period from 01 August to 31 January, in each season from 1979 to 1989, respectively. To enable convenient and frequent reference to these Figures as the reader progresses through the following, primarily verbal description, each can be folded out for simultaneous viewing. It is assumed that the reader will be making regular reference to these Figures, and few explicit references to them will be made in the text.

Consistent with our primarily synoptic analysis of each season's EPV evolution, we often focus in what follows on the behaviour of individual disturbances to the vortex,

and in particular on anticyclonic, or low EPV perturbations. Accordingly, the terms 'perturbation' and 'disturbance' will generally be used to describe a region of *low* EPV magnitude (i.e. low latitude origin), a 'lobe' refers to an EPV perturbation of high latitude origin (the ridge of an EPV wave on the vortex edge) and a 'tongue' is an extrusion of high latitude EPV from one of these lobes (the result of Rossby wave breaking, or contour buckling) around the eastern flank of an A/C disturbance and into the middle latitudes.

5.1 1979

Wave activity in the winter/spring season of 1979 was examined in the studies of Mechoso and Hartmann (1982) and Hartmann *et al* (1984), and the 1979 final warming was analysed by Yamazaki and Mechoso (1985). The present analysis was hampered somewhat by poor data quality, which resulted in particularly noisy analyses, and data for many days were missing (see Trenberth and Olson, 1988).

Although the 1979 season, which coincided with the easterly phase of the QBO, has a reputation for having been dynamically very active, the present analysis suggests it was not particularly so. Nonetheless, an early completion of the seasonal transition was observed, reflected by particularly warm temperatures in the lower stratosphere. Why such an early final warming occurred is not clear. The present analysis reveals that after a rather average early winter period, the spring season was characterised by a background of moderately disturbed conditions upon which was superimposed a series of rather regularly spaced bursts of planetary wave activity. Peak amplitudes at 10 hPa associated with these events increased monotonically after the beginning of August, to climax in a large amplitude (but not extraordinarily so) event in early October. The EPV analyses suggest that each event was accompanied by a somewhat greater degree of apparent upper level Rossby wave breaking than is typically evident in the seasons examined. Overall, we are led to speculate that it may have been their regularity and unusually marked impact on the mean flow (i.e. their overall efficiency

at breaking down the vortex) which brought about the early final warming, rather than the number and magnitude of the events *per se*. As noted above, the following discussion is intended to be read in conjunction with the information contained in Figure A.1(a), and very few explicit references will be made to the Figure in the text.

The early winter period (up to the end of July) was about average, as noted above, and noticeable wave activity first began in late April, before a moderate SW1 event at the beginning of June and a rather large TW1 event in early July. This latter event coincided with the poleward and downward movement of the jet in the upper stratosphere (see Randel, 1992).

Although the jet shift occurred by mid-July the first two weeks of August were characteristic of LW behaviour (as described in Section 4.4 above). A TW2 event developed rapidly in the space of a few days centred on 01 August (01/08), and travelled eastward with an average period of about 16 days (Figure A.1(a)), but the EPV analyses suggest it caused little in the way of Rossby wave breaking at any level.

The period from mid-August to late September was rather typical of the ES stage described in Section 4.4 above. After 14/08 a disturbance, shown in the analyses as a patch of low EPV beyond the vortex edge, intensified as it travelled eastward from the western Indian Ocean (WIO), to peak over New Zealand (NZ) by 22/08, the vortex centre being displaced towards South America (SAm) at upper levels and minor upper level vortex erosion evident over the eastern Pacific Ocean (PO). The following four weeks saw a succession of smaller scale disturbances developing over the Atlantic Ocean (AO) and intensifying as they each tracked rapidly east to New Zealand (NZ) to replace the previous dissipating disturbance, each apparently producing some erosion of the outer edge of the vortex at upper levels only, accompanied by an oscillating but amplifying displacement of the vortex towards the South Atlantic Ocean (SAO). The reflection of this series of travelling disturbances was a vacillating quasi-stationary W1/W2 event which reached maximum amplitude around 21/09, with time-averaged geopotential ridge near $160^{o}E$, and which appeared to cause significant vortex edge erosion at the upper levels only, a broad surf zone signature appearing over the

Australia (AU) and PO mid-latitudes.

Following this ES stage, the behaviour of subsequent disturbances became more typical of the LS stage described in Section 4.4.

After 20/09, rather than another relatively small scale disturbance over the WIO, a large region of low EPV developed further west, and intensified rapidly as it moved eastward into the WIO region. With this intensification, while the previous disturbance (over NZ) persisted rather than dissipating as it continued east, the two disturbances on opposite sides of the hemisphere rapidly distorted the vortex into a marked W2 pattern (10 hPa TW2, with period around 14 days, reached its peak amplitude for the season on 27/09). As the vortex continued to rotate eastwards, the PO disturbance caused marked contour buckling at the outer edge of the vortex at upper levels, enhancing the surf zone signature over the CPO by 01/10. In the process, this PO disturbance weakened somewhat, while the other continued to intensify as it crossed into the CIO by 01/10, causing a weak upper level tongue over AU.

The interaction between these two disturbances and the vortex during early October is particularly noteworthy, and appears reminiscent of the boreal vortex intrusion event studied by Plumb *et al* (1993).

As the pattern rotated eastwards after 01/10 the EPO disturbance retained its intensity as it crossed the AO (see Figure A.1(a)), while that in the IO intensified further, peaking as it reached the AU region by 06/10 (see Figure 5.1(a)). In the process, the A/C associated with each disturbance squeezed (or gouged) the vortex from either side, apparently splitting the vortex core, so that it took on an hour-glass shape by 07/10, with one lobe pushed off the pole toward Africa (AF) at 75^oS 30^oE, the other centred over the EPO Antarctic coast (75^oS 140^oW). This behaviour was evident at all levels above $425K$. At lower levels the major lobe appeared to be that south of AF, while at upper levels most of the vortex material was associated with the EPO lobe, and at all levels a tongue extended from just beyond the edge of the EPO lobe out into the CPO and west over the AU and NZ (ANZ) region.

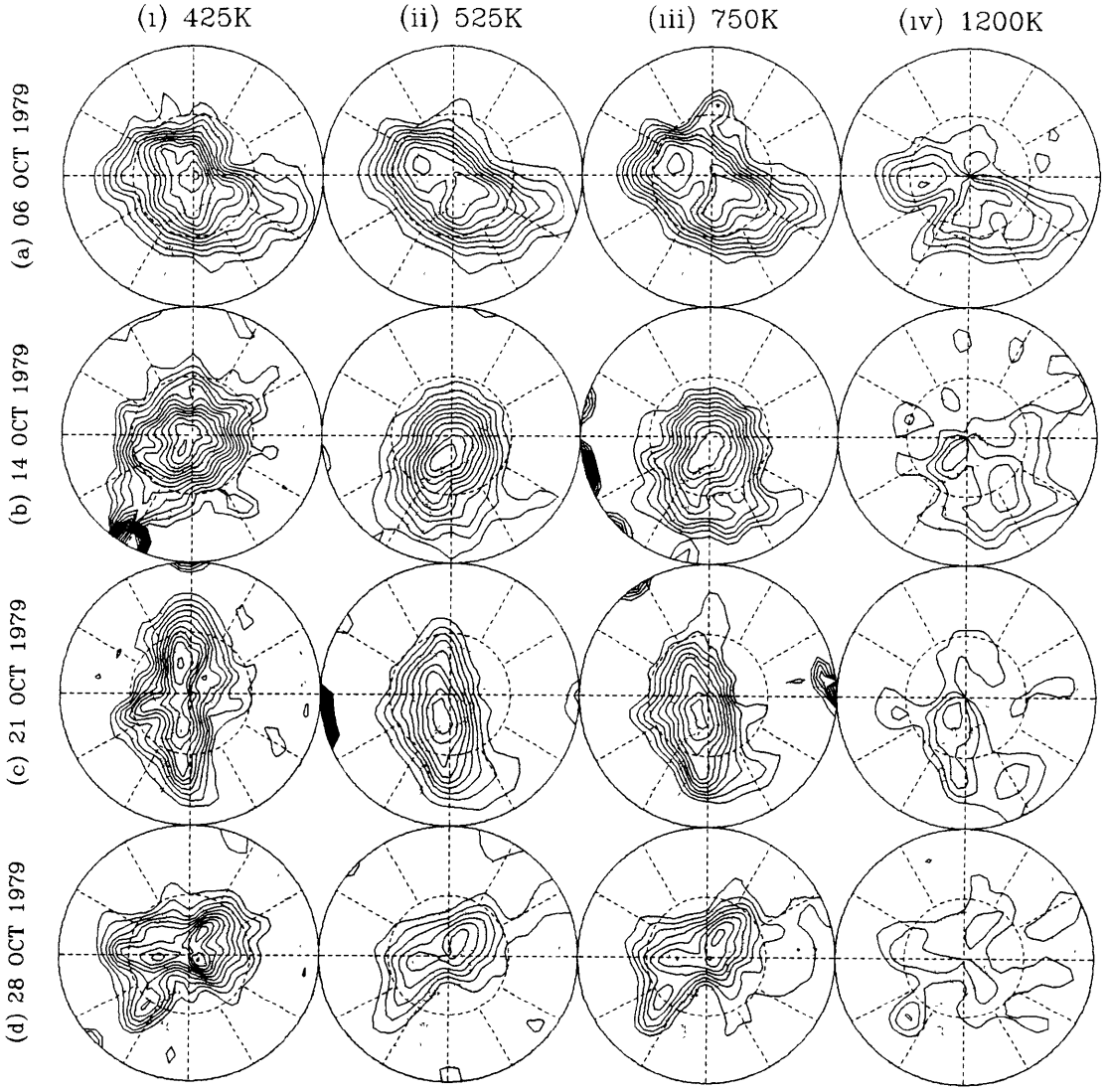

Figure 5.1: Isentropic Analyses of Ertel Potential Vorticity (in PVU) Depicting the Polar Vortex on (a) 06, (b) 14, (c) 21, and (d) 28 October 1979, for (i) $425K$, (ii) $525K$, (iii) $750K$ and (iv) $1200K$ Surfaces. Each plot is a south polar stereographic projection, with Greenwich Meridian at 9 o'clock, outer boundary at $30°S$, inner dashed circle at $60°S$. The lowest contour in each plot broadly represents the fringe of the vortex. Lowest contour value and contour interval for each plot are, respectively, (i) 13 and 2, (ii) 40 and 10, (iii) 150 and 20, and (iv) 1000 and 200 PVU. Large contour gradients at lower latitudes are due to data noise.

During the second week, the AU A/C progressed into the PO, gouging but weakening as it did so and its movement slower at upper levels than lower down so it appeared to develop a marked baroclinic structure. At the same time the AO disturbance reintensified as it migrated more rapidly east across the IO, pinching off the minor vortex lobe at upper levels to form another tongue over AU and NZ by 14/10 (Figure 5.1(b)). At lower levels, on the other hand, the rapid eastward movement of the IO disturbance resulted in the vortex lobes being squeezed together again and pushed toward SAm. The overall result was a strong baroclinic wavenumber 1 signature developing by 14/10 with a tongue extending into the mid-latitudes across the PO, the vortex itself sloping markedly north and west with height at upper levels.

This sequence of events is that examined by Yamazaki and Mechoso (1985), and which brought about the meridional temperature gradient reversal at 10 hPa ($20K$ polar warming between 10/10 and 18/10). Their analyses also support the two stage nature of the process, the wave 2 vortex split prior to 06/10 most evident in their upper level analyses, while the remerger was witnessed by (zonal mean) upper level flow acceleration from 06/10 to 10/10, and the eventual baroclinic W1 development was supported both by the strong upward EP fluxes noted on 14/10 and by their harmonic analysis. Newman (1986) also associates this wave event with the 30 hPa temperature gradient reversal on 14/10.

By 18/10 the PO disturbance crossed into the AO, having weakened markedly as it approached SAm, while that in the IO had intensified slightly as it moved rapidly into the ANZ region, the weakened upper vortex again displaced towards the EPO.

With the vortex at upper levels greatly weakened by this early October wave event, the following five weeks saw the downward progression of the vortex destruction process characteristic of our TT stage.

After 18/10 the AO disturbance again began to reintensify as it continued eastward, the ANZ disturbance weakening only slightly, and the vortex took on a TW2 character, with a more marked tongue being produced over the CPO/NZ by 21/10 under the gouging influence of the NZ/WPO A/C (Figure 5.1(c)). While the EPV

analyses suggest that the low level vortex erosion was confined to the vortex edge region, a marked and rapid decrease in isentropic EPV values at the vortex centre at lower levels between 21/10 and 24/10 indicates that the erosion process may have been more marked, and that lateral mixing may have been occurring on scales beneath the resolution of the analyses. (The implications of a similar occurrence in 1987 will be discussed further in Chapter 7 below.)

This gouging event also brought about the virtual destruction of the $1200K$ vortex remains, most of which were extruded out into the sub-polar and middle latitudes after 21/10, the residue apparently to decay radiatively over the following few weeks. The two disturbance pattern at lower levels then persisted until the end of the month with little change in amplitudes (Figure 5.1(d)).

The late October TW2 pattern collapsed by 01/11 and during the following ten days the greatly weakened vortex at lower levels was subjected to only weak smaller scale disturbances. After further radiative decay, the final destruction sequence occurred dynamically during mid-November. By 10/11 two disturbances had developed and lay over CIO and E/CPO, the former intensifying as it moved eastward, the latter decaying as it reached SAm. As the pattern continued to rotate, the SAm disturbance reintensified as it crossed the AO into the WIO, while the other, having peaked S of AU, remained relatively strong in the CPO. The associated A/Cs began gouging the vortex remains from either side, contorting the vortex into a Z shape by 17/11 (see Figure 5.2(a)), and by 21/11 the vortex above $450K$ had been rather evenly split in two, its remains apparently extruded towards AF and CPO respectively, as polar easterlies set in above $450K$ by 24/11 (see Figure 5.2(b)), the final warming complete.

Overall, then, and keeping in mind of course that there was little in the way of polar ozone depletion, the 1979 season showed only average wave activity, but the final warming was accomplished particularly early, with three wave events of interest from our perspective.

The series of wave events up to the end of September began to erode the vortex at upper levels, but appears to have caused little damage lower down. The first signs of

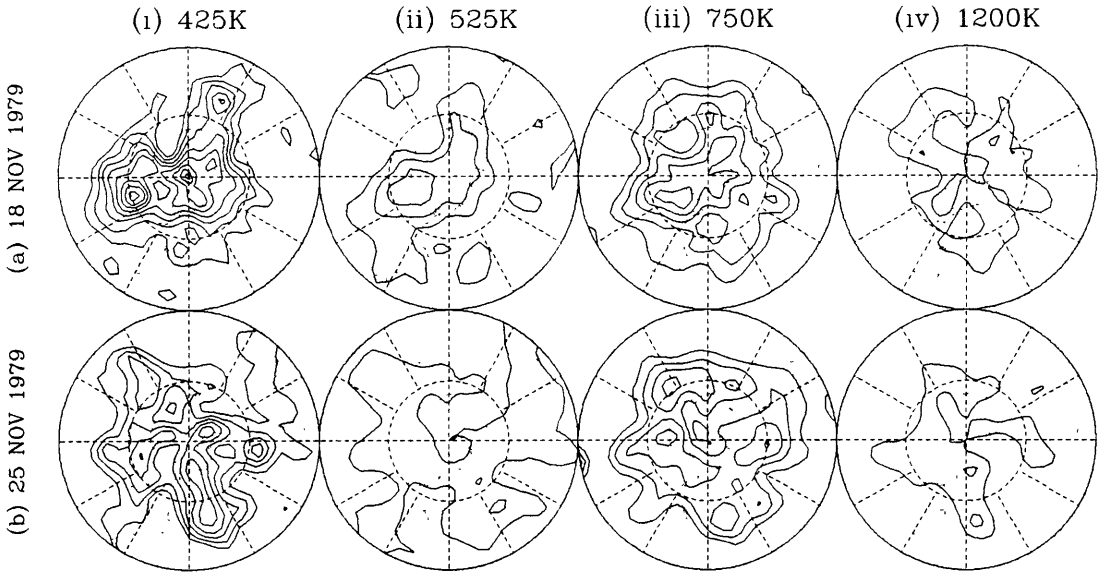

Figure 5.2: As in Figure 5.1, except for (a) 18, and (b) 25 November 1979.

significant low level erosion accompanied the second peak of the large double-peaked wave event of October, which displayed the typical W1/W2 anticorrelated vacillation and brought about the destruction of the vortex remains at upper levels. The EPV analyses suggest significant low level vortex edge erosion occurred by 14/10, in the form of the PO tongue described above. The analyses suggest, however, that this event probably had little effect on the vortex interior. As the October event waned and SW1 gave way to TW2 on 21/10, the analyses suggest that significant low level extrusion of inner vortex material into the Pacific mid-latitudes may have occurred. Finally, a month later, the W2 low level vortex destruction process resulted in the vortex remains being squeezed into the AO/IO and NZ/PO regions between 18/11 and 25/11.

5.2 1980

Although the 1980 winter/spring season has been included in numerous climatological studies of either stratospheric wave activity or the final warming, it has received very little separate attention, other than an examination of the upper stratospheric zonal wind and stationary wave evolution by Hirota *et al* (1983). This is presumably because

the spring stratosphere was cool and dynamically very quiet, coinciding with the westerly phase of the QBO. Like 1979, the present analysis was hampered somewhat by apparently poor quality of the NMC analyses prior to mid-October, the time after which radiosonde data were no longer included in the analysis scheme.

High latitude temperatures in the lower stratosphere were cooler than average, so the polar jet in mid-winter was particularly strong although rather compact. Significant dynamical activity in the spring season commenced late, following the jet shift in early September, with a moderate wave event later in the month. The peak wave event of the season occurred in early October, but with the vortex still strong at its commencement, only weakened the upper level vortex. It was not until another pulse in early November that the upper vortex was essentially destroyed and the polar warming occurred, the lower levels following suit after a last weak wave event in late November. The following discussion is to be read in conjunction with the Hovmoller diagram of Figure A.2(a).

The early winter period up to the end of July displayed little in the way of significant wave activity except for a very marked eastward travelling TW1 event which peaked during early June, and which was the largest event recorded in the pre-August period between 1979 and 1990. This event was one of two closely examined by Farrara *et al* (1992), who noted that the wave displayed equivalent barotropic structure with largest amplitude in the middle stratosphere. It initially amplified as its ridge (in geopotential) crossed the ANZ region, and completed a full rotation about the hemisphere before dissipating at the end of the month.

The LW stage of the 1980 season persisted through the first week of September. A weak amplification of TW1 occurred during early August, the reflection of three unevenly spaced eastward travelling EPV perturbations which each reached maximum intensity over the WPO. Afterwards August was dynamically inactive, the quietest of the eleven years examined.

By 30/08 the vortex displayed a weak baroclinic TW2 structure, with broad regions of low EPV centred over AF and the PO. Then, during the first few days of

September, as the PO perturbation weakened as it approached SAm, the former intensified as it crossed the IO, to peak south of AU at low levels by 06/09. This disturbance amplified rapidly and sloped westward with height, producing a broad upper level tongue over ANZ by 05/09. Randel (1992) shows this event to reach large amplitude at 1 hPa, and it coincides with the rapid poleward/downward shift of the jet in the upper stratosphere.

After 06/09 wave amplitudes began to increase, characteristic of the ES stage. Up to 15/09 the vortex itself generally retained a rather elliptic TW2 shape at all levels, although the EPV analyses suggest this resulted from the sequential amplification and decay of three rapidly moving perturbations (period about 5 days) spread around the hemisphere at low levels. Coinciding with a gradual drift of the vortex centre off the pole towards the AO (increasing the W1 component of the flow), these generally peaked in the NZ/WPO region. By 15/09 the low level vortex had a W3 appearance, with perturbations south of Africa (AF), AU and over the CPO, whereas at upper levels it was W1/W2, the vortex displaced towards the AO and large scale disturbances centred over the EAO and WPO. Associated with the eastward progression and intensification of these disturbances as they crossed the IO, a minor but noteworthy low level wave breaking signature at the outer edge of the vortex was evident at most levels over ANZ between 08/09 and 10/09, with another at low levels over the IO between 10/09 and 12/09.

A disturbance over the C/EIO by 18/09 advanced to the NZ/WPO region by 21/09, apparently producing vortex edge erosion all the way down to $425K$ over the CPO (Figure 5.3(a)). With another disturbance developing over the WIO by this time, the upper level vortex had drifted off the pole towards SAm somewhat, producing a brief W1 peak.

By 24/09 the next disturbance had intensified in the AF region, that over the WIO having migrated rapidly across to the EIO region and weakened, and the WPO disturbance spanned the PO, still producing signs of a tongue at most levels, now over the EPO from the tip of SAm (Figure 5.3(b)). With the dominance of the PO

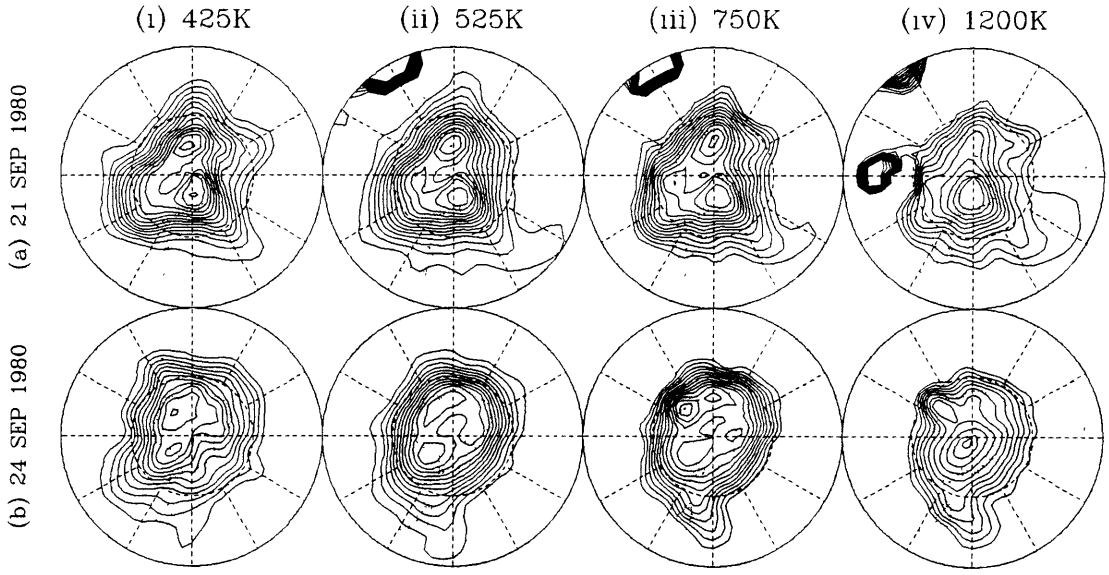

Figure 5.3: As in Figure 5.1, except for (a) 21 and (b) 24 September 1980.

and AO/AF disturbances, the vortex had drifted back towards the pole, weakening the W1 signature and producing a peak in W2.

The following three week period, which contained the largest wave event of the 1980 spring season, might best be described as a mixed ES/LS stage. While it had all the hallmarks of W2 LS-type behaviour, the vortex at the beginning of the event was apparently too strong for the activity to bring about its destruction at upper levels. This wave event involved the typical interaction with the vortex of three or four EPV perturbations continually going through their separate life cycles of growth, development and decay, so that two dominated at any time, the key feature being the relative weakness of the decay stage as one of the perturbations crossed SAm around 08/10.

After 24/09 the perturbation over the PO continued gouging the vortex edge at all levels before weakening rapidly as it crossed SAm. The next significant vortex erosion occurred as the disturbance visible on 24/09 in Figure 5.3(b) in the AF region intensified while crossing the IO, to peak 10 days later over the W/CPO and produce an upper level tongue across the PO between 01/10 and 07/10. Although the erosion process eased, this disturbance did not weaken much as it crossed into the AO around 08/10. By 10/10 the next major perturbation, which began to amplify over the WIO

around 02/10, had intensified rapidly crossing the IO to lie well south of AU and produce a new PO tongue at most levels, while the vortex centre had drifted towards the AO.

The vortex, squeezed between AO and AU perturbations and a third redeveloping south of AF, took on a distinct W2/W3 shape, displaced towards the AO. By 14/10 the upper level circulation was W1/W2 (major lobes near $90°E$ and $90°W$, and vortex centre towards SAm), with significant breaking still occurring from the lobe over SAm/EPO.

After mid-October the behaviour became more typical of the LS stage, and a similar progression brought about all but the final destruction of the upper level vortex. Every three or four days, as each perturbation in turn reached maximum intensity over the NZ/WPO region, it produced wave breaking over ANZ and across the PO, the signature being more marked with increasing height, and occurring earlier (hence further west) at upper levels than lower down, during each event. By 03/11 the vortex at $1200K$ was very weak and displaced towards SAm, surrounded by a ring of low EPV near $60°S$ with an outer ring of higher EPV near $45°S$. Hirota *et al* (1983) show that the 1 hPa circulation became easterly everywhere at this time.

With the vortex at upper levels all but destroyed by 03/11, the TT stage commenced. By 07/11, perturbations in the WPO and AO/AF regions at upper levels had distended the upper vortex remains into a pole-centred Z shape, with erosion from lobes south of AF, and over the EPO. As the pattern rotated the AO disturbance spiralled in towards the pole as it progressed eastward (bringing about the temperature gradient reversal at 30 hPa), to be south of ANZ (at $70°S$) on 11/11 from where it moved SE onto the pole, the upper vortex destruction essentially complete above $1000K$ by 15/11. At lower levels this was seen as a continuing erosion process by three or four disturbances tending to peak in the ANZ region, so the vortex was gradually displaced further towards SAm as the period progressed.

A broad perturbation over the EIO on 15/11 amplified as it moved SE into the ANZ region by 19/11, distorting the vortex into a W2 pattern, displaced towards

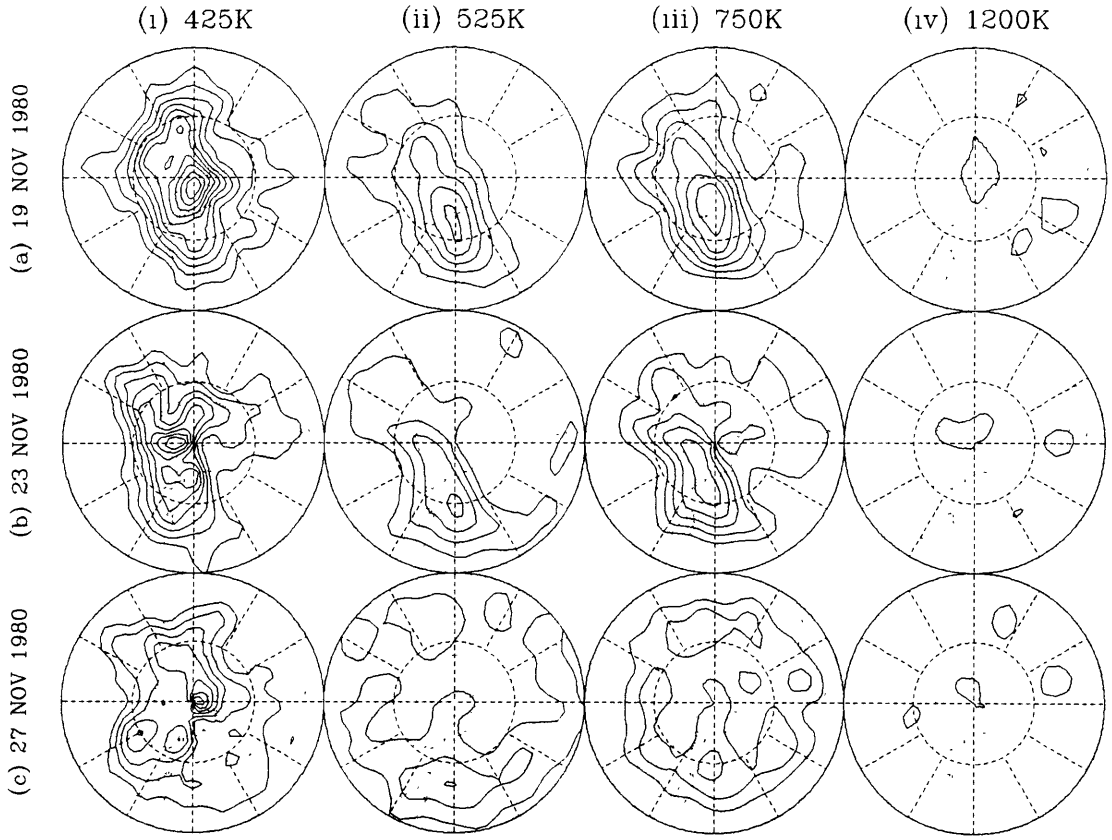

Figure 5.4: As in Figure 5.1, except for (a) 19, (b) 23, and (c) 27 November 1980.

SAm, and producing a weak tongue over the WPO/ANZ region (Figure 5.4(a)). This distortion resulted in the vortex destruction down to $850K$, as evidenced by the flow reversal at 10 hPa shown by O'Neill and Pope (1990). This broad disturbance and another over the AO then grossly distorted the vortex remains (Figure 5.4(b)) by 23/11 (bringing about the 30 hPa wind reversal), and merged over the pole at levels above $450K$ by 25/11, with the bulk of the vortex pushed into the AO/PO near $90°W$, while a smaller lobe was extruded into the CIO (Figure 5.4(c)), the residue subsequently to decay radiatively and be sheared out in the mid-latitude flow.

The character of the vortex erosion process in 1980 was quite different from that seen in 1979. In 1979 there appeared to be virtually no low level erosion until the TT stage in late October, during which the low level circulation was essentially destroyed by just two wave events. In 1980 on the other hand, the picture presented by the EPV analyses suggests a much more gradual weakening process, comprising a series

of minor erosion events starting in early September, but apparently with no extrusion of inner vortex material at low levels before the final wave event in late November, which destroyed the low level vortex and deposited its remains in sub-polar and middle latitudes. This series of minor wave breaking events occurred around 09/09 (ANZ), 11/09 (IO), 22/09 (PO), 11/10 (EPO), 22/10 (EPO), 26/10 (SAm), 03/11 (SAm), 07/11 (EPO), 11/11 (CPO) and 15/11 (WPO), culminating in the final low level vortex destruction between 19/11 and 27/11, most of the vortex debris being ejected initially into the AO/PO region, but with a lesser remnant perhaps ending up over the IO.

5.3 1981

Several authors have examined different aspects of the 1981 season. Hirota *et al*(1983) analysed the 1 hPa evolution of the geostrophic wind distribution and stationary wave 1 and 2 amplitudes. Shiotani and Hirota (1985) reexamined the evolution of the upper stratospheric wind field and analysed EP flux behaviour (total, W1 and W2) during the season, and O'Neil and Pope (1990) briefly examined the evolution of the 10 hPa wind field and the 850K EPV distribution. In many respects 1981 was a very average and unremarkable year and coincided with the easterly phase of the QBO.

Two features were noteworthy, however. The first of these is the observed dominance of stationary wave 2 for a brief period during early August. The second was the nature of the upper level vortex erosion process, with no clearly identifiable LS stage. Only two major wave events occurred during the season, one in late September and a lesser event in early October. Had the first occurred a few weeks later it may have been strong enough and the vortex already weak enough to bring about rapid destruction at upper levels. Instead it merely served to weaken the vortex somewhat. The second event, while showing signs of impending upper level destruction, appears to have collapsed just before rapid destruction may have resulted. Examination of the analyses suggests that this latter event may have produced greater erosion of the

vortex at lower levels than aloft. It was a relatively small wave event in November which finally destroyed the upper level vortex, further weakening the low level circulation, and just a few weeks later the already greatly weakened low level vortex was destroyed. The following discussion is to be read in conjunction with Figure A.3(a).

The early winter period displayed about average wave activity, starting with a weak burst at the beginning of April, followed by the two largest events of the period in late April and early May, before tapering off with two minor events centred on early June and early July, each being dominated by the W1 component.

The early August period, typical of the LW stage, saw three perturbations travelling around the hemisphere, the only noteworthy feature of the overall pattern being that, rather than amplification in the ANZ region, there was a tendency for the disturbances to amplify as they cross the AU region, then decay before amplifying again as they cross the AO, i.e. the dominant forcing was SW2 rather than SW1. On virtually all other occasions between 1979 and 1988 (no information was available for 1989) when W2 amplitude exceeded that of W1 for periods of more than a few days, W2 was travelling.

Otherwise, the early August behaviour was typical of the LW stage, culminating by 15/08 with two of the three disturbances intensifying almost simultaneously, one south of AF and the other in the ANZ region, both amplifying rapidly and sloping westward with height to produce a strong upper level wave breaking signature over the IO, and another, not so strong, over the CPO region. This event coincided with the jet shift discussed by Shiotani and Hirota (1985), who noted that W2 EP fluxes (which accounted for the bulk of the total flux) pointed strongly upward in the mid-latitude stratosphere at the time, the region of upward pointing flux vectors apparently propagating upward from the lower stratosphere between 12/08 and 15/08 (see their Figure 6), suggesting a low level source, and producing the familiar flux divergence dipole. Our observation of the uniqueness of the event with respect to SW2 forcing (which indicates direct low level forcing, consistent with Shiotani and Hirota's EP flux behaviour) suggests caution in interpreting the observed behaviour

as typical.

Overall wave amplitudes, particularly W1, tended to increase after the above event, signalling the start of the ES stage. While the 'three disturbance' behaviour continued, the tendency for the disturbances to amplify near AF diminished. Another upper level wave breaking pattern was evident on 27/08, with a tongue extending across the CPO to NZ, the upper level vortex distorted into a marked W2 shape, and displaced somewhat towards the AO. The next significant but short-lived upper level wave breaking event occurred after 08/09, and involved erosion of the vortex edge by a disturbance in the EPO, to produce a tongue over SAm and across the PO, with contour buckling occurring down to $475K$, but only involving contours beyond the vortex boundary at the lower levels.

After 11/09, the preferred intensification region switched quite rapidly back to a more normal location in the EIO (note the rapid phase shift reflected in the Hovmoller diagram of Figure A.3(a)). The familiar cyclic behaviour of three or four perturbations producing vacillations between W1, W2 and W3 set in, persisting until the end of October. Whereas the harmonic composition of the pattern shows the typical W1/W2 vacillations, the occurrence and frequency of minor wave breaking events appeared once again to be largely determined by the locations of the smaller scale disturbances.

O'Neill and Pope (1990) claim that this period showed the same characteristics as the 1982 season, September featuring travelling A/Cs, one of which became quasi-stationary and grew in place at the beginning of October, lasting until the end of the month (the MOPF evolution). The present analysis supports the presence during October 1982 of a persistent (slow-moving) A/C, which, as noted in Section 4.4 above and discussed further in the following Section, we view as the result of continued cyclic amplification and replacement of EPV perturbations. For October 1981, however, the present analysis strongly suggests the pattern was considerably more mobile, contrary to O'Neill and Pope's claim.

By 17/09 the vortex had taken on a marked W2 pattern at upper levels (W3 lower down), with contour buckling beyond the vortex edge to the east of a rather baro-

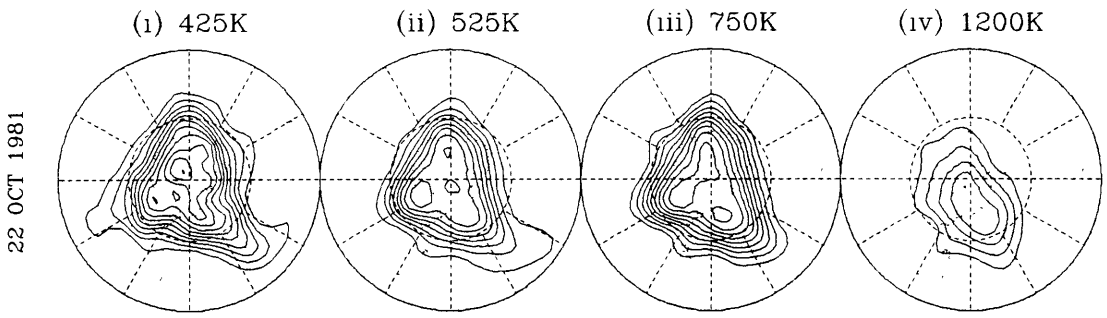

Figure 5.5: As in Figure 5.1, except for 22 October 1981.

clinic disturbance in the CIO/AF region. This event was associated by Shiotani and Hirota (1985) with strong upward pointing EP flux vectors in the lower stratosphere. After 17/09 the IO disturbance lost its baroclinic structure, the upper level perturbation apparently travelling more rapidly eastwards than at lower levels, and weakened somewhat over the WPO as the next perturbation intensified rapidly in the CIO, the vortex being displaced markedly toward the CPO by 24/09, with wave breaking commencing over AU from the edge of the upper level vortex. As the lobe moved over NZ by 27/09, the breaking signature extended downwards, then weakened as the lobe crossed the WPO. Renewed breaking then occurred as the next perturbation arrived in the PO by 06/10. By 10/10 the vortex at upper levels had weakened and shrunk and was displaced towards the EPO, with a surf zone extending westwards from the WPO to AF.

After 10/10 the vortex once again took on a W2 shape with a disturbance intensifying over the AO and another in the NZ region, the A/C associated with this latter disturbance renewing the wave breaking process and beginning to produce contour buckling at upper levels over the CPO on 14/10. Rapid EPV relaxation at the $1200K$ vortex core suggests this may have been more marked than the analyses suggest. This event was short-lived and by 18/10 the vortex was again rather axisymmetric at upper levels, although displaced towards the EPO, while at lower levels there was more evidence of weak erosion at the edge over the AO and IO.

The same process was repeated over the following eight days, this time the most marked contour buckling signature clearly visible at the lowest levels over the CPO

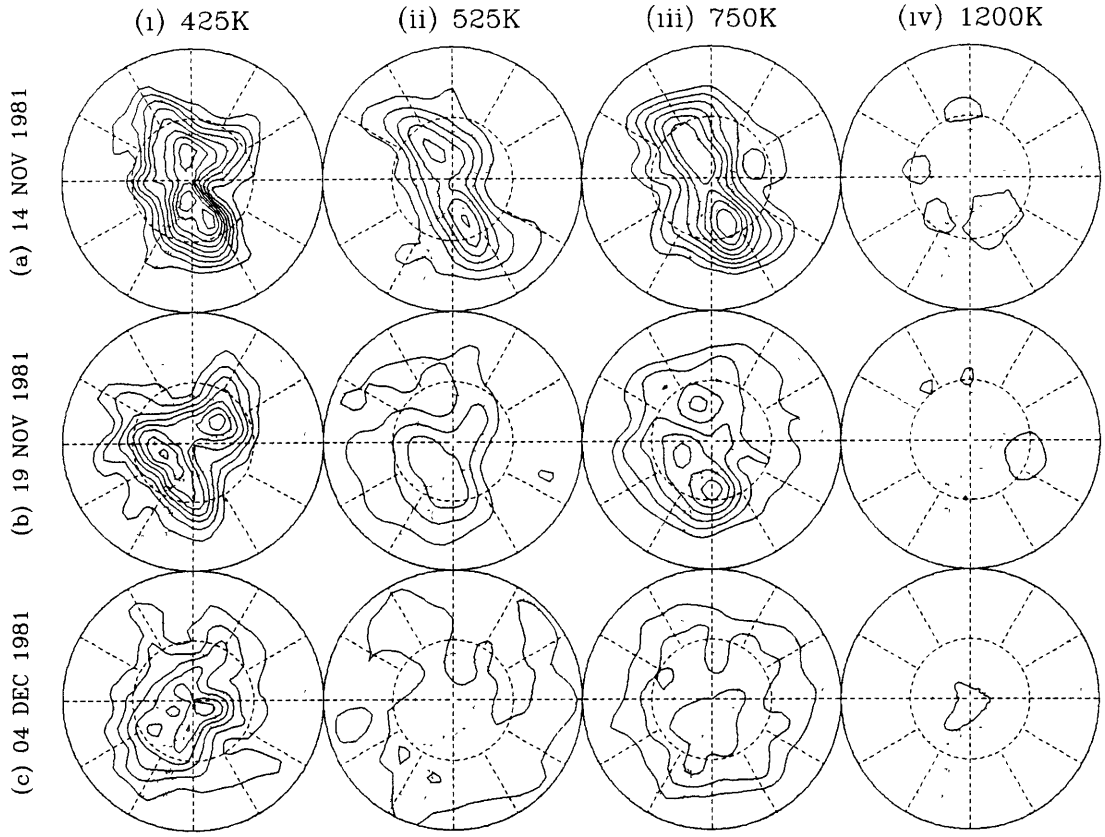

Figure 5.6: As in Figure 5.1, except for (a) 14 and (b) 19 November, and (c) 04 December 1981.

(see Figure 5.5). By 26/10 the vortex was back on the pole and weak but essentially axisymmetric at upper levels, remaining so until 30/10, by which time the high latitude temperature gradient reversal had reached down to 10 hPa (Mechoso, 1990). It is of note that this latter marked wave breaking event, although relatively short-lived, occurred well after the peak W1 amplitude, reinforcing the impression gained from the present analysis that it may not be so much W1 amplitude alone which determines the degree of vortex erosion in the southern hemisphere stratosphere, but a combination of W1 and the shorter scale (W2/W3) travelling disturbances.

After the gradual weakening of the upper level vortex during September and October, the upper level temperature gradient reversal signalled the start of our TT stage. Yet another cyclic episode occurred after 30/10, this time the effect being greatest aloft, where a disturbance gouged a tongue from the weak vortex remains

out over the E/CPO by 09/11. After this a disturbance in the IO intensified and pushed SE to the S of NZ, moving onto the pole at $1200K$ to complete the drawn out seasonal transition there, the vortex remains above $900K$ drifting into the AO/EPO region, while at lower levels the greatly weakened vortex was pinched between the NZ disturbance and another intensifying in the AO, and split into a pole-centred hour glass shape by 14/11 (Figure 5.6(a)).

After 14/11 the AO disturbance moved rapidly ESE into the IO, extruding a tongue of high EPV into the IO at low levels, while squeezing the bulk of the vortex remains towards the SAm/AO by 19/11 (Figure 5.6(b)). Over the following two weeks the pattern drifted eastward around the hemisphere, being sheared out and decaying in the process, the bulk to be in the SAm region by 04/12 (Figure 5.6(c)). Notably, a period of only a few weeks had separated the upper level vortex destruction from the breakdown at lower levels.

This overall evolution in 1981, then, was rather average, apart from the occurrence of the largest wave event of the season during September rather than October. Because of the early peak in wave activity, there was essentially no LS stage to the evolution, and only a brief period between upper and lower level circulation reversal. In regard to potential ozone dilution events, despite a number of apparent instances of low level erosion of the vortex edge (e.g. 27/09 (ANZ), 06/10 (AF), 18/10 (AO, IO)) there was little indication of significant erosion from within the vortex at low levels until the final vortex destruction process during and after mid-November. The only likely exception may have been the breaking event centred on 22-26/10 over the C/EPO.

5.4 1982

The 1982 season has been examined by many authors. Among these Mechoso and Farrara (1986), Mechoso *et al* (1988) and Mechoso (1990) all focussed on the 1982 evolution in climatological studies of the final warming in the middle/upper strato-

sphere, and Yamazaki (1987) examined the 1982 season in a comparative study of the observed evolution in each hemisphere. Manney *et al* (1991) closely examined TW2 during 1982 in their analysis of the behaviour of TW2 in the southern hemisphere. Although dynamically rather quiet in the early winter period, polar temperatures were rather warm during September for a season in which the QBO was in its westerly phase, and very warm in October, consistent with the occurrence of one of the largest wave events of the decade. The following discussion is to be read in conjunction with Figure A.4(a).

The early winter period was dynamically quiet, with almost negligible wave activity in April, a small event in May and another at the beginning of July. The latter event, which produced significant wave amplitude at 1 hPa, was followed by the poleward/downward shift of the jet.

After the early jet shift, a brief but relatively large amplitude TW2 event occurred at the beginning of August (which Manney *et al* (1991) found to be coherent between troposphere and stratosphere), followed by a W1/W2 event in the middle of the month. Despite this, the EPV analyses suggest that August was more typical of the LW stage than ES stage, and little was evident in the way of Rossby wave breaking before September.

September comprised the ES stage, in which the behaviour was characterised by three EPV disturbances rather evenly distributed about the hemisphere during the month, as evidenced by relatively large TW3 power at $60^{o}S$ (see Figure A.4(a)). Although the first few weeks of the month involved the familiar sequential amplification and decay of disturbances as they travelled across the IO and PO, little was evident in the way of contour buckling at the vortex edge other than at the highest analysis levels.

By 18/09 eastward travelling disturbances were present in the AO and ANZ regions at upper levels, and the vortex had a marked W2 appearance, with erosion from its outer edge occurring at upper levels. As the pattern progressed, the ANZ disturbance continued to intensify, and by 22/09 the vortex at upper levels was deformed into a

crescent shape with marked gouging by the A/C associated with the PO disturbance and a tongue evident at most levels over the EPO. The PO disturbance then weakened rapidly while amplification took place in the EIO, this disturbance moving into the AU region accompanied by a movement of the upper level vortex off the pole towards SAm by 26/09. As the disturbance subsequently moved into the PO, producing upper level erosion of the vortex edge as it went and the vortex moving further towards the EAO, another disturbance began to intensify in the WIO by 30/09.

The first three weeks of October displayed exemplary LS stage behaviour. As described in Section 4.4 above, the progression involved the cyclic intensification of disturbances as they tracked from the WIO into the ANZ region, then decelerated as they tracked further east, gouging vortex edge material out in the PO mid-latitudes, before being replaced by the next intensifying disturbance. In this manner the vortex was kept displaced from the pole towards SAm/AO and rapid weakening occurred at upper levels towards the end of the month.

The PO disturbance decayed after 30/09 as it approached SAm, while the IO disturbance amplified further as it crossed rapidly into the PO region by 05/10, having caused upper level vortex edge erosion over ANZ/WPO prior to this. It in turn decayed, to be immediately followed by yet another which tracked rapidly into the CPO to renew the gouging process by 09/10. With the redevelopment of a disturbance in the AO by this stage the vortex was distorted into a wave 2 shape displaced toward the EAO. As the PO A/C continued to gouge the vortex, a significant portion of the upper level vortex was apparently extruded into the mid-latitude EPO by 14/10, the erosion process extending down to $475K$ by this stage. After 14/10 the erosion eased somewhat as the PO disturbance moved east and weakened. The next ten days then saw a succession of smaller scale disturbances amplify in turn in the IO and track rapidly east, causing upper level vortex edge erosion over the ANZ region, to reach maximum amplitude in the PO before decaying, the series of events keeping the vortex displaced towards the AO. Eventually, with the upper level vortex considerably weakened, one of these disturbances pushed in towards the pole south

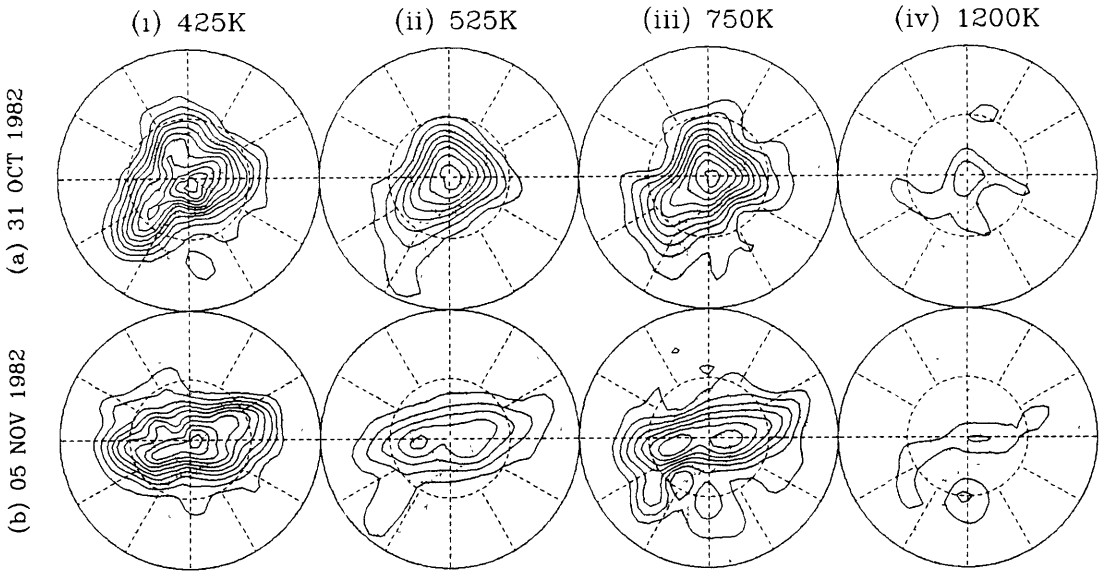

Figure 5.7: As in Figure 5.1, except for (a) 31 October, and (b) 05 November 1982.

of NZ after 19/10, producing dramatic erosion of the vortex at upper levels, with a weaker signature at lower levels over the ANZ region.

After 23/10 and the effective destruction of the upper level vortex, which brought about the start of the TT stage, the low level vortex (and the upper level remains) gradually moved back over the pole. The NZ disturbance continued gouging as it moved eastwards, producing a tongue out over SAm/EPO by 26/10. This process was repeated by the next travelling across the PO, which produced another tongue over SAm/PO by 30/10 (see Figure 5.7(a)). At this stage, as the PO disturbance weakened, those over the AU and AF regions on 31/10 amplified together, the former moving rapidly into the PO, and the two together squeezing the vortex into a Z shape, with lobes south of NZ and in the CAO by 05/11 (Figure 5.7(b)), and with further wave breaking signs from each lobe on 06/11. As the vortex rotated, a three disturbance pattern re-emerged, each producing more vortex erosion at the lowest levels by 15/11 (Figure 5.8(a)). Subsequently the vortex appeared from the analyses to rotate rather passively under the influence of these three disturbances, maintaining a convoluted W3 shape (Figure 5.8(b)) until the majority of the remnants was squeezed out into the PO/AO region during the first weeks of December (Figure 5.8(c)).

Overall, 1982 was in many respects similar to 1979. Although generally quieter in

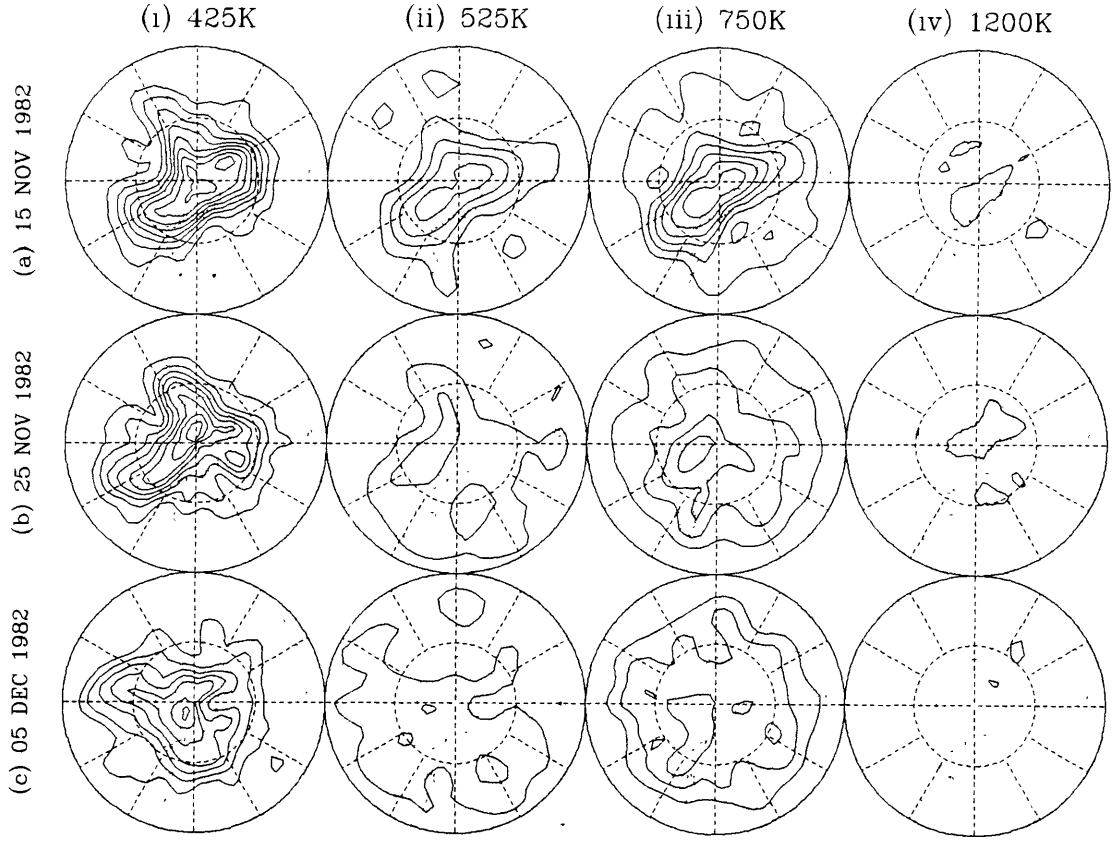

Figure 5.8: As in Figure 5.1, except for (a) 15 and (b) 25 November, and (c) 05 December 1982.

the early winter it showed the same monotonic increase in 10 hPa wave amplitudes leading up to a major wave event in October, which brought about the virtual destruction of the vortex at upper levels, before much erosion had occurred at low levels. Although signs of low level vortex edge erosion were evident during late September (22-26/09 (EPO) and October (14/10 (SAm/EPO), 23-31/10 (ANZ/SAm)), it was not until November that the low level vortex was rapidly weakened by a marked wave breaking event (05/11). Then, after a relative lull, the bulk of the vortex remains was pushed into the AO/PO mid-latitudes during early December.

5.5 1983

The only previous analysis focussing on the 1983 season was that of Shiotani *et al* (1990), who closely examined the prominent behaviour of TW2 during the season. With the QBO in its westerly phase, the polar spring stratosphere was generally rather cool, the overall spring dynamical activity about average. The prominent behaviour of TW2, with a quite regular period of around 9 days (Shiotani *et al*, 1990) was brought about, after a rather slow start to seasonal wave activity, by the most striking and regular cyclic behaviour of EPV perturbations (generally 3) seen in the eleven years examined. Shiotani *et al* noted that after its poleward/downward shift, the jet was unusually strong and narrow, and they speculate that the resulting large curvature on its flanks may have been responsible, via an instability mechanism, for enhancing subsequent TW2 amplitudes. The following description is to be read in conjunction with Figure A.5(a).

The early winter period was rather quiet, like 1982, with negligible wave activity until late May, which saw a small and primarily W1 event, followed by two more small brief bursts in late June and early July, then a moderate event in late July.

After the late July event, early August was quiet in the lower and middle stratosphere, typical of the LW stage. During the period, however, a small wave event, involving a W1/W2 vacillation, amplified rapidly with height at upper levels, and by about 25/08 the upper jet shift was complete. (The jet movement commenced in late July with the former wave event, after which it was rather slow and gradual, ending with the mid-August event.)

The last week of August and first week of September saw the transition to the ES stage, during which gradually increasing perturbation amplitudes, with preferential amplification in the IO/AU region, led to two cycles of the typical anticorrelated vacillation of W2 and W1.

After the first week of September preferential amplification in the IO/AU region diminished rapidly (the W1 component collapsed), and there was a brief period of

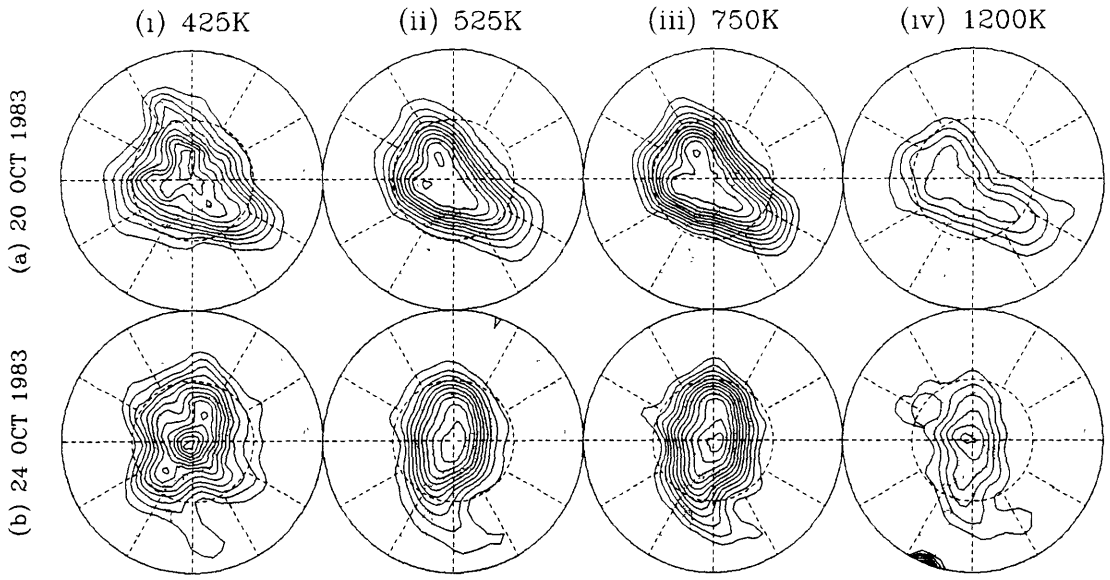

Figure 5.9: As in Figure 5.1, except for (a) 20 and (b) 24 October 1983.

primarily TW3 behaviour at lower and middle levels from 10/09 to 15/09, seen in the analyses as two larger scale perturbations at low levels over the AF and ANZ regions, and a third smaller scale disturbance over SAm/EPO). After 15/09 the smaller scale feature, moving more rapidly then the others, apparently merged with that to its east, and marked contour buckling at and beyond the vortex edge occurred at upper levels over the EPO/WAO region around 18/09 and 26/09 in association with two marked peaks in TW2, the latter event extending down to $425K$.

After 26/09 the PO disturbance to the west of the breaking lobe weakened markedly as it approached SAm, while the other amplified as it approached the ANZ region, the vortex at most levels being displaced from the pole towards the AO/AF region by 04/10. This disturbance, in turn, weakened as it crossed the PO while the other again began to intensify as it passed south of AF on 04/10, the vortex completing its elliptic excursion by moving back onto the pole temporarily, before perfoming another under the influence of the newly intensified disturbance, which lay over the EIO by 08/10. Strengthening further, this disturbance began to produce significant vortex edge erosion as it moved into the PO by 12/10, while the vortex was displaced substantially towards the EAO at all levels, weakening rapidly aloft.

The following three weeks saw a W2 LS stage, with two more TW2 cycles which

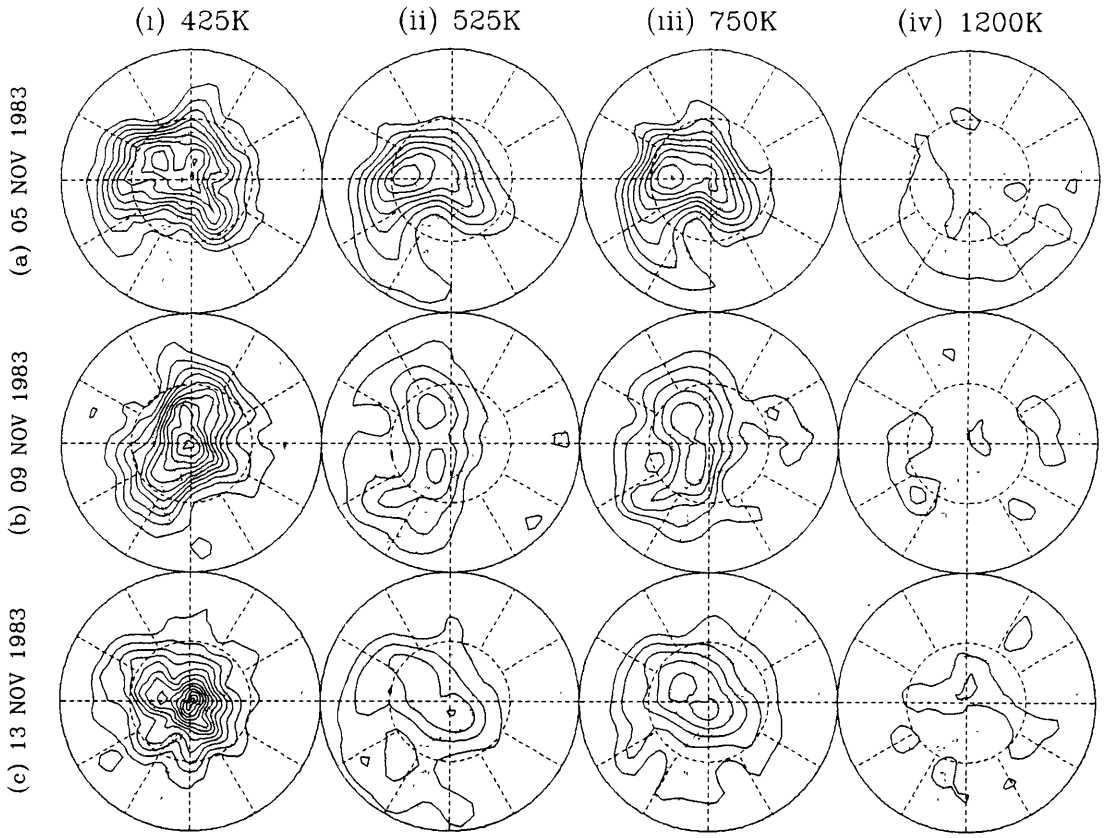

Figure 5.10: As in Figure 5.1, except for (a) 05, (b) 09 and (c) 13 November 1983.

brought about all but the final destruction of the upper level vortex.

After 12/10, while the AO disturbance intensified as it crossed AF, the PO disturbance remained strong, and by 16/10 upper level vortex erosion was occurring from the AO lobe. The upper level erosion process became more marked and began to involve both lobes over the next two weeks as the TW2 pattern rotated, with the lobe in the PO being eroded more severely at any time, and the erosion process extending downward with time, culminating in a marked event over the EPO between 20/10 and 24/10 (see Figure 5.9). By 01/11 the vortex at upper levels had been displaced towards the EPO and all but destroyed, the small core being surrounded by an extensive surf zone. With the high latitude meridional temperature gradient reversal occurring on 31/10 at 30 hPa (Newman, 1986), the evolution entered the TT stage.

After 01/11 the disturbance over the WPO/NZ continued eastward while maintaining its intensity, and caused spectacular erosion at all levels, extruding a marked

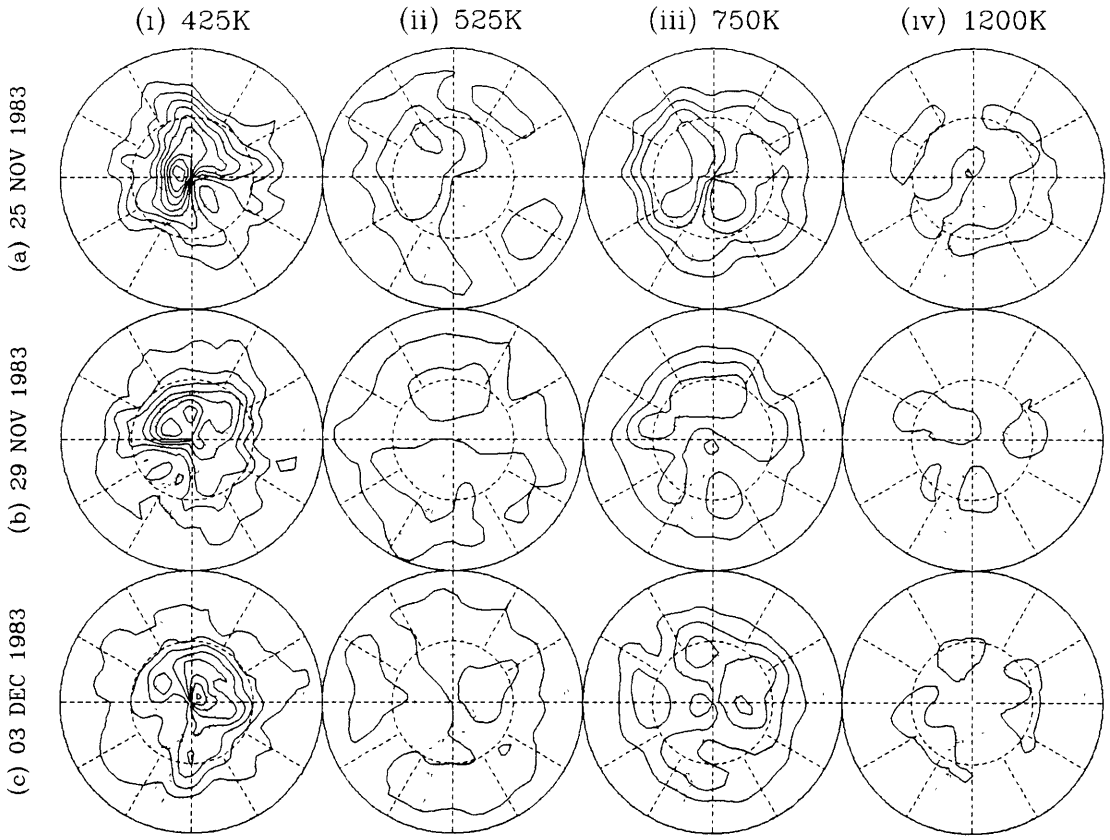

Figure 5.11: As in Figure 5.1, except for (a) 25 and (b) 29 November, and (c) 03 December 1983.

tongue into the AO/SAm/EPO region and shearing out the vortex remains above $900K$, to occupy the pole at upper levels by 05/11 (Figure 5.10(a)). While the lower level analyses suggest once again that the erosion process only involved material from the vortex edge region, a rapid decrease in EPV values at the vortex core accompanying this event suggests extrusion and mixing from within the vortex core. After 05/11 the A/C associated with this process weakened rapidly over WAO, while the next disturbance, over the CPO by 09/11 (Figure 5.10(b)), renewed the low level erosion process as it progressed across the PO/SAm region, to begin to weaken in turn as it crossed the AO on 13/11 (Figure 5.10(c)). This was followed by a weak repetition of the process around 17/11, then a brief lull before a final wave event gently pushed the still relatively substantial remains of the vortex below $800K$ off the pole towards the AO/AF region by 25/11 (Figure 5.11(a)), to be sheared out and radiatively decay over the following weeks (Figure 5.11(b) and (c)). Notably, this final push appears

to have affected all levels down to $425K$, an unusually deep breakup.

Overall, then, the remarkable prevalence and persistence of TW2 throughout the spring season appears to have brought about a relatively slow weakening of the vortex at upper levels, but relatively rapid weakening lower down. While three weeks separated the upper from lower level destruction process, the impression gained from the EPV analyses is that, were it not for the mid-November lull in wave activity, the low level circulation might have followed the upper level demise much sooner. The general picture which emerges from the present analysis is one in which large SW1 events, in which TW2 is present but plays a secondary role, cause the most rapid erosion at upper levels but not so much lower down, whereas large amplitudes of smaller scale disturbances in the presence of only moderate SW1 tends to do as much damage lower down as aloft.

With respect to potential for ozone dilution, the first significant low level wave breaking event, which occurred around 26/09 (EPO), appears to have affected only the vortex edge region. However, the more marked event peaking around 24/10 (EPO) has some potential for extrusion of ozone hole material into mid-latitudes, as has the 05/11 event (EPO/AO) and perhaps that leading up to 13/11 (AO). The final vortex destruction process during late November saw the vortex remains pushed towards the AO/AF region, apparently to drift slowly eastward over the next few weeks. In view of the appreciable ozone hole in 1983, it appears quite likely that this process may have produced a noticeable ozone dilution effect.

5.6 1984

The seasonal evolution in 1984 has not previously been considered in isolation. Although the QBO was in its easterly phase, the polar winter/spring stratosphere showed only average temperatures and overall wave activity. A noteworthy feature was the relative uniformity of the level of wave activity throughout the season, the early winter period being almost as active as the spring period and weak but signifi-

cant activity persisting through mid-winter. Another peculiarity was that, like 1981, the largest event of the spring season was a mixed W1/W2 event which occurred in early September while the vortex was still strong, with no clearly dominating event thereafter. The present analysis suggests that this September event might be better described as two closely separated periods of MOPF W1 October type behaviour (LS stage), the first occurring in late August, the second in the first three weeks of September (see Figure A.6(a)), after which the behaviour reverted to that more characteristic of the MOPF September period (ES stage). Like 1981 there was therefore no rapid vortex erosion period; rather the vortex destruction was more gradual and continuous throughout. Also similar to the 1981 season but more pronounced, after initial weakening of the upper vortex during September, the essentially W2 decay process appeared to occur at a similar rate at all levels, the final breakup occurring gradually throughout the lower and middle stratosphere by mid-December. The following discussion is to be read in conjunction with Figure A.6(a).

As suggested above, the early winter period in 1984 was particularly active, significant wave activity commencing at the beginning of May and persisting throughout the season, with a moderate pulse at the end of May (SW1) and then a large event which grew after mid-June to a marked peak (mixed W1/W2) at the beginning of July. Oddly enough, despite the large wave event at 10 hPa, its signature at 1 hPa was rather weak, and it was well afterwards, during the latter half of July, which saw a period of anti-correlated vacillation between relatively weak W1/W2 amplitudes, that the poleward/downward shift of the jet occurred.

With the jet shift having occurred by the end of July, wave amplitudes after the first week of August already showed the characteristics of ES Stage behaviour, a minor upper level wave breaking signature present by 10/08 over SAm, and another over the EAO by 20/08, with larger scale EPV perturbations over the WAO and NZ regions and a smaller one in the IO.

As noted above, the four week period after 20/08 was best described as two brief periods of LS stage behaviour, the IO disturbance amplifying rapidly as it crossed

into the AU region, while the others weakened, then it in turn weakened over the PO while the next amplified in the IO to take its place as the dominant disturbance. The overall result was a MOPF October type quasi-stationary A/C over the AU region at upper levels, although it lasted only until the end of the month. Weak erosion from the edge of the upper level vortex was evident over AU around 28/08. This first period was then rapidly followed by another of the same type of behaviour.

The mobile disturbance which produced the AU erosion, unlike its two predecessors, retained its intensity as it moved into the WPO by 03/09. At the same time a second disturbance had begun to amplify over the AO by 03/09, causing marked upper level erosion over the AF region, and continued to amplify as it crossed the IO, while the PO disturbance eventually weakened somewhat over the EPO. By 12/09 the IO disturbance had reached the AU region, and continuing eastwards began to weaken in the PO after 18/09. As it did so, the next amplified in the IO and travelled rapidly eastward to the AU region, where it in turn decelerated and commenced the upper level gouging process by 25/09. By this stage a third but smaller disturbance had amplified crossing the IO, and moving more rapidly east than the former, began to produce contour buckling near the vortex edge at the lowest levels over AU, while that to the east continued upper level vortex erosion over the CPO, accompanied by a displacement of the vortex towards the WAO by 28/09.

By 28/09 the next disturbance had begun to amplify in the AO. At the same time the leading disturbance in the EPO began to weaken while that to its west took over, moving into the PO by 03/10, by which stage the temperature gradient reversal had occurred at 10 hPa. After 03/10 the PO disturbance weakened, while the next intensified rapidly as it moved eastwards into the WPO, producing marked upper level vortex erosion by 07/10, and extruding a large tongue of inner vortex material out over the PO region, accompanied by a displacement of the upper level vortex remains towards the AO. This disturbance weakened thereafter, while another amplified as it crossed the IO to AU, beginning to produce low level erosion over ANZ by 11/10 and

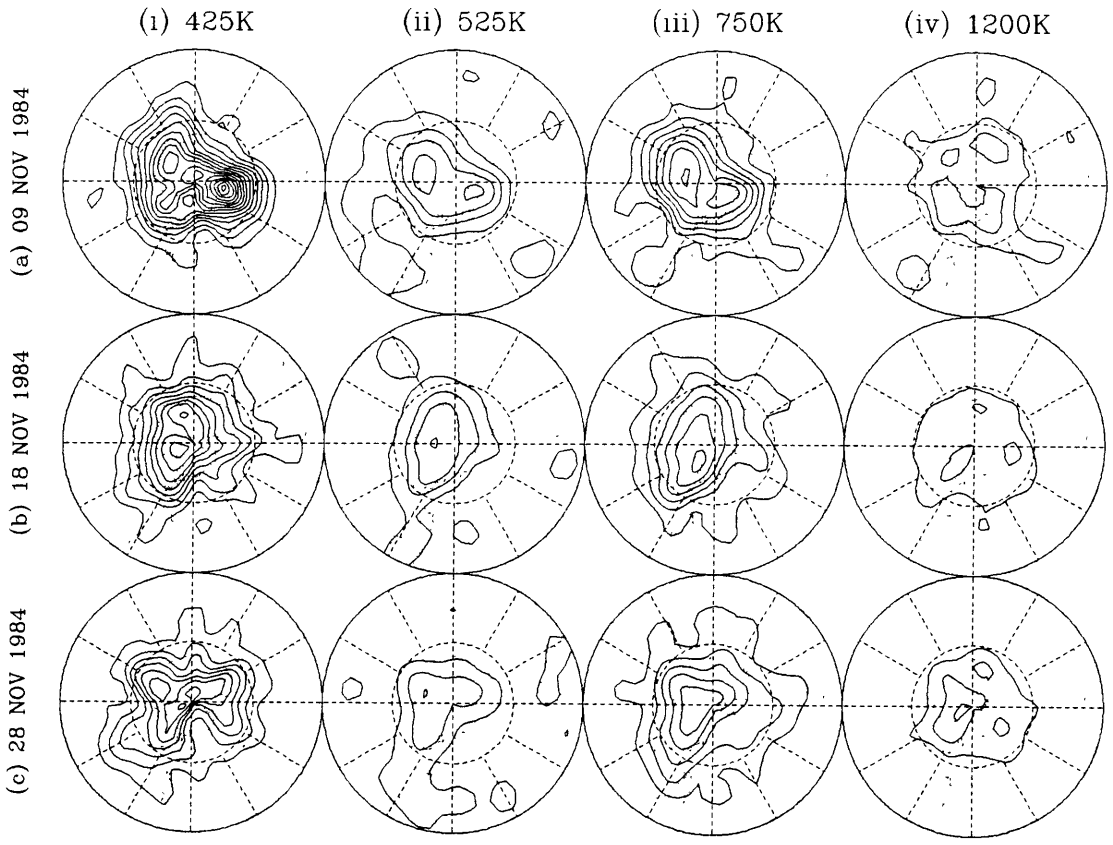

Figure 5.12: As in Figure 5.1, except for (a) 09, (b) 18 and (c) 28 November 1984.

minor erosion at all levels as it crossed into the EPO by 15/10, by which time the next disturbance had amplified south of AF.

This three disturbance cyclic behaviour continued for the rest of the month, no individual disturbance growing to produce a devastating effect on the vortex, but each in turn producing apparent minor erosion from the vortex edge at most levels. In this manner, by the end of the month the temperature gradient reversal had reached down to 30 hPa, and the vortex had been greatly weakened at all levels, rather than primarily at the upper levels, so it retained a much weakened but still cylindrical structure, as opposed to the climatological conical shape displayed by late October.

The beginning of November essentially brought about an ill-defined commencement to the TT stage. The rather gentle dynamical erosion process characteristic of the preceding four weeks continued into November, wave amplitudes steadily decreasing, with each disturbance producing limited low level erosion (see Figure 5.12).

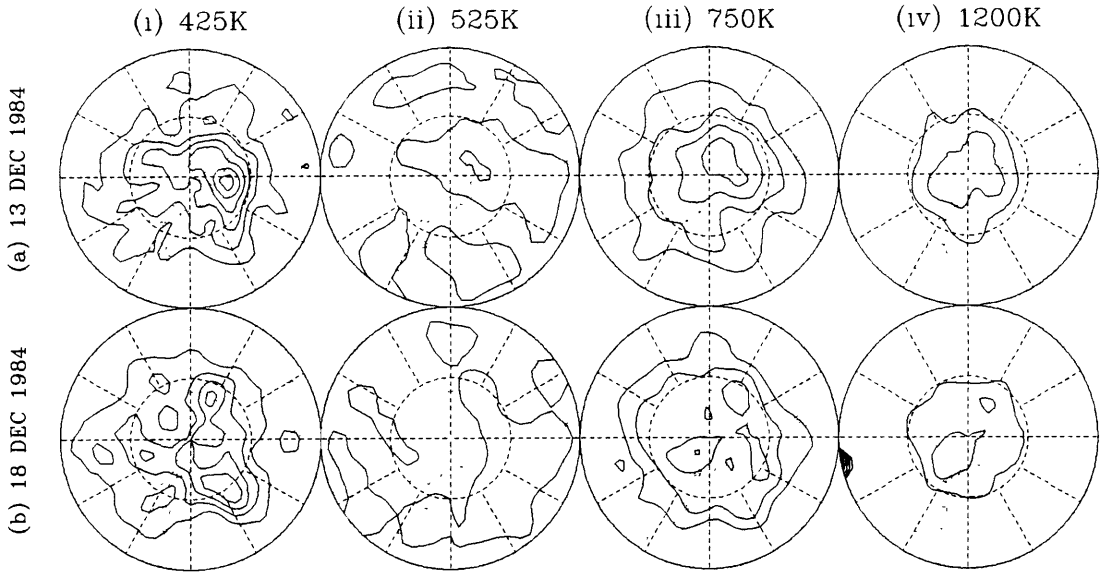

Figure 5.13: As in Figure 5.1, except for (a) 13 and (b) 18 December 1984.

The wind reversal at 10 hPa had occurred by 13/11, and the low level vortex remains were displaced from the pole in the first week of December, to be gradually sheared out in the hemispheric flow thereafter (see Figure 5.13).

The 1984 evolution was rather unusual, and from the synoptic viewpoint appeared to occur in reverse fashion to that of 1982, with LS type behaviour seen in late August and September, followed by ES type behaviour for the remainder of the season, so no rapid vortex destruction phase occurred.

The EPV analyses convey the impression that rather than one or two marked low level events with significant potential for ozone dilution, the season contained numerous minor erosion events. Of these minor events, the most marked wave breaking signatures at low levels were observed around 17/10 (AO/SAm), and during the period between 30/10 and 09/11 (from EPO to AF), the latter of these the more promising with respect to ozone dilution. Finally the vortex remains were gradually dissipated during December.

5.7 1985

The spring season in 1985 has not been previously examined in detail, although Farrara *et al* (1992) examined a large TW1 event which occurred in June, and Manney *et al* (1991) closely examined the behaviour of TW2 during the spring season. Coinciding with the westerly phase of the QBO, polar stratospheric temperatures were about average in early spring, but much colder than average during October. Overall wave activity was relatively high, although other than the large event in June, this activity was characterised by a series of rather brief bursts of moderate amplitude occurring regularly throughout the spring, without any single large event being observed. The most noteworthy feature of the year was the prevalence of TW3 compared to any of the other years examined. The following discussion is to be read in conjunction with Figure A.7(a).

The early winter period was very quiet at first before the very large wave event which peaked in mid-June. Farrara *et al* (1992) found it to be primarily attributable to slow eastward moving W1, W2 amplitudes becoming significant towards the end of the month. The poleward/downward shift of the jet occurred in three stages. The first two accompanied the June event and another smaller event in mid-July, while the third followed in late August.

Early August was typical of the LW stage, with a three disturbance pattern travelling eastwards with a rather regular period of around eight days, apparently causing very little vortex erosion at any level. After 20/08 wave amplitudes increased rather suddenly, marking the onset of the ES stage. The TW3 pattern gave way to TW2, as a disturbance in the AO on 20/08 moved rapidly into the IO region, apparently to merge with that to its east and the combined disturbance amplified markedly. As it crossed the IO the third disturbance amplified somewhat as it approached SAm, distorting the vortex into a marked TW2 pattern by 28/08, with wave breaking signs visible beyond the vortex edge at upper levels over the EPO by 31/08. Manney *et al* (1991) note that TW2 showed coherence between troposphere and stratosphere at

this time, suggesting this event, which saw the completion of the jet shift, was forced from below.

After 31/08 the TW2 pattern weakened rapidly, the evolution during the following few weeks reminiscent of a period of rather weak MOPF October behaviour (LS stage), as a series of otherwise minor perturbations amplified markedly as each approached the CPO, to decay again crossing SAm after producing upper level vortex erosion over the EPO. This short-lived sequence ended after 20/09 when a perturbation continued into the AO without weakening, and by 24/09 produced vortex edge erosion over the AO. According to Manney *et al* (1991) this event was forced in the troposphere. It was also short-lived, and by the end of September the EPV distribution had reverted to the familiar three perturbation pattern which, with increasingly preferential amplification of successive disturbances over the CPO, saw a very large TW3 peak give way to domination by the SW1 component by 06/10, with marked vortex edge erosion at all levels occurring at this stage to the east of a disturbance over the CPO (Figure 5.14(a)). The wave breaking process continued over the SAm/WAO region until the disturbance weakened in the EPO after 10/10, renewed erosion commencing over the EPO as the next disturbance amplified and moved into the CPO by 13/10. As this disturbance continued eastwards without decaying, another began to amplify rapidly south of AF, and the pattern took on a TW2 shape, with marked vortex erosion at upper levels over the AO by 15/10.

Although this latter event brought about the temperature gradient reversal at 10 hPa, it was not until the last half of October that rapid weakening of the upper level vortex occurred, characteristic of the LS stage. After 19/10 the PO disturbance began to weaken over the AO while the other, having further amplified crossing the IO, lay south of NZ and was producing substantial erosion over the CPO. This marked erosion signature continued as the disturbance moved rapidly across the PO before weakening as it approached SAm on 22/10. The next perturbation to its east amplified in the NZ region and repeated the cycle, before it in turn collapsed crossing SAm around 26/10, leaving the vortex at upper levels greatly weakened, the temperature gradient

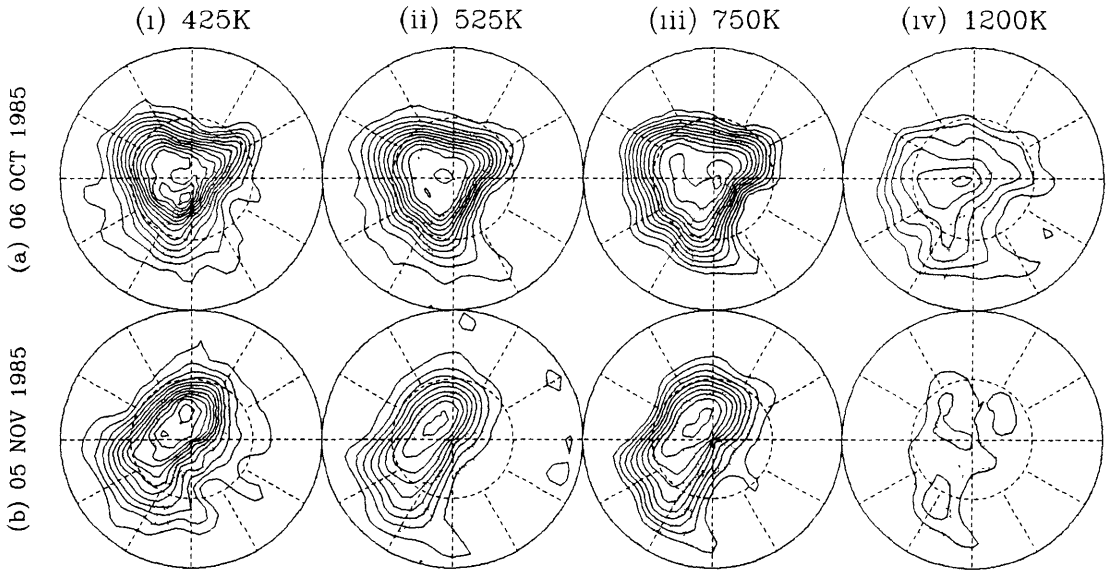

Figure 5.14: As in Figure 5.1, except for (a) 06 October and (b) 05 November 1985.

reversal reaching the 30 hPa level around 02/11.

With the upper vortex greatly weakened by 26/10, the TT stage commenced. As the PO disturbance collapsed near SAm by 26/10, another had amplified over the IO, and lay over the ANZ region by 30/10, with the remains of the upper level vortex displaced towards SAm. This disturbance amplified further as it crossed into the PO region by 05/11, producing further vortex edge erosion throughout the lower levels (Figure 5.14(b)). As the pattern rotated eastward and the erosion process continued, the next disturbance amplified over the IO by 08/11. By 13/11 the vortex at lower levels had been grossly distorted into a marked Z shape, with the A/Cs associated with each disturbance lying in the ANZ and WAO regions, and producing two marked tongues over the PO and AO regions respectively (Figure 5.15(a)).

After 15/11 the erosion process eased as the perturbations decayed, and the following week saw little in the way of dynamical activity (see Figure 5.15(b)). While the previous two weeks of activity had brought about a marked weakening of the low level vortex, at 10 hPa the circulation still remained westerly.

By 22/11 radiative decay finally brought about the 10 hPa flow reversal, after

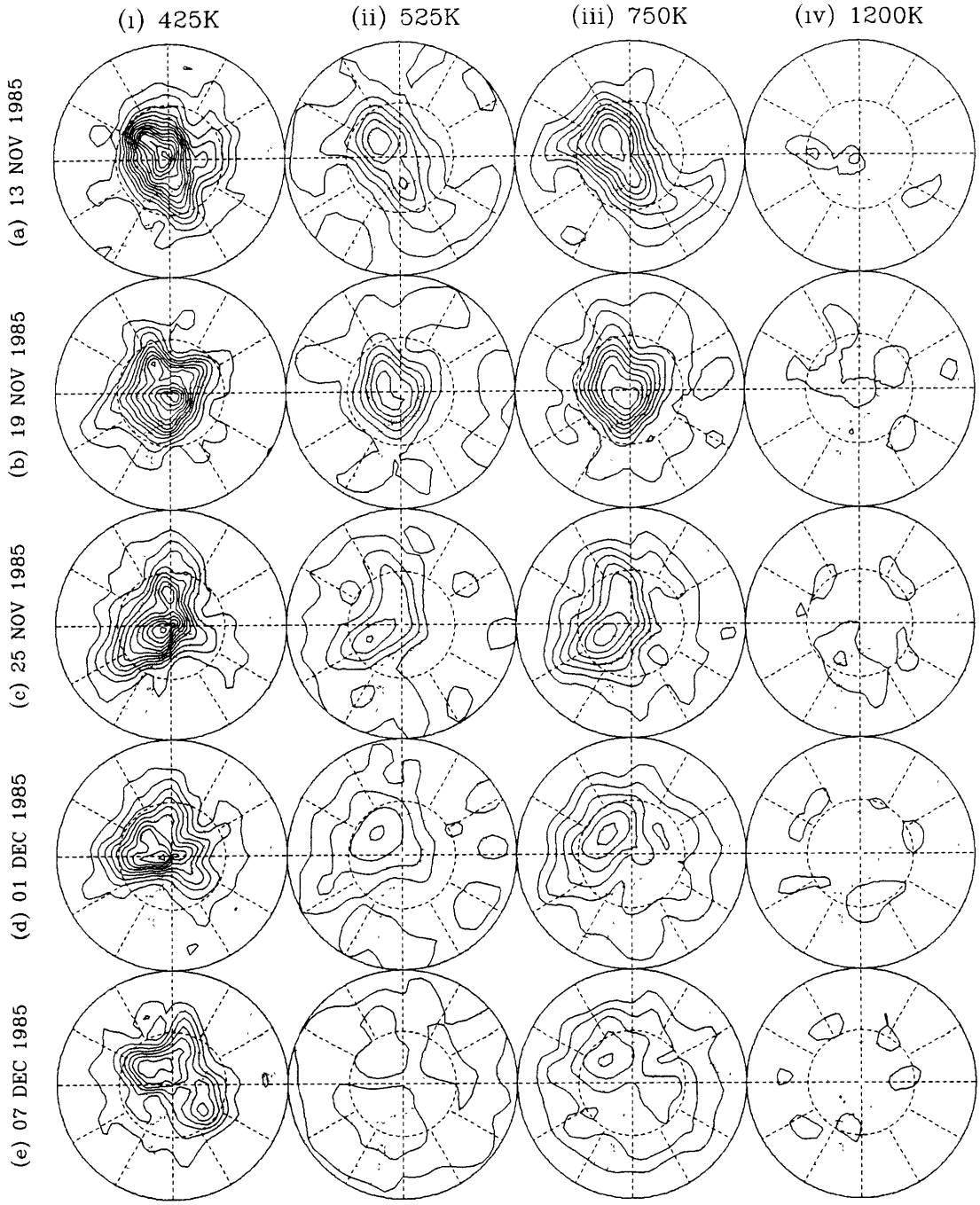

Figure 5.15: As in Figure 5.1, except for (a) 13, (b) 19 and (c) 25 November, and (d) 01 and (e) 07 December 1985.

which a low level TW2 event further weakened the vortex remains (Figure 5.15(c)).

It was not until the first week of December, however, that disturbances south of AU and SAm gently squeezed the bulk of the vortex residue below $800K$ off the pole. (Figure 5.15(d) and (e)), apparently to disperse gradually during the following three

weeks.

Overall, despite the fact that the season was not dynamically quiet, it lacked the sufficiently large and primarily SW1 event apparently required for rapid and early destruction of the vortex at upper levels. Instead, the series of rather regular TW2/TW3 events during the season produced a gradual weakening of the vortex at all levels, the essential collapse of significant wave activity allowing a primarily radiative decay during late November, before a very weak event pushed the vortex remains below $800K$ off the pole in early December.

On the basis of the EPV analyses, it seems unlikely that the minor low level erosion accompanying the October events would have caused much extrusion into mid-latitudes of ozone hole material, but the November wave breaking events of 05-13/11 (which was accompanied by significant EPV relaxation at the vortex core) and 25-28/11 may have produced significant ozone dilution, before the vortex remains were deposited in sub-polar latitudes during early December.

5.8 1986

The dynamical evolution of the austral stratosphere in 1986 has not previously been examined in isolation, although examination of the chemical evolution over Antarctica was the focus of the 1986 NOZE expedition (see *Geophysical Research Letters*, Volume 13, Number 12, 1986). Coinciding with the easterly phase of the QBO, the stratosphere was rather warm throughout the winter/spring period, and while no very large wave events were observed, the overall level of wave activity was high and rather continuous throughout the spring season. This continuous large scale perturbation of the vortex in a series of apparently well organised LS type events resulted in rapid vortex erosion. However, despite the low level vortex being displaced from the pole by a wave event in mid-November, it retained its integrity and drifted back by the end of the month, eventually to be more gradually dissipated during December. The following discussion is to be read in conjunction with Figure A.8(a).

After a rather late start, the early winter period displayed about average wave activity, significant wave amplitudes first evident in early May and leading up to a moderate and primarily W1 event in early June. After this it was rather quiet, with just a pair of small amplitude bursts of W1 activity in late June and early July. This July event, although not very large at 10 hPa, appears to have been responsible for the first stage of a gradual and drawn out poleward/downward shift of the jet core, which continued until early September. It is also noteworthy that the polar jet was significantly weaker at upper levels during mid-winter than in the other years examined, with maximum zonal mean zonal wind speeds at 1 hPa of about 90 ms^{-1}, compared with typical values of about 110 ms^{-1}. The last week in July saw a brief TW2 event of moderate amplitude, after which wave amplitudes throughout the season remained relatively large, suggesting the commencement of the ES stage despite the incomplete movement of the jet core by August.

As shown in Figure A.8(a), August behaviour was dominated by a persistent and steadily eastward moving (period about 15 days) episode of TW2 activity of significant amplitude, against an apparently weak background of SW1/SW2 (perturbations tending to reach maximum amplitude primarily in the WPO region, but to a lesser extent also in the EAO). This remarkably perturbed August activity produced signs of brief periods of vortex erosion at most levels at one time or another, the most notable being at low levels over the SAm/EPO region around 06/08 and at upper levels over SAm around 18/08.

The beginning of September, by which time the jet shift was complete, saw an apparent change in the disturbance behaviour to that more closely resembling a drawn out series of three mixed W1/W2 LS stage events. While the TW2 character persisted and was in many respects similar to that seen in 1983 but with even larger TW2 amplitudes involved, it was joined by a number of sustained pulses of SW1, apparently accompanying the passage over the CPO region of one of the two TW2 disturbances (but not the other).

This pattern of behaviour is seen in the Hovmoller diagram of Figure A.8(a). One

of the two large scale disturbances in the TW2 pattern apparently moved steadily eastwards, underwent only marginal amplification and decay, and completed three circuits of the hemisphere between August 10 and October 30. The other, however, underwent a marked amplification and decay cycle, first amplifying in the IO to reach maximum intensity in the CPO, then decaying rapidly as it crossed SAm. Hence the overall process saw an alternation between W1 and W2 LS stage behaviour, with an average period of around 26 days. Closer examination of the EPV analyses and Figure A.8(a) suggests, nonetheless, that from the synoptic viewpoint the process is still best described by the sequential amplification and decay of three perturbations. This sequence of events brought about an accelerating erosion of the upper level vortex in a series of wave breaking events, with an increasingly large corresponding signature seen at the vortex edge at lower levels as time progressed. The first weak signs of low level wave breaking were visible in the analyses of 31/08 to 04/09 in the SAm/AO region. After brief upper level erosion at the vortex edge occurred over the PO/ANZ region between 04/09 and 08/09, a major perturbation amplified as it crossed the IO between 16/09 and 20/09, to produce a marked wave breaking signature at upper levels across ANZ on 20/09, continuing the erosion process as it crossed into the CPO and producing a substantial surf zone signature across the PO by 28/09, the signature extending down to $525K$. This event greatly weakened the upper level vortex, apparently extruding inner vortex material out into mid-latitudes. Weakening thereafter, the PO perturbation was rapidly replaced by the next which moved rapidly across the IO and into the CPO by 04/10, renewing the erosion process. This was followed in turn by another on 09/10 while yet another perturbation amplified in the AF region to begin eroding the vortex over the EIO. After 09/10 the PO perturbation continued eastwards without decaying, causing further erosion at lower levels over the AO region, while at upper levels the vortex was displaced towards the EIO by 14/10. After 14/10, while the AO perturbation retained its intensity, the gouging process eased, commencing instead from the PO lobe by 19/10 under the influence of the amplifying ANZ perturbation. After 19/10 the ANZ disturbance weakened rapidly as it crossed into the PO, and by 24/10 a broad surf zone spanned the IO at lower

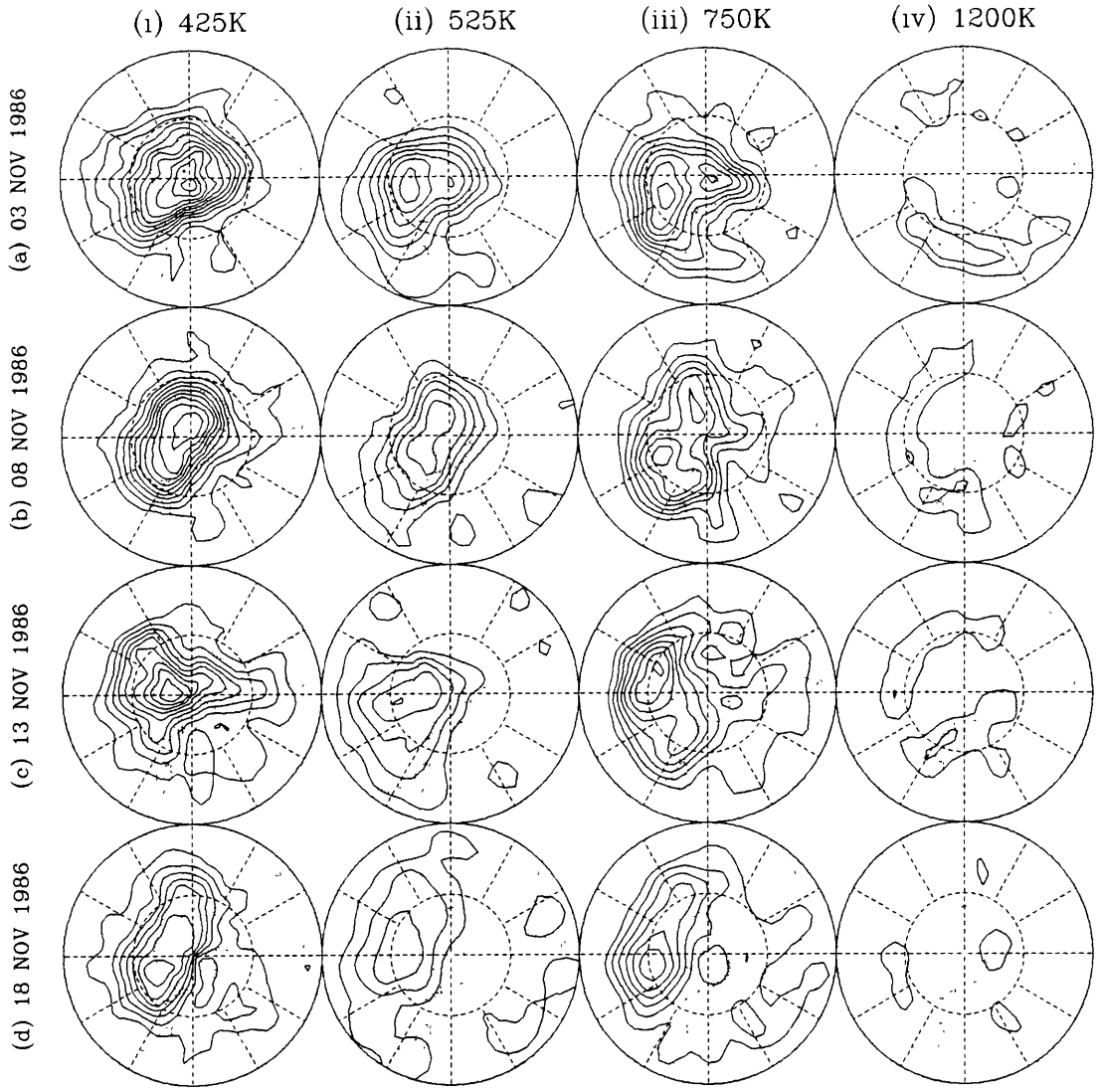

Figure 5.16: As in Figure 5.1, except for (a) 03, (b) 08, (c) 13, and (d) 18 November 1986.

levels, with the vortex rather axisymmetric but displaced towards the EPO, while at upper levels the vortex had been split in two, most of its material having been extruded into the IO/AO mid-latitudes by the IO disturbance.

The next significant wave activity occurred during the first few days of November, and a disturbance in the PO gouged a tongue from the low level vortex out over SAm/EPO by 03/11 (see Figure 5.16(a)) having extruded the remains of the upper level vortex into mid-latitudes. The event was short-lived, the erosion easing as the disturbance moved into the AO. By 08/11 two more disturbances had amplified and

lay over the PO and AU regions (Figure 5.16(b)). As the AO disturbance moved into the IO by 11/11, it and the AU disturbance, progressing eastwards, together began to squeeze the still substantial low level vortex remains towards the AO between 13/11 (Figure 5.16(c)) and 18/11 (Figure 5.16(d)). Perhaps because the remains were so substantial, however, the analyses suggest they retained their integrity, drifting back over the pole by the end of the month, thereafter to decay only gradually during December.

Overall, the 1986 season was rather active, the cyclic behaviour of the EPV disturbances seen as a combination of TW2 and SW1 appearing to work together to bring about an early flow reversal at upper levels. Despite a number of minor low level wave breaking events throughout the season (06/08 (SAm), 31/08-04/09 (SAm/AO), 24-28/09 (C/EPO), 09-14/10 (SAm/AO), 19/10 (PO)) it was not until the event around 03/11 (SAm) that the analyses indicate much potential for ozone dilution. In view of the seemingly rather reversible nature of the mid-November wave event, and the gradual decay thereafter, it is unclear from the analyses how much ozone dilution potential might be associated with the final breakup.

5.9 1987

The dynamical evolution in 1987 was highly anomalous. Coinciding with the occurrence of severe polar ozone depletion and an intensive polar observations campaign (the AAOE), various aspects of the evolution have been the subject of numerous investigations (see e.g. *Journal of Geophysical Research*, Volume 94, Numbers D9 and D14, 1989). Of these, the most relevant with respect to the overall dynamical evolution are that of Randel (1988), who contrasted the anomalous 1987 dynamical behaviour with the mean climatology of the preceding six years, and that of Newman *et al* (1990), who compared the 1987 season with that of 1988 (see Section 5.10 below). Coinciding with the westerly phase of the QBO, the polar lower stratosphere after August became very cold (or, more accurately, warmed much more slowly than

usual) particularly during November, which was up to $14K$, or four standard deviations, cooler than 1980-1986 climatology. It was also the quietest spring season, dynamically, of the eleven examined in the present analysis, being marginally less perturbed than 1980. The following discussion is to be read in conjunction with Figure A.9(a).

The early winter period up to the end of July was dynamically quiet, though not uniquely so, being similar in many respects to the early winter periods of 1982 and 1988. After two weak pulses of activity in May a moderate and primarily W1 event occurred in late June, before a very quiet July. By the end of July, polar temperatures were close to normal, and while the vortex circulation was a little larger than usual at upper levels, the jet was no more intense.

The August period displayed typical LW stage behaviour. Significant wave activity first began at the beginning of the month, appearing in the EPV analyses as eastward travelling perturbations, the first of which reached peak amplitude over the EPO around 10/08, the next a pair which peaked together (reflected by a brief SW2 component to the wave pattern) over the ANZ and AO regions around 26/08, this latter event showing signs in the EPV analyses of wave breaking at upper levels, and coinciding with a rather rapid poleward/downward shift of the polar jet. The EPV analyses also suggest this W2/W3 event involved the typical three perturbation behaviour, a shorter scale disturbance moving more rapidly eastwards than the others, to catch up to that to its east, enhancing the W2 signature.

After the beginning of September the behaviour became more typical of the ES stage. Of three weak travelling perturbations, one began to amplify as it crossed into the AU region by 06/09, peaking over the WPO by 10/09 and causing marked erosion at the vortex edge above $750K$ over the E/CPO. Rapidly decaying thereafter, the process was renewed by a second disturbance following closely behind, while another began to amplify over AF, in turn producing upper level erosion over the EIO by 16/09 as the TW2 pattern rotated. After 19/09 the pattern collapsed, leaving a weak W3/4 signature which persisted for the next few weeks.

In the last week of September, with the vortex still very strong, a preferential amplification sequence involving the three to four disturbance pattern began (period 3 to 4 days) which displayed the features of the LS stage (a MOPF W1 October sequence). One after another each of the disturbances amplified as it crossed AF into the IO, to reach peak amplitude in the ANZ region, then decay rapidly on reaching the EPO, each producing increasingly more marked vortex erosion before decaying, and the erosion process extending down to lower levels as time progressed. The harmonic projection of this sequence of events at upper levels was a brief peak in TW2 and TW3, followed by increasing W1 amplitude, which culminated in the largest wave event of the year (SW1) in early to mid-October. The first wave breaking signature at lower levels which resulted from this sequence was observed over SAm/WAO on 07/10, and the next was over SAm/EPO around 10/10, due to a rather baroclinic disturbance in the CPO which amplified rapidly with height to be well south of AU at $1200K$, forcing the weakened upper level vortex towards SAm and producing marked wave breaking over the C/WPO. These first two events were rapidly followed by another in the same region around 14/10 and perhaps yet another on 17/10 (no NMC data were available from 16/10 to 18/10, but the occurrence of an event on 17/10 is consistent with the analyses from before and after and with the independent TOMS analyses).

Following this latter event the W1 pattern collapsed, being replaced by a more typical W2 type LS stage. After 17/10 the PO perturbation continued into the AO, weakening only slightly, before reamplifying over the EAO by 25/10, while over the PO the apparent merger and amplification of two smaller scale perturbations had occurred, the vortex moving back over the pole and a peak in TW2 occurring.

After 25/10 the pattern continued to rotate, further erosion evident at upper levels over the EPO/SAm region after 27/10, then the ANZ region after 29/10. After 31/10 the erosion process eased, and by 06/11 the much weakened vortex at upper levels was again pole centred, the temperature gradient reversal had occurred at 10 hPa, and the signature at lower levels was once again W3/W4. Brief amplification of a disturbance as it crossed the IO produced further erosion at upper levels by 10/11

but failed to destroy the vortex remains there, before the pattern settled down again.

With the vortex greatly weakened at upper levels, the evolution entered the TT stage, which saw wave amplitudes increase during the last half of November before bringing about the low level vortex destruction.

With the vortex relatively undisturbed on 15/11, two eastward travelling low level disturbances began to amplify crossing the IO and EPO regions by 19/11. As they reached AU and SAm, respectively, a third began to amplify south of AF after 20/11, deforming the vortex into a W2/W3 pattern by 24/11. The IO disturbance thereafter amplified rapidly as the others decayed somewhat, and decelerated as it crossed the IO, producing marked gouging of the low level vortex to the south of ANZ by 28/11 (Figure 5.17(a)) and pushing the vortex remains off the pole above 10 hPa, bringing about the zonal wind reversal. As the pattern rotated, the weaker disturbance over the AO again intensified, and by 02/12 the low level vortex was squeezed between the two disturbances (Figure 5.17(b)) and distorted into an hourglass shape, the larger lobe displaced towards the EPO, the smaller towards the CIO. As the pattern continued to rotate, the A/C associated with each disturbance continued extensive gouging of the vortex remains, and by 06/12 (Figure 5.17(c)) that over the PO had produced a tongue out over the EPO, while the IO A/C had produced a weaker tongue out over the EIO. This process continued as the pattern rotated (Figure 5.17(d)), and by 14/12 (Figure 5.17(e)) the bulk of the vortex remains had been extruded into the mid-latitudes between the EPO and WIO, the lesser lobe being deposited over the region from the WPO to the EIO.

Overall, 1987 was a very quiet season, the vortex remaining remarkably undisturbed at low levels until late in the evolution, and the final warming was the latest observed in the eleven years examined.

There was no evidence of significant low level wave breaking which might have produced an ozone dilution effect, prior to October. The sequence of low level erosion events which occurred between 07/10 and 15/10 appears from the analyses to have involved only the outer edge of the vortex, as do the other minor events occurring

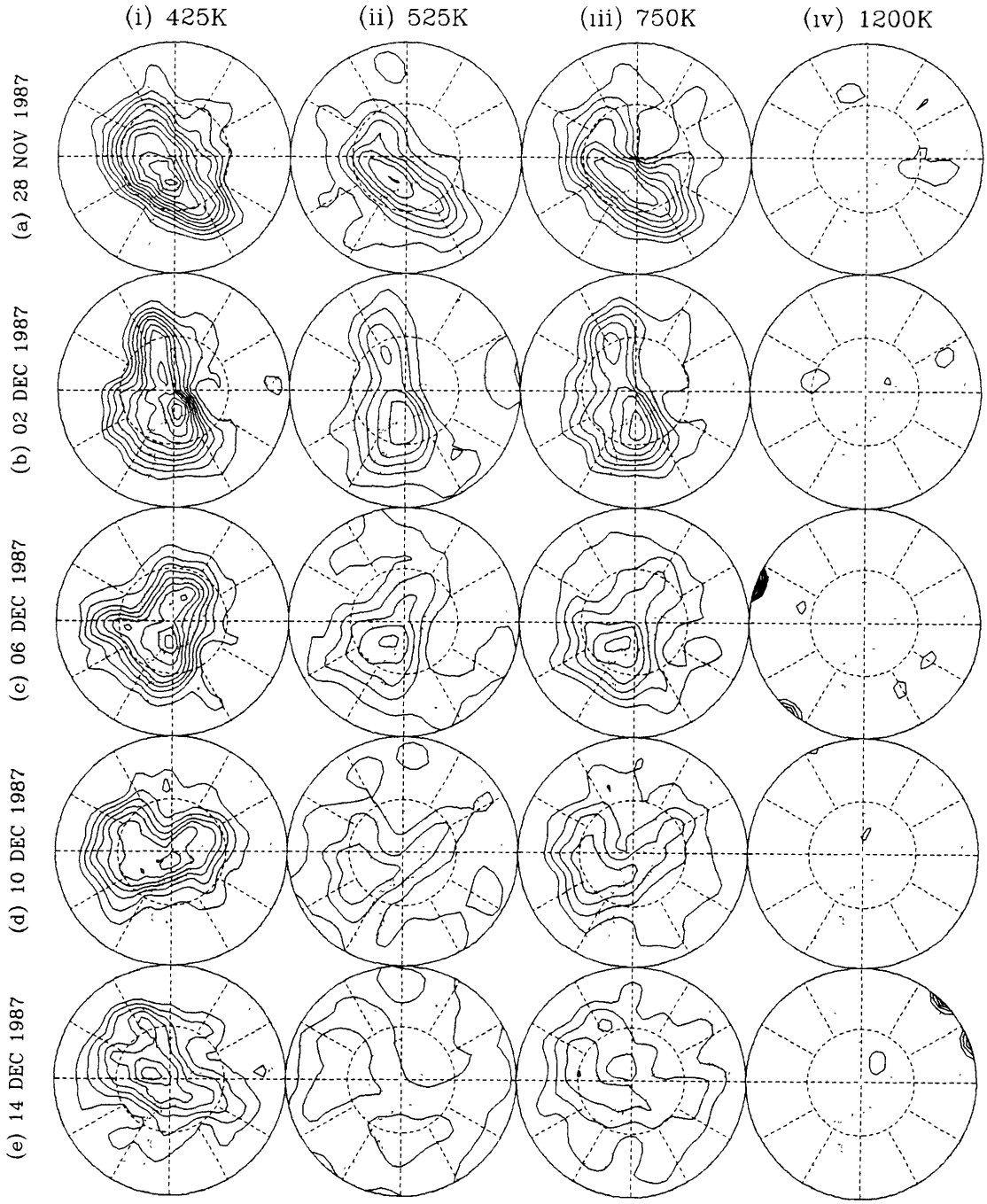

Figure 5.17: As in Figure 5.1, except for (a) 28 November, and (b) 02, (c) 06, (d) 10, and (e) 14 December 1987.

prior to mid-November. The distortion of the low level vortex which occurred between 17/11 and 24/11 also appears from the analyses to have produced little in the way of extrusion of inner vortex material, but the apparently significant erosion observed between 24/11 and 30/11 over the region to the south of ANZ may be worthy of

closer examination. Finally, the sequence of events comprising the vortex destruction process after 02/12 is the subject of the detailed analysis of Chapter 7 below.

5.10 1988

Just as 1987 was anomalously cool and dynamically quiet, 1988, which coincided with the easterly phase of the QBO, was equally anomalous for the outstandingly high level of wave activity throughout the spring season, and the very warm polar stratosphere which accompanied the wave activity. Kanzawa and Kawaguchi (1989a, 1989b) examined the seasonal evolution of temperature and total ozone at Syowa (69^oS 40^oE) during 1988, Hirota *et al* (1990) examined the dynamical evolution in the August/September period, and, as noted in the preceding Section, Newman *et al* (1990) contrasted the dynamical evolution throughout the 1988 season to that of 1987.

After an unusually quiet early winter period, wave activity essentially exploded at the start of August with a series of 7 large amplitude SW1 events spaced about two weeks apart, to bring about the earliest completion to the seasonal transition since 1979. The following discussion is to be read in conjunction with Figure A.10(a).

As noted above, the early winter period was very quiet, with very small wave events in mid-April, mid- to late July, and early June. By the end of June the stratosphere was dynamically very average, and although the vortex was slightly larger than most years (like 1987) the jet was not particularly intense. At the start of July wave amplitudes began to increase, an anticorrelated W1/W2 event producing a small peak in SW1 around 10/07, then a peak in W2 (apparently quasi-stationary) around 17/07. These two small events appear to have been responsible for the poleward/downward shift of the jet by the end of the month.

By the beginning of August three disturbance LS stage behaviour had commenced (MOPF W1 October) and a large disturbance lay in the NZ region. The vortex was

displaced towards the AO with a strong SW1 signature which peaked on 02/08, the first of the series of large W1 events during the season. After 02/08 the NZ disturbance moved east and weakened, while another south of AF by 07/08 began to intensify rapidly as it moved east across the IO to reach peak intensity in the AU region around 13/08, producing signs of erosion near the vortex edge at all levels. The following week saw three cycles of the sequential amplification and decay of a three disturbance pattern, together comprising a single episode of MOPF October behaviour (see Figure A.10(a)). The AU disturbance decayed as another small scale disturbance amplified over the IO to move rapidly eastward and take its place a little further to the east, this one in turn decaying, to be replaced by a third, each disturbance producing limited erosion at the outer edge of the vortex with its passage across the AU region. Around 19/08 the third of these disturbances had begun to amplify over the WIO. As it progressed eastward to take the place of the second in the AU region by 25/08, the first, once more back over the WIO, did not amplify in turn there. Instead the second began to reintensify further west over the AO. Subsequently, the new AU disturbance, rather than decaying as it crossed the PO, retained its identity while the other amplified rapidly approaching AF to peak in the IO region, rather than over AU, around 31/08 to commence a second episode of MOPF SW1 behaviour there. This second episode continued throughout the spring period, the zonal scale of each disturbance at peak intensity becoming gradually larger as the season progressed, and the location of maximum amplitude drifting slowly eastward again to lie in the ANZ region by mid-October. The overall effect of this continuing process was an accelerated erosion of the upper level vortex, and a much slower but gradual weakening of the vortex at lower levels.

By early October the vortex at upper levels was already greatly weakened and between 09/10 and 26/10 the upper level remains were further eroded and eventually pushed off the pole into the PO region, bringing about the circulation reversal above $900K$.

This process also marked the beginning of the TT stage, which saw rapid destruc-

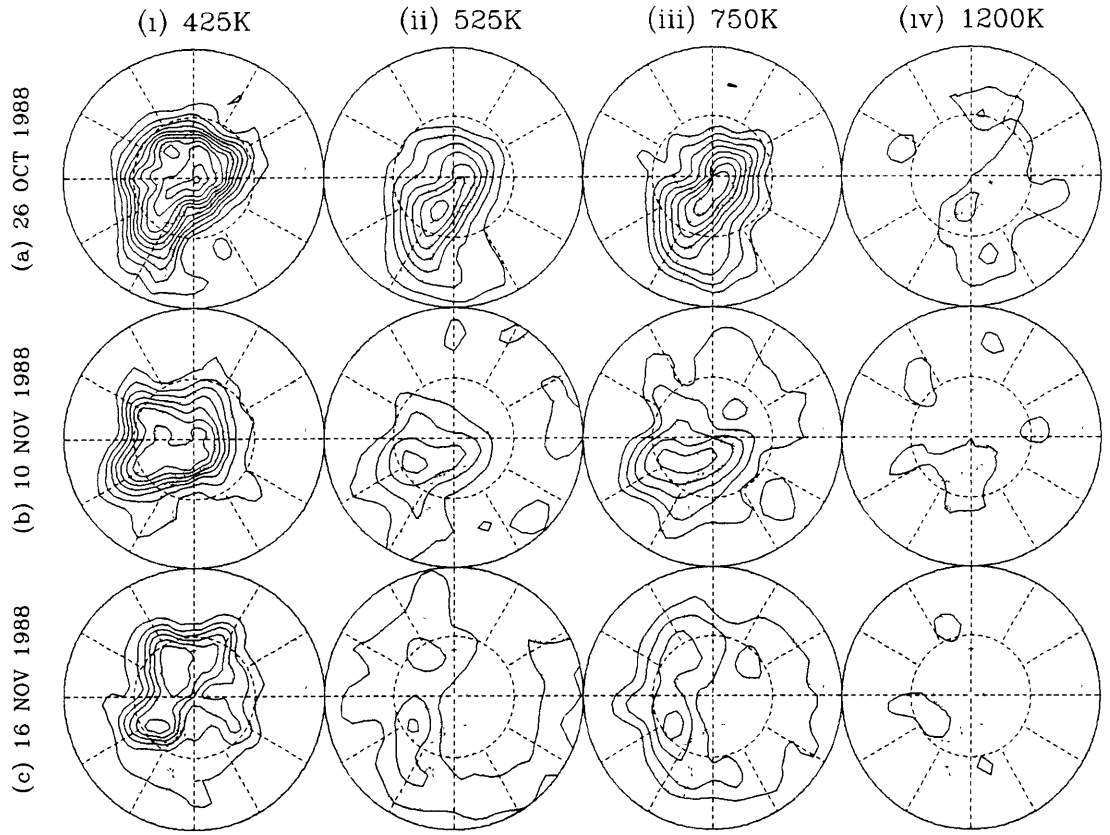

Figure 7.18: As in Figure 5.1, except for (a) 26 October, and (b) 10 and (c) 16 November 1988.

tion of the low level vortex over the next three weeks. The disturbance responsible for finally displacing the upper level vortex from the pole began to produce significant low level erosion as it passed south of AU after 20/10, producing a marked tongue over the SAm/PO region by 26/10 (Figure 5.18(a)). While the erosion process from this A/C eased after 29/10, another followed soon after, extruding a tongue of vortex material out over the PO region between 01/11 and 04/11, before a third disturbance, south of AF on 10/11 (Figure 5.18(b)), tracked southeast as it crossed the IO to move in over the pole after 13/11, pushing the vortex remains towards the AO/IO region (Figure 5.18(c)), to be sheared out over the following weeks in the earliest completion to the seasonal transition since 1979.

With respect to potential ozone dilution events, the EPV analyses suggest that almost continual, although subtle, low level vortex edge erosion probably occurred throughout September and early October, but there is no evidence of any large scale

wave breaking events at low levels during this early period. The first suggestion of a significant event was that centred on 26/10, althought it is not clear from the EPV analyses whether this involved inner vortex material. It seems more likely that limited extrusion of ozone hole material may have accompanied the minor event of 01/11 to 04/11 (EPO), and the final breakup after 10/11, despite the rather moderate ozone hole in 1988, is worthy of closer examination.

5.11 1989

Little independent information is available on the 1989 evolution, other than that provided by Randel (1992) and Farrara *et al* (1992). 1989 was a rather average year overall, polar stratospheric temperatures being about normal and no very large wave events were observed, although several moderate events occurred against a background of continual light activity, and the season culminated in a large event in late October. The season coincided with a weak westerly phase of the QBO. The following discussion is to be read in conjunction with the information displayed in Figure A.11(a).

The early winter period displayed about average activity overall, the stratosphere almost continually perturbed by a series of rather small amplitude events, before a moderate burst in late July. Despite this activity, almost none of it reached the highest levels of the stratosphere and by the end of July the jet was still strong and broad.

August was characteristic of the LW stage, and saw a continuation of the earlier rather light wave activity. Although there is little indication in the Randel (1992) analysis of a significant event towards the end of the month, Figure A.11(a) depicts the development of a rather localised and minor TW2 event during the last week of August, which the upper level EPV analyses suggest may have caused an episode of Rossby wave breaking over the ANZ region down to $750K$ between 27/08 and 30/08, and which coincided with a rapid shift of the jet. Little of dynamical significance

appears to have occurred during the following few weeks, despite brief deformation of the vortex into a marked TW2 pattern around 11/09.

Following the brief August event the evolution entered the ES stage. A rather marked and persistent three disturbance pattern developed by 14/09, dominating the flow until the second week of October. During the last week of September preferential amplification became evident, at first in both the IO and EPO regions (a TW2 pulse) then just the IO/AU region, and a weak vortex erosion signature was observed at low levels in the EPV analyses around 25/09 over the AO, then at most levels over the PO on 28/09.

During the first week of October, two of the three perturbations amplified almost simultaneously over the AO and WIO regions, merging as they travelled east into the AU region by 10/10. By this stage the third disturbance began to amplify over the AO, and the vortex was distorted into a marked TW2 pattern, upper level erosion occurring to the east of the AU disturbance as it crossed the WPO by 16/10, displacing the upper vortex towards the AO.

After 16/10 the evolution became characteristic of a W1 LS stage, and was accompanied by the largest wave event of the season during the latter stages of month (the largest and most sustained late October event in the eleven years examined). The PO disturbance began to weaken while the other continued to intensify as it crossed into the IO, and by 19/10 the erosion process had commenced over the AU/EIO region. Amplifying further, the low level disturbance moved across the ANZ region and into the CPO by 26/10, the upper level gouging became more marked, rapidly weakening the vortex there and producing a tongue across the PO, the erosion signature extending down to the lower levels. As this first perturbation over the PO weakened rapidly after 26/10, it was followed by a rapid succession of two others, each amplifying and commencing the erosion process a little further to the east than that preceding it. In this manner, an apparently significant amount of vortex material was extruded out to lower latitudes, the successive tongues visible in the analyses of 30/10 over SAm/EPO (Figure 5.19(a)), and 03/11 over SAm (Figure 5.19(b)). Following the latter event a

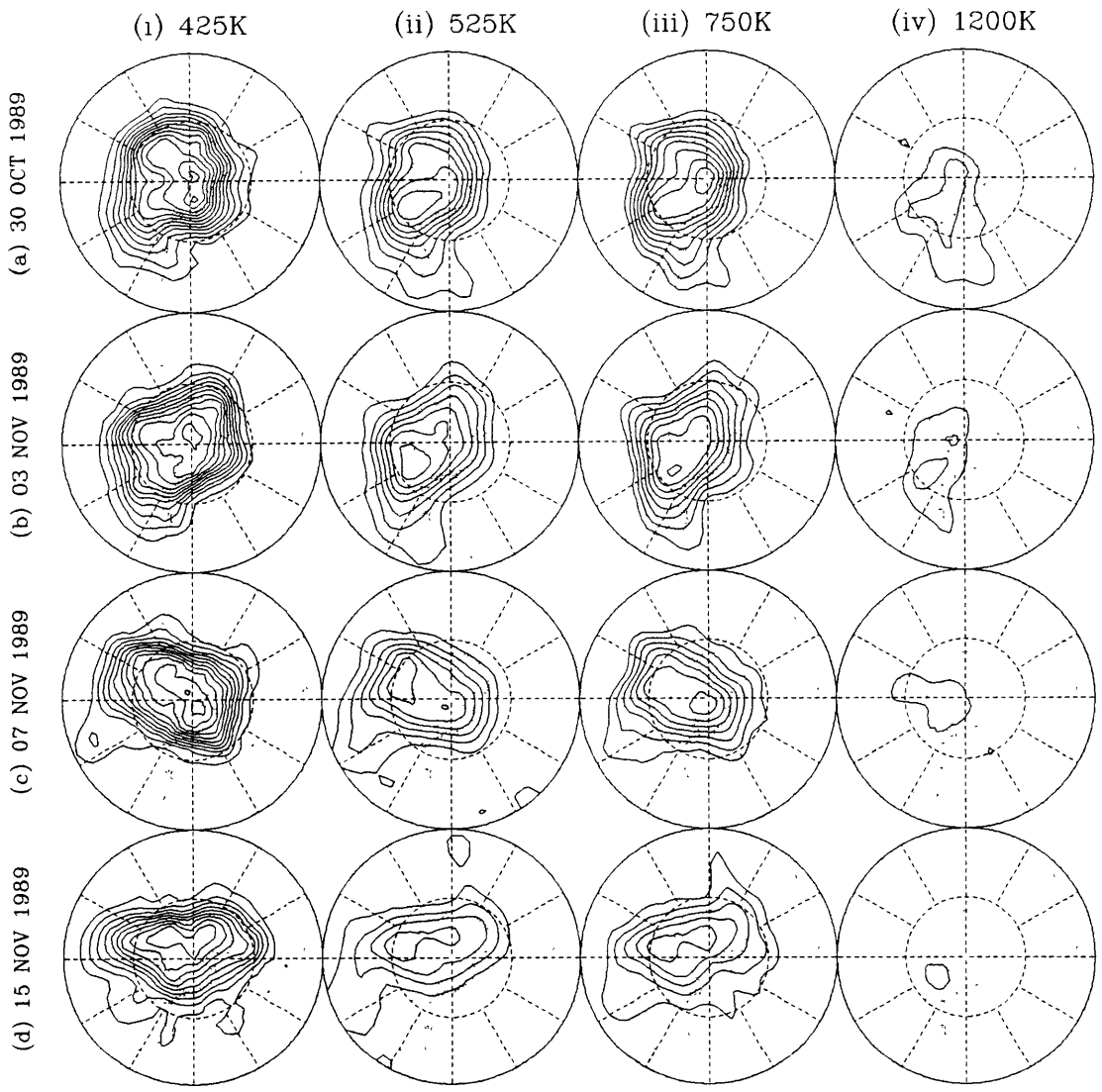

Figure 5.19: As in Figure 5.1, except for (a) 30 October, and (b) 03, (c) 07 and (d) 15 November 1989.

fourth disturbance crossed the IO and completed the upper level vortex destruction process, moving over the pole at $1200K$ after 07/11 (Figure 5.19(c)). After the upper level destruction, a series of rather small scale disturbances travelling rapidly eastwards along the vortex edge consecutively enhanced the erosion signature over the AO region by 15/11 (Figure 5.19(d)), bringing about a progressive decay of the vortex at low levels, but the subsequent destruction of the low level circulation up to early December is perhaps best described as a process of primarily radiative decay, after which the closing stages of the evolution becomes poorly defined in the analyses.

The analyses suggest the first event with any potential for ozone dilution was that which occurred around 26/10, after which the low level vortex destruction commenced with the series of rather minor events centred on 30/10, 03/11 and 07/11, each of which probably had small potential, followed by the weak episodes leading up to 15/11 which, although each was small, may together have produced a more significant effect. In view of the apparently primarily radiative decay after this, it is not clear from the synoptic analysis alone how much potential existed for ozone dilution accompanying the final vortex breakup.

Chapter 6

Ozone Evolution in the Austral Spring Stratosphere: 1979 to 1989

In Chapter 4 above we discussed the dynamical climatology of the southern hemisphere stratosphere, and in Chapter 5 the dynamical evolution in each year from 1979 to 1989 was considered in more detail, leading to the identification of a number of potential ozone dilution events which occurred in each spring season. By employing the coordinate transformation technique decribed in Chapter 3 we can obtain a picture of the ozone evolution during each of these events which coincides with the availability of SAGE ozone data, and hence assess their ozone dilution potential. We can also use the direct approach to analyse those events which occurred up to a week or two before or after a SAGE hemispheric sweep was made, although with an expected reduction in confidence. Of course, the direct approach can not be used for events which occurred at other times, and this presents a major problem for the earlier years.

Figure 6.1 shows the periods in each spring season (August to December) from 1979 to 1989 for which SAGE data south of $10^{o}S$ are available, and the observation latitude for each ozone vertical profile. Each curve shown is made up of a series of (barely discernible) crosses, each cross in each of the plots denoting a single vertical profile.

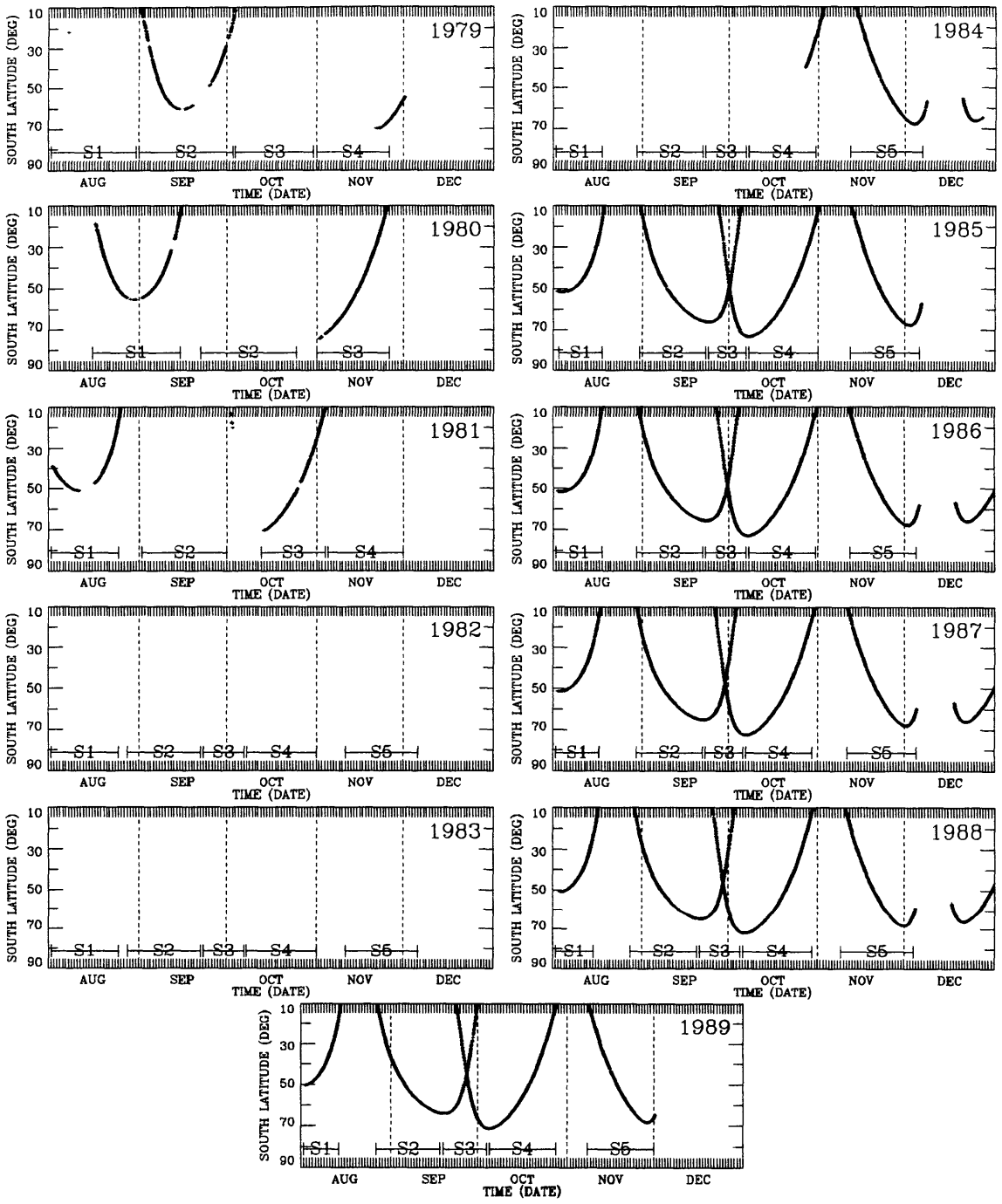

Figure 6.1: Southern hemisphere SAGE ozone data availability during the spring seasons from 1979 to 1989, showing the observation latitude of each available ozone vertical profile south of $10°S$ vs time. One cross is plotted for each available profile. Also shown are the 'sweep' subdivisions (S1 to S5), both actual and 'virtual', selected for each season (see text for details).

Evident in Figure 6.1 is the almost continuous coverage by the SAGE II instrument after October 1984. This has enabled us to divide all the available data into several hemispheric sweeps for each season (also shown in Figure 6.1) and perform the coordinate transformation technique on the data for each sweep, to provide the basis for an examination of virtually all of the potential ozone dilution events occurring after October 1984. The results of this examination will be presented in Chapters 7 and 8 below. Before proceeding with this, however, it is instructive for two reasons to consider the overall ozone evolution in each of these years.

Firstly, by comparing the period mean, zonally averaged and vertically integrated ozone distribution obtained from the SAGE data reconstructions for each sweep, with the corresponding meridional distribution of TOMS total ozone, we can assess the overall effectiveness of the reconstruction technique, gaining some insight into its strengths and limitations. Also, by performing the coordinate transformation on all the ozone sonde data available for the period of each SAGE II sweep and comparing the resulting $\chi/\hat{q}$ isentropic distributions with those obtained using the SAGE data, we are able to uncover some of the reasons for discrepancies between the SAGE total ozone reconstructions and the TOMS distributions.

Secondly, by contrasting the reconstructed SAGE ozone distributions from one sweep to the next we can improve our understanding of the climatological evolution of the ozone distribution, and by relating, to the observed dynamical evolution each year (as discussed in Chapters 4 and 5), the differences seen between the ozone evolution from one year to the next, we can extract possible clues to the impact of the dynamical evolution on the ozone evolution. Besides being of value for its own sake, this all then becomes helpful when we attempt to piece together a picture of the likely ozone evolution in the years prior to the commencement of SAGE II, when not only are there significant gaps in SAGE data coverage, but we find direct use of the transformation technique to be considerably less effective, apparently due to the inferior quality of both the available SAGE I data and the early NMC data.

The gaps in SAGE I coverage are evident in Figure 6.1, and result, as noted in Chapter 3, from a spacecraft power supply problem, so that there are only one or two useful coverage periods in each of the years from 1979 to 1981. The commencement of operation of SAGE II in October 1984 resulted in only one complete sweep for that season as well. More critical is the total lack of SAGE data in 1982 and 1983. Direct examination, based on actual SAGE observations, of all the potential ozone dilution events prior to October 1984, and falling more than a week or two outside the SAGE I sweep periods, is therefore precluded. Nonetheless, we wished to attempt at least a qualitative examination of the ozone transport associated with each of these events, so we needed first to speculate at the ozone distribution which might have been observed during these periods.

Although there is a number of ways in which this might have been done, the technique eventually employed was selected because it was relatively simple to apply and it allowed us to test the impressions, gained from the examination of the later years, about the impact of the dynamical evolution on the ozone evolution, while providing speculative but essentially credible ozone distributions for the periods for which no SAGE data were available.

The first step in building up a picture of the ozone evolution in each of the years prior to 1985 was to perform reconstructions, as for the sweeps subsequent to 1984, on the data for the available SAGE sweeps. As noted above, the quality of the SAGE I reconstructions was often inferior to those obtained using the SAGE II data. While for most the result was deemed to be acceptable, significant problems were apparent for some, and the resulting distributions were modified to produce a more believable result.

The second step in the procedure adopted for the years prior to 1985 was to divide the periods for which no SAGE data were available into 'virtual' sweep periods of generally two to four weeks, as alluded to in Section 4.1 above. These imaginary sweep periods for each season are shown in Figure 6.1. For each of these periods, a set of 'first guess' $\chi/\hat{q}$ relationships was then selected from those derived using the data

from the actual SAGE sweeps, the selection being based initially on either temporal continuity, where possible, or dynamical similarity between the seasonal evolution leading up to the particular 'virtual' sweep and that observed at some other time for which SAGE data were available. These 'first guess' relationships were then used, with the isentropic pressure and EPV distributions for the period of the 'virtual' sweep, to obtain a period and zonal mean meridional distribution of reconstructed total ozone, for comparison with TOMS total ozone. In some cases use of the 'first guess' relationships led immediately to a good fit to the TOMS data, suggesting the dynamical reasoning might be well founded, and the resulting ozone distribution to be perhaps close to that which would have been observed. In some cases, however, this was not so, apparently primarily because of a significant secular trend in the ozone data, so the process was repeated using other sets of $\chi/\hat{q}$ relationships, until an acceptable fit to the TOMS data was obtained. This, of course, introduced a rather large degree of subjective tuning into the process, and the resulting ozone distributions must be regarded as highly speculative: we do not claim, for any of these periods for which ozone data were unavailable, to have determined the ozone distribution as it actually occurred during a given 'virtual' sweep, but only to have arrived at a realistic distribution which might have occurred, which provides a reasonable fit to the observed total ozone distribution, and with which we can at least perform a speculative examination of the potential ozone dilution events occurring at these times.

The purpose of the present Chapter, then, is to provide the details of this portion of the present work. In Section 6.1 we present the results of applying the reconstruction technique to the SAGE II data for the 1985 to 1989 seasons. We discuss the performance of the technique and the ozone evolution observed in each season, relating it to the observed dynamical evolution, pointing out a number of interesting features apparent in the ozone evolution, and comparing some of the features of the picture obtained with the previously assembled climatologies of Nagatani *et al* (1988) and Dutsch (1978). In Section 6.2 we consider the ozone reconstructions obtained for the SAGE sweeps prior to 1985, describing the problems apparent with some,

the modifications made, and discussing the main features of the ozone distributions obtained. In Sections 6.3 and 6.4 we deal with the speculative ozone distributions for the 'virtual' sweep periods when no SAGE data were available. In Section 6.3 we describe the means by which a picture of the ozone evolution in each of the years from 1979 to 1981 and 1984 was put together using the $\chi/\hat{q}$ relationships from the available SAGE sweeps, discussing the main features of the resulting distributions, and the level of confidence which might be placed in them. Finally, in Section 6.4 we present and briefly discuss the highly speculative proxy distributions obtained for each of the 'virtual' sweep periods in 1982 and 1983, the years for which no SAGE data were available.

6.1 Observed Springtime Ozone Evolution: 1985 to 1989

For each of the years from 1985 to 1989, all the available SAGE data from the start of August to early December were binned into five sweeps. The corresponding value of normalised EPV ($\hat{q}$) for each SAGE observation at each isentropic level was then interpolated in space and time from the dynamical analyses, and the reconstruction technique described in Section 3.4 was performed on the data for each sweep at each level. As noted above, the sweep periods for each season are shown in Figure 6.1 (denoted S1 to S5), and approximately correspond to the periods for which the climatology of the springtime dynamical evolution was discussed in Chapter 4 above (as depicted in Figure 4.1) i.e. early August (S1), late August to mid-September (S2), late September to early October (S3), October (S4) and mid- to late November (S5). (The reconstruction technique was also initially applied to the late December data for each year but was found to be unsuccessful. This was as expected, since by this stage of the dynamical evolution virtually the entire stratosphere displays a surf zone signature, rendering the EPV coordinate degenerate. Since by late December the seasonal transition is essentially complete, the SAGE data for this period were

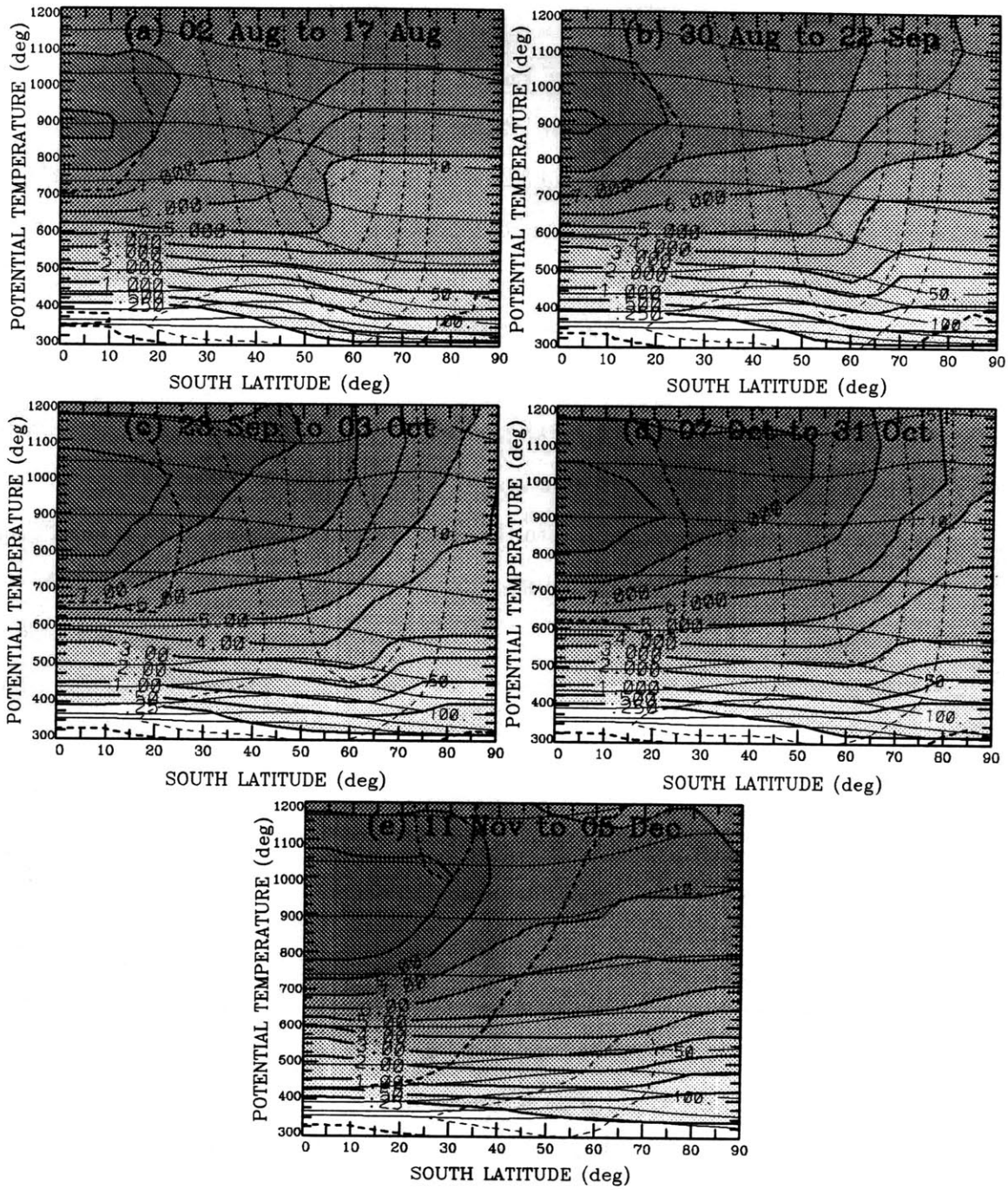

Figure 6.2: Reconstructed cross-sections (potential temperature vs latitude) of ozone mixing ratio (OMR, in $ppmv$), pressure (hPa) and zonal wind (ms^{-1}), for each SAGE sweep in the spring season of 1985. The OMR distribution is denoted by shading and labelled thick contours. Thin solid contours, from the bottom up, are 200, 150, 100, 70, 50, 30, 20, 10, 7 and 5 hPa isobars. Dashed contours are isotachs, from 0 ms^{-1} (the heavy contour) at 20 ms^{-1} intervals.

omitted from further consideration.)

Having obtained the χ vs $\hat{q}$ fitted curves for each level and sweep, meridional distributions (potential temperature vs latitude) of zonal mean, period mean $\hat{q}$, p and u were calculated for each sweep, and the $\hat{q}$ distributions converted, using the $\chi/\hat{q}$ relationships, to provide corresponding meridional distributions of reconstructed χ. These zonal mean, period mean ozone distributions for each sweep in 1985 through 1989 are shown, respectively, in Figures 6.2 through 6.6. In each of the plots the ozone distribution is shaded, the heavy labelled contours being isopleths of OMR. The thin solid contours are isobars, added to enable visualisation of the temperature and OMR distributions in the isobaric coordinate system, and the dashed lines are isotachs, the jet axis approximately corresponding to the mean position of the vortex edge. Using the technique described in Section 3.5 above, corresponding meridional distributions of reconstructed total ozone were then calculated, as were those of TOMS total ozone. These are shown for each sweep in each of the five years in Figures 6.7 to 6.11, the reconstructed distribution shown by a solid curve, TOMS dashed.

6.1.1 Overall Performance of the Reconstruction Technique on SAGE II Data

Figures 6.7 to 6.11 show that the overall agreement in the extra-tropics between TOMS and reconstructed period mean, zonal mean total ozone is rather close, and in some cases very close. In general, the reconstructions accurately capture the location, shape and approximate magnitude of the mid-latitude total ozone maximum, they reproduce the polar minimum well, and in most cases provide a close fit to the observed meridional gradient at sub-polar latitudes.

Comparison of the individual χ vs $\hat{q}$ plots for each sweep in each year with similar plots constructed using the available ozone sonde data for each period revealed two general shortcomings of the reconstructions, one due to the technique itself and the other to the SAGE data.

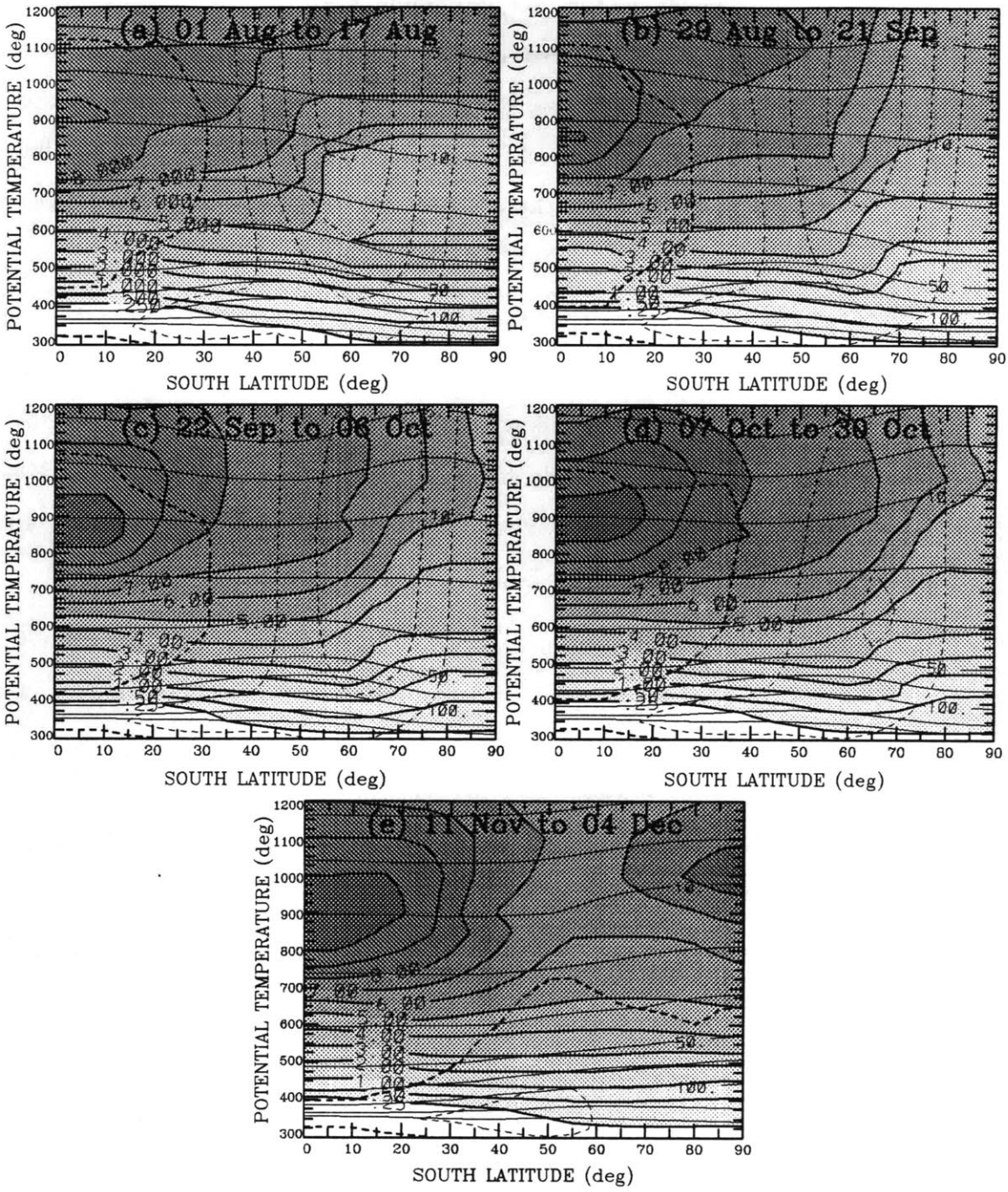

Figure 6.3: As in Figure 6.2, except for the SAGE sweeps of 1986.

The first of these is the failure of the technique to represent accurately the OMR distribution in the tropical middle stratosphere. At almost all levels where maximum OMR is found at mid-latitudes, the curve fitting technique leads to overestimation of tropical values and consequently to overestimation of the tropical ozone column.

This problem is found for all reconstruction periods, both for SAGE I and SAGE II data. Although it might be partially overcome by the use of a superior curve fitting technique, this has not been attempted here since it is not of concern to us: our interest lies beyond the tropical region. (Neither the use of the non-linear balance winds in the evaluation of EPV nor the adopted transformation technique itself are appropriate for the tropics.)

Secondly, and also as noted in Chapter 3 above, comparison of the available ozone sonde data with the SAGE II data at the lowest stratospheric levels, where the ozone sondes are at their optimum performance, suggests that SAGE II overestimates OMR, increasingly so with increasing latitude and with decreasing altitude below the $340K$ surface. In the lower stratosphere above $340K$ the two systems produce similar results, providing reason for confidence in each observation technique.

Apart from these two shortcomings, however, and despite additional minor problems pertinent to specific sweep periods which are discussed below, the application of the transformation technique to the SAGE II data provides us with detailed reconstructions of the OMR distribution in which, on the basis of their close agreement with the TOMS total ozone distribution, we can place a high level of confidence.

6.1.2 Overall Picture of the Winter/Spring Ozone Evolution: 1985 to 1989

Using the reonstruction technique on the available SAGE II data, we were able to obtain a useful and detailed picture of the ozone evolution during each of the seasons between 1985 and 1989. The overall springtime evolution is much as expected from previous examinations of ozone climatology. The highest values of OMR are found in the photochemical source region in the tropical middle/upper stratosphere throughout the season, decreasing gradually poleward at upper levels and rapidly downwards (with the OMR ridge sloping upward towards the pole in isobaric coordinates), but with a mid-latitude downward bulge in the middle and lower stratosphere by mid-

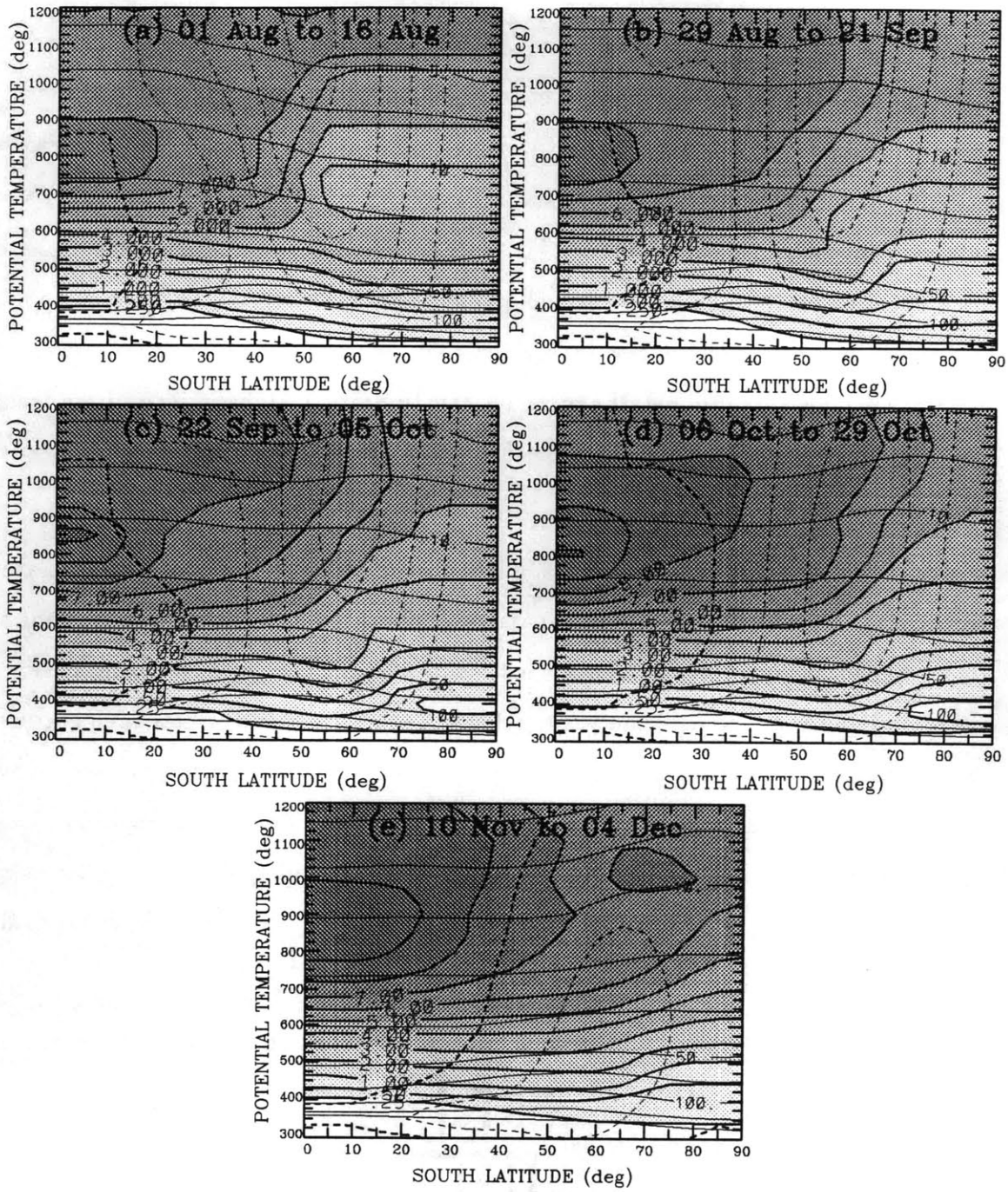

Figure 6.4: As in Figure 6.2, except for the SAGE sweeps of 1987.

winter (in either isentropic or isobaric coordinates) which results from the descending branch of the residual circulation and produces the mid-latitude maximum in total ozone. The downward bulge is located further poleward with decreasing altitude, but below about $500K$ is replaced by an isentropic OMR gradient which is initially

poleward at all latitudes.

As the season progresses, maximum OMRs in the tropical source region increase to a semi-annual maximum around spring equinox, and the high mixing ratios from the source region spread out into mid-latitudes and downward, due both to an increase in photochemical equilibrium values and poleward/downward transport by the wave-induced residual circulation. At high latitudes in the middle and upper stratosphere, low isentropic OMRs and weak vertical gradients are observed, understood to be due to gradual photochemical decay, within the cold, poorly illuminated polar vortex, of OMRs which are already low, the material having descended diabatically from levels above the OMR maximum during the formation of the vortex during early winter (Russell *et al*, 1993).

By spring equinox, the return of sunlight to the still cold and materially isolated vortex interior enables rapid chlorine-catalysed photochemical destruction of ozone to commence in the lower stratosphere. This occurs between the vortex base and between $600K$ and $700K$ in the extreme years, where the very cold mid-winter temperatures have resulted in the formation of polar stratospheric clouds, enabling heterogeneous processing of the chlorine reservoir compounds into active forms. The rapid low level ozone destruction is realised in the formation during September of the Antarctic ozone hole, the depletion process continuing into October until the active chlorine is again taken up in reservoir compounds.

As the spring progresses further and the vortex shrinks and weakens under the influence of large scale radiative warming and mechanical erosion by the increasing wave activity, high OMRs extend further southward and the location of the mid-latitude total ozone maximum migrates slowly poleward. Finally, as first the wave-induced polar warming and then the vortex breakup extend downward from the upper stratosphere, the isentropes sink and high OMRs flood onto the pole, mixing with the lower values there and smearing out the mid-latitude ozone maximum and polar minimum into a broad high latitude total ozone plateau, the seasonal transition complete.

Three features of particular interest emerge from the overall picture of the ozone

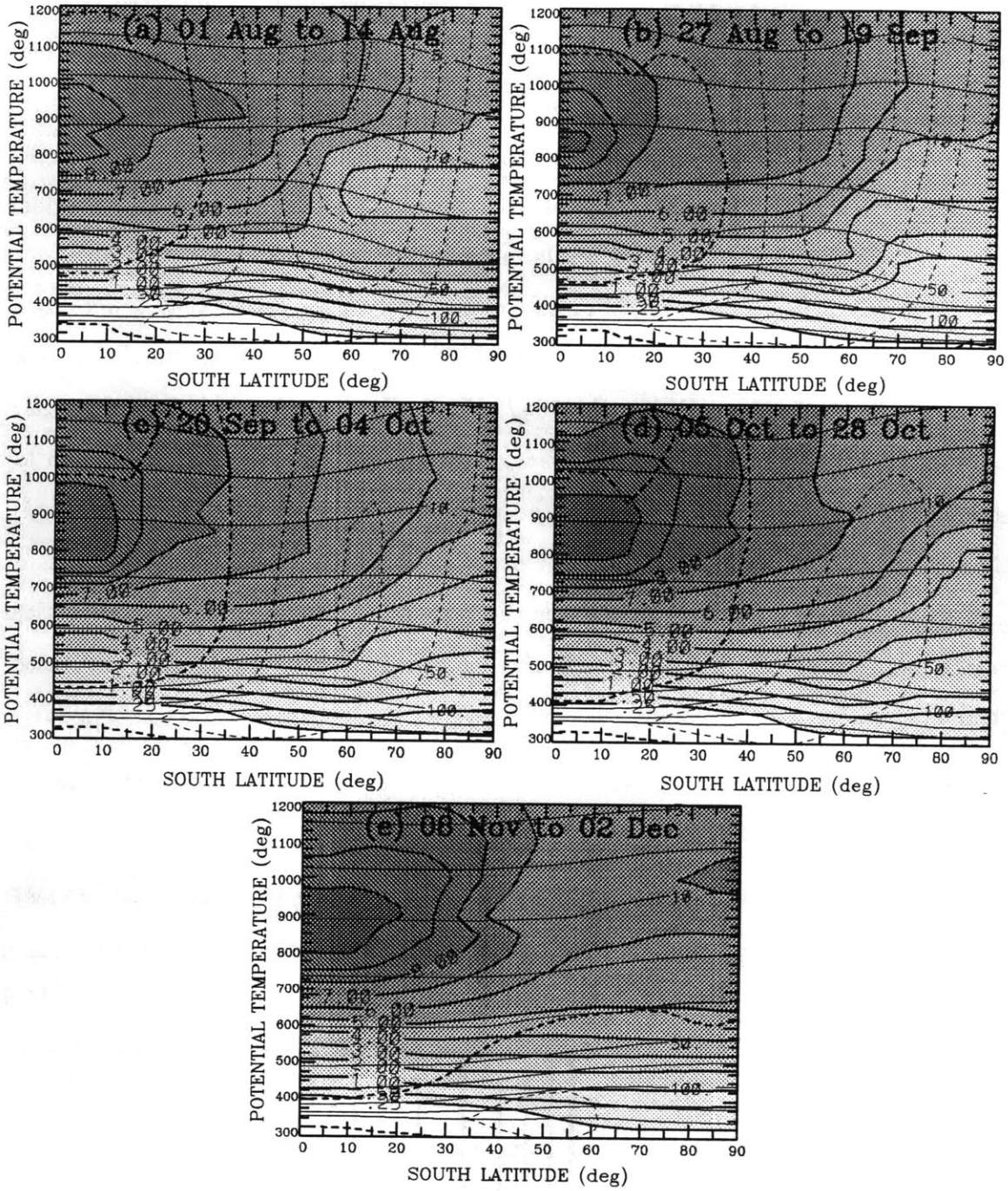

Figure 6.5: As in Figure 6.2, except for the SAGE sweeps of 1988.

evolution presented by the SAGE II analysis, two of which are evident in Figures 6.2 to 6.6.

1. The tropical OMR maximum lies at or below the 10hPa level.

The most widely employed climatology of OMR is that of Nagatani *et al* (1988),

whose analysis of SBUV data from 1979 to 1986 shows the ozone maximum to lie above the $10hPa$ level, generally around $7hPa$. The analysis of Dutsch (1978), in which he employed BUV, Umkehr and sonde data, also shows the ozone maximum above the $10hPa$ level, although a secondary maximum is evident in his October analyses just below the $10hPa$ level, as derived from the sonde and Umkehr data. Previous examinations of LIMS ozone data for January 1979 (see e.g. Gille and Russell, 1984) also depict the ozone maximum at or above the $10hPa$ level, rather than lower down. With the exception of 1979, the present analysis of SAGE data suggests the tropical OMR maximum lies at or below the $10hPa$ level. Examination of individual SAGE profiles shows that this is not an artefact of the reconstruction technique. While for many purposes this small difference in the location is rather arbitrary (ours included), it may have important implications for ozone photochemistry and radiation studies and we are led to suggest that perhaps the SAGE instrument, with its fine vertical resolution (compared to SBUV, BUV and Umkehr measurements), more accurately depicts the actual distribution.

2. Lower stratospheric mid-latitude isobaric OMR maxima are almost constant throughout the season (they don't peak in October).

There is a climatological tendency for the mid-latitude maximum values of OMR at all levels below about $600K$ to remain essentially constant on each isobaric surface after early August (decreasing monotonically with time on isentropic surfaces). This is not a new observation (the isobaric SBUV analysis of Nagatani *et al* (1988) shows that lower stratospheric OMR maxima occur in June, then remain rather constant during the spring period) but is contrary to the classical and still commonly held view of the springtime total ozone evolution. The observed southern hemisphere subpolar total ozone maximum in October has been viewed historically as being due to strong poleward/downward transport into the lower stratosphere of air rich in ozone by the residual circulation accompanying the spring wave activity maximum. While the spring wave activity no doubt enhances the downward transport of ozone into the lower stratosphere at this time, the overall rather constant values of isobaric OMR

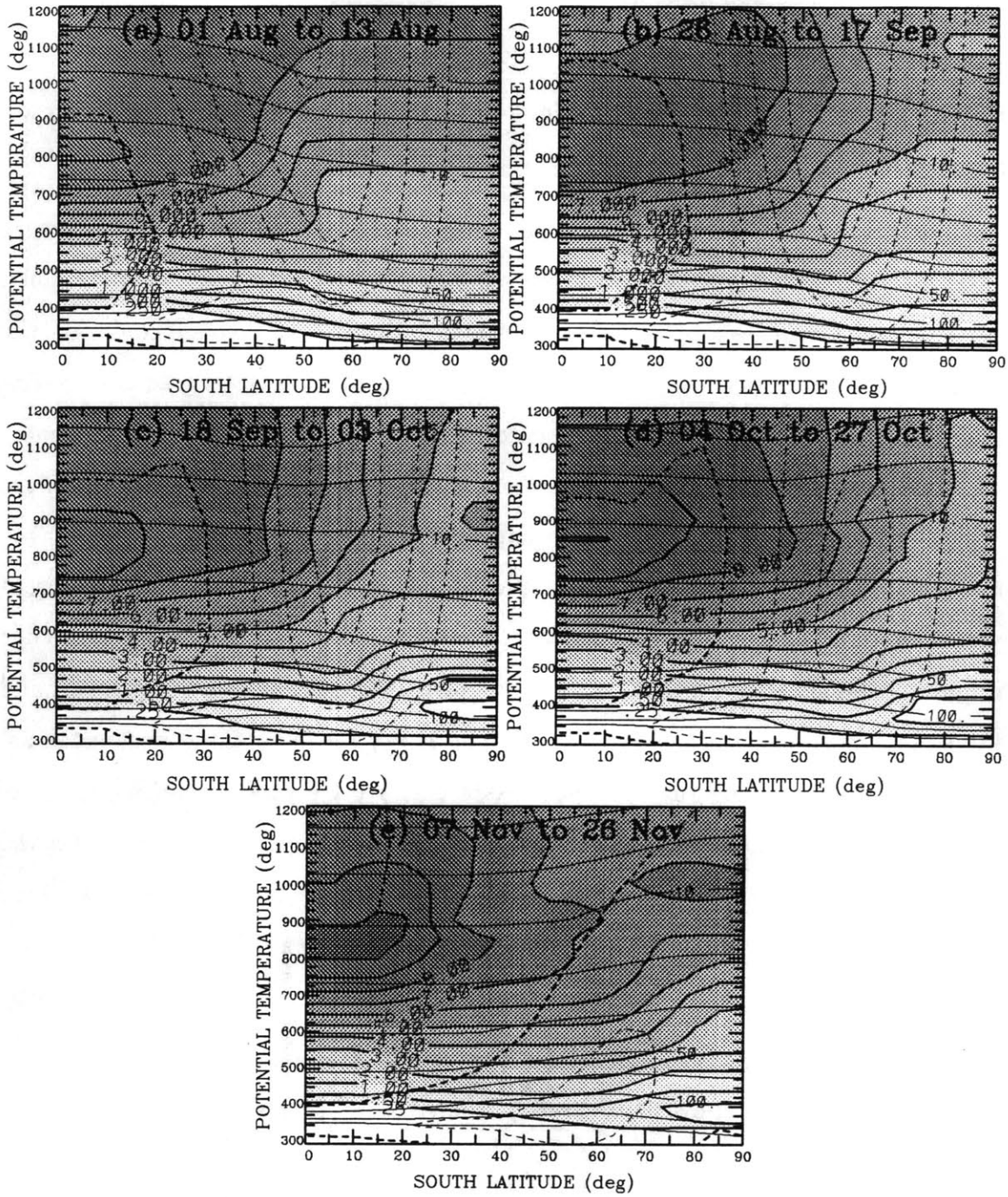

Figure 6.6: As in Figure 6.2, except for the SAGE sweeps of 1989.

at lower levels indicates that meridional mixing and photochemical destruction of ozone at these levels together must generally remove ozone from the region as rapidly as it is supplied by the downward mass flux, and that the springtime total ozone maximum is the result of midlatitude isobaric OMR increases at higher levels (i.e

primarily poleward and downward advection aloft rather than downward advection lower down).

3. The vertical (geometric) gradient of OMR reverses crossing the vortex edge.

The third feature which emerges from the present analysis, but the omnipresence of which is not entirely evident in Figures 6.2 to 6.6, primarily because of the zonal averaging, but also because of inadequate high latitude SAGE coverage during the August period, is a rather sharp mid- to high latitude vertical OMR gradient reversal observed in the vicinity of the the vortex edge between $600K$ and $900K$ in almost all SAGE profiles in the early spring. Only weak signs of this gradient reversal are evident in the Figures (e.g. note the S shape of the $5ppmv$ contour in Figure 6.2(a) in the vicinity of the jet axis). The simplest and most likely explanation of the feature is the steep meridional gradient in OMR separating elevated values at the vortex edge from lower values poleward, the vertical gradient inside the vortex being small, and the equatorward slope with height of the vortex edge. Under these circumstances, a vertical profile cutting through the edge of the inverted cone comprising the vortex wall would produce the observed features, the only requirement being that the meridional gradient at the edge must be rather steep. If this is in fact the cause, then it points to a rather simple technique for accurately locating the vortex edge (at a single level) using a single vertical profile.

Having considered the overall seasonal ozone evolution suggested by the SAGE II reconstructions, we next discuss the reconstructed distributions for each sweep period in more detail.

6.1.3 S1 Reconstruction (Early August)

Although the comparisons between TOMS and reconstructed total ozone shown in Figures 6.7(a) to 6.11(a) suggest the technique performs quite well during the early August period, the reasonable agreement evident in the Figures at the higher latitudes

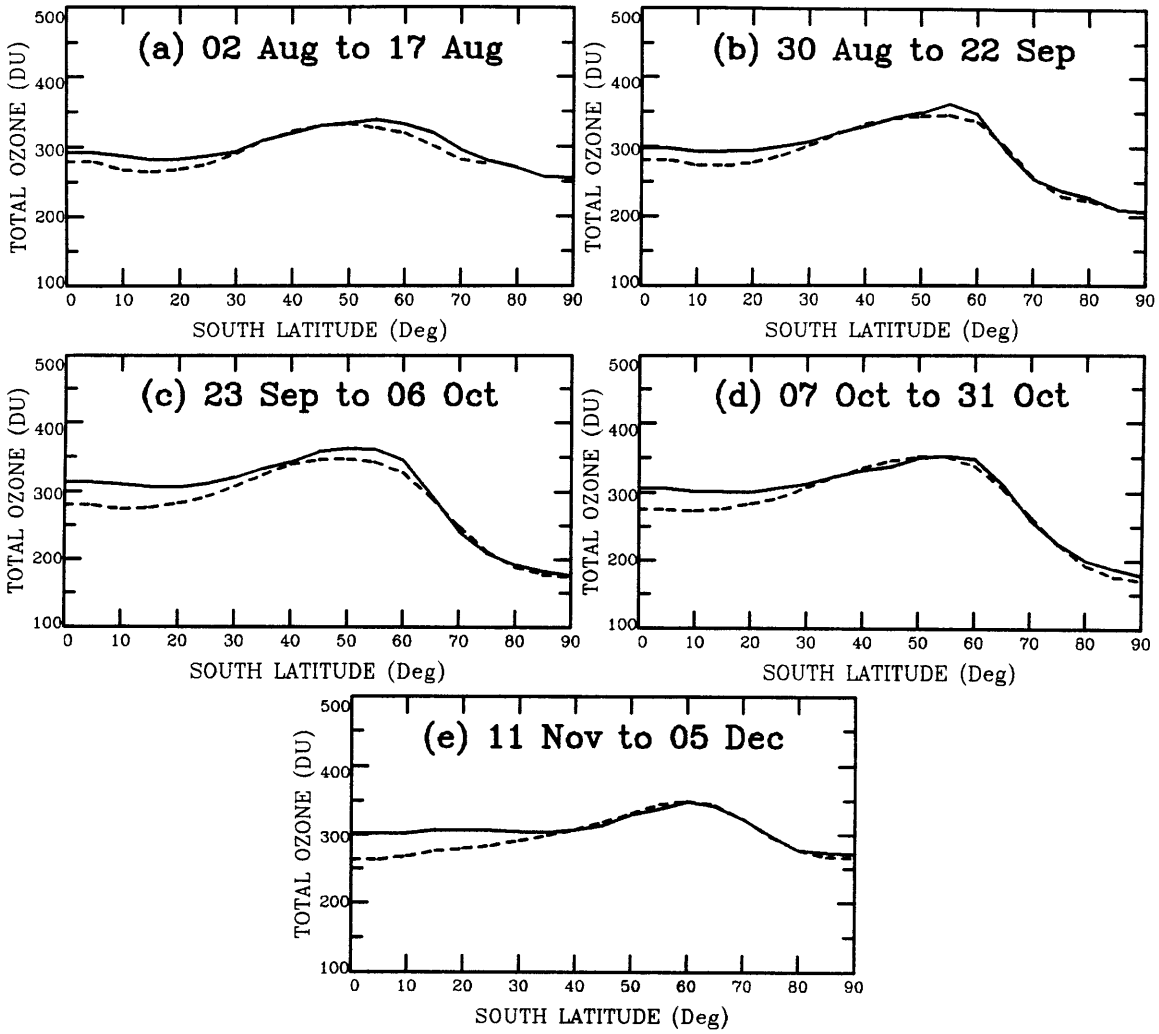

Figure 6.7: Meridional distributions of zonal mean temporal mean reconstructed (solid curves) and TOMS (dashed curve) total ozone (DU), for each SAGE sweep in the spring season of 1985: (a) S1, (b) S2, (c) S3, (d) S4 and (e) S5 (precise period of each sweep as indicated on the plots).

is largely fortuitous. (Note that, with the pole in darkness, TOMS data are only available to about $74^{o}S$.)

As discussed in Chapter 4, during early August the stratosphere is generally dynamically quiet so meridional excursions of air parcels tend to be small, particularly in the lower and middle stratosphere, and the SAGE sweeps extend only to about $52^{o}S$. Consequently, few data are available from further poleward than the outer edge of the vortex. This problem is not so great at upper levels in those years when there

is significant wave activity in early August. The high latitude upper level meridional structure evident in Figure 6.5(a), for example, demonstrates that in August 1988 there were SAGE observations near 50^oS which were well within the vortex. The problem is much more severe lower down, where both the vortex radius and disturbance amplitudes are smaller. In the reconstruction technique, as applied, isentropic OMRs at the limits of the $\hat{q}$ sampling domain are extrapolated to the 'dynamical' equator ($\hat{q} = 0.0$) and pole ($\hat{q} = 1.0$) by assuming no meridional variation beyond the edges of the sampling domain. This extrapolation is evident in each of Figures 6.2 to 6.6 as perfectly flat OMR isopleths at either very low or high latitudes, and for the S1 period generally leads to the fortuitous correspondence between TOMS and reconstructed total ozone.

Comparison of the SAGE χ vs $\hat{q}$ plots at the lowest levels ($\theta < 500K$) with corresponding plots for the available ozone sonde data for each S1 period showed that the SAGE reconstructions fail to capture a significant poleward meridional OMR gradient at high latitudes (the sonde data show that OMR increases steadily all the way to the pole during early August). Hence use of the technique leads to underestimation of the contribution to the ozone column from these levels during the period. On the other hand, further aloft (from 500 to $650K$) the sonde data indicate a meridional gradient reversal and a region of negligible (or possibly reversed) vertical OMR gradient inside the vortex, with average OMR around $3ppmv$ (broadly in agreement with the mid-winter climatology of Dutsch (1978)). The reconstructions are also blind to this feature, so the technique leads to significant overestimation of the contribution to the ozone column from these levels. The combined result of these two offsetting effects is for the reconstruction technique to produce an ozone mixing ratio distribution whose vertical integral closely resembles the observed period and zonally averaged total ozone distribution, but which would not be very suitable for ozone transport studies. Obviously, the preferred approach, particularly for the S1 period in each year, would be to use both ozone sonde and SAGE data for the coordinate transformation. As noted in Chapter 3 above, the late acquisition of the sonde data precluded this in the present study, but since our primary focus is on ozone dilution events which occur

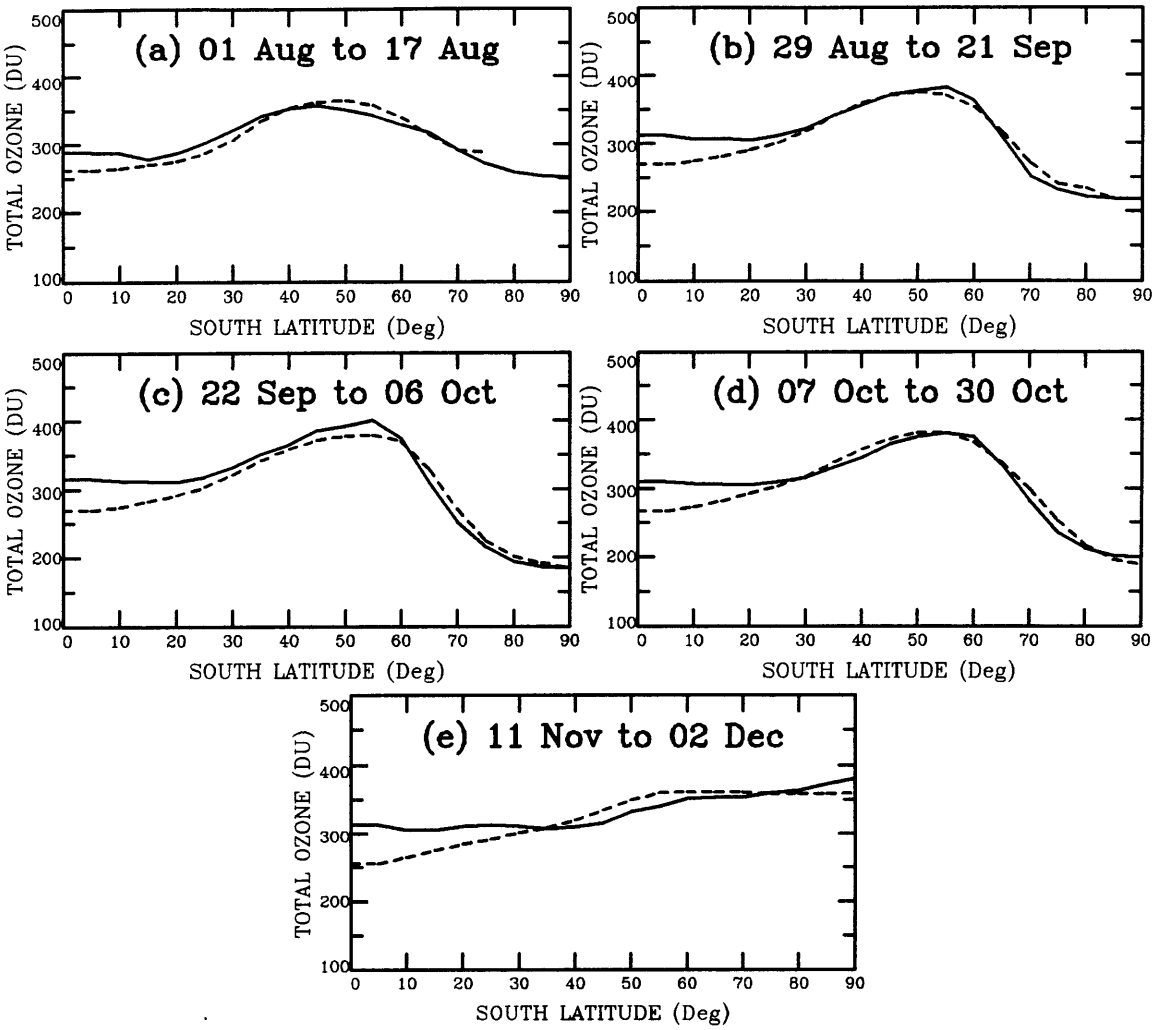

Figure 6.8: As in Figure 6.7, except for the SAGE sweeps of 1986.

later in the spring when SAGE coverage is considerably better and wave amplitudes are generally larger, the shortcoming for the S1 period does not present much of a problem.

Figures 6.7(a) to 6.11(a) show that during the S1 period, total ozone was generally low in the odd years 1985, 1987 and 1989 and high in 1986 and 1988. Closer examination of the OMR distributions for each year suggests that the consistent feature of the odd (even) years was relatively low (high) OMRs in middle latitudes between about $475K$ and $650K$ (25 to 70 hPa), coinciding with a less (more) pronounced mid-latitude temperature maximum at these levels. All other things being equal, this suggests more wave dissipation, hence more EP flux convergence, in subtropical

latitudes in the middle stratosphere leading up to mid-August in 1986 and 1988 than in the other years. The $10hPa$ wave amplitude behaviour, as discussed in Chapter 5 above, leaves no clear distinction between the odd and even years with respect to overall wave activity in the winter and early spring, but it may be significant that, unlike in the odd years, in 1986 and 1988 significant wave amplitudes were observed north of 40^oS in the period prior to mid-August, the wave 2 component was significantly larger in these years and the tropical QBO was in its easterly phase. Figures 6.2(a) to 6.6(a) show that the polewardmost location of the early August zero wind line for the even years was near 30^oS between $700K$ and $900K$ whereas during the other years it tended to lie north of 20^oS, at lower levels during 1987 and 1989, and near $900K$ in 1985. Together these features are consistent with, although not necessarily indicative of, greater downward mass flux in the mid-latitude middle and lower stratosphere in the even years.

While the S1 total ozone distributions for 1986 and 1988 were very similar, the OMR distributions were quite different. As well as apparently larger mixing ratios in the tropical source region, OMRs were higher in 1988 than in 1986 at sub-tropical latitudes above about $600K$ and generally lower below $600K$, the opposite tending to be the case at higher latitudes. This picture is consistent with, but once again not necessarily indicative of, more mid-latitude EP flux convergence at lower levels prior to mid-August in 1988 than in 1986, and we are led to speculate that, were all other things equal, perhaps the large wave 1 amplitudes observed during late July and early August 1988 assisted in bringing about significant wave dissipation (whether by Rossby wave breaking or wave absorption) at lower levels than in 1986.

In each of the years 1985, 1987 and 1989 the total ozone maximum was about the same, but the peak in these years lay near 50^oS, 45^oS and 40^oS, respectively. It seems most likely that this was due to the vortex at upper levels in mid-winter being larger in 1989, and smaller in 1985, than in 1987. Assuming, as is suggested on the grounds of both observational and theoretical evidence, that the preferred location of the stratospheric wave activity remains essentially fixed relative to the vortex edge

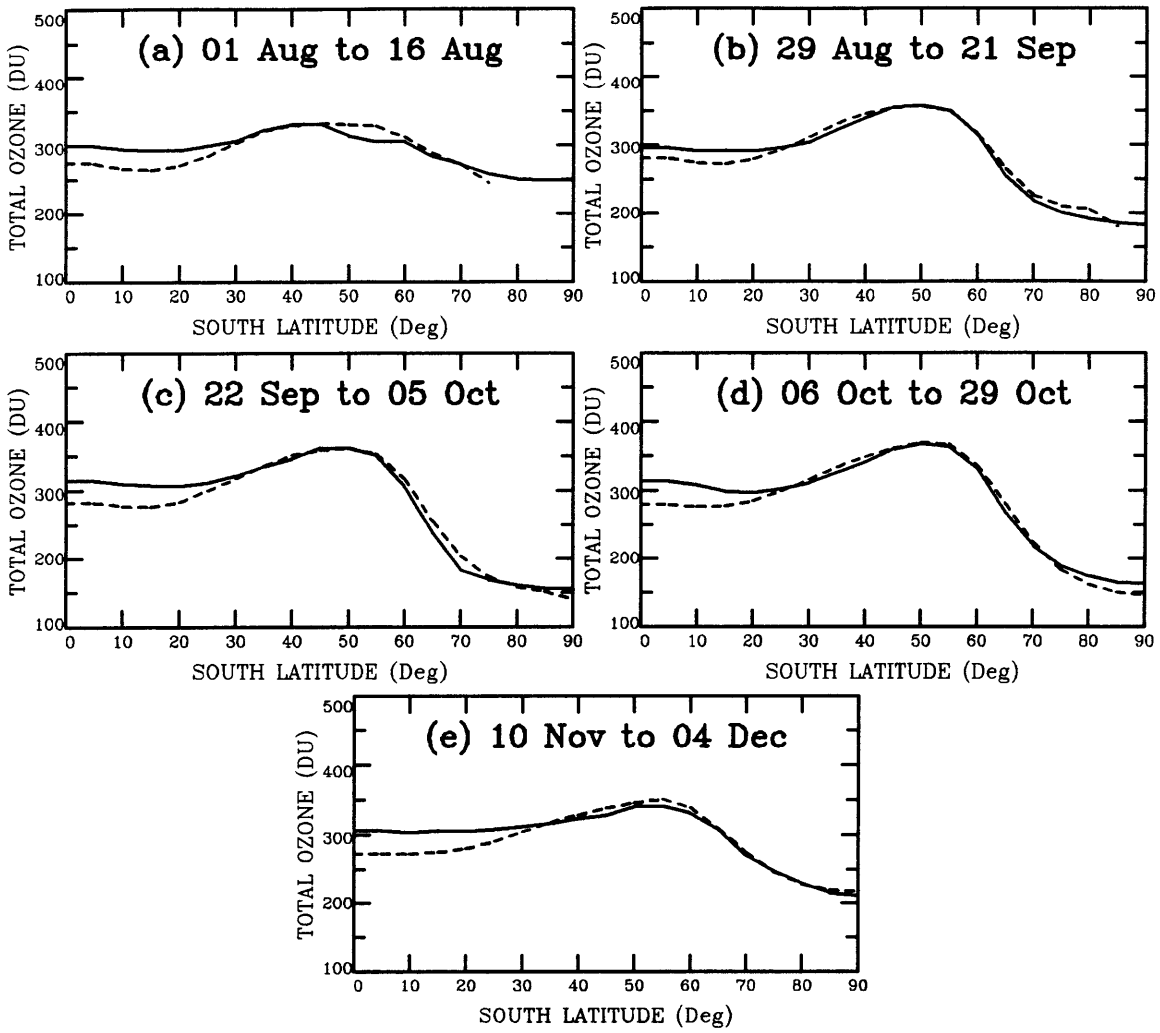

Figure 6.9: As in Figure 6.7, except for the SAGE sweeps of 1987.

(because the high meridional EPV gradient at the vortex edge acts as a wave guide for the vertical propagation of Rossby waves, and any in-situ stratospheric forcing would be related to the structure of the polar jet), then focussing of the wave activity successively further north from 1985 to 1989 might be expected to be accompanied by maximum wave dissipation, and the resultant downflux of high ozone, successively further north. Moreover, a more northerly location of the wave activity might also be expected generally to result in interaction of the waves with the tropical critical layer at progressively lower levels. In this context it is of interest that, while the $10hPa$ wave amplitude plots of Randel (1992) for the successive years perhaps suggest the wave activity prior to mid-August each year was located marginally further north

in succeeding years, his $1hPa$ plots leave the matter in little doubt, both as far as the meridional location of the wave activity and its vertical penetration, his plot for 1989 showing that virtually none of the activity reached $1hPa$, as noted in Chapter 5 above. It is perhaps not surprising, then, that there was so much ozone in the sub-tropics in 1989 (the same zonally averaged value of total ozone at a lower latitude implying a much greater amount of hemispherically integrated ozone). In fact, zonal mean total ozone in early August 1989 between 25^oS and 30^oS was as high as in any of the eleven years examined, being very similar in 1979 and 1981.

6.1.4 S2 Reconstruction (Late August to mid-September)

With the SAGE observation latitude reaching around 64^oS by the end of the sweep and wave amplitudes generally increasing as the period progressed, the reconstruction technique was effective in achieving almost complete meridional coverage of the ozone distribution during S2. The resulting OMR cross-sections and zonal mean total ozone distributions for the five years are shown in Figures 6.2(b) to 6.11(b).

As for the August sweep, total ozone is generally much higher in mid-latitudes in 1986 and 1988 than in the other years, consistent with the higher level of overall wave activity in the even years. The meridional total ozone distributions in 1986 and 1988 are again very similar, the mid-latitude peak having increased markedly from early August, particularly in 1988, when maximum isobaric OMRs at lower levels were actually observed to increase rather consistently from one sweep to the next, as opposed to the climatological tendency, noted above, to remain rather constant. This increase in 1988 is seen as a direct result of the extraordinary level of persistent wave activity during the spring period. Similarly, the August/September period in 1986 was particularly active, although total wave activity was considerably lower than in 1988. It is noteworthy that the total ozone evolution was so similar given this substantial difference. Closer examination of the OMR distributions again reveals that in the sub-tropics 1988 OMRs were lower than in 1986 at lower levels and higher aloft. The particularly high total ozone in 1986 appears due to particularly high

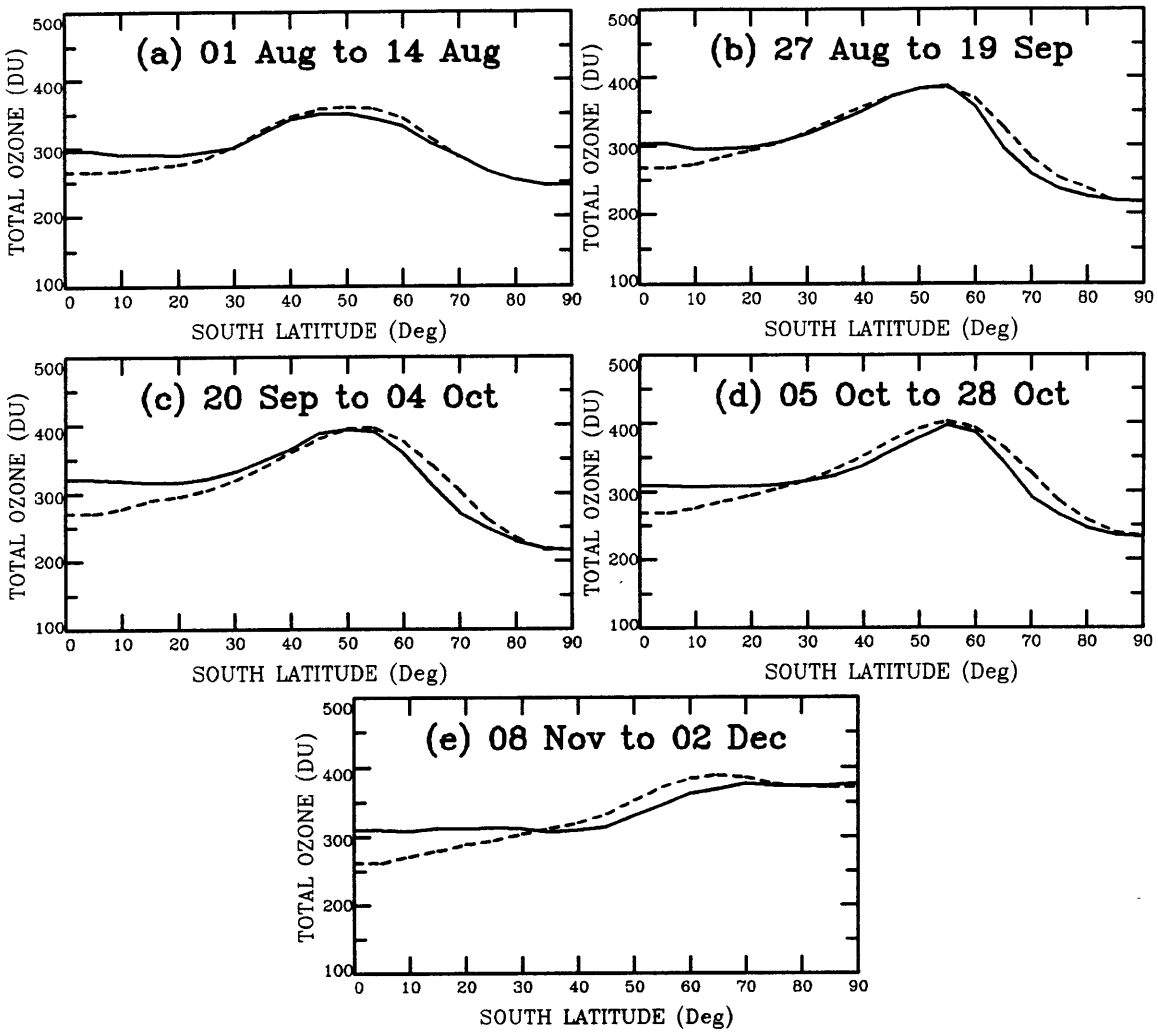

Figure 6.10: As in Figure 6.7, except for the SAGE sweeps of 1988.

ozone in mid-latitudes below $450K$, suggestive of relatively low level EP flux convergence and consistent with the observation, as discussed in Chapter 5 above, of an inordinate number of low level wave breaking events occurring at lower levels throughout the spring season. In view of the high level of wave 2 activity in the 1986 season, we are led to speculate that, at least in the southern hemisphere spring, large amplitude shorter scale disturbances (wave 2 and 3) acting in concert with wave 1 may have a more marked impact on the mean flow evolution and the strength of the residual circulation at lower levels than large amplitude wave 1 by itself.

Also evident in Figures 6.3(b) and 6.5(b) is the formation stage of the Antarctic ozone hole, evidenced by the upward bulge in e.g. the $2ppmv$ contour inside the

vortex between $450K$ and $550K$ in each plot. As suggested by the two plots, the depletion up to early September 1988, while the lower stratosphere was still quite cool (slightly cooler than in 1986, as evidenced by the more marked downward dip of the isobars over the pole at these levels), was greater than in 1986, and, as noted by Krueger *et al* (1989), similar to that in 1987. Krueger *et al* conclude that it was the virtual cessation of the depletion process after early September which brought about the shallow ozone hole in 1988, rather than a slower day-to-day depletion rate throughout the season.

The total ozone distributions for 1985, 1987 and 1989 were once again similar, the total ozone peak in 1985 further south and that in 1989 further north than in 1987, but each about the same magnitude. Once again, this appears to be related to the size of the vortex circulation each year. Also evident in the Figures are the signs of ozone hole formation, particularly marked in 1987 and 1989.

It is of interest that total ozone was so low during early September 1985, given that this was a rather active period in the evolution (as noted in Chapter 5 above) as opposed the the relatively quiet corresponding periods in 1987 and 1989. Were the resulting total ozone distribution solely dependent on the overall level of wave activity leading up to the period, peak total ozone levels might be expected to lie somewhere between those of, say, 1987 and 1986, rather than being so similar to 1987. Although the study of Manney *et al* (1991) suggests rather typical EP flux convergence behaviour during the 1985 season, the present synoptic analysis (summarised in Chapter 5 above) indicates little in the way of low level wave breaking events during the early spring (like 1987 and 1989, and unlike 1986 and 1988), despite the relatively high level of overall wave activity in 1985. The observed low peak total ozone values therefore reinforce the impression gained from the present analysis that it may not be the overall level of wave activity, *per se*, which is critical in determining the total ozone distribution, but the occurrence of significant wave dissipation at low levels, which is not necessarily in direct proportion to the overall level of wave activity.

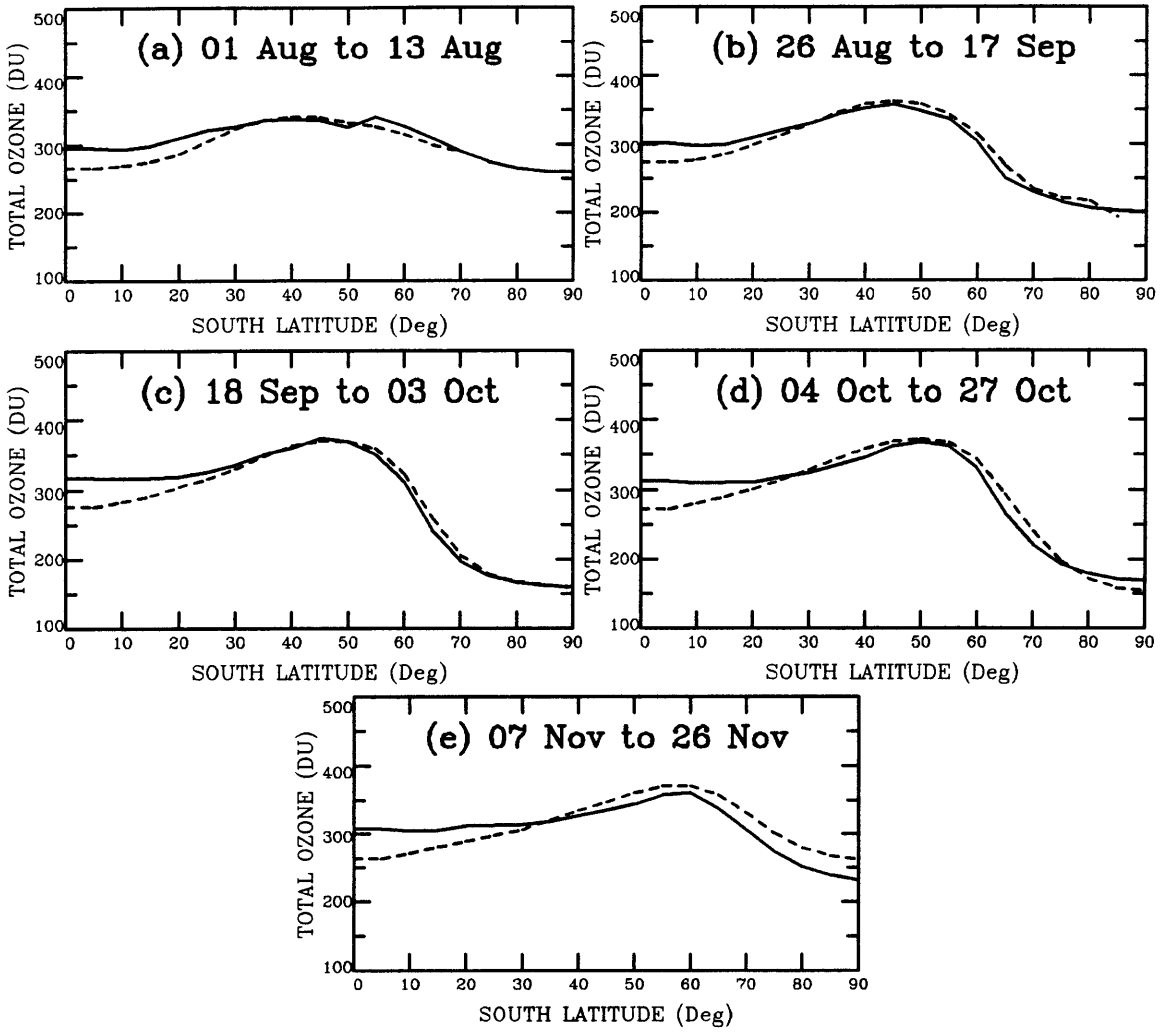

Figure 6.11: As in Figure 6.7, except for the SAGE sweeps of 1989.

6.1.5 S3 Reconstruction (Late September to early October)

S3 is the shortest period 'full hemispheric coverage' sweep of the season, and its end sees the Antarctic ozone hole at full maturity and the mid-latitude total ozone peak approaching its annual maximum (see Figures 6.2(c) to 6.11(c)).

Like the behaviour earlier in each season there is a marked difference between the even years (1986 and 1988) and the odd years (1985, 1987 and 1989), with much greater total ozone in the former, consistent with greater overall wave activity during the August/September period, the occurrence of large wave events at the end of

September, and the indications from the EPV analyses of low level wave breaking almost throughout September in the even years.

The difference between the mean total ozone distributions seen in 1986 and 1988 is larger than for the earlier sweeps, particularly at high latitudes, with higher ozone observed in 1988. In 1986 the Antarctic ozone hole continued to deepen significantly during September, and with the upper level vortex only gradually weakening, isentropic OMRs and temperatures in the polar middle and upper stratosphere increased only slowly. The overall result was a continuing decline in polar total ozone as the month progressed. In 1988, on the other hand, the extraordinary level of wave activity rapidly weakened the vortex at upper levels, dynamically warming the polar middle and upper stratosphere, and the resultant meridional transport and large scale diabatic response transported high ozone poleward and downward, markedly increasing isobaric OMRs at middle and upper levels over the pole. Below $500K$, however, the SAGE data show that the polar ozone depletion process continued throughout the month and into October. The overall effect was an essentially constant polar total ozone column during September, and a greater sub-polar increase than that seen in 1986. The present analysis shows then, that, consistent with the analysis of McMurdo ozone sonde data by Deshler *et al* (1990), in 1988 the ozone hole continued to deepen significantly during September, contrary to the conclusion of Krueger *et al* (1989), based on total ozone data alone, that the depletion process essentially ceased after early September. We explain the observed almost constant total ozone during the month as a result of the offsetting effects of the deepening ozone hole and the upper level influx of high ozone resulting from the intense wave activity.

The period and zonal mean total ozone distributions were again similar in the odd years, except for two noteworthy differences.

While south of $60°S$ the distributions in 1987 and 1989 very similar, with the deep ozone hole in each year obvious in Figures 6.4(c) and 6.6(c), polar total ozone in 1985 was considerably higher, the difference apparently almost totally attributable to milder ozone depletion in the polar lower stratosphere.

The other noteworthy difference was a much greater increase in mid-latitude total ozone from S2 to S3 in 1989 than in 1987 or 1985. The 1989 increase relative to 1987 is consistent with the observation noted in Chapter 5, of apparent low level Rossby wave breaking evident in the EPV analyses during the latter part of September 1989, whereas there were no indications of this prior to October in 1987. However, low level wave breaking events were also observed in late September 1985, so this does not explain why mid-latitude ozone remained relatively low in 1985.

6.1.6 S4 Reconstruction (October)

The meridional distributions for the S4 period are shown in Figures 6.2(d) to 6.11(d). The period coincides with the annual peak in mid-latitude total ozone, and the extreme annual minimum over the pole, which occurs in association with the fully developed Antarctic ozone hole. As for the earlier sweeps, total ozone at middle and high latitudes is considerably higher in the even years than in the odd years.

The contrast between 1986 and 1988 has increased further from that in S3, total ozone in 1988 being higher than in 1986 poleward of about $45°S$, consistent with the much greater wave activity throughout the 1988 season, which led both to an earlier final warming (as noted in Chapter 5) and a shallower ozone hole than in 1986.

As for S3 during the odd years, polar ozone was higher in 1985 than in 1987 or 1989, and the mid-latitude maximum was lower, again consistent with wave dissipation further south in 1985. The difference between mid-latitude total ozone in 1987 and 1989 was not as marked as for S3, the OMR cross-sections being very similar. This 'catch up' behaviour in 1987 is again consistent with the observed occurrence of low level wave breaking in association with the marked wave event of early October 1987, whereas in 1989 only upper level wave breaking was evident during October prior to the event towards the end of the month, as discussed in Chapter 5.

6.1.7 S5 Reconstruction (Mid- to Late November)

With respect to the analysis of potential mid-latitude ozone dilution accompanying the low level vortex breakup each year, S5 is generally the most important of the SAGE reconstruction periods in the present work. As can be seen by close examination of Figures 6.7(e) to 6.11(e), the technique performs better in some years than in others, based on the agreement between TOMS and reconstructed total ozone. While it appears to do well in 1985 and 1987 while the vortex remains intact at low levels, it generally underestimates the total ozone column throughout the extra-tropical region in 1989, the year of primarily radiative decay during the latter half of November, and tends to underestimate mid-latitude ozone in 1986 and 1988 (also overestimating polar ozone in 1986), the two years in which the vortex was displaced from the pole by mid-November.

The general underestimation in November 1989 is due to a gradually increasing component of unaccounted-for EPV relaxation in the analyses, which erroneously shifts the high OMR region in the lower stratosphere (500 to $600K$) too far equatorward, expanding the ozone hole and smearing out the mid-latitude maximum. Nonetheless, since the meridional gradient in total ozone at higher latitudes is quite well represented in the reconstructions, they are adequate for our subsequent purposes. The mismatch in 1986 and 1988 results from EPV relaxation in the analyses after mid-November each year. This decrease in the effectiveness of the reconstructions does not render them useless, but introduces a requirement for additional care in interpretation of the results.

6.2 Reconstructions for the SAGE Sweeps in 1979 to 1981, and 1984

As described above, the SAGE I data from the available sweeps in 1979, 1980 and 1981, and the SAGE II data from the sweep in 1984 (see Figure 6.1) were used, in

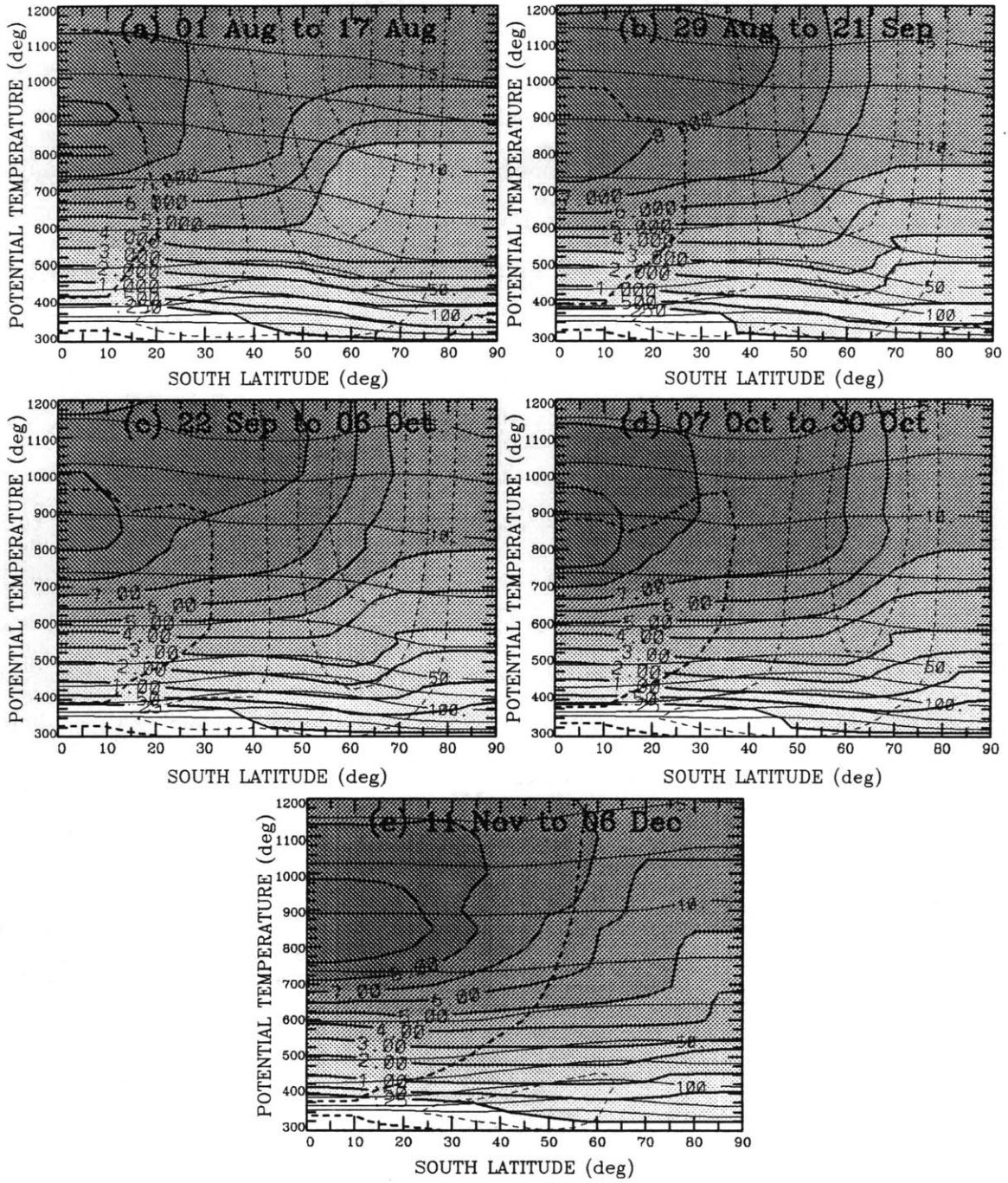

Figure 6.12: As in Figure 6.2, except for the sweeps (SAGE and 'virtual') of 1984.

some cases after modification, to produce ozone reconstructions for each period. For each of these available sweeps, we now present the reconstructed ozone distributions, giving details of modifications and why they were made, and discussing the resulting distributions.

6.2.1 S5 1984 (Mid-November to Early December)

The meridional cross-sections of OMR and total ozone reconstructed using the available SAGE data from this period are shown in Figures 6.12(e) and 6.16(e) respectively. The adopted distributions were obtained by applying the reconstruction technique without modification. As is evident in Figure 6.16(e), the technique performed quite well for the period. Comparison with Figures 6.11(e) for S5 1989 reveals that by this stage of the season the total ozone distribution was very similar to that in 1989 except that there was substantially more ozone poleward of the mid-latitude maximum. Comparison with Figure 6.7(e) for S5 1985 shows that, although the shape of the total ozone distribution was similar to that in 1985, total ozone was much higher in 1984 everywhere beyond the tropics. Close examination of Figure 6.12(e) reveals that the relatively high total ozone levels were primarily due to higher ozone at the lowest levels, below $450K$ (like in 1986) whereas at upper levels the ozone distribution was rather average. This low level feature is consistent with the picture gained from the dynamical analyses of a series of low level wave breaking events occurring throughout the season, and serving to elevate the ozone levels in the lower stratosphere.

6.2.2 S1 1981 (August)

All of the SAGE I data from August 1981 were combined into a single sweep, and the reconstruction technique applied without modification to produce the distributions shown in Figures 6.13(a) and 6.17(a). As shown in the latter Figure, the technique works reasonable well for the period, although it tends to overestimate the ozone column north of about $60°S$, and the close agreement south of $60°S$ is fortuitous and due to poor latitudinal coverage, as for the SAGE II S1 periods discussed earlier. The reasons for the overestimation at lower latitudes have not been ascertained. Only two ozone sonde profiles were available for the period (from Aspendale, Australia), and these show generally good agreement with SAGE. It seems most likely that the problem results from the inadequacy of the curve fitting technique employed to

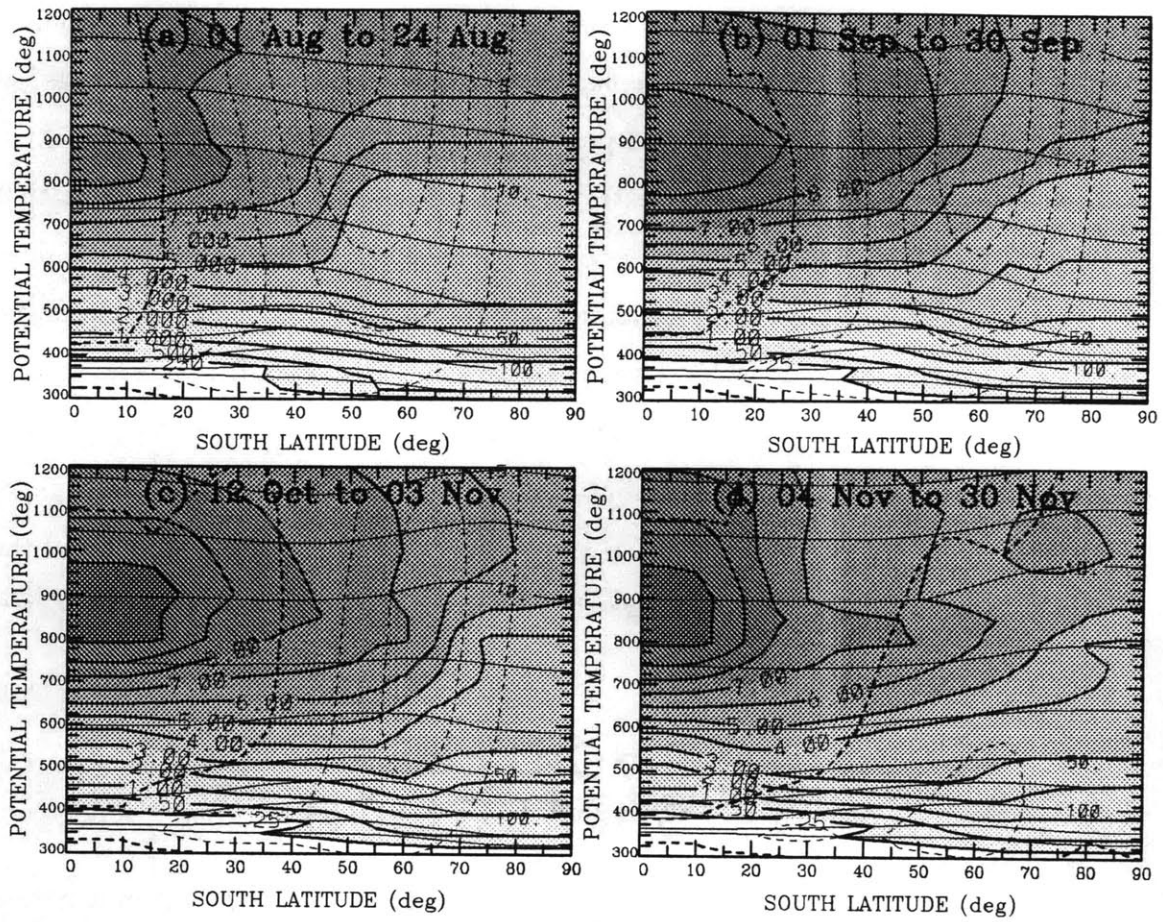

Figure 6.13: As in Figure 6.2, except for the sweeps (SAGE and 'virtual') of 1981, and the season was divided into only four sweeps, instead of the five shown in Figure 6.2.

depict accurately the steep $\chi/\hat{q}$ gradients present at lower latitudes below $500K$. Comparison of the total ozone distribution with those in August of the later years shows that total ozone was very high everywhere, somewhat at odds with the rather average wave activity prior to late August, if we are to neglect a possible contribution from a significant long-term photochemical trend. However, as in 1989, the $1hPa$ wave amplitude data of Randel (1992) show little of the activity observed at $10hPa$ reached the stratopause, suggesting the wave driving of the mean flow in the middle and lower stratosphere may have been more marked than usual, perhaps contributing to the elevated total ozone levels.

The most extraordinary feature of the resulting OMR distribution is the appar-

ently very high ozone values at lower levels during August 1981, particularly at middle and higher latitudes. Experimental replacement of all $\chi/\hat{q}$ relationships for levels below $400K$ with those from the S1 1988 period led to a marked underestimation of the total ozone column throughout the extratropical region, leading us to conclude that the high values indicated by SAGE were essentially correct. Just why they were so high is not clear from the present dynamical analysis, and unless the early winter period saw unusually marked low level wave dissipation, the observation appears to defy dynamical explanation, suggesting a photochemical cause. (The underlying question of a significant photochemical contribution to differences in the lower stratosphere between the SAGE I years and SAGE II years arises regularly in the remainder of the present Chapter, but rather than addressing it directly here, the matter is considered separately later.)

6.2.3 S3 1981 (Mid-October to Early November)

Application of the derived relationships for this period in 1981 resulted in a period and zonally averaged meridional distribution of total ozone with an unrealistically high and sharp peak near $60^{o}S$ and anomalously high ozone over the pole ($60DU$ higher than that indicated by TOMS). Comparison of the $\chi/\hat{q}$ correlation curves at lower levels with the available ozone sonde data (two profiles from Aspendale during October, and two each from Aspendale and Syowa during November) suggested that SAGE I during this period substantially overestimated OMR below $340K$, the departure between SAGE and sonde increasing with increasing latitude. Since the low level $\chi/\hat{q}$ relationships for the October sweep of 1988 (S4) showed better agreement with the sonde data, these relationships were used to replace the SAGE I fitted curves below $360K$, and the reconstruction was repeated. The resulting OMR and total ozone distributions are shown in Figures 6.13(c) and 6.17(c). As can be seen from the latter Figure, the agreement is reasonable after modification at the lowest levels, although the modified distribution still overestimates total ozone near the pole.

Close comparison of the mean TOMS distribution for the sweep with that of

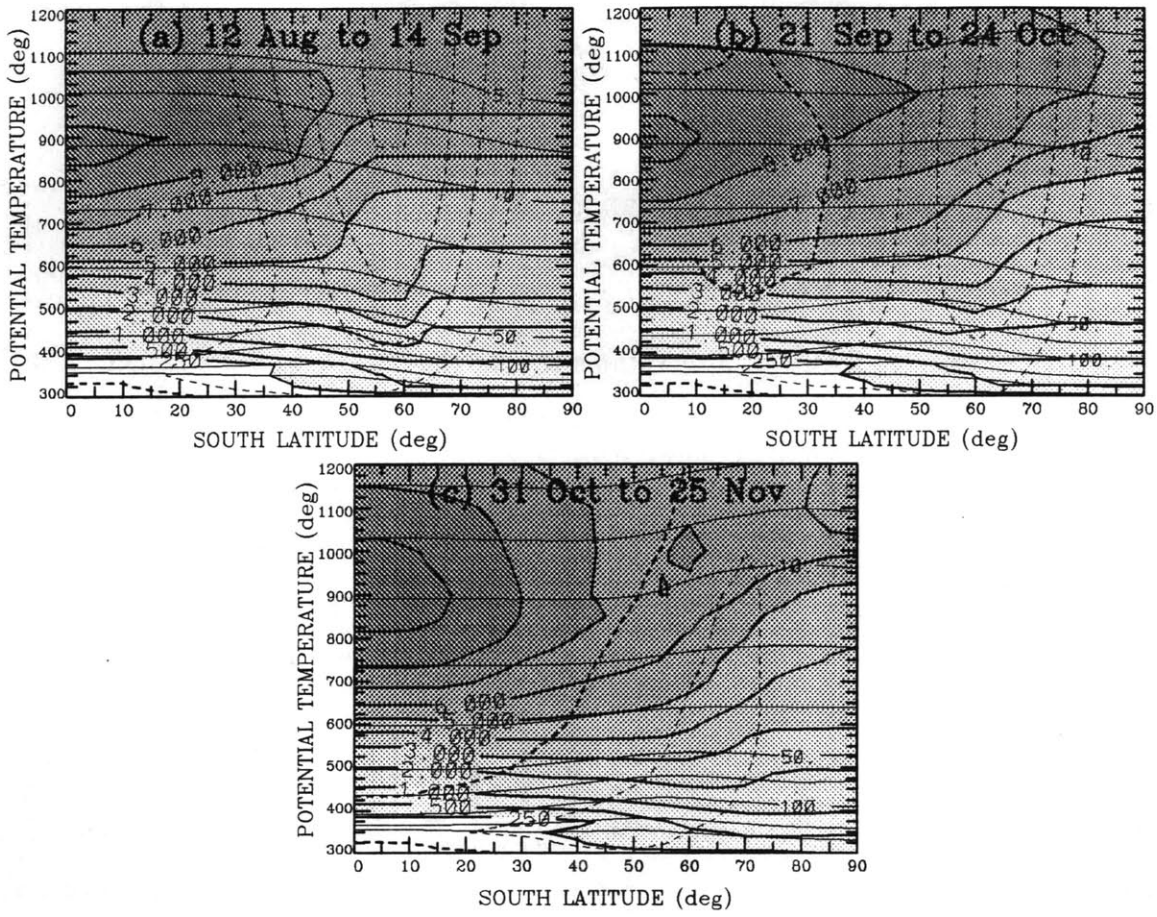

Figure 6.14: As in Figure 6.2, except for the sweeps (SAGE and 'virtual') of 1980, and the season was divided into only three sweeps, instead of the five shown in Figure 6.2.

S4 in 1988 reveals the two were very similar. Comparison of the associated OMR distributions suggests that while the more advanced vortex decay at upper levels by October 1988 resulted in substantially higher ozone over the pole aloft, at lower levels there was generally more ozone at middle and higher latitudes in 1981, consistent with a weaker ozone hole and, in the absence of a significant long term contribution due to changing photochemistry, perhaps indicative of more low level downflux of ozone at sub-polar latitudes in the 1981 season. While by no means providing conclusive evidence, the observed high ozone values at the lower levels in October 1981 once again reinforce the impression that the total ozone evolution may be dependent on the degree of low level wave breaking occurring throughout the season, rather than the overall level of wave activity itself (recall that in Chapter 5 a number of low level

wave breaking episodes were noted after mid-September in 1981, and the October wave event appeared to cause as much vortex erosion at low levels as aloft).

6.2.4 S1 1980 (Mid-August to Mid-September)

Because of the apparent poor quality of the NMC-based EPV analyses during 1980, a number of missing SAGE I observations during the period, and the rather limited SAGE latitudinal coverage, all the SAGE data from mid-August to mid-September 1980 were combined and treated as a single sweep, so that $\chi/\hat{q}$ relationships could be derived with some confidence despite a rather large degree of data scatter. The resulting reconstructions produced excessive total ozone at all latitudes (30 to $50DU$ more than TOMS). With only two ozone sonde profiles available from the period (both from Aspendale, one for which $\chi/\hat{q}$ data were available only up to $525K$) and both flights made with a low EPV airmass aloft, the sonde data for the period were of only limited use for comparison purposes. On the basis of comparison with all the sonde data available for the whole season (three profiles for October and another two for November) and the broad features of the ozone distribution during the August/September period in each of the other years examined, it became evident that the gross overestimation of the total ozone distribution during the sweep was most probably largely due to two factors.

The first was apparent substantial overestimation of low level OMRs by SAGE I during the period, primarily at mid-latitudes, evidence for which was found in much lower sonde ozone below $400K$, and much lower SAGE ozone at the same levels in August 1981, despite the apparent occurrence of particularly high ozone at low levels in August 1981. As a trial, the $\chi/\hat{q}$ relationships derived from the SAGE data for the sweep were replaced with those from the S1 1981 sweep, and the reconstruction repeated. The effect of the substitution was to produce close agreement with TOMS in the middle latitudes, but it did not explain the polar discrepancy.

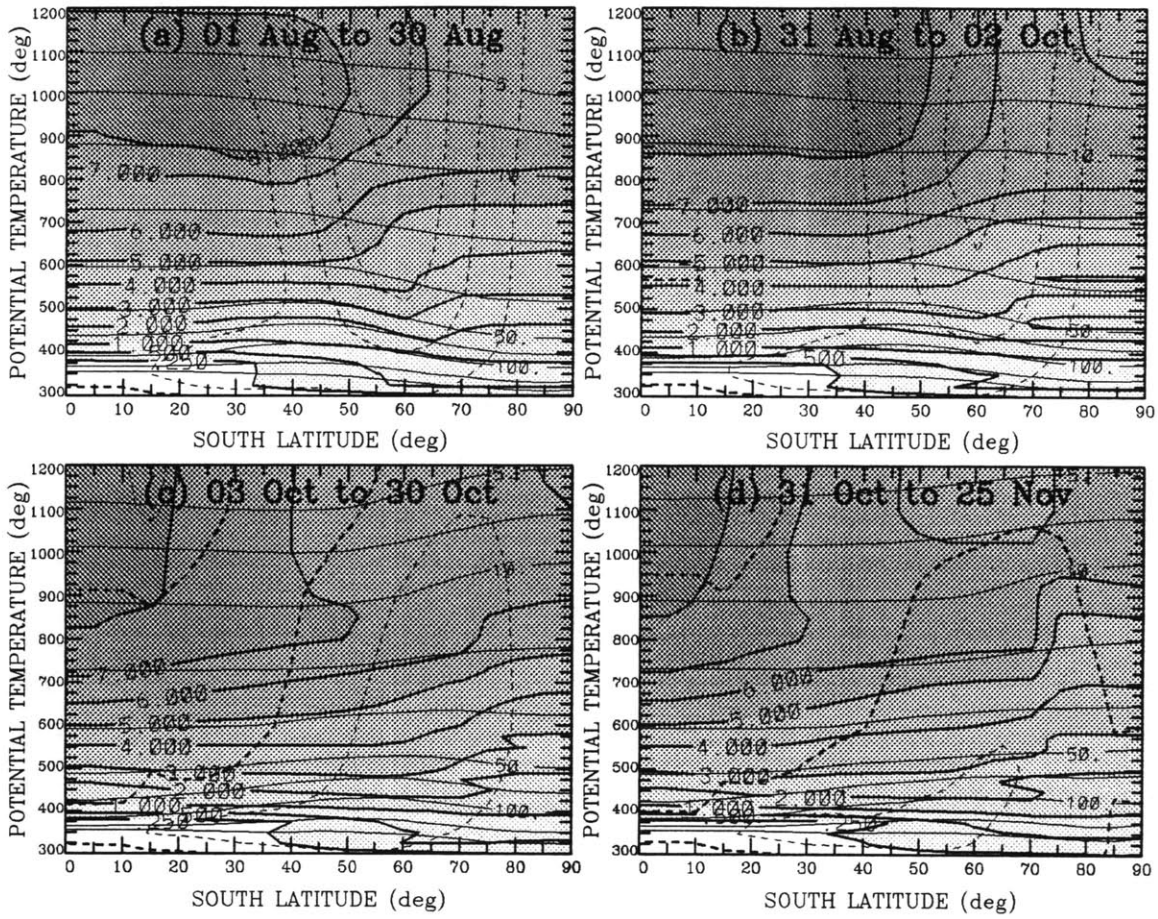

Figure 6.15: As in Figure 6.2, except for the sweeps (SAGE and 'virtual') of 1979, and the season was divided into only four sweeps, instead of the five shown in Figure 6.2.

This polar discrepancy was subsequently attributed to the inadequate latitudinal coverage of the sweep, as for the S1 periods in the later years. The southernmost SAGE observations were made at around $56^{o}S$ (see Figure 6.1) at the end of August when the vortex at low levels was pole-centred and relatively undisturbed, so the ozone levels recorded by SAGE corresponded to those at the outer edge of the vortex only. Whereas during early August isentropic ozone levels increase all the way to the pole below $500K$ so the S1 sweeps for the later years tend to underestimate polar ozone in the lower stratosphere, the 1980 S1 sweep extends into September. By this time, despite the relatively mild polar ozone depletion observed in 1980, a lower level polar minimum has formed. The failure of the SAGE observations to penetrate the vortex edge during the sweep therefore led to overestimation of polar ozone at most levels.

To overcome this problem and produce a semi-quantitatively credible, if speculative, ozone distribution for the period, the $\chi/\hat{q}$ relationships for the levels between $400K$ and $550K$ were rederived while forcing the fitted curves to produce polar ozone values about midway between those observed by SAGE during September 1979 and those in October 1981. Although the subjective interference involved makes the resulting ozone distributions speculative, it provides a credible distribution and a reasonably close fit to the TOMS data.

So the ozone distribution adopted for the sweep was that obtained from the SAGE reconstructions with both of the above modifications made. The resulting mean meridional OMR and total ozone distributions are shown, respectively, in Figures 6.14(a) and 6.18(a) and the reasonable agreement with TOMS is evident in the latter. While the overlap of the sweep period with the S1 and S2 periods of the later years prevents exact comparison, it is evident that total ozone was generally rather high in 1980, like 1981 but with a rather sharply peaked total ozone maximum near $55°S$ contrasting to the broader maximum centred near $50°S$ which was seen in 1981. Figure 6.18(a) shows that the reconstruction tends to overemphasise the sharpness of this mid-latitude peak somewhat (note the sharp meridional gradient on the poleward side of the maximum with too little total ozone between $65°S$ and $70°S$). This is a direct result of the crude technique used to force the polar minimum between $400K$ and $550K$, which decreases OMRs too rapidly poleward on the southern side of the OMR maximum (see Figure 6.14(a)). Although the total ozone levels were considerably greater at middle and higher latitudes than at the same stage in 1985, the overall shape of the ozone distribution was very similar, suggesting perhaps that, like in 1985, the small but strong vortex at upper levels after the rapid jet shift at the start of September 1980 may have confined the wave activity, and its dissipation, further south than in most years.

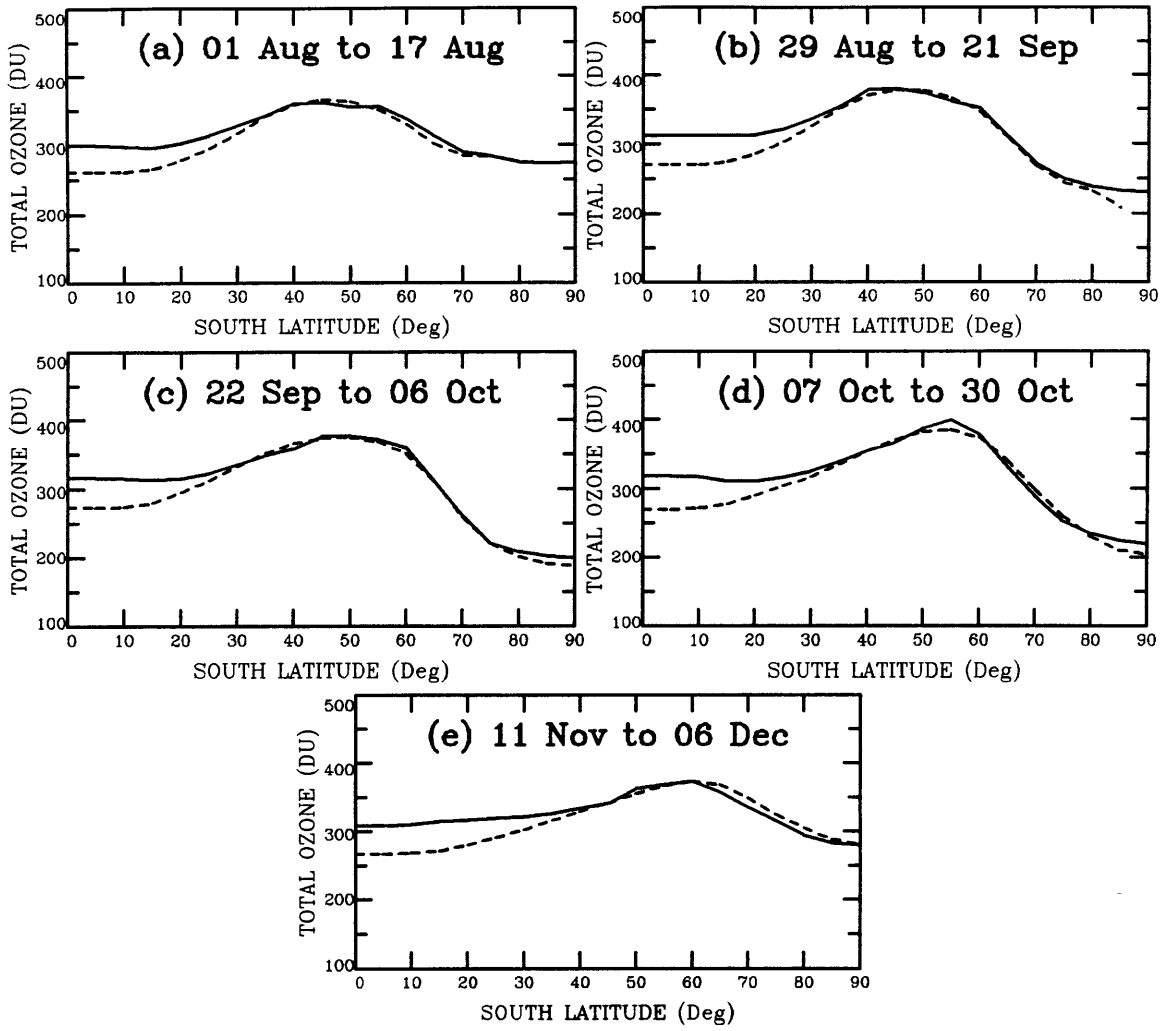

Figure 6.16: As in Figure 6.7, except for the sweeps (SAGE and 'virtual') of 1984.

6.2.5 S3 1980 (November)

The available SAGE data for this sweep were used, without modification, to perform the reconstruction depicted in Figures 6.14(c) and 6.18(c). The problems with spuriously high ozone at the lowest levels found for S1 were not evident in the data for the sweep and the direct reconstructions produced a total ozone distribution which agreed quite well with TOMS. The shape of the distribution shown in Figure 6.18(c) is by this stage of the season rather typical of November in those years when the vortex breakup does not occur during the period, the only substantial difference between November 1980, and e.g. the November sweep of 1989, being higher total ozone at

middle and high latitudes in 1980. Comparison of Figure 6.14(c) with Figure 6.6(e) for 1989 shows the ozone levels at these latitudes in 1980 were lower at middle and upper levels than in 1989, but much higher below $500K$ (by up to a factor of two).

6.2.6 S2 1979 (September)

As for the S1 period in 1980, despite the execution of two hemispheric sweeps by SAGE I in September 1979, because of poor quality of the EPV analyses, many days with missing NMC data and a number of missing SAGE observations during each sweep, all the data were combined into a single sweep and the reconstruction technique was used to produce the distributions shown in Figures 6.15(b) and 6.19(b). Once again, the technique works reasonably well, producing close agreement between TOMS and reconstructed total ozone. The most noteworthy feature of the ozone distribution is the broad mid-latitude ozone maximum and very high values everywhere, particularly at high latitudes, where total ozone levels were more than $100DU$ greater than during the same period in 1987. Another noteworthy feature is that referred to earlier: unlike most years examined, the tropical ozone maximum shown in Figure 6.15(b) lies above the $10hPa$ level. Comparison of this Figure with those corresponding to the SAGE sweeps at a similar stage in each of the other years suggests that the generally very high total ozone levels were primarily due, as for the sweeps of 1980 and 1981 considered above, to much higher ozone at the lower levels, although the 1979 cross-section indicates elevated OMRs at higher levels as well. Just why there was so much ozone in September 1979 remains unclear. As noted in Chapter 5 above, overall wave amplitudes during the season were not particularly anomalous, although frequent signs of upper level wave breaking were observed throughout the season, perhaps suggesting stronger wave driving of the mean flow there than in other years. Nonetheless, a propensity for low level wave breaking events early in the season was not observed, the occurrence of which, at least in the SAGE II years, appears to coincide with high ozone at lower levels. So assuming the relatively poor quality of the EPV analyses during 1979 did not lead to misinterpretation of the dynamical

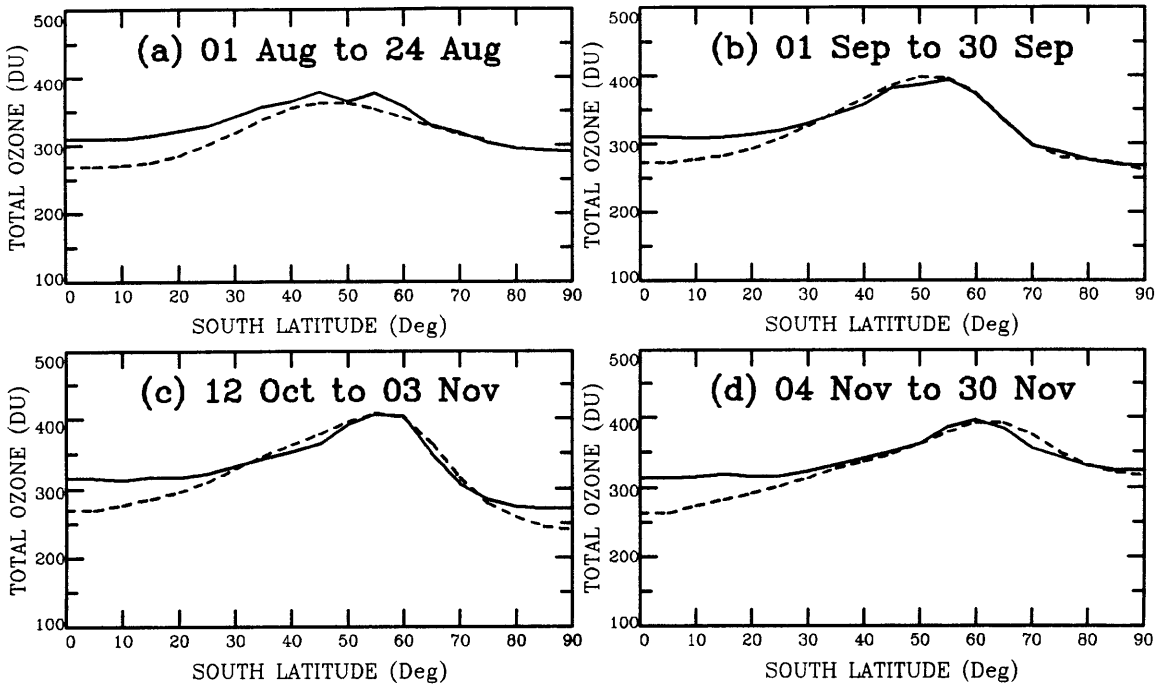

Figure 6.17: As in Figure 6.7, except for the sweeps (SAGE and 'virtual') of 1981, and the season was divided into only four sweeps, instead of the five shown in Figure 6.7.

evolution at lower levels, we are led to suspect some other cause, such as either anomalously high ozone production in the tropical stratosphere in 1979, or significant photochemical ozone depletion in the later years compared to 1979.

6.3 Speculative Reconstructions for the 'Virtual' Sweeps of 1979 to 1981, and 1984

As noted above, having performed reconstructions on the available SAGE data for the years from 1979 to 1981 and 1984, the remainder of each season was divided into appropriate 'virtual' (i.e. imaginary, or hypothetical) sweep periods (see Figure 6.1). We now turn to the more problematic and much more speculative selection of representative OMR distributions for these designated 'virtual' sweep periods, in each of the years for which at least one SAGE sweep was made.

The adopted distributions have been chosen, where possible, on the basis of intraseasonal continuity from one actual SAGE sweep to the next, in which case a reasonable level of confidence might be placed in the resulting distribution. Where this was not possible, we have attempted to arrive at adopted distributions which, although more speculative, are largely consistent with the observed dynamical evolution and the overall total ozone evolution depicted by TOMS. The four spring seasons involved are treated below in order of decreasing confidence in the results, or in increasing order of speculative input required to arrive at the adopted distributions.

We reiterate that although the adopted distributions generally display close agreement with the observed period and zonal mean TOMS distributions (at extratropical latitudes), this is because they have been chosen to do so. Although they provide a picture of the ozone evolution in each season which is consistent with the observed dynamical evolution, comprises our best guess at the evolution as it actually occurred and is probably semi-quantitatively correct, we do not claim necessarily to have uncovered the details of the ozone evolution in each season as it would have been observed.

6.3.1 1980: S2 (Late September to Late October)

Falling between the actual SAGE S1 and S3 sweeps for 1980, the isentropic OMR distribution adopted for the S2 period was that obtained simply from the mean of the adopted $\chi/\hat{q}$ relationships from the sweep before and that after. The resulting meridional distributions of OMR and total ozone are shown in Figures 6.14(b) and 6.18(b). While the agreement of period mean, zonal mean reconstructed total ozone with TOMS is generally quite close, the selected distribution shows too much ozone at polar latitudes. This is explained as the failure of the adopted distribution to describe the annual minimum in the polar lower stratosphere which occurs during the period. A trial reconstruction using the S3 $\chi/\hat{q}$ relationships alone approximately halved the high latitude discrepancy, implying that the polar OMRs depicted by the adopted distribution in the layer between about $380K$ and $550K$, the ozone

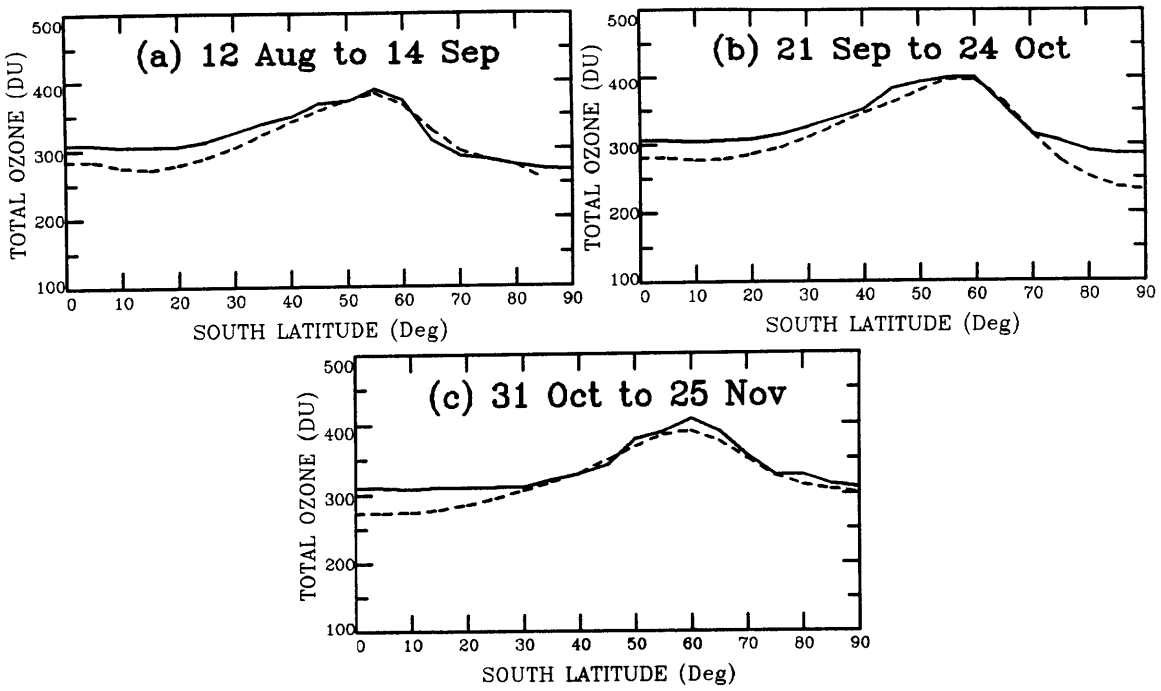

Figure 6.18: As in Figure 6.7, except for the sweeps (SAGE and 'virtual') of 1980, and the season was divided into only three sweeps, instead of the five shown in Figure 6.7.

hole region, are too high on average by about $0.75 ppmv$ (from 0.25 to $1.00 ppmv$). Rather than further contriving the result, the distribution shown in Figure 6.14(b) was adopted as is, so this shortcoming in the polar lower stratosphere is to be borne in mind. Comparison of Figure 6.14(b) with Figure 6.14(a) and (c) also indicates that the adopted reconstruction for S2 probably results in too much ozone at upper levels in middle and high latitudes, although this is not particularly critical to either the total ozone column or to subsequent ozone dilution considerations.

6.3.2 1981: S2 (September) and S4 (November)

As for the 1980 S2 period, the OMR distribution which resulted from the mean of the adopted $\chi/\hat{q}$ relationships for the S1 and S3 periods in 1981 was taken as representative of the S2 period. The resulting distributions of OMR and total ozone are shown in Figures 6.13(b) and 6.17(b). In this case, with the S3 period falling in October and coinciding with the polar ozone minimum, rather than November

when polar ozone has begun to increase, the simple temporal interpolation was more effective in describing the S2 ozone distribution, as suggested in Figure 6.17(b) by the close agreement with TOMS, although it must be kept in mind that the resulting ozone distribution will have inherited to some extent the fortuitous high latitude agreement with TOMS noted for the S1 distribution.

With the polar vortex at lower and middle levels remaining intact throughout November despite being displaced from the pole in the middle of the month (as discussed in Chapter 5), and in the absence of any SAGE data after late October, the adopted 1981 S3 $\chi/\hat{q}$ relationships were also adopted to represent the ozone distribution during November. The results are displayed in Figures 6.13(d) and 6.17(d). As can been seen by inspection of the latter plot, the adopted reconstructed total ozone distribution produces reasonable agreement with TOMS at most latitudes, but fails to represent accurately the broad structure of the total ozone maximum and places the maximum somewhat further north than actually observed.

While at first sight the above mismatch appears to be rather minor, closer inspection of Figure 6.13(d) and comparison with similar sweep periods from other years suggests the overall reconstruction is probably rather poor and the relatively close agreement with TOMS largely coincidental. The problem stems from implicitly assuming conservation of χ and $\hat{q}$ at each isentropic level during the combined seven week period of the actual S3 sweep (from which the $\chi/\hat{q}$ relationships were taken) and the S4 'virtual' sweep (on which they were used). The effect is most easily seen in the broadening of the region between the $3ppmv$ and $4ppmv$ isopleths from S3 to S4 in Figures 6.13(c) and (d). Below $500K$, with conservation of χ with respect to analysed $\hat{q}$ at each isentropic level having been implicitly assumed since the S3 period, while rather strong lower stratospheric warming has occurred in response to the wave activity at middle and higher latitudes, the reconstruction depicts significant increases in isobaric OMRs. On the other hand above $500K$ a marked change in the shape of the meridional $\hat{q}$ profile has resulted in depicted decreases in isobaric OMRs

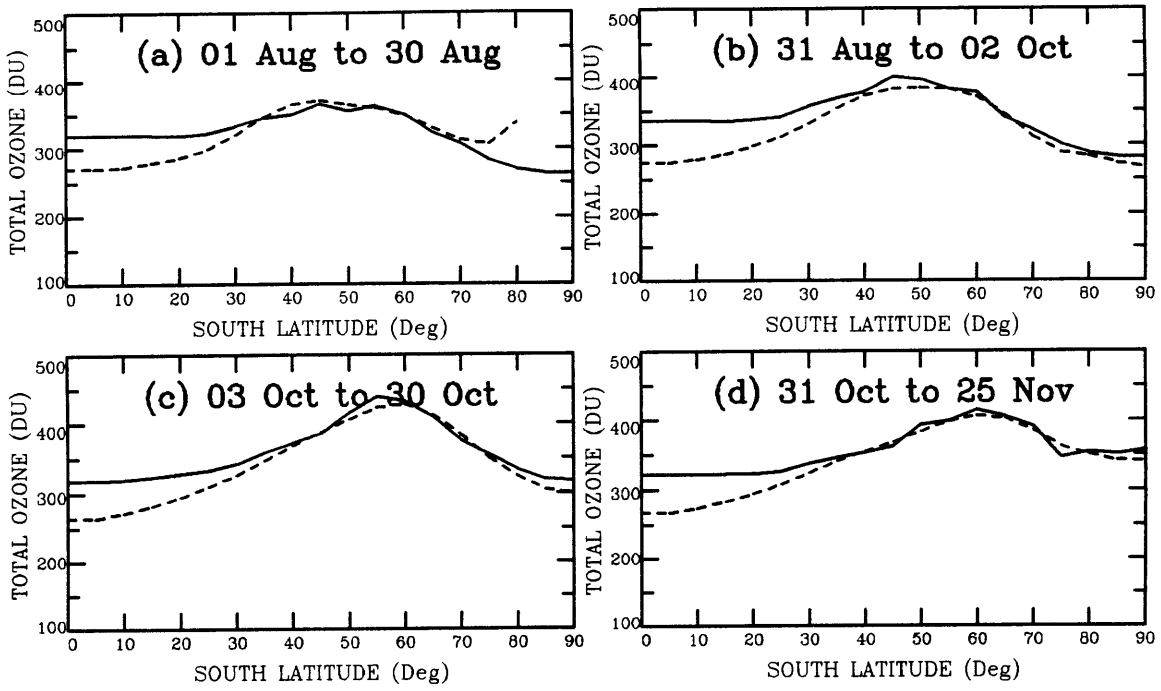

Figure 6.19: As in Figure 6.7, except for the sweeps (SAGE and 'virtual') of 1979, and the season was divided into only four sweeps, instead of the five shown in Figure 6.7.

at middle latitudes in the reconstruction. Both of these changes are contrary to the typical evolution observed in the later years at this stage of the season, but because they tend to offset one another, the agreement with TOMS remains quite close. In spite of the relatively poor quality of the reconstruction, however, it nonetheless provides a useful basis for subsequent examination of potential ozone dilution events.

6.3.3 1979: S1 (August), S3 (October) and S4 (November)

For a number of reasons it was not possible to piece together a picture of the seasonal evolution of the ozone distribution in 1979 in which much confidence could be placed. As noted in Chapter 5 above, the season was dynamically anomalous, with respect to the apparent efficiency of the not-so-extraordinary level of wave activity in effecting the mean flow evolution. Similarly, the ozone evolution was anomalous, remarkably high ozone being observed throughout the season. Added to these factors, data from only one SAGE sweep were available for direct analysis and the EPV analyses were

generally of inferior quality to those of the later years. Altogether, the process of reconstructing a picture of the ozone evolution as it might have occurred was a rather difficult task, and the adopted distributions, shown in Figures 6.15(a), (c) and (d) and 6.19(a), (c) and (d) must be considered highly speculative.

Since, of the years for which SAGE data were available, only in 1980 and 1981 was hemispherically integrated ozone similar to (although still lower than) that in 1979 both early in the season and late in the season, only SAGE $\chi/\hat{q}$ relationships from the sweeps in the early years were used to attempt ozone reconstructions for the 'virtual' sweeps of 1979.

For S1 the distribution adopted was that obtained by taking the mean of the adopted $\chi/\hat{q}$ relationships from the SAGE sweeps of August/September 1980 (S1) and September 1979 (S2). As shown in Figure 6.19(a), the resulting total ozone distribution privided a reasonable match to TOMS south of $45^{o}S$, but tended to smear out the mid-latitude ozone maximum, and probably underestimated polar total ozone somewhat, a reflection of the use of September relationships for the August period.

Selection of a likely ozone distribution for the S4 period was not so strightforward. A trial reconstruction performed using the $\chi/\hat{q}$ relationships from the 1979 S2 period resulted in far greater polar ozone than indicated by TOMS, and overly elevated values in mid-latitudes. The high latitude discrepancy appeared to be due to inadequate allowance for a lower stratospheric springtime polar ozone decrease, and the mid-latitude discrepancy to the failure, by using the September relationships, to account for the decrease with time in isentropic OMRs at mid-latitudes, primarily at the lowest levels. To account semi-quantitatively for these variations, a second reconstruction was performed, again using the OMRs derived from the 1979 S2 period everywhere above $400K$ and equatorward of $75^{o}S$, but replacing the previous values elsewhere with those derived using the 1980 S3 $\chi/\hat{q}$ relationships. The resulting rather contrived distribution was adopted to represent the period and is shown in Figures 6.15(d) and 6.19(d). As is evident in the latter plot, the total ozone distribution quite closely resembles that observed by TOMS, but because of the level of contrivance involved

in its derivation, particular details of the OMR distribution shown in the former plot must be considered highly speculative. For example, in view of the high ozone observed at middle and upper levels during S2 (Figure 6.15(b)) the reconstruction almost certainly underestimates OMRs above about $600K$ at most latitudes. On the other hand, the apparent marked increase in isobaric OMRs at middle and high latitudes in the $400K$ to $500K$ region between S2 and S4 is probably exaggerated.

The adopted distribution for the S3 period was derived from the mean of the $\chi/\hat{q}$ relationships used for the adopted S4 distribution and those from the SAGE sweep of September (S2), and is shown in Figures 6.15(c) and 6.19(c). Since the S4 relationships were used, the resulting distribution probably suffers the same problems as those just noted for S4, although perhaps to a lesser degree since only half weighting was used.

6.3.4 1984: S1, S2, S3 and S4

Because 1984 was dynamically very average in most respects other than the rather even distribution of overall wave activity throughout the winter/spring period (as opposed to a general spring peak) no individual season for which SAGE data were available promised to be a particularly useful candidate for dynamical similarity. In view of this rather average dynamical evolution, and since observed hemispherically integrated ozone during the SAGE I coverage period (the first 3 years of the analysis period) was significantly larger than during the SAGE II period (the latter 5 years), the general approach adopted for building up an approximate picture of the 1984 ozone evolution was to select two actual SAGE sweep periods from a similar stage of the season, one from prior to 1984 and one from the later years, one of these from a dynamically active season and one from a quieter period, and to use these to calculate a 'first guess' average distribution.

Since the only SAGE I sweep in August was that of 1981, the $\chi/\hat{q}$ relationships from S1 in 1981 were chosen as one of the two to be used for estimation of the S1 (early

August) distribution in 1984. The early to mid-winter period in 1984, as noted in Chapter 5 above, was particularly active, however, whereas the corresponding period in 1981 was rather quiet, so the second set of $\chi/\hat{q}$ relationships used was that from the S1 sweep in 1986, dynamically the most active of the August periods for which SAGE II data were available. Use of these two sets of $\chi/\hat{q}$ relationships resulted in the ozone distributions shown in Figures 6.12(a) and 6.16(a), which were adopted as representative of the period.

For the S2 period (late August to mid-September), S2 in 1979 was the more appropriate selection from the two available SAGE I sweeps (recall the S1 1980 $\chi/\hat{q}$ relationships had required somewhat subjective modification prior to use). In view of the extraordinarily high ozone in 1979, the second set chosen was that from S2 in 1987, the year with extraordinarily low ozone. The ozone distribution thus derived and adopted is shown in Figures 6.12(b) and 6.16(b).

In view of the close agreement between TOMS and reconstructed ozone for the S2 period, and to maintain a degree of temporal continuity, the S3 (late September to early October) and S4 (October) distributions for 1984 were derived again using the 1979 S2 $\chi/\hat{q}$ relationships, with the 1987 S3 and S4 relationships respectively. In these latter cases, however, the simple mean of the two sets of relationships resulted in overestimation of total ozone at most latitudes (implying the ozone distribution during the latter part of the 1984 season was more like that in 1987 than 1979), so the calculations were repeated using a 2:1 weighting towards the 1987 relationships. The resulting distributions, which were adopted as representative of the respective 'virtual' sweep periods, are shown in Figures 6.12(c) and (d) and 6.16(c) and (d). As can be seen in Figure 6.16, the agreement of the mean meridional distribution of reconstructed total ozone with TOMS is quite close for each of the virtual sweeps. The finer details of the associated OMR distributions in Figure 6.12 are nonetheless highly speculative and the agreement could arguably be fortuitous. Other than apparently tending to show too much ozone at upper levels, however, the resulting speculative

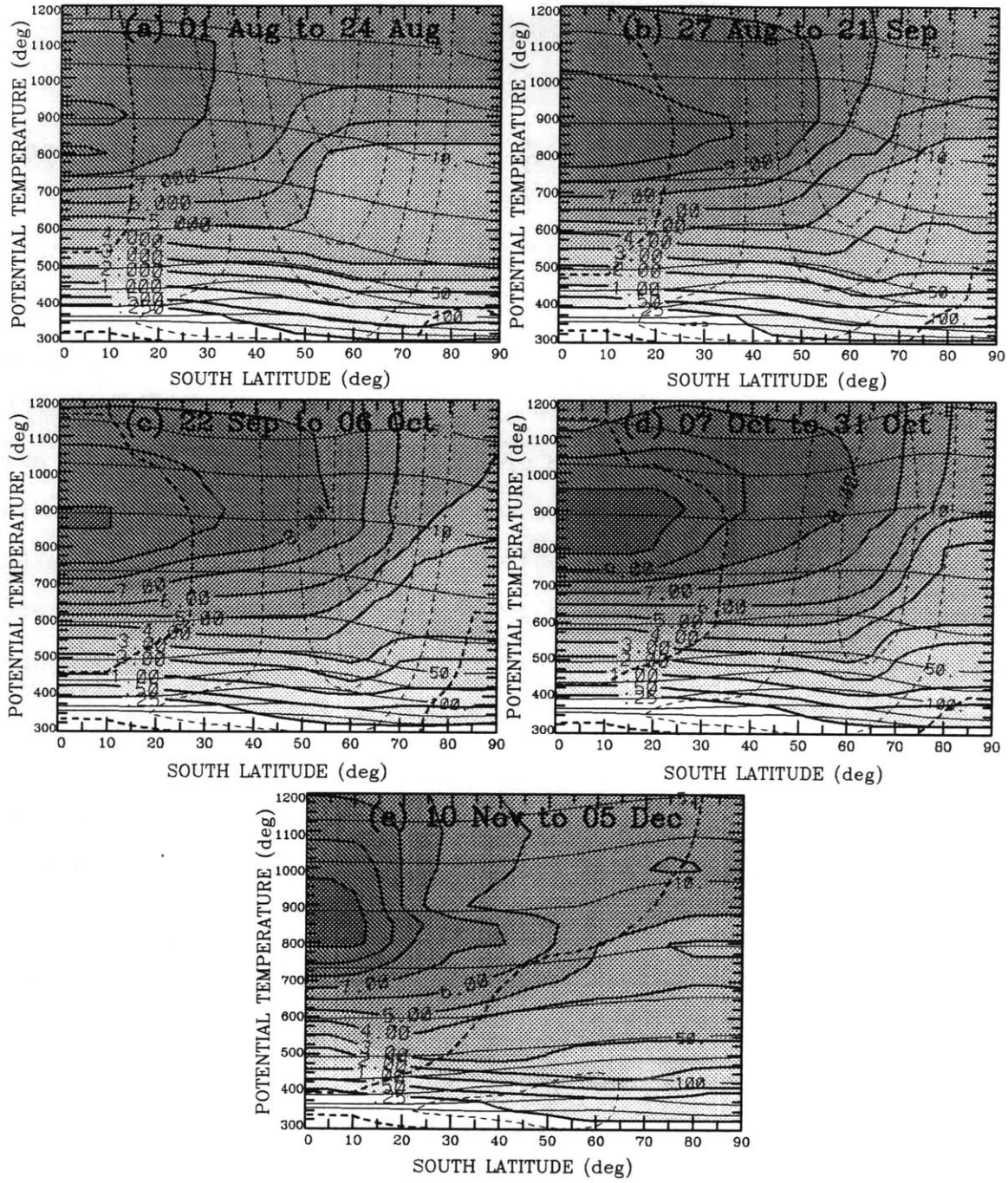

Figure 6.20: As in Figure 6.2, except for the 'virtual' sweeps of 1983.

distributions in Figure 6.12 portray an ozone evolution which is rather consistent both with those observed in the later years, and with the distribution observed for the S5 period of 1984. Close agreement was also seen between daily reconstructions and hemispheric maps of TOMS total ozone, and this suggests that the adopted dis-

tributions may indeed quite closely resemble the three dimensional ozone distribution which would have been observed, particularly during the later sweeps.

6.4 Speculative Reconstructions for 1982 and 1983

Although at the outset an attempt was made to build up a picture of the likely ozone evolution during 1982 and 1983 based upon dynamical similarity with other seasons for which SAGE data were available, this proved to be largely fruitless, indicating either that the broad overall consistency between the dynamical evolution and the ozone evolution during the SAGE II coverage period from 1985 to 1989 was more due to 'good luck than good management', or that the relationship between the dynamical and ozone evolutions in 1982 and 1983 was particularly anomalous. While it is of course possible that the former is the case, highly anomalous behaviour in the 1982 and 1983 seasons has been identified previously. Primarily in 1982, but to a lesser extent in 1983, global mean stratospheric temperatures were unusually high, thought perhaps to be connected with the very strong ENSO event which peaked in 1982 (WMO, 1988), and the volcanic eruption of El Chichon during March 1982 greatly perturbed the global stratospheric aerosol column, the Antarctic signature peaking in 1983 (McCormick and Trepte, 1987).

In view of the overall lack of success in building a description of the ozone evolution in these two years based primarily on dynamical reasoning, the approach eventually adopted was to use the $\chi/\hat{q}$ relationships from the available SAGE sweeps, and essentially by trial and error to come up with an OMR distribution for each 'virtual' sweep during 1982 and 1983 which resulted in a reconstructed meridional total ozone distribution approximately fitting the observed TOMS distribution.

Accordingly, the ozone distributions selected as 'representative' of each virtual sweep period are highly speculative, and little confidence can be placed in their detailed features simply on the strength of their overall fit to the TOMS data. Nonetheless, because each results from blending observed stratospheric OMR distributions

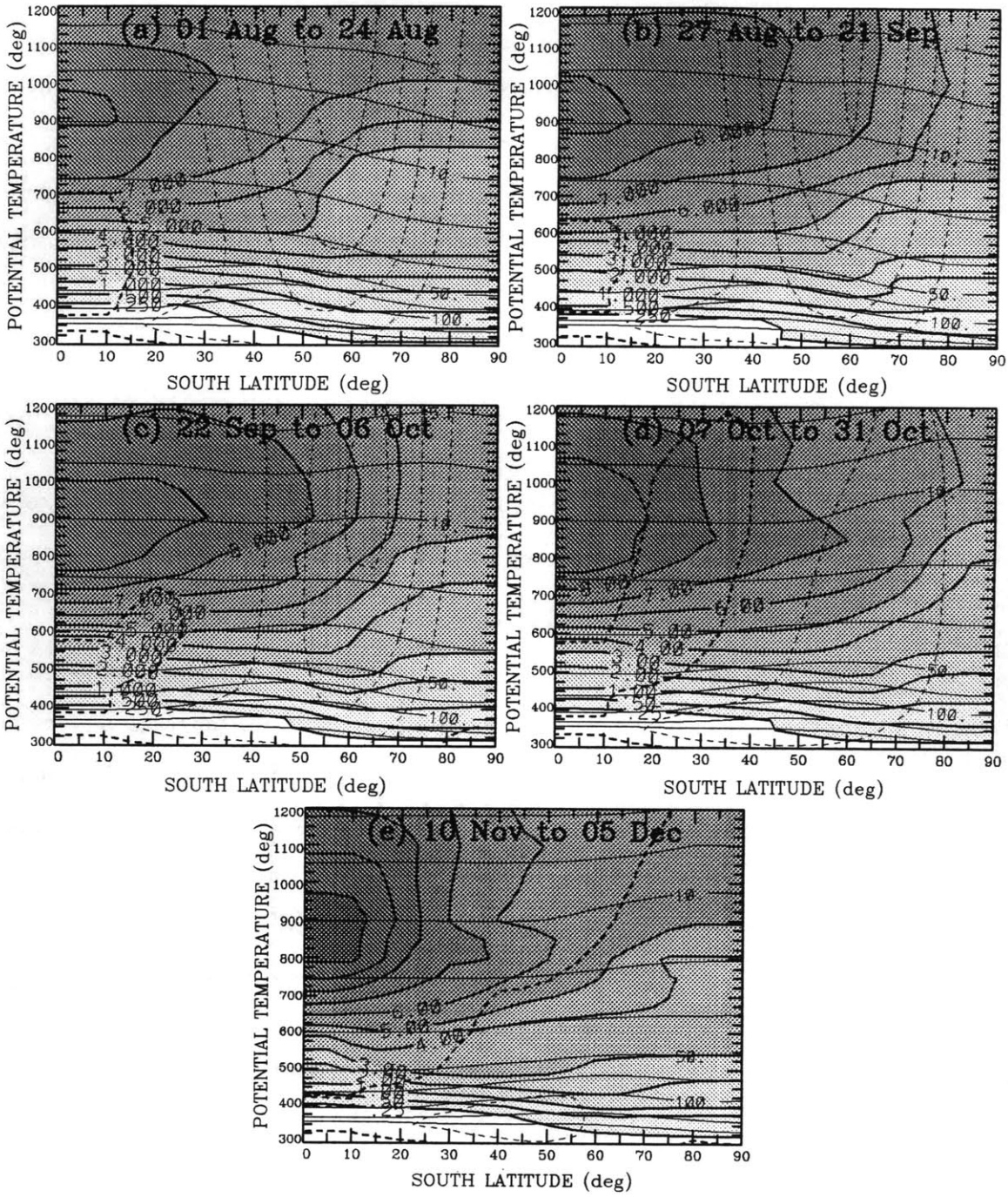

Figure 6.21: As in Figure 6.2, except for the 'virtual' sweeps of 1982.

generally taken from the same stage of the season in other years, the grosser features depicted should closely resemble those which would have been observed, and we claim that the product therefore serves as a useful surrogate for real ozone data, for the subsequent semi-quantitative examination of potential ozone dilution events occurring

in these years (dealt with in Chapter 8 below). In view of the fact that no SAGE data were available for these two years whatsoever and that an average of only 6 ozone sonde profiles in 1982, and 3 in 1983, were available for the entire southern hemisphere per month, we claim that the speculative distributions are better than nothing. In this final Section, we present the adopted distributions for 1982 and 1983, describing how they were obtained, briefly discussing the main features of the speculative ozone evolution in each year, and how reliable these features appear to be.

6.4.1 1982

The adopted zonal and temporal mean meridional distributions of OMR and total ozone for the five 'virtual' sweeps of 1982 are shown in Figures 6.21 and 6.23 respectively.

The season up to the end of August was dynamically rather quiet, as noted in Chapter 5 above, and quite similar to mid-winter in 1981. So, too, was the overall temperature distribution, except that the upper levels in 1982 were warmer and the polar middle stratosphere cooler. Nonetheless, use of the 1981 S1 $\chi/\hat{q}$ relationships resulted in too much ozone at all but polar latitudes. Since the difference was greater than could be explained by the temperature differences alone, this suggested lower ozone was present in the extra-polar lower stratosphere during the period in 1982. The best fit to the TOMS data was achieved by taking the mean of the $\chi/\hat{q}$ relationships from S1 in 1985 and 1986 and is shown in Figures 6.21(a) and 6.23(a). By adopting the distributions shown, the resulting reconstructions of course inherited the high latitude problem of overestimation at mid-levels and underestimation below, present in all the SAGE II August reconstructions.

The gradual buildup of wave activity during September was also reminiscent of the 1981 season, although, as noted in Chapter 5, was unaccompanied in 1982 by signs of low level wave breaking. A trial using the adopted $\chi/\hat{q}$ relationships from S2 in 1981 produced a reasonable fit to the data, but with too little ozone in mid-latitudes

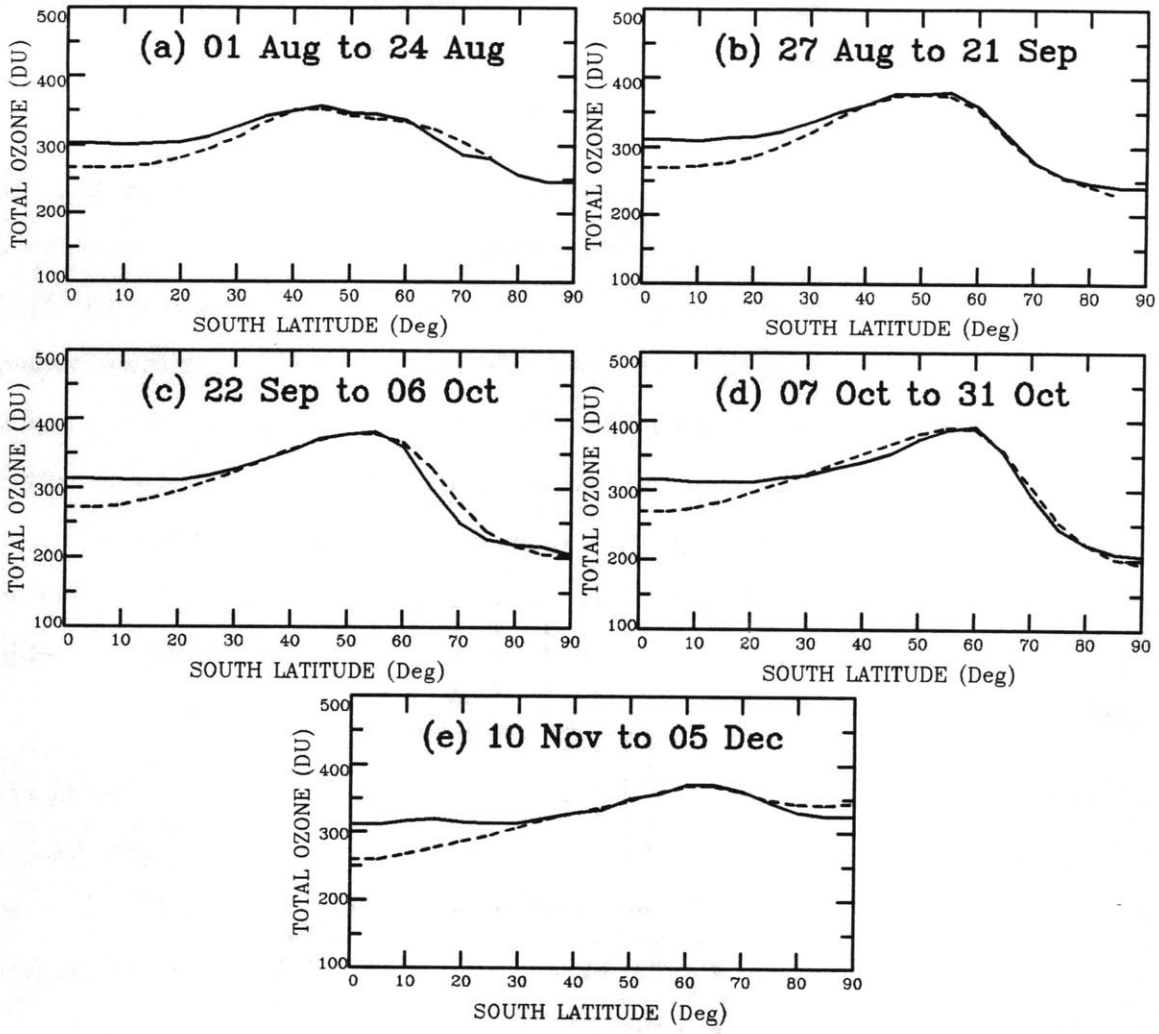

Figure 6.22: As in Figure 6.7, except for the 'virtual' sweeps of 1983.

and too much over the pole, whereas using the mean of S2 from 1985 and 1986 led to substantial underestimation at most latitudes. Rather than employing the modified 1981 relationships, however, the mean of S2 in 1979 and S2 in 1985 was adopted, with which the best overall fit to TOMS was achieved.

The general underestimation of total ozone which resulted from using the S2 1985/1986 relationships, the S1 equivalents of which provided good agreement with TOMS in August, suggests that in the absence of other factors (e.g. aerosol induced diabatic cooling) strong mid-latitude tracer downflux must have occurred during early September 1982 i.e. strong wave driving of the mean flow. In view of the absence of detectable low level Rossby wave breaking during the period, and the absence of a

strong vertical EP flux signature associated with the early September wave activity (Mechoso *et al*, 1988; Manney *et al*, 1991) this seems unlikely, however, and a clear explanation is not evident.

Trial use for the S3 period in 1982 of each of the sets of relationships from S3 in 1985 and 1989, in turn, understandably produced much too little ozone poleward of the ozone maximum while generally leading to overestimation equatorward. That this was a reflection of a smaller polar ozone depletion in 1982 rather than warmer polar temperatures was shown when the 1986 and 1988 relationships (both warmer periods in the polar lower stratosphere) each produced the same effect. On the other hand, use of the relationships from either 1979 or 1981 led to gross overestimation at higher latitudes (and in the former case everywhere). The best fit for the S3 period was eventually achieved using the mean of the adopted $\chi/\hat{q}$ relationships from S3 in 1981 and S2 in 1989.

For the S4 period the best fit was obtained using a combination of the adopted $\chi/\hat{q}$ relationships from S3 in 1981 and S4 in 1985, although it is evident in Figure 6.23(c) and (d) that the rather sharp sub-polar peak in lower stratospheric OMRs observed in both 1981 and 1985 but somewhat exaggerated in the 1981 reconstructions (see Figure 6.17(c)) was not present in 1982.

While use of the S3 relationships from 1980 for the S5 period in 1982 produced a reasonable fit, they overplayed total ozone near the latitudinal maximum ($60°S$) and in the polar region, and underplayed the mid-latitude column. The distribution eventually adopted combined S3 from 1981 above $400K$ with S4 from 1988 elsewhere. As shown in Figure 6.23(e), while the extratropical total ozone distribution appeared to be reasonably well described, several features evident in Figure 6.21(e) are unrealistic, the most obvious of these being the sharp low latitude peak in the $4ppmv$ contour, and the rather large region between the $3ppmv$ and $4ppmv$ contours. the same comments made in relation to the 1981 S4 reconstruction are also relevant to this adopted distribution.

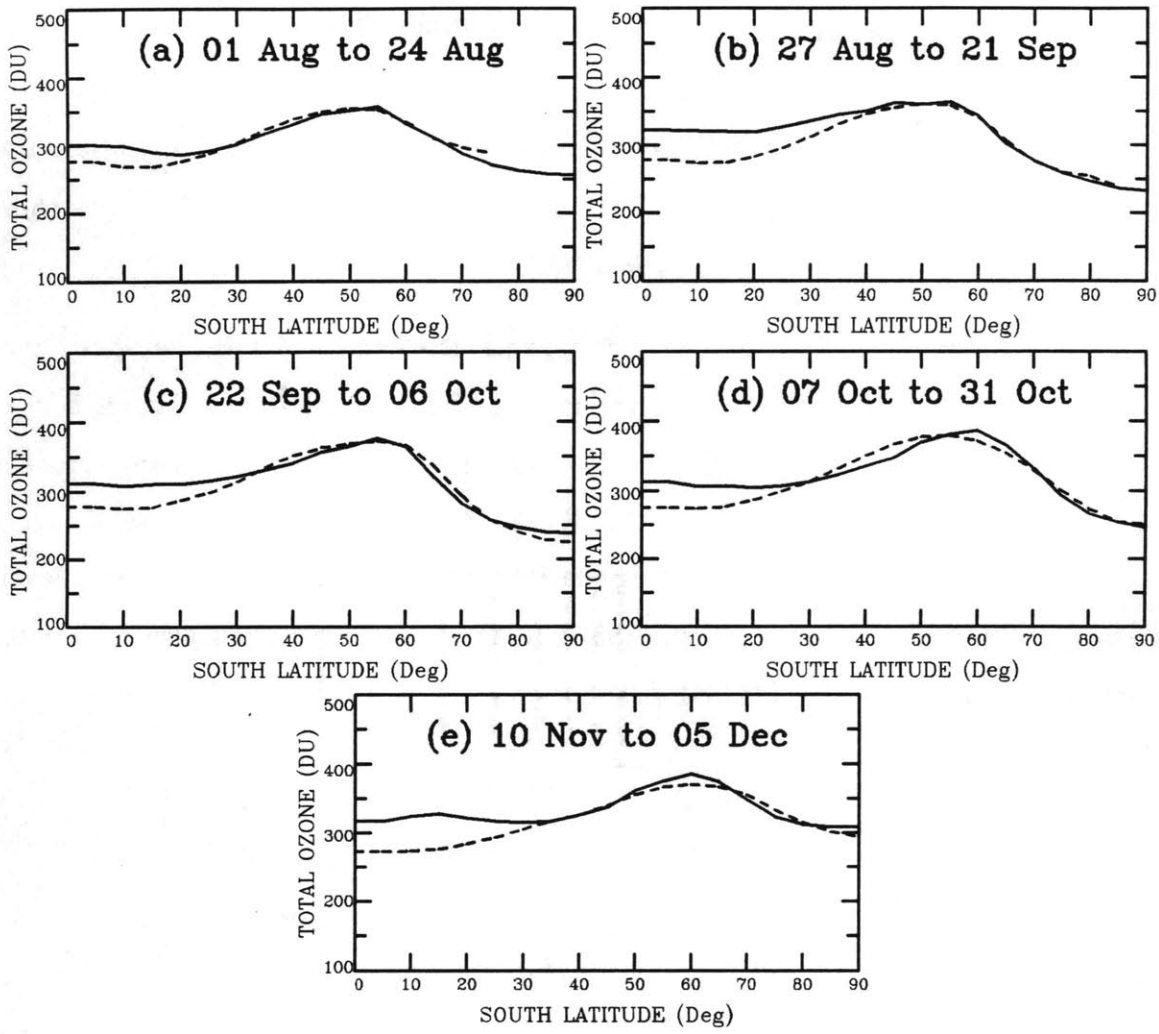

Figure 6.23: As in Figure 6.7, except for the 'virtual' sweeps of 1982.

6.4.2 1983

The adopted zonal and temporal mean meridional distributions of OMR and total ozone for the five 'virtual' sweeps in 1983 are shown in Figures 6.20 and 6.22.

The S1 reconstruction was obtained by applying the mean of the S1 $\chi/\hat{q}$ relationships from 1981 and 1986. This was the same choice as for S1 in 1984, and suggests that the lower mid-latitude total ozone peak observed in August 1983 may have been due to cooler temperatures in the lower stratosphere in 1983 (they were considerably warmer at the highest levels).

The S2 reconstructions of Figures 6.20(b) and 6.22(b) were obtained with an OMR distribution very similar to that of the September 1981 (S2) reconstruction i.e. using the mean of the adopted S1 and S3 $\chi/\hat{q}$ relationships from 1981, except that, since this overestimated total ozone slightly at all extratropical latitudes, the S3 relationships were modified by replacing all the 1981 data below $425K$, rather than just those below $340K$, with the data from S4 in 1988.

The same modified 1981 S3 $\chi/\hat{q}$ relationships were combined with the S3 relationships from 1985 to produce the distribution for S3 in 1983 shown in Figures 6.20(c) and 6.22(c), while the S4 $\chi/\hat{q}$ relationships from 1988 were adopted unchanged for the S4 period (see Figures 6.20(d) and 6.22(d)). Finally, the S5 reconstruction of Figure 6.20(e) and 6.22(e) was obtained using the 1981 S3 $\chi/\hat{q}$ relationships, but with levels below $425K$ replaced by those from S5 in 1984. This distribution also suffers the problems apparent in the 1981 S4 distribution.

Chapter 7

Detailed Analysis of the December 1987 Ozone Dilution Event

We now come to the primary concern of the present work, the Antarctic ozone hole dilution effect. In this Chapter we present the detailed analyis of the event during the first few weeks of December 1987, which was first identified by a marked and sudden decrease in total ozone over southeastern Australia and was later attributed to an extrusion of ozone-depleted air from within the polar vortex out into the middle latitudes of the southern hemisphere, accompanying the breakup of the vortex in the lower stratosphere during the first week of December.

Using the full suite of analysis techniques described in Chapters 2 and 3 above, we assess the contributions to the observed mid-latitude ozone decline attributable, respectively, to vertical and horizontal advection. We decompose the contribution due to vertical motion into components arising from different horizontal scales of motion and vertical 'forcing' domains, and we separate the contribution due to horizontal advection into 'natural' and 'ozone hole' components. By performing the detailed analysis we are able to estimate the contribution to the observed decrease which was the direct result of an ozone hole dilution event, and that which would most likely have occurred anyway in the absence of an Antarctic ozone hole.

In Section 7.1 below we briefly recount the results of the earlier investigations, and show the need for closer analysis if we are to settle the question of whether or not the event was at least partially due to ozone dilution. In Section 7.2 we deal with the means by which a hemispheric picture of the ozone evolution was obtained for the early December period. We describe the difficulties encountered, the technique employed to circumvent them, and the factors likely to influence the accuracy of the picture obtained. In Section 7.3 we describe the detailed examination and breakdown into different components of the implied ozone transports during the early December period, while in Section 7.4 the transports occurring during the latter half of the month are briefly discussed. Finally, in Section 7.5 we summarise the key findings and discuss their implications from the ozone dilution perspective.

7.1 Background: The Need for a Closer Examination of the 1987 Event

As noted in Chapter 1, Atkinson and Easson (1988) first noticed a sudden and marked decrease in total ozone, measured by Dobson spectrophotometer at Melbourne, Australia between 11 and 13 December 1987, the low values persisting for the remainder of the month and producing record low December mean total ozone at the station. Figure 7.1(a) shows the sudden decrease observed by Atkinson and Easson, and its impact on the monthly mean ozone column. Similar sudden, but less marked, decreases were also observed at other Australian Dobson stations within a few days of the Melbourne decrease. Atkinson and Easson noted that the event closely followed the polar vortex breakup at low levels during the preceding week, hinting at a possible connection but pursuing the matter no further.

Atkinson *et al* (1989), who subsequently examined the event more closely, used TOMS total ozone data to show the large areal extent of the ozone decrease between 08 and 14 December (see Figure 7.1(b)). Using NMC data they also examined the evolution of EPV in the lower stratosphere during the period, noting the close cor-

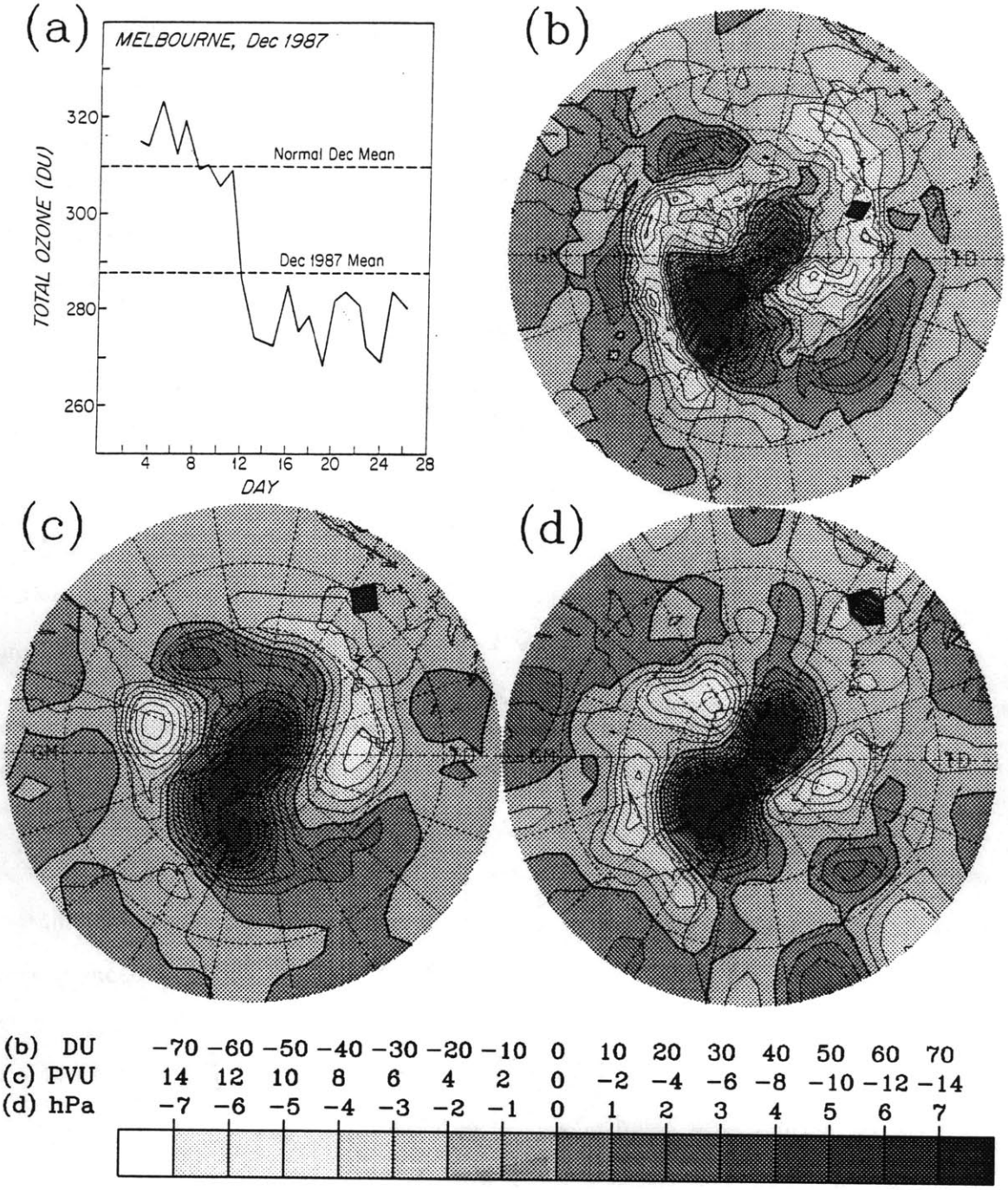

Figure 7.1: The 1987 Ozone Dilution Event. (a) Daily averaged total ozone (DU) at Melbourne, Australia for December 1987, and the long term and 1987 December mean. (b) Hemispheric distribution of the change in TOMS total ozone (DU) between 3 day means centred on 08 and 14 December. (c) As for (b) except for the change in $500K$ EPV. (d) As for (b) except for the change in $500K$ pressure. Shading between contours is as indicated by the key. Grid lines at 20^o intervals, Greenwich Meridian to the left, edge of plot at equator.

respondence between the areal distribution of the $500K$ EPV change (Figure 7.1(c)) with that of the total ozone change, which suggested the ozone decrease might be due to the quasi-horizontal transport of ozone hole air out into the mid-latitudes as the vortex broke up. They also used NMC-based balanced wind fields to examine parcel trajectories in the lower stratosphere during the period and found that some of the air parcels near Melbourne on 14 December appeared to have originated in the vicinity of the vortex edge over the southern Indian Ocean ten days before, just prior to the vortex beakup. On the strength of all their evidence, Atkinson *et al* claimed *prima facie* evidence that the 1987 mid-latitude ozone decrease was the first observed occurrence of a direct impact of the ozone hole on southern mid-latitudes.

In view of the scarcity of available ozone data for direct confirmation, and the possibility that the observed ozone decrease might be explicable in terms of vertical advection from lower levels of air naturally low in ozone, Atkinson *et al* were cautious not to claim irrefutable proof of an ozone hole connection.

That the total ozone decrease observed between 08 and 14 December 1987 might be at least qualitatively explained as a result of the broad scale vertical motion field is evident from Figure 7.1(d), which shows the observed pressure change on the $500K$ isentropic surface between the two dates. The similarity between the areal distribution of the pressure change and that of both the EPV change and the total ozone change is clearly evident. Such a broad scale vertical motion field is inevitable, and must occur in response to a relatively localised EPV redistribution, if the atmosphere is to preserve thermal wind balance. This is perhaps most easily seen by consideration of the quasigeostrophic omega equation, as expressed by the 'QPV tendency' form, Equation 2.22. By virtue of the elliptic properties of the inverse Laplacian-type operator on the left hand side of Equation 2.22, we can qualitatively reexpress the equation to obtain the simplified, loosely qualitative relationship

$$\tilde{\omega} \sim f_0 \frac{\partial}{\partial p}\left(\frac{\partial q_p}{\partial t}\right), \tag{7.1}$$

or over an appropriately short period and in the southern hemisphere, where f_0 is

negative and q_p is generally so,

$$\Delta p|_{x,y,\theta} \sim \frac{\partial}{\partial p}(\Delta|q_p|). \tag{7.2}$$

Equation 7.2 says simply that a local vertical gradient of QPV change will be accompanied by a local isentropic pressure change. Of course, with the gross simplification of Equation 2.22 to obtain Equation 7.1 we have also lost the smoothing property of the differential operator: the smoothed response which actually occurs will generally be seen over a broader region than a more localised QPV change.

Given a hypothetical situation relevant to the 1987 event in which an outbreak of a high latitude airmass into mid-latitudes occurs, concentrated in a relatively localised vertical domain in the lower stratosphere, then in mid-latitudes at lower levels, with $\partial/\partial p(\Delta|q_p|)$ negative, Δp will be negative, and the vertical motion response will comprise isentropic uplift, while at higher levels adiabatic subsidence will occur. At higher latitudes, where the outbreak will be seen as a general decrease in q_p magnitude, the opposite response will be seen, with adiabatic descent below and ascent above the levels at which the outbreak is concentrated. (The former of these components of the high latitude response, when the origin of the outbreak is the polar upper stratosphere, is of course the simple mechanism explaining the marked temperature increase observed with, and definitive of, a stratospheric sudden warming.)

So it is plain that the isentropic pressure change distribution observed in the lower stratosphere between 08 and 14 December 1987 is qualitatively consistent with the observed EPV outbreak in the lower and middle stratosphere. (Although the above simplified picture resulted from consideration of QPV changes, the same general response can be shown to result from changes in EPV).

That the observed pressure change distribution might also explain qualitatively the observed total ozone behaviour follows equally simply by consideration of Equation 3.9, which expresses the total ozone column as the total vertical integral with respect to log-pressure of the ozone partial pressure, itself the product of the pressure and OMR. Let us assume for simplicity that a high latitude outbreak occurs at

some level in the lower to middle stratosphere, below the OMR maximum, which is sufficiently localised in the vertical that contributions to the change in total ozone due to horizontal advection at a given location can be neglected (i.e. isentropic OMR values remain essentially fixed). Then in mid-latitudes at pressure levels below the hypothetical mid-latitude destination of the outbreak, where OMR increases with height, ozone partial pressures will decrease due to isentropic uplift of lower OMRs from below, whereas at levels above the outbreak but below the OMR maximum they will increase, and above the OMR maximum they will decrease, both as the result of adiabatic subsidence. Since we might expect, consistent with the downward control principle (Haynes *et al*, 1991), that the bulk of the response will be realised below the outbreak level where the much greater atmospheric mass is more easily able to bring about the required adjustment without the need for gross changes in the overall mass distribution (i.e. by Occam's razor), and since in any case much of the ozone column resides at the lower stratospheric levels (where ozone partial pressures are greatest to begin with), then the overall mid-latitude signature will be a total ozone decrease. If the EPV outbreak is centred at the level of the OMR maximum further aloft, then ozone partial pressures will decrease everywhere in the column, maximising the efficiency (though not necessarily the magnitude) of the negative total ozone response. On the other hand, if the EPV outbreak is centred too far below the ozone partial pressure maximum, say near the tropopause or lower, then the total ozone signature will reverse. Of course, at higher latitudes at the origin of the EPV outbreak, the opposite signal can be expected.

Accordingly, with the 1987 EPV outbreak apparently concentrated in the middle stratosphere, the observed distribution of the change in total ozone can be explained qualitatively by, and might conceivably have been substantially due to, broad scale vertical motion, itself the direct result of the EPV outbreak. Hence closer analysis of the event is required than was achieved by the previous investigations if we are to determine conclusively whether or not a contribution to the observed 1987 mid-latitude ozone decline was due to the extrusion into mid-latitudes of air low in ozone from within the polar vortex.

7.2 Reconstructing a Picture of the Ozone Evolution on 02 and 14 December 1987

Much of what follows in this and the next Section in relation to the analysis technique employed has been described in Chapters 2 and 3 above, but is generally recapitulated and in some cases expanded upon here, to tie together the various components of the analysis in one place, and to demonstrate their need in the context of the difficulties encountered in the analysis of the 1987 event. A brief account of the early stages of the analysis, with some preliminary results, is contained in Atkinson and Plumb (1993).

As noted above, the observed mid-latitude decrease in total ozone during the second week of December 1987 closely followed the polar vortex breakup at lower levels. The synoptic evolution of the EPV distribution during the period was briefly described in Chapter 5 above and the vortex destruction phase was depicted in Figure 5.17(b) to 5.17(e), the $525K$ plots from the Figure strongly suggesting that the bulk of the vortex remains were deposited in the Atlantic Ocean region between 02 and 14 December. The EPV analyses also suggest that tongues of ozone hole material may have been extruded into the mid-latitudes, and importantly, over the populated regions of South America, New Zealand and southern Australia (see Figure 5.17(ii)). These are the features on which the following analysis will tend to focus. While Atkinson *et al* (1989) examined the period between 08 and 14 December, in the present analysis we shall consider the expanded 12 day period between 02 and 14 December.

7.2.1 Direct Reconstruction of the Ozone Distribution on 02 December

The first step in the analysis was to come up with a three dimensional picture of the ozone and pressure (temperature) distributions on 02 December. The latter was

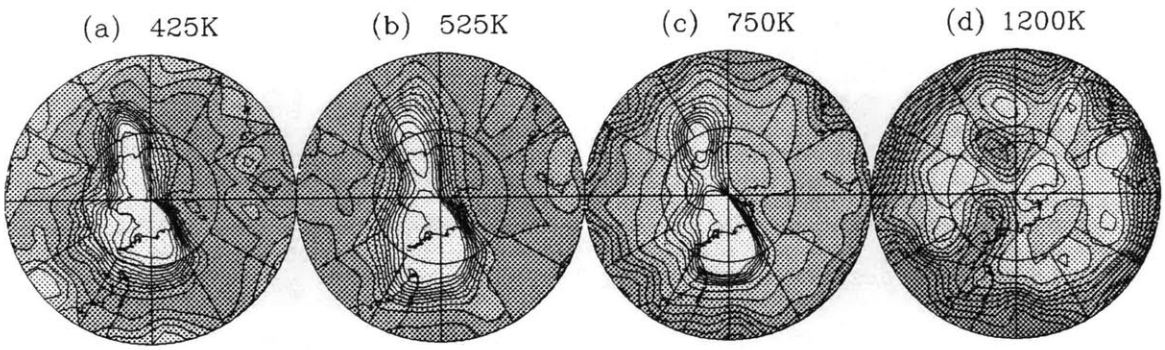

Figure 7.2: Reconstructed OMR Distribution on 02 December 1987 at (a) $425K$, (b) $525K$, (c) $750K$ and (b) $1200K$, with light shading for low ozone, dark for high ozone. In (a) the lowest contour is drawn at $0.35ppmv$ with additional contours every $0.05ppmv$. The corresponding values are, respectively for (b), 1.4 and $0.15ppmv$, for (c), 5.0 and $0.2ppmv$, and for (d), 6.2 and $0.2ppmv$. 30^o grid spacing, Greenwich Meridian to left, outer edge at 30^oS.

simply obtained using the NMC data for the day. To obtain the approximate ozone distribution, the reconstruction technique described in Chapter 3 was performed on the normalised EPV distribution for 02 December, using the $\chi/\hat{q}$ relationships for the 1987 SAGE II S5 period (10 November to 04 December) described and presented in Chapter 6 above.

Hemispheric plots of the OMR distribution obtained for each of the four isentropic surfaces depicted in Figure 5.17(b) (425, 525, 750 and $1200K$) are shown in Figure 7.2. Evident at the lower levels (Figure 7.2(a) and (b)) is the Antarctic ozone hole, which coincides with the polar vortex interior and where OMRs according to the reconstruction are below $0.35ppmv$ at $425K$, and $1.4ppmv$ at $525K$. This is surrounded by a region of strong meridional OMR gradient between the vortex and the circumpolar OMR maximum (with values around $0.85ppmv$ at $425K$ and $3.8ppmv$ at $525K$) and then a gradual OMR decline equatorward. At $525K$ and nearby levels (not shown) the reconstruction tends to place the OMR maximum somewhat further equatorward than it may actually lie, as a result of an element of the EPV relaxation observed during November which has remained unaccounted for by the normalisation procedure. We shall discuss the likely impact of this below. At $750K$ (Figure 7.2(c))

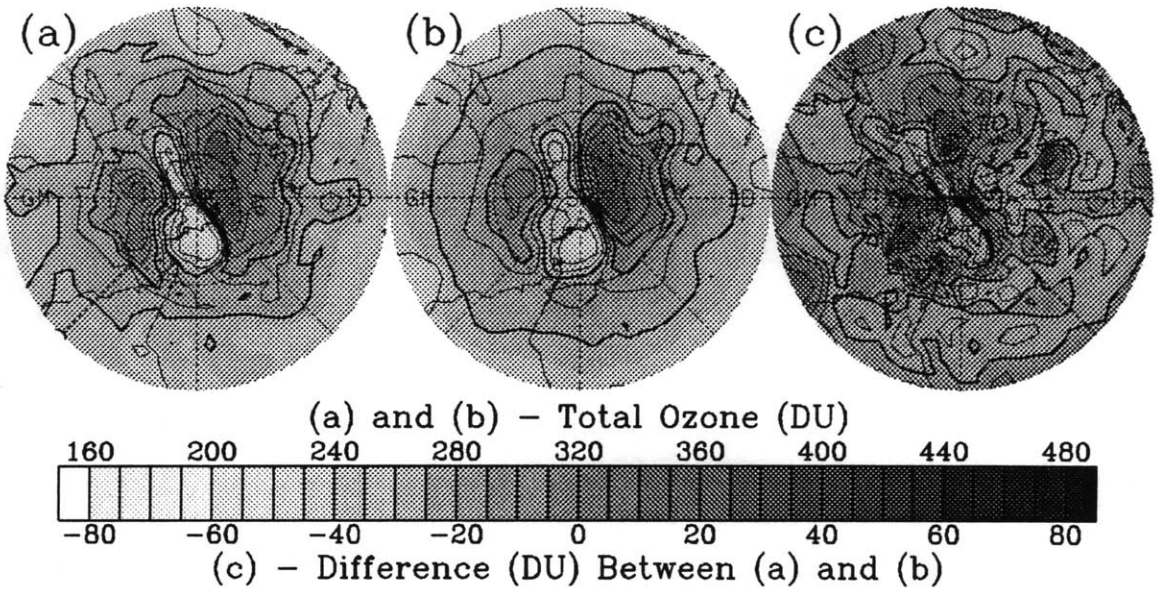

Figure 7.3: Total Ozone Distribution on 02 December 1987 from (a) TOMS and (b) Reconstruction. Contours are drawn every $20DU$ with heavy contours at 280 and $320DU$ for reference. (c) Total ozone difference (TOMS minus reconstruction), with $10DU$ contour interval, heavy contour at $0DU$, and darker/lighter shading denoting under/overestimation by the reconstruction. Grid lines at 45^o intervals, Greenwich Meridian to the left, outer edge at equator.

the pattern is similar, but the polar minimum shown (just below $5ppmv$) is understood to be due, as noted in Subsection 6.1.2 above, to the combined effects of strong diabatic descent during early winter, and subsequent gradual photochemical ozone relaxation within the isolated vortex, rather than the ozone hole mechanism, and instead of a mid-latitude maximum there is a gradual monotonic increase towards the tropics. At $1200K$ (Figure 7.2(d)) the OMR distribution is already rather chaotic with only weak gradients present and typifies the well-mixed state which has followed the vortex breakup at upper levels during the latter half of November, as noted in Chapter 5. In fact the reconstruction at this level, which continues to associate low OMR with high EPV magnitude so long after the vortex destruction, is probably mostly fictitious. As noted earlier, the short diabatic and ozone photochemical time

scales at the upper levels render invalid the conservation assumptions on which the coordinated transformation and reconstruction technique is based. Nonetheless this is rather unimportant for our purposes since the highest levels make such a small contribution to the total ozone column.

Using the technique described in Section 3.5, the pressure and reconstructed OMR distributions were used to produce a hemispheric map of reconstructed total ozone on 02 December. This is shown, alongside the TOMS distribution for the day (interpolated to 12 UTC), and a map of the difference between the two, in Figure 7.3. Close agreement between reconstructed and TOMS total ozone is evident, with typical departures of less than $10DU$ (less than 3%), and the largest departures (around $50DU$) associated with the failure of the reconstruction to depict the small scale total ozone extrema seen by TOMS e.g. near 50^oS 35^oW, or to capture adequately either the steep OMR gradients at the vortex edge or the precise location of the edge. While the former two of these are due to the limitations of the reconstruction technique (e.g. the apparent mislocation of the mid-latitude OMR maximum at levels around $525K$, noted above), the third apparently results primarily from the asynoptic nature of the NMC analyses. Almost all of the other small scale maxima or minima in Figure 7.3(c) are due to the understandable failure of the reconstruction to represent the small scale features in the total ozone distribution seen by TOMS, but which lie beneath the resolution of the EPV analyses upon which the reconstruction is based.

7.2.2 Direct Reconstruction of the Ozone Distribution on 14 December

As noted in Chapter 3 above, and particularly unfortunate from our perspective, no SAGE data were available for the blackout period between 05 and 16 December 1987, because the alignment of the satellite during this period prevented observations from being made. (This was one of the reasons why 02 December was selected as the start date of the analysis period). As evident in Figure 6.1 this condition occurs at

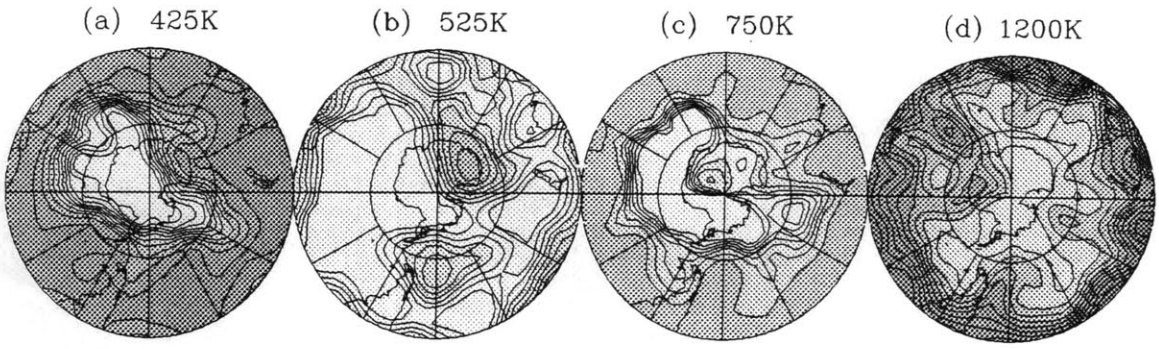

Figure 7.4: As for Figure 7.2, except for the 14 December 1987 reconstruction based on the NMC EPV analyses of 14 December.

approximately the same time in each year of SAGE II coverage. In view of the lack of SAGE data during mid-December, a reconstruction was performed on the NMC EPV data for 14 December using the same $\chi/\hat{q}$ relationships as were employed for the 02 December reconstruction. Figures 7.4 and 7.5 show that this reconstruction was somewhat less successful than that for 02 December, as evidenced by the relatively large differences (some in excess of $85DU$) between TOMS and reconstructed total ozone in Figure 7.5(c), the reconstruction generally underestimating the total ozone column around the fringes of the mid-latitude ozone maximum. (Note the much smaller areas enclosed by the thick contours in Figure 7.5(b), and the dominance of positive differences in Figure 7.5(c).) Nonetheless, the distributions are qualitatively very similar, the shape and location of the regions of high and low total ozone corresponding remarkably well.

The mismatch results from the EPV relaxation problem referred to in Sections 1.2 and 2.6 above, and its effect on the reconstruction is most clearly seen by comparing Figure 7.2(b) with Figure 7.4(b). As is evident in Figure 5.17, accompanying the breakup of the vortex in 1987 is a rapid decrease in vortex maximum EPV in the lower and middle stratosphere, and a coinciding increase in the area enclosed by the lowest isopleth in each of the plots. This is the typical signature of 'surf zone' formation, thought to be mainly due both to Rossby wave breaking and mechanical mixing, and the diabatic response to dynamically-induced departures from radiative equilibrium, although the debate continues as to which might be the more dominant

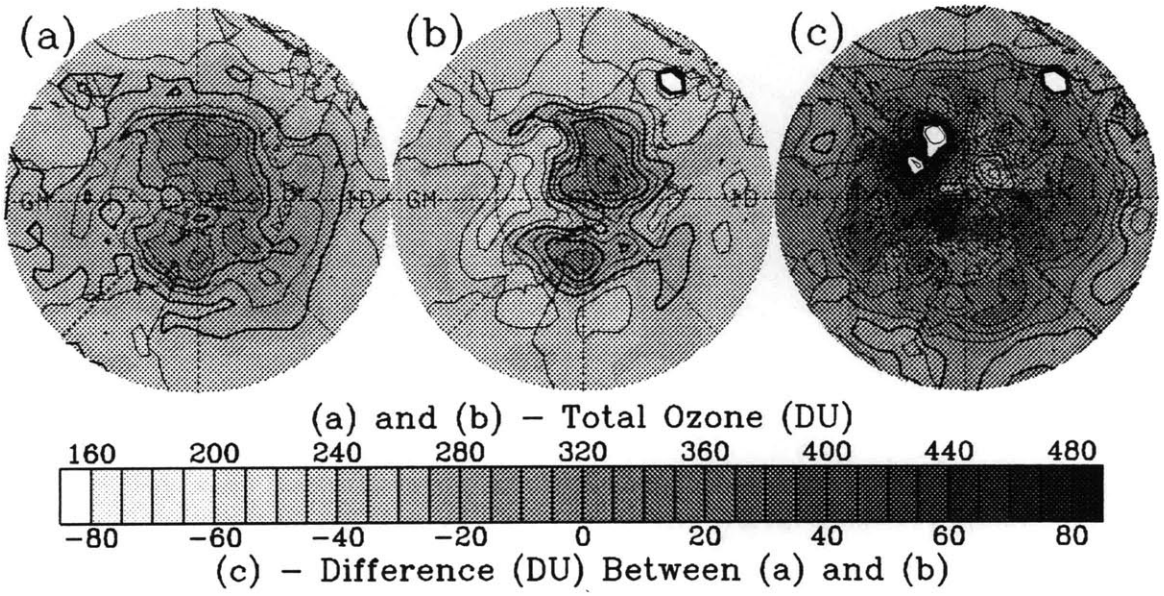

Figure 7.5: As for Figure 7.3 except for the 14 December 1987 reconstruction based on the NMC EPV analyses of 14 December. (The white hexagonal area over NW Australia is due to missing data, and the additional white areas denote differences greater than $85DU$.)

process (see e.g. Butchart (1987), O'Neill and Pope (1990) or Pierce *et al* (1993)). Fairlie and O'Neill (1988) encountered a similar relaxation of EPV associated with a sudden warming in the northern hemisphere which, on the basis of comparison with rocketsonde data, they attributed to the inadequacy of the satellite-derived data in resolving a relatively sharp jump in static stability in the middle stratosphere, which they associated with the downward progression of the warming. We shall consider this possibility further below. It has also been suggested (P.A. Newman, personal communication) that such episodes of EPV relaxation might be explained by the occasional updating of the regression coefficients for the first guess temperature retrievals in the NMC CAC data acquisition scheme. While this is possible, the tendency for the episodes to coincide with large wave events argues against it.

7.2.3 The Use of CAS to Describe the EPV Distribution on 14 December

For the purposes of investigating the ozone dilution effect of the 1987 event, the EPV relaxation presents a problem. While use of normalised EPV rather than EPV itself as our 'meridional' coordinate in the reconstructions appears largely to combat the problem associated with large wave events prior to the vortex breakup, even the normalising procedure fails to cope with the pronounced non-conservation of 'analysed' EPV which accompanies the breakup itself. This is because the shape of the meridional distribution of normalised EPV changes markedly during the period, smoothing out meridional gradients, so the OMR reconstructions become highly sensitive to small differences in EPV in the base maps. In an endeavour to ameliorate the EPV relaxation problem we employed CAS, as described in Section 2.6 above, to obtain advected contour distributions for 14 December upon which to base the OMR reconstruction. As noted in Chapter 3 above, we make no direct attempt to account for the contribution to this EPV relaxation which may arise from diabatic processes occurring at the time. This is partly because the diabatic contribution is so difficult to quantify, even were we to resort to detailed modelling, but also because by basing the reconstruction on the CAS output, the resulting OMR distribution appears to be less sensitive to unaccounted-for diabatic fluxes, than when the EPV analyses themselves are used. We shall discuss this point further below.

For the 1987 event, 24 CAS simulations were performed, one for each of the isentropic levels involved in the reconstruction (i.e. $300K$ to $1200K$). Each simulation was initialised with 20 to 25 evenly incremented contours from the analyses of 02 December, and the contour fields were advected for 12 days (time increment 0.05 day) using trilinearly interpolated winds from the balanced wind fields derived from the NMC analyses each day. The simulations were performed on the Pittsburgh SCC CRAY YMP, each requiring between 10 and 30 minutes CPU time. To provide an example of the CAS output, Figure 7.6 shows the advected contour distributions on the four representative surfaces of Figure 5.17, at four day intervals commencing with

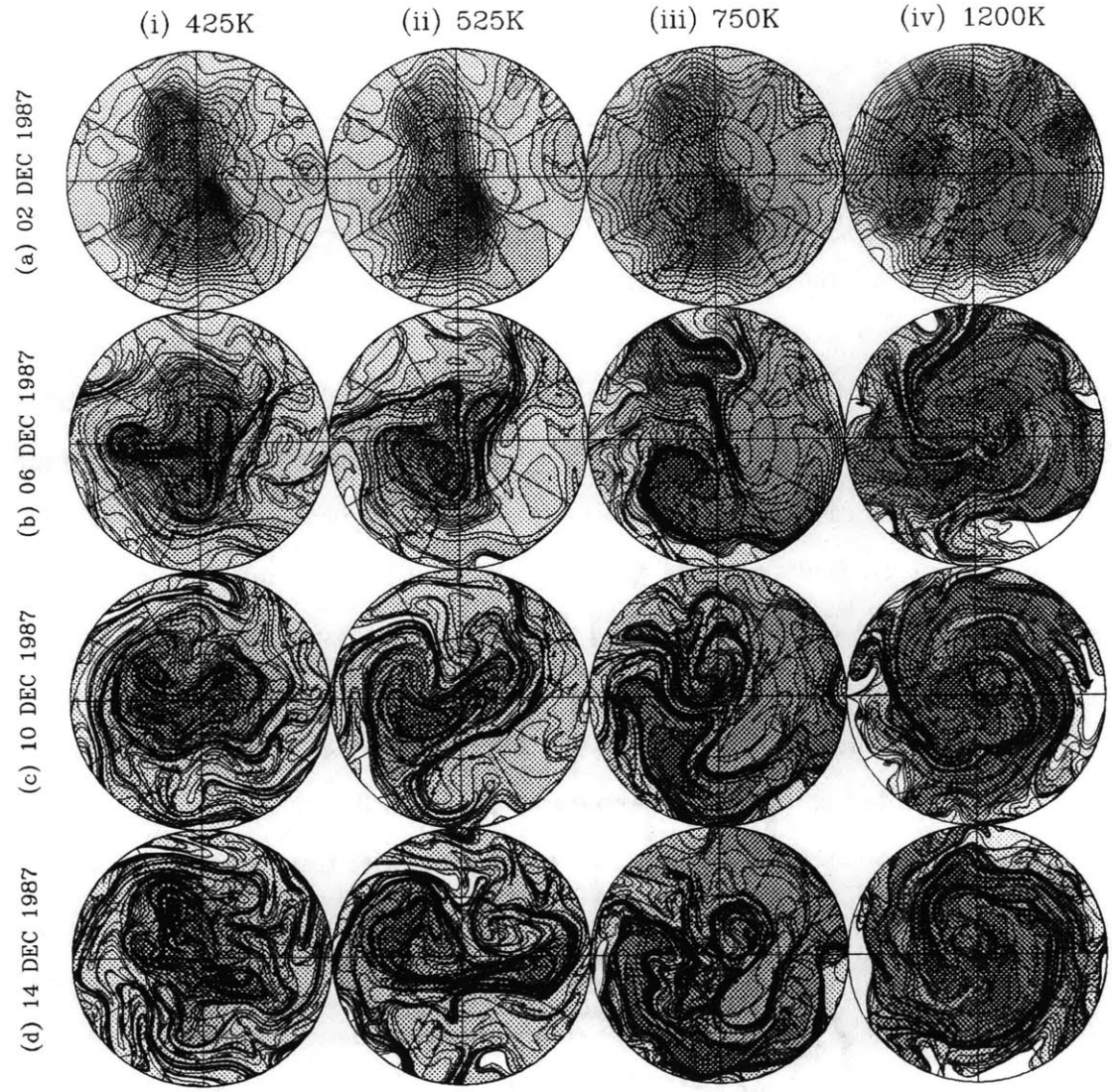

Figure 7.6: Advected EPV contours for CAS simulation initialised on 02 December, at (i) $425K$, (ii) $525K$, (iii) $750K$ and (iv) $1200K$, for (a) 02 December (NMC analyses), (b) 06, (c) 10 and (d) 14 December 1987. The plots shown correspond to the NMC analyses shown in Figure 5.17, except that different contour levels are shown. Darker shading denotes higher EPV magnitude.

the analysed contour fields of 02 December. Together the plots correspond to the EPV analyses shown in Figure 5.17(b) to (e). The full set of contours which were advected to ensure adequate spatial resolution of the resulting OMR distributions is shown in each plot, but to enable easier qualitative comparison with Figure 5.17, the

regions between contours have been shaded. (Without the shading it is difficult to distinguish between regions of high and low EPV.) Figure 7.6 shows the remarkable degree to which the contours at each level are sheared out and/or wrapped up on different spatial scales, demonstrating the aforementioned potential enstrophy cascade, whereas the coarser resolution EPV analyses suggest the vortex retains its integrity to a much greater extent. Significant differences exist between the grosser features of the evolution according to the analyses and those depicted by the CAS simulations, particularly at the higher levels. We shall discuss these below.

Having completed the CAS simulations, the resulting contour distributions for 14 December at each level were inverted and reinverted, as described in Section 2.6, to obtain corresponding gridded fields of 'advected' EPV at 5^o by 5^o resolution.

7.2.4 The Difference Between the NMC and Regridded CAS EPV Distributions for 14 December

Figure 7.7 shows the hemispheric plots of analysed EPV and regridded 'advected' EPV for 14 December, at $425K$, $525K$, $750K$ and $1200K$. (The regridded data correspond to the contour distributions shown in Figure 7.6(d)). At each isentropic level, the same minimum contour level and contour interval is shown for both the analysis and the regridded data. The smaller total number of contours in the NMC analyses demonstrates the extent to which relaxation of 'analysed' EPV has occurred between 02 and 14 December. Other significant differences also exist between the CAS plots and the NMC analyses. Each of the CAS plots shows steeper EPV gradients than the corresponding analysis, for three possible reasons. The CAS data, regridded at 5^o by 5^o resolution, may still comprise a higher resolution picture of the EPV distribution than the analyses. Further, even the CAS simulations may substantially underplay the extent of the potential enstrophy cascade. Thirdly, perhaps a significant contribution to the EPV relaxation in the analyses results from diabatic processes or observational error.

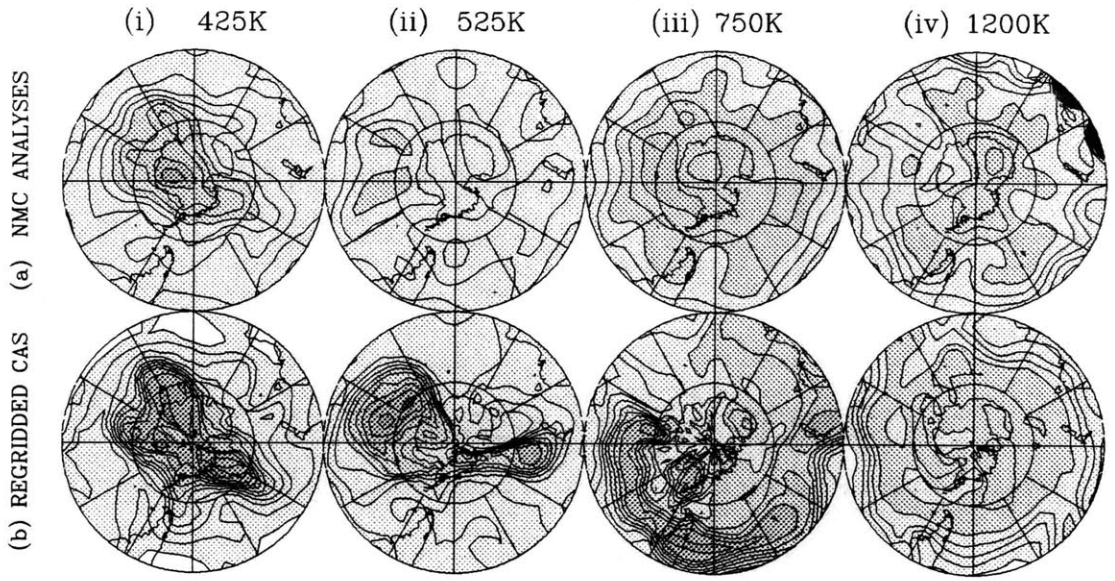

Figure 7.7: EPV distributions of 14 December 1987 at (i) $425K$, (ii) $525K$, (iii) $750K$ and (iv) $1200K$ obtained from (a) the NMC analyses, and (b) the CAS simulations, but after inversion to obtain gridded data. Grid lines at 30^o intervals, Greenwich Meridian to the left, outer edge at 30^oS, and darker shading denotes higher EPV magnitude.

Other than the steeper gradients present in the regridded data, the $425K$ simulation displays rather remarkable similarity to the NMC analysis. At $525K$ the broadscale features are similar in the two plots, but differences exist in the structure of the EPV tongues extending from the two vortex lobes. Whereas the analysis suggests the South American tongue to be a major feature, CAS depicts it only to involve material from the outer edge of the vortex. Just as significant is the difference in the structure of the tongue in the Australia/New Zealand region. While the analyses perhaps suggest it extends westward across Australia into the Indian Ocean, the CAS simulation curves it southwestward from the Tasman Sea, wrapping it rather tightly around the anticyclonic circulation associated with the patch of low EPV to the south of New Zealand. At $1200K$ the correspondence between the analyses and the regridded CAS data is poorer, understandable in view of the already chaotic nature of the flow and the rather rapid diabatic timescales in the upper stratosphere. At $750K$, however, where the technique is expected to perform moderately well, there is

virtually no correspondence between the analysis and the advected distribution. The analysis suggests the vortex remnants remain well south over the Atlantic Ocean and extend across West Antarctica, whereas CAS depicts them as having been sheared out over South America and across the Pacific Ocean north of $50^{o}S$, reaching beyond the Australian region.

The causes of the discrepancies are most likely to be due to degradation in the quality of the NMC analyses, inaccuracies in the CAS advecting wind fields, and to diabatic changes to isentropic EPV during the 12 day period prior to 14 December.

7.2.5 Likely Causes and Their Impact on the Ozone Distribution

Overall, there are five most likely causes of the differences between the EPV analyses for 14 December and the regridded CAS distributions, one or more of which contributes significantly. These are (i) degradation of the overall quality of the EPV analyses between 02 and 14 December, (ii) differences in the effective spatial resolution of the regridded CAS fields and the NMC analyses, (iii) inadequate representation of the potential enstrophy cascade by CAS, (iv) inaccuracies in the derived balanced wind fields which lead to erroneous 'bulk' advection by CAS, and (v) diabatic processes. Because our concern here is the material tracer evolution rather than the EPV distribution *per se*, each of these possibilities, although they might have a similar impact on the depicted EPV distribution, could have a markedly different impact on the OMR distribution, hence on the quality of a subsequent reconstruction of the OMR distribution. While the effect of each is at best difficult to quantify, we shall now consider the likelihood of each, and the qualitative impact each might have on an ozone reconstruction based on the CAS data, compared to that based on the EPV analyses.

Degradation of NMC Analysis Quality

The fact that the ozone reconstruction for 02 December produced rather close agreement with the TOMS distribution suggests that the NMC analyses for that day successfully captured the essential features of the EPV distribution. In view of the larger differences associated with the direct reconstruction for 14 December, the possibility arises that these might be due to much poorer performance overall of the NMC analyses on 14 December, arising, for example, from either of the two potential causes noted at the end of Subsection 7.2.2 above. Were this the case, then as long as the NMC geopotential height fields continued to represent effectively the horizontal geopotential gradients, so the derived balanced winds did not suffer, then the CAS simulations may still provide an accurate picture of the tracer evolution during the period. Under these circumstances an ozone reconstruction based on CAS should show closer correspondence to TOMS than that based on the EPV analyses. i.e. The use of CAS may largely overcome the problem. (The aforementioned lack of agreement at $750K$ suggests this is probably not the case, at least at mid-stratospheric levels.)

Whether such a data quality degradation is a significant contributor to the poor performance of the ozone reconstruction might be tested to a limited extent by examination of the EPV evolution depicted by an alternative data set, but this has not been attempted, since it is unlikely that any of the alternatives (e.g. ECMWF) could be considered sufficiently independent in any case, in that they depend to a large extent on the same satellite retrievals upon which the NMC analyses are based. Instead we will consider, *a posteriori*, the differences between the resulting reconstructed total ozone distribution and the observed TOMS distribution, to gain more insight into the extent to which this effect might contribute.

Discrepancies Due to Different Spatial Resolution

If the major contribution to the observed EPV relaxation in the analyses, and the differences in the horizontal gradients of EPV between the analyses and the regridded data, results from the poorer spatial resolution of the EPV analyses (i.e. the 'knobbly glass' view of the satellite), then an ozone reconstruction based on

the regridded CAS data would be expected to provide a better representation of the true ozone distribution than one based on the EPV analyses. Of course, this is also dependent on the advecting wind fields, which are derived from the daily NMC analyses during the period, providing a sufficiently accurate picture of the flow evolution. So long as the coarse grain view of the EPV evolution depicted by the analyses is correct, then because the balanced winds are largely determined by the coarser features of the EPV distribution (via the inverse differential operator involved in the invertibility relationship) this should be the case. (Waugh and Plumb (1993) finds the flow evolution depicted by CAS to be rather insensitive to the spatial resolution of the input wind fields.)

To test whether a significant contribution to the observed EPV relaxation in the analyses resulted from their limited spatial resolution, the $525K$ EPV contour distribution obtained for 14 December from the CAS simulations were inverted and reinverted at varying spatial resolution from 1^o by 1^o to 45^o by 45^o. Were $525K$ EPV actually conserved during the period, were the CAS simulations perfect, were the actual effective resolution of the EPV analyses, as measured in degrees latitude by degrees longitude, constant with latitude, and were the EPV relaxation entirely due to inadequate spatial resolution of the NMC analyses, then at some point as the resolution of the CAS regridding process was gradually decreased, the regridded EPV distribution should correspond to that of the EPV analyses for the day. (This would then ascertain precisely the effective resolution of the satellite data).

For the trial reinversions at resolutions higher than 5^o by 5^o, the regridded contour distributions showed very little relaxation at the vortex core (from the vortex maximum on 02 December), while producing gradients at the vortex edge which were steeper than those of the analyses (progressively so with increasing resolution). At 7.5^o by 7.5^o, the vortex edge gradients were similar to the analyses but the vortex core relaxation was much less marked. (Whereas the analysed map maximum EPV at $525K$ decreased from around $87PVU$ on 02 December to about $57PVU$ on 14 December, the 7.5^o by 7.5^o regridding produced a 14 December maximum still in ex-

cess of $80PVU$.) To produce significant core relaxation in the regridded distributions required the resolution to be decreased to below 30^o by 30^o, which also resulted in much weaker gradients at the vortex edge than in the analyses (the edge became so vague as to be unidentifiable) and also produced much higher EPV at low latitudes than shown in the analyses.

Of course, none of the aforementioned assumptions upon which the test was based is expected to be exactly met. The worst of these is that of constancy with latitude of the effective resolution of the analyses, as measured in degrees longitude, since the actual resolution is expected to be better described as constant in area. While the problem might have been overcome by spherical harmonic filtering of the high resolution regridded data at varying triangular truncation, this was not attempted because it appeared unnecessary: it became evident that although the potential enstrophy cascade might contribute to the EPV relaxation observed in the analyses, it was not the major cause, unless it was also significantly underplayed by CAS.

Under-representation of the Potential Enstrophy Cascade by CAS

In the (hypothetical) absence of other influences, and in view of the above lack of success in explaining the EPV relaxation in the analyses using the CAS contour distribution, the possibility remains that even the CAS simulations fail to depict the true extent of the potential enstrophy cascade. While it seems unlikely, on the basis of the extensive testing of the CAS technique by Waugh and Plumb (1993), that CAS could fail to the degree implied (were all other potential influences in fact negligible), it is impossible to determine the precise extent to which CAS might underplay the cascade process. (In this context, it may be important that all the tests carried out by Waugh and Plumb were performed for situations in which the vortex was strong, and clearly dominated the hemispheric flow pattern (i.e mid-winter/early spring). The effectiveness of CAS in depicting the flow evolution in situations appropriate to late spring/early summer, when the vortex is much weaker and more perturbed and the details of the flow are likely to be more dependent on the smaller-scale features of the EPV distribution, has not yet been ascertained.) Nonetheless, even

were this the major problem, then the regridded data should still provide a better ozone reconstruction than the EPV analyses themselves.

Erroneous Bulk Advection by CAS

Quite apart from each of the above possibilities and a likely contribution from diabatic processes, which we consider last, is the possibility, suggested by the mismatch at $750K$, that at least some of the disparity between the analyses and the regridded CAS data arises as a result of erroneous bulk advection by CAS. An example at lower levels where this might be the case is the southwest extension, noted above, of the New Zealand tongue at $525K$ in Figure 7.7(b)(ii), whereas the analysis of Figure 7.7(b)(i) perhaps suggests more westward advection. Using the NMC data alone, it is not possible to determine which presents the more accurate picture of the flow evolution, or how commonly discrepancies of this nature might arise. Again, this might be tested using another data set but this has not been attempted (again the question of independence arises). Whereas each of the preceding potential problems should generally lead to CAS serving as a better basis for an ozone reconstruction for 14 December, erroneous bulk advection by CAS presents a serious threat to the accuracy of a resulting ozone reconstruction. If this is a major contributor to the disparity between the NMC analyses and the regridded CAS fields, then an ozone reconstruction based on the CAS data would be expected to do a worse job of depicting the medium scale features of the ozone distribution (but would possibly still describe the larger scale picture better because it would not suffer the sensitivity to EPV relaxation experienced using the analyses).

Diabatic Processes

Apart from the primarily observational factors is the possibility that the NMC analyses quite accurately depict the EPV evolution as it occurred, and that both the EPV relaxation and the discrepancies between the analyses and the regridded CAS data for 14 December result primarily from diabatic changes to isentropic EPV occurring during the period.

Such diabatic effects would then be included in the analyses but entirely unaccounted for by the CAS simulation, other than, importantly, in the manner in which they would feed into the advecting velocity distributions. Under these circumstances, and because of (rather than in spite of) this neglect of diabatic processes, the CAS simulations may still perform better as the basis of the ozone reconstruction, than the EPV analyses themselves. While we do not attempt to establish this quantitatively here, that it might be the case can be seen by considering heuristically the relative impact of such diabatic processes on the EPV and ozone distributions.

In the lower stratosphere (where we need to do well) when the vortex breaks up and the smaller scales tend to dominate the dynamics, local net heating rates and the associated gradients in net heating might be expected to be dominated by relatively small scale dynamically-induced departures from radiative equilibrium. On the other hand, the corresponding temperature perturbations will tend to be rather small compared to mean temperatures. Radiative EPV destruction/creation rates, in the absence of frictional processes, are solely dependent on the local gradient of net heating, whereas ozone photochemical destruction/production rates are expected to be primarily dependent on local temperature. Hence, against a background of large scale and rather slow temperature-dependent photochemical changes to OMR at a given isentropic level, smaller scale and relatively large radiative changes to EPV might be expected, so these direct radiative changes are likely to have a more profound effect on the isentropic EPV distribution than the photochemical changes in ozone will have on the overall OMR distribution. In the presence of frictional processes, the disparity would most likely be even greater.

In addition, vertical EPV gradients with respect to potential temperature are proportionately much greater than vertical ozone gradients (exponential vs rather linear) whereas the meridional variations in each are of similar proportion. Hence dynamically-induced diabatic fluxes of EPV can be expected to have a more marked impact on the isentropic EPV distribution than fluxes of ozone on the isentropic OMR distribution.

Consequently, it is quite likely that the assumption of material conservation of OMR on each isentropic surface, which is implicit in the use of the CAS-advected distributions for the ozone reconstructions, is closer to the truth than assuming conservation of normalised EPV which is implicit in using the EPV analyses for the 14 December reconstruction. If so, then CAS should do a better job for the reconstruction than the EPV analyses if the relaxation problem noted is primarily due to diabatic processes (i.e. ozone is a much better conserved tracer than EPV at the time in question). Of course, regardless of whether or not the advected contour distributions represent the material distribution better than the analyses, they will not account for the photochemical or diabatically-induced changes to isentropic OMR which occurred during the period, but we bear this in mind in the work that follows.

7.2.6 CAS-Based Reconstruction of the Ozone Distribution on 14 December.

Overall, then, by basing the 14 December reconstruction on the regridded CAS data instead of the EPV analyses for the day, it was anticipated that the problems due to sensitivity of the reconstruction technique to the 'observed' EPV relaxation might be considerably reduced, provided that the input velocity fields adequately describe the evolution of the bulk advection pattern during the period. Perhaps the major shortcoming of employing the CAS data would be their failure to account for photochemical production/destruction and diabatic fluxes of ozone which occurred during the period. We shall consider the likely impact of this later.

The ozone reconstruction was repeated on the regridded advected EPV (or more appropriately, approximate material) distribution. Figure 7.8 shows the resulting hemispheric distributions of OMR at the four isentropic levels shown for the earlier reconstructions, and the reconstructed total ozone distribution is compared with TOMS in Figure 7.9. Immediately apparent in Figure 7.8 is the much greater correspondence of the overall features of the OMR distribution on 14 December with

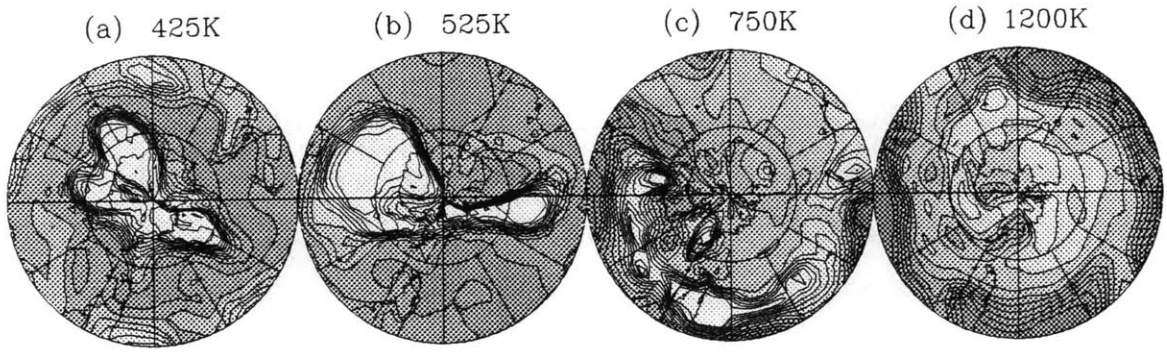

Figure 7.8: As for Figure 7.2, except for the 14 December 1987 reconstruction based on the regridded data from the CAS simulation initialised on 02 December.

those of the 02 December reconstruction (Figure 7.2), brought about by enforcing material, and hence OMR, conservation between the two dates. Equally apparent, by comparison of Figure 7.9 with Figure 7.5, is a marked improvement in the agreement between the CAS-based reconstruction and TOMS, the overall bias being greatly reduced. However, the CAS reconstruction produces too great a range of total ozone values; the high latitude total ozone maxima are too high and mid-latitude values generally too low. This provides further insight into which of the factors discussed in the preceding Section might play a significant role.

Firstly, if the CAS simulation indeed significantly underplays the potential enstrophy cascade, preserving significant meridional OMR gradients, particularly in the lower stratosphere, when they have in fact been considerably decreased by small scale insentropic mixing, a pattern would result which is qualitatively consistent with that shown in Figure 7.9(c).

A second possibility is that the temperatures in the lower stratosphere, as depicted by the NMC isobaric temperature analysis for 14 December, are too warm in the region of the total ozone maximum and too cold in the mid-latitudes. Examination of e.g. Figure 6.4(e) suggests that during the SAGE S5 sweep in 1987, OMR increases at a rate of 3 to $4\%/K$ in the lower stratosphere. If we assume that the mismatch in Figure 7.9(c) results from incorrectly specifying isentropic OMRs (for our purposes equivalent to incorrectly specifying isentropic pressures) throughout a region in the

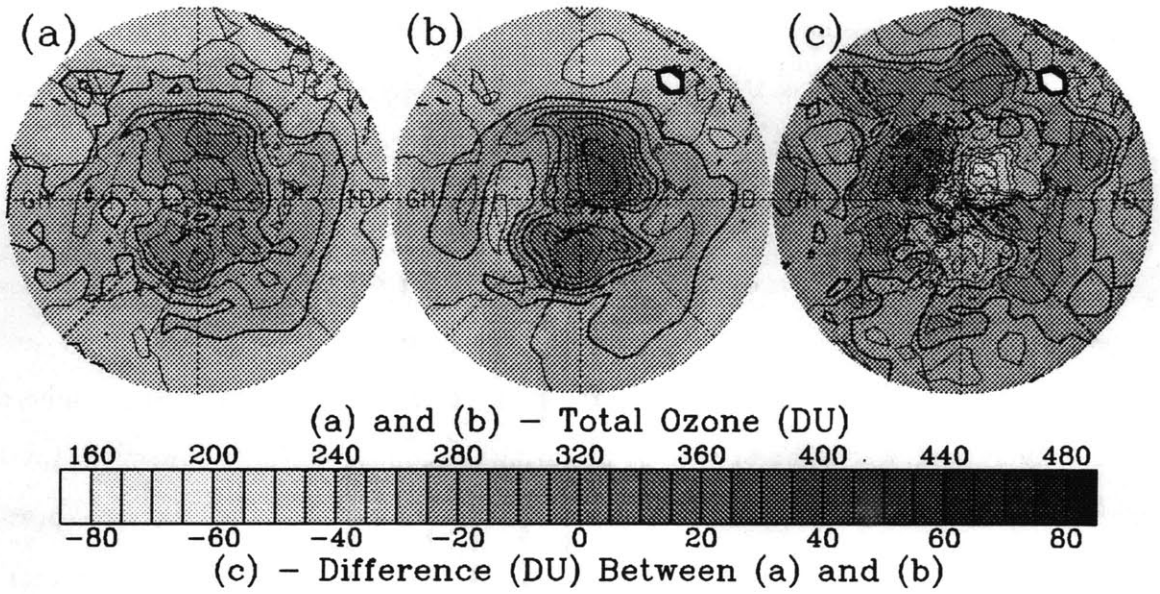

Figure 7.9: As for Figure 7.3, except for the 14 December 1987 reconstruction based on the regridded data from the CAS simulation initialised on 02 December.

lower stratosphere which accounts for, say, 50% of the total ozone column, then to produce a mismatch of around $10DU$ (say 3% of the column), this requires a mismatch of about 6% in isentropic OMR throughout the region, or a few degrees in potential temperature, which in turn equates to about a degree in temperature. The implication, then, is that in the vicinity of the total ozone maxima the NMC temperatures throughout the lower stratosphere would be required to be several degrees too warm, and a few degrees too cold in mid-latitudes. This in turn would suggest either that the NMC temperature and geopotential height fields would be significantly out of hydrostatic balance, or that the derived wind fields overestimate the strength of the larger scale circulations, which would then feed back on the CAS simulations, resulting in the potential enstrophy cascade probably being underplayed.

As it turns out, the latter possibility does not present a direct problem for our subsequent analysis of the ozone dilution event, since we will remove the effects of such temperature errors later when we separate the reconstructed total ozone decrease into components arising from vertical and horizontal advection.

A third possibility is that the discrepancies arise from our failure to account for 'nonconservation' of isentropic OMRs. As discussed above, there are two possible contributions, one resulting from photochemical changes (true nonconservation) and one from diabatic fluxes (apparent nonconservation). The latter of these is the more easily dealt with.

We discussed earlier the dynamically-induced adiabatic temperature changes associated with local EPV tendencies. That the ozone reconstruction generally under/overestimates the ozone column where the temperatures in the lower stratosphere are relatively cold/warm can be seen by picturing the zonal mean structure of the total ozone distribution shown in Figure 7.9(c) and comparing it with the isentropic pressure distribution of Figure 6.4(e). If a diabatic response has accompanied these temperature perturbations, then in the lower stratosphere, where we would tend to look first if we are to explain significant changes in total ozone, radiative warming/cooling might be expected to have occurred where the temperatures are low/high. This would diabatically raise the isentropes through the warm air and sink them through the cold air, bringing lower OMRs to higher potential temperature surfaces in mid-latitudes and the opposite in the region of the total ozone maximum. This of course will contribute to a further increase in the total ozone maximum and work to decrease the mid-latitude ozone column, the opposite signal to that which we are endeavouring to explain. If, instead, we examine the response further aloft, above the level at which the EPV rearrangement is concentrated, but below the OMR maximum, the opposite process will occur and the expected diabatic response may indeed contribute to the observed mismatch. It is also more likely that a significant diabatic response will be experienced at the higher levels, where the radiative time scale is so much shorter. So perhaps some of the mismatch results from the failure of the technique to account for diabatic fluxes of ozone further aloft. As it turns out, we will also remove the effects of such a potential contribution later, when we attempt to separate from the other contributions the ozone hole dilution component (in the lower stratosphere) of the changes in reconstructed total ozone.

The other factor, a possible contribution to the mismatch arising from ozone destruction/creation during the period, is difficult to assess quantitatively. In view of the rather slow photochemical time scale for ozone in the lower stratosphere where we concentrate our attention (of the order of a few months), the short period considered (12 days) and the expectation that the photochemical time scale at a given level should be essentially determined by mean temperature rather than the more local dynamically-induced temperature perturbations, this is not expected to be a major concern for our purposes. This is because, although such photochemical ozone changes during the period might be as much as 10 to 15 % at ozone hole levels, such changes should occur over the largest spatial scales, so while they may lead to absolute inaccuracies in our representation of the ozone distribution, they should not have a significant bearing on the three-dimensional structure of the dynamically-induced ozone changes which are the focus of the present work.

A final potential contribution to the discrepancies noted between TOMS and reconstructed total ozone distributions, and that which may produce perhaps a significant contribution to the mismatches which occur on both 02 December and 14 December, results from applying the S5 sweep $\chi/\hat{q}$ relationships, which provide a close but not perfect description of the ozone distribution for the overall S5 period, to reconstruct the distribution on two individual days falling well after the midpoint of the sweep. A proportion of this component, that due to a latitudinally dependent but otherwise rather constant bias in both reconstructions, can be simply removed by considering the areal distribution of the changes in ozone witnessed between 02 and 14 December by the reconstructions, and comparing this with the changes seen by TOMS. Accordingly, in the following Section we focus on these changes between 02 and 14 December.

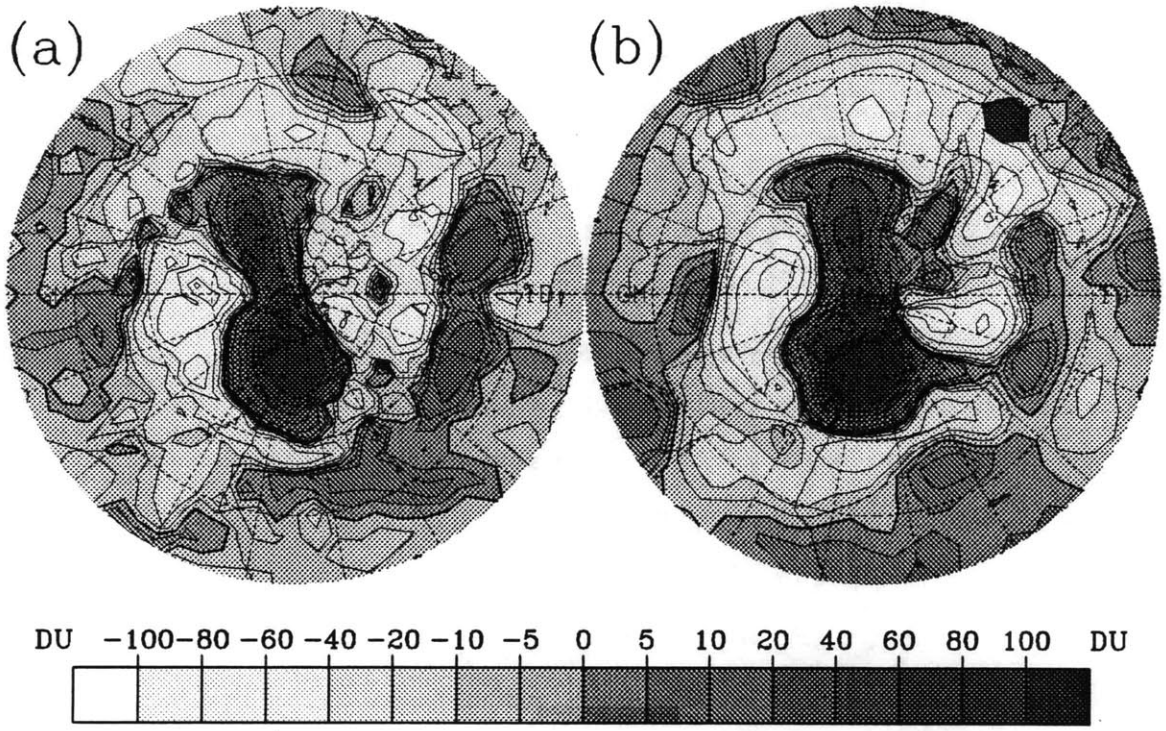

Figure 7.10: Hemispheric distribution of the total change in total ozone between 02 and 14 December, from (a) TOMS and (b) reconstructions. Contours shown at 0 (heavy), and ± 5, 10, 20, 40, 60, 80 and $100 DU$. Shading between contours is as indicated by the key. Grid lines at 20° intervals, Greenwich Meridian to left, outer edge at equator.

7.3 Detailed Examination of the Ozone Changes between 02 and 14 December

Figure 7.10 shows the areal distribution of the change in total ozone during the 02 to 14 December period, as witnessed by TOMS and depicted by the reconstructions (using the EPV analyses from 02 December and the CAS data for 14 December). The picture provided by the reconstructions of the total ozone evolution during the 12 day period is similar overall to that shown by TOMS, and this inspires confidence in the differences between the reconstructed OMR distributions for the two days. The two

most noteworthy features in each of the plots are the region of large ozone increase centred over the Palmer Peninsula, closely approximating the shape of the ozone hole on 02 December, and the region of marked decrease in the southern Atlantic Ocean, which corresponds to the location on 14 December of the bulk of the ozone hole remains. Each plot shows the mid-latitude tongues of ozone decrease, which correspond to those seen in Figure 7.1(b), one across South America from the region of large decrease in the Atlantic, the other seeming to extend from the lesser 'pinched off' lobe of the vortex/ozone hole located over the southwest Pacific Ocean, out across New Zealand and southern Australia and into the Indian Ocean. Significant differences also exist between the plots. Associated with the overestimation by the reconstruction of the total ozone maximum in the vicinity of the Antarctic coast to the south of Australia in Figure 7.9, Figure 7.10(a) shows a TOMS decrease while the reconstruction shows an increase, and the reconstruction tends to exaggerate the magnitude of the mid-latitude decreases over the central and eastern Pacific and Indian Oceans. Generally, however, the patterns are quantitatively similar, and we next proceed with the closer examination of the event based on the changes in NMC isentropic pressure and reconstructed OMR distributions between the two days.

7.3.1 Individual Contributions from Vertical and Horizontal Motion

Using the technique described in Section 3.6 above, the respective contributions to the reconstructed change in the hemispheric total ozone distribution, arising from quasi-horizontal advection of OMR on isentropic surfaces, and vertical motion of the isentropes, were first isolated. Figure 7.11 shows these respective contributions. Immediately apparent in Figure 7.11(a) is the broad region of total ozone increase (up to $40DU$) at high latitudes which results from adiabatic subsidence associated with the movement of the low level vortex remains off the pole, and the total ozone decreases resulting generally from relatively modest isentropic uplift in rather localised regions in the middle latitudes. Even more obvious by comparison of the two plots in

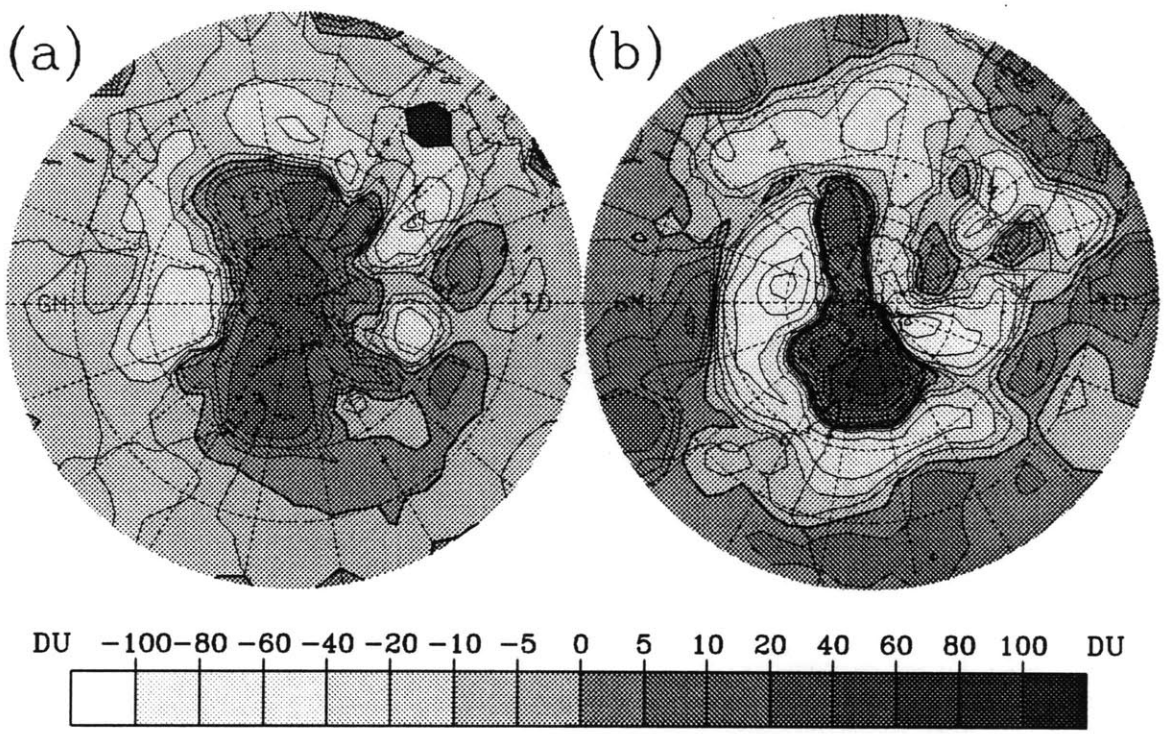

Figure 7.11: As for Figure 7.10, except for the contribution to the total change in reconstructed total ozone arising from (a) vertical advection and (b) horizontal advection.

the Figure is the overwhelming tendency for the 'horizontal' component to dominate the overall changes, the pattern of the changes due to horizontal advection in Figure 7.11(b) being qualitatively similar to that of the observed changes in Figure 7.10(a). A noteworthy exception in view of the previous analysis by Atkinson *et al* (1989), and which we examine more closely below, is the region of marked ozone decrease near Melbourne.

The overall dominance of the observed pattern by the horizontal component is explained as a consequence of the final warming in the southern hemisphere stratosphere comprising a drawn-out downward progression, the breakup of the vortex at upper levels preceding that at lower levels, and having already occurred by the start of December in 1987. Ozone reconstructions for the November period (not shown) demonstrate that accompanying the upper level weakening and destruction process (the LS stage) which comprises the final warming in the classical sense, the

hemispheric distribution of the total ozone changes is primarily attributable to the vertical motion component. Because ozone partial pressures are relatively small at the higher levels, so horizontal transports there produce a relatively modest impact on the total ozone distribution, the deep and broadscale vertical motion response throughout the lower and middle stratosphere, where most of the ozone column lies, results in the vertical motion component dominating the observed changes. By the beginning of December 1987 this stage of the dynamical evolution has occurred, and the destruction of the vortex at lower levels, where meridional gradients are large, produces a much stronger effect on the total ozone column attributable to horizontal transports, than that due to vertical transports. This overall pattern of behaviour, in which the vertical motion component dominates the response to the breakup at upper levels, whereas the horizontal component dominates that at low levels, is seen in each of the years considered in the broader search for dilution events, to be covered in Chapter 8 below. We speculate that in this respect the ozone reponse accompanying the seasonal transition in the southern hemisphere is probably quite different to the northern hemisphere case, where the vortex breakup tends to occur almost simultaneously throughout much of the stratosphere.

To illustrate the vertical structure of the reconstructed total ozone changes from 02 to 14 December, Figures 7.12 to 7.16 show meridional cross-sections of the overall change in ozone partial pressure and total pressure, and each of the components due to vertical and horizontal motion respectively. Figure 7.12 is a cut along the Greenwich Meridian, passing through the ozone hole remnants. Figure 7.13 slices through the centre of the region of mid-latitude decrease in the Indian Ocean. Figure 7.14 shows the structure of the Melbourne decrease. Figure 7.15 shows that of the lesser pinched off lobe of the vortex, and Figure 7.16 is a slice through the South American 'tongue'.

These Figures provide a representative description of the dynamical evolution throughout the hemisphere during the period and its impact on the ozone distribution, as well as providing further insight into the limitations of the reconstruction technique.

In each of the Figures the vertical coordinate is potential temperature, which has

been scaled logarithmically in each plot, so that, by Equation 3.10, the 'equal area' property approximately holds for the contribution from a given change in ozone partial pressure to the total ozone change at a given location. Each plot shows the ozone partial pressure change distribution shaded, the shaded regions separated by thin contours, whereas the distribution of the total pressure change is shown by contours of intermediate thickness (labelled in Part (b) of each Figure), with those for pressure increase (subsidence) shown dashed. The heaviest contours in each plot denote zero change in either variable. In Part (b) of each Figure, because all horizontal advection has been suppressed, the contours for zero change in ozone partial pressure and total pressure coincide, and in Part (c), with all vertical motion eliminated, there are of course no changes in total pressure anywhere.

Although rather obvious from the earlier consideration of the EPV evolution and the distribution of the TOMS total ozone change in Figure 7.10(a), Figure 7.12 clearly establishes that the South Atlantic total ozone decrease, centred near $60°S$, was the direct result of advection into the region of the bulk of the ozone hole remains. Figure 7.12(b) and (c) show that by far the dominant contribution to the total ozone decrease was that due to isentropic advection of low OMRs, with a relatively small contribution from vertical motion (about 25%) because the impact on total ozone of the subsidence aloft largely cancels that below due to isentropic uplift. Figure 7.12(c) shows that the bulk of the horizontal component of the decrease occurred at ozone hole levels, rather than being due to 'natural' poleward advection of low OMRs at the lowest levels, or equally 'natural' equatorward advection at levels above $600K$, although both of these effects contributed to the reconstructed decline. Figure 7.12(b) also suggests that, in line with the previous discussion of the dynamical adjustments accompanying EPV changes, the polar outbreak at this longitude was focussed around $650K$, with ascent below and descent aloft. At lower levels ridging (poleward EPV advection) occurred in mid-latitudes around $340K$. Figure 7.12(c) shows that its effect on the total ozone change was greatest near $50°S$, whereas north of $40°S$ OMRs generally increased during the period, implying equatorward advection of air from higher latitudes, but not from within the ozone hole.

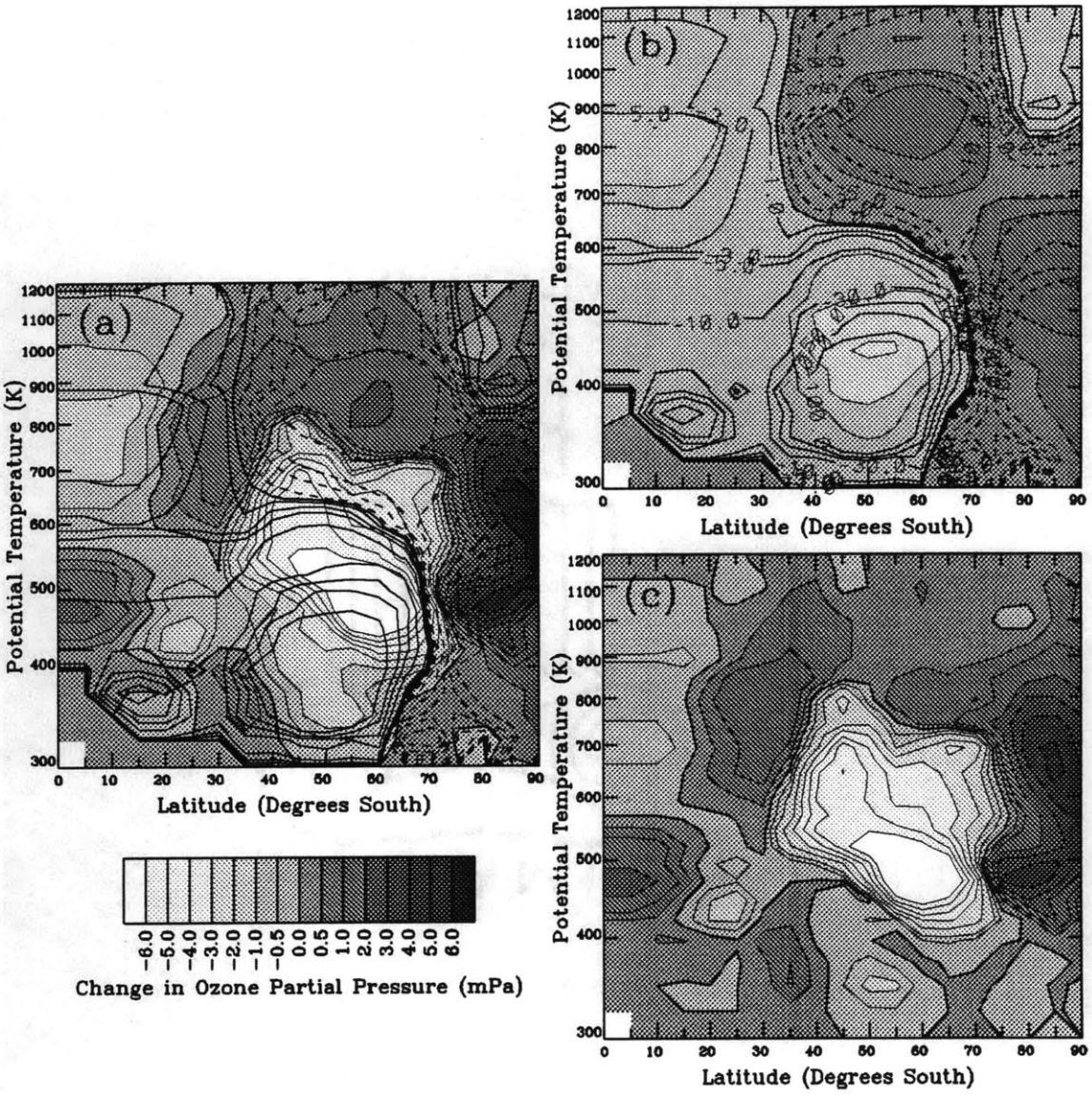

Figure 7.12: Meridional cross-section (log potential temperature vs latitude) at $0°E$, of the change in reconstructed ozone partial pressure (mPa - thin solid contours, shading as indicated by the key, and with regions of positive and negative change separated by the thickest contour) and total pressure (DPa - thicker contours, positive values dashed) between 02 and 14 December. (a) Total change. (b) Component due to vertical advection. (c) Component due to horizontal advection. Isallobars are the same in (a) and (b) but are labelled in (b) only.

Of particular interest at $90°E$ (Figure 7.13) is the structure of the total ozone decrease which was apparent in Figure 7.10 near $35°S$, and which is about equally

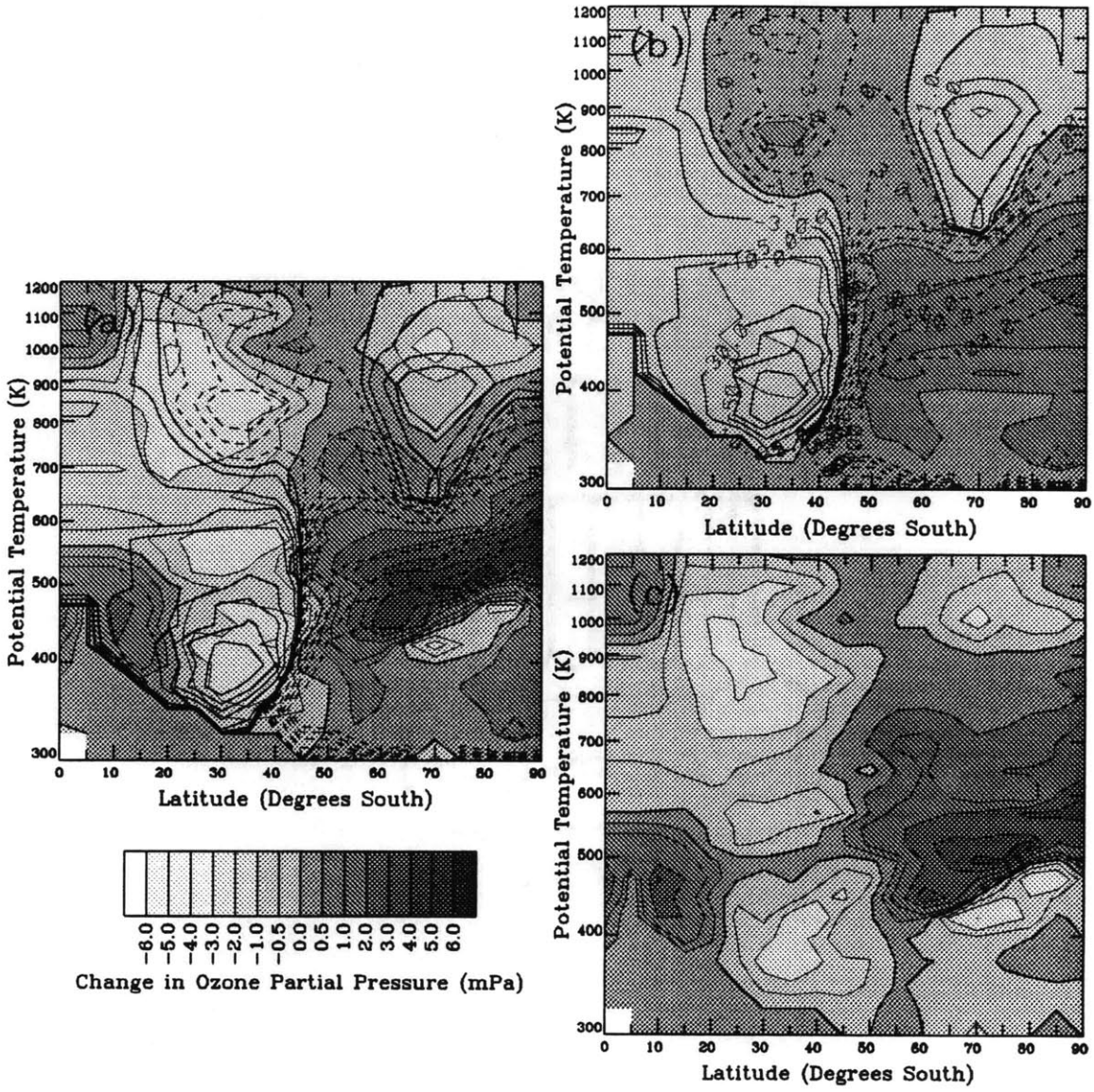

Figure 7.13: As for Figure 7.12 except for the cross-section at $90°E$.

attributable to horizontal and vertical advection. Figure 7.13(c) shows some of the horizontal contribution arose from advection of low ozone at the lower levels, and the structure of the pressure change distribution suggests both that it was poleward advection (with ascent aloft) of air from lower latitudes rather than a polar outbreak, and that the ascent contributed significantly to the overall change (i.e the feature was not caused by ozone dilution). The region of ozone decrease above $600K$ in the subtropics also contributes to the overall decrease at $35°S$. While the reconstructions are not expected to perform well at lower latitudes anyway, this feature produces a

total ozone change of opposite sign to that shown by TOMS over the northeast Indian Ocean north of $30°S$. It resulted from equatorward advection of polar air, producing substantial isentropic OMR changes. Since this upper level feature is the reflection in the 14 December reconstruction of the shearing out and rapid westward advection of the vortex remains which was discussed earlier in the context of the $750K$ CAS simulation, and since TOMS indicates an opposite tendency in total ozone in the region, this in turn suggests the CAS-indicated OMR changes are probably erroneous and either that diabatic and photochemical ozone changes were not negligible during the period, or that the balanced wind fields overplayed the strength of the easterlies at and near the $750K$ level, producing an error in bulk advection by CAS. A small component of the total ozone decrease at $35°S$ is suggested to have resulted from a decrease in OMR between $500K$ and $600K$. This results from equatorward advection by CAS of material which initially lay poleward of the OMR maximum at these levels. Hence it comprises a potential ozone dilution contribution to the overall decrease. We noted above, however, that the reconstructions may place the OMR maximum too far north at these levels, so the signature requires closer inspection before an ozone hole connection can be positively identified. We shall deal with this further below.

Figure 7.14, which shows the meridional cross-section at $145°E$, disects the Melbourne region ($38°S$), the observed total ozone decrease at which first inspired the earlier investigation of the ozone dilution event by Atkinson *et al* (1989). In this context the result of the reconstruction is particularly interesting: it suggests quite plainly that very little of the mid-latitude ozone decrease observed in the Melbourne area was likely to be attributable to an ozone dilution effect. There are several interesting features in the cross-section at mid-latitudes.

The first of these is the region of ozone decrease centred around $340K$, which, with OMR increasing monotonically towards the pole at the lowest levels, was obviously due to low level ridging. (To some extent this feature results from an unfortunate choice for the start date of the analysis period, because on 02 December a synoptic scale upper tropospheric cold pool was passing over the Melbourne region, with ridg-

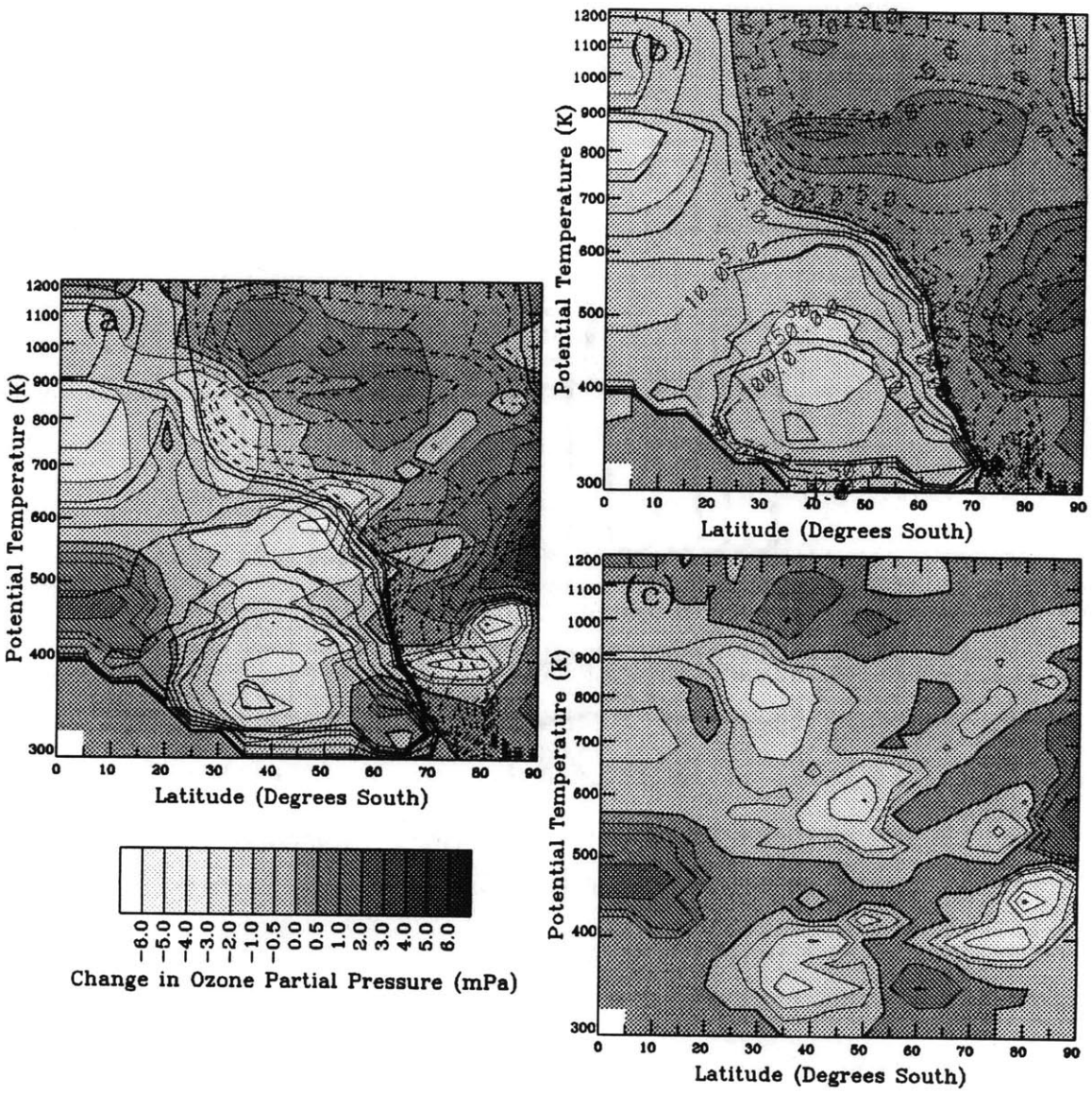

Figure 7.14: As for Figure 7.12 except for the cross-section at $145°E$.

ing to east and west. Hence the ridging indicated might better be described as the retreat of a trough.) The contribution from horizontal advection associated with this event, which extended upward to $425K$, comprised a significant component of the overall total ozone decrease.

The second noteworthy feature is the ozone decrease centred near $30°S$ around $800K$ in Figure 7.14(c) and which results from the shearing out and rapid westward advection of the vortex remains by CAS. As for the $90°E$ cross-section, because the reconstruction overestimates the total ozone decrease at $30°S$ compared with TOMS,

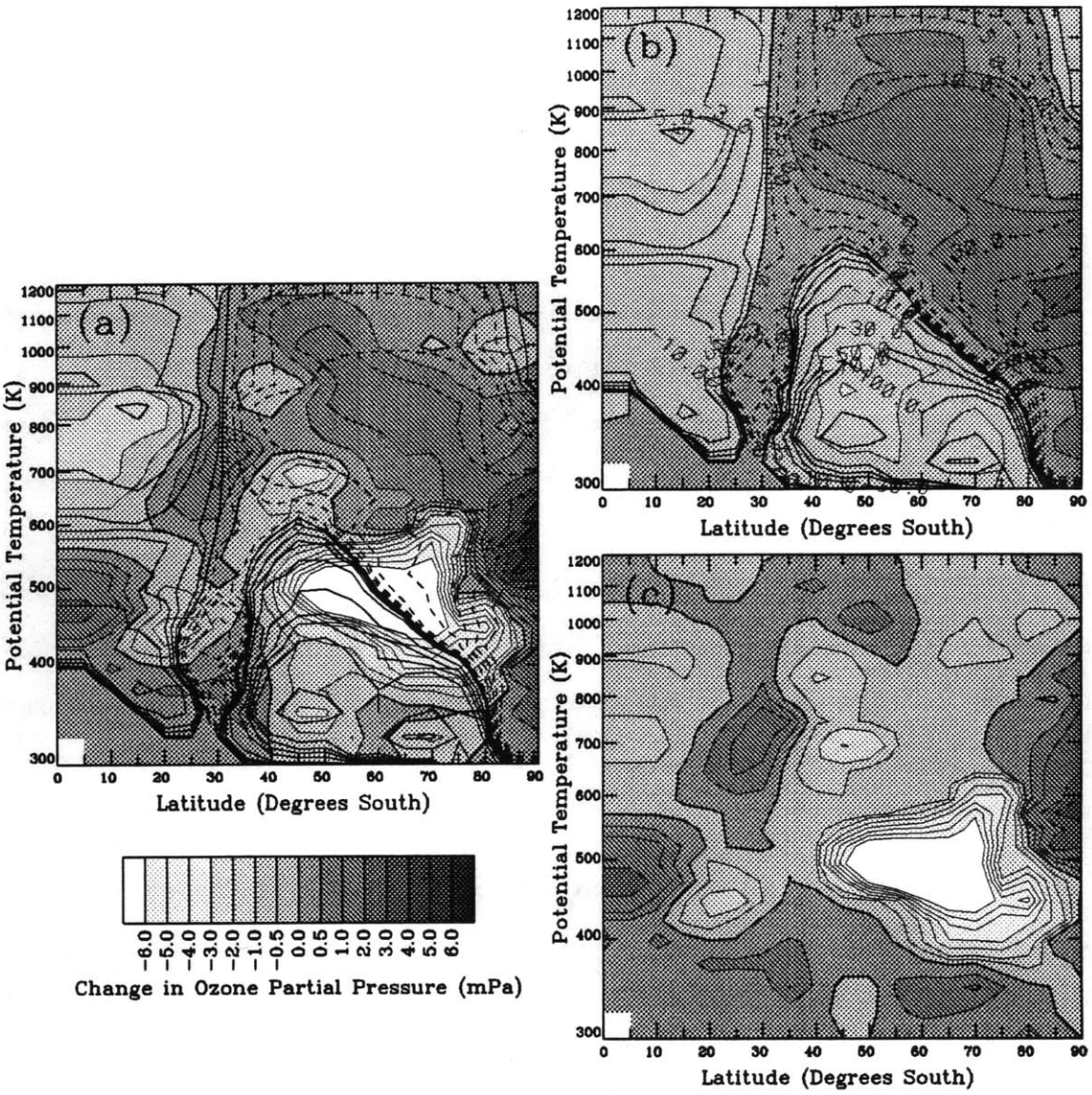

Figure 7.15: As for Figure 7.12 except for the cross-section at $165°W$.

the feature may be erroneous.

The ozone decrease centred near $50°S$ at $600K$ is the reflection of the tongue extending from the pinched-off lobe of the vortex over the southwest Pacific Ocean, and it is noteworthy that this feature extends down to about $475K$. While the decrease shown results from the advection into the region of material which initially lay poleward of the reconstructed OMR maximum at these levels, the generally modest ozone changes suggested and the uncertainty about the accurate placement of the OMR maximum by the reconstruction suggests closer examination of the feature is

required before an ozone hole connection can be established.

Consistent with the low level ridging and the EPV outbreak at higher levels (in the NMC-based analysis of 14 December), is the broad mid-latitude region of isentropic uplift in Figure 7.14(b), which provided the largest contribution to the overall total ozone decrease.

While Figure 7.15 shows the structure of the changes at $165°W$ to be rather complex, the major feature is the pinched-off lobe of the vortex. Figure 7.15(c) shows a marked region of ozone decrease centred $500K$, which indicates a significant amount of ozone-depleted air to have extended north of $45°S$ at this longitude. Figure 7.15(b) suggests the peak of the outbreak sloped equatorward with height at $165°W$ between about $400K$ and $600K$. The pressure change cross-section shown, with subsidence dominating the ozone changes at high latitudes, but ascent below the outbreak dominating at mid-latitudes, produces an overall total ozone change signature which is typical of an EPV outbreak, with a high latitude increase giving way to a decrease at mid-latitudes, as evident in Figure 7.11(a).

The cross-section at $80°W$ shown in Figure 7.16 passes through the mid-latitude tongue of ozone decrease which extends from the ozone hole remnants in the Atlantic Ocean across South America and into the Pacific Ocean. The dominating feature of the pattern is the large ozone increase at high latitudes, which reflects the movement of the vortex away from the region during the 12 day period.

The more interesting features from the ozone dilution perspective are the contributions to the ozone decrease near $40°S$. That between $700K$ and $800K$ in Figure 7.16(c) is due to the advected vortex remains. Once again, the indications by TOMS of an overall increase in total ozone north of about $30°S$ suggests the equatorward extent of this region to be overplayed by CAS, although the close overall agreement beteween TOMS and the reconstruction south of $30°S$ tends to support it. The reconstructed ozone decreases below $500K$ are the result of poleward advection of lower OMRs, so except for the small potential contribution from the levels between $500K$ and $600K$, which awaits closer scrutiny, the reconstruction shows no evidence of a

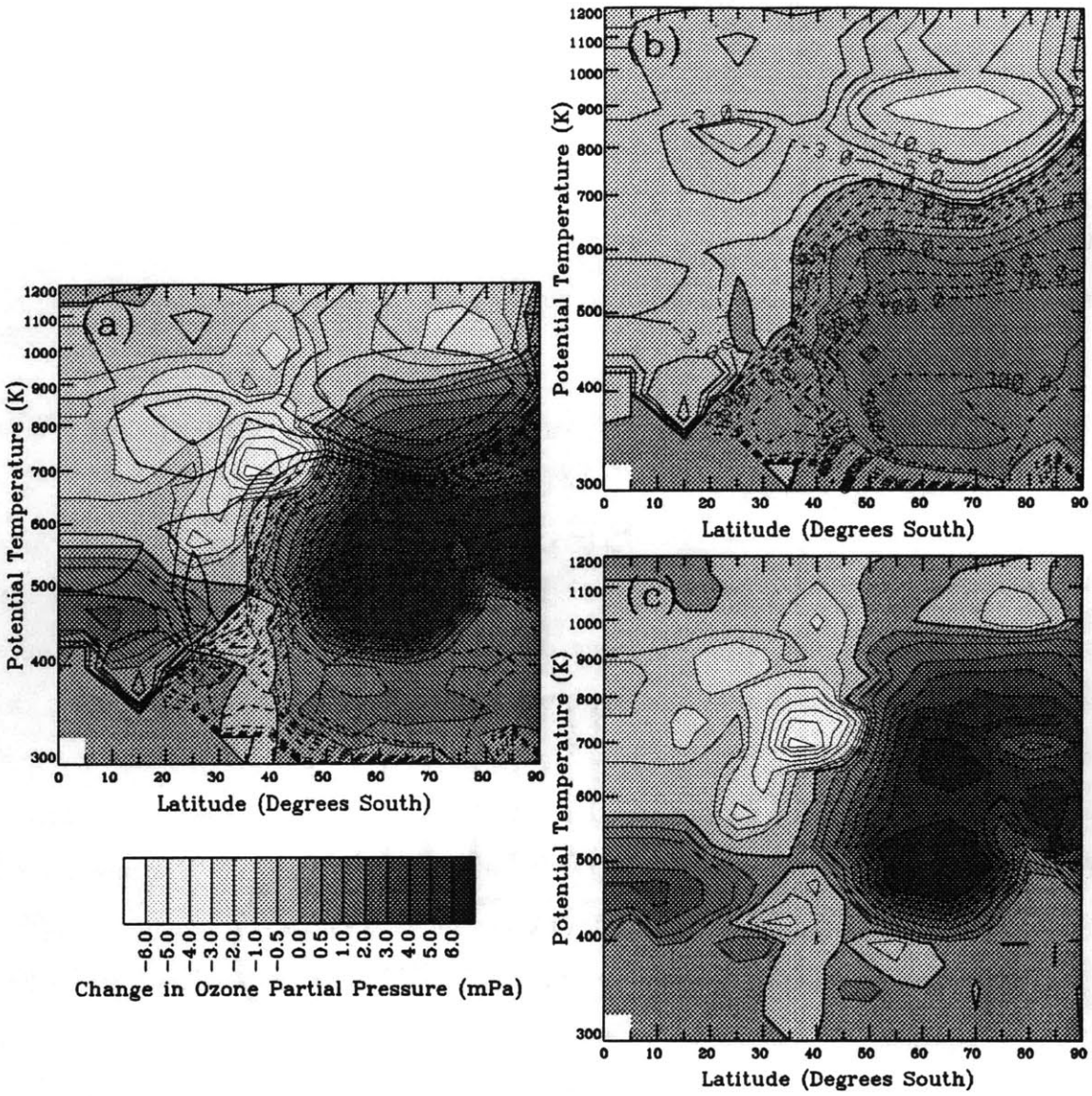

Figure 7.16: As for Figure 7.12 except for the cross-section at $80^{o}W$.

direct ozone hole connection to the observed total ozone decrease.

Overall, then, of all the regions shown in Figure 7.11(b) where quasi-horizontal advection led to an ozone decrease component, those over the Indian Ocean, South America and the eastern Pacific regions were, according to the reconstructions, almost entirely due either to poleward advection at low levels of low OMRs from subtropical latitudes, or to equatorward advection of polar air accompanying the CAS-depicted vortex breakup, but at levels too high to have an ozone hole connection. Only the decreases over the southwest Pacific and Atlantic Oceans were primarily due to the

breakup of the ozone hole, while a smaller but perhaps significant component of the decrease over New Zealand and southeastern Australia was due to an ozone hole dilution effect.

Having separated the reconstructed distribution of the total ozone changes into vertical and horizontal advection components and examined them in some detail, we shall now examine each contribution in more detail.

7.3.2 Further Decomposition of the Contribution from Vertical Motion

While the analysis described in the preceding Subsection enables us to identify the spatial structure of the localised ozone changes which brought about the changes in reconstructed total ozone, it provides only qualitative insight into the dynamical mechanisms responsible for the vertical motion component, and how these are tied to the contribution from horizontal advection. It would be of interest, for example, to determine whether the broad scale ascent in the lower and middle stratosphere, which was responsible for a substantial proportion of the total ozone change in the Melbourne region, was primarily due to the low level ridging or the higher level EPV outbreak. Were the former the case, then the observed response might well have been largely predicted on the basis of analysis of tropospheric data alone, without the need to resort to the poorer quality stratospheric data set. Were the latter the case, however, this would not be possible, implying the the situation was one in which the observed total ozone change could not necessarily be deduced by consideration of, for example, changes in tropopause height, or geopotential height or temperature at some isobaric level in the upper troposphere. Accordingly, we have used the technique described in Section 2.5 above on the observed distribution of the changes in QPV during the period, to gain further insight into the horizontal scales and vertical domains of the dynamical rearrangements primarily responsible for the vertical motion component of the reconstructed total ozone change.

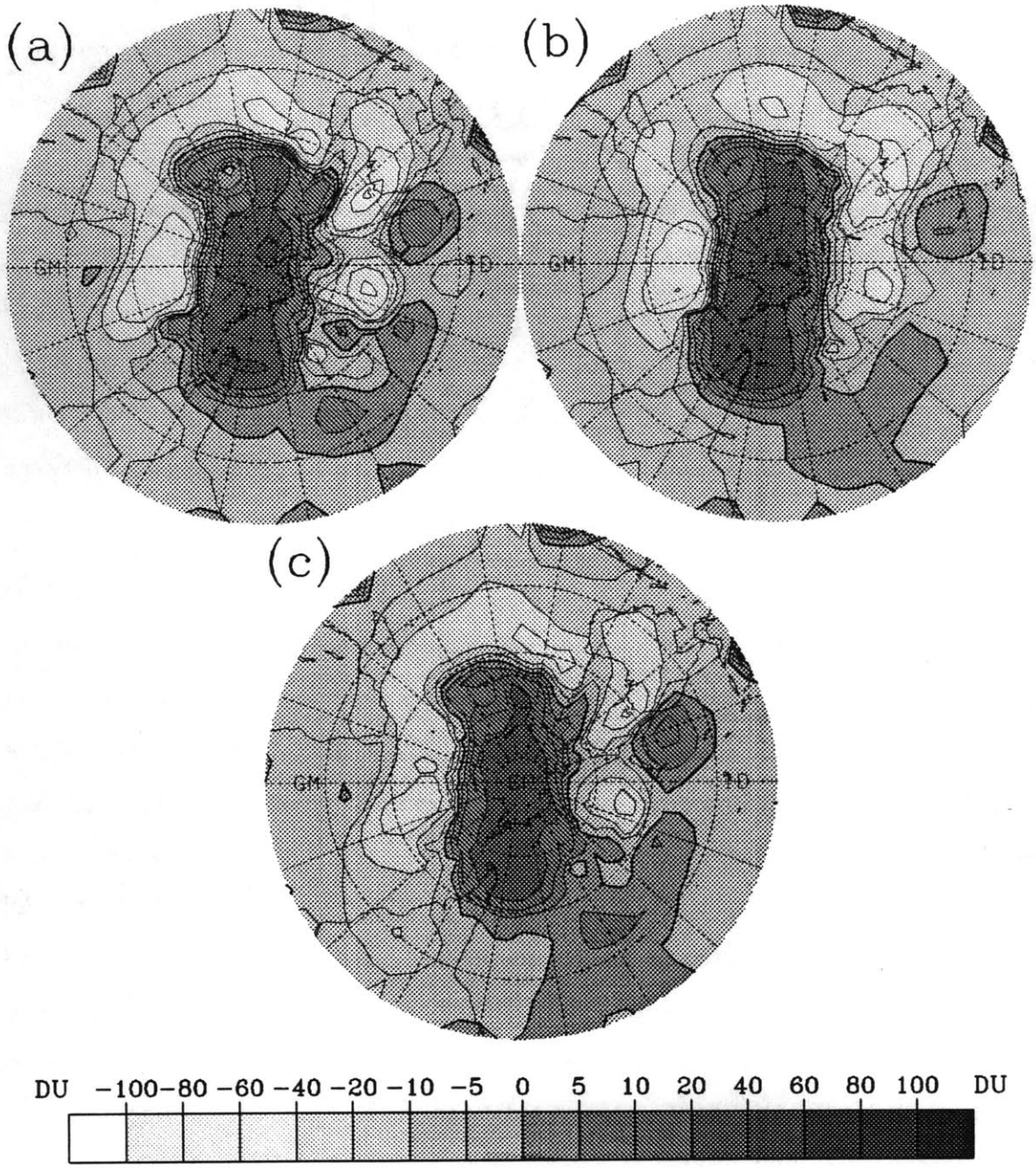

Figure 7.17: As for Figure 7.11, except for the contribution to the total change in reconstructed total ozone arising from vertical advection, as calculated by solution of the quasi-geostrophic omega equation for (a) QPV 'forcing' from the full vertical domain, at T20 resolution, (b) QPV 'forcing' from the full vertical domain, at T10 resolution, and (c) QPV 'forcing' only in the region above $225hPa$, at T20 resolution.

As a first step, and to confirm that the omega equation inversion technique was

effective in duplicating the impact of the observed pressure changes on the total ozone distribution, a full domain inversion was performed at T20 truncation. The resulting vertical advection component of the total ozone change around the hemisphere is shown in Figure 7.17(a). The similarity of the plot to Figure 7.11(a) demonstrates the overall effectiveness of the technique, the small differences apparent being due to small scale dynamical forcing at effective wavenumbers greater than about 14. (To confirm that the discrepancies were indeed due to the exclusion of small scale features and not the inversion technique itself or hydrostatic imbalance in the NMC data, the observed pressure change distribution used to produce Figure 7.11(a) was itself harmonically filtered and the reconstruction repeated. The differences between the resulting distribution and that of Figure 7.17(a) were very small.)

The full domain inversion was then repeated at T10 truncation to eliminate the contributions from QPV forcing at the smaller synoptic scales (effective wavenumber greater than about 7). The resulting vertical motion contribution to the distribution of total ozone change is shown in Figure 7.17(b). That the overall features of Figure 7.17(a) and (b) are so similar demonstrates the primary importance of the planetary and medium scale dynamical rearrangements occurring during the vortex breakup, in determining the overall vertical motion field and its effect on the ozone column. Of some interest is the expected result that the largest differences between the two plots tend to coincide with those regions in which the analysis of the previous Subsection revealed a significant contribution to the total ozone change from a low level source. (Note, for example, the smaller change indicated in the Melbourne region when the smaller scales are eliminated.)

Additional inversions were then performed at increasingly severe truncation (not shown), and it was found that, while the few gravest scales of dynamical rearrangement accounted qualitatively for the broad features of the observed distribution, quantitative agreement decreased rapidly below T10 resolution.

A number of inversions was next performed to investigate the contributions to the observed vertical motion response, and their impact on the ozone distribution,

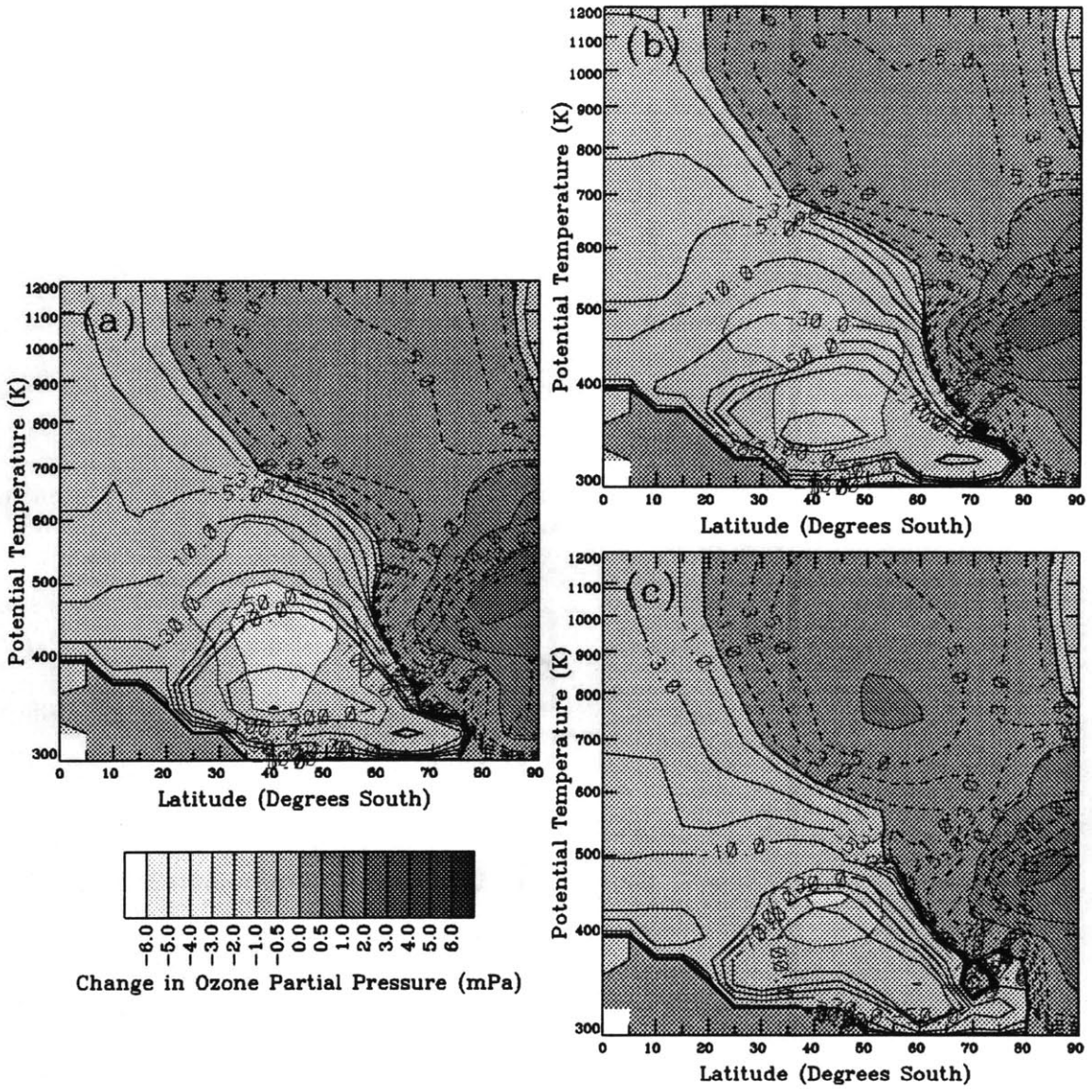

Figure 7.18: Meridional cross-sections at $145^{o}E$ (as in Figures 7.12 to 7.16), except for the vertical motion components shown in Figure 7.17 i.e. (a) full vertical domain at T20, (b) full vertical domain at T10 and (c) forcing above $225hPa$ at T20.

which arose from QPV changes occurring in different vertical sub-domains. The results of the most illuminating of these is shown in Figure 7.17(c), which depicts the distribution of total ozone change resulting from the vertical motion field due to stratospheric QPV advection only. The recomposition was performed at T20 with all forcing below $225hPa$ removed. This level was chosen as approximately representative of the mid-latitude tropopause during the period. Comparison of the plot with Figure

7.17(a) shows that the majority of the total ozone vertical motion response was due to stratospheric dynamics, the dynamical changes occurring in the troposphere having a relatively small impact.

Returning to the vertical motion contribution to the reconstructed total ozone change in the Melbourne region, Figure 7.18 shows meridional cross-sections which correspond to that shown in Figure 7.14(b), except they are for the three omega equation solutions shown in Figure 7.17. Figure 7.18(a) is generally very similar to Figure 7.14(b). However, it shows larger pressure (and ozone) decreases in mid-latitudes between $340K$ and $400K$, suggesting the low level ridging (below $340K$) is too strong in the omega equation solution. This is a symptom, quite often seen in the omega equation inversions for other periods, of the disparity noted at the end of Section 2.5 above, and which appears to result either as a consequence of the use of linear interpolation with respect to pressure, or to an internal inconsistency in the NMC geopotential height analyses between the 70 and $100hPa$ levels. The effect on the solutions is nonetheless minor. The T20 inversion also fails to capture the magnitude of the vertical motion response at upper levels or its detailed structure, in this case because of spherical harmonic truncation of the more dominant smaller scale features present in the analyses.

The differences between Figure 7.18(a) and 7.18(b) highlight a significant contribution to the Melbourne ozone decline from the synoptic scale component of the QPV changes, and Figure 7.18(c) shows that, while the tropospheric dynamics at this location had quite a strong impact on the vertical motion contribution, the overall broad structure of the response was attributable to the QPV changes in the stratosphere.

7.3.3 Isolation of the Ozone Dilution Component of the Total Ozone Changes

The ultimate objective of the reexamination of the 1987 event was to determine quantitatively the contribution to the observed mid-latitude ozone decline during

December 1987 which arose as the direct result of advection into the region of ozone-depleted air from within the Antarctic ozone hole. Despite the overall insight gained from the above examination, it was insufficient to arrive at an accurate assessment of this contribution at all locations. The major reason that this was so is that the ozone dilution component, virtually everywhere other than the south Atlantic and southwest Pacific regions, where the two lobes of the low level vortex were advected, appears to have been small at most. So whereas we might confidently conclude that in these former two regions the ozone dilution signal indicated by the reconstructions is considerably larger than the errors we can reasonably expect using the reconstruction technique (although we have not quantified these expected errors), elsewhere the signal obtained is so small as to be arguably due entirely to inaccuracies associated with the analysis technique.

To overcome this problem and better assess the 'Antarctic ozone hole dilution' component of the mid-latitude total ozone decrease, the analysis was further refined, by focussing on the particular question of ozone dilution.

Although we have not quantified the likely errors associated with the analysis technique, because in most cases this is not practicable, we have devoted considerable attention to identifying their potential sources. A large proportion of these likely errors, discussed earlier, can be eliminated by excluding from consideration the ozone changes occurring as a result of quasi-horizontal transport everywhere above and below ozone hole levels, and by excluding entirely the component due to vertical transport. Accordingly, an ozone reconstruction was performed which employed the CAS-advected OMR distributions for 14 December for the levels between $380K$ and $575K$ (the approximate vertical domain of the ozone hole), but the OMR distribution derived from the EPV analysis of 02 December at other levels, and the tropopause and isentropic pressure distributions of 02 December at all levels. The hemispheric distribution of the change in total ozone between this contrived reconstruction and the previous 02 December reconstruction was then calculated and is shown in Figure 7.19.

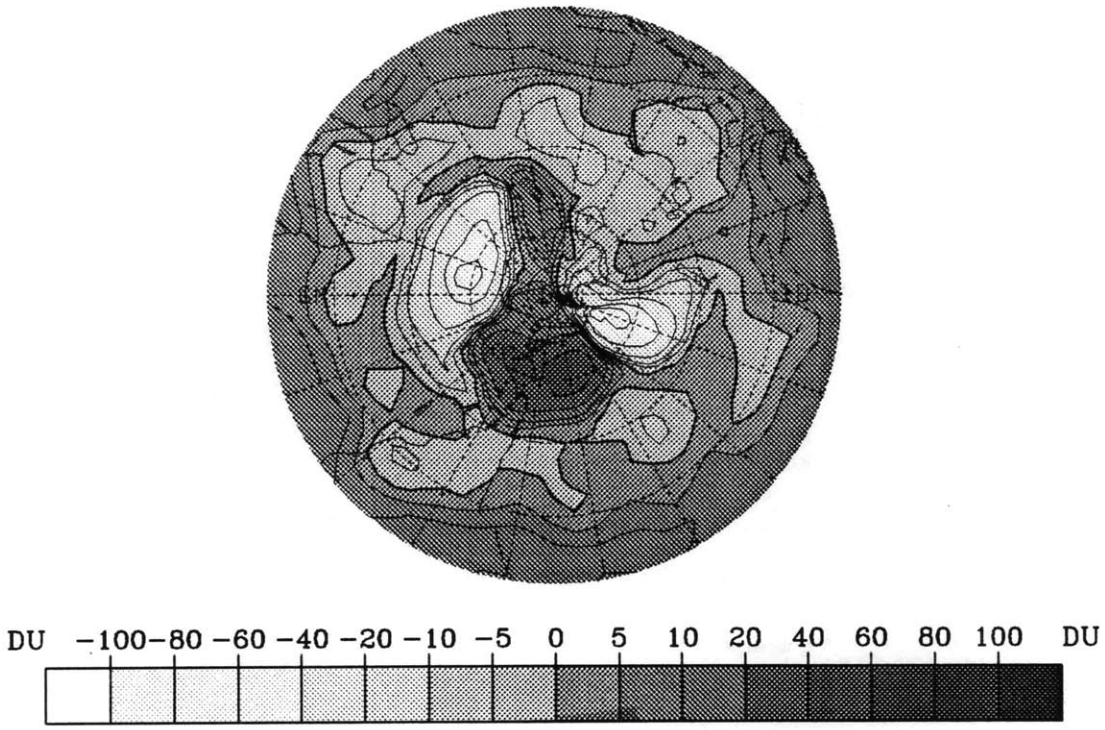

Figure 7.19: As for Figure 7.11, except for the contribution to the total change in reconstructed total ozone arising from horizontal advection occurring between $380K$ and $575K$.

While the contrivance serves to eliminate the 'natural' ozone changes due to horizontal advection at the upper and lower levels which considerably clouded the picture shown in Figure 7.11(b), and thus eliminates the likely errors associated with the reconstruction technique's representation of these features, closer examination of the vertical structure of the changes shown in Figure 7.19 revealed that a significant component of the remaining structure is the result of poleward advection associated with low level ridging episodes, some of which where discussed earlier. For example, the region of ozone decrease in the central Pacific evident in Figure 7.19 is entirely due to such an episode. Even were these contributions to have been eliminated, there remain the questions as to what proportion of the surviving changes might result from the abovementioned possible mislocation of the OMR maximum between $500K$ and $600K$, and, even were the reconstruction technique perfect, what fraction of the changes would have occurred anyway in the absence of Antarctic ozone depletion.

This latter question is where the lack of a control distribution limits our ability to quantify precisely the mid-latitude impact of the Antarctic ozone hole.

It was presumed at the outset of the investigation that the availability of SAGE I data for the 1979 to 1981 period would enable us confidently to reconstruct such a control distribution. However, it soon became apparent that this was not so straightforward a task. In the first place it is likely, on the basis of evidence from Antarctic total ozone observations prior to the 1980s (Farman *et al* (1985), Chubachi (1993), Komhyr *et al* (1986), Schoeberl *et al* (1989b)) that the Antarctic ozone depletion process was already well underway by 1979 (Farman *et al*, 1985) and that the SAGE I reconstructions themselves reflect a significant component of springtime Antarctic depletion. That a natural Antarctic ozone minimum has probably always existed was noted by Dobson (1966) and it seems likely, on the basis of dynamical reasoning, that at ozone hole levels a local isentropic OMR minimum has always existed within the polar vortex. Just what values of OMR would have been present prior to the vortex breakup in 1987 in the absence of Antarctic ozone depletion is far from certain, however. Given the uncertainties associated with describing the unperturbed ozone distribution, the fall back option was to assess the mid-latitude impact from the 1987 event, relative to that which might have been experienced under similar dynamical conditions had it occurred during the SAGE I period.

For 1979 the only appropriate SAGE data for comparison were those from the last ten days in November (see Figure 6.1), but since the low level vortex destruction occurred early in this period, and because ozone levels were seemingly anomalously high during the 1979 season, as discussed in Chapter 6 above, they were not considered. While data from the S3 period in 1981 were available, these were from October, a full month before the vortex breakup. The logical choice was the S3 period of 1980, which fell in November, with the high and mid-latitude SAGE observations made not long before the vortex breakup at low levels (as for S5 in 1987). 1980 was also dynamically very quiet, as noted in Chapter 5 above, the dynamical evolution being the most similar to that in 1987 of all the seasons examined. Nonetheless, the dy-

namical cross-sections from the 1980 sweep were by no means similar to those for the 1987 sweep, particularly below $500K$, with significantly greater OMRs present both at high and middle latitudes in 1980. Taking into account the significantly warmer temperatures at lower levels in November 1980, the differences were even greater (compare Figure 6.4(e) with Figure 6.14(c)), not only in the polar region but also in association with the circumpolar ozone maximum, where ozone partial pressures in the lower stratosphere were about twice as high as those in 1987 . In view of the similarity in the dynamical evolution of each season (except for the apparently greater incidence of low level Rossby wave breaking and the somewhat more advanced stage of low level vortex decay in 1980), this again raises questions about whether the presence of the Antarctic ozone hole might influence ozone levels in the region of the ozone maximum, which would then provide an additional source for mid-latitude ozone dilution. Investigating this matter in depth is beyond the scope of the present work, although we shall consider it further in Chapter 9 below. For our present purposes, we have assumed that the only reflection of Antarctic ozone depletion has been a lowering of OMRs in the lower stratosphere (between $380K$ and $575K$) within the polar vortex interior, and that in the absence of Antarctic ozone depletion the observed ozone levels within the vortex would have been similar in 1987 to those in 1980. This implies, as is evident from the distributions shown in Figures 6.4(e) and 6.14(c), that in the absence of an ozone hole in 1987 there would have been only a small decrease poleward of the OMR maximum at each 'ozone hole' level above $450K$ and essentially no decrease below. (At $450K$ the OMR maximum for S5 in 1987 was about $1.5ppmv$, the same as the polar minumum for S3 in 1980, while at lower levels the OMR maximum in 1987 was lower than the polar values in 1980).

To isolate approximately the ozone dilution component of the reconstructed ozone change between 02 and 14 December, the OMR distribution for each day was recalculated by 'fiddling' the OMR distribution between $380K$ and $600K$. Below $450K$ the OMRs poleward of the vortex edge were forced to remain constant at the vortex edge value. Above $450K$, since the 1987 mid-latitude values were higher than the 1980 polar values, the OMRs were allowed to decrease poleward until they reached

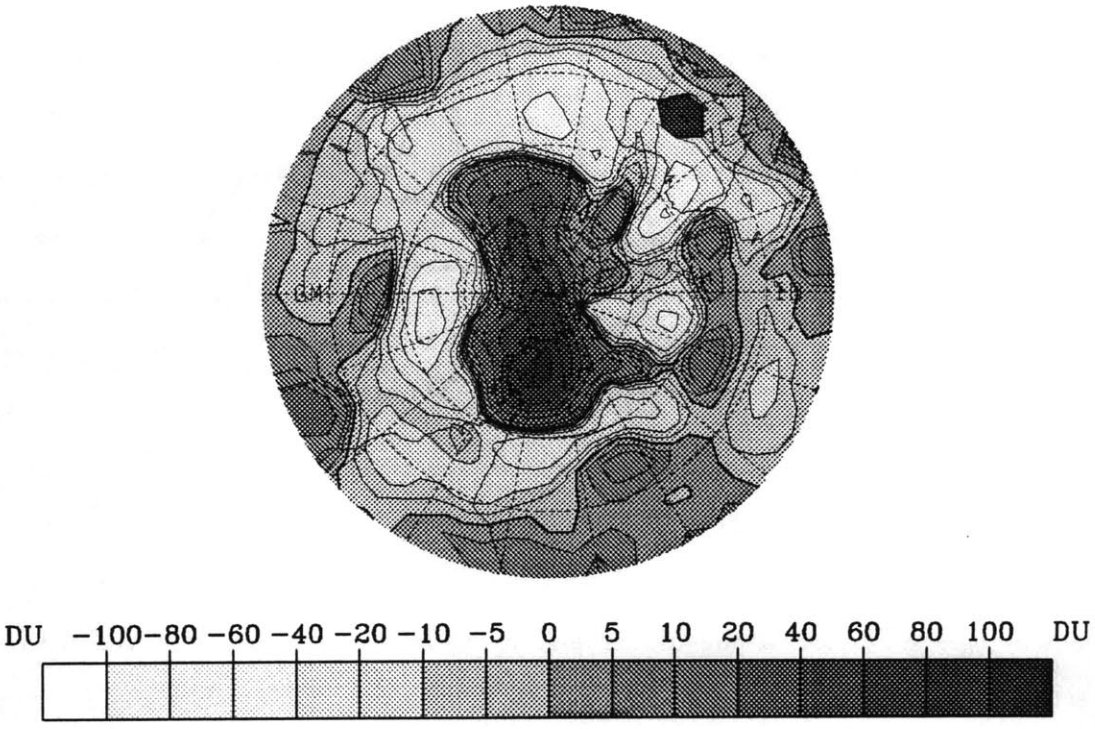

Figure 7.20: As for Figure 7.10(b), except for the CAS-based 'no ozone hole' scenario reconstructions.

the 1980 minimum after which they were held constant. In this manner the adopted distribution produced OMR values which were less than or equal to the 1980 values, hence comprised a conservative 'no ozone hole' scenario. By introducing this interference 'poleward' (i.e. in dynamical space) of the vortex edge rather than poleward of each isentropic OMR maximum, we were also able to remove the effects of the possible error, referred to earlier, resulting from the reconstructions locating the OMR maximum too far equatorward.

To demonstrate that the observed hemispheric distribution of the TOMS-observed total ozone change between 02 and 14 December could be explained almost everywhere in terms of 'natural' influences, Figure 7.20 shows the reconstructed total ozone change between the two days for the 'no ozone hole' simulation, for comparison with the TOMS and reconstructed distributions of Figure 7.10. Remarkable similarity is apparent between all three plots, the only detectable differences, as expected, being in the structure and magnitude of the areas of ozone decrease in the Atlantic and

southwest Pacific regions.

Figure 7.21 shows the difference in the total ozone distributions for 14 December obtained from the full CAS-based reconstruction and that of the subjectively modified 'no ozone hole' distribution. It therefore shows only the ozone dilution component of the reconstructed 14 December total ozone distribution. Plainly apparent is an ozone dilution signature as far north as $35°S$, albeit small north of $45°S$, the reconstructions suggesting, for example, that the south island of New Zealand experienced a marginal decrease in total ozone (about 1%) due to ozone dilution. Of course, the accuracy of the picture obtained is strongly dependent on the accuracy of the CAS-depicted flow development, on the accuracy of our subjective specification of the edge of the ozone hole, and that of the polar 'no ozone hole' OMR values chosen. However, because the influence of the higher and lower levels has been removed, and as a result of the subjective interference at the other levels, the result is expected to be rather insensitive to other errors associated with the reconstruction technique. In particular the influence of nonconservation of OMR should be small (perhaps 5% of the magnitude of the indicated component, not this fraction of the entire ozone column).

The sensitivity of the result to the accuracy of the bulk advection by CAS is obvious but, as noted earlier, can not be assessed directly without reference to an alternative data set, and then not with certainty. In this context the discrepancy noted in Subsection 7.2.4 above, between the southwest advection of the New Zealand tongue by CAS at $525K$ and the more extensive and easterly orientation suggested by the analyses, is of interest. The ozone decrease over the Australian region can be explained from the present analysis entirely in terms of 'natural' processes, but in view of the uncertainties surrounding the advecting winds for the CAS simulations, an ozone dilution component of the decrease can not be ruled out. The same uncertainties apply to the ozone decrease observed over South America.

The sensitivity of the solution to the location chosen at each level to represent the vortex edge was tested by moving the cutoff point to both higher and lower values of

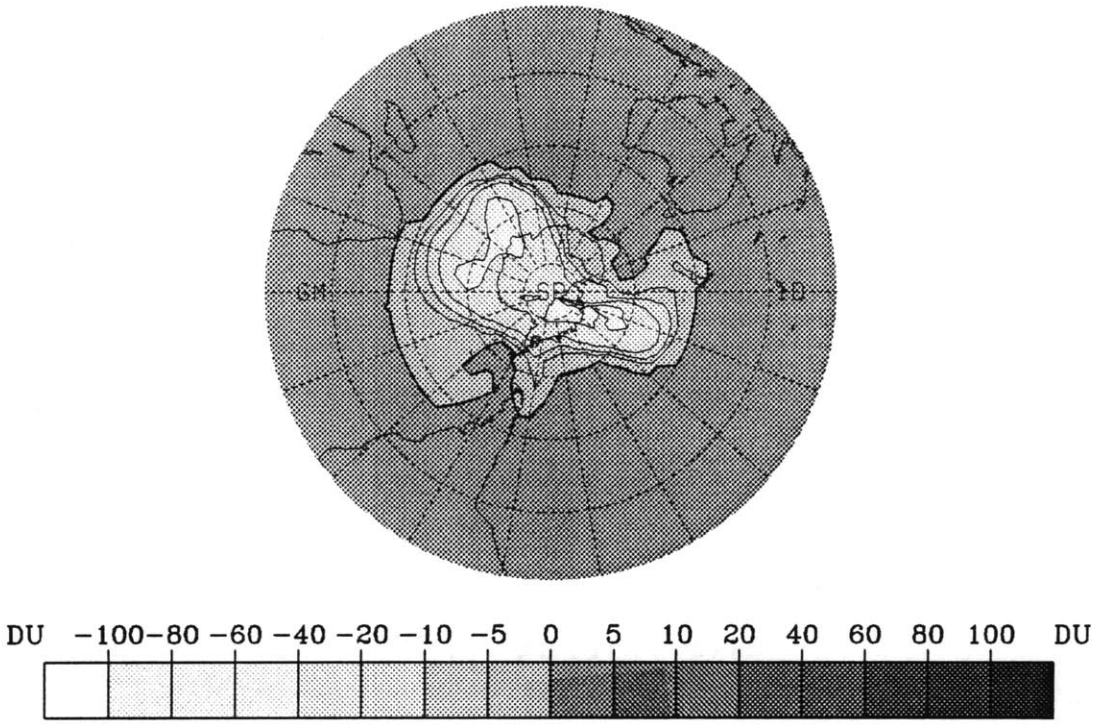

Figure 7.21: Hemispheric distribution of the difference in total ozone on 14 December between the unmodified CAS-based reconstruction and the 'no ozone hole' scenario reconstruction, showing the areal extent and magnitude of the ozone hole dilution component of the event. Plot parameters as for Figure 7.10.

$\hat{q}$. Poleward movement naturally further confined the extent of the ozone dilution region, although it is noteworthy that it required a large and unrealistic poleward shift to move the boundary more than a few degrees. On the other hand a very marginal shift in the opposite direction produced a marked increase in the area affected, a tongue appearing across South America and out over the eastern Pacific Ocean, for example. Colocating the cutoff point with the OMR maximum produced a response virtually everywhere south of $30°S$, largely due to the influence, suspected to be spurious, of the $550K$ and $575K$ levels. Nonetheless this sensitivity has rather profound implications for the ozone dilution effect, were a connection to be established between Antarctic ozone depletion and the maximum OMR values observed on isentropic surfaces in the lower stratosphere.

Finally, the sensitivity of the solution to the 'no ozone hole' polar OMRs chosen

was tested by replacing the 1980 minima above $450K$ with those from the October 1981 SAGE sweep (which were considerably higher). While little proportionate difference was apparent in the regions of large decrease (over $20DU$), the magnitude of the decrease in the fringe region approximately doubled, and the region expanded slightly, the result of the fringe region being due almost entirely to the effects of horizontal transport above about $500K$.

Overall, since springtime Antarctic ozone depletion is understood to have already been significant in 1980, we conclude that Figure 7.21 provides a conservative estimate of the Antarctic ozone hole dilution effect on 14 December 1987, and that the region actually affected is unlikely to have been more restricted than that shown, nor is the magnitude likely to have been smaller. On the contrary, the region affected may have been considerably larger and the actual magnitude up to a factor of two or so greater than shown in Figure 7.21.

Of course, the above analysis has considered only the early December period. Despite the dynamically rather dramatic vortex breakup, the vortex interior appears to have remained remarkably intact up to 14 December, and other than separation of the two lobes into separate entities, seemed to display resilience to marked erosion and mixing out into the mid-latitude environment during the period. In view of this preserved integrity it may be that the more critical period with respect to mid-latitude ozone dilution was the period following that examined above.

In the following Section we consider briefly the evolution after 14 December and its implications for ozone dilution.

7.4 Ozone Dilution after 14 December

The period after 14 December falls too far after the SAGE S5 sweep for either CAS, initialised before the vortex breakup, to be practicable, or for the assumptions, implicit in using this sweep for the reconstructions, to remain acceptably valid for such

an extensive period. Also, with EPV itself becoming degenerate as a coordinate following the vortex breakup, the reconstruction technique, as adopted here, would not be expected to be useful for examination of the later period. Nonetheless the question of the subsequent fate of the ozone hole remnants and their potential for more widespread mid-latitude ozone dilution, are worthy of closer examination.

Accordingly, a number of simplified CAS simulations was performed to investigate the likely fate of the ozone hole remains after 14 December. At $425K$, $475K$, $525K$ and $575K$ levels, the ozone reconstructions from 02 December were used to identify a single EPV contour in each of the NMC-based analyses which approximately corresponded to the edge of the Antarctic ozone hole on that day. A 29 day CAS simulation was then performed on each contour to provide a qualitative picture of the flow evolution during the month. Figure 7.22 shows the advected contour distributions at each of the four levels at three day intervals commencing on 13 December and ending on 31 December. The region 'poleward' of the advected contour (vortex material) is shaded black in each plot for visual clarity.

Clearly evident in Figure 7.22(a) is the limited extent of the vortex breakup by 13 December. By this stage the two lobes have separated somewhat at the higher levels, and the major lobe is beginning to roll up and intrude a tongue of extra-vortical air as it moves eastward into the Indian Ocean. By 14 December at $575K$, and 16 December at $525K$, the northeastward outbreak of the lobe in the southwest Pacific region reaches its easternmost extent, after which the low EPV airmass which has pushed poleward over eastern Antarctica begins to dominate the flow pattern and the extruded vortex air first stagnates, then subsequently drifts back towards the west, being sheared out into long thin filaments as it does so. At lower levels where the poleward excursion of low EPV is weaker at first, and in the Atlantic and Indian Ocean regions aloft, the vortex mass still dominates the flow and the pattern continues to drift eastwards, although shearing out at each level as it does so. It is not until about 19 December that the low EPV region moves over the pole from the southwest Pacific region at the lower levels, splits the vortex, and takes control of

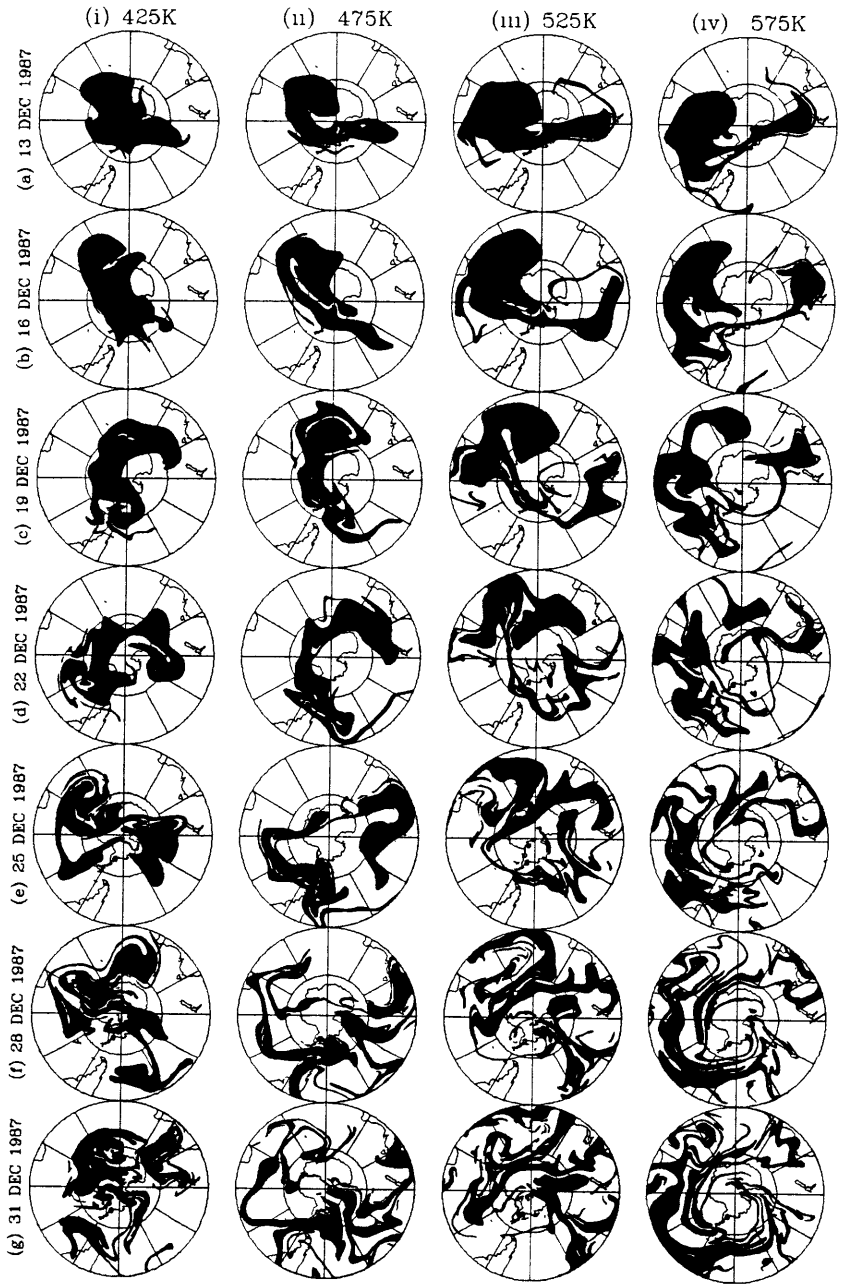

Figure 7.22: CAS-advected distribution of the vortex debris at (i) $425K$, (ii) $475K$, (iii) $525K$ and (iv) $575K$ levels at three day intervals from (a) 13, to (g) 31 December 1987. The simulations were each initialised on 02 December and 'vortex material' is shaded black. Grid lines are drawn at 30^o intervals, Greenwich Meridian to left, and outer edge of plot is at $30^o S$.

the wind distribution throughout the hemisphere at upper levels. (Note the gradual

flow reversal over the Atlantic Ocean after which the winds are easterly everywhere aloft, not unlike solid body rotation but with the shearing process continuing slowly as time progresses.) By the end of the month the vortex mass above $450K$ has been rather well mixed out into the middle latitudes. (Although the northward extent of the plots in Figure 7.22 is $30°S$, little of the debris extends beyond $20°S$.) Below $450K$ on the other hand, the situation is better described by extra-vortical intrusions weakening, but not dispersing, the polar vortex. Despite apparent episodic outbreaks at $425K$ there is a tendency for the debris to wrap back in around the vortex remains as time progresses.

The CAS simulations were not continued past the end of the month but it seems likely that the contour distributions shown in Figure 7.22(g) for December 31 approximate the maximum extent of the vortex destruction process. While the details of the tracer evolution are not expected to be accurate, we assume that the broad features and qualitative nature of the development depicted by CAS are correct.

The overall picture presented by the simulations suggests that a more substantial mid-latitude ozone dilution effect was experienced after 14 December than before, with the ozone hole remains above about $450K$ (representing about half the mass of the ozone hole), being rather evenly dispersed throughout the extratropical region of the hemisphere in the space of a few weeks. Below about $450K$ the vortex remains appear to have been split into two around 20 December and extruded temporarily into mid-latitudes, but instead of being sheared out and dispersed there, CAS suggests the bulk of the remains thereafter tended to be wrapped back in around the polar region, essentially reforming the vortex circulation and limiting the extent of mid-latitude dilution.

A significant and credible feature of the CAS simulations is the rapid shearing in the vertical of the vortex remains accompanying the breakup, which would tend to camouflage the total ozone signature locally, and produce small scale laminations in ozone vertical profiles like those observed in the northern hemisphere mid-latitudes (Reid and Vaughan, 1993). So while the initial stages of the breakup, say up to 20

December, would have produced rather sudden and marked local decreases in total ozone at some locations in association with the outbreak of each of the vortex lobes, these signatures would rapidly have been smeared out at mid-latitudes, producing a small overall decrease at most mid-latitude locations.

Although, as already noted, the CAS simulations are not expected to be accurate in detail, support for the overall features of the flow development is found in Figure A.9(b), which shows the daily time series of zonal mean TOMS total ozone vs latitude for the season. As for the Hovmoller diagram of Figure A.9(a) discussed in Chapter 5 above, the data have been normalised to enhance the colour contrast in the plot. The Antarctic ozone hole shows up as the region of red colouring, the circumpolar total ozone maximum by shades of blue. Figure A.9(c) is an equivalent plot of zonal mean $525K$ EPV. The vortex breakup is clearly evidenced by the influx of high total ozone over the pole and the rapid and marked total ozone decrease at mid-latitudes during the first few weeks of December in Figure A.9(c), and by the EPV gradient reversal in Figure A.9(b). Figure A.9(c) also shows that, although at, e.g. $45^{o}S$, the total ozone decrease has already occurred by around 12 December, at lower latitudes the decrease occurred more gradually and later, consistent with (but not by no means proof of) the outward mixing process shown by the CAS simulations. Figure A.9(c) also shows that after the sudden large increase in total ozone over the pole after 10 December (the low level vortex destruction), the polar values decreased rapidly and markedly again at the end of the month, consistent with the regrouping in the polar region of the vortex remains below $450K$. (Additional support comes from plots similar to Figure A.9(b) but for $425K$ and $375K$ which show the rapid return of the highest EPV to the polar region after a temporary excursion into mid-latitudes during the latter part of December.

Should the CAS simulations correctly depict the essential features of the vortex breakup process during December, the question remains as to the approximate magnitude of the associated mid-latitude ozone dilution effect during the latter stages of the month. While this question has been addressed by the numerous detailed modelling

studies noted in Chapter 1 above, the present analysis enables us to make a crude and simple estimate of the likely effect without resort to such detailed modelling.

Assuming the gross features of the CAS simulations to be essentially correct, then we might approximate the vortex breakup as one in which the vortex remained intact over the pole below $450K$, while above this it was rapidly and evenly dispersed throughout the hemisphere south of $30°S$. Let us assume, on the basis of the SAGE reconstructions, that the total ozone column within the vortex immediately prior to the breakup exhibited a 30% reduction in total ozone due to the ozone hole mechanism, and that this overall 30% decrease was due to, say, 50% depletion of 60% of the column (the approximate proportion of the unperturbed column lying in the altitude range of the ozone hole, and the approximate fractional depletion of the layer suggested by comparison between polar OMRs from the SAGE 1987 S5 period and the 1980 S3 period.) Let us further assume that half of this 60% of the unperturbed column lay below $450K$, the other half aloft, and that the ozone hole occupied the region south of about $65°S$ (10% of the area of the hemisphere). This then suggests a fivefold dilution of the ozone deficit above $450K$ in the mixing process (since half the area of the hemisphere lies south of $30°S$). If the unperturbed polar column was about $300DU$, then in the absence of further photochemical losses during the mixing process, the mid-latitude impact of the fivefold dilution of a $45DU$ polar deficit would be around $10DU$, or say 3% of the total ozone column everywhere south of $30°S$. If we very crudely take into account natural photochemical destruction of ozone during the period, by assuming an average relaxation of the ozone-depleted air (and the surrounding air) towards zero ozone content with an e-folding time of say 80 days, and we further assume both that the ozone hole debris remains unmixed with its environment at molecular scales and that diabatic transports are negligible, then the overall fractional decrease of the mid-latitude ozone column due to ozone dilution will be closer to 2% by the end of December and perhaps 1.5% by the end of January.

7.5 Summary and Implications

In the course of the above analysis of the 1987 Antarctic ozone hole dilution event, in which the ozone evolution during the 12 day period from 02 to 14 December was examined in detail, we have demonstrated the remarkable utility of the overall reconstruction technique used, particularly in view of the scarcity of available ozone data and the EPV relaxation observed in the NMC-based analyses during the period. Despite their limitations, the reconstructions presented above provide a detailed description of the ozone evolution which shows generally close agreement with the TOMS total ozone evolution, and provides the means by which to isolate individual components of the evolution for closer examination.

The reconstructions show that most of the ozone changes during early December 1987 were due to quasi-horizontal transport, with the vertical motion contribution playing a significant, but secondary, role.

Much of the vertical motion component occurred in response to large scale dynamical processes occurring in the stratosphere, with tropospheric dynamics generally exerting a much smaller influence, as expected in view of the downward control principle.

Despite the overall large change in reconstructed total ozone due to quasi-horizontal advection, most of the changes were due to 'natural' ozone transports i.e. they would most probably have been observed in the absence of an Antarctic ozone hole. In particular, the observed total ozone decrease over southeastern Australia, linked by Atkinson *et al* (1989) to an ozone dilution effect, can be explained in terms of natural processes. The notable exceptions to this general behaviour were the decreases observed over the south Atlantic and southwest Pacific regions, which extended as far north as $35^{o}S$ by 14 December and which produced a decrease in total ozone of perhaps a few percent over the south island of New Zealand by then.

While the event may actually have been areally more extensive than this, the accuracy limitations of the technique, and a lack of complete understanding of the

chemically unperturbed ozone distribution which would have been observed in the absence of Antarctic ozone depletion, prohibits a more precise assessment. It is apparent, however, that the true ozone dilution effect experienced during early December is unlikely to have been much less pronounced than was shown by the analysis, although the fringe regions affected may have been slightly different. Of course, if a connection can be made between ozone depletion and the particularly low OMR values observed in the region of the lower stratospheric circumpolar maximum, a matter beyond the scope of the present work, then the potential for mid-latitude ozone dilution would be greatly enhanced.

Although, due to practical constraints, the detailed analysis was not extended beyond 14 December, the simplified CAS simulations performed to cover the latter part of the month suggest that a greater ozone dilution effect would most probably have been experienced during the latter period. However, rather than a marked signature being felt in a few relatively localised regions, the latter effect is expected to have comprised a much more widespread decrease of a few percent.

We conclude, then, that the 1987 polar vortex breakup did cause a mid-latitude ozone dilution effect. The question remains as to whether this was typical of the breakup process each year or an extreme case, and whether a similar process may have occurred prior to the vortex breakup in 1987 or other years. This broader question is the subject of the following Chapter.

Chapter 8

The Ozone Dilution Effect: 1979 to 1989

In the previous Chapter we closely examined the breakup of the polar vortex during December 1987, focussing on the first two weeks of the month, but also considering the subsequent evolution. There appears little doubt from the analysis that the 1987 vortex breakup produced a small but not insignificant ozone dilution effect at southern mid-latitudes. The question remains as to whether the same process occurs every year, and if so, whether its magnitude is solely dependent on the severity of the Antarctic ozone depletion, or whether interannual variability in the dynamics plays an important part in determining the extent of mid-latitude dilution. Equally important is the question of whether significant episodic dilution events might occur each season prior to the vortex breakup. Each of these matters has been touched on in the discussion, in Chapter 5 above, of the dynamical evolution each season. In the present Chapter we examine the issues more closely.

In Section 8.1 we deal with the former. By applying to the NMC-based EPV analyses the adopted $\chi/\hat{q}$ relationships, detailed in Chapter 6 above, from the last of the sweep periods for each season, we have reconstructed the ozone evolution leading up to and during the early stages of the vortex breakup each year. As was

the case for the 1987 event, rapid EPV relaxation in the analyses soon after the commencement of the breakup each year severely limits the usefulness of analysis-based ozone reconstructions for the latter stages of each event. Whereas we were able to circumvent this problem to some extent for the 1987 breakup by performing full CAS simulations of the approximate material evolution up to mid-December, this was not practicable for the other years, so we were unable to examine these cases as closely as the 1987 event. Nonetheless, with the detailed ozone reconstructions from the earlier stages of the breakup each year and a number of simplified but extended-period CAS simulations, as were performed for the examination of the latter stages of the 1987 event, we have arrived at a crude estimate of the extent of mid-latitude ozone dilution accompanying the vortex breakup in most of the other years.

In Section 8.2 we address the matter of ozone dilution events occurring prior to the vortex breakup each year. The potential dilution events identified in Chapter 5 have been examined in more detail using ozone reconstructions based on the EPV analyses. Unlike those for the post-breakup period, these reconstructions, the technique for which was essentially developed for use on the pre-breakup period, serve as an effective tool for examining the large scale ozone transports occurring. Their only serious limitation is the coarse resolution of the EPV analyses, which are incapable of depicting the smaller scale features of the flow. To ease this limitation and enable us to examine the evolution at finer scales, additional simplified CAS simulations have been performed, and the implications of these simulations will be discussed to augment the analysis based on the ozone reconstructions.

Finally, in Section 8.3 the overall results of the examination are summarised and we discuss their implications for mid-latitude ozone dilution during the 1980s.

8.1 Ozone Dilution Associated with the Vortex Breakup Each Year

8.1.1 1989

As discussed in Section 5.11, the breakup of the polar vortex at low levels after mid-November 1989 was rather ill-defined in the EPV analyses, appearing to be due as much to radiative decay as dynamically-induced destruction.

Figure 8.1 shows a sequence of the TOMS total ozone distribution and corresponding analysis-based ozone reconstruction (using the 1989 S5 $\chi/\hat{q}$ relationships) at six day intervals from 21 November to 09 December. The reconstructions for 21 and 27 November, despite the underestimation of zonal and period mean total ozone for the sweep noted in Section 6.1 above, capture all but the small scale features of the TOMS distribution. The effect of rapid EPV relaxation in the analyses for the lower stratosphere after 27 November is clearly evident however, and leads to an erroneous enlargement of the area of the polar minimum and smears out the mid-latitude total ozone maximum, as noted in Section 6.1. The effect becomes more marked as time progresses.

As noted in Section 5.11, there was little evidence, from the EPV analyses at ozone hole levels, of a significant outbreak of polar air associated with the vortex breakdown before the second week of December, after which the dynamical evolution becomes rather poorly defined in the analyses. While there is a suggestion in the analyses, and in the TOMS and reconstructed ozone distributions for 09 December (Figure 8.1(d)), of extrusion of ozone hole material into the Pacific mid-latitudes, the reconstruction is of inadequate quality to confirm this. (The three dimensional structure of the ozone reconstructions (not shown) suggests the area of observed total ozone decrease might be explained by a combination of isentropic uplift, ridging at levels below the ozone hole, and outbreak of the vortex remains above ozone hole levels.)

To gain a more detailed picture of the dynamical evolution at ozone hole levels at

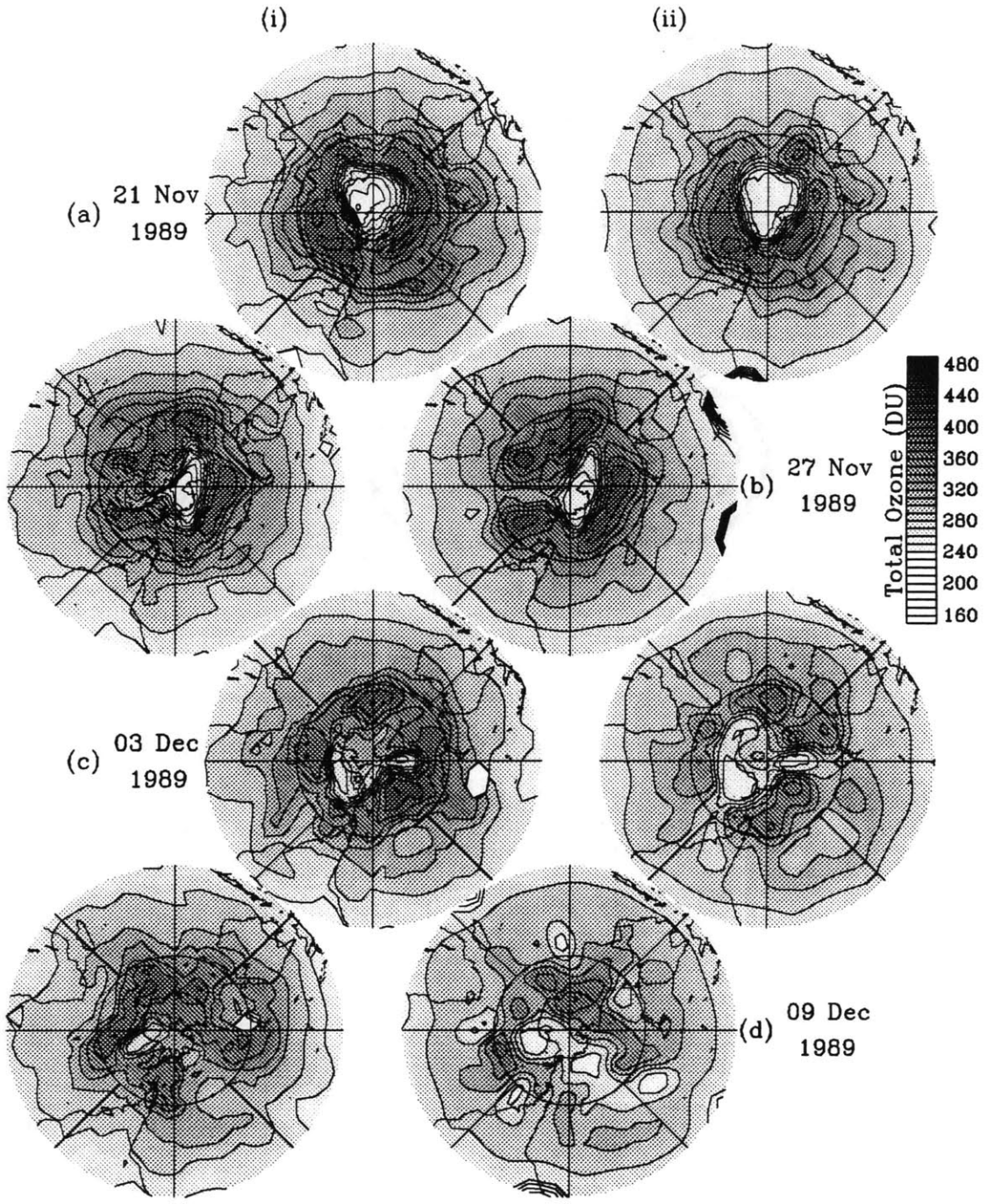

Figure 8.1: Hemispheric distribution of (i) TOMS (*left*) and (ii) reconstructed (*right*) total ozone on (a) 21 and (b) 27 November, and (c) 03 and (d) 09 December 1989. Contours are drawn at $20DU$ intervals, shading as indicated in the key. Polar stereographic projection, Greenwich Meridian to left, grid lines at 45° intervals, and outer edge of each plot at equator.

this latter stage of the season, four simplified, but extended-period, CAS simulations

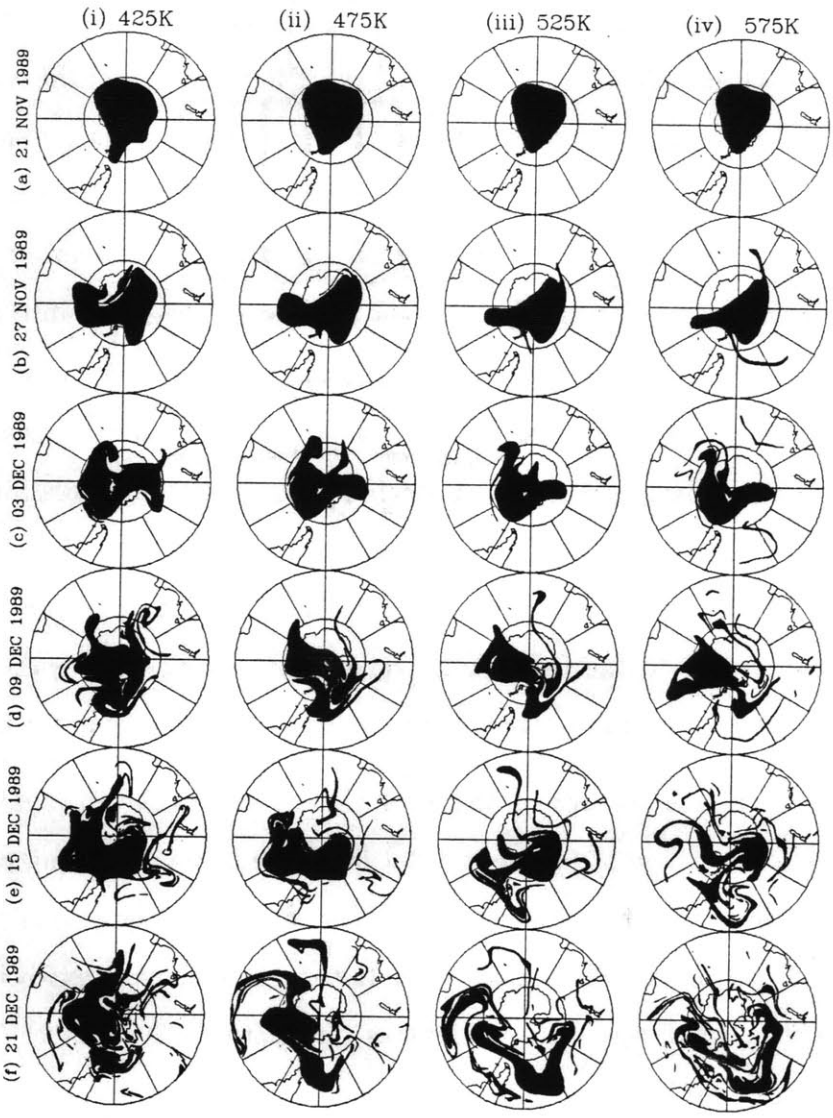

Figure 8.2: As for Figure 7.22, except for (a) 21 and (b) 27 November, and (c) 03, (d) 09, (e) 15 and (f) 21 December 1989.

were performed, as for the 1987 breakup, wherein at $425K$, $475K$, $525K$ and $575K$ levels, a single contour approximating the inner edge of the vortex (the boundary of the ozone hole) at each level on 21 November, was advected for 30 days. Figure 8.2 shows the CAS-depicted evolution of these contours from 21 November to 21 December.

The simulations suggest the ozone hole remains to have stayed essentially intact, as indicated by the EPV analyses, up to the end of the first week of December, but that after this the vortex lobe near the date line on 03 December was split from the main

vortex mass above $500K$ and extruded out into mid-latitudes over South America and into the Atlantic Ocean. At lower levels, while the distended lobe of the vortex passed over the tip of South America around 09 December, it remained essentially attached to the main vortex mass. After 15 December, however, a stronger disturbance pushed in over the pole from the Indian Ocean, and the vortex remains above $500K$ were sheared out into the mid-latitudes, the bulk moving initially out into the eastern Pacific region and over South America by 21 December. On this occasion the implied temporary dilution event over South America was more significant, extending from $425K$ to $575K$, but sheared westward with height. Although the simulations ended on 21 December, it appears likely that the vortex remains above $475K$ after 21 December would have been almost entirely sheared out and mixed into the middle and high latitude flow according to the CAS runs, while below $475K$, despite the temporary outbreak over South America, most of the vortex remains reformed in the polar region.

Although the above picture of the evolution is somewhat speculative, Figure A.11(c) shows a two stage zonal mean total ozone decrease extending equatorward from the polar region, the first coinciding with the CAS-depicted extrusion into mid-latitudes by 09 December, the second with the more significant extrusion after 15 December, with a weak signature evident as far north as 30^oS at the end of the month. That the vortex above $475K$ was sheared out into the middle latitudes is supported by Figure A.11(b), which shows that after mid-December the vortex remains did not reform over the pole, while similar plots for levels below $500K$ (not shown) support the CAS-suggested evolution at these levels.

Overall, then, the picture obtained suggests that the eastern Pacific/South America region probably experienced two transient ozone dilution events during December, the first around 08 December and lasting perhaps a few days, and a second and more significant event after 15 December, which may have lasted a week or so at a given location, if the details of the CAS-depicted evolution are correct. Apart from these two transient events, it is likely that a smaller, more gradual and evenly distributed ozone dilution effect would have spread throughout the mid-latitudes by early Jan-

uary, in association with the destruction and shearing out of the ozone hole remains above about $475K$.

The Antarctic ozone hole in 1989 was similar in overall magnitude to that in 1987. The SAGE reconstructions for S5 in 1989 suggest that OMR values within the polar vortex at levels below $450K$ were actually about 10% lower than those at the same time in 1987, while they were perhaps 10% higher at ozone hole levels above $450K$, both within the vortex and at the mid-latitude maximum (the latter, at least, consistent with the effects on the residual circulation of the large wave event in late October discussed in Section 5.11). Let us assume, then, that by early December the overall ozone deficit within the polar vortex remains was similar to that in 1987 (say 50% depletion of 60% of the overall column, or about $90DU$) but that this comprised a 60% reduction of the 30% of the column comprising the lower half of the ozone hole, and a 40% reduction of the 30% comprising the upper half. Let us further assume, consistent with the apparently higher base of the 'total mixing' region in 1989 (about $475K$ as opposed to about $450K$ in 1987), that only the top 1/3 of the ozone hole was mixed into the mid-latitudes by early January. The implied overall mid-latitude dilution effect, then, neglecting photochemical changes during the period, would have been of the order of $5DU$ (1/5 x 2/3 x 40% x 50% x $300DU$), or about half as severe as the 1987 dilution effect.

On the other hand the transient events suggested by CAS to have occurred during December over the eastern Pacific/South America region, taking into account the significant vertical shear associated with each event, may have produced temporary ozone dilution over this region of as much as $40DU$, or 10 to 15% of the ozone column. (This is not to say that total ozone over the region would have decreased by this amount, or even at all necessarily, but only that, temporarily, the total ozone column may have been as much as 10 to 15% lower than it would have been in the absence of Antarctic ozone depletion.)

Because we were unable to perform CAS-based ozone reconstructions for the period, and because, even were we able to, we cannot be entirely certain that the finer

details of the CAS-depicted evolution at this stage of the season are correct, it was not possible to reconstruct the total ozone evolution during the period at a sufficient level of accuracy to make useful comparisons with that observed. Hence the picture of the ozone evolution suggested above must remain somewhat speculative. This is also the case for each of the other years examined below.

8.1.2 1988

There was only moderate springtime Antarctic ozone depletion in 1988, comprising a net decline of 10 to 15% during September, compared to 50% in 1987 (Schoeberl *et al*, 1989b). Accordingly, despite the early and apparently rather dramatic breakup of the vortex at low levels during the latter half of November, there was little potential for a marked mid-latitude ozone dilution effect accompanying the breakup. Nevertheless, were the vortex remains deposited essentially intact in mid-latitudes brfore being sheared out, there would have been some potential for a transient effect.

Figure 8.3 shows TOMS and reconstructed total ozone distributions on four November days spanning the initial stages of the breakup at low levels. Despite the adverse effect on the reconstructions after 07 November of gradual EPV relaxation accompanying the breakup, the similarity between the TOMS and reconstructed total ozone distributions throughout the period suggests both that the S5 $\chi/\hat{q}$ relationships accurately described the OMR distribution for the period and the EPV analyses capture the broader features of the dynamical transports occurring at the time. The results of a set of simplified 30-day CAS simulations like those for 1987 and 1989, but initialised on 01 November (see Figure 8.4) also show close agreement with the evolution described by the analyses up to mid-November (compare Figure 8.4 (b), (c) and (d) with Figure 5.18 (b) and (c)). The CAS simulations suggest that after 13 November about half the vortex remains above $500K$ were sheared out rather evenly across the South America/Atlantic Ocean region as the pattern rotated, while after 25 November the mass remaining above about $450K$ was split into two, being sheared out above $475K$ as in 1989, according to Figure A.10(b) and similar plots (not shown) for other levels,

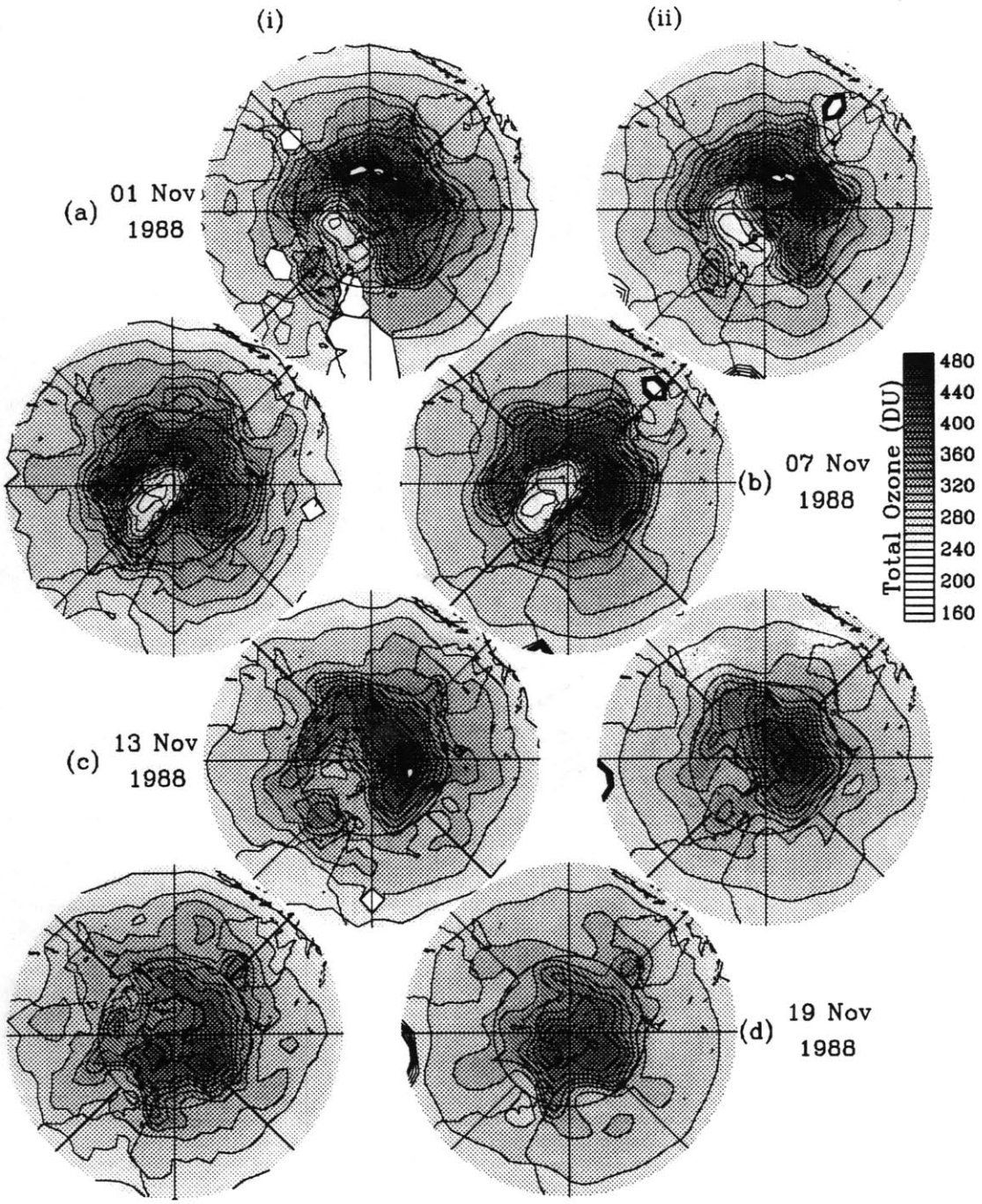

Figure 8.3: As for Figure 8.1, except for (a) 01, (b) 07, (c) 13 and (d) 19 November 1988.

while below $475K$ they tended to regroup over the pole.

Under these circumstances, for a similar crude calculation as was performed for the 1987 and 1989 breakups, we assume an overall 10% reduction in polar total ozone just prior to the breakup, attributable to 25% depletion of 40% of the column (the

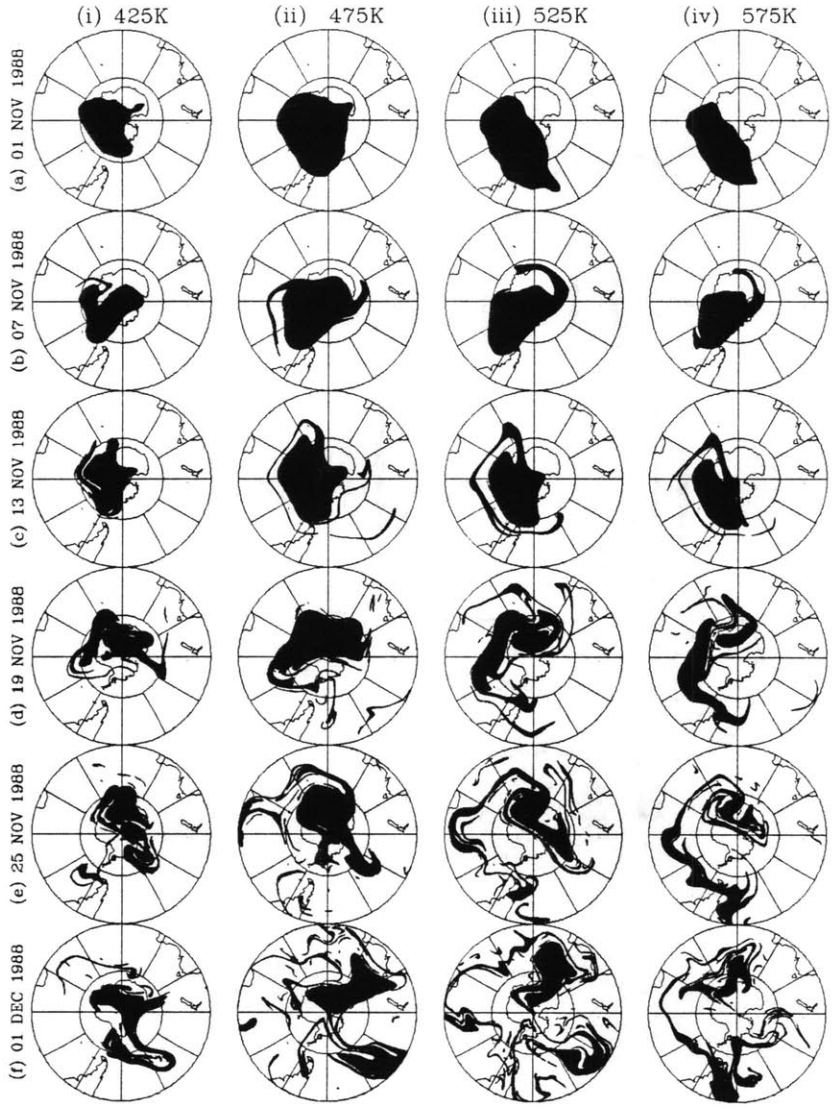

Figure 8.4: As for Figure 7.22, except for (a) 01, (b) 07, (c) 13, (d) 19 and (e) 25 November, and (f) 01 December 1988.

magnitude suggested by the $\chi/\hat{q}$ relationships for the sweep, with the upper limit of the depletion at about $525K$ in 1988), or about $30DU$. Assuming further that $10DU$ of this was present above $475K$, then fivefold dilution of this deficit, neglecting subsequent photochemical relaxation, would produce a mid-latitude ozone dilution effect of, at most, a few DU, or less than 1% of the mid-latitude column. Qualitative support for a lack of marked mid-latitude dilution is perhaps seen in Figure A.10(c), which shows little change in zonal mean mid-latitude total ozone after the initial stages of the breakup during mid-November.

Prior to the dispersion of the vortex remains there were two transient events of interest. The first of these was the apparent extrusion of vortex material out over the South America/Atlantic Ocean region around 19 November. Since this was essentially confined to levels above $500K$, and since the top of the ozone hole lay near $525K$ in 1988, it is unlikely that a significant dilution component accompanied this event. On the other hand, the final vortex splitting process at the end of November may have produced a small transient effect (up to about $10DU$ decrease) over the central Pacific mid-latitudes or in the Australia/New Zealand region, although the simulations were not carried far enough to confirm this.

8.1.3 1986

As discussed in Section 5.8, despite the rather early displacement of the vortex mass from the pole at low levels in mid-November, the EPV analyses suggested that it remained rather intact during the latter stages of November, to drift back over the pole at the end of the month, gradually decaying thereafter. As for the 1988 breakup, despite marked EPV relaxation in the analyses accompanying the mid-November wave event, the total ozone reconstructions for the subsequent period (see Figure 8.5) compare well with the TOMS distributions, which suggests, in view of the rapid vertical shearing of the features in the EPV distribution, that the S5 $\chi/\hat{q}$ relationships rather accurately describe the ozone distribution during the period.

Consistent with the impression gained from the EPV analyses, simplified 40-day CAS simulations initialised on 18 November suggest a fundamentally different character of the 1986 breakup to those of the three later years (see Figure 8.6). Rather than one or two dynamical events tending to split the vortex core and shear out the remains, the CAS-depicted evolution after mid-November is better described as a series of smaller scale events gradually stripping away the material from the outer edge of the vortex, so that by late December a significant portion of the vortex mass at ozone hole levels remained essentially pole-centred and relatively undisturbed. This fundamental difference is most easily seen by comparing the time series of zonal mean

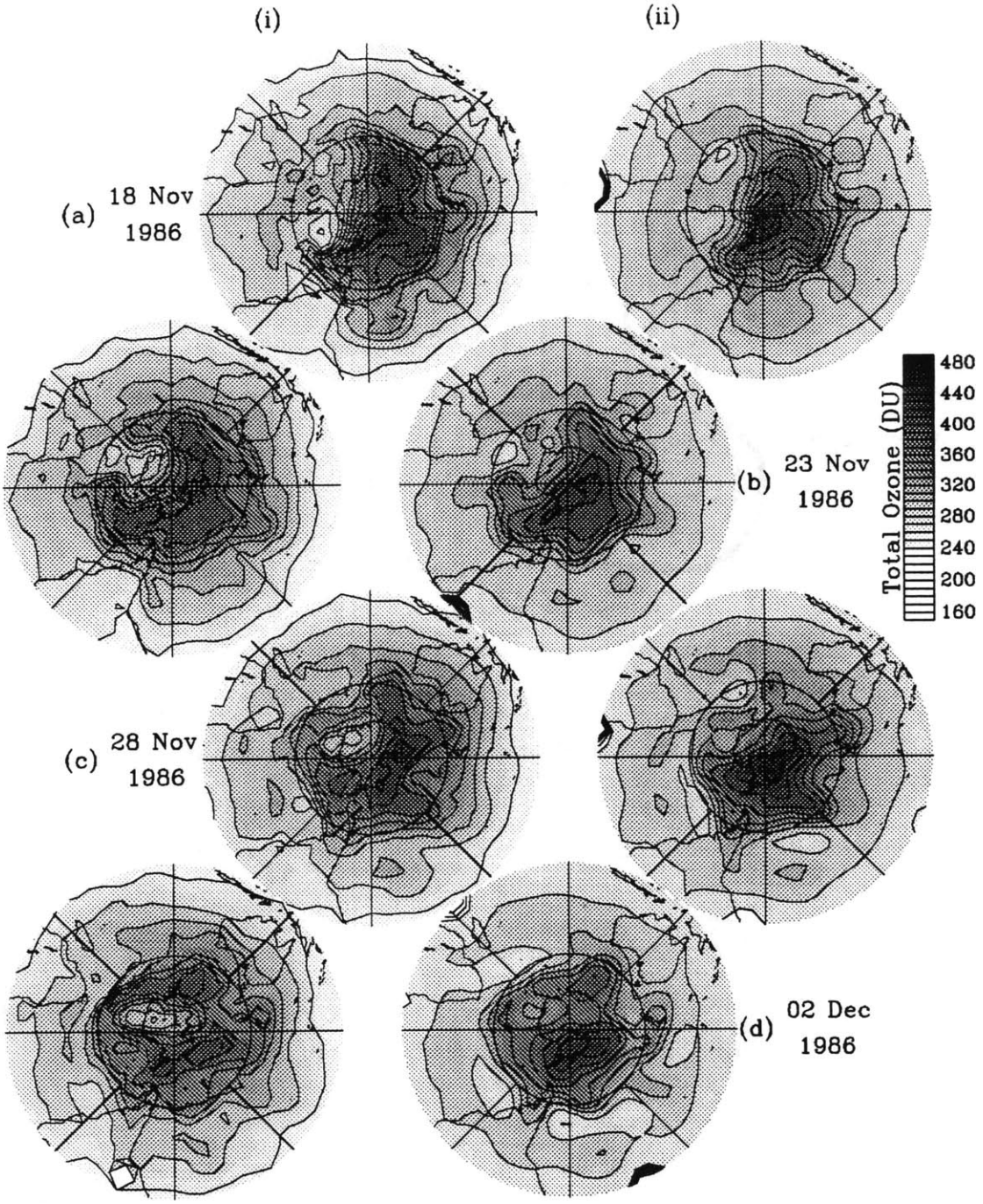

Figure 8.5: As for Figure 8.1, except for (a) 18, (b) 23 and (c) 28 November, and (d) 02 December 1986.

$525K$ EPV after mid-November (Figure A.8(b) with that for 1987 (Figure A.9(b)), no marked and lasting gradient reversal seen in 1986. Evident in Figure A.8(c) is the absence of a marked mid-latitude signature of zonally averaged TOMS total ozone decrease, but rather a gradual decrease occurs after mid-November, again consistent

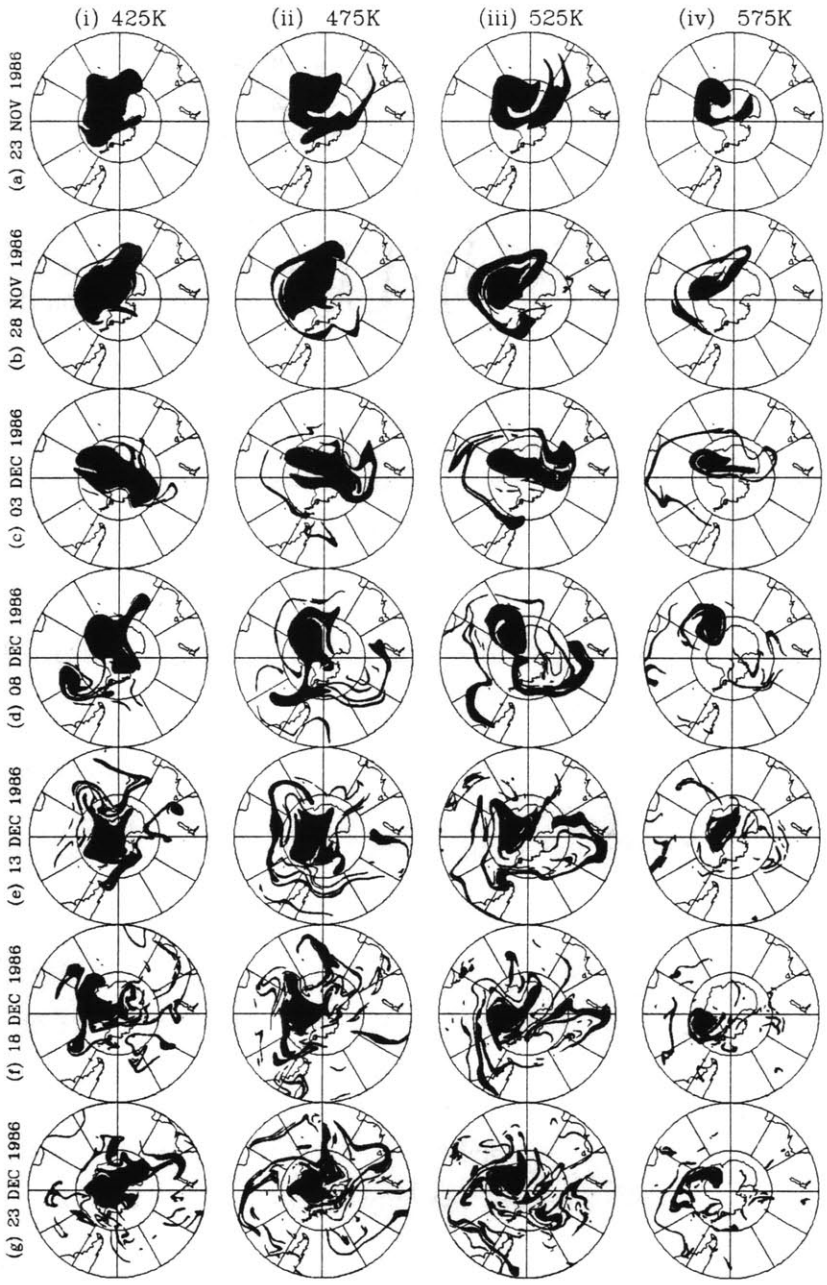

Figure 8.6: As for Figure 7.22, except for (a) 23 and (b) 28 November, and (c) 03, (d) 08, (e) 13, (f) 18 and (g) 23 December 1986.

with a drawn out decay of the polar vortex.

In view of this apparently gradual filamentation of the ozone hole remains, it seems unlikely that any significant transient ozone dilution events would be identifiable in association with the vortex decay in 1986. With regard to a more widespread effect throughout the extratropical region, the 1986 S5 ozone data suggest Antarctic ozone

depletion was essentially confined to the region below about $500K$, and was about mid-way in severity between that of 1987 and 1988 at these levels. If, say, 40% depletion of 40% of an unperturbed polar column of $300DU$ is assumed for November, this amounts to about a $45DU$ deficit. Consistent with the CAS simulations, if it is further assumed that only 1/3 of the ozone hole mass above $450K$ was evenly diluted throughout the hemisphere south of $30°S$ by late December, this amounts to less than $2DU$ dilution at mid-latitudes, or about 1/2% of the mid-latitude column, a rather insignificant amount.

8.1.4 1985

As noted in Section 5.7, the breakup of the vortex at lower levels in 1985 occurred after the beginning of December, when the bulk of the remains was first displaced towards the western Indian Ocean, apparently to dissipate over the following weeks.

Figure 8.7 shows TOMS and reconstructed total ozone distributions at six day intervals from 19 November to 07 December 1985, the period leading up to and including the early stages of the vortex breakup. The close agreement between the TOMS and reconstructed distributions each day demonstrates the effectiveness of the reconstructions for this period, not only in describing the period and zonally averaged total ozone distribution presented in Section 6.1, but also the daily evolution throughout the extra-tropical region, the only significant disparity being a tendency for the reconstructions to underplay the mid-latitude ozone maximum and show too much ozone within the polar vortex. Nonetheless, the differences are small, and the similarity between TOMS and the reconstruction on 07 December confirms the movement of the low level vortex remains out over the Antarctic coast southwest of Africa.

After 07 December the features in the EPV analyses become less well-defined, so a set of 30-day CAS simulations, initialised on 01 December, was performed as for the later years, to investigate the subsequent fate of the ozone hole remains. The results

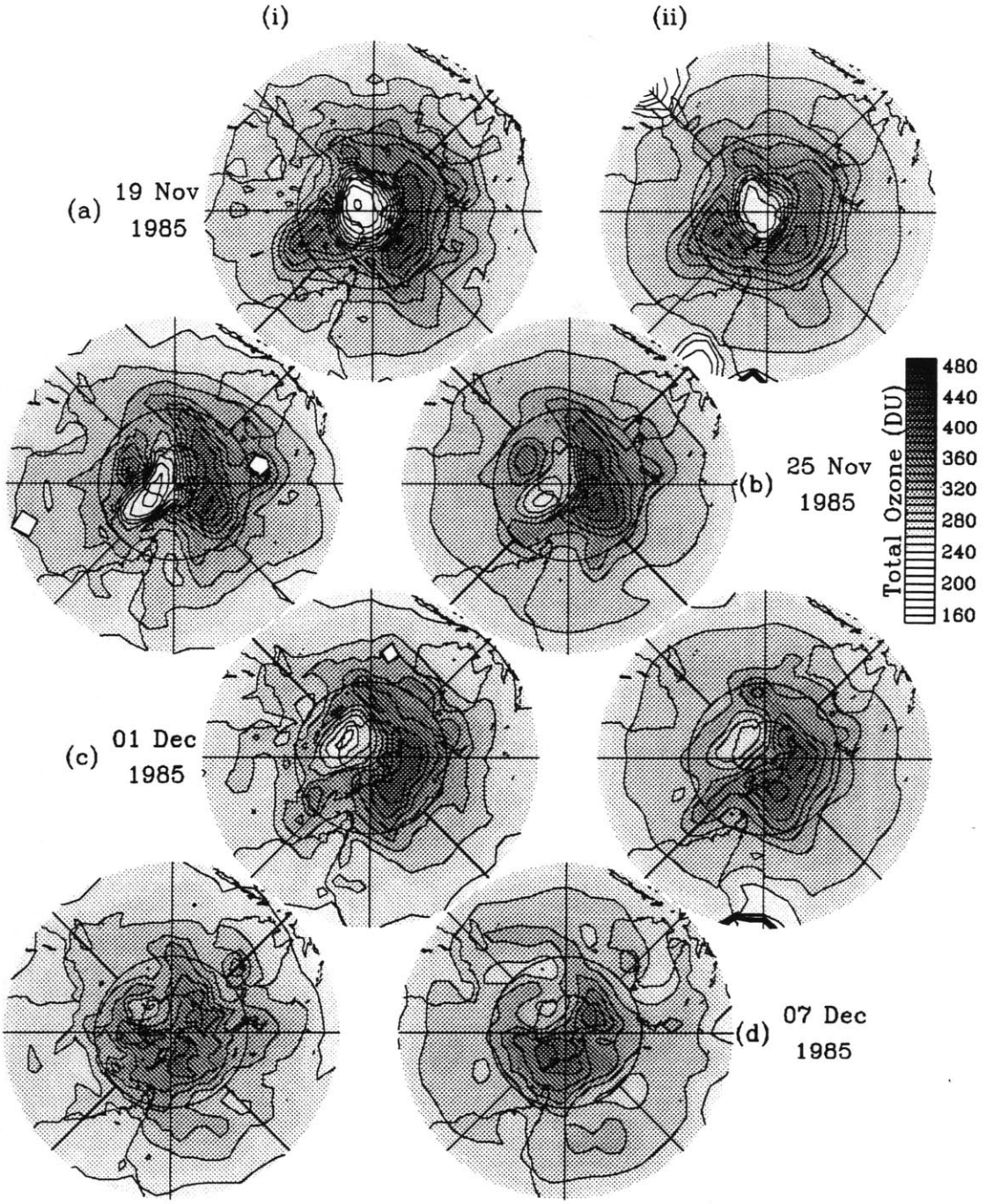

Figure 8.7: As for Figure 8.1, except for (a) 19 and (b) 25 November, and (c) 01 and (d) 07 December 1985.

of the simulations are shown in Figure 8.8, and suggest that the lesser remnant of the vortex, extruded out over the Pacific Ocean in the first week of December, probably caused a transient ozone dilution event over the eastern Pacific/South America region between 08 and 20 December, the remnant stagnating somewhat over South America

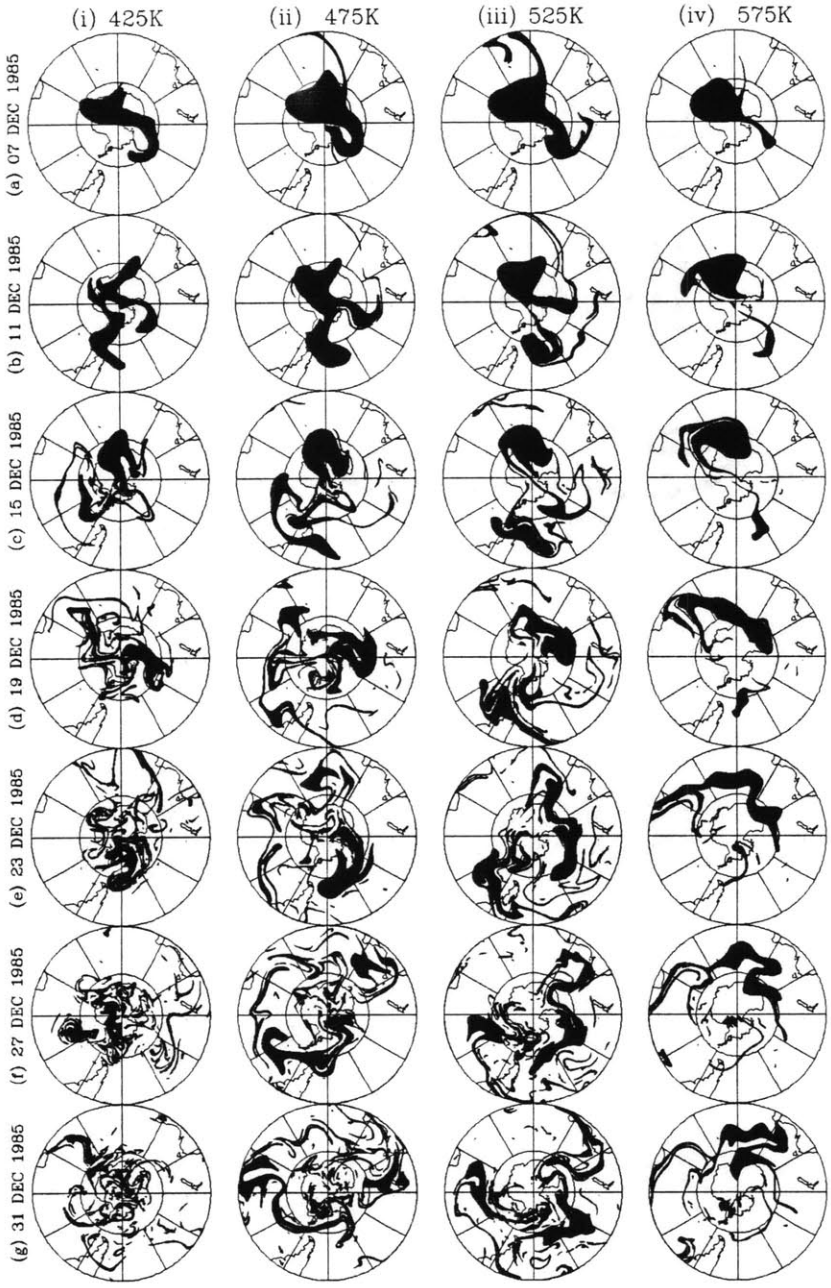

Figure 8.8: As for Figure 7.22, except for (a) 07, (b) 11, (c) 15, (d) 19, (e) 23, (f) 27, and (g) 31 December 1985.

during the period, as it was gradually sheared out above $450K$. The simulations also suggest that the Indian Ocean lobe was gradually sheared out into the hemisphere after mid-December, so that by the end of the month rather even mixing had taken place above $450K$, while below $450K$ the remains tended to collect again in the polar region. In this respect the latter stages of the breakup process were very similar

to 1987. (Note the qualitative similarity between the zonal mean TOMS and $525K$ EPV evolution after early December in 1985 shown in Figure A.7 and that for 1987 in Figure A.9.)

The ozone data for the S5 period suggest that Antarctic ozone depletion at the end of November was about mid-way between that of 1986 and 1987, and confined to the region below about $550K$. Assuming say 45% depletion of 50% of the Antarctic column, and that the upper half was evenly sheared out into the hemisphere during mid-December, this implies an average dilution effect at midlatitudes of around $6DU$, or about 2% of the ozone column, a significant decrease. On the other hand, the CAS-depicted transient event over South America after 10 December likely caused local decreases of perhaps 20 to $25DU$ greater than would have occurred in the absence of Antarctic ozone depletion.

8.1.5 1984

As for the 1985 breakup, the daily reconstructions of the total ozone distribution for S5 in 1984 showed close correspondence with the TOMS distribution up to mid-December (see Figure 8.9), by which stage the low level vortex dissipation stage was well underway, as noted in Section 5.6. Figure 8.9(d) clearly shows the remnants of the ozone hole (below $500K$) over the western Pacific Ocean. A set of 28-day CAS simulations, initialised on 03 December, was performed as for the later years, and the results are shown in Figure 8.10. An interesting feature of the simulations is the manner in which the bulk of the vortex remains above $550K$ is rapidly sheared out over the African region, with little remaining over the Pacific Ocean by mid-December (where the bulk lies at lower levels). However, the NMC-based analyses suggest that the vertical structure was more coherent, with the Pacific remnant on 18 December dominating (recall Figure 5.13(b)). The rather close correspondence between TOMS and the analysis-based reconstruction in the Pacific region for 18 December (Figure 8.9(d)) suggests that, at least on this occasion, the analyses perhaps more correctly describe the broad-scale features of the material evolution than CAS.

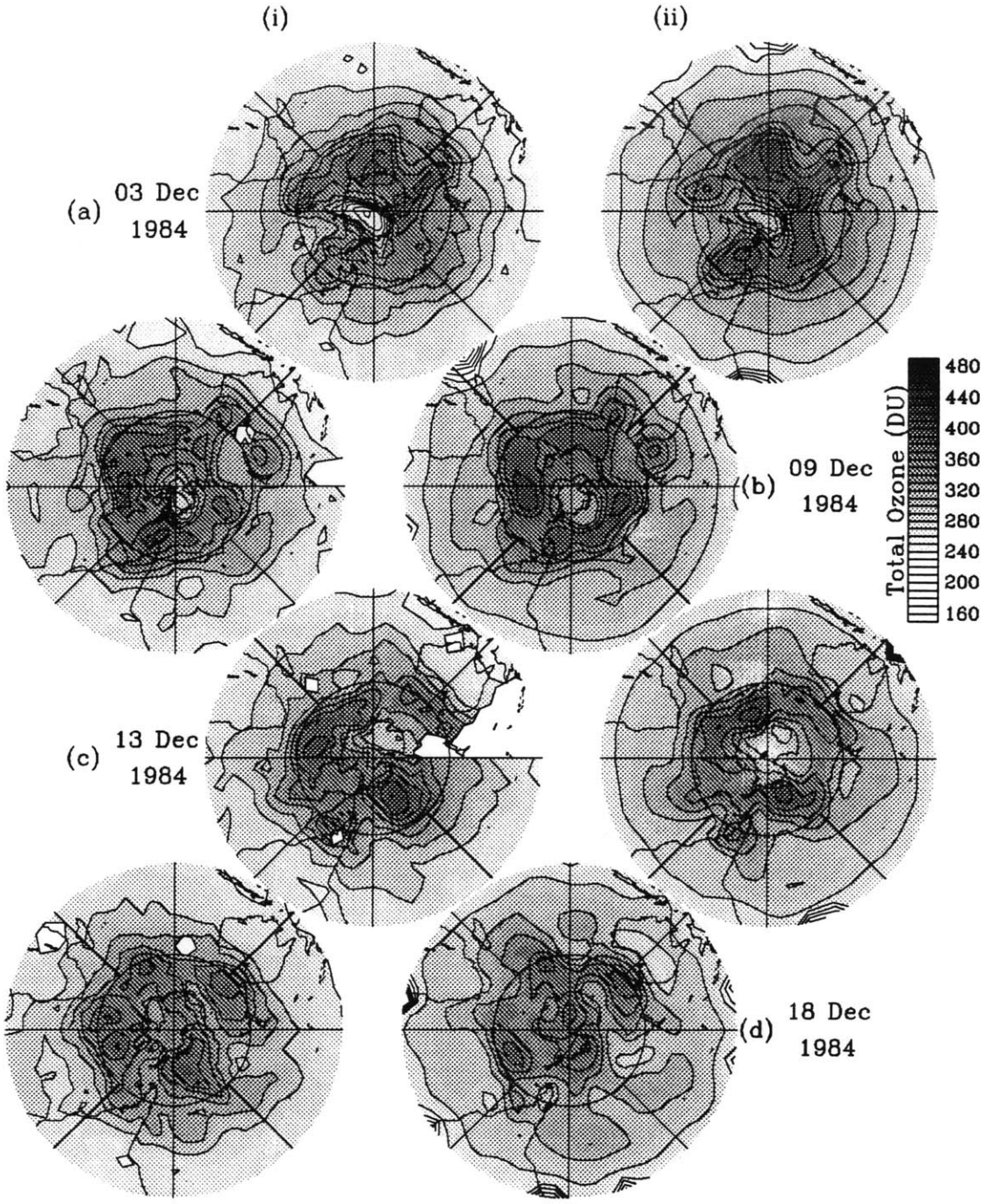

Figure 8.9: As for Figure 8.1, except for (a) 03, (b) 09, (c) 13 and (d) 18 December 1984.

Notwithstanding this discrepancy, the CAS simulations suggest rather gradual but thorough shearing out of the ozone hole remains at each level shown during the latter part of December, although there is once again a tendency for the debris below about $450K$ to regroup in the polar region.

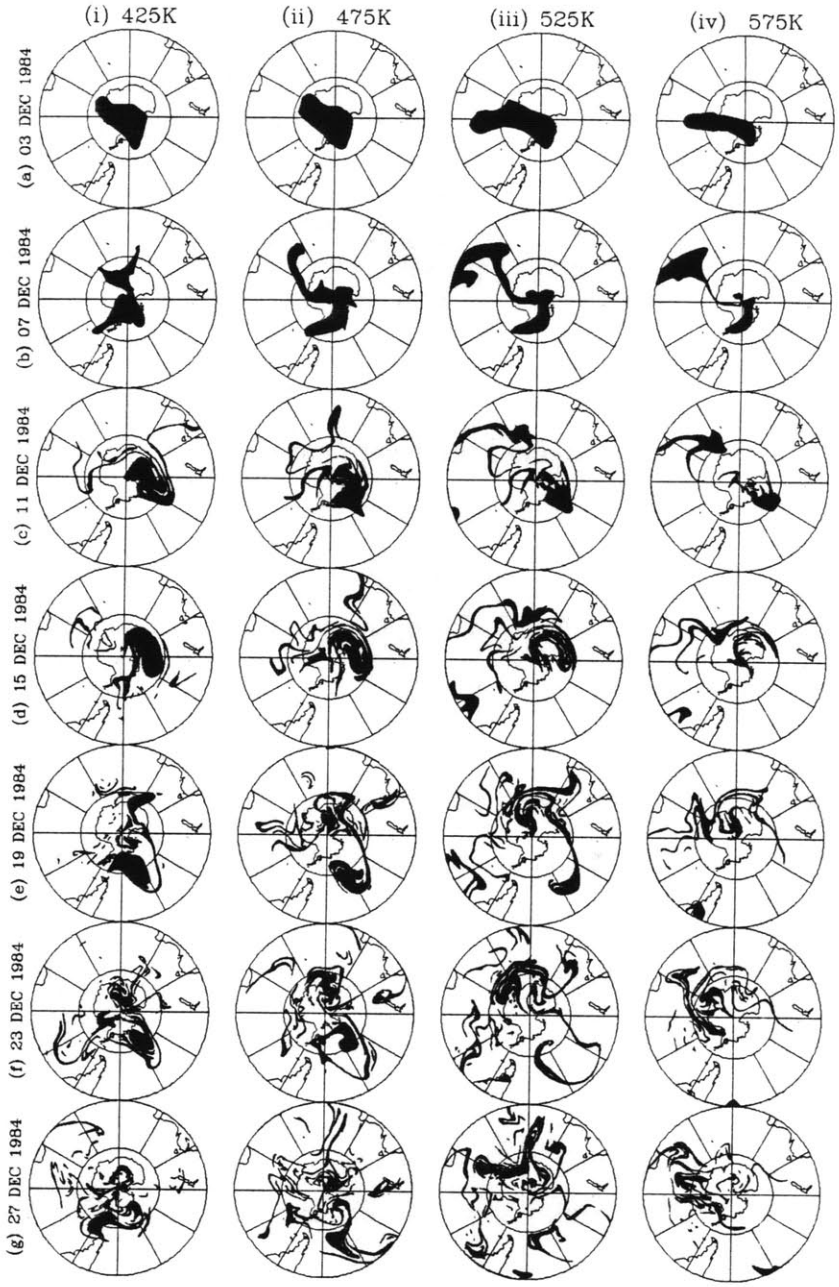

Figure 8.10: As for Figure 7.22, except for (a) 03, (b) 07, (c) 11, (d) 15, (e) 19, (f) 23, and (g) 27 December 1984.

The SAGE data for the S5 period suggest that the extent of the 1984 ozone hole was very similar to that in 1986. Although Bowman (1990) shows mimimum total ozone by the end of November in 1986 to have been about $260DU$, as opposed to about $230DU$ in 1984, we explain this in terms of the very late breakup of the upper level circulation in 1984 relative to that at lower levels (as noted in Section 5.6) so

that, whereas in 1986 high ozone had already moved in over the pole at upper levels, substantially increasing the polar column, in 1984 the upper level vortex was still rather isolated at this time and total ozone remained relatively low. This cautions against using polar total ozone levels to infer the date of dispersion of, or to define the lateral extent of, the Antarctic ozone hole, a point to which we shall return later.

Assuming, then, an integrated ozone hole deficit of about $25DU$ for the levels above about $450K$, and thorough mixing out above this level (fivefold dilution), the expected mid-latitude signal, again neglecting photochemical decay, would have been of the order of $5DU$, or almost 2% of the mid-latitude column, once again a significant effect. On the further assumption that the CAS-indicated extrusion into the African region at levels above $500K$ during the first week of December was erroneous, and that instead the bulk of the ozone hole material at these levels was extruded into the Pacific region with that from the lower levels after mid-December (see Figure 8.10(e)) then the zonal mean total ozone decrease at this time, which can be seen propagating away from the polar region in Figure A.6(c), can be partially explained as mid-latitude ozone dilution. (Note the corresponding 'smoke plume' in analysed zonal mean $525K$ EPV in Figure A.6(b).)

8.1.6 1983

In Section 6.4 we noted the highly speculative nature of the $\chi/\hat{q}$ relationships adopted for the S5 virtual sweep period in 1983, and our reservations about the accuracy of their details. Figure 8.11, which shows TOMS and reconstructed total ozone at four day intervals from 17 to 29 November 1983, demonstrates the usefulness of the speculative relationships in describing the daily distribution of total ozone, despite these reservations. Although the Antarctic ozone hole is rather poorly represented in the reconstructions for the latter stages of the period, it is nonetheless remarkable how well the other features are represented. Indeed, the poor correspondence in the structure of the ozone hole, particularly for 25 and 29 November, is best explained by significantly less ozone within the vortex between $425K$ and $550K$ in 1983 compared

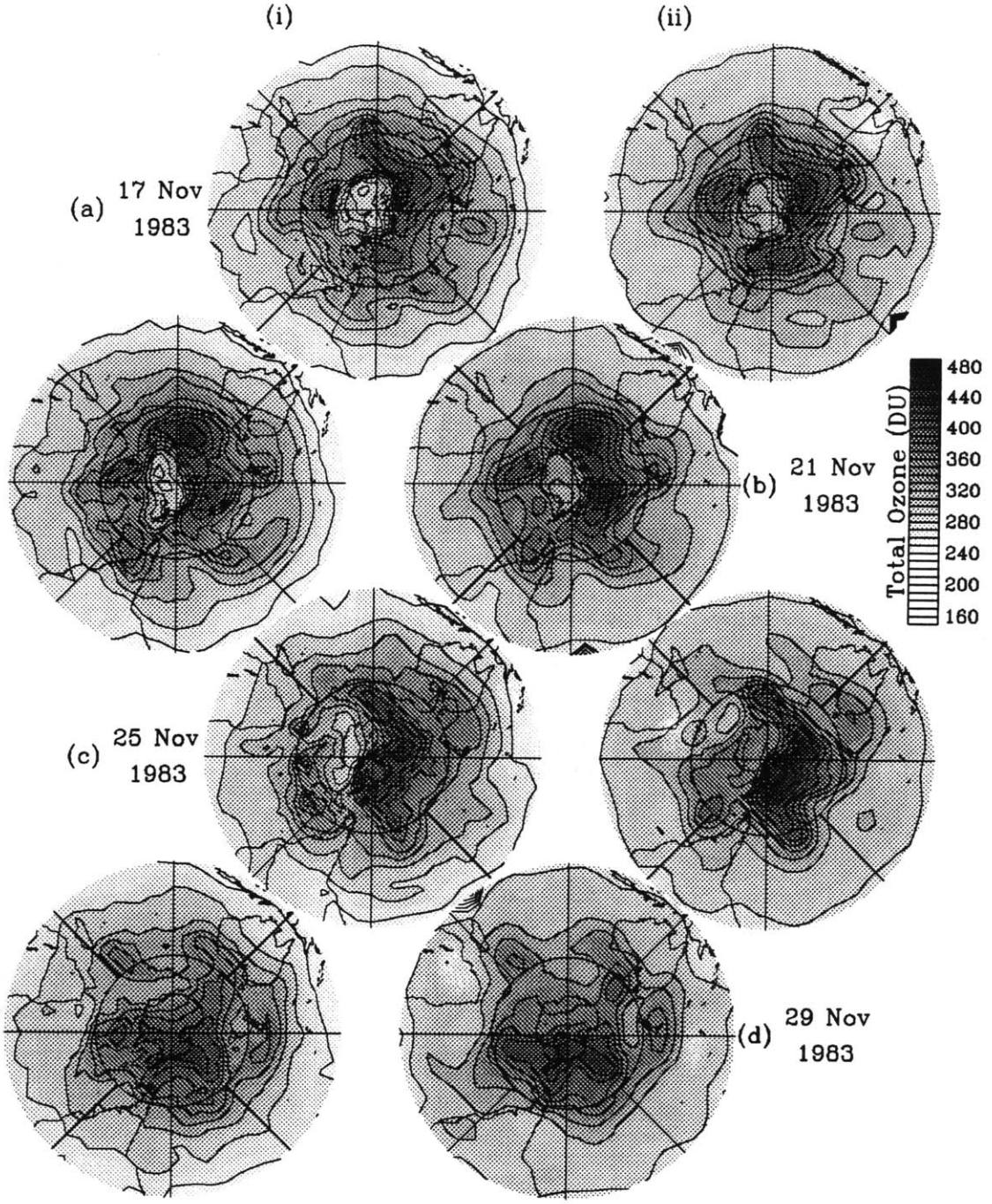

Figure 8.11: As for Figure 8.1, except for (a) 17, (b) 21, (c) 25 and (d) 29 November 1983.

to October 1981 (recall that the October 1981 $\chi/\hat{q}$ relationships were used above $400K$).

As discussed in Section 5.5 above, the vortex at low levels was displaced off the pole towards the Indian Ocean during the last week of November, apparently to

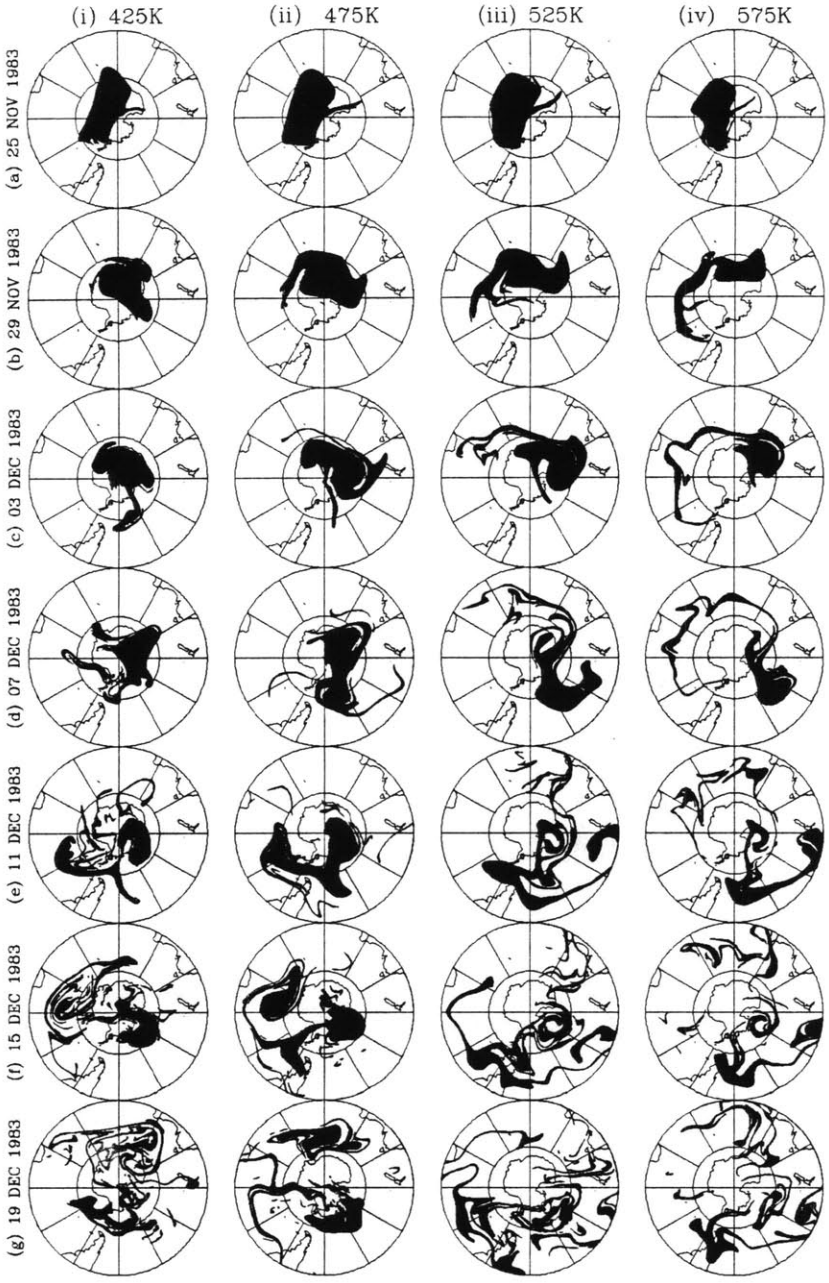

Figure 8.12: As for Figure 7.22, except for (a) 25 and (b) 29 November, and (c) 03, (d) 07, (e) 11, (f) 15, and (g) 19 December 1983.

dissipate over the following weeks. The results of a set of simplified 30-day CAS simulations, initialised on 21 November, are shown in Figure 8.12, and are consistent with the earlier interpretation of the EPV analyses. The vortex mass first began to be sheared out above $500K$ after 25 November as the pattern rotated eastward. Then the remains above $400K$ were rather evenly split in two after 07 December and

gradually mixed with the mid-latitude environment during the rest of the month. Perhaps the most noteworthy feature indicated by the $425K$ simulation, referred to in Section 5.5, was the deep extent of the mixing process, the vortex at $425K$ being rather well mixed out by late December, and unlike in the other years, tending not to regroup over the polar region by the end of the month. Of note in Figure A.5(b) is the equatorward propagation of a zonal mean total ozone decrease accompanying the initial displacement of the vortex remains off the pole. The analysis of Bowman (1990) and the mismatch between reconstructed and TOMS polar ozone during the first half of November suggests the polar ozone depletion in 1983 was similar to that in 1984. Only a few ozone sonde ascents were made within the vortex during October in each of the two years (from Syowa). These suggest similar ozone levels below $475K$ and above $600K$ in 1983 but much lower values in the intervening layer. This, however, seems irreconcilable with the similarity in total ozone in each year. Assuming that, as was assumed for 1984, by mid-November 1983 the Antarctic ozone depletion amounted to about a $45DU$ deficit within the vortex, $30DU$ of which was present above $400K$, and was mixed evenly out into the hemisphere south of $30°S$, then the expected mid-latitude ozone dilution signature, neglecting photochemical processes, would be about $6DU$, or about 2% of the mid-latitude column, once again a significant effect. (Had the 1983 dynamics acted on the 1987 ozone hole remains, the mid-latitude effect may have been as great as 5%.) Apart from this overall hemisphere-wide signature, if the CAS simulations correctly portray the mixing process up to mid-December, then a temporary decrease of 10 to $15DU$ would have been experienced over South America during the second week of December.

8.1.7 1982

Whereas the highly speculative OMR distribution assumed for the breakup period in 1983 produced total ozone reconstructions which agreed rather well with the TOMS evolution (apart from the OMR structure at lower levels within the vortex), the similarly speculative distribution adopted for the 1982 breakup period was not as

successful at describing the observed evolution. Figure 8.13 shows TOMS and reconstructed total ozone distributions at five day intervals from 10 to 25 November 1982. Not only do they inadequately describe the structure of the ozone hole, they are also less successful in describing the medium scale features of the distribution at mid-latitudes, suggesting the agreement between the period and temporally averaged distributions to have been rather fortuitous. Nonetheless, the larger scale features are still well explained, attesting to the overall robustness of the reconstruction technique.

In Section 5.4 the 1982 breakup at low levels, as depicted by the EPV analyses, was described as primarily radiative during the latter part of November, before the remains were squeezed out into the western hemisphere in early December. A set of 30-day CAS simulations initialised on 20 November provided qualitative agreement with the interpretation of the EPV analyses, but suggest that the vortex above $525K$ was split in two during the last week of November, the lesser remnant being advected into the Australian mid-latitudes and subsequently sheared out, while the remainder above $400K$ was gradually and rather evenly sheared out during December, although with a tendency to be advected initially towards the South American region. Although the CAS simulations terminated on 20 December, by this stage the vortex above $475K$ had been evenly dispersed throughout the extratropical region, while below $475K$ the remains were regrouping, as appears typical, over the polar region. This interpretation is once again supported qualitatively by the EPV gradient obliteration after late November at $525K$ in Figure A.4(b), while below $475K$ (not shown) the highest zonal mean EPV returned to the polar region.

In the absence of reliable information from the present analysis on the ozone hole structure in 1982, it is assumed, based on the Bowman (1990) analysis, that Antarctic ozone depletion in 1982 was relatively mild and shallow, say 15% depletion of 30% of the column, or a polar ozone deficit of only about $15DU$ by late November. If it is also assumed that no more than 1/3 of this was due to ozone depletion above $475K$, but that this fraction was eventually totally mixed out into the region south of $30°S$, then the maximum potential for mid-latitude ozone dilution would have been about

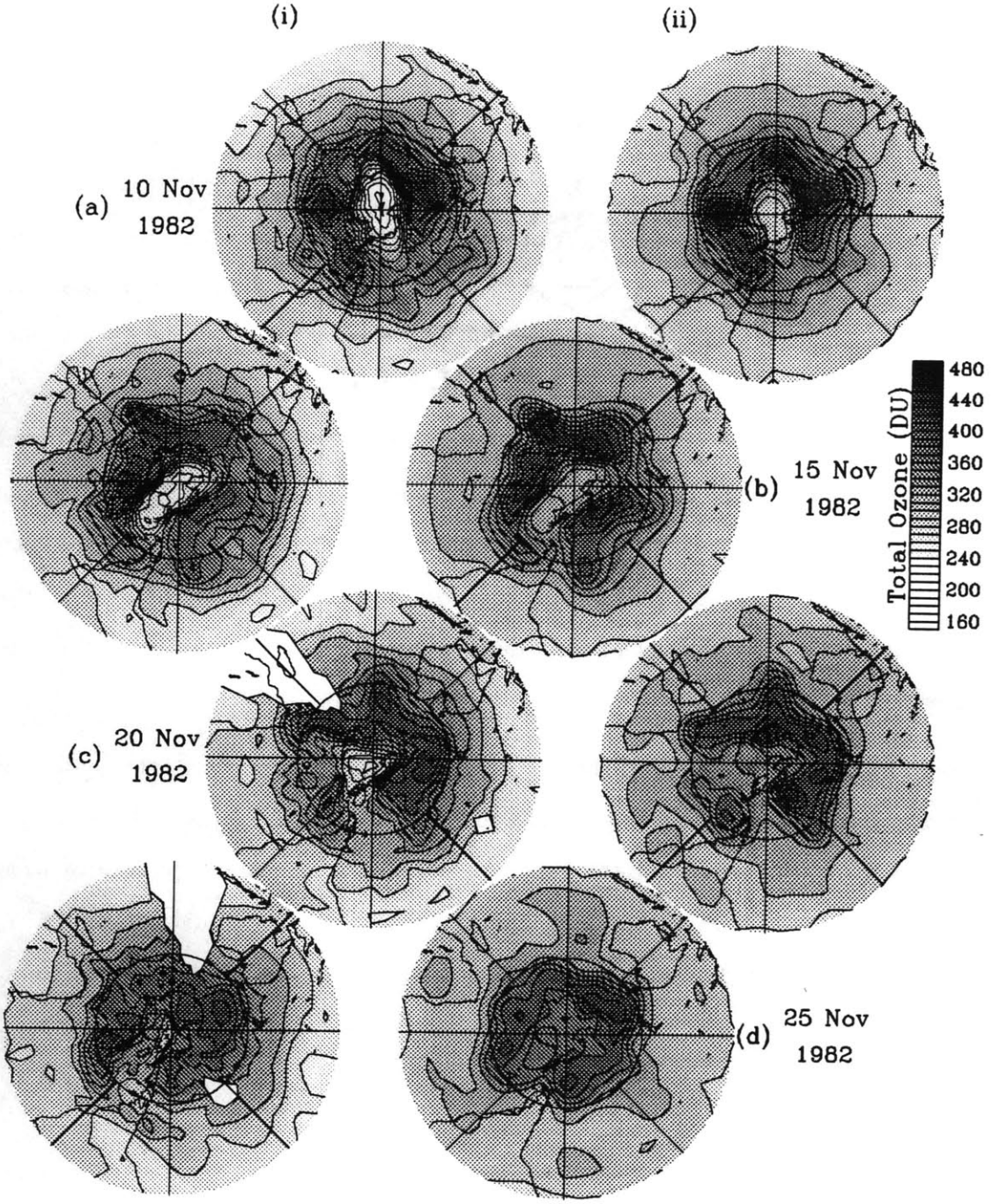

Figure 8.13: As for Figure 8.1, except for (a) 10, (b) 15, (c) 20 and (d) 25 November 1982.

$1DU$ or less than 1/2% of the mid-latitude column. i.e There is little scope for mid-latitude ozone dilution accompanying the 1982 vortex breakup. As was the case for the 1988 breakup, Figure A.4(c) shows virtually no signs of a zonal mean mid-latitude ozone decrease after late November, consistent with the above speculative

interpretation.

8.1.8 The Early Years

We discussed in Section 7.3 the uncertainty about the extent of Antarctic ozone depletion occurring during the first few years of the present analysis period, and have crudely assessed the approximate extent of ozone dilution accompanying the vortex breakup in the later years relative to these earlier years. i.e. We have essentially assumed negligible Antarctic depletion in the earlier years in order to arrive at quantitative estimates for the later years. As noted above, however, there is evidence to suggest that significant springtime ozone depletion was already underway by the start of the decade, the implied estimates ranging from around $30DU$ to $70DU$ for October over Antarctica (compared with an *additional* reduction of more than $100DU$ in October 1987).

Irrespective of the extent of the depletion by the early eighties, examination of the dynamical evolution in these years and its implications for ozone transport, if not dilution, is worthwhile for the sake of gaining a more general picture of what comprises the typical vortex breakup, and the extent of interannual variability. In the remainder of the present Section, then, we consider briefly the implied ozone transport associated with the breakup in the latter two of these first three years.

8.1.8.1 1981

As described in Section 5.3, the EPV analyses for 1981 suggest the polar vortex remains were displaced from the pole after mid-November, to drift eastwards and gradually dissipate over the following weeks. TOMS and reconstructed total ozone distributions at five day intervals from 09 to 24 November 1981 are shown in Figure 8.14, and demonstrate that, despite once again failing to portray correctly the polar ozone minimum, the reconstructions for the period show rather close agreement with the TOMS evolution elsewhere. The most interesting feature of the evolution dur-

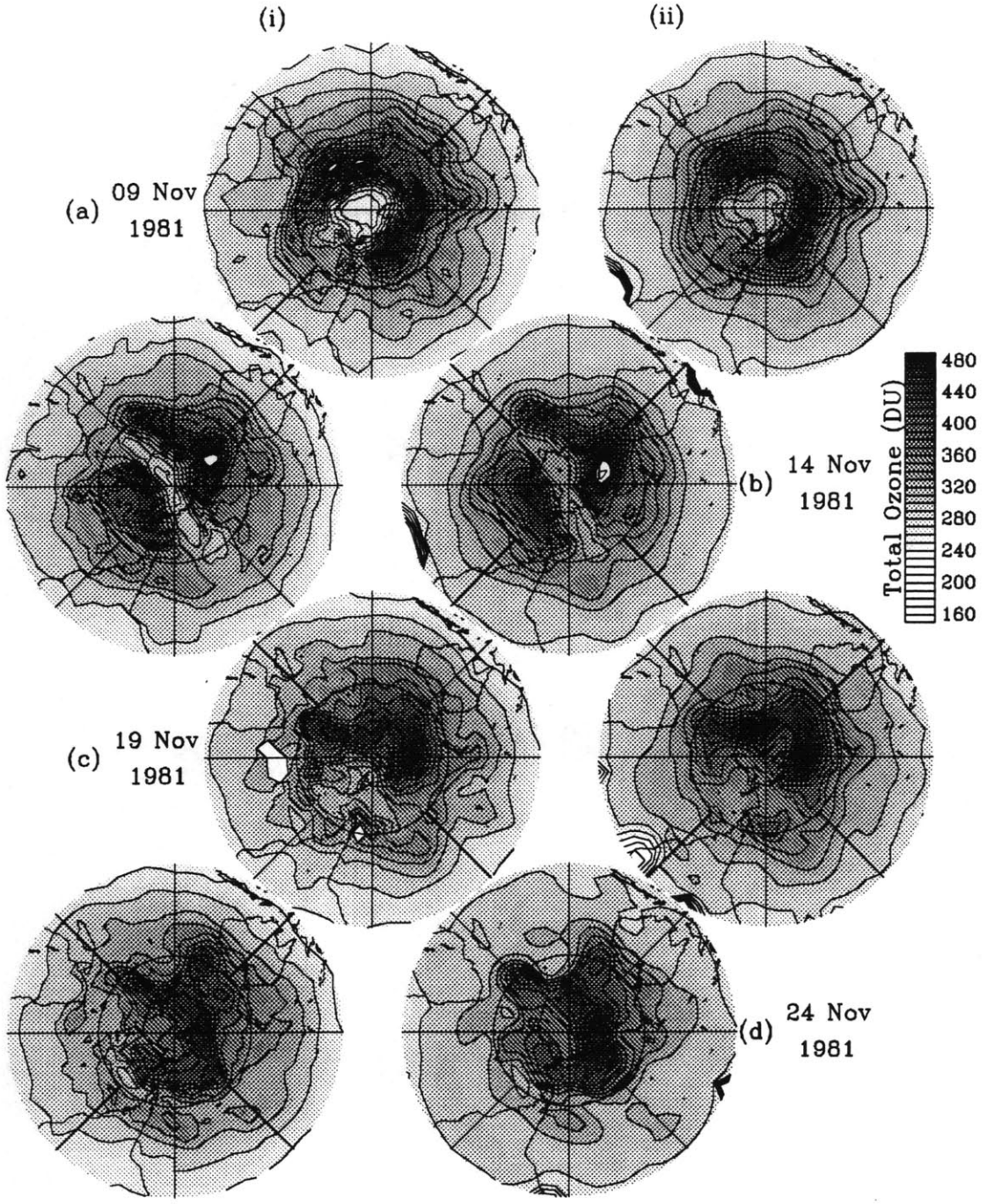

Figure 8.14: As for Figure 8.1, except for (a) 09, (b) 14, (c) 19 and (d) 24 November 1981.

ing the period is the virtual disappearance of the polar total ozone minimum by 19 November. Bowman and Mangus (1993), who use the TOMS data alone to interpret the dynamical evolution in the lower stratosphere, state *"by 20 November, the breakdown of the vortex and the mixing of the ozone hole is essentially complete."*

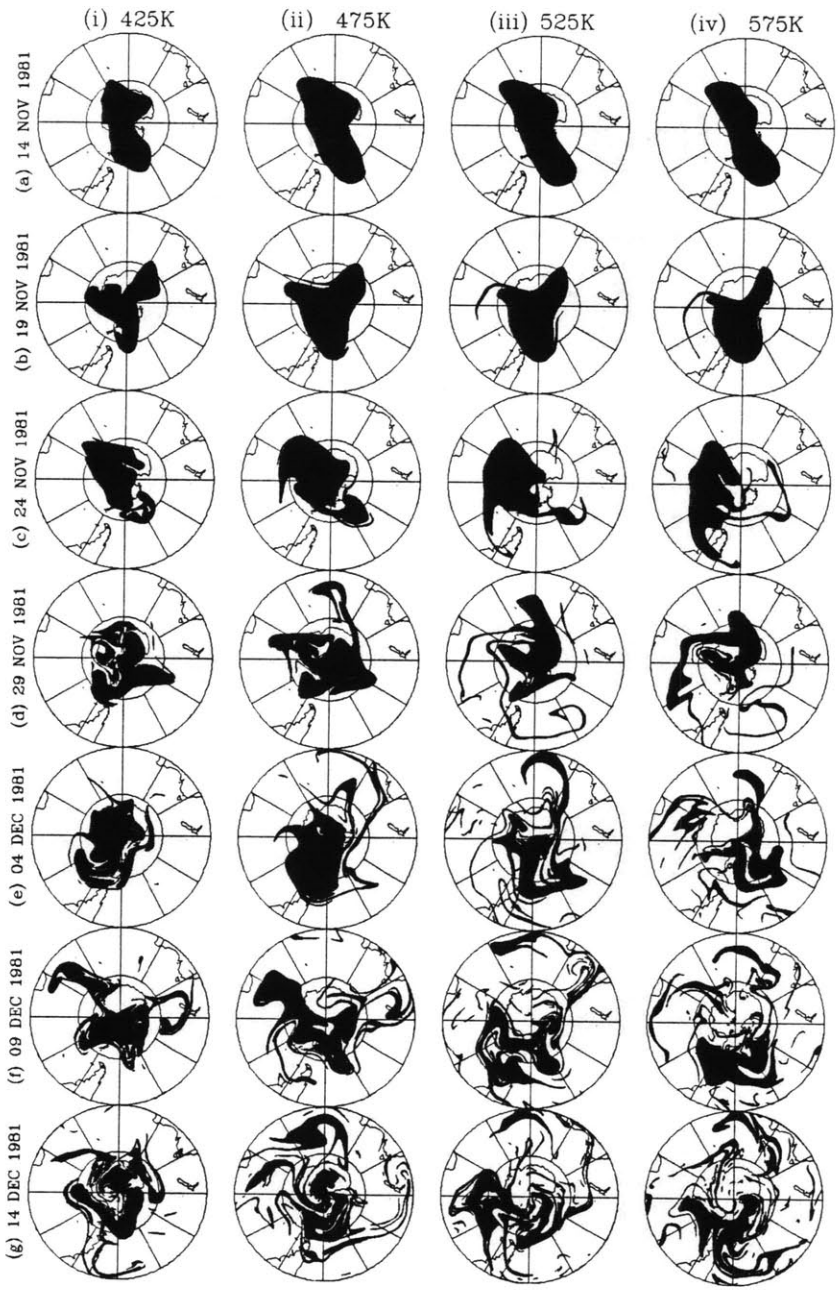

Figure 8.15: As for Figure 7.22, except for (a) 14, (b) 19, (c) 24 and (d) 29 November, and (e) 04, (f) 09, and (g) 14 December 1981.

The EPV analyses for the period (see Figure 5.6(b)), the close agreement between TOMS and reconstructed total ozone distributions, and additional support for the dynamical evolution indicated by the analyses from a set of CAS simulations initialised on 14 November (see Figure 8.15) demonstrate clearly that the interpretation of Bowman and Mangus is incorrect. On 19 November, the vortex remains below

$575K$ (comprising the ozone hole in its entirety) are still intact and almost pole-centred, and the virtual disappearance of the polar total ozone minimum is due to poleward ozone flux at upper levels and adiabatic subsidence at lower levels in association with the vortex destruction aloft. Bowman (1990) drew a similarly erroneous conclusion in regard to the ozone hole breakup in 1983, claiming that it rapidly fragmented and disappeared between November 27 and 29, by which stage *"the transition to the summertime ozone pattern is complete"*. As noted earlier, the ozone hole was essentially intact on 29 November 1983 (recall Figure 8.12(b)), the mixing process occurring only gradually during December. These cases clearly demonstrate the fallacy of interpreting total ozone as a materially-conserved property of the flow, particularly at this stage of the season when extensive vertical shearing of the flow makes the barotropic assumption, implicit in the work of Bowman (1990) and Bowman and Mangus (1993), entirely inappropriate.

The results of the CAS simulations shown in Figure 8.15 suggest the mixing process at ozone hole levels essentially commenced after 20 November, and extended gradually downwards with time, but was still incomplete by the termination of the CAS simulations on 25 December (not shown). In some respects the flow evolution appears to have been similar to that in 1986, with a rather gradual stripping of the vortex remains during December rather than one or two events in which the entire vortex mass was sheared out. In the process it is likely that a number of smaller scale transient dilution events occurred at mid-latitudes (e.g. over southern Australia and South America after 04 December, and perhaps in the New Zealand region around 09 December). By late December the vortex fragments below $475K$ had tended to regroup in the polar region while above this level, other than a small unsheared remnant back over the polar region, the vortex material had been rather evenly mixed out into the hemisphere (see Figure A.3(b)). The lack of complete mixing indicated by the CAS simulations is also supported somewhat by the mid-latitude behaviour of zonal mean total ozone in Figure A.3(c), which shows transient fluctuations consistent with meridional excursions of the still coherent vortex core during December.

8.1.8.2 1980

The sequence of TOMS and reconstructed total ozone distributions at 4 day intervals from 15 to 27 November 1980 in Figure 8.16 shows that, other than exaggerating the magnitude of the mid-latitude ozone maxima, the reconstructions provide a rather close fit to the TOMS data up to late November. A set of 40-day CAS simulations initialised on 19 November (not shown) suggested that the vortex remains, initially advected over the South American region by 23 November (as noted in Section 5.2), were rapidly sheared out above $500K$ during the following two weeks. (Note the rapid reversal of the EPV gradient in Figure A.2(b) which coincides with the equatorward propagation of a weak total ozone decrease during late November and early December in Figure A.2(c).) At lower levels, with a westerly flow regime persisting south of $30°S$, the shearing process was much slower, and by the end of the simulation on 29 December, most of the rather coherent debris was confined to the region south of $45°S$ at $475K$, while at $425K$ most was south of $60°S$.

Despite the modest Antarctic ozone depletion in 1980, the initial advection after 19 November of the low level vortex remains out over South America would most likely have produced a temporary but perhaps significant ozone dilution effect there. However, the extent and vertical structure of the Antarctic depletion in 1980 are not known, so the magnitude of the mid-latitude dilution effect can not be accurately assessed. Nonetheless, to provide a qualitative impression of its likely impact, and also to demonstrate how subtle an effect the presence of the ozone hole has on the overall total ozone distribution (hence how inappropriate it is to use total ozone data to infer the dynamical behaviour of the Antarctic ozone hole), the reconstructions for 23 and 27 November were repeated after imposing 1987 Antarctic ozone hole OMRs within the 1980 polar vortex between $380K$ and $575K$. i.e The reverse process from that used to examine the magnitude of the 1987 ozone dilution event was carried out.

The resulting total ozone distributions on the two days are shown in Figure 8.17, for comparison with the two earlier reconstructions and the TOMS distributions in Figure 8.16. While the visible effect on the reconstruction for 23 November is signifi-

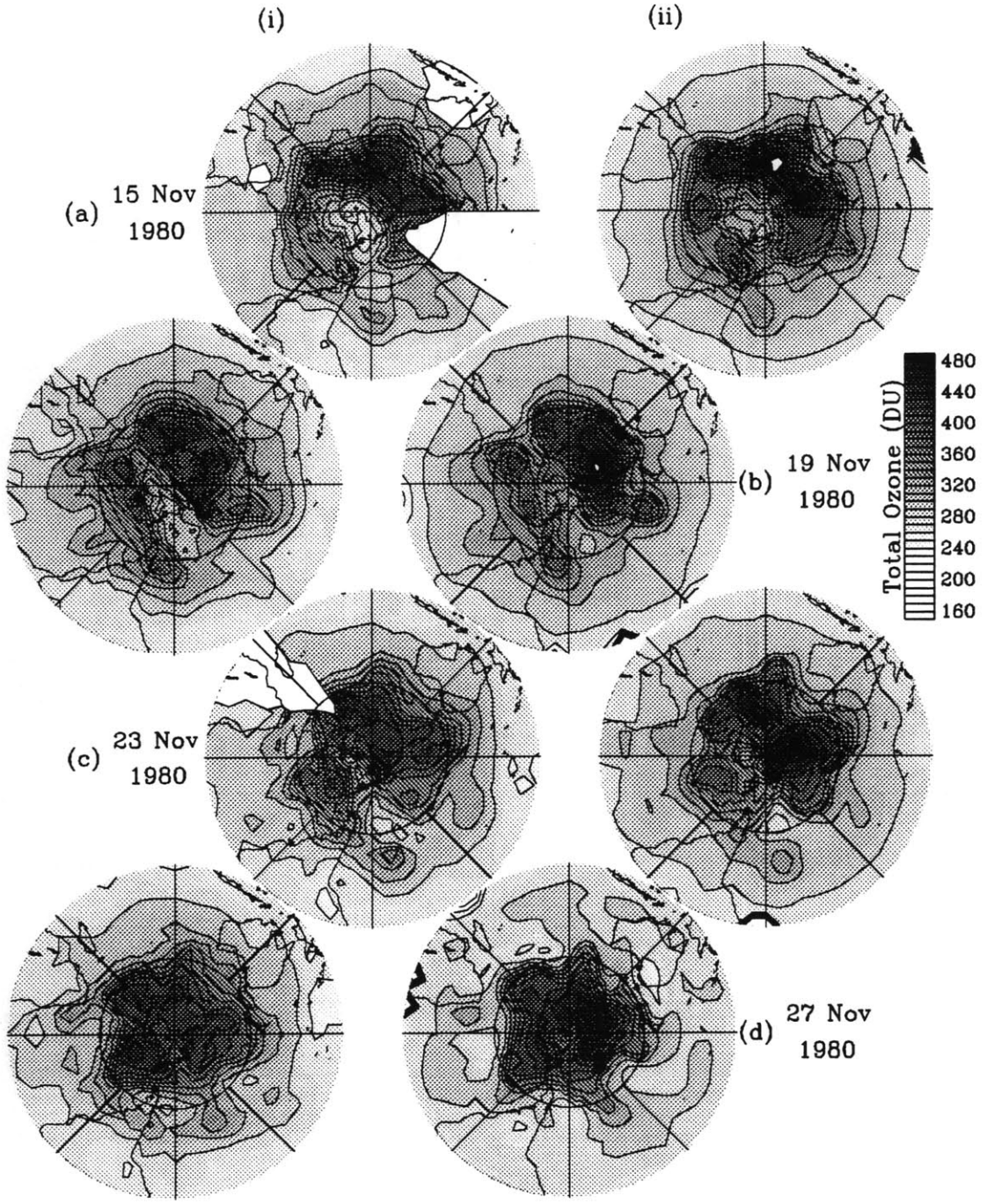

Figure 8.16: As for Figure 8.1, except for (a) 15, (b) 19, (c) 23 and (d) 27 November 1980.

cant because at this stage the vortex is vertically coherent throughout the lower and middle stratosphere, by 27 November a major portion of the ozone hole lies beneath ozone-rich air advected over the polar region at higher levels as the vortex remains were pushed out over South America, so the effect on the total ozone distribution,

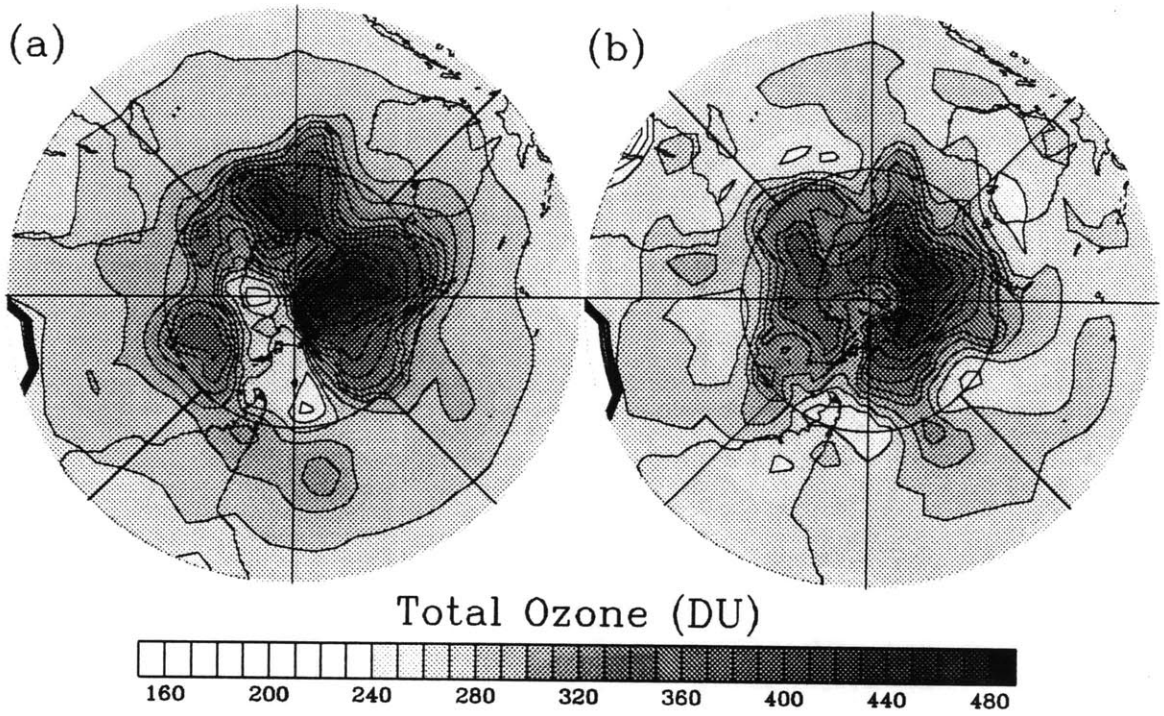

Figure 8.17: Total ozone reconstructions, with the 1987 Antarctic ozone hole OMRs imposed within the polar vortex between $380K$ and $575K$ for (a) 23 and (b) 27 November 1980.

while as large, is not as noticeable, being seen more as a decrease in the maximum values in the south Atlantic Ocean region than in the development of the low ozone area over South America. The true extent of the effect of the imposed ozone hole is seen more clearly in Figure 8.18, which shows the difference between the reconstructions before and after the imposition of the ozone hole for each day.

If we suppose that by 1980 springtime Antarctic ozone depletion was already underway, with an overall deficit of, say, $50DU$ (which is about half the decrease observed between 1980 and 1987), and, less validly but for simplicity, that the structure of the decrease was the same as that in 1987 (it is more likely that the 1980 ozone hole would have affected only the lower levels significantly), then halving the total ozone values shown in Figure 8.18 provides a (very) crude estimate of the likely impact of the 1980 ozone hole on the total ozone distributions on each of the days shown. (Note that, were this the case, then the 1987 ozone dilution estimates provided in Chapter 7 need to be increased by 50%, and those for the other years discussed above by more

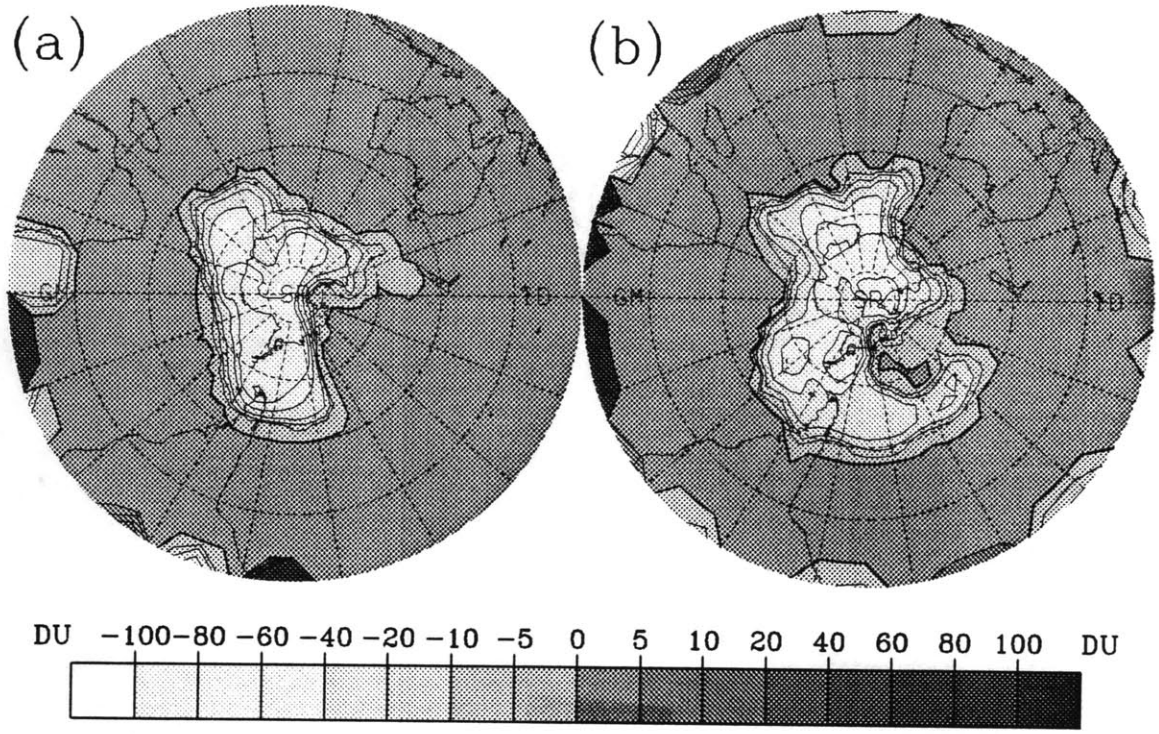

Figure 8.18: The difference in total ozone between the unmodified and '1987 ozone hole' reconstructions for (a) 23 and (b) 27 November 1980.

than this proportion.)

8.1.8.3 1979

A speculative examination of the 1979 polar vortex breakup similar to those carried out for the remaining years was essentially prevented by the overall poor quality of the total ozone reconstructions for the period, itself due to the poor quality of the NMC-based EPV analyses used in the present work. Further, simplified extended-period CAS simulations, although carried out, were unsuccessful due to noisy balanced wind fields, which tended to play havoc with the advected contour distributions. Hence an examination of the 1979 evolution after the initial stages of the vortex breakup was not carried out. Figure 8.19 shows a sequence of TOMS and reconstructed total ozone distributions at (approximately) seven day intervals from 04 to 24 November 1979, and has been included to show the effect of the poor quality EPV analyses on the reconstructions. (It is stressed that we do not mean by the above comments

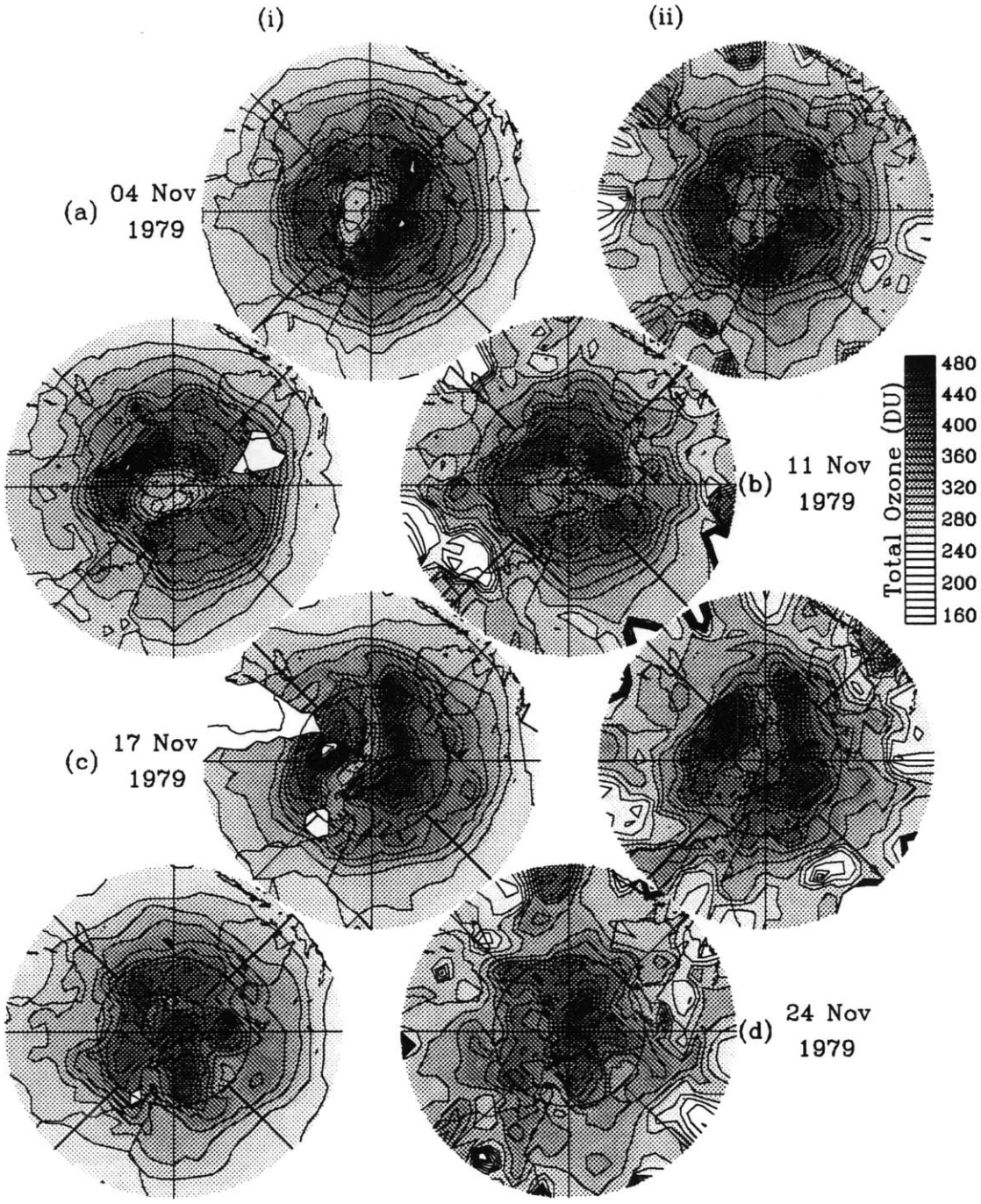

Figure 8.19: As for Figure 8.1, except for (a) 04, (b) 11, (c) 17 and (d) 24 November 1979.

to denigrate the NMC product, but merely our use of it: a superior technique for derivation of both the EPV and velocity distributions would have circumvented many of the problems experienced.) Nonetheless, despite the problems, the plots shown demonstrate that, even when used on the particularly noisy 1979 data, the coordinate

transformation technique still produces a surprisingly close fit to the TOMS data in the extratropical region.

8.2 Ozone Dilution Prior to the Vortex Breakup Each Year

To examine the issue of ozone dilution occurring each season prior to the vortex breakup at ozone hole levels, a closer inspection was made of each of the potential dilution events identified in the eleven season analysis of the dynamical evolution considered in Chapter 5 above.

For each event, the OMR and implied total ozone evolutions during the period of interest were reconstructed using the EPV analyses and the corresponding adopted $\chi/\hat{q}$ relationships from the relevant sweep period. As noted above, these reconstructions for the period prior to the vortex breakup each year did not suffer the EPV relaxation effects of those for the latter stages of the season, and provided a picture of the evolution which, at resolvable scales, closely resembled that witnessed by the TOMS instrument, suggesting a high level of confidence could be placed in the picture obtained.

Of all the events examined using the analysis-based ozone reconstructions alone, none provided firm evidence of the irreversible extrusion into mid-latitudes of material from within the Antarctic ozone depletion region (i.e from *inside* the polar vortex at lower levels) prior to the vortex breakup. While there were occasions during many of the seasons examined of 'bulk' extrusion of material from within the vortex at levels above the ozone hole, and of apparent extrusion at lower levels of material from the outer edge of the vortex, the analysis based solely on the ozone reconstructions leads us to conclude that there were no *broad-scale* mid-latitude ozone dilution events prior to the breakup of the vortex at low levels in any of the seasons examined.

Of course, the limited spatial resolution of the EPV analyses precluded an assess-

ment, based solely on the ozone reconstructions, of the likelihood of ozone dilution occurring at smaller spatial scales prior to the vortex breakup each year.

To address this question, simplified CAS simulations were performed for each of the potential events identified in Chapter 5. As for the vortex breakup periods considered in the preceding Section, the ozone reconstructions for each event were used to identify the EPV contour, at each of several levels, which best represented the material boundary of the ozone depletion region at that level. The appropriate EPV contour, initialised using the EPV analysis from several days before the event of interest, was then advected using CAS to provide a picture of the tracer evolution during the event at scales unresolved by the EPV analyses. Whereas the effectiveness of CAS for the post-breakup period is not known precisely, so we claim only qualitative representation of the real flow evolution for this latter period, it is thought generally to perform well in the pre-breakup period when the vortex is still strong, so we can place greater confidence in the CAS-depicted evolution at each level.

Overall, despite the lengths gone to, via the development of the ozone reconstruction technique, to obtain a detailed picture of the three-dimensional distribution of OMR during each event examined, and despite our confidence in the CAS-depicted evolution for the pre-breakup period each year, this part of the analysis achieved only limited success.

We can conclude that, prior to the LS stage of the dynamical evolution (as described in Chapter 5) in each of the seasons examined, the vortex interior at ozone hole levels remains essentially isolated from its surroundings, insofar as there were no occasions in any of the seasons examined in which quasi-horizontal advection resulting from Rossby wave breaking at ozone hole levels led to the extrusion of material from within the vortex interior out into the region beyond the vortex edge. Of course, we have not addressed the question of transports which might arise as a result of gradual diabatic downwelling through the vortex, gravity wave activity, or other vehicles for vertical transport such as Kelvin-Helmholtz instability.

During the TT stage of the evolution in each season, once the upper level vortex

breakdown is essentially complete, numerous occasions were found on which the CAS simulations suggest extrusion of ozone hole material into the mid-latitudes, but each of these comprised transient events of such limited horizontal and vertical scales according to the simulations, that, without the benefit of CAS-based reconstructions, quantitative assessment of the magnitude of the associated mid-latitude ozone dilution effect is precluded. The examination of this period therefore provides only qualitative insight, as was the case for the vortex breakup period discussed earlier.

With regard to the question of ozone dilution during the LS stage of the evolution each year, the direct success achieved by the present analysis was even more marginal. Despite numerous cases of Rossby wave breaking at the vortex edge, suggested by the EPV analyses and noted in Chapter 5 above, and similar indications from the CAS simulations for many of these events, there were no occasions in the many seasons examined for which *conclusive* evidence was found of *significant* extrusion of ozone hole material into the mid-latitudes during the LS stage of the evolution. In fact the CAS simulations suggest the vortex interior at low levels remains extremely robust and resistant to wave-induced erosion: whereas numerous extrusions were evident from the vortex edge at various times, none involved material from deep within the vortex interior.

Whether or not each of the potential dilution events identified actually involved extrusion of ozone hole material into mid-latitudes depends critically on, and is highly sensitive to, the precise location of the boundary of the ozone depletion region. Even the detailed reconstruction technique used is incapable of defining this boundary to the level of accuracy required.

Notwithstanding the overall inconclusiveness of the analysis in this respect, the CAS simulations of the potential dilution events and a series of additional simulations for other periods during each season provide insight into the nature of the vortex erosion process during the season, and also enable us to demonstrate how more simplistic approaches to the vortex isolation/ozone dilution issue can be entirely inadequate and misleading.

In the remainder of the present Section, then, we deal with these matters. We consider primarily the broad pattern of behaviour evidenced by the CAS simulations in each of the four stages of the dynamical evolution described in Section 4.4 above and treat in more detail only a few of the individual events examined, to demonstrate the subtlety of the pre-breakup ozone dilution issue, and the fallacy of attempting to use the total ozone distribution as a basis for the identification of ozone dilution events.

8.2.1 The LW Stage

As discussed in Section 4.4, the LW stage of the dynamical evolution covers the late winter period during which the vortex is large and strong, and stratospheric wave amplitudes are rather small. CAS simulations for the LW period of each season examined suggest that the vortex remains almost completely isolated from the surrounding environment, particularly at the lower levels (i.e. the ozone depletion region).

Figures 8.20 and 8.21 show the typical evolution of CAS-advected EPV contours in the lower stratosphere during the period. The former, which is from a 12-day simulation at the $450K$ level initialised on 01 September 1987, depicts the typical evolution at and within the vortex edge, while the latter, from a 12-day simulation at $525K$ initialised on 20 August 1987, typifies the evolution at and equatorward of the edge. Apparent in each of these Figures is the lack of contour folding (or buckling) and stretching in the vicinity of the vortex edge (close to the polar jet axis). For the $525K$ run, the edge lies close to the innermost contour, while for the $450K$ run it lies between the two outermost contours. (For each case the vortex edge was located using the dynamical analyses and ozone reconstructions for the period, and for the $450K$ simulation the location inferred was consistent with $425K$ edge located by Hartmann *et al* (1989) using ER-2 flight data of 02, 04 and 09 September 1987 from the AAOE mission.) On the other hand, both within and beyond the vortex edge, the simulations suggest that a slow but essentially continual mixing process

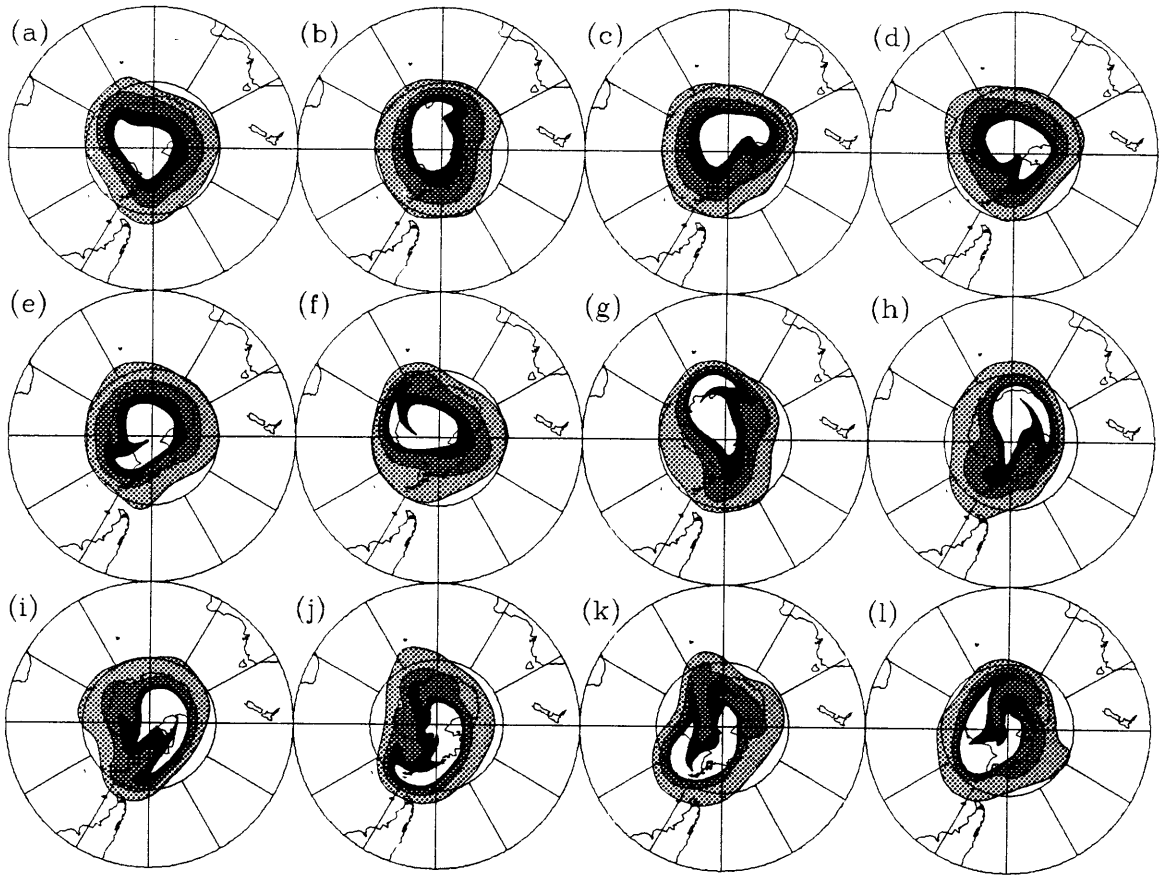

Figure 8.20: Results of a 12-day $450K$ CAS simulation initialised on 01 September 1987, and showing the advected contour distribution from (a) 02, to (l) 13 September, at one day intervals. The vortex edge lies between the two outermost contours. Polar stereographic projection with Greenwich Meridian to left, 30^o grid spacing and outer edge of plot at 30^oS.

typically occurs, consistent with the particle displacement calculations of Schoeberl *et al* (1989) and Bowman (1993), which reveal a minimum in meridional mixing at the vortex edge. (Although each of these also used NMC data for their calculations, Pierce and Fairlie (1993) find the same feature in GCM output.) Away from the vortex edge, the EPV contours occasionally buckle under the influence of small amplitude perturbations, the resulting folds to be stretched out into thin filaments. Consistent with the impressions gained from the synoptic analysis of Chapter 5, it appears to be the perturbations of relatively small spatial scales which tend to cause the initial contour buckling, rather than those of the graver scales. Noteably, at this time of the season the resulting filaments tend to wrap back in around the vortex, with very

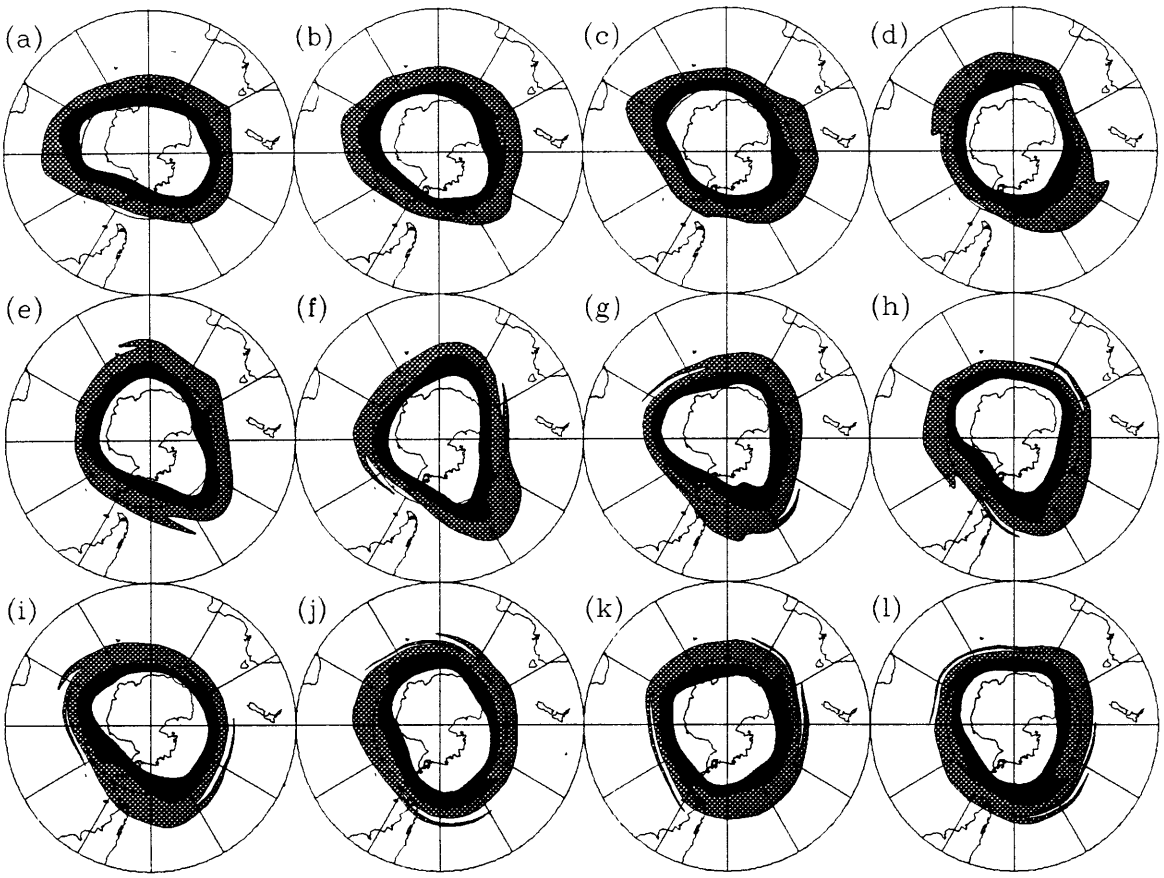

Figure 8.21: As for Figure 8.20, except for a $525K$ simulation initialised on 20 August 1987, showing the advected contour distribution at one day intervals from (a) 21 August, to (l) 01 September, and the inner contour approximately corresponds to the vortex edge.

limited net meridional excursions, and meridional transport through the vortex edge appears to be negligible.

Contrary to the results of Bowman (1993), the CAS simulations suggest this behaviour to be quite general down to levels at least as low as $400K$. (Simplified CAS simulations were not performed for lower levels, at which, Tuck (1989) argues, much greater meridional exchange occurs.)

8.2.2 The ES Stage

The CAS simulations performed for the ES stage of each season suggest that the behaviour at lower levels remains essentially the same as that for the LW period, with only very gradual contour buckling and filamentation near the vortex edge, but more frequent occurrences both equatorward and poleward. Despite the generally increasing planetary wave amplitudes during the period, however, the filaments which form beyond the jet axis at the outer edge of the vortex are only rarely advected beyond the sub-polar region, tending instead to continue to be wrapped back in around the vortex.

At higher levels, the increasing wave amplitudes distinguishing the the ES stage from the LW stage serve to bring about a gradual erosion of the vortex edge, not only by causing contour folding at larger horizontal scales, but by advecting the resulting filaments out into mid-latitudes and around the equatorward flanks of the associated anticyclones. Figure 8.22 shows a typical case of the ES stage upper level edge erosion process. For this simulation three EPV contours from the equatorward side of the vortex edge at $1000K$ were advected for 12 days from 20 August 1981. Most of the contour folding and stretching during the first few days of the simulation is due to rapid shearing out of small scale perturbations present in the initial contour pattern and which are most likely a satellite data artefact. After 25 August, however, and as noted in Section 5.3 above, an amplifying large scale perturbation tracks across the Australia/New Zealand region, deforming the contours near the vortex edge over the western Pacific, and drawing out a narrow tongue which is subsequently advected around the anticyclone into the middle latitudes. As evidenced by the innermost contour in Figure 8.22, the vortex interior remains essentially isolated during the event, and despite limited contour folding at the edge, none of the material from the interior escapes to lower latitudes.

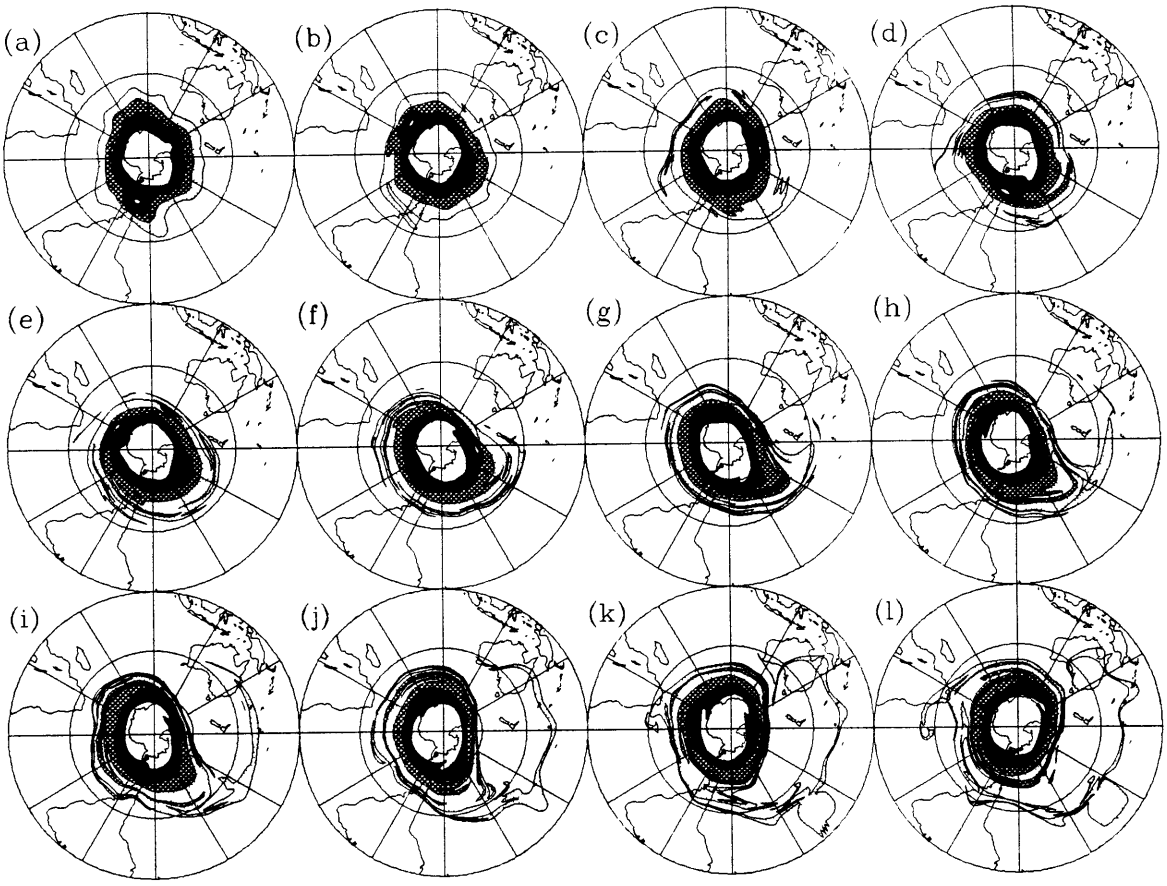

Figure 8.22: As for Figure 8.21, except for a $1000K$ simulation initialised on 19 August 1981, showing the advected contour distribution at one day intervals from (a) 20, to (l) 31 August, and the plot boundary is at the equator.

8.2.3 The LS Stage

As discussed in Section 4.4, the LS stage sees peak wave amplitudes and rapid erosion of the vortex at upper levels, while at lower levels the increasing wave amplitudes generally begin a much more gradual erosion of the vortex edge. It is also the period during which the analysis of Chapter 5 suggested the possibility arises of extrusion of ozone hole material into mid-latitudes. Accordingly, we have focussed more attention on this than the earlier stages of the seasonal evolution.

The CAS simulations performed for each season confirm, as was suggested from the analysis of the EPV evolution, that as the perturbation amplitudes increase, and as the vortex is progressively weakened, subsequent distrubances tend to have a

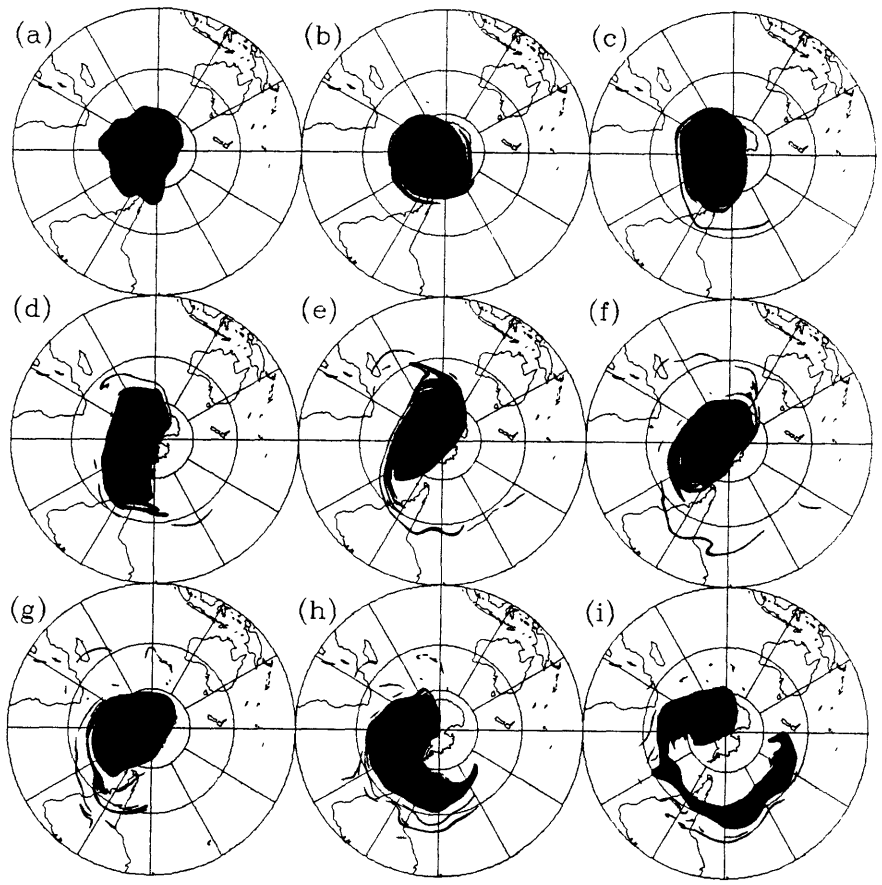

Figure 8.23: As for Figure 8.22, except for a 25-day $1000K$ simulation initialised on 01 October 1982, showing the advected contour distribution at 3 day intervals from (a) 01, to (i) 25 October. The shaded region represents the vortex interior.

more profound effect on the vortex interior at upper levels. The contour folding and extrusion process becomes more marked, occurs at larger spatial scales, and begins to involve material from deeper within the vortex, with 'McIntyre and Palmer'-type Rossby wave breaking events extruding significant amounts of the vortex interior into mid-latitudes.

Perhaps the clearest, but otherwise not exceptional, example of this type of behaviour is the sequence of events leading up to the the final warming of 1982, which was closely examined by Mechoso *et al* (1988) and was discussed in Sections 4.4 and 5.4 above. Figure 8.23 shows the results of a 25-day CAS simulation at the $1000K$ level, initialised on 01 October, for which a single contour representing the boundary of the vortex interior was advected. The simulation shows that the sequence of trav-

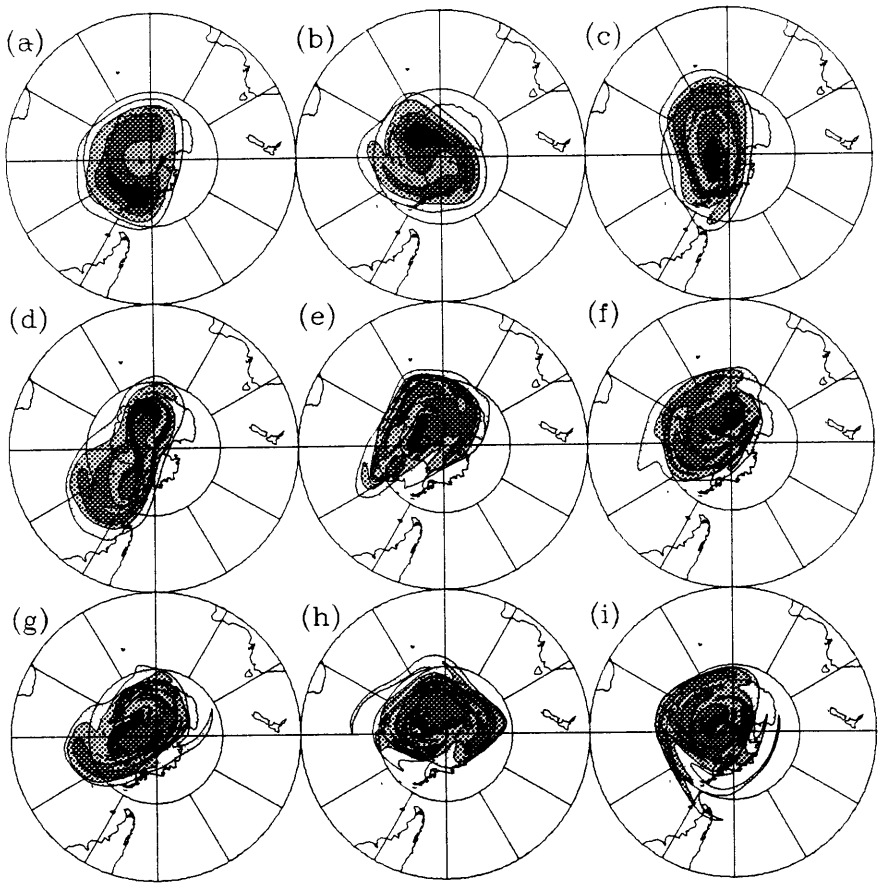

Figure 8.24: As for Figure 8.20, except for a 25-day $525K$ simulation initialised on 01 October 1982, showing the advected contour distribution at 3 day intervals from (a) 01, to (i) 25 October. The boundary of the vortex interior lies near the second outermost contour.

elling disturbances (discussed in Section 5.4) had relatively little effect on the vortex interior before later in the month, contrary to the suggestion in the EPV analyses of significant extrusion of material from within the vortex interior out into the Pacific around 14 October. On 19 October, however, in an almost explosive intensification episode, a disturbance near $60°S$ $150°W$ (Figure 8.23(g)) amplified rapidly, moved southeastward, and by 25 October had extruded a broad tongue of material comprising more than half the vortex mass out into the middle latitudes over the Pacific and Atlantic Oceans.

Despite the rather dramatic effect of the large amplitude LS stage disturbances at upper levels, lower down in the ozone hole region the vortex interior tends to

remain remarkably robust and resistant to the action of the disturbances. The major difference between the evolution at lower levels during the LS stage from that during the ES stage is a tendency for the EPV filaments which form beyond the ozone hole boundary to be peeled away from the vortex edge and subsequently sheared out and deposited in mid-latitudes.

Figure 8.24 shows the results of a 25-day CAS simulation of the 1982 October event at the $525K$ level, also initialised on 01 October. The second outermost contour approximately corresponds to the boundary of the vortex interior, while the outer contour shown represents the outer edge (the equatorward edge of the region of steep meridional EPV gradients). Despite mixing within the vortex core and contour folding at the boundary of the interior, the filaments formed there are subsequently wrapped back in around the region, the potential for extrusion of interior air out into the surrounding region being rather limited. As noted above, the behaviour beyond the core is substantially different, with much more frequent folding events occurring and significant meridional excursions of the filaments so formed into mid-latitudes.

The rapid transition in the behaviour of the contours over the small range of latitudes which separates the vortex interior from the outer edge, and the relative imprecision with which the ozone reconstruction technique allows us to locate the lateral edge of the ozone depletion region (except for the few occasions on which high resolution aircraft data are avaliable), are what makes it impossible, from the present analysis, to state definitely the extent of mid-latitude ozone dilution accompanying these LW stage dynamical events. It is this very sensitivity, however, and the much greater impact of the wave events on the tracer distribution at the higher levels, which makes it relatively easy to show, with the help of the ozone reconstructions and the CAS simulations, that endeavouring to assess the extent, or even the occurrence, of ozone dilution events on the basis of tongues of low total ozone visible in TOMS imagery, and even cruder techniques than that used here for locating the ozone hole boundary, is entirely inadequate.

Figure 8.25 shows TOMS and reconstructed total ozone distributions on 24 Oc-

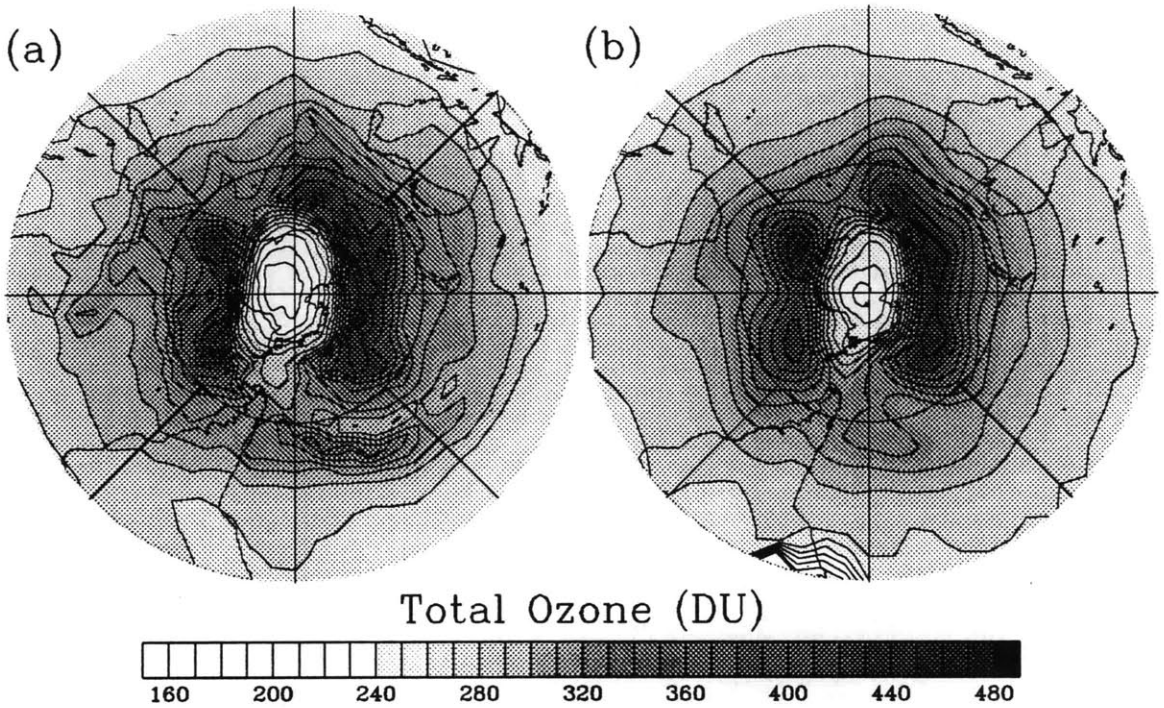

Figure 8.25: (a) TOMS and (b) reconstructed total ozone distribution for 24 October 1983. Plot parameters are as for Figure 8.17.

tober 1983. The feature of interest in the TOMS distribution in Figure 8.25(a) is the tongue of relatively low ozone extending from just south of the tip of South America out into the central Pacific Ocean near $40°S$. Bowman and Mangus (1993) and Bowman (1993) highlighted this event as an extreme example of the transport into mid-latitudes of ozone-depleted air from within the ozone hole prior to the vortex breakup. Bowman implies 14% of the ozone hole mass was involved in the extrusion event. While we cannot entirely rule out a very small (and almost certainly unnoticeable) ozone dilution effect, our analysis of the three dimensional structure of the event quite clearly demonstrates that the observed tongue of low ozone is entirely due to a combination of the deep extrusion of vortex material into mid-latitudes at levels well above the ozone hole and the *poleward* advection of low OMRs to the southeast of a relatively minor outbreak at the lower levels.

Bowman selected, apparently rather subjectively, the $275DU$ total ozone contour (obtained from asynoptic TOMS for 01 October) as defining the boundary of the Antarctic ozone hole at $450K$ on that day. He then used NMC-derived wind fields

to calculate extended-period trajectories for a selection of particles initially lying within this boundary, and implied that a resulting tongue of advected particles which was extruded out over South America and the Pacific mid-latitudes by the last week of October, and which shares the approximate shape and location of the tongue of low total ozone shown in Figure 8.25(a), establishes that the wave event extruded a significant fraction of the ozone hole out into the mid-latitudes.

Although the ozone reconstruction in Figure 8.25(b) fails to capture the details of the feature shown in the TOMS distribution, the tongue is crudely represented despite the use of a rather speculative ozone distribution for the period (recall the discussion of Section 6.4). The primary reason for the under-representation of the feature by the reconstruction is in this case the limited spatial resolution of the EPV analyses, rather than the speculative nature of the $\chi/\hat{q}$ relationships used.

To capture the details of the flow evolution at smaller scales, a set of CAS simulations, initialised from the EPV analyses of 16 October 1983, was performed for the 425, 475, 525, 575, 750 and $1000K$ surfaces, wherein a contour at each level was carefully selected to represent the maximum likely equatorward extent of the ozone depletion region on 16 October. The CAS-depicted location of these contours on 24 October is shown in Figure 8.26. Plainly evident in the Figure is the very limited extent of the outbreak at levels below $575K$, in the region of Antarctic ozone depletion. Also evident is the much more significant extent of the extrusion at higher levels. Perhaps more importantly, the location of the low level extrusion does not correspond with that of the tongue of *low* total ozone, but rather closely matches that of the tongue of *high* ozone further to the northeast. This is just the signature which might be expected, neglecting the vertical motion response, were the origin of the tongue at lower levels to lie near the circumpolar OMR maximum rather than within the ozone hole region. (Although impossible to ascertain from the diagrams presented by Bowman and Mangus, close inspection of their Figures suggests they experience the same mismatch.) Despite our uncertainty in placing precisely the lateral boundary of the ozone hole region at the start of the simulation, there seems little doubt that

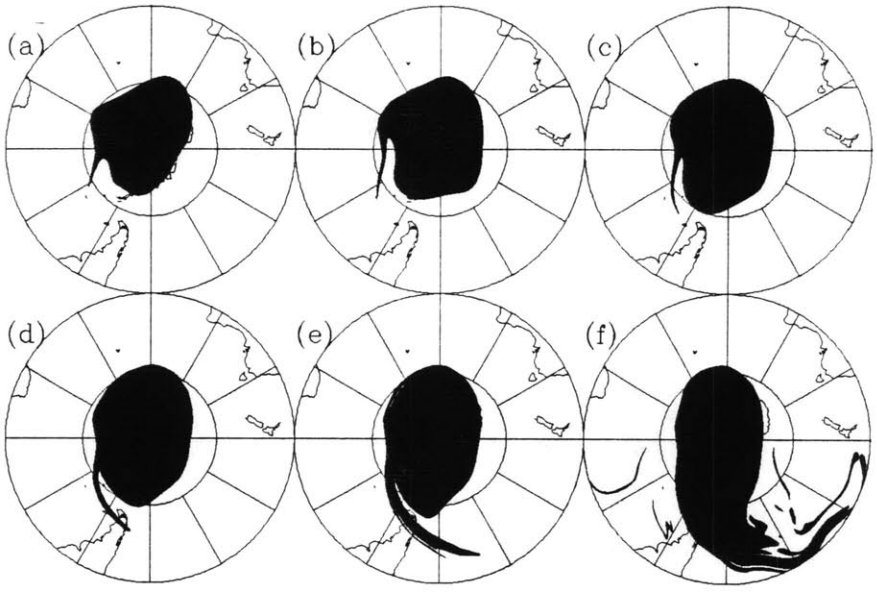

Figure 8.26: The location of the boundary of the vortex interior on 24 October 1983, at (a) $425K$, (b) $475K$, (c) $525K$, (d) $575K$, (e) $750K$, and (f) $1000K$, as depicted by 15-day CAS simulations initialised on 16 October. Gridding and map orientation are as in Figure 8.20.

the tongue of low ozone visible in the TOMS imagery is entirely unattributable to an ozone hole dilution effect. Because of this uncertainty, however, we are unable to conclude whether or not the tongue of high total ozone further east comprised an element of ozone dilution. The subtlety of the event makes the reconstruction technique inadequate in this regard.

From the above analysis, then, it is plain that the technique employed by Bowman and Bowman and Mangus, an approach which appears to have recently gained some credence, is entirely inadequate for assessing the extent of mass exchange between the ozone hole and its surroundings.

Had the event of 20 to 25 October 1983 not been accompanied by a much stronger signature at the higher levels, it is unlikely that it would have attracted the attention of Bowman and Mangus in the first place. Of interest in this regard, and reinforcing the claim that TOMS total ozone imagery, when considered in isolation, can be misleading for the identification of potential dilution events, Figure 8.27 shows TOMS

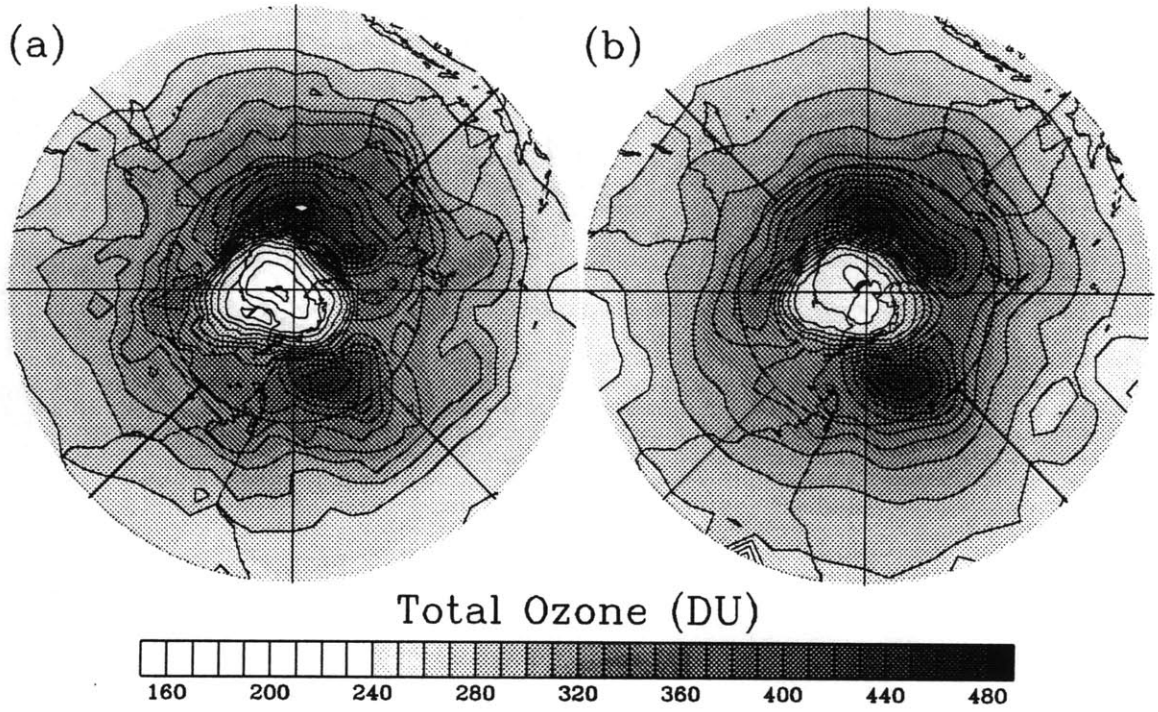

Figure 8.27: As for Figure 8.25, except for 28 October 1983.

and reconstructed total ozone distributions on 28 October 1983, a few days after the event, while Figure 8.28 shows the results of the same CAS simulation shown in Figure 8.26, but four days later on 28 October. In this case there are similar indications of equatorward advection of (the same) polar material at low levels, by this time across the dateline and over the Tasman Sea, but without a much greater extrusion at higher levels there is almost no indication in the TOMS analysis of anything of significance occurring. (As on 24 October, the slightly elevated total ozone levels along the path of the extruded filament are perhaps indicative of northwestward advection of higher OMRs, rather than ozone hole dilution.) Once again, of course, the event is so marginal that we are unable to conclude whether or not it caused an ozone dilution effect.

Numerous other LS stage examples were found of possible minor episodes of mid-latitude ozone dilution, but without exception, these proved as subtle as the above event, and no cases were found which provided incontravertible evidence. Noteably, on most of these occasions the CAS simulations suggest the outbreaks to comprise a two stage process. The first stage involves contour folding and filamentation at the

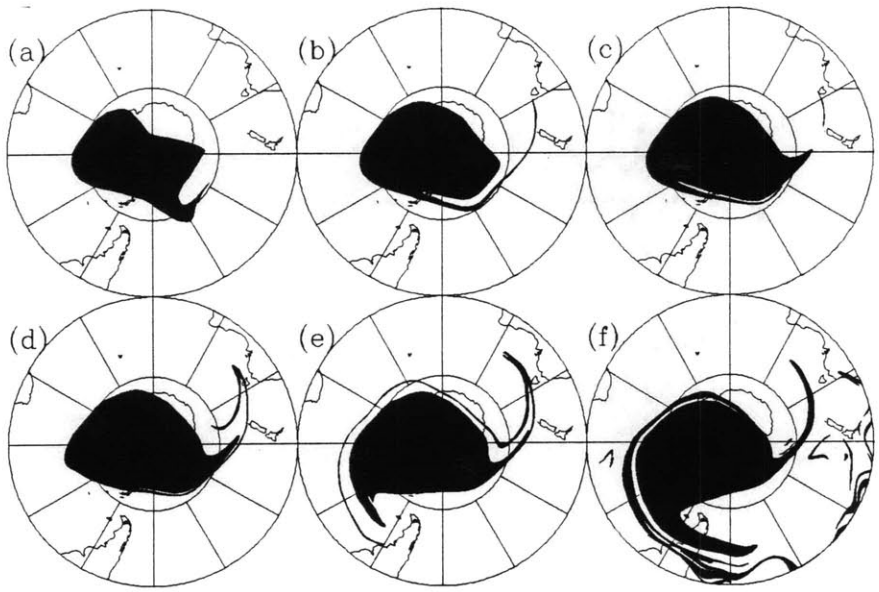

Figure 8.28: As for Figure 8.26, except for 28 October 1983.

vortex edge, generally the result of a relatively small-scale perturbation. Subsequently, a week or so later, the second stage involves a larger-scale perturbation causing the filament to be rapidly advected into mid-latitudes. Events in which the filamentation and rapid equatorward advection occur together as a single process appear to be much rarer.

8.2.4 The TT Stage

By the commencement of the TT stage, as discussed in Section 4.4 above, the vortex circulation at upper levels has been all but destroyed (the final warming, in the classical sense, has occurred), and the vortex at low levels begins to weaken rapidly under the influence of both diabatic processes and continuing dynamical activity at these levels. The CAS simulations performed for the TT stage for each season suggest that despite the more rapid weakening of the vortex circulation and the tendency for disturbance amplitudes to remain large at the lower levels, the vortex nonetheless remains rather resilient to bulk erosion, and large-scale wave breaking events do not occur: despite gross deformations of the vortex remains on some occasions, these tend to be largely elastic and reversible, and although occasional intrusions of external air

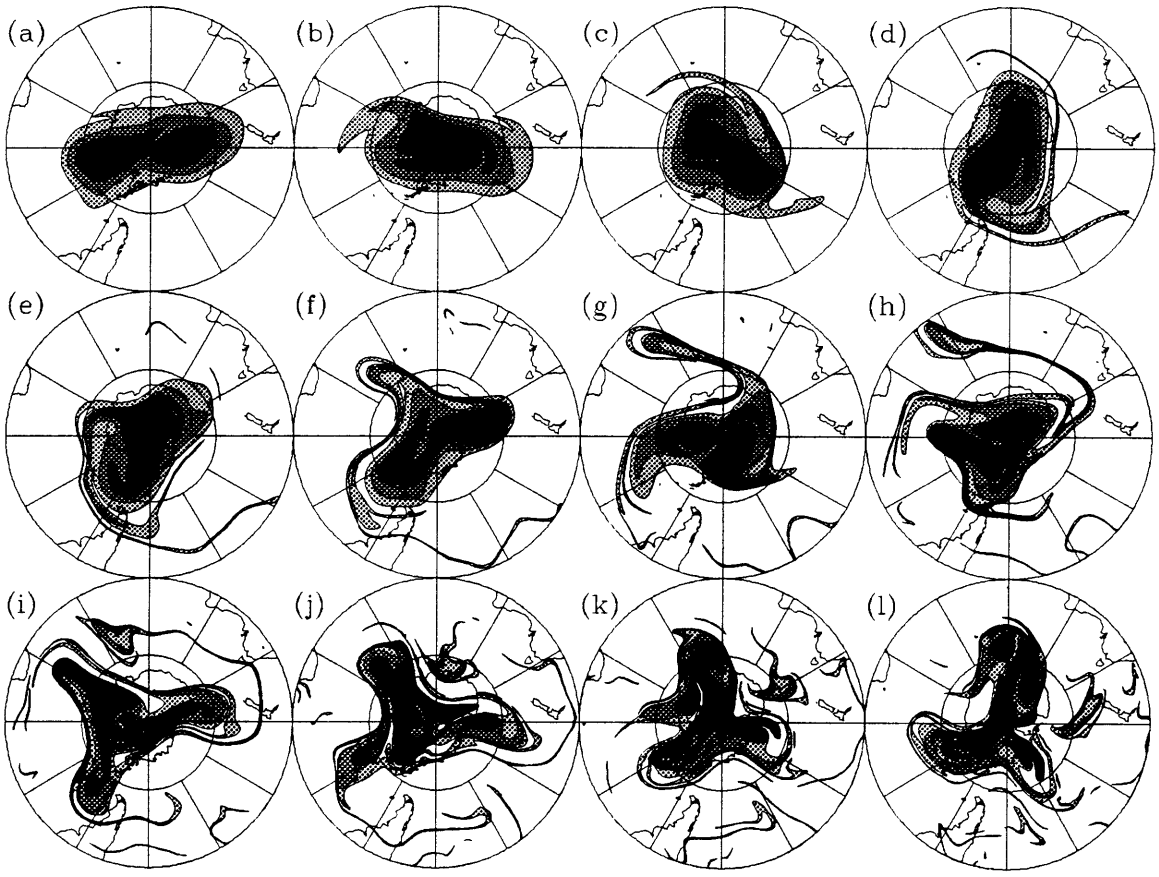

Figure 8.29: As for Figure 8.24, except for a 27-day $525K$ simulation initialised on 01 November 1982, and showing the advected contour distribution at 2 day intervals from (a) 05, to (l) 27 November.

into the vortex interior are indicated by the CAS simulations, material from deep within the vortex is not extruded into the mid-latitudes prior to the final breakup.

On the other hand, the CAS simulations suggest that on some occasions limited amounts of material from near but apparently within the ozone hole boundary are extruded into the mid-latitude flow. However, on all but one of these occasions in the seasons examined, the material was rapidly sheared into a thin sloping sheet (in three dimensions) as it was advected equatorward. Hence each event, by itself, would be expected to produce a negligible impact on the total ozone column. The only exception to this behaviour, according to the CAS runs, was an outbreak of ozone hole material over the Indian Ocean between 15 and 20 November 1982, in which one lobe of the convoluted wave 3 vortex was pinched off, subsequently to drift eastward

and be slowly sheared out over the following two weeks. Figure 8.29 shows the flow evolution at the $525K$ level depicted by a 27-day CAS simulation initialised on 01 November 1982. While the EPV analyses for the period provide only limited support for the existence of the feature, hence so too do the total ozone reconstructions (see Figure 8.13), there is perhaps a suggestion in the TOMS imagery for the period around 20 November of a local impact on the total ozone column in the central Indian Ocean. (Although not obvious in Figure 8.13(c)(i), there is a total ozone minimum near $40^{o}S$ $60^{o}E$ on 20 November. As discussed above, however, this is by no means strong evidence for the reality of the event.)

As well as the relatively rare but almost certain dilution events (albeit rather insignificant) noted above, on numerous occasions marginal events were observed in the CAS simulations, similar to those discussed for the LS stage. As was the case for the LS stage, however, the analysis technique employed is incapable of distinguishing whether these more subtle events comprise an ozone dilution component.

8.3 Summary and Implications

In the analysis described above, we have addressed the issues of mid-latitude ozone dilution occurring prior to, and accompanying, the breakup of the Antarctic ozone hole during the 1980s.

We considered first the vortex breakup period each year, when the greatest likelihood of mid-latitude ozone dilution is expected. While the coordinate transformation and ozone reconstruction techniques, when combined with the use of full CAS simulations, allowed us to carry out a detailed assessment of the extent of mid-latitude ozone dilution accompanying the initial stages the 1987 vortex breakup, our inability to perform similar full CAS simulations for the other years severely limited the prospects for a similar assessment of the breakup period of the other years. Nonetheless, the reconstructions of the ozone distribution immediately prior to the vortex breakup, together with a qualitative picture of the flow evolution following the breakup each

year obtained from a series of simplified CAS simulations, enabled us to arrive at a crude estimate of the likely extent of mid-latitude ozone dilution accompanying the vortex breakup each season. This also provided some insight into the degree of inter-annual variability generally to be expected, and the principal factors which determine the extent of mid-latitude ozone dilution in a particular year.

Our crude assessment is that the extent of mid-latitude ozone dilution accompanying the dispersion into mid-latitudes of the Antarctic ozone hole debris following the breakup each year is probably as strongly dependent on the dynamical nature of the breakup as it is on the severity of the springtime Antarctic ozone depletion. The CAS simulations suggest that there is considerable interannual variability, not only in the thoroughness of the dispersion at those levels where the vortex is dynamically destroyed, but also in the depth of the destruction process. Whereas in 1986, for example, a significant fraction of the vortex debris at ozone levels appears to have remained essentially confined to the polar region and may not have been dispersed into the middle latitudes at all, in 1983 the process appears to have been not only much more thorough, but also extended down to about the $425K$ level. Of course, quantitative mass flux calculations have not been performed to confirm the general impressions gained from the CAS simulations.

Nonetheless, to arrive at a crude semi-quantitative estimate of the overall effect on the mid-latitude column of the Antarctic ozone depletion each year, we assumed that our qualitative interpretation of the dispersion process accompanying the post-breakup period each year to be essentially correct. We also assumed that our assessment of the three-dimensional structure of the Antarctic ozone hole each year, relative to that in the first few years of the decade, is essentially correct. Accordingly, and neglecting the effects of photochemical changes to ozone during the dispersion process, we estimated that the resulting overall mid-latitude ozone dilution in early summer would have been of the order of 3% of the mid-latitude column in 1987, around 2% in 1983 and 1985, slightly less than this in 1984 and 1989, and less than 1% in the other years since 1981. Making equally crude allowance for slow photo-

chemical relaxation of lower stratospheric ozone levels in the mid-latitudes during the early summer period, these values would be about 1/3 smaller.

Considering this effect entirely in isolation, the implied and generally increasing overall ozone hole dilution effect during the 1980s might explain a linear downward decadal trend of up to a few percent in zonally averaged summertime mid-latitude total ozone. In this context, it is of note that Niu *et al* (1992), who performed a seasonal trend analysis on the recently revised TOMS total ozone data set (from 1979 to 1990) found a mean southern hemisphere mid-latitude decadal trend in total ozone which was about two percent larger (more negative) in summer than for the spring period. (Their estimates for the summer period were $-2.78 \pm 0.14\%$ at 35^oS and $-4.29 \pm 0.18\%$ at 45^oS, while the respective springtime trends were $-0.82 \pm 0.25\%$ and $-2.59 \pm 0.35\%$. The summer estimates were between 1/2 and 1% smaller (less negative) than the corresponding estimates for the winter months.) On the basis of the above analysis, we speculate that a substantial contribution to the difference between the mid-latitude decadal trends for the spring and summer periods might be due to the gradual onset at mid-latitudes during the 1980s of an annual zonal mean summertime Antarctic ozone hole dilution effect.

As well as the more general and effectively 'irreversible', zonal mean impact of the ozone hole breakup each season, we considered more briefly the occurrence of localised, more marked but temporary mid-latitude dilution events due to the local passage of still-coherent remnants of ozone hole material accompanying the initial stages of the breakup each year. The CAS simulations suggest that these transient events do occur, and that their occurrence and severity are dependent on the dynamical nature of the vortex breakup and on the vertical structure of the Antarctic ozone depletion. Our inability to perform CAS-based reconstructions for the relevant periods prevented closer examination of each of the events identified, however. Nonetheless, the CAS simulations performed suggest that, in general, significant transient events are more likely to accompany the vortex breakup when the low level vortex remains are split in two prior to their advection into mid-latitudes, that there appears to be a tendency

for such events to occur over the Pacific and South American regions, and that on occasions they may comprise as much as a 10 to 15% decrease in total ozone, lasting locally from a few days (if embedded in a westerly flow) to a few weeks (if the remnant stagnates over the region prior to gradual dispersion).

To address the issue of mid-latitude ozone dilution prior to the vortex breakup each year, we examined each of the potential dilution events identified in the examination of the dynamical evolution described in Chapter 5, by performing analysis-based reconstructions for each period and augmenting these with simplified CAS simulations of the flow evolution.

The examination based on the ozone reconstructions alone indicated that there were no occasions prior to the ozone hole breakup in any of the years examined on which broad-scale ozone dilution events occurred (i.e. events clearly resolvable in the EPV analyses.)

The CAS simulations, however, provided a more detailed picture of the flow evolution by depicting features unresolvable in the EPV analyses, and so allowed us to describe distinct characteristics of each of the four stages of the dynamical evolution discussed in Section 4.4, which were not as apparent from the examination of the EPV analyses themselves.

The CAS simulations showed that during the LW stage of the evolution each year the Antarctic ozone hole remains almost completely isolated from its surroundings, insofar as quasi-horizontal advection from within the vortex interior into the surrounding region, due to Rossby wave breaking events, is not observed. i.e. Mid-latitude ozone dilution events do not occur at this stage of the season. The simulations also suggest that meridional transports in the sub-polar region surrounding the vortex are small in the LW period, and despite contour folding and filamentation, the filaments tend to wrap back in around the vortex.

During the ES stage of the evolution, despite a somewhat greater degree of contour folding and filamentation than in the LW stage, the CAS simulations suggest the

Antarctic ozone hole region remains essentially isolated from its surroundings. Beyond the vortex edge, however, the filaments formed tend to be more commonly advected into mid-latitudes, suggesting gradual mechanical erosion of the outer edge of the vortex.

With the arrival of the LS stage, and the largest disturbance amplitudes of the season, this tendency for the contour filaments from the vortex edge region to be advected into mid-latitudes increases further, and begins to involve material from near the boundary of the ozone hole. While on some occasions the material deposited in mid-latitudes may have originated within the ozone hole, the ozone reconstruction technique, employed solely on the SAGE data, is not sufficiently accurate to determine whether some of these events might comprise a small ozone dilution component. On the other hand, the CAS simulations showed no evidence for the extrusion of material from deep within the ozone hole out into mid-latitudes i.e. all the cases noted were marginal.

While the imprecision of the ozone reconstruction technique adopted led to our failure to reach a definite conclusion in regard to the extent of ozone dilution during the LS stage, it enabled us to show, equally importantly, that more simplistic approaches to the ozone dilution issue, such as that adopted by Bowman and Mangus (1993) and Bowman (1993), are entirely inadequate. If such events occur at all during the LS stage of the evolution, they are particularly subtle, and the question is only likely to be resolved by detailed examination of the three dimensional evolution at higher spatial resolution than that achieved in the present work.

The CAS simulations, combined with the ozone reconstructions, show that after the commencement of the TT stage of the evolution, relatively frequent extrusions of ozone hole material into the mid-latitudes almost certainly occur as the disturbances progressively erode material from the vortex edge. With apparently only one exception in all the seasons examined, however, the amount of material eroded during each event was small and the filaments were rapidly sheared out in both the vertical and horizontal, so it seems unlikely that these events would produce a noticeable impact

on the mid-latitude ozone column.

Overall, then, the qualitative examination of the pre-breakup period leads us to speculate that extrusion of ozone-depleted polar air into mid-latitudes prior to the vortex breakup each year does not have a significant impact on the mid-latitude ozone column, either in the short term through transient events, or in the longer term by producing a gradually accumulating mid-latitude deficit as the season progresses. This is not because dilution events do not occur, but because they appear to involve a rather insignificant fraction of the ozone hole mass. Of course, without more detailed examination than has been performed here, this interpretation remains open to question.

Chapter 9

Conclusions

In the present work, described above, we have performed an observational investigation of the Antarctic ozone hole dilution effect: the extrusion of ozone-depleted air from within the ozone hole out into the middle latitudes of the southern hemisphere, prior to and accompanying the annual breakup of the polar vortex in the lower stratosphere.

The first objective of the investigation was to perform a detailed analysis of a previously-identified event which accompanied the vortex breakup during early December 1987. The analysis has provided a clearer understanding of the nature of the 1987 event. Overall, we conclude as follows.

1. Accompanying the breakup of the polar vortex at lower levels during early December 1987, a small but significant ozone dilution effect was experienced at southern mid-latitudes.

More specifically,

(a) The observed hemispheric distribution of the local changes in total ozone between 02 and 14 December was primarily attributable to quasi-horizontal ozone transports, with a smaller but significant contribution

due to vertical motion of the isentropes.

While the observed hemispheric pattern of total ozone changes during the period is reproduced qualitatively by consideration of horizontal transports alone, close quantitative agreement between the observed and reconstructed changes requires inclusion of allowance for the vertical motion component, particularly at higher latitudes where the latter contributes as much as 30% of the overall response. The dominance of the horizontal component at this stage of the season is explained as a consequence of the vortex breakup at upper levels, which is responsible for most of the seasonal transition in the stratospheric temperature distribution (the isentropic pressure distribution), having already occurred prior to the beginning of December 1987.

(b) The hemispheric distribution of the vertical motion component of the total ozone changes between 02 and 14 December was primarily attributable to large-scale dynamical processes occurring in the stratosphere.

This, and the relative smallness of the vertical motion contribution compared to that due to horizontal transports, reinforces the view that examination of local changes in tropopause height or isobaric temperature in the upper troposphere, for example, can only enable a crude qualitative estimate of the broadscale total ozone changes occurring at this stage of the season, and quantitative assessment, and understanding, requires detailed consideration of the dynamical processes occurring in the stratosphere.

(c) The hemispheric distribution of the contribution to the observed total ozone changes during the period due to quasi-horizontal advection was primarily attributable to 'natural' ozone transports.

In the absence of Antarctic ozone depletion, the broad pattern of total ozone changes throughout the hemisphere during early December 1987 would have been similar to that observed. In this respect, the ozone reconstructions suggest that the observed total ozone decreases over southeastern Australia and South America can be explained entirely in terms of natural processes. This result is of particular interest since it was the observed sudden decrease over the former region which originally prompted

the earlier examination of the event by Atkinson *et al* (1989). Nonetheless, while the reconstructions show that the observed decreases over these regions can be explained 'naturally', persisting uncertainties about the accuracy of the CAS simulations performed for the period mean that a small ozone dilution component at these locations cannot be ruled out.

(d) Despite the dominance of 'natural' transports in bringing about the total ozone changes observed at most locations, a significant temporary ozone dilution effect involving a total ozone deficit of up to about $40DU$ (10 to 15% of the mid-latitude ozone column) was experienced over the southwest Indian Ocean and southwest Pacific Ocean by 14 December 1987, with a smaller effect present across the Atlantic Ocean as far north as 35^oS and the southwest Pacific (including New Zealand) and western Indian Oceans as far north as 40^oS.

The above estimates were made by assuming no Antarctic ozone depletion occurred during the spring period in 1980. They are therefore rather conservative. In the more likely situation that by 1980 springtime Antarctic ozone depletion was already underway, with a peak total ozone deficit in early October of, say, $50DU$, then the actual magnitude of the 1987 ozone dilution component might be substantially (say up to 50%) larger than that suggested above. Under these circumstances the region affected is unlikely to have been much different, however. Additional uncertainties are associated with the precise boundary of the region affected by the event by 14 December, which derive from uncertainties both about the accuracy of the CAS simulations employed for the analysis, and about the precise boundary of the Antarctic ozone depletion region immediately prior to the vortex breakup. Nonetheless, in this respect as well, the results are considered conservative: while a larger region may have been affected, it is unlikely to have been significantly smaller.

Because the detailed analysis of the early December 1987 period indicated that the full potential for mid-latitude ozone dilution may not have been achieved by mid-

December, the subsequent CAS-depicted dynamical evolution was examined more briefly, with the following conclusion.

2. It is very likely that a small but significant Antarctic ozone hole dilution effect, comprising perhaps a few percent reduction in total ozone below normal levels, spread gradually throughout the middle latitudes of the southern hemisphere during the latter half of December 1987, thereafter to decay slowly due to natural photochemical processes.

Although the results of the brief analysis suggest this to be a reasonable conclusion, it remains tentative, since it was arrived at by only crude and qualitative interpretation of the CAS-depicted material evolution and equally crude allowance for photochemical processes. Confirmation that such a longer-term effect was experienced at mid-latitudes during the summer of 1987 requires more detailed chemical/dynamical modelling of the stratospheric material evolution during the period.

Having established that the dynamical destruction of the ozone hole during December 1987 produced a mid-latitude ozone dilution effect, the broader issue was then considered of ozone dilution accompanying the breakup in the other years of the 1980s, and of dilution events prior to the vortex breakup each year. In relation to these broader issues, we conclude as follows.

3. There were no occasions during the 1980s of deep, broadscale mid-latitude ozone dilution events in the spring season prior to the vortex breakup at low levels.

That is, based solely on the analysis-derived ozone reconstructions for the eleven seasons examined, no events were identified in which material from within the polar vortex at ozone hole levels was extruded into mid-latitudes at scales resolvable by the EPV base analyses.

4. During the late winter and early spring, prior to the appearance of large amplitude disturbances in the stratosphere and rapid weakening of the vortex at upper levels, the prospects for either sub-polar or mid-latitude ozone dilution, even at small scales, appear to be negligible.

Of the numerous CAS simulations performed, none suggested signs of extrusion of material from within the ozone hole into the surrounding regions. Although the simulations suggest that the vortex interior is subjected to almost continuous mixing during the period, as is the region beyond the vortex edge, and that the degree of mixing, at least beyond the edge, tends to increase as the season progresses, the two regions appear to remain almost entirely isolated from one another, implying almost complete chemical containment within the ozone hole region. However, we can not rule out the occurrence of other processes by which exchange of material might be effected between the vortex interior and its surroundings, a matter not considered in the present work.

5. During the latter part of the spring season, up to the final breakup of the Antarctic ozone hole each year, the extent of mid-latitude dilution appears to remain insignificant, despite evidence from the CAS simulations of a gradually-increasing tendency as the season progresses for narrow filaments of ozone hole material to be extruded into mid-latitudes.

Once again this finding is somewhat tentative. Firstly, the ozone reconstruction technique adopted, despite the efforts made to arrive at detailed three-dimensional descriptions of the ozone distribution, does not define the edge of the Antarctic ozone depletion region with sufficient accuracy to determine which of the many marginal extrusion events observed actually involved ozone-depleted material and which only comprised material from just beyond the edge. Despite the large disturbance amplitudes at this stage of the season, and the rather common occurrence of small scale extrusions from the vortex edge, the vortex interior appears to remain remarkably robust and resilient to erosion. It is only toward the end of the period, once the vortex at upper levels has been destroyed and the circulation at lower levels weakens rapidly, that firmer evidence was found for the extrusion of ozone-depleted material

into mid-latitudes. Even for these latter events, however, the extrusion process depicted by the CAS simulations occurs at such fine scales (in all cases but one), that without detailed mass flux calculations, which have not been attempted, quantitative assessment of their mid-latitude impact is unattainable. Notwithstanding these uncertainties, the subjective impression gained from examination of the numerous CAS-depicted events observed at this stage of the season was that the overall amount of ozone hole material involved is insignificant.

6. Despite the inadequacy of the adopted technique for determining quantitatively the extent of pre-breakup ozone dilution, or even in many cases for determining whether an event involved an element of ozone dilution at all, its use demonstrates that cruder techniques for the analysis of these subtle dynamical events, such as that employed by Bowman (1993), are entirely inadequate.

Specifically, because of the strong meridional gradient at the vortex edge in the extent of the CAS-indicated mixing process, accurate location of the lateral edge of the Antarctic ozone depletion region *at the vertical levels examined* is essential if the matter of ozone hole isolation prior to the vortex breakup is to be resolved. Further, the detailed vertical structure of these subtle events which is indicated by the CAS simulations suggests that quantitative evaluation of the extent of ozone hole confinement requires consideration of the full three-dimensional structure of each event. Hence making quantitative assessments by assuming not only that total ozone is a conserved property in the stratosphere, but also that the dynamical processes occurring are essentially barotropic, as does Bowman (1993), is entirely inappropriate and can lead only to erroneous conclusions.

7. Accompanying and subsequent to the low level breakup of the polar vortex each year, a significant impact on mid-latitude ozone can occur, but its magnitude is as much dependent on the dynamical nature of the vortex breakup as it is on the severity of springtime Antarctic ozone depletion in that year.

This finding, also, is rather tentative, in that it is based on the subjective impressions gained from the CAS simulations. Its correctness relies both on the accuracy of our interpretation of the CAS depictions of the material evolution, and on the effectiveness of CAS in correctly representing the material evolution during the breakup period of each season, which has not been independently assessed.

(a) Transient Events.

The analysis reveals that significant transient mid-latitude dilution events can occur in some years in association with the vortex breakup. With an Antarctic ozone depletion similar to that in 1987, for example, these events can produce localised temporary ozone deficits of as much as 10 to 15% of the mid-latitude ozone column, lasting from a few days to a few weeks, and generally occurring during December. In those years when the weakened vortex is displaced from the pole intact, it tends to be advected initially no further than the sub-polar region and subsequent stripping and dispersion of its remains comprises a small-scale filamentation process, with little potential for subsequent sudden and marked local decreases in mid-latitude total ozone. On the other hand, when the vortex breakup is accompanied by a splitting of the vortex remains (as in 1987 and 1989 for example), the lesser remnant tends to be advected further north, and the CAS simulations suggest this can produce localised but significant transient dilution events at middle latitudes.

(b) An Overall Dilution Effect.

According to the CAS simulations a smaller but more widespread and longer-term dilution effect is to be expected each summer, but the extent of the effect, although logically dependent on the severity and areal extent of the Antarctic ozone depletion, appears to be equally sensitive to both the depth and the completeness of the vortex destruction process. With the base of the ozone hole lying beneath the lowest level at which the breakup occurs each year, the lower the base of the destruction process, the more severe the mid-latitude impact, and the analysis suggests significant interannual variability in the depth of the breakup. Similarly, there appears to be considerable interannual variability in the thoroughness of the subsequent dispersion of the ozone

hole debris throughout the middle and high latitudes. Hence we estimated that in 1983, despite a relatively moderate ozone hole, with the thorough vortex destruction extending down to below $425K$, the summertime mid-latitude impact would have been marginally greater than that in 1989, even though a more severe ozone hole was observed in 1989, because of the relative shallowness of the breakup that year. In 1986 on the other hand, although the breakup was quite deep, most of the ozone hole debris remained confined to higher latitudes, preventing a noteworthy mid-latitude dilution effect from being experienced.

8. The differences observed by Niu *et al* (1992) between overall spring-time and summertime trends in southern mid-latitude total ozone during the 1980s might be largely attributable to an overall trend in summertime mid-latitude ozone dilution during the period.

During the spring period prior to the vortex breakup we have implied a negligible mid-latitude impact of Antarctic ozone depletion is likely. Our assessment for the summer period, neglecting all other influences on mid-latitude ozone levels, would imply a decadal decrease in mid-latitude ozone at this time of year of up to a few percent, and this is not inconsistent with the magnitude of the differences between spring and summer trends observed by Niu *et al* (1992) to have occurred between 1979 and 1990. Of course, this suggestion is highly speculative, and the observed differences may well be the result of some other influence, with the broad agreement between our crude estimate and the observed behaviour being merely coincidental.

Preparatory to carrying out the latter part of the investigation, it was necessary first to examine the dynamical evolution in the austral spring stratosphere in each of the years examined, and also to build up a picture, using the available SAGE ozone data and the coordinate transformation technique, of the ozone evolution in each season. Nothing new and conclusive arose from the dynamical analysis, the primary purpose of which was to identify the potential ozone dilution events which occurred each season. The analysis performed has nonetheless reinforced the view

that current understanding of the dynamical mechanisms responsible for the observed behaviour in the southern hemisphere stratosphere is far from complete. Not only is the question of the sources of the observed wave behaviour a highly contentious issue yet to be adequately resolved, the present examination suggests that non-linear processes probably play an important role in the stratospheric evolution, despite the expectation that, with such a strong westerly flow regime present in the springtime, linear theory should provide most of the answers. While the dynamical analysis was by no means rigorous, the examination of the ozone evolution, which suggests the ozone distribution to be perhaps as sensitive to the dynamical behaviour occurring at smaller scales as it is to the planetary scale activity, lends support to the impressions gained from the dynamical analysis. Irrespective of the precise impact of the dynamics on the ozone distribution, the examination of the ozone evolution led to the identification of several unexpected features.

9. According to the SAGE ozone measurements, the tropical ozone mixing ratio maximum during the spring period generally occurs at levels at or below the $10hPa$ level, not at or above this level as suggested by previous analyses of ozone climatology.

In view of the high vertical resolution and expected accuracy of the SAGE data in the middle and upper stratosphere, we suggest that the SAGE instrument better describes the actual behaviour in this respect than the earlier analyses.

10. The annual maximum in total ozone at southern mid-latitudes during October is not, as is held by conventional wisdom, generally the result of the downward diabatic flux of high ozone mixing ratios into the lower stratosphere accompanying the seasonal wave amplitude maximum, but is rather generally due to both poleward and downward transport occurring at higher levels. In the lower stratosphere maximum mid-latitude ozone mixing ratios tend to decrease monotonically with time on isentropic surfaces and remain essentially constant on isobaric surfaces.

11. Large differences are evident in springtime ozone mixing ratios in

the austral lower stratosphere, not only at high latitudes but also in middle latitudes, as measured by the SAGE I instrument (1979 to 1981) and the SAGE II instrument (1984 to the present), and as previously noted by McCormick *et al* (1992).

Substantial differences (implying, if real, a decadal trend of up to 50%) were noted at mid-latitudes in the lower stratosphere ($400K$ to $500K$) between the ozone values observed by the two instruments. The availability of ozone sonde data during the early 1980s is very limited, but while the evidence from these data is very weak and may not be significant, they tend to support rather than contradict the SAGE data. It is not clear from the present analysis if the indicated decreases at the lowest levels are real, or due to SAGE I data degradation at the lower levels (the SAGE I instrument, which sampled less wavelengths than SAGE II, was more prone to aerosol-induced errors at the lower levels than SAGE II). The decreases indicated are nonetheless consistent with those identified in the SAGE data trend analysis of McCormick *et al* (1992), the northern hemisphere counterparts of which they found to be consistent with trends derived from Hohenpeissenberg ozone sonde data. The implications of these changes at the lowest stratospheric levels are intriguing. While in the present analysis we have not considered the early winter period, our examination suggests the sub-polar decreases are probably not attributable to the Antarctic ozone depletion mechanism. We speculate that if they can be connected to another, as yet little understood, ozone depletion mechanism occurring at sub-polar (and/or tropical) latitudes (e.g. via chlorine conversion by liquid sulphuric acid droplets), then the present analysis, which has indicated that considerable mid-winter mass exchange occurs between middle and sub-polar latitudes, suggests potential for a different mid-latitude ozone dilution process. Were this the case it might help to explain the observed mid-winter ozone decline at middle latitudes.

Overall, then, the investigation conducted was largely successful in that it has enabled a crude assessment to be made, based solely on observational data, of the

mid-latitude ozone dilution issue. Nonetheless, it has raised as many questions worthy of further attention as it has answered.

Of particular relevance and importance, in relation to the present work, are several questions concerning the meteorological data set used, the SAGE ozone data, the CAS technique, and the coordinate transformation technique employed.

We have noted inaccuracies in the total ozone reconstructions, particularly for the latter stages of the seasonal transition, which may derive from inaccuracies in the NMC data set upon which much of the examination was based. We also noted that it may not be possible to assess the extent of these errors precisely, because all operational data sets are based to a greater or lesser extent on the same satellite temperature retrievals, which have limited vertical (hence spatial) resolution. Nonetheless, the accuracy issue is important and needs to be pursued if similar investigations are to be performed with confidence. Perhaps the high resolution data set becoming available from the UARS satellite, or the even higher resolution insitu data occasionally provided by high altitude aircraft missions, can be used to shed more light on the issue.

The question of SAGE data accuracy, particularly for SAGE I at the lower stratospheric levels, has been touched on above, and warrants further attention. Noteably, and as pointed out by Schoeberl and Lait (1993), the intrinsic power of the coordinate transformation technique now provides a new and valuable opportunity for simultaneous intercomparison and validation of observations from virtually any platform, essentially irrespective of observation time (within reason) or location, and not only those for ozone, but also any other suitably long-lived atmospheric tracer.

Use of the CAS technique for tracer studies is a relatively novel innovation which also has great potential for advancing understanding of the dynamical processes and transports occurring, both in the real atmosphere and atmospheric models, over a broad spectrum of spatial scales. The questions raised about the accuracy of the CAS technique also require attention. Not only do we need to know its effectiveness at portraying the flow evolution in relatively chaotic flows where the dominant scales

of motion fall close to or beneath the grid resolution of perfectly accurate advecting wind fields, but also its effectiveness in depicting the evolution in not so chaotic flows when significant errors are present in the advecting wind fields.

We noted that our difficulty in distinguishing between ozone dilution events during the latter part of the spring period and those which did not affect the ozone hole interior stemmed from the inadequacy of the ozone reconstruction technique adopted. The question remains as to whether the required level of accuracy can be achieved using the SAGE data and a refined version of the coordinate transformation technique, or whether additional or alternative data sets are required. In regard to the former possibility, numerous options are available. Among these are the use of a different or higher spatial resolution meteorological data set for the derivation of the base EPV fields, a not-so-crude technique for vertical interpolation, a superior technique for obtaining the $\chi/\hat{q}$ relationships, reversion to a q coordinate rather than the $\hat{q}$ coordinate, and introducing allowance for diabatic drift (as described e.g. by Schoeberl and Lait, 1993). It seems likely that the introduction of these modifications might largely overcome the problems. In regard to the latter possibility, incorporation of all available ozone data, including SBUV, sondes and aircraft, or alternatively by repeating the analysis using e.g. NO_2 data instead of ozone are possibly worthy of consideration.

As well as these matters concerning the pre-breakup vortex isolation question, we noted above that, accompanying the vortex breakup, ozone dilution can occur both as transient events and as a longer-term impact on mid-latitude ozone levels. While full CAS simulations of the breakup period for other than 1987 were not practicable in the present work, they would allow a more quantitative assessment to be made of each of the transient events identified in the other years, and this may comprise a worthwhile task which merely requires sufficient supercomputer access to perform the simulations (about 10 hours per simulation). The subtler effect of longer-term ozone dilution will be more difficult to quantify precisely, requiring either accurate mass flux calculations (which are in principle obtainable from the CAS output) and more

detailed allowance for photochemical processes, or the use of a sophisticated three-dimensional model, initialised with the observed pre-breakup ozone distribution, and driven by the observed dynamics.

As noted above, understanding of the observed dynamical behaviour in the austral spring stratosphere is far from complete and many fundamental issues are yet to be resolved, such as the cause of the mid-winter lull in wave activity, the source(s) of the transients, the reasons for such a marked degree of interannual variability, not only in wave amplitudes and structure, but also, apparently, in the vortex decay process during spring. Surprisingly little is known of the details of the ozone evolution, or the precise impact of the dynamics on the ozone distribution. A small but important step in this direction would be the assembly of a more careful and thorough climatology than that achieved in the present work, by applying the reconstruction technique to all the available ozone data from the last decade or so.

Finally, and with particular relevance for the nations of the southern hemisphere, two additional points are of note, each of which derives from the remarkable utility of the ozone reconstruction technique as demonstrated in the present work. The first is that, given suitably accurate dynamical model predictions for the austral stratosphere, and sufficient access to SAGE or alternative ozone profile data from the recent past, the possibility of forecasting total ozone levels throughout the extratropical regions of the southern hemisphere appears to be in reach. Secondly, and perhaps more importantly, whereas conventional wisdom holds that a ground-based ozone sonde network involving numerous stations rather evenly distributed about the hemisphere (a near impossibility in the southern hemisphere) is necessary for adequate monitoring of lower stratospheric ozone, on the basis of the present work it is evident that a high quality network of about seven lidar or ozone sonde stations, required to be strategically distributed in latitude only, and producing one or two ozone vertical profiles per week, would serve as an adequate basis for routine monitoring of the lower stratosphere. Of course, this would probably not suffice for adequate tropospheric monitoring, and continued routine satellite monitoring is essential for adequate cov-

erage above the lower stratosphere.

In closing, and in relation to the outstanding questions concerning mid-latitude ozone dilution, the NASA ASHOE and MAESA missions planned for the southern hemisphere during 1994 will provide an excellent opportunity, not only for advancing understanding of the chemistry behind mid-latitude ozone depletion, but also to investigate several of the issues raised above. While the conclusion of the missions in October will probably preclude the opportunity for examining the post-breakup period, they will no doubt provide a wealth of information with which to examine more closely such issues as the extent of pre-breakup ozone hole isolation, and the effectiveness of CAS, when employed on operational meteorological analyses for the southern hemisphere, in accurately depicting the small scale features of the flow evolution.

Appendix A

Colour Graphics

Figures A.1 to A.11 show the daily evolution, from 01 August to 31 January in each of the seasons examined (1979 to 1989) of $525K$ EPV and TOMS total ozone.

Part (a) of each Figure is a Hovmöller diagram of daily $525K$ EPV (versus longitude) at $50°S$. Blue colouring (or darkest shading) depicts high EPV (polar air) and red colouring (or medium shading) depicts low EPV (tropical air). The diagram shows the daily evolution of the zonal structure of mid-latitude wave activity during the season, the red/orange regions showing the 'disturbances' and the blue regions the vortex 'lobes' discussed in Chapter 5.

Part (b) of each Figure shows the seasonal evolution of zonal mean EPV (versus latitude). The polar vortex shows up as blue and tropical air as red/orange. Also apparent are any significant polar outbreaks which occurred during the season, and for some years a gradient reversal associated with the movement of the vortex remains off the pole, or the extrusion of significant tongues of high EPV from the vortex out into mid-latitudes, is visible as a green mid-latitude 'smoke plume' in the plot.

Part (c) shows the corresponding zonal mean evolution of TOMS total ozone versus latitude. The polar ozone minimum shows up as red colouring, the mid-latitude ozone maximum as blue. The expected signature of significant mid-latitude ozone dilution events (which also results from dynamically-induced total ozone changes not

necessarily attributable to ozone dilution) is a 'saw tooth' of rapid decrease in mid-latitudes, sometimes preceded by a rapid increase over the pole a few days early and propagation of a temporary ozone decrease through the ozone maximum region, to produce the 'saw tooth' at mid-latitudes.

Each of (a), (b) and (c) in each Figure is a 'normalised' pixel plot. For maximum visual impact, all values are first normalised and the plot mean and standard deviation are calculated (the respective values are shown in the bottom right corner of each plot). Assuming the values in each plot to be normally distributed about the mean, each point is next assigned a percentile value from the cumulative frequency distribution, which is then converted to an integer pixel value from 0 to 221 by linear interpolation from the percentile range. Missing values and those more than three standard deviations from the mean are set to -1 (black). Finally, the full pixel range is divided equally among 36 colours, which are shown in the colour bar at the bottom of each Figure and which have been assigned to accentuate the middle of the range.

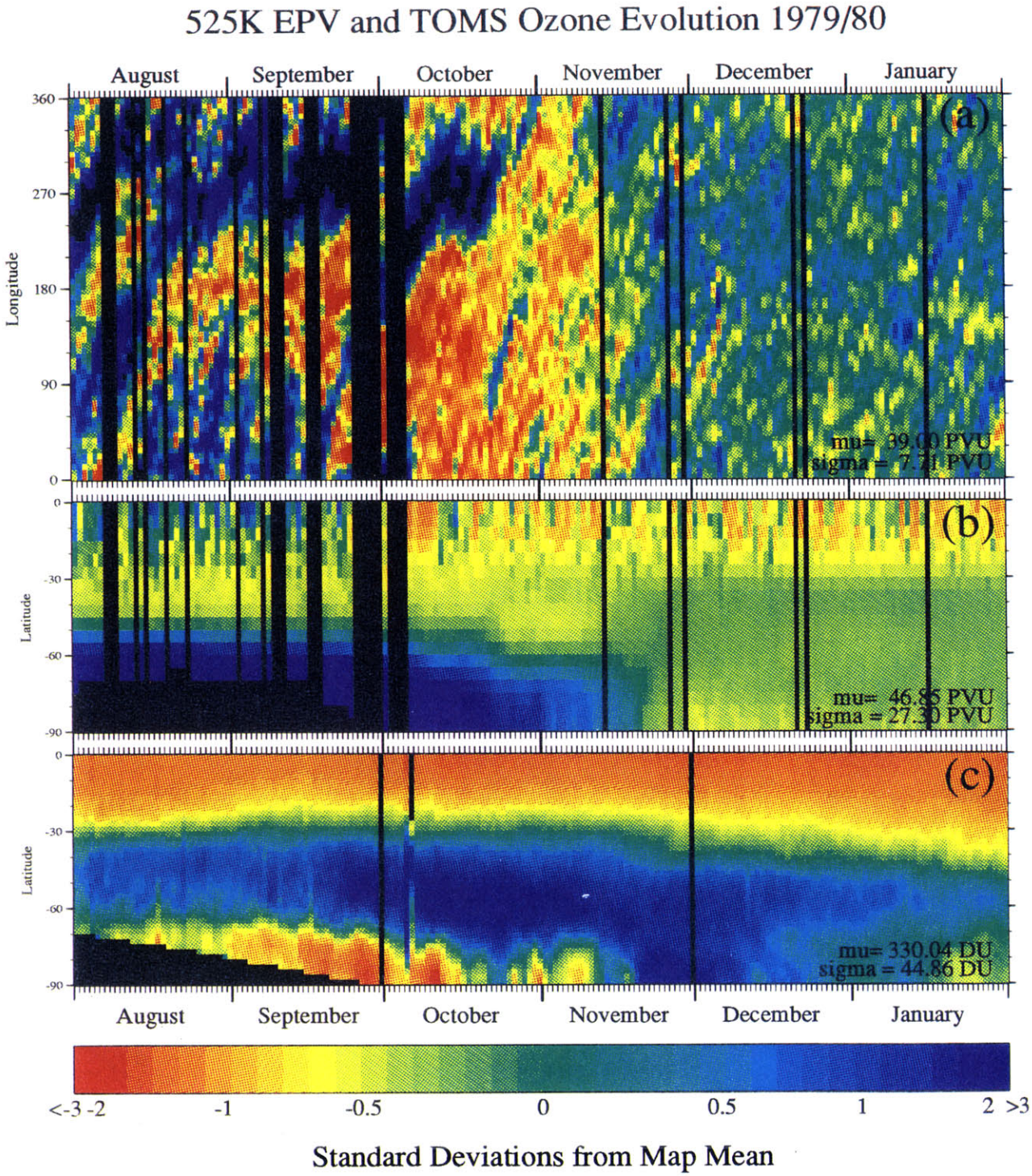

Figure A.1: Daily evolution of $525K$ EPV and total ozone during 1979: (a) $525K$ EPV at $50^{o}S$, (b) zonal mean $525K$ EPV, and (c) zonal mean TOMS total ozone. See text for details.

Fold this page out to reveal Figure A.1.

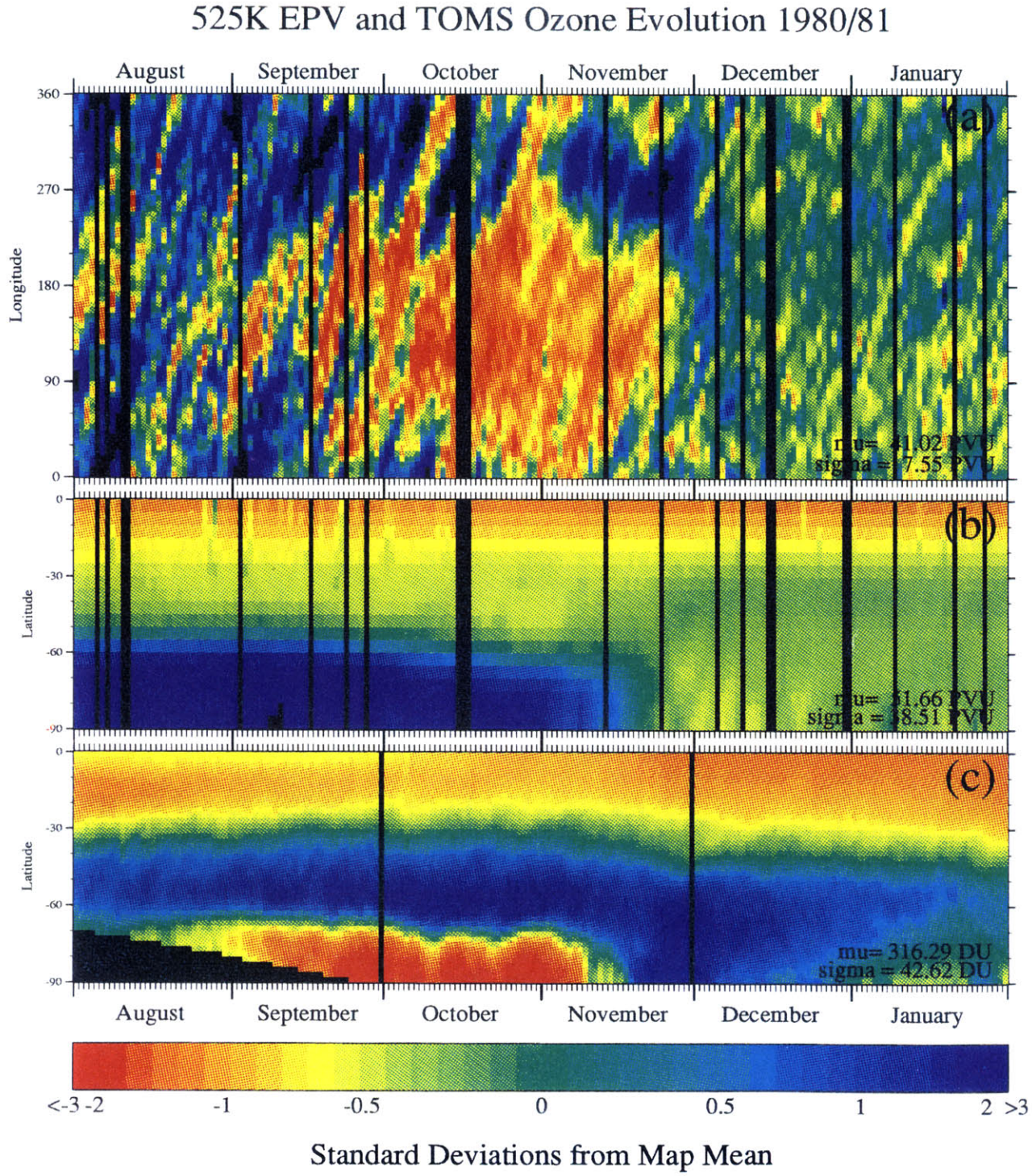

Figure A.2: Daily evolution of $525K$ EPV and total ozone during 1980: (a) $525K$ EPV at $50^{o}S$, (b) zonal mean $525K$ EPV, and (c) zonal mean TOMS total ozone. See text for details.

Fold this page out to reveal Figure A.2.

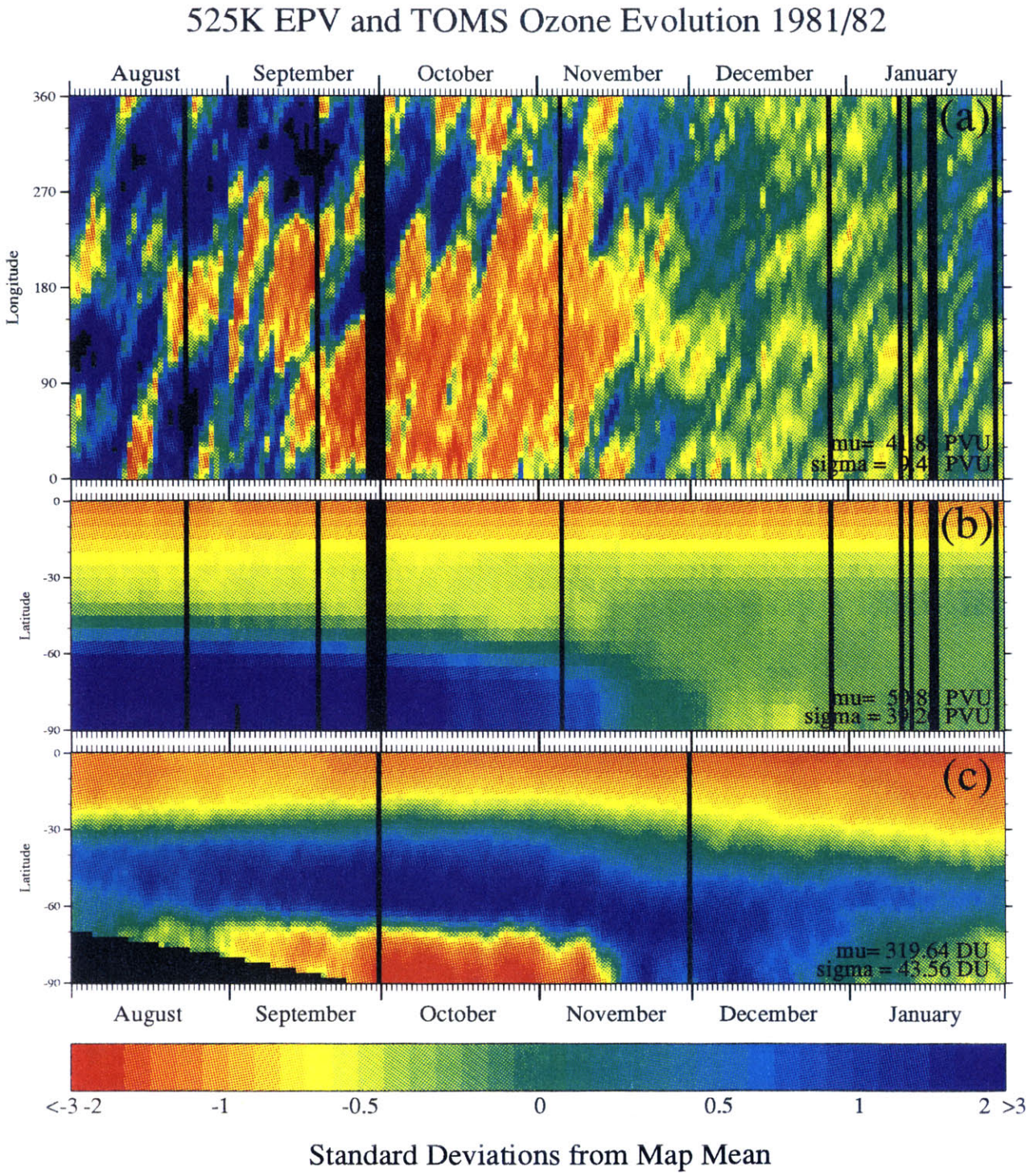

Figure A.3: Daily evolution of $525K$ EPV and total ozone during 1981: (a) $525K$ EPV at $50°S$, (b) zonal mean $525K$ EPV, and (c) zonal mean TOMS total ozone. See text for details.

Fold this page out to reveal Figure A.3.

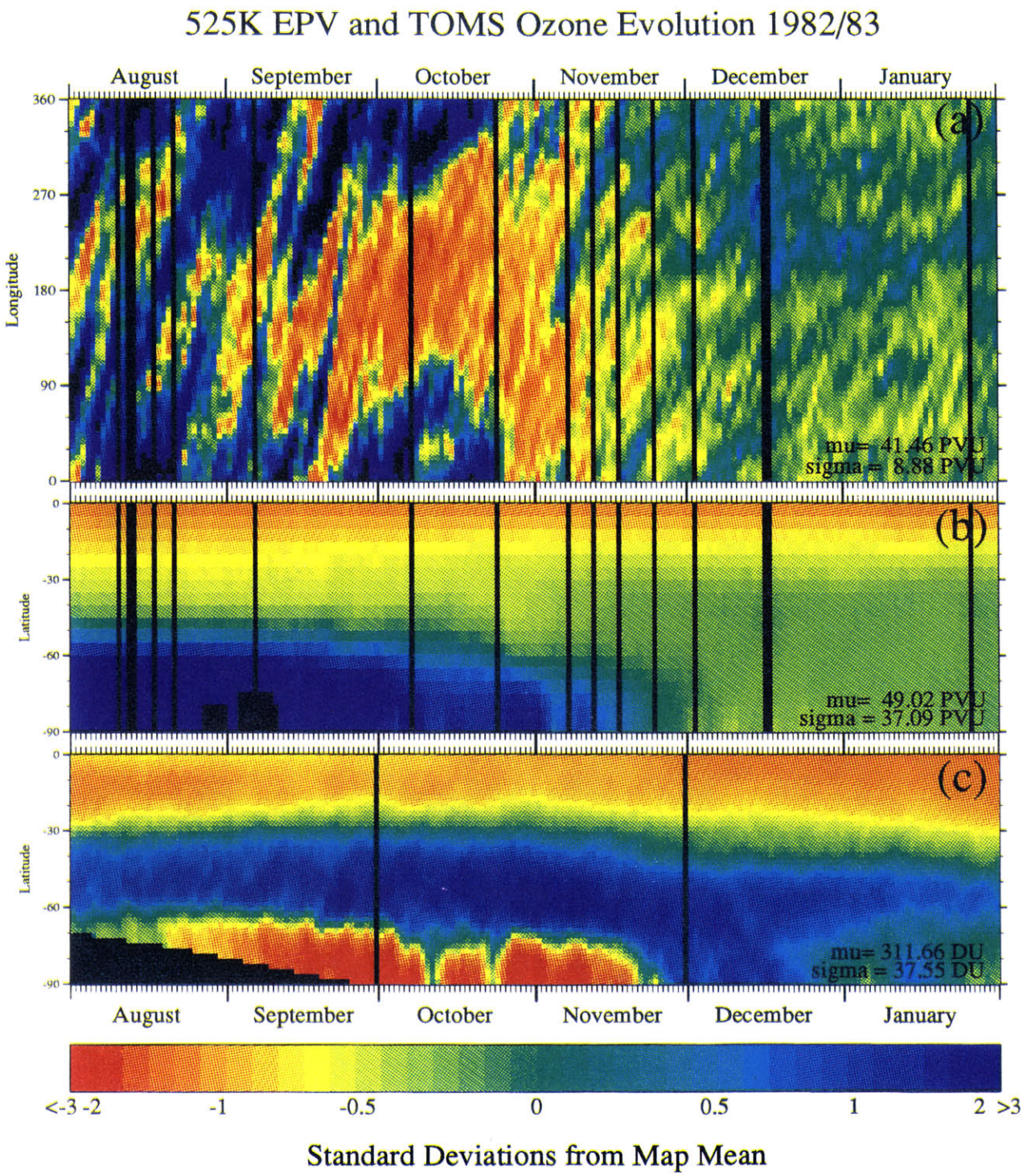

Figure A.4: Daily evolution of $525K$ EPV and total ozone during 1982: (a) $525K$ EPV at $50°S$, (b) zonal mean $525K$ EPV, and (c) zonal mean TOMS total ozone. See text for details.

Fold this page out to reveal Figure A.4.

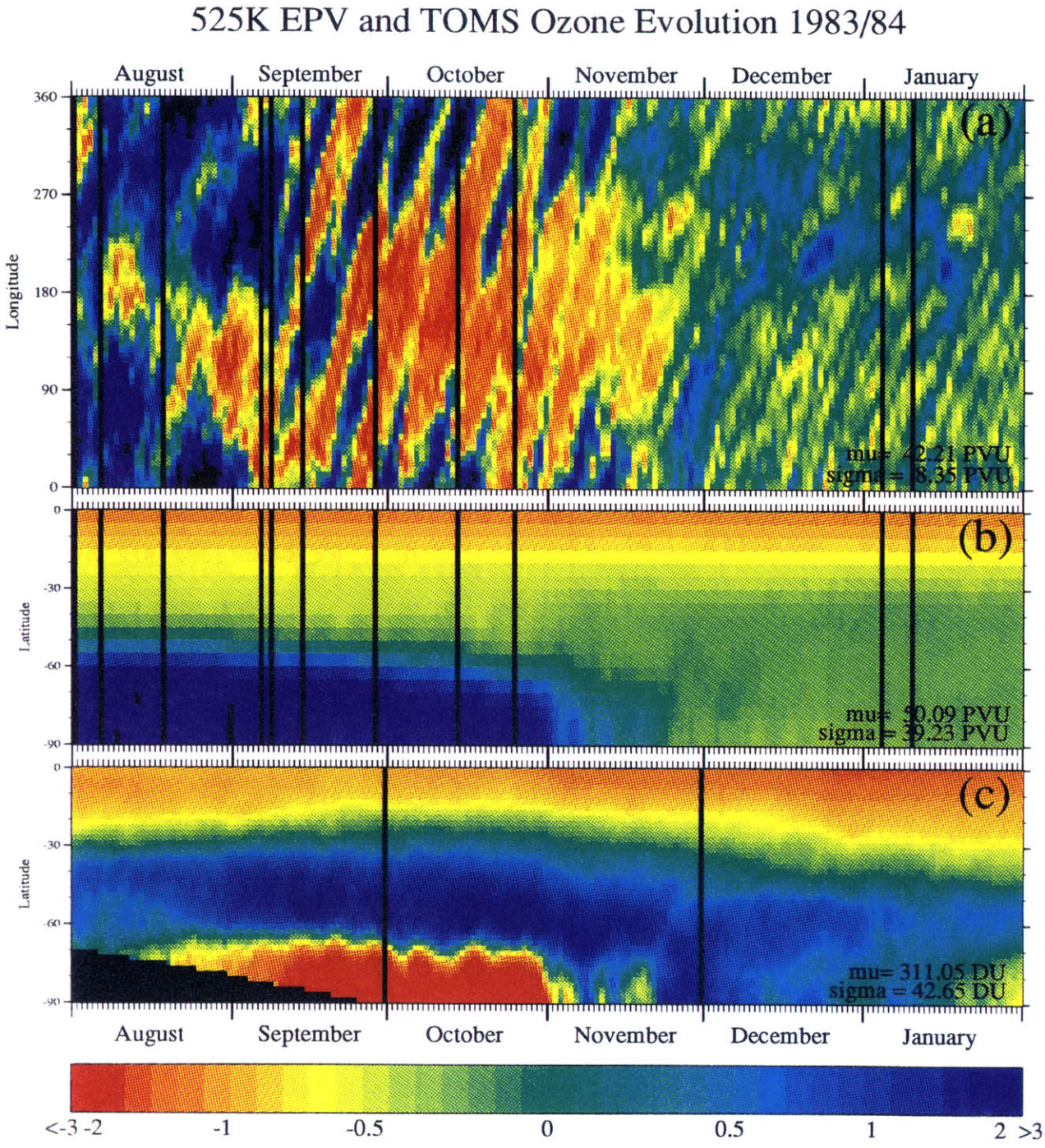

Figure A.5: Daily evolution of $525K$ EPV and total ozone during 1983: (a) $525K$ EPV at $50^{o}S$, (b) zonal mean $525K$ EPV, and (c) zonal mean TOMS total ozone. See text for details.

Fold this page out to reveal Figure A.5.

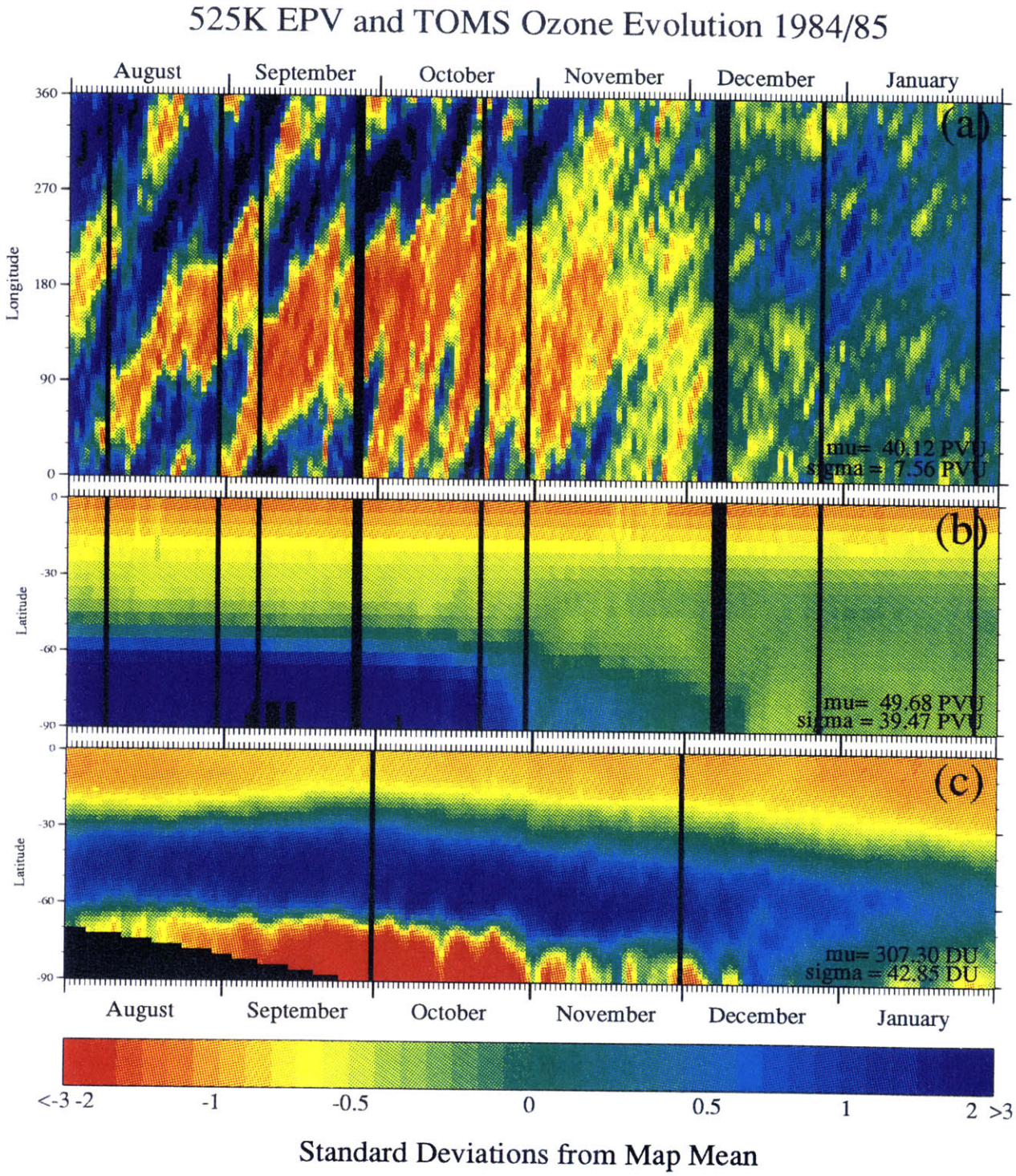

Figure A.6: Daily evolution of $525K$ EPV and total ozone during 1984: (a) $525K$ EPV at $50^{o}S$, (b) zonal mean $525K$ EPV, and (c) zonal mean TOMS total ozone. See text for details.

Fold this page out to reveal Figure A.6.

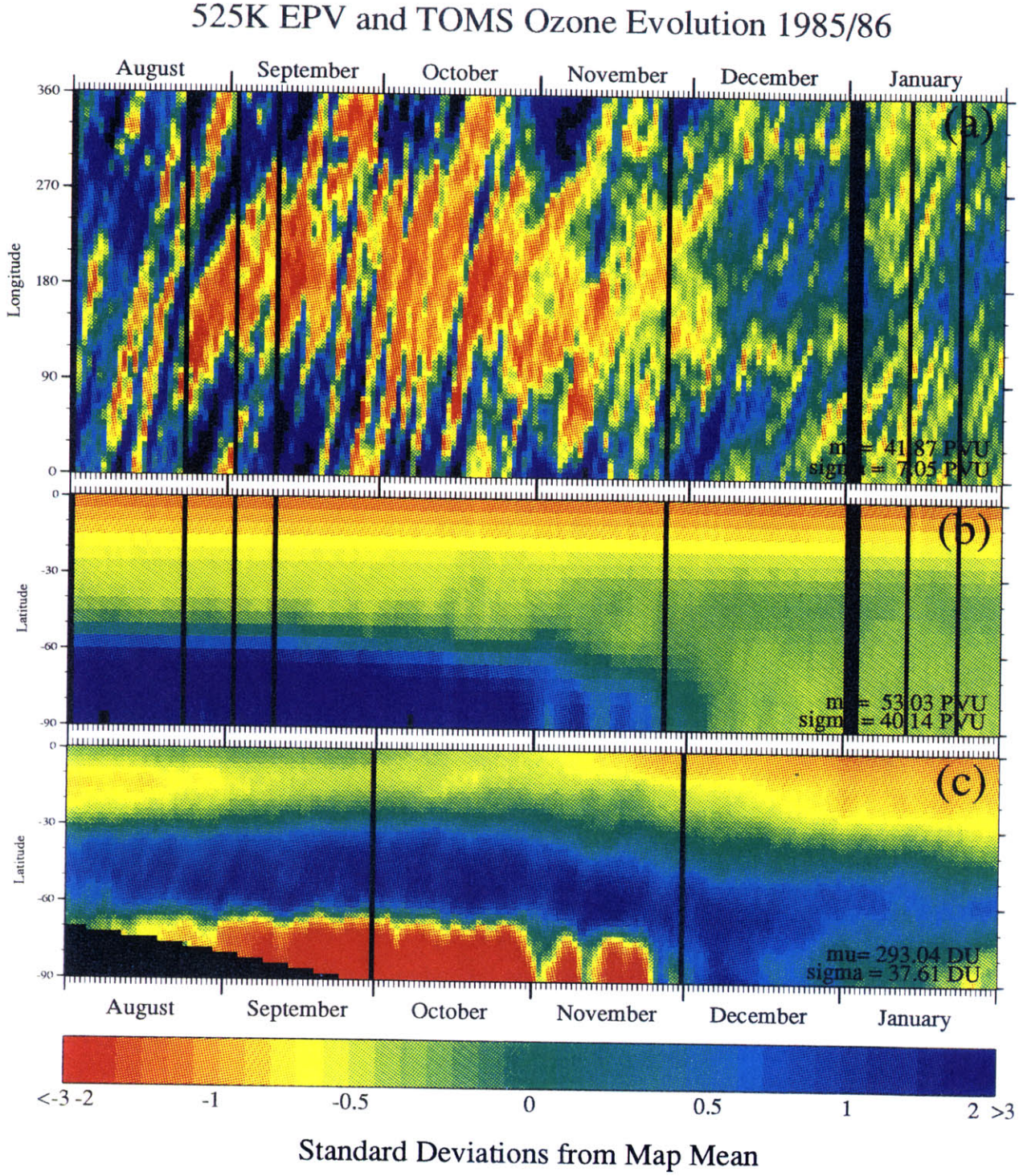

Figure A.7: Daily evolution of $525K$ EPV and total ozone during 1985: (a) $525K$ EPV at $50°S$, (b) zonal mean $525K$ EPV, and (c) zonal mean TOMS total ozone. See text for details.

Fold this page out to reveal Figure A.7.

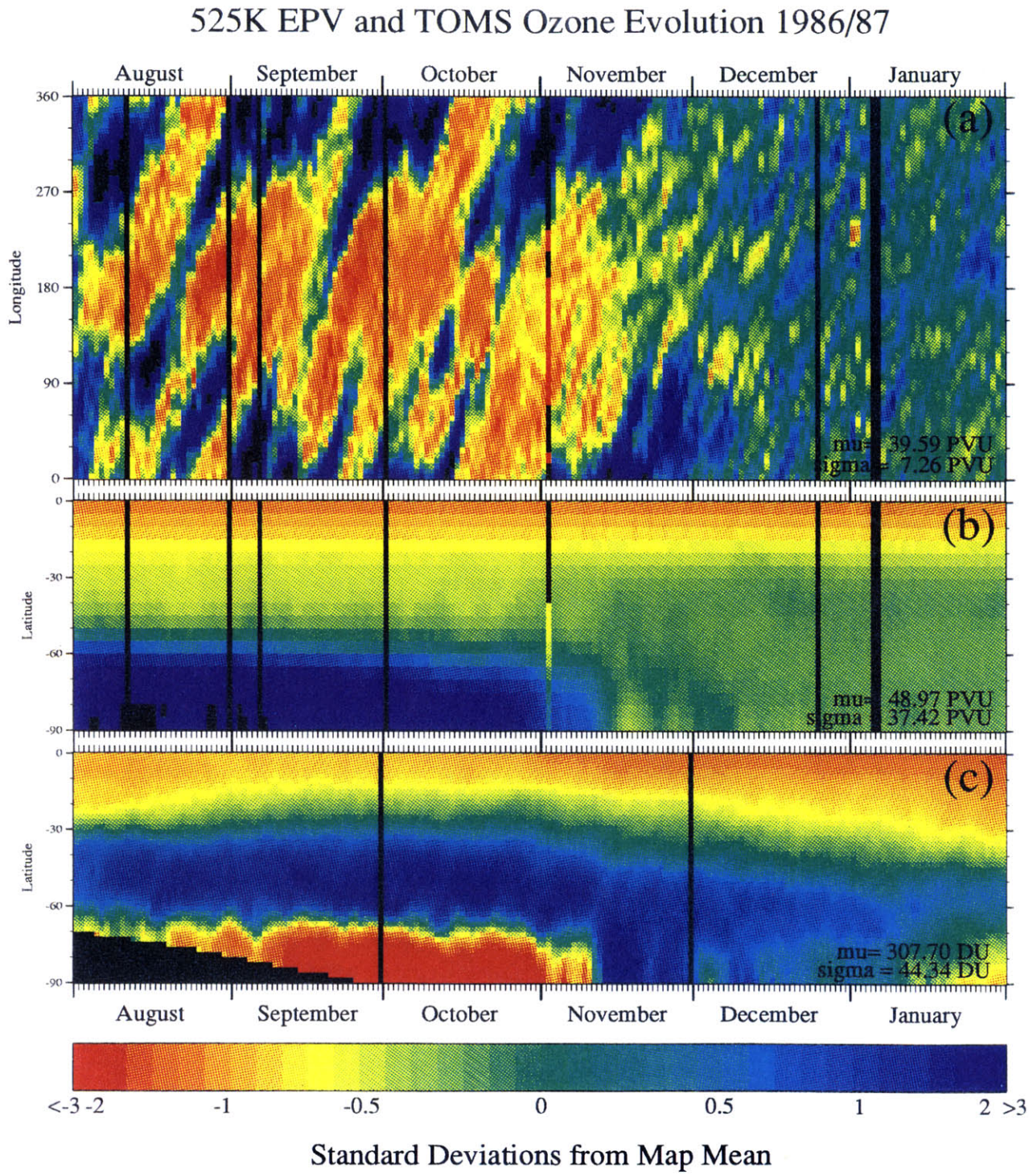

Figure A.8: Daily evolution of $525K$ EPV and total ozone during 1986: (a) $525K$ EPV at $50^{o}S$, (b) zonal mean $525K$ EPV, and (c) zonal mean TOMS total ozone. See text for details.

Fold this page out to reveal Figure A.8.

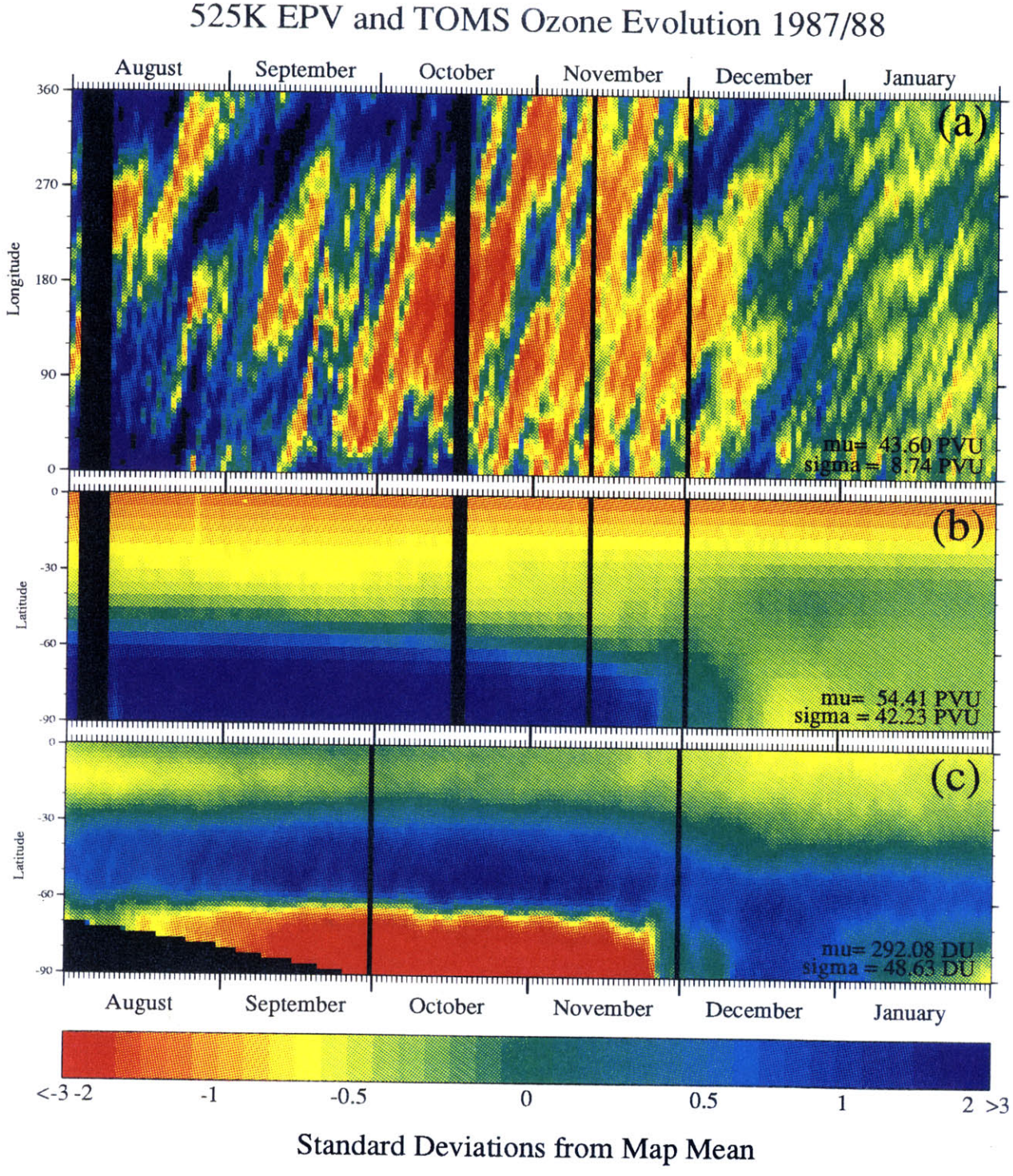

Figure A.9: Daily evolution of $525K$ EPV and total ozone during 1987: (a) $525K$ EPV at $50°S$, (b) zonal mean $525K$ EPV, and (c) zonal mean TOMS total ozone. See text for details.

Fold this page out to reveal Figure A.9.

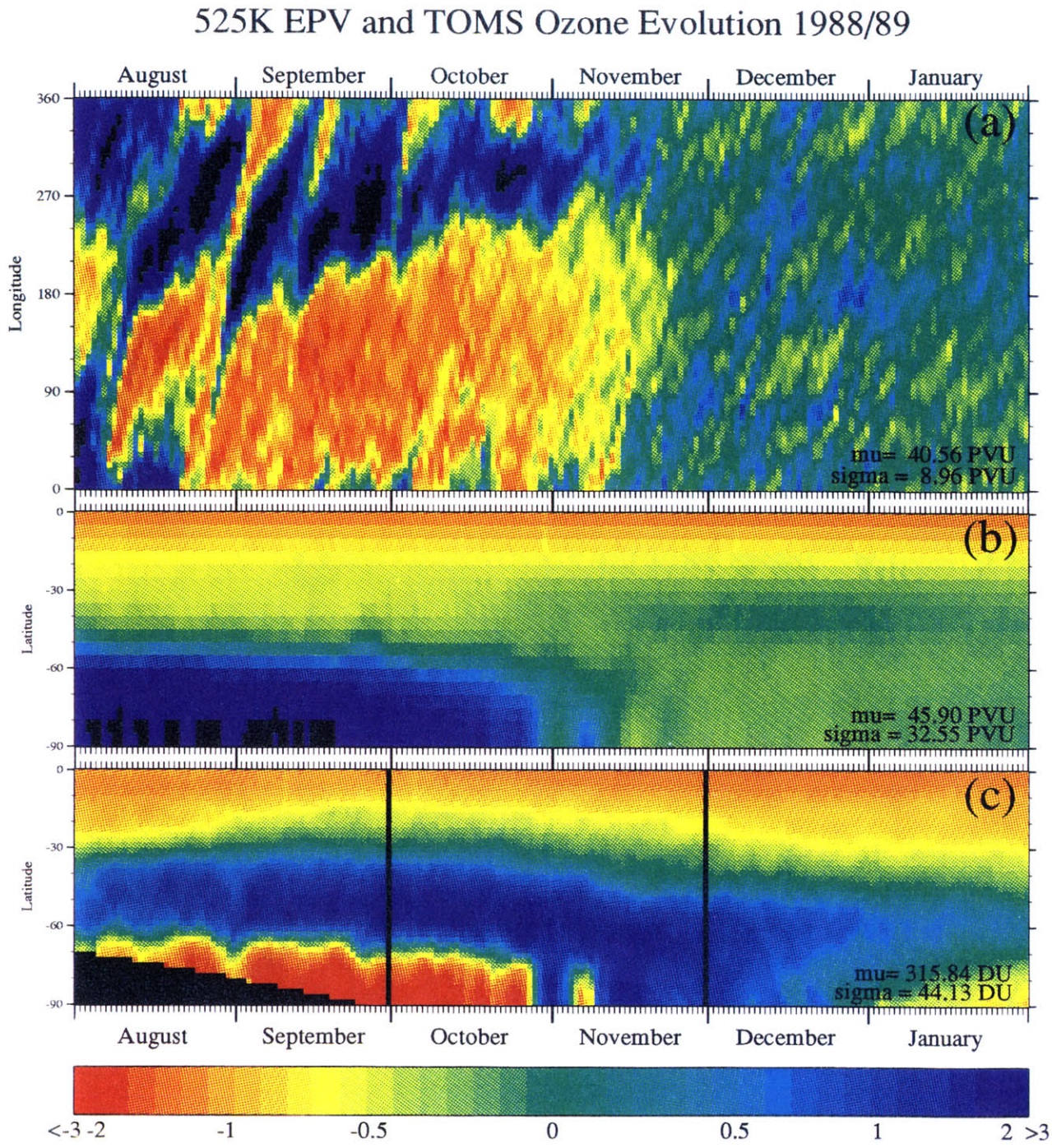

Figure A.10: Daily evolution of $525K$ EPV and total ozone during 1988: (a) $525K$ EPV at $50^{o}S$, (b) zonal mean $525K$ EPV, and (c) zonal mean TOMS total ozone. See text for details.

Fold this page out to reveal Figure A.10.

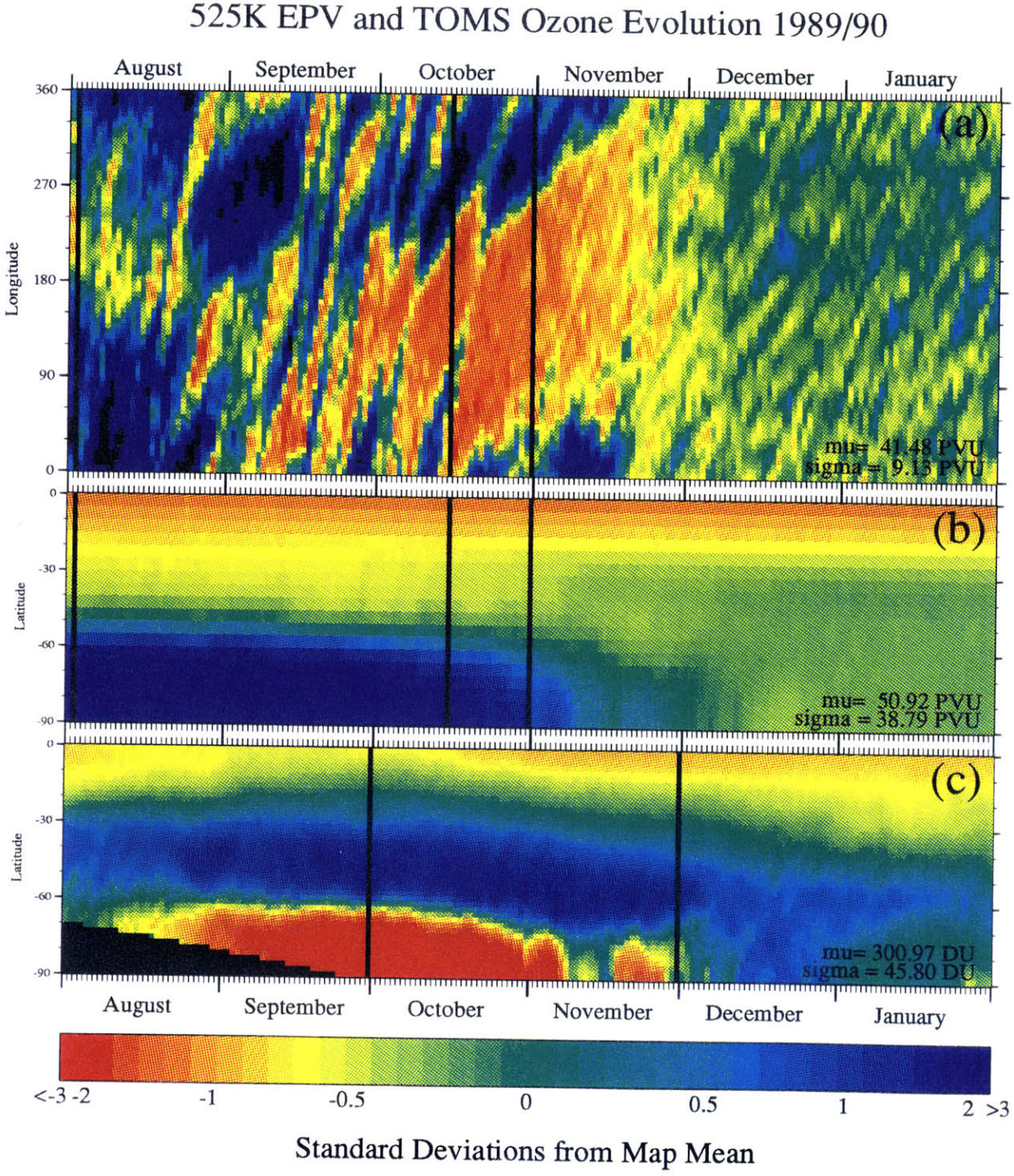

Figure A.11: Daily evolution of $525K$ EPV and total ozone during 1989: (a) $525K$ EPV at $50^{o}S$, (b) zonal mean $525K$ EPV, and (c) zonal mean TOMS total ozone. See text for details.

Fold this page out to reveal Figure A.11.

Appendix B

References

Anderson, J.G., W.H. Brune and M.H. Proffitt (1989) 'Ozone destruction by chlorine radicals within the Antarctic vortex: the spatial and temporal evolution of $ClO - O_3$ anticorrelation based on insitu ER-2 data.' *J. Geophys. Res.*, **94**, 11465-11479.

Anderson, J.G., D.W. Toohey and W.H. Brune (1991) 'Free radicals within the Antarctic vortex: the role of CFCs in Antarctic ozone loss.' *Science*, **251**, 39-46.

Andrews, D.G. (1987a) 'Transport mechanisms in the middle atmosphere: an introductory survey.' In G. Visconti and R. Garcia (eds.) *"Transport Processes in the Middle Atmosphere."* Reidel, Dordrecht, Holland, 169-181.

Andrews, D.G. (1987b) 'On the interpretation of the Eliassen-Palm flux divergence.' *Quart. J. Roy. Meteor. Soc.*, **113**, 323-338.

Andrews, D.G., J.R. Holton and C.B. Leovy (1987) *"Middle Atmosphere Dynamics."* Academic Press, Boston, 489 pp.

Andrews, D.G. and M.E. McIntyre (1976) 'Planetary waves in horizontal and vertical shear: the generalised Eliassen-Palm relation and the mean zonal acceleration.' *J. Atmos. Sci.*, **33**, 2031-2048.

Andrews, D.G. and M.E. McIntyre (1978) 'An exact theory of non-linear waves on a Lagrangian mean flow.' *J. Fluid Mech.*, **89**, 609-646.

Atkinson, R.J. and J.R. Easson (1988) 'A reevaluation of the Australian total ozone data record.' In R.D. Bojkov and P. Fabian (eds.) *"Ozone in the Atmosphere: Proceedings of the Quadrennial Ozone Symposium 1988 and Tropospheric Ozone Workshop."* Deepak, Hampton VA, 168-171.

Atkinson, R.J., W.A. Matthews, P.A. Newman and R.A. Plumb (1989) 'Evidence for the mid-latitude impact of Antarctic ozone depletion.' *Nature*, **340**, 290-293.

Atkinson, R.J. and R.A. Plumb (1993, in press) 'An observational study of the ozone dilution effect: ozone transport in the austral spring stratosphere.' *Proc. Quadrennial Ozone Symp., Charlottesville, VA, June 1992.*

Barnett, J.J. and M. Corney (1985) *"Middle Atmosphere Reference Model Derived from Satellite Data."* Handbook MAP, **16**, 47-85.

Bowman, K.P. (1990) 'Evolution of the total ozone field during the breakdown of the Antarctic circumpolar vortex.' *J. Geophys. Res.*, **95**, 16529-16543.

Bowman, K.P. (1993, submitted) 'Large scale isentropic mixing properties of the Antarctic polar vortex from analyzed winds.' *J. Geophys. Res.*

Bowman, K.P. and N.J. Mangus (1993, in press) 'Observations of deformation and mixing of the total ozone field in the Antarctic polar vortex.' *J. Atmos. Sci.*

Bretherton, F.P. (1966) 'Critical layer instability in baroclinic flows.' *Quart. J. Roy. Meteor. Soc.*, **92**, 325-334.

Brewer, A.W. (1949) 'Evidence for a world circulation provided by the measurements of helium and water vapour distributions in the stratosphere.' *Quart. J. Roy. Meteor. Soc.*, **75**, 351-363.

Butchart, N. (1987) 'Evidence for planetary wave breaking from satellite data: the relative roles of diabatic effects and irreversible mixing.' In G. Visconti and

R. Garcia (eds.) *"Transport Processes in the Middle Atmosphere."* Reidel, Dordrecht, Holland, 121-136.

Butchart, N. and E.E. Remsberg (1986) 'The area of the stratospheric polar vortex as a diagnostic for tracer transport on an isentropic surface.' *J. Atmos. Sci.*, **43**, 1319-1339.

Charney, J.G. and P.G. Drazin (1961) 'Propagation of planetary scale disturbances from the lower into the upper atmosphere.' *J. Geophys. Res.*, **66**, 83-109.

Charney, J.G. and M.E. Stern (1962) 'On the stability of internal baroclinic jets in a rotating atmosphere.' *J. Atmos. Sci.*, **19**, 159-172.

Chipperfield, M.P. and J.A. Pyle (1988) 'Two dimensional modelling of the Antarctic lower stratosphere.' *Geophys. Res. Letters*, **15**, 875-878.

Chubachi, S. (1993) 'Relationship between total ozone amounts and stratospheric temperature at Syowa, Antarctica.' *J. Geophys. Res.*, **98**, 3005-3010.

Deland, R.J. (1973) 'Analysis of Nimbus 3 SIRS radiance data: travelling planetary waves in the stratosphere temperature field.' *Mon. Wea. Rev.*, **101**, 132-140.

Deshler, T., D.J. Hoffmann, J.V. Hereford and C.B. Sutter (1990) 'Ozone and temperature profiles over McMurdo Station, Antarctica in the spring of 1989.' *Geophys. Res. Letters*, **17**, 151-154.

Dobson, G.M.B. (1956) 'Origin and distribution of the polyatomic molecules in the atmosphere.' *Proc. Roy. Soc. Lond.*, **A236**, 189-193.

Dobson, G.M.B. (1966) 'Annual variation of ozone in Antarctica.' *Quart. J. Roy. Meteor. Soc.*, **92**, 549-552.

Dritschel, D.G. (1988) 'Contour surgery: a topological reconnection scheme for extended integrations using contour dynamics.' *J. Computer Phys.*, **77**, 240-266.

Dritschel, D.G. (1989) 'Contour dynamics and contour surgery: numerical algorithms for extended, high resolution modelling of vortex dynamics in two-dimensional, inviscid, compressible flow.' *Computer Phys. Rep.*, **10**, 77-146.

Dunkerton, T.J., C.-P. Hsu and M.E. McIntyre (1981) 'Some Eulerian and Lagrangian diagnostics for a model stratospheric warming.' *J. Atmos. Sci.*, **38**, 819-843.

Dutsch, H.U. (1978) 'Vertical ozone distribution on a global scale.' *Pure Appl. Geophys.*, **116**, 511-529.

Fairlie, T.D. and A. O'Neill (1988) 'The stratospheric major warming of winter 1984/85: observations and dynamical influemces.' *Quart. J. Roy. Meteor. Soc.*, **114**, 557-578.

Farman, J.G., B.G. Gardner and J.D. Shanklin (1985), 'Large losses of total ozone in Antarctica reveal seasonal ClOx/NOx interaction.' *Nature*, **315**, 207-210.

Farrara, J.D. M. Fisher, C.R. Mechoso and A. O'Neill (1992) 'Planetary scale disturbances in the southern stratosphere during early winter.' *J. Atmos. Sci.*, **49**, 1757-1775.

Farrara, J.D. and C.R. Mechoso, (1986) 'An observational study of the final warming in the southern hemisphere stratosphere.' *Geophys. Res. Letters*, **13**, 1232-1235.

Fels, S.B. (1985) 'Radiative-dynamical interactions in the middle atmosphere.' *Adv. Geophys.*, **28A**, 277-300.

Fishman, J., K. Fakhruzzaman, B. Cros and D. Nganga (1991) 'Identification of widespead pollution in the southern hemisphere deduced from satellite analyses.' *Science*, **252**, 1693-1696.

Fishman, J, C.E. Watson, J.C. Larsen and J.A. Logan (1990) 'Distribution of tropospheric ozone determined from satellite data.' *J. Geophys. Res.*, **95**, 3599-3617.

Fleig, A.J., A.J. Krueger, P.K. Bhartia, B.M. Schlesinger, R.P. Cebula and C.G. Wellemeyer (1993, in preparation) *"Nimbus 7 Total Ozone Mapping Spectrometer (TOMS) Data Product Users Guide."* NASA Ref. Publ.

Fleig, A.J., R.D. McPeters, P.K. Bhartia, B.M. Schlesinger, R.P. Cebula, K.F. Klenk, S.L. Taylor and D.F. Heath (1990) *"Nimbus 7 solar backscatter ultraviolet (SBUV) ozone product users guide."* NASA Ref. Publ. 1234, 128 pp.

Garcia, R.R. and S. Solomon (1985) 'The effect of breaking gravity waves on the dynamics and chemical composition of the mesosphere and lower thermosphere.' *J. Geophys. Res.*, **90**, 3850-3868.

Garcia, R.R. and S. Solomon (1987) 'A possible relationship between the interannual variability in Antarctic ozone and the quasi-biennial oscillation.' *Geophys. Res. Letters*, **14**, 848-851.

Geller, M.A. and M.-F. Wu (1987) 'Troposphere-stratosphere general circulation statistics.' In G. Visconti and R. Garcia (eds.) *"Transport Processes in the Middle Atmosphere"*, Reidel, Dordrecht, Holland, 3-17.

Gelman, M.E., F.G. Finger, A.J. Miller, K. Johnson and R.M. Nagatani (1984) 'Developing a stratospheric climatology from NMC analyses.' *Adv. Space Res.*, **4**, 29-32.

Gelman, M.E., A.J. Miller, K. Johnson and R.M. Nagatani (1986) 'Detection of long-term trends in global stratospheric temperature from NMC analyses derived from NOAA satellite data.' *Adv. Space Res.*, **6**, 17-26.

Gelman, M.E., A.J. Miller, R.M. Nagatani and H.D. Bowman II (1983) 'Mean zonal wind and temperature structure during the PMP-1 winter periods.' *Adv. Space Res.*, **2**, 159-162.

Gille, J.C. and J.M. Russell III (1984) 'The limb infrared monitor of the stratosphere: experiment decription, performance and results.' *J. Geophys. Res.*, **89**, 5125-5140.

Grose, W.L., R.S. Eckman, R.E. Turner and W.T. Blackshear (1990) 'Antarctic ozone depletion and potential effects on the global ozone budget.' In A. O'Neill (ed.) *"Dynamics, Transport and Photochemistry in the Middle Atmosphere of the Southern Hemisphere."* Kluwer, Netherlands, 237-252.

Hartmann, D.L. (1976) 'The structure of the stratosphere in the southern hemisphere during late winter 1973 as observed by satellite.' *J. Atmos. Sci.*, **33**, 1141-1154.

Hartmann, D.L. (1977a) 'On potential vorticity and transport in the stratosphere.' *J. Atmos. Sci.*, **34**, 968-977.

Hartmann, D.L. (1977b) 'Stationary planetary waves in the southern hemisphere.' *J. Geophys. Res.*, **82**, 4930-4934.

Hartmann, D.L. (1979) 'Baroclinic instability of realistic zonal-mean states to planetary waves.' *J. Atmos. Sci.*, **36**, 2336-2349.

Hartmann, D.L. (1983) 'Barotropic instability of the polar night jet stream.' *J. Atmos. Sci.*, **40**, 817-835.

Hartmann, D.L. (1990) 'Dynamical properties of the Antarctic circumpolar vortex inferred from aircraft observations.' In A. O'Neill (ed.) *"Dynamics, Transport and Photochemistry in the Middle Atmosphere of the Southern Hemisphere."* Kluwer, Netherlands, 117-134.

Hartmann, D.L., K.R. Chan, B. Gary, M.R. Schoeberl, P.A. Newman, R.L. Martin, M. Lowenstein, J.R. Podolske and S.E. Strahan (1989a) 'Potential vorticity and mixing in the south polar vortex during spring.' *J. Geophys. Res.*, **94**, 11625-11640.

Hartmann, D.L., L.E. Heidt, M. Lowenstein, J.R. Podolske, J. Vedder, W.L. Starr and S.E. Strahan (1989b) 'Transport into the south polar vortex in early spring.' *J. Geophys. Res.*, **94**, 16779-16795.

Hartmann, D.L., C.R. Mechoso and K. Yamazaki (1984) 'Observations of wave-mean flow interaction in the southern hemisphere.' *J. Atmos. Sci.*, **41**, 351-362.

Harwood, R.S. (1975) 'The temperature structure of the southern hemisphere stratosphere, August to October, 1971.' *Quart. J. Roy. Meteor. Soc.*, **101**, 75-92.

Haynes, P.H., C.J. Marks, M.E. McIntyre, T.G. Shepherd and K.P. Shine (1991) 'On the "downward control" of extratropical diabatic circulations by eddy-induced mean zonal forces.' *J. Atmos. Sci.*, **48**, 651-678.

Haynes, P.H. and M.E. McIntyre (1987) 'On the evolution of vorticity and potential vorticity in the presence of diabatic heating and frictional or other forces.' *J. Atmos. Sci.*, **44**, 828-841.

Herman, J.R., R. Hudson, R. McPeters, R. Stolarski, Z. Ahmad, X.Y. Gu, S. Taylor and C. Wellemeyer (1991) 'A new self-calibration method applied to TOMS and SBUV backscattered ultraviolet data to determine long term global ozone change.' *J. Geophys. Res.*, **96**, 7531-7545.

Hirooka, T. and I. Hirota (1985) 'Normal mode Rossby waves observed in the upper stratosphere. Part II. Second antisymmetric and symmetric modes of zonal wavenumbers 1 and 2.' *J. Atmos. Sci.*, **42**, 536-548.

Hirooka, T. and I. Hirota (1989) 'Further evidence of normal mode Rossby waves.' *Pure Appl. Geophys.*, **130**, 277-289.

Hirota, I. and T. Hirooka (1984) 'Normal mode Rossby waves observed in the upper stratosphere: Part 1: First symmetric modes of wavenumbers 1 and 2.' *J. Atmos. Sci.*, **41**, 1253-1267.

Hirota, I., T. Hirooka and M. Shiotani (1983) 'Upper stratospheric circulations in the two hemispheres observed by satellites.' *Quart. J. Roy. Meteor. Soc.*, **109**, 443-454.

Hirota, I., K. Kuroi and M. Shiotani (1990) 'Midwinter warmings in the southern hemisphere stratosphere in 1988.' *Quart. J. Roy. Meteor. Soc.*, **116**, 929-941.

Holton, J.R. (1992) *"An Introduction to Dynamic Meteorology."* 3rd Ed., Academic Press, 511 pp.

Hoskins, B.J., I. Draghici and H.C. Davies (1978) 'A new look at the omega equation.' *Quart. J. Roy. Meteor. Soc.*, **104**, 31-38.

Hoskins, B.J., M.E. McIntyre and A.W. Robertson (1985) 'On the use and significance of isentropic potential vorticity maps.' *Quart. J. Roy. Meteor. Soc.*, **111**, 877-946.

James, I.N. (1988) 'On the forcing of planetary-scale Rossby waves by Antarctica.' *Quart. J. Roy. Meteor. Soc.*, **114**, 619-637.

Juckes, M. N. and M.E. McIntyre (1987) 'A high-resolution one-layer model of breaking planetary waves in the stratosphere.' *Nature*, **328**, 590-596.

Kanzawa, H. (1989) 'Warm stratopause in the Antarctic winter.' *J. Atmos. Sci.*, **46**, 435-438.

Kanzawa, H. and S. Kawaguchi (1990a) 'Large stratospheric sudden warming in Antarctic late winter and shallow ozone hole in 1988.' *Geophys. Res. Letters*, **17**, 77-80.

Kanzawa, H. and S. Kawaguchi (1990b) 'Large stratospheric sudden warming in Antarctic late winter and shallow ozone hole in 1988: Observation by Japanese Antarctic Research Expedition.' In A. O'Neill (ed.) *"Dynamics, Transport and Photochemistry in the Middle Atmosphere of the Southern Hemisphere."* Kluwer, Netherlands, 135-148.

Karoly, D.J. and D.S Graves (1990) 'On data sources and quality for the southern hemisphere stratosphere.' In A. O'Neill (ed.) *"Dynamics, Transport and Photochemistry in the Middle Atmosphere of the Southern Hemisphere."* Kluwer, Netherlands, 19-32.

Karoly, D.J. and B.J. Hoskins (1982) 'Three dimensional propagation of planetary waves.' *J. Meteor. Soc. Japan*, **60**, 109-122.

Kiehl, K. and S. Solomon (1986) 'On the radiative balance of the stratosphere.' *J. Atmos. Sci.*, **43**, 1525-1534.

Ko, K.W.K., R.-L. Shia, S. Zhou, D.K. Weisenstein and N.-D. Sze (1993, submitted) 'Antarctic ozone hole: dilution effect simulated by an interactive two-dimensional model.' *Proc. Quadrennial Ozone Symp., Charlottesville, VA, June 1992.*

Kodera, K. and K. Yamazaki (1990) 'A possible influence of sea surface temperature variation on the recent development of the ozone hole.' In A. O'Neill (ed.) *"Dynamics, Transport and Photochemistry in the Middle Atmosphere of the Southern Hemisphere."* Kluwer, Netherlands, 149-158.

Komhyr, W.D., R.D. Grass and R.K Leonard (1986) 'Total ozone decrease at South Pole, Antarctica, 1964-1985.' *Geophys. Res. Letters*, **13**, 1248-1251.

Komhyr, W.D., S.J. Oltmans, J.A. Lathrop, J.B. Kerr and W.A. Matthews (1993, submitted) 'The latitudinal distribution of ozone to 35 kilometer altitude from ECC ozonesonde observations, 1982-1990.' *Proc. Quadrennial Ozone Symp., Charlottesville, VA, June 1992.*

Krueger, A.J., R.S. Stolarski and M.R. Schoeberl (1989) 'Formation of the 1988 Antarctic ozone hole.' *Geophys. Res. Letters*, **16**, 381-384.

Kurzeja, R.J. (1984) 'Spatial variability of total ozone at high latitudes in winter' *J. Atmos. Sci.*, **41**, 695-697.

Lait, L.R., M.R. Schoeberl and P.A. Newman (1989) 'Quasi-biennial modulations of the Antarctic ozone depletion.' *J. Geophys. Res.*, **94**, 11559.

Lait, L.R., M.R. Schoeberl, P.A. Newman, M.H. Proffitt, M. Lowenstein, J.R. Pedolske, S.E. Strahan, K.R. Chan, B. Gary, J.J. Margitan, E. Browell, M.P. McCormick and A. Torres (1990) 'Reconstruction of O3 and N2O fields from ER-2, DC-8 and balloon observations.' *Geophys. Res. Letters*, **17**, 521-524.

Lait, L.R. and J.L. Stanford (1988) 'Fast, long-lived features in the polar stratosphere.' *J. Atmos. Sci.*, **45**, 3800-3809.

Lehmann, P., D.J. Karoly, P.A. Newman, T.S. Clarkson and W.A. Matthews (1992a) 'Long-term winter total ozone changes at Macquarie Island.' *Geophys. Res. Letters*, **19**, 1459-1462.

Lehmann, P., D.J. Karoly, P.A. Newman, T.S. Clarkson and W.A. Matthews (1992b) 'An investigation into the causes of stratospheric ozone loss in the southern Australasian region.' *Geophys. Res. Letters*, **19**, 1463-1466.

Leovy, C.B., C.-R. Sun, M.H. Hitchman, E.E. Remsberg, J.M. Russell, L.L. Gordley, J.C. Gille and L.V. Lyjak (1985) 'Transport of ozone in the middle stratosphere: evidence for planetary wave breaking.' *J. Atmos. Sci.*, **42**, 230-244.

Leovy, C.B. and P.S. Webster (1976) 'Stratospheroc longwaves: comparison of thermal structures in the northern and southern hemispheres.' *J. Atmos. Sci.*, **33**, 1624-1638.

Levy II, H., J.D. Mahlman and W.J. Moxim (1985) 'Tropospheric ozone: the role of transport.' *J. Geophys. Res.*, **90**, 3753-3772.

Logan, J.A. (1985) 'Tropospheric ozone: seaonal behaviour, trends and anthropogenic influence.' *J. Geophys. Res.*, **90**, 10463-10482.

Madden, R.A. (1979) 'Observations of large scale travelling waves.' *Rev. Geophys. Space Phys.*, **17**, 1935-1949.

Manney, G.L. (1993, submitted) 'Non-linear barotropic instability of idealized stratospheric jets.' *J. Atmos. Sci.*

Manney, G.L., J.D. Farrara and C.R. Mechoso (1991) 'The behaviour of wave 2 in the southern hemisphere stratosphere during late winter and early spring.' *J. Atmos. Sci.*, **48**, 976-998.

Manney, G.L., T.R. Nathan and J.L. Stanford (1988) 'Barotropic stability of realistic stratospheric jets.' *J. Atmos. Sci.*, **45**, 2545-2555.

Manney, G.L., T.R. Nathan and J.L. Stanford (1989) 'Barotropic instability of basic states with a realistic jet and a wave.' *J. Atmos. Sci.*, **46**, 1250-1273.

Marks, C.J. (1988) 'Linear wavetrains in models of the stratosphere.' *Quart. J. Roy. Meteor. Soc.*, **114**, 297-323.

Matsuno, T. (1970) 'Vertical propagation of stationary planetary waves in the winter northern hemisphere.' *J. Atmos. Sci.*, **27**, 871-883.

Matsuno, T. (1971) 'A dynamical model of the stratospheric sudden warming.' *J. Atmos. Sci.*, **28**, 1479-1494.

McCormick, M.P. and C.R. Trepte (1987) 'Polar stratospheric cloud optical depth observed between 1978 and 1985.' *J. Geophys. Res.*, **92**, 4297-4307.

McCormick, M.P., R.E. Veiga and W.P. Chu (1992) 'Stratospheric ozone profile and total ozone trends derived from the SAGE I and SAGE II data.' *Geophys. Res. Letters*, **19**, 269-272.

McCormick, M.P., J.M. Zawodny, R.E. Veiga, J.C. Larsen and P.H. Wang (1989) 'An overview of SAGE I and SAGE II ozone measurements.' *Planet. Space Sci.*, **37**, 1567-1586.

McIntyre, M.E. (1980) 'Towards a Lagrangian mean description of stratospheric circulations and chemical transports.' *Phil. Trans. Roy. Soc. London*, **A296**, 129-148

McIntyre, M.E. (1982) 'How well do we understand the dynamics of stratospheric warmings?' *J. Meteor. Soc. Japan*, **60**, 37-65.

McIntyre, M.E. (1989) 'On the Antarctic ozone hole' *J. Atmos. Terr. Phys.*, **51**, 29-43.

McIntyre, M.E. (1990) 'Middle atmosphere dynamics and transport: some current challenges to our understanding.' in A. O'Neill (ed.) *"Dynamics, Transport*

and Photochemistry in the Middle Atmosphere of the Southern Hemisphere." Kluwer, Netherlands, 1-7.

McIntyre, M.E. and T.N. Palmer (1983) 'Breaking planetary waves in the stratosphere.' *Nature*, **305**, 593-600.

McIntyre, M.E. and T.N. Palmer (1984) 'The surf zone in the stratosphere.' *J. Atmos. Terr. Phys.*, **46**, 825-849.

McPeters, R.D., D.F. Heath and P.K. Bhartia (1984) 'Average ozone profiles for 1979 from the Nimbus-7 SBUV instrument.' *J. Geophys. Res.*, **89**, 5199-5214.

McPherson, R.D., K.H. Bergman, R.E. Kistler, G.E. Rash and D.S. Gordon (1979) 'The NMC operational global data assimilation scheme.' *Mon. Wea. Rev.*, **107**, 1445-1461.

Mechoso, C.R. (1990) ' The final warming of the stratosphere.' In A. O'Neill (ed.) *"Dynamics, Transport and Photochemistry in the Middle Atmosphere of the Southern Hemisphere."* Kluwer, Netherlands, 55-70.

Mechoso, C.R. and D.L. Hartmann (1982) 'An observational study of travelling planetary waves in the southern hemisphere.' *J. Atmos. Sci.*, **39**, 1921-1935.

Mechoso, C.R., D.L. Hartmann and J.D. Farrara (1985) 'Climatology and interannual variability of wave, mean flow in the southern hemisphere.' *J. Atmos. Sci.*, **42**, 2189-2206.

Mechoso, C.R., A. O'Neill, V.D. Pope and J.D. Farrara (1988) 'A study of the stratospheric final warming of 1982 in the southern hemisphere.' *Quart. J. Roy. Meteor. Soc.*, **114**, 1365-1384.

Miles, T. and W.L. Grose (1986) 'Transient medium-scale wave activity in the summer stratosphere.' *BAMS*, **67**, 674-686.

Miles, T. and W.L. Grose (1989) 'Upper stratosphere polar jet instability in the southern hemisphere.' *Geophys. Res. Letters*, **16**, 239-242.

Miller, A.J. (1989) 'A review of satellite observations of atmospheric ozone.' *Planet. Space Sci.*, **37**, 1539-1566.

Nagatani, R.M. and A.J. Miller (1987) 'The influence of lower stratospheric forcing on October Antarctic ozone decrease.' *Geophys. Res. Letters*, **14**, 202-205.

Nagatani, R.M., A.J. Miller, K.W. Johnson and M.E. Gelman (1988) *"An eight year climatology of meteorological, and SBUV ozone data."* Tech. Report NWS40, U.S. Department of Commerce, NOAA, 125 pp.

Newman, P.A. (1986) 'The final warming and polar vortex disappearance during the southern hemisphere spring.' *Geophys. Res. Letters*, **13**, 1228-1231.

Newman, P.A. and W.J. Randel (1988) 'Coherent ozone-dynamical changes during the southern hemisphere spring, 1979-1986.' *J. Geophys. Res.*, **93**, 12585.

Newman, P.A., M.R. Schoeberl and L.R. Lait (1990) 'Comparison of the southern hemisphere springs of 1988 and 1987.' In A. O'Neill (ed.) *"Dynamics, Transport and Photochemistryin the Middle Atmosphere of the Southern Hemisphere."* Kluwer, Netherlands, 71-90.

Niu, X., J.E. Frederick, M.L. Stein and G.C. Tiao (1992) 'Trends in column ozone based on TOMS data: dependence on month, latitude and longitude.' *J. Geophys. Res.*, **97**, 14661-14669.

Oltmans, S.J. and J. London (1982) 'The quasi-biennial oscillation in atmospheric ozone.' *J. Geophys. Res.*, **87**, 8981-8989.

O'Neill, A. and V.D. Pope (1988) 'Simulations of linear and non-linear disurbances in the stratosphere.' *Quart. J. Roy. Meteor. Soc.*, **114**, 1063-1110.

O'Neill, A. and V.D. Pope (1990) 'The seasonal evolution of the extra-tropical stratosphere in the northern and southern hemispheres: systematic changes in potential vorticity and the non-conservative effects of radiation.' In A. O'Neill (ed.) *"Dynamics, Transport and Photochemistry in the Middle Atmosphere of the Southern Hemisphere."* Kluwer, Netherlands, 33-54.

Pawson, S., R.S. Harwood and J.D. Haigh (1992) 'A study of the radiative dissipation of planetary waves using satellite data.' *J. Atmos. Sci.*, **49**, 1304-1317.

Pedlosky, J. (1987) *"Geophysical Fluid Dynamics."* 2nd Ed., Springer-Verlag, 710 pp.

Phillpot, H.R. (1969) 'Antarctic stratospheric warming reviewed in the light of 1967 observations.' *Quart. J. Roy. Meteor. Soc.*, **95**, 328-348.

Pierce, R.B., W.T. Blackshear, T.D. Fairlie, W.L. Grose and R.E. Turner (1993, submitted) 'The interaction of radiative and dynamical processes during a simulated sudden stratospheric warming.' *J. Atmos. Sci.*

Pierce, R.B. and T.D. Fairlie (1993, in press) 'Chaotic advection in the stratosphere: implications for the dispersal of chemically perturbed air from the polar vortex.' *J. Geophys. Res.*

Pitari, G., G. Visconti and M. Verdecchia (1992) 'Global ozone depletion and the Antarctic ozone hole.' *J. Geophys. Res.*, **97**, 8075-8082.

Plumb, R.A. (1989) 'On the seasonal cycle of stratospheric planetary waves.' *Pure Appl. Geophys.*, **130**, 233-242.

Plumb, R.A., D.W. Waugh, R.J. Atkinson, P.A. Newman, L.R. Lait, M.R. Schoeberl, E.V. Browell, A.J. Simmons, M. Lowenstein and D.W. Toohey (1993, submitted) 'Intrusions into the lower stratospheric Arctic vortex during the winter of 1991/92.' *J. Geophys. Res.*

Prata, A.J. (1984) 'The 4-day wave.' *J. Atmos. Sci.*, **41**, 150-155.

Prather, M.J., M.M. Garcia, R. Suozzo and D. Rind (1990) , 'Global impact of the Antarctic ozone hole: dynamical dilution with a 3-D chemical transport model.' *J. Geophys. Res.*, **95**, 3449-3471.

Prather, M.J. and A.H. Jaffe (1990) ' Global impact of the Antarctic ozone hole: chemical propagation.' *J. Geophys. Res.*, **95**, 3473-3492.

Press, W.H., B.P. Flannery, S.A. Teukolsky and W.T. Vettering (1986) *"Numerical Recipes: The art of scientific computing."* Cambridge University Press, 963 pp.

Randel, W.J. (1987a) 'A study of planetary waves in the southern winter troposphere and stratosphere. Part 1: Wave structure and vertical propagation.' *J. Atmos. Sci.*, **44**, 917-935.

Randel, W.J. (1987b) 'The evaluation of winds from geopotential height data in the stratosphere.' *J. Atmos. Sci.*, **44**, 3097-3120.

Randel, W.J. (1988a) 'The seasonal evolution of planetary waves in the southern hemisphere stratosphere and troposphere.' *Quart. J. Roy. Meteor. Soc.*, **114**, 1385-1409.

Randel, W.J. (1988b) 'The anomalous circulation of the southern hemisphere stratosphere during spring 1987.' *Geophys. Res. Letters*, **15**, 911-914.

Randel, W.J. (1992) *"Global Atmospheric Circulation Statistics, 1000 - 1 mb."* NCAR Tech. Note NCAR/TN-366+STR, 256 pp.

Randel, W.J. and L.R. Lait (1991) 'Dynamics of the 4-day wave in the southern hemisphere polar stratosphere.' *J. Atmos. Sci.*, **48**, 2496-2508.

Randel, W.J., D.E. Stevens and J.L. Stanford (1987) 'A study of planetary waves in the southern winter troposphere and stratosphere. Part 2: Life cycles.' *J. Atmos. Sci.*, **44**, 936-949.

Reed, R.J. (1949) *The Effects of Atmospheric Circulation on Ozone Distribution and Variations."* Sc.D. Thesis, Massachusetts Institute of Technology, Cambridge MA, U.S.A., 105 pp.

Reid, S.J. and G. Vaughan (1991) 'Lamination in ozone profiles in the lower stratosphere.' *Quart. J. Roy. Meteor. Soc.*, **117**, 825-844.

Robinson, W.A. (1986) 'The behaviour of planetary wave 2 in preconditioned zonal flows.' *J. Atmos. Sci.*, **43**, 3109-3121.

Rodriguez, J.M., M.K.W. Ko and N.D. Sze (1988) 'Antarctic chlorine chemistry: possible global implications.' *Geophys. Res. Letters*, **15**, 257-260.

Rodgers, C.D. (1976) 'Evidence for the 5-day wave in the upper stratosphere.' *J. Atmos. Sci.*, **33**, 710-711.

Rodgers, C.D. and A.J. Prata (1981) 'Evidence for a travelling 2 day wave in the middle atmosphere.' *J. Geophys. Res.*, **86**, 9661-9664.

Russell, J.M. III, A.F. Tuck, L.L. Gordley, J.H. Park, S.R. Drayson, J.E. Harries, R.J. Cicerone and P.J. Crutzen (1993) 'HALOE Antarctic observations in the spring of 1991.' *Geophys. Res. Letters*, **20**, 719-722.

Salby, M.L. (1984) 'Survey of planetary-scale travelling waves: the state of theory and observations.' *Rev. Geophys. Space Phys.*, **22**, 209-236.

Salby, M.L. and P.F. Callaghan (1993) 'Fluctuations in total ozone and their relationship to stratospheric air motions.' *J. Geophys. Res.*, **98**, 2715-2727.

Schoeberl, M.R. (1978) 'Stratospheric warmings, observations and theory.' *Rev. Geophys.*, **16**, 521-538.

Schoeberl, M.R. and D.L. Hartmann (1991) 'The dynamics of the stratospheric polar vortex and its relation to springtime ozone depletion.' *Science*, **251**, 46-52.

Schoeberl, M.R. and A.J. Krueger (1986) 'Overview of the Antarctic ozone depletion issue.' *Geophys. Res. Letters*, **13**, 1191-1192.

Schoeberl, M.R. and L.R. Lait (1993) 'Conservative coordinate transformations for atmospheric measurements.' In J. Gille and G. Visconti (eds.) *"The Use of EOS for Studies of Atmospheric Physics"*, North-Holland, 419-431.

Schoeberl, M.R., L.R. Lait, P.A. Newman, R.L. Martin, M.H. Proffitt, D.L. Hartmann, M. Lowenstein, J.R. Pedolske, S.E. Strahan, J. Anderson K.R. Chan and B. Gary (1989a) 'Reconstruction of constituent distribution and trends in the

Antarctic polar vortex from ER-2 flight observations.' *J. Geophys. Res.*, **94**, 16815-16845.

Schoeberl, M.R., L.R. Lait, P.A. Newman and J.E. Rosenfield (1992) 'The structure of the polar vortex.' *J. Geophys. Res.*, **97**, 7859-7882.

Schoeberl, M.R., R.S. Stolarski and A.J. Krueger (1989b) 'The 1988 ozone depletion: comparison with previous year depletions.' *Geophys. Res. Letters*, **16**, 377-380.

Shaw, D.B., P. Lonneberg, A. Hollingsworth and P. Unden (1987) 'Data assimilation: the 1984/84 revisions of the ECMWF mass and wind analysis.' *Quart. J. Roy. Meteor. Soc.*, **113**, 533-566.

Shine, K. (1989) 'Sources and sinks of zonal momentum in the middle atmosphere diagnosed using the diabatic circulation.' *Quart. J. Roy. Meteor. Soc.*, **115**, 265-292.

Shiotani, M. and J. Gille (1987) 'Dynamic factors affecting the ozone mixing ratio in the Antarctic winter stratosphere.' *J. Geophys. Res.*, **92**, 9811-9824.

Shiotani, M. and I. Hirota (1985) 'Planetary wave-mean flow interaction in the stratosphere: a comparison between northern and southern hemispheres.' *Quart. J. Roy. Meteor. Soc.*, **111**, 309-334.

Shiotani, M., K. Kuroi and I. Hirota (1990) 'Eastward travelling waves in the southern hemisphere stratosphere during spring 1983.' *Quart. J. Roy. Meteor. Soc.*, **116**, 913-927.

Stolarski, R.S., P. Bloomfield and R.D. McPeters (1991) 'Total ozone trends deduced from NIMBUS-7 TOMS data.' *Geophys. Res. Letters*, **18**, 1015-1018.

Stolarski, R.S., A.J. Krueger, M.R. Schoeberl, R.D. McPeters, P.A. Newman and J.C. Alpert (1986) 'Nimbus 7 satellite measurements of the springtime Antarctic ozone decrease.' *Nature*, **322**, 808-811.

Sze, N.D., M.K.W. Ko, D.K. Weisenstein, J.M. Rodriguez, R.S. Stolarski and M.R. Schoeberl (1989) 'Antarctic ozone hole: possible implications for ozone trends in the southern hemisphere.' *J. Geophys. Res.*, **94**, 11521-11528.

Trenberth, K.E. and J.G. Olson (1988) *"Evaluation of NMC Global Analyses, 1979-1987."* NCAR Tech. Note NCAR/TN-299+STR, 82 pp.

Tuck, A.F. (1989) 'Synoptic and chemical evolution of the Antarctic vortex in late winter and early spring, 1987.' *J. Geophys. Res.*, **94**, 11687-11737.

Vaughan, G. A. Howells and J.D. Price (1993, submitted) 'Connection between total ozone fields and lower stratospheric dynamics.' *Proc. Quadrennial Ozone Symp., Charlottesville, VA, June 1992.*

Vaughan, G. and J.D. Price (1991) 'On the relation between total ozone and meteorology.' *Quart. J. Roy. Meteor. Soc.*, **117**, 1281-1298.

Venne, D.E. (1985) 'The horizontal structure of travelling planetary-scale waves in the upper stratosphere.' *J. Geophys. Res.*, **90**, 3869-3879.

Venne, D.E. (1989) 'Normal-mode Rossby waves observed in the wavenumber 1-5 geopotential fields of the stratosphere and troposphere.' *J. Atmos. Sci.*, **46**, 1042-1055.

Venne, D.E. and J.L. Stanford (1979) 'Observation of a 4-day temperature wave in the polar winter stratosphere.' *J. Atmos. Sci.*, **36**, 2016-2019.

Venne, D.E. and J.L. Stanford (1982) 'An observational study of high-latitude stratospheric planetary waves in winter.' *J. Atmos. Sci.*, **39**, 1026-1034.

Waugh, D.W. and R.A. Plumb (1993, in press) 'Contour advection with surgery: a technique for investigating fine scale structure in tracer transport.' *J. Atmos. Sci.*

Waugh, D.W., R.A. Plumb, R.J. Atkinson, M.R. Schoeberl, L.R.Lait, P.A. Newman, M. Lowenstein, D.W. Toohey and C.R. Webster (1993, submitted) 'Transport

of material out of the stratospheric Arctic vortex by Rossby wave breaking.' *J. Geophys. Res.*

Whitten, R.C. and S.S. Prasad (eds.) (1985) *"Ozone in the Free Atmosphere."* Van Nostrand Reinhold, New York.

Wirth, V. (1990) *"The Seasonal Cycle of Stationary Planetary Waves in the Southern Stratosphere: a Numerical Study."* M.S. Thesis, Massachusetts Institute of Technology, Cambridge MA, USA, 90 pp.

WMO (1962-1992) *"Ozone Data for the World."* **1-30**, Atmospheric Environment Service, Downsview, Ontario, Canada.

WMO (1985) *"Atmospheric Ozone 1985: Assessment of our Understanding of the Processes Controlling its Present Distribution and Change."* WMO Global Ozone Research and Monitoring Project, Report No. 16, WMO, Geneva.

WMO (1988) *"Report of the International Ozone Trends Panel: 1988."* WMO Global Ozone Research and Monitoring Project, Report No. 18, WMO, Geneva, 829 pp.

Yamazaki, K. (1987) 'Observations of the stratospheric final warmings in the two hemispheres.' *J. Meteor. Soc. Japan*, **65**, 51-65.

Yamazaki, K. and C.R. Mechoso (1985) 'Observations of the final warming of the southern hemisphere during 1979.' *J. Atmos. Sci.*, **42**, 1198-1205.

Young, R.E. and H. Houben (1989) 'Dynamics of planetary-scale baroclinic waves during southern hemisphere winter.' *J. Atmos. Sci.*, **46**, 1365-1383.

Zhang, R., P.J. Woodridge, J.P.D. Abbott and M.J. Molina (1993, submitted) 'Physical chemistry of the H_2SO_4/H_2O binary system at low temperatures:stratospheric implications.' *J. Phys. Chem.*